S333 WORKING GROUP
PHASE 1 SYNTHESIS REPORT

September 27, 2023

Prepared by

S333 Working Group Members

SOUTH FLORIDA WATER MANAGEMENT DISTRICT

EVERGLADES NATIONAL PARK

UNITED STATES ARMY CORP OF ENGINEERS

FLORIDA DEPARTMENT OF ENVIRONMENAL PROTECTION

ARTHUR R. MARSHALL LOXAHATCHEE NATIONAL WILDLIFE REFUGE

CONTENTS

EXECUTIVE SUMMARY

Water deliveries to Everglades National Park (ENP) through S333 structure when L29 canal stage is low are generally elevated in total phosphorus (TP). To understand the drivers and provide insight for addressing these elevated TP levels, ENP's South Florida Natural Resources Center invested in a sediment characterization study. Further, the South Florida Water Management District (SFWMD) invested in a hydrodynamic study using Computational Fluid Dynamic (CFD) modeling to estimate and assess velocities for estimating sediment entrainment potentials. The goal of these Phase I studies was to evaluate TP levels and sediment transport/accumulation (marsh to canal and in-canal) characteristics to support recommendations for an initial suite of engineering, maintenance, and/or operational solutions (EMOs), for addressing the elevated TP levels at S333. The Phase I studies were designed to be preliminary studies that could lead to a need for additional studies (Phase II) in the future.

This synthesis report presents the findings from the sediment characterization study, coupled with CFD modeling, focusing on the entrainability of marsh and canal sediments. Evaluation of the flocculent material will be a focus of future studies. The current findings yielded the information that provided the basis for the initial recommended EMOs. Findings suggest that dried sediments in the S333 bay and upstream canal were small (diameter less than 250 microns [μm]) enough to be entrained at fairly low velocities (≥ 1.5 centimeters per second [cm/s]) under low stage conditions (< 9 feet [ft] National Geodetic Vertical Datum of 1929 [NGVD29]). Surface water samples collected in front of S333 demonstrated decreasing TP and total suspended solid concentrations with height from the canal bed.

CFD modeling demonstrated that under the hydrologic conditions experienced during surface water sampling events, velocities were high enough to entrain canal bed sediments. In several of the surface water sampling events, flow coming down the L67A canal exceeded controlled discharge through the S333 gate, and the excess incoming flows moved west in L29 when the S12 structures were open. During water sampling events, flows moving down L67A promoted saltation and bedload sediment transport towards S333. Very little water flowed from L29 east toward S333 during this study. Hence, flow directionality in L29 coupled with the apparently bound nature of TP in the sediments suggest L29 is acting as a TP sediment trap, while high flow rates and associated velocities down L67A appear to be promoting bedload transport towards S333. These transport mechanics can be evaluated with future studies associated with the initial EMOs during an initial period of implementation.

Similarities observed in bulk density, organic matter, and TP concentrations in sediments from the marsh and in the S333 compartment (defined as a 6,560 square meter [m^2] area extending from the S333 structures to the nexus of the L67A and L29 canals) might be explained by flow along canal embankment exchanging with the marsh-edge in the northwest corner of the S333 bay. However, sediment samples deeper in the marsh had relative higher median size (d_{50}) levels that indicate the mineral sediment fractions (non-organic) would be relatively less susceptible to entrainment and transport to the canals when compared to the L67A compartment (defined as a 10,655 m^2 area extending from the S333 compartment to 457 meters (m) upstream in the L67A canal) sediments under the same levels of flows. Thus, this exchange is likely restricted to the canal embankment and marsh-edge interaction during high stage wet periods.

A little more than 8,000 cubic meters (m^3) of sediments was observed in the S333 compartment and upstream 457 m (1,500 ft) in L67A and L29. In the top 5 centimeters (cm) of these sediments, about 1,306 m^3 are within the particle size that is entrainable under relatively low velocities. Approximately 521 kilograms (kg) of TP were apparently bound to these sediments. Removal of these sediments has a potential to reduce TP concentrations during low stage water deliveries through S333.

In conclusion, L67A bedload transport processes are one of the potential sources of TP rich sediments to S333. Other TP sources could include solids (such as organic matter) and floc material that are suspended in the water column that also flow through S333. During the flow direction (tilt current meter) evaluation period of the sediment study, the results indicate L29 waters moved westward to the S12 structures and away from the S333 structures. These flow dynamics indicate that L29 sediment dynamics may have a minor contribution to S333 TP concentrations and dynamics. S333 compartment sediment TP and bulk density similarity to the marsh levels might be explained by marsh-edge and canal embankment water exchanges during the wet season. Removal of sediments accumulated in the S333 compartment and L67A compartment (10,655 m^2 area extending from the S333 compartment to 437 m upstream in the canal), and possibly upstream in the L29 compartment (defined as a 9,995 m^2 area extending from the S333 compartment to 457 m upstream in the L29 canal) as well, has the potential to reduce TP available for water column entrainment. These transport processes should be explored more in the future.

Informed by the sediment and hydrodynamic studies, the recommended solution for immediate implementation includes canal maintenance dredging and installation of low-sill weirs in both the L-67A and L-29 canals, implemented in steps, and should consider the S333 and L67A compartments as first priorities. A monitoring and assessment program is recommended to monitor the effectiveness of this recommended solution for optimization and to inform future actions. In addition, because the recommended solution targets TP from consolidated sediment, a feasibility study on the potential use of innovative technologies to help address elevated TP levels from the flocculent material is being recommended. And finally, advancing the studies to confirm or verify the results from the sediment characterization studies and further evaluate regional nutrient transport and better understand nutrient origins and dynamics in the general system, is recommended. Longer-term recommendations are also presented for consideration.

INTRODUCTION AND BACKGROUND

Due to the elevated TP concentrations in the vicinity of the S333 structure, the agency leadership from the Florida Department of Environmental Protection (FDEP), SFWMD, U.S. Department of the Interior (DOI), and U.S. Army Corps of Engineers (USACE), collectively referred to as the Coordinating Agencies, formed the S-333 Working Group through a collaborative interagency approach. The sole purpose of the working group is to expeditiously make unanimous recommendations to the agency leadership on a suite of potential research projects that could provide information to better understand the localized phenomenon contributing to the phosphorus peaks, or support engineering, operational, or maintenance solutions to redress the phosphorus peaks passing through the S333 structure.

Investigation of the TP dynamics for inflows across the northern boundary of the ENP revealed an annual pattern of low and high concentrations (**Figure 1**) associated with high and low L29 canal water stages, respectively, during specific times of the year. In short, the lowest TP concentrations were observed late in the wet season (May–October), while the highest TP concentrations were observed near the end of the dry season (November–April). The working hypothesis for this cyclic pattern is that these changes in TP concentrations are driven by rainfall and flow dynamics within a complex water management system. Rainfall TP concentrations are generally less than 10 µg/L (Surratt et al. 2012; Ahn and James 2001) as such, rainfall on WCA3A tends to support the lower concentrations observed in the marsh. During high WCA3A stages, marsh runoff into the canal conveys a portion of water above the sediment/floc interface and less sediment/floc transport occurs. This water is characterized by lower TP concentrations, whereas sediment/floc is characterized by higher TP concentrations. During this wet period, TP inputs into the L67A are characterized by low TP levels. During the dry season when the WCA3A marsh water levels recede and

canal and marsh disconnect, water transport toward S333 becomes dominated by L67A waters, with higher TP concentrations than those observed in the marsh.
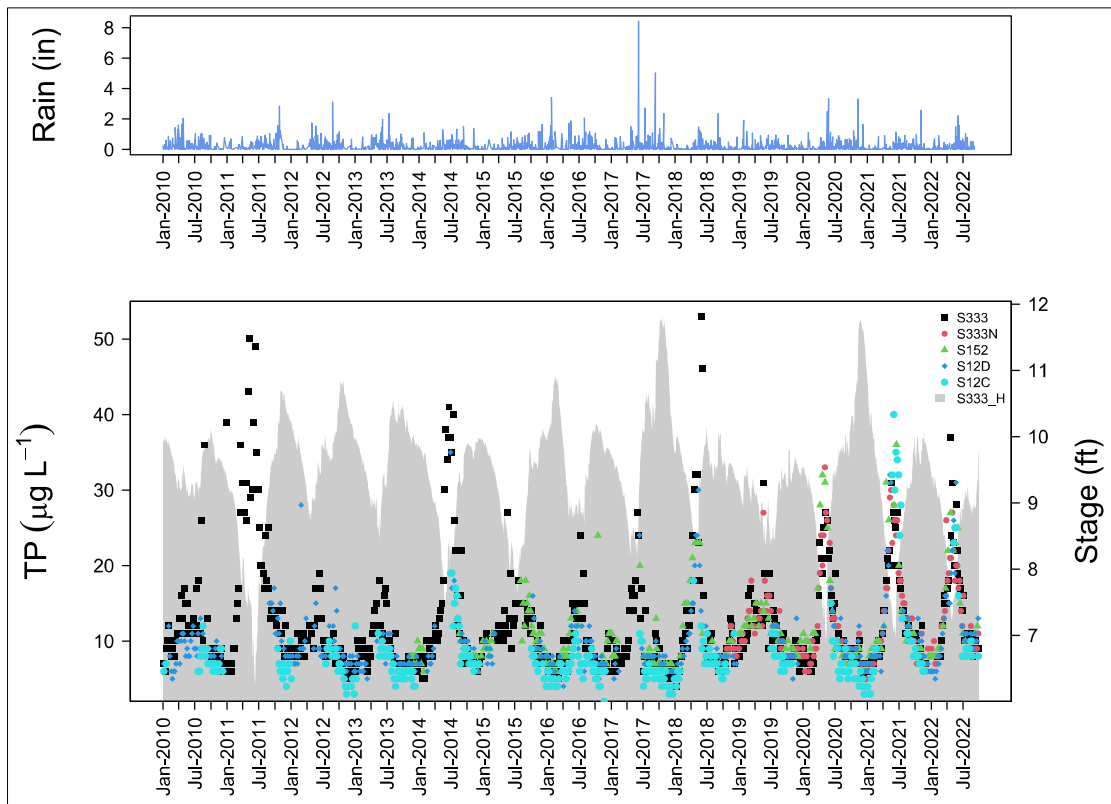
Figure 1. (a) Rain in WCA3 and (b) stage at S333 headwater and TP concentrations at S333, S333N, S152, S12D, and S12C. Data were secured from DBHYDRO , the SFWMD's environmental corporate database. (Note: in – inches and µg L^{-1} – micrograms per liter.)

Through interagency discussions and data evaluation since 2011, a low canal water stage threshold for TP was identified. This threshold was determined to be 9.2 ft NGVD29 at the headwater of the S333 structure and was considered during the development of the most recent water management operations plan, the Combined Operations Plan (COP; USACE 2020). Below this threshold, TP concentrations rarely decline below 8 µg/L. The COP Adaptive Management and Monitoring Plan was developed with the primary objective of identifying the monitoring necessary to inform decision-makers, the COP partner agencies, and the public on progress towards achieving restoration success, as well as address uncertainties related to project performance. COP adaptive management options regarding COP project uncertainty around water quality in Northeast Shark River Slough included short duration, event-based operations to help manage potential water quality concerns for water delivered to ENP. The COP management options were developed to reduce high canal TP concentrations coming out of the dry season by adjusting operations to change spatial and/or temporal quantity and distribution of water, while minimizing the effect on the overall volume of water delivered to ENP. To support the decision-making process, a water quality group consisting of DOI, SFWMD, FDEP, and other agencies with expertise in water quality (led by USACE) conducts discussions to evaluate conditions for potential recommendations to implement the options. Recommendations from the water quality team will be shared with USACE water managers and then brought forth to the periodic scientist meeting for WCA3A prior to implementation of these water quality

strategies. USACE, after receiving input, shall make the operational decision whether to implement the water quality strategy in consideration of water quality and all authorized project purposes. After three years of COP operations, the full suite of specific operational options has not been implemented and only one of the measures was applied, shifting water west from S12D to S12C late in the season during Water Year 2023, with no water quality benefits observed. The federal and state agencies involved in the process have prioritized sending water to ENP with the purpose of improving ecological conditions, and operational options such as reducing flows to mitigate water quality impacts proved difficult to implement. Therefore, an operational solution(s) alone would not be sufficient or desirable to mitigate the high TP levels during low canal stages and additional engineering and maintenance solutions would be likely and necessary to do so.

From a water quality perspective, an additional critical concern comes in the form of the S333 and now S333N structure gate design (**Figure 2**). The S333 and now S333N structure gates (**Figure 2**) were designed to meet multiple and, at times, conflicting objectives (e.g., flood control, water supply, environmental needs). These operate by lifting the gate open from the bottom (canal floor), promoting flow intake from canal bottom that can induce near canal bed scouring and entrain nutrient rich sediments. These entrained sediments appear to be increasing water column TP concentration and thus TP loads delivered to ENP. This concern is most apparent under low stage conditions.
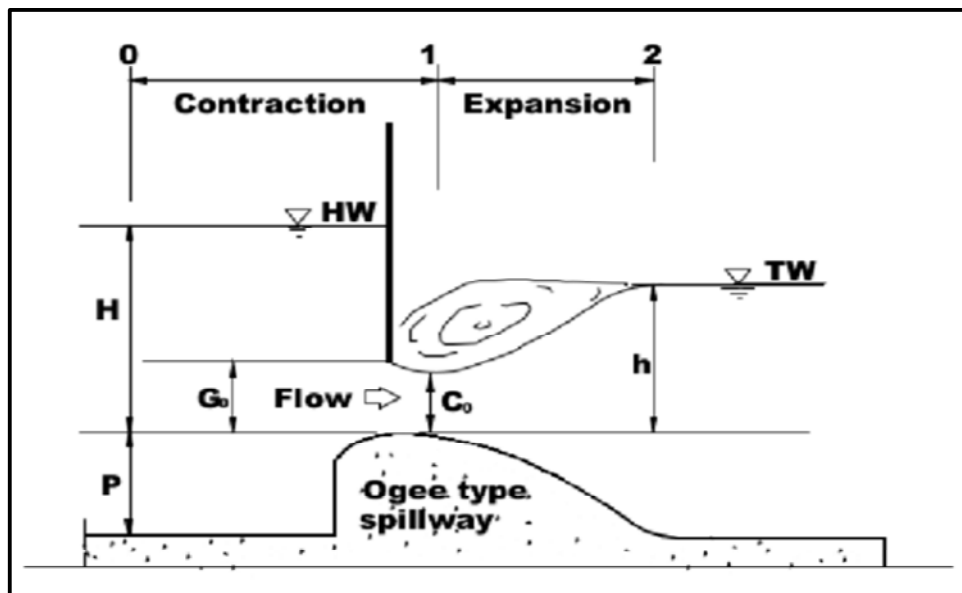
Figure 2. S333 gated structure design. Spillway with a lift-gate resting on a sill three feet from canal floor. (Note: HW – headwater elevation, TW – tailwater elevation, H – Headwater depth above sill crest, h – Tailwater depth above sill crest, G_o – Gate opening, C_o – Critical depth, and P – Height of spillway.)

Given the standing high TP concentrations concerns in waters delivered to ENP during low canal stages, the S333 Working Group developed an outline of research projects (SFWMD 2021) consisting of two sequential phases (Phase I and Phase II) focused on sediment characterization upstream of the S333 structure and hydrodynamic influences of sediment transport on S333 structure operations, to ultimately recommended EMOs. The Phase I studies were limited in scope with an emphasis on canal maintenance through initial localized EMOs. In the development of the Phase I studies, it was acknowledged that additional studies in a potential Phase II would be needed to fully understand TP sources and regional

influences. However, the information obtained under Phase I is informative to the initial recommendation presented in Part II of this report.

In Phase I, ENP investigated sediment characteristics and flow dynamics (results summarized in **Section 1.0** of **Part I** below) and SFWMD investigated hydrodynamics through computational modeling (results summarized in **Section 2.0** of **Part I** below). This report synthesizes ENP and SFWMD investigations and is aimed at informing potential EMOs for reducing TP concentrations to protective levels. The recommended EMOs are presented in **Part II** of this report.

PART I: PHASE I STUDIES

1.0 SEDIMENT CHARACTERIZATION STUDIES

The sediment characterization studies included three agreements with individual principal investigators: two from Florida International University, and one from the University of Florida. These three studies (1) investigated sediment transport at the S333 gated structure and upstream in the L67A and L29 canals; (2) performed an acoustic survey of the sediments along the canal floor to quantify sediment volume; and (3) developed sediment physiochemical profiles local to S333 to include L67A, L29, the bay in front of S333, and in the marsh. Additionally, ENP investigated flow profiles and direction in L67A and L29, and at the S333 gate.

Pertinent information from the sediment characterization investigations focuses on sediment particle size distribution, sediment volume at S333 and upstream along L67A and L29 canals, mass of TP in these sediments, TP in the surface water, and flow velocities and directionality. These data were identified as essential for informing the hydrodynamic studies and/or EMOs. The first section of the report focuses on presenting the results from the sediment characterization, flow profiles, and flow direction and concludes with an estimation of the potential sediment TP mass and resulting concentration reductions that EMOs might realize. The complete individual principal investigators sediment study reports are provided in Attachment 1, including the S-333 Working Group's comments on the reports and responses provided by ENP through consultation with the principal investigators.

Methods

Site Description

In 2022, sediment samples were collected near the S333 structure, upstream of S333 in the L29 and L67A canals, and in the WCA3A adjacent marsh (**Figure 3**). This sampling occurred during April and May in the canals, and during September in the marsh. A total of 91 sampling sites were selected for the sampling events from April through September 2022, including 12 sites in the marsh, 10 transects in the L67A canal, 12 transects in the L29 canal, and 8 transects near S333 (**Figure 3**). For each transect in canals, three sites (middle of the canal, two-thirds from the middle of canal) were sampled for sediments. All seven surface water sampling events were conducted when water levels at headwater of S333 structure were below 9.2 ft NGVD29 (**Figure 4**).

Figure 3. Locations of sampling events during 2022 include 12 sites in the WCA3A marsh, 10 transects in the L67A canal, 12 transects in the L29 canal, and 8 transects near the S333 structure.

Figure 4. Hydrologic conditions associated with the 7 surface water quality sampling events.
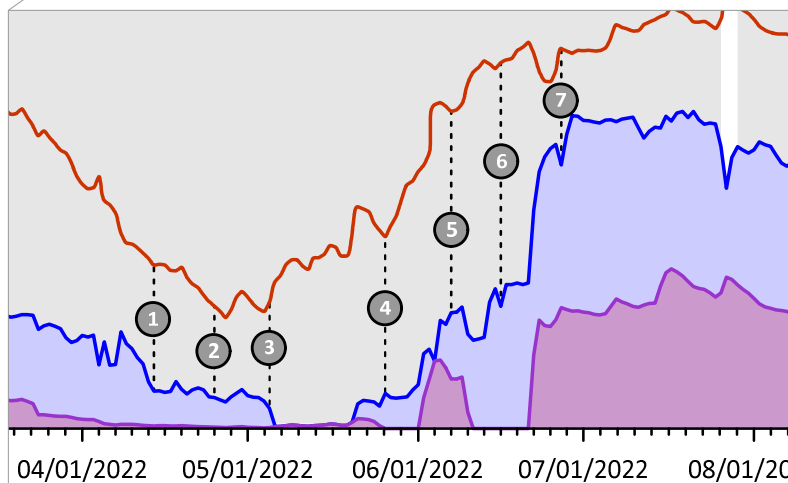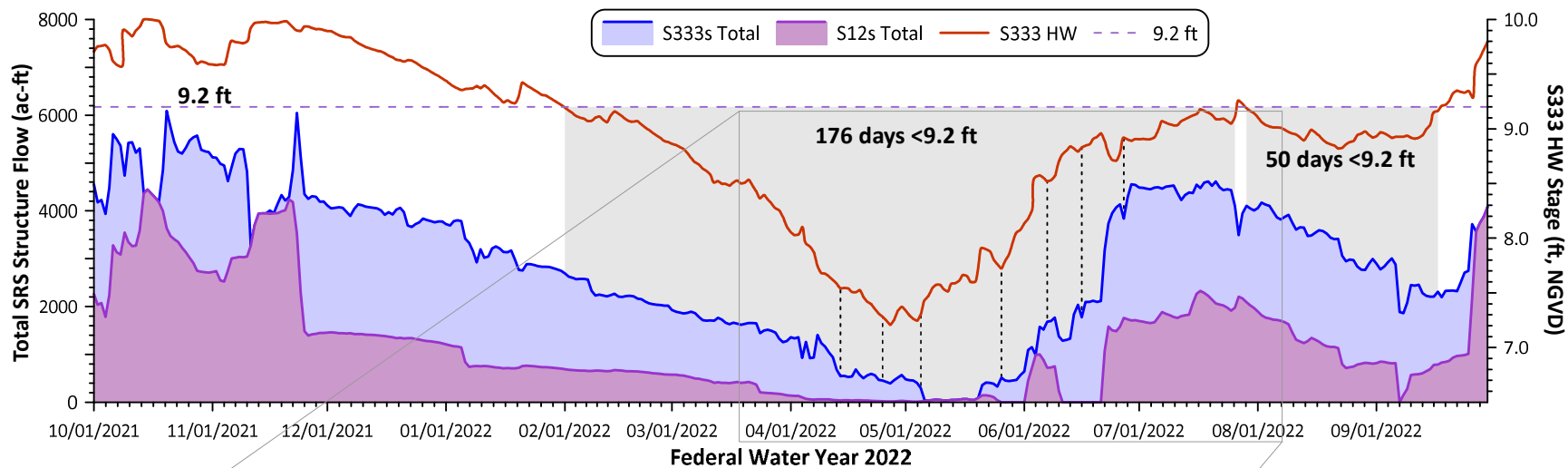
Water Quality Sampling Events

Event Number	Event Date	S333 Stage (ft, NGVD)	Total S333 Flow (ac-ft)	Total S12s Flow (ac-ft)	Total Flow (ac-ft)
1	04/14/2022	7.54	509	36	545
2	04/25/2022	7.28	430	20	450
3	05/05/2022	7.31	281	14	295
4	05/26/2022	7.72	514	0	514
5	06/07/2022	8.52	965	720	1,685
6	06/16/2022	8.83	1,778	0	1,778
7	06/27/2022	8.92	2,076	1,762	3,838

Sediment Core Sampling

A universal core head was screwed onto an extension rod, lowered into the canal, pushed into the sediment as deep as possible, and slowly extracted. The core was capped and stored vertically in a large cooler until transported back to the lab and then stored vertically in a cooler room at 4 degrees Celsius (°C) until processed. A similar procedure was used to collect sediment cores in the marsh.

Cross-sectional Water Sampling

Water samples were collected in front (~23 m) of S333 on a horizontal transect across vertical transects to form a cross-section (**Figure 5**) during seven water sampling events on April 14, April 25, May 5, May 26, June 7, June 16, and June 27, 2022. Water samples were analyzed for particle size distribution, TP, total suspended solids (TSS), and total dissolved phosphorus (TDP). The water samples were collected using the telescopic sampling pole and portable pump. The samples were collected at heights of 30, 60, 100, 160, 250, and 500 cm from the canal bed. Additionally, one sample from the water surface was taken at 50 cm depth for every vertical transect.
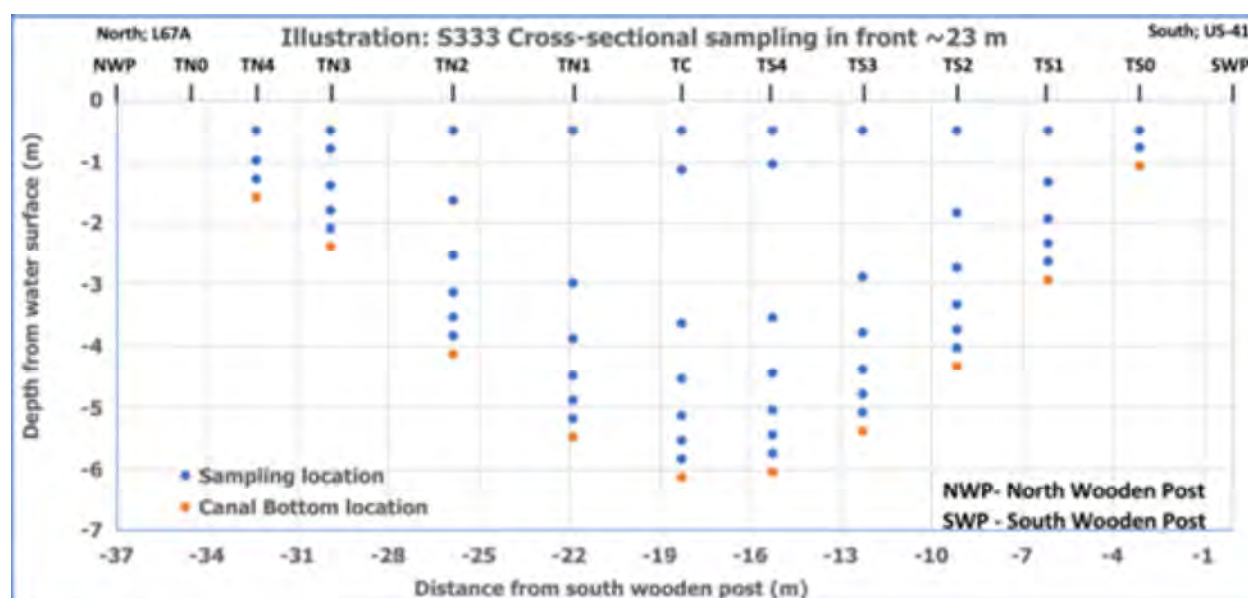
Figure 5. Illustration of water sample collection on 7 sampling events during April–June 2022 at ~23 m in front of S333. (Note: SWP – towards US-41, NWP– towards the L67A canal, TC– central vertical transect, TS – southern vertical transects, and TN – northern vertical transects).

Canal Flow Profile and Direction Measurements

Flow measurements were taken during seven water sampling events (April 14, April 25, May 5, May 26, June 7, June 16, and June 27, 2022) at ~457 m upstream of S333 across the L29 and L67A canals. Flows were also measured across the canal ~23 m in front of the S333 gate. The flow measurements were done using an acoustic Doppler current profiler (ADCP) from Teledyne RD Instruments using Model-Workhorse running at 1,200 kilohertz (KHz) frequency following the instructions within the manufacturer's operation manual. Analysis of ADCP data was conducted using Teledyne RD Instruments WinRiver II software (https://hydroacoustics.usgs.gov/movingboat/WinRiverII.shtml) and QRev USGS software (https://hydroacoustics.usgs.gov/movingboat/QRev.shtml) for comparison.

Tilt current meters (TCMs) from Lowell Instruments LLC were installed at ~305 m upstream of S333 in the center of the L29 and L67A canals to continuously measure flow speed and direction from March through October 2022. The TCM measures current using the drag-tilt principle. The data logger is buoyant and is anchored to the bottom of the canal via a short flexible tether. Moving water tilts the data logger in the direction of flow. The TCM contains a 3-axis accelerometer and 3-axis magnetometer for measuring tilt and bearing. The resulting orientation data is converted to current by applying calibration coefficients.

Analytical Methods

The physical and chemical analyses performed on sediments and water samples included sediment bulk density (BD), particle size distribution, TSS, TP, TDP, and phosphorus (P) fractionation.

Physical Parameters

The dry BD of each 0-5-cm sediment core was calculated by dividing the mass of sediment core by its volume. TSS were measured following Baird et al. (2017).

Laser Diffraction

The particle size distributions in water and sediments were determined using the laser diffraction method. In this method, a laser diffraction particle size analyzer (LS 13 320, Beckman Coulter, Brea, CA) was used. Briefly, either 125 milliliters (mL) of water or 5 mL of dried sediment sample (< 1 millimeter [mm]) were loaded into the liquid or dry powder module of the analyzer. For each water sample, the measurement duration was set to 60 seconds, while the duration for sediment samples was ~120 seconds. Minor uncertainties may occur if results are compared to laser analyses performed on wet samples.

Chemical Parameters

Sediment TP concentration was determined following a modified EPA 365.3 colorimetric method (USEPA 1982). The sequential fractionation procedure for P in sediment involves a series of chemical extractions that partition TP into different forms or fractions. These fractions represent different pools of P with varying availability and potential for releasing P into the water. For this study, sediment TP was differentiated into seven forms using a modified sequential fractionation procedure (Irick et al. 2013; Zhang and Kovar 2009). These P fractions were extracted sequentially by different reagents as follows:

- Water-soluble P using water (H_2O)
- Exchangeable P using 1-molar (M) ammonium chloride (NH_4Cl)
- Aluminum (Al)-bound P using 0.5-M ammonium fluoride (NH_4F)
- Iron (Fe)-bound P using 0.1-M sodium hydroxide (NaOH)
- Organic P using 0.1-M NaOH + digestion
- Calcium (Ca)-/magnesium (Mg)-bound P using 0.5-M hydrochloric (HCl)
- Recalcitrant residual P using 6-M HCl

The P fractions were aggregated into apparently available-P and apparently bound-P categories in relationship to canal bed sediment interaction with overlying canal water. These aggregations have implications for potential release to surface water based on P availability and reactivity. Apparently available-P refers to aggregated fractions (water-soluble P and exchangeable P) that can be easily released or exchanged into the flowing water. Apparently bound-P, on the other hand, refers to remaining aggregated fractions (Al/Fe-bound P, Ca/Mg-bound P, organic P, and residual P) that are bound to sediment minerals, organic matter, or other forms of chemical complexes, and are relatively resistant to

be released to the surface water. However, one should recognize that organic P and P fractions bound to clay particles (small lighter particles) would be available for entrainment within the flowing waters.

Water samples were analyzed for TDP and TP (USEPA method 365.1 following dry ashing according to Solórzano and Sharp 1980). Particulate phosphorus (PP) was calculated as the difference between TP and TDP.

Spatial and Statistical Data Analysis

The Quantum Geographic Information System (QGIS) software (version 3.30.2) was used to generate maps for sampling sites and to summarize and present results. Total P mass present in 5-cm core depths for 1-m^2 area at sample collection points was interpolated for the desired area in the canal and the marsh using inverse distance squared weighting (IDW) tool and a grid size of one square meter. The summation of mass over the desired area provided total TP mass present in 5-cm depth. A similar method was applied for estimating sediment volume using IDW. As IDW does not provide prediction standard errors, they are not reported. Differences in the TP mass and sediment volume results obtained from estimating the mass and volume from the entire surveyed area or by summing S333, L67A, and L29 individual compartments (defined in the *Results* section for sediment volume and total phosphorus mass) area can occur. Clipping surveyed area by the compartment polygons may exclude individual pixels, based on software's design, which might lead to decreased total pixels.

Statistical analyses were conducted following a rank-based nonparametric multiple contrast test procedure (mctp) using "nparcomp" package via the "mctp" function (Noguchi et al. 2020). Statistically significant differences for the mctp test were indicated using different letters among compartments. Kruskal Wallis (Mann-Whitney U) rank sum test was used to test for differences among locations across parameters.

Entrainable Sediment and TP Mass Determination

Laser particle size differential volume (LPSDV) curves (**Figure 6**) were used with a 200-μm threshold to estimate the mass of entrainable sediment. Below 200 μm, bedload sediments are considered entrainable at velocities greater than 1.5 cm/s (0.05 foot per second [ft/s]) (Hjulstrom 1935). Based on the hydrodynamic modeling output, low-stage low and medium flow velocities were estimated to be between 1.5 to 19.8 cm/s (0.05 to 0.65 ft/s) in the L67A canal. These velocities are associated with the modeled 750 to 1,500 cubic feet per second (cfs), which are flow conditions experienced historically during low canal water stages conditions.

Analyses of the LPSDV curves (**Figure 6**) resulted in 25 to 85% of the particle sizes being below the 200-μm threshold. The individual percent entrainable fraction was multiplied by the mass of the top 5 cm of the individual sediment cores to estimate the mass of entrainable sediments per core. TP mass associated with this entrainable sediment mass was determined by multiplying the TP concentration for the core by the entrainable sediment mass. Consistent with total sediment and TP mass determination, IDW was applied to the entrainable fraction of sediments and TP to determine entrainable masses for each compartment (L67A canal, L29 canal, and S333).
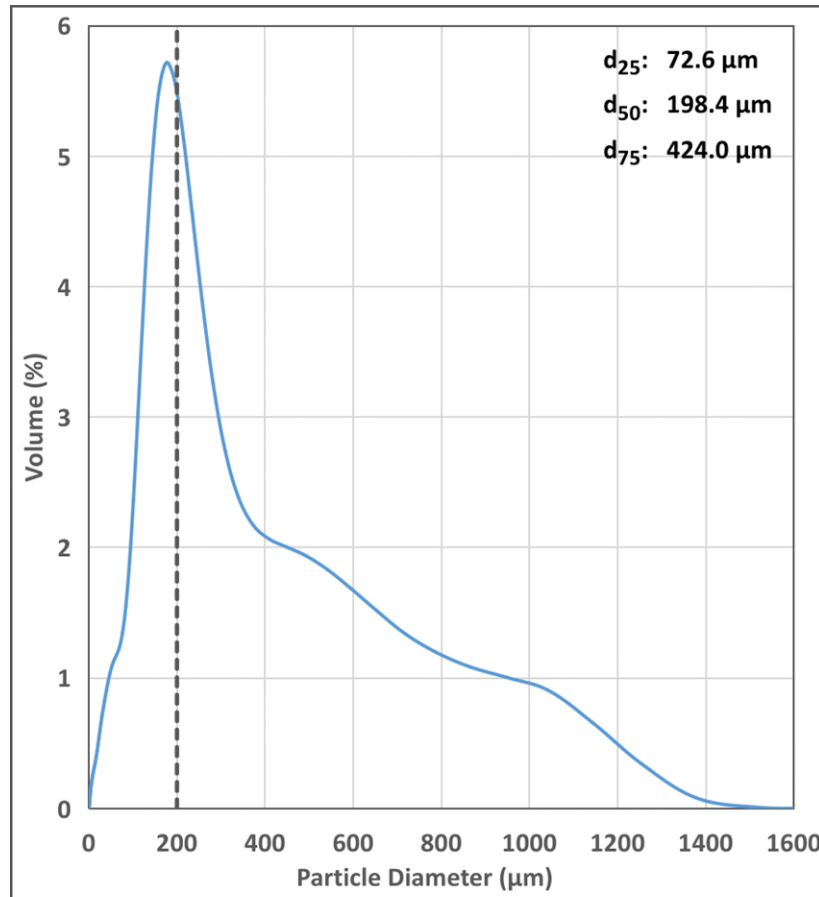
Figure 6. Illustration of LPSDV curve along with the 200-μm threshold used to estimate the mass of entrainable sediments. The volume under the curve represents 100% of the particle volume. (Note: d_{25}, d_{50}, and d_{75} represent the relative sizes of particles with d_{25} being the 25th percentile, d_{50} the median, and d_{75} the 75th percentile.)

Results

Sediment Volume and Total Phosphorus Mass

The L29 canal compartment extends 457 m upstream from S333 for a total area of 9,995 m^2 and a sediment volume of 3,232 m^3 (**Figure 7**). The L67A canal compartment extends 457 m upstream of S333 for a total area of 10,655 m^2 and a sediment volume of 3,071 m^3. Total area for compartment S333 was 6,560 m^2 with a sediment volume of 2,013 m^3.

Total P mass in the top 5 cm of sediments was 307 kg for the L29 canal compartment, 153 kg for the L67A canal compartment, and 77 kg for compartment S333 (**Figure 8**). The sediment TP mass decreased from west to east in the L29 canal and increased from north to south in the L67A canal. The S333 area sediment typically showed lower TP mass near the S333 gate and higher near the marsh.

L29 canal sediment BD decreased from west to east (**Figure 9**). Different from sediment TP mass, S333 sediment BD was relatively lower near the marsh and higher near the structure. L67A canal sediment BD was greater than that of the L29 and S333 samples. Based on the power model fit, sediment BD was highly correlated with organic matter content (**Figure 10**). TP mass was similar among the 12 marsh sediment samples (**Figure 11**).
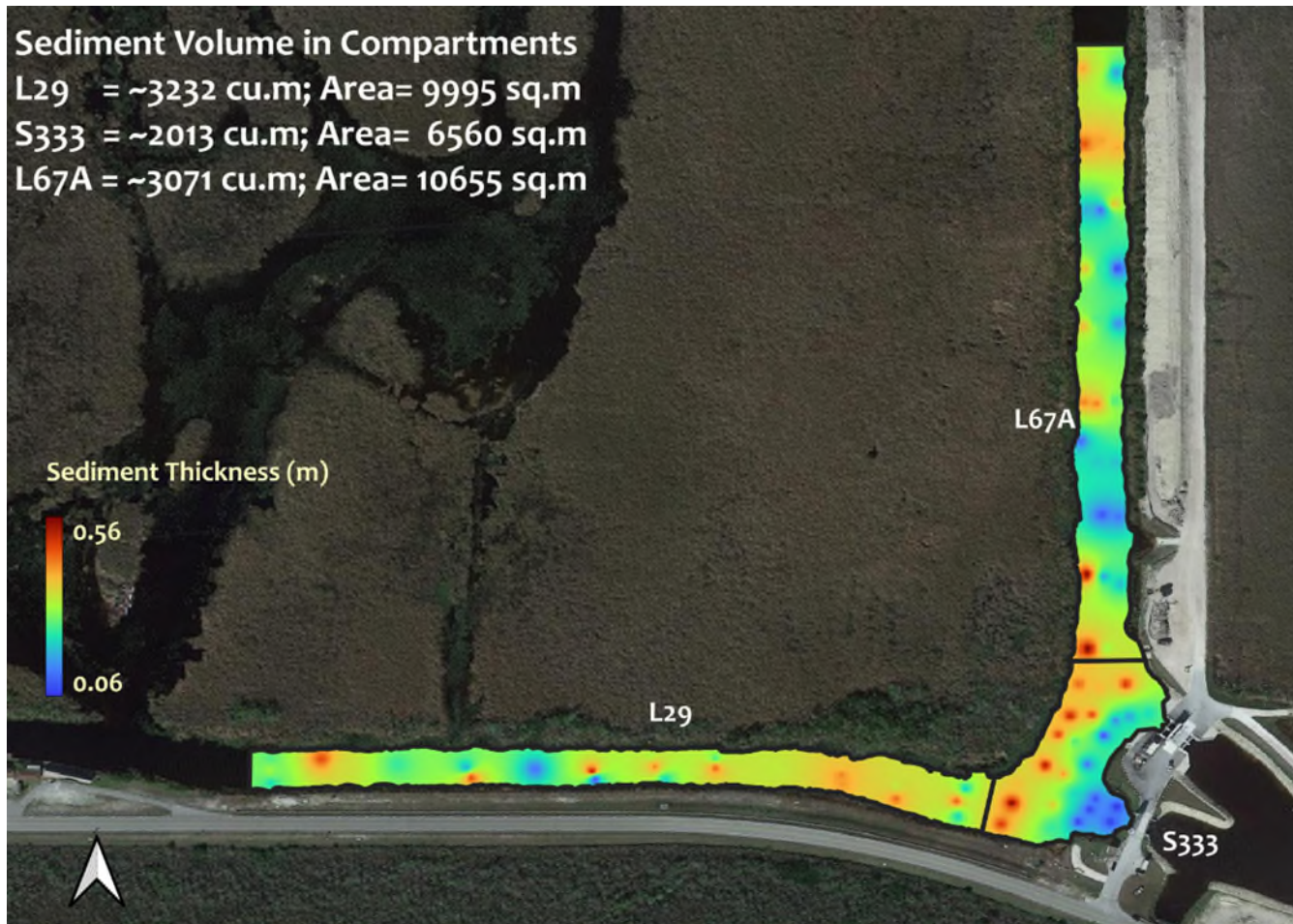
Figure 7. Sediment volume in L29 canal, S333, and L67A canal compartments.
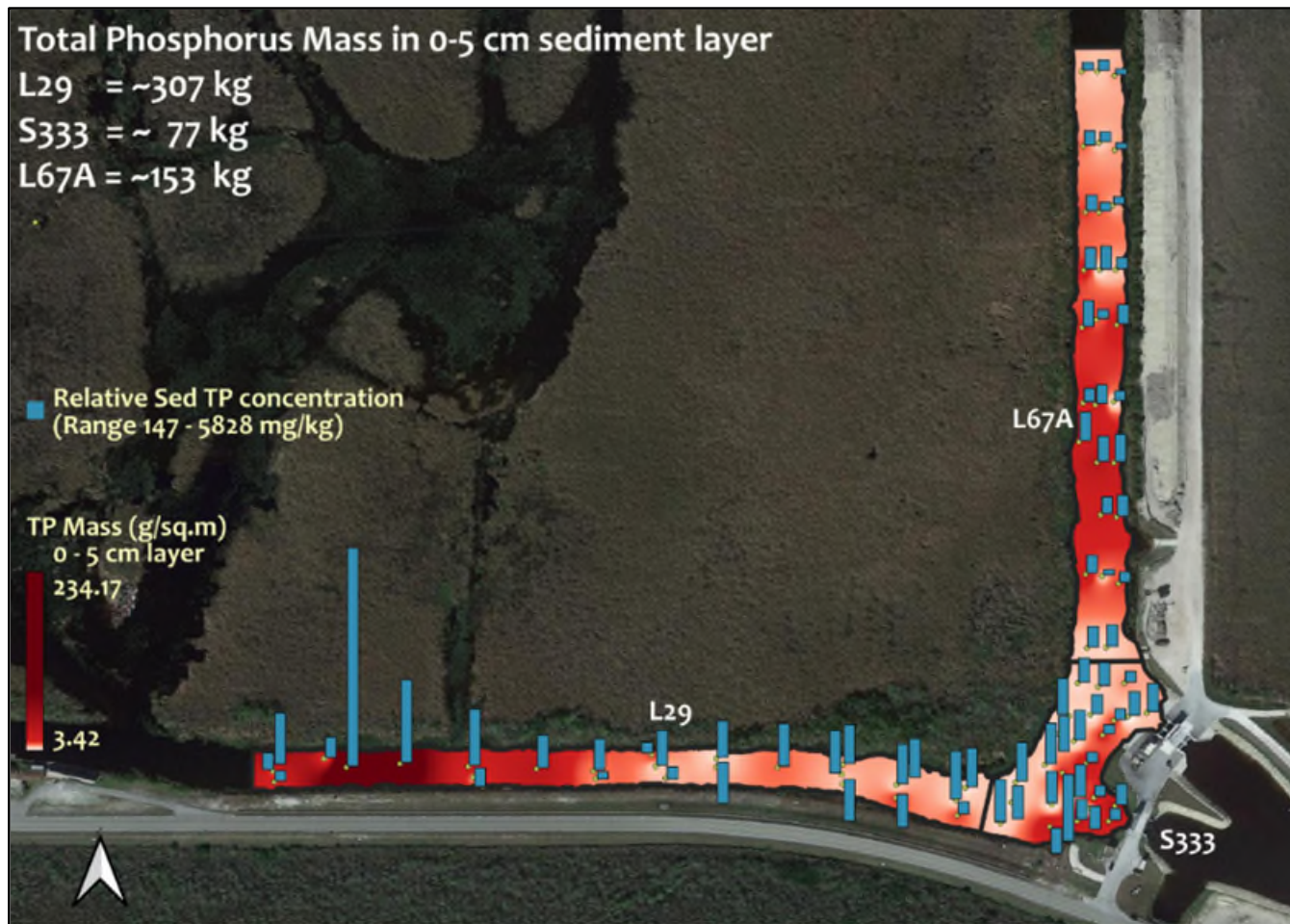
Figure 8. TP concentration bar plot of sediment surface (0-5 cm) in the L29 canal, near the S333 structure, and the L67A canal. The height of each bar represents relative TP concentration for the sampling location in grams per square meter (g/m). Total phosphorus mass (kg) contained in sediment surface (0-5 cm) in the L29 canal, near the S333 structure, and the L67A canal are also indicated.
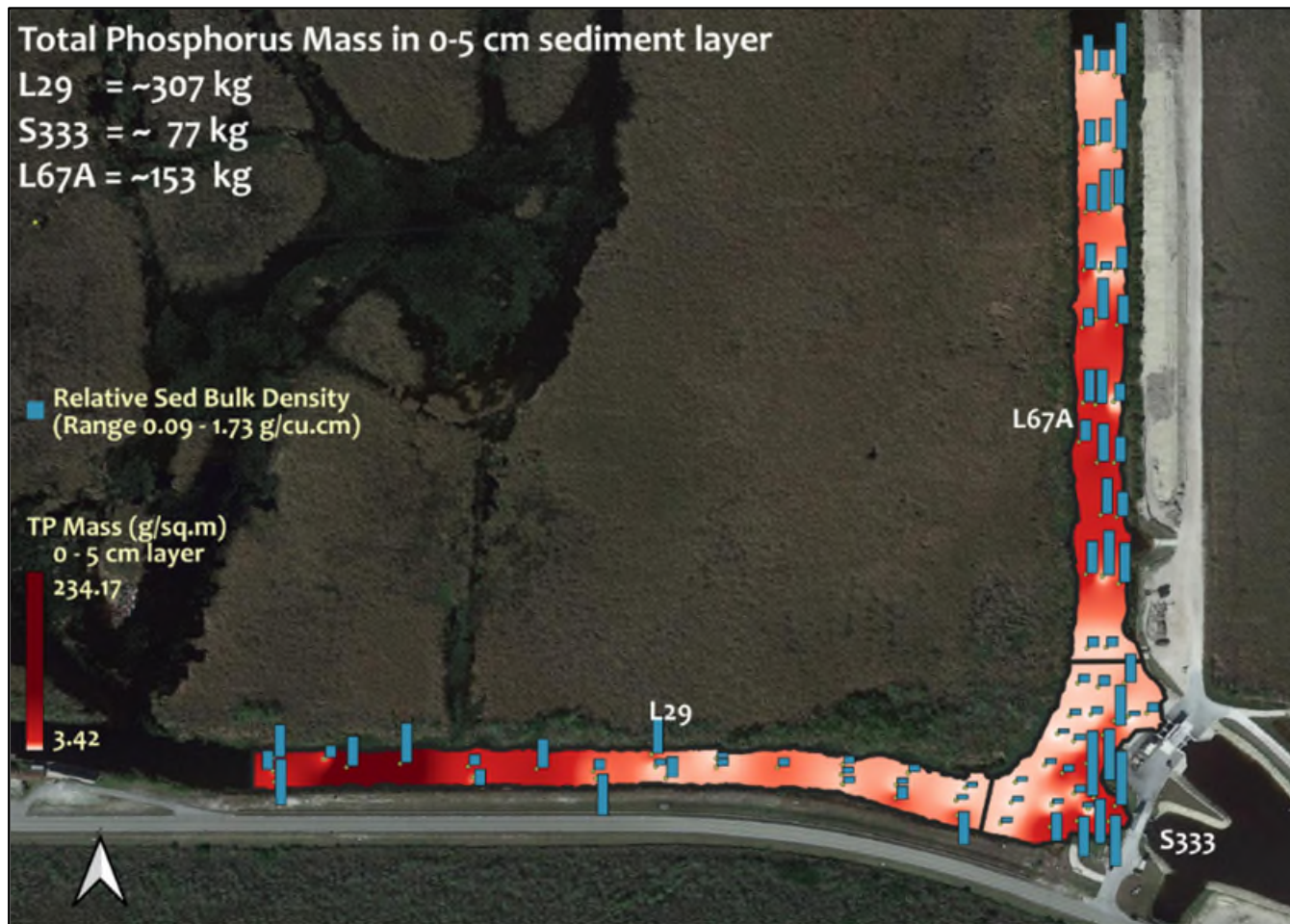
Figure 9. BD bar plot of sediment surface (0-5 cm) in the L29 canal, near the S333 structure, and in the L67A canal. The height of each bar represents relative BD from the sampling location. TP mass (kg) contained in sediment surface (0-5 cm) in the L29 canal, near the S333 structure, and in the L67A canal are also indicated.
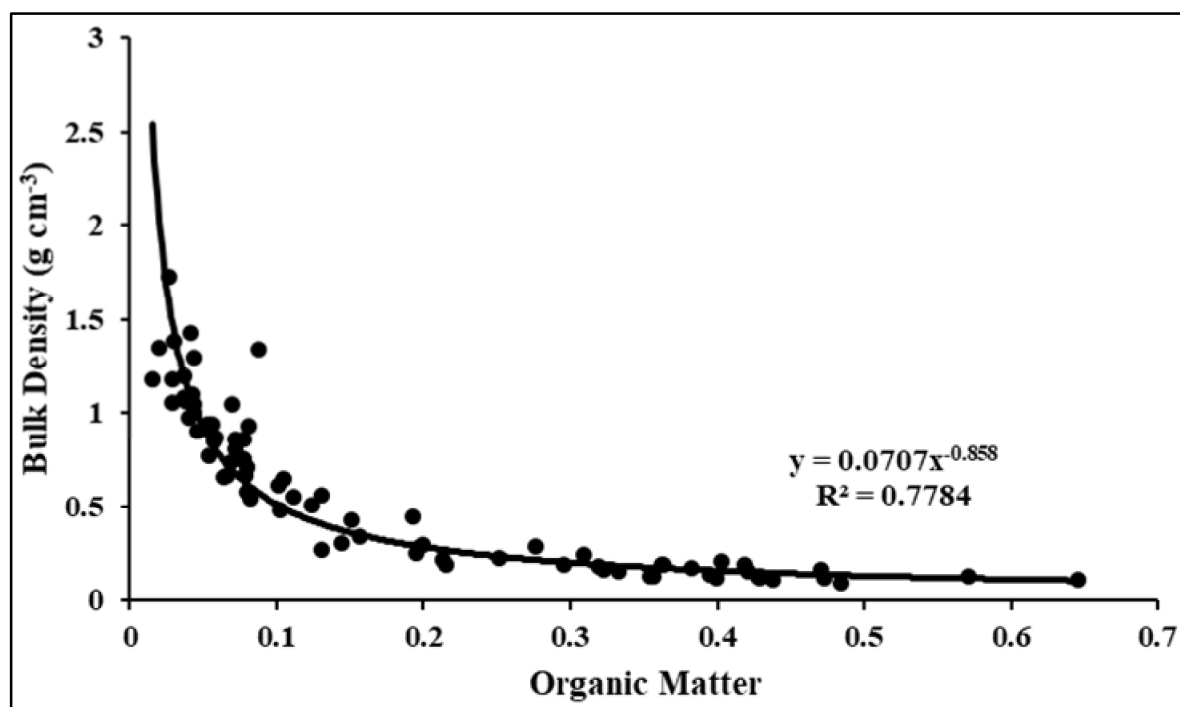
Figure 10. BD and organic matter scatterplot of sediment surface (0-5 cm) near the S333 structure, and in the L29 and L67A canals.
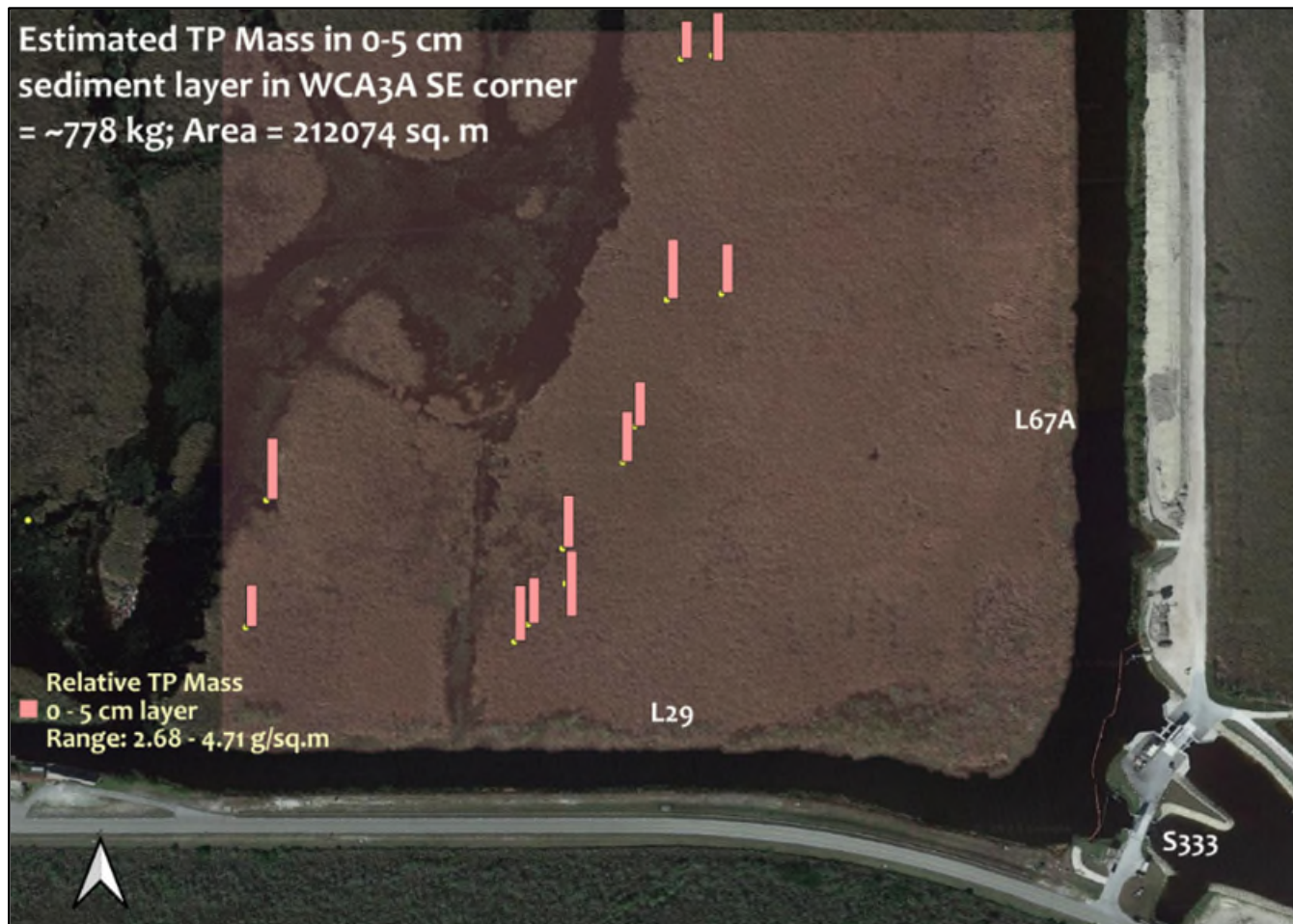
Figure 11. TP concentration bar plot of sediment surface (0-5 cm) at adjacent marsh near the S333 structure, and in the L29 and L67A canals. The square shade represents marshland area used for estimation. The height of each bar represents relative TP mass for the sampling location in g/m^2.

Sediment Particle Size Distribution

Sediment particle size distribution, represented as the median particle size or d_{50}, varied among compartments (**Figure 12**). Statistically, marsh d_{50} (median = 277 µm; interquartile percentile (IQP) = 251, 324 µm) was greater than all canal compartments (mctp; probability [p] < 0.01), while S333 d_{50} (median = 143 µm; IQP = 130, 188 µm) was similar to the L67A canal (median = 166 µm; IQP = 145, 224 µm) and L29 canal (median = 188 µm; IQP = 169, 206 µm). Maximum d_{50} across the compartments were less than 450 µm.
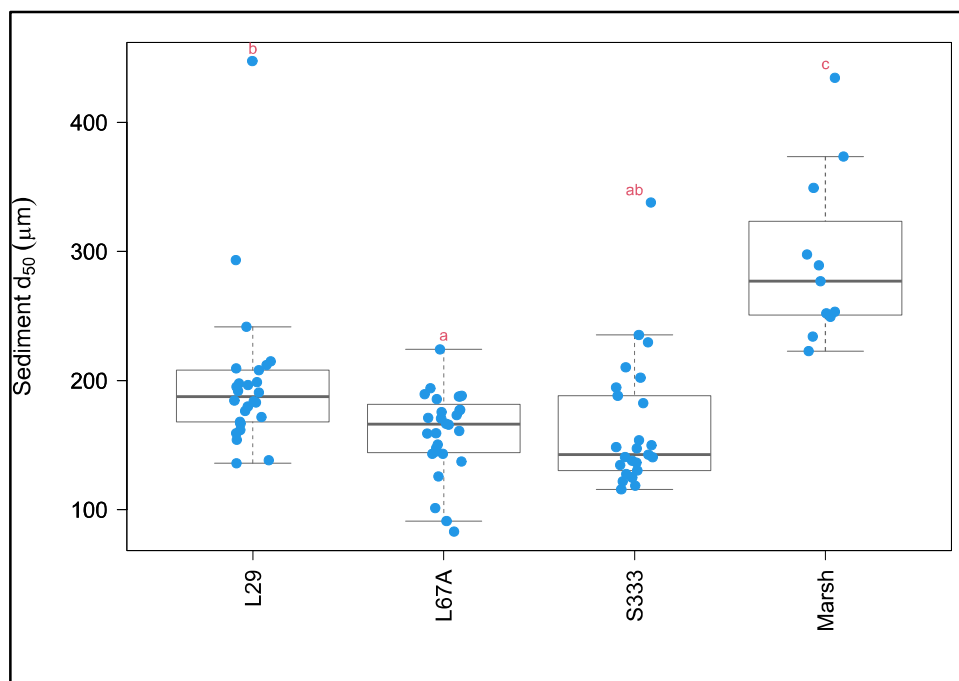
Figure 12. Sediment particle size represented as d_{50} across the four compartments. Differences in letters above boxes indicates statistically significant differences between compartments.

Total Phosphorus Fractions

TP present in sediment samples was differentiated into seven forms by P fractionation analysis: (1) water-soluble P, (2) exchangeable P, (3) Al-bound P, (4) Fe-bound P, (5) organic P, (6) Ca/Mg-bound P, and (7) residual P. TP concentrations in sediment samples followed an order by compartment of L29 > Marsh > S333 > L67A (**Figure 13A**). Residual P, Ca/Mg-bound P, and Al-bound P were the major P forms present in the sediment canal samples (L29, L67A, and S333), with little water-soluble, organic, and exchangeable P present (**Figure 13B**). The majority of P in sediment marsh samples was present as Al-bound P and residual P, and a modest amount of Ca/Mg-bound P, Fe-bound P, water-soluble P, and exchangeable P were also present (**Figure 13B**). In canal sediments ~98 % was bound-P and ~2 % in available-P form. Marsh sediments had ~87 % in bound-P and ~13 % in available-P form.
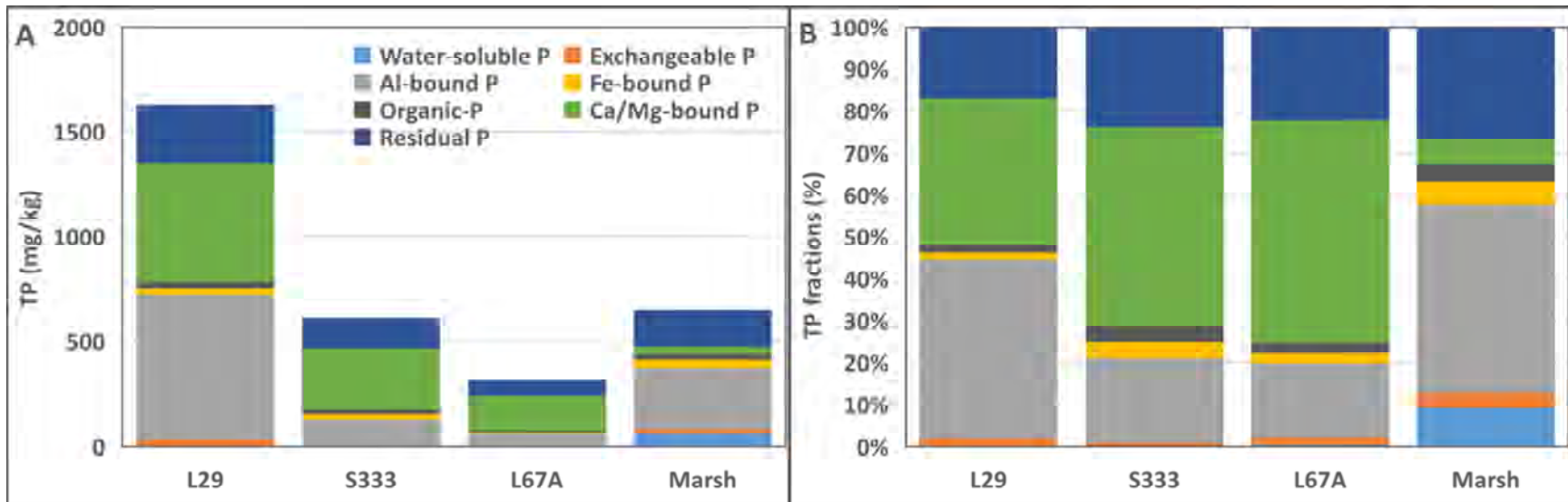
Figure 13. Distribution of various forms of P expressed as (A) concentrations and (B) percentages of TP in sediments.

Phosphorus and Total Suspended Solids Concentrations: Sediment and Surface Water

Sediment TP concentrations showed some variability across compartments (**Figure 14**). Compartment L67A (median = 401 milligram per kilogram [mg/kg]; IQP = 254, 769 mg/kg) had the lowest TP concentrations (mctp; p < 0.001), while the S333 compartment (median = 651 mg/kg; IQP = 510, 882 mg/kg) was similar to the L29 (median = 1,005 mg/kg; IQP = 510, 1,131 mg/kg) and marsh (median = 693 mg/kg; IQP = 641,723 mg/kg) compartments.
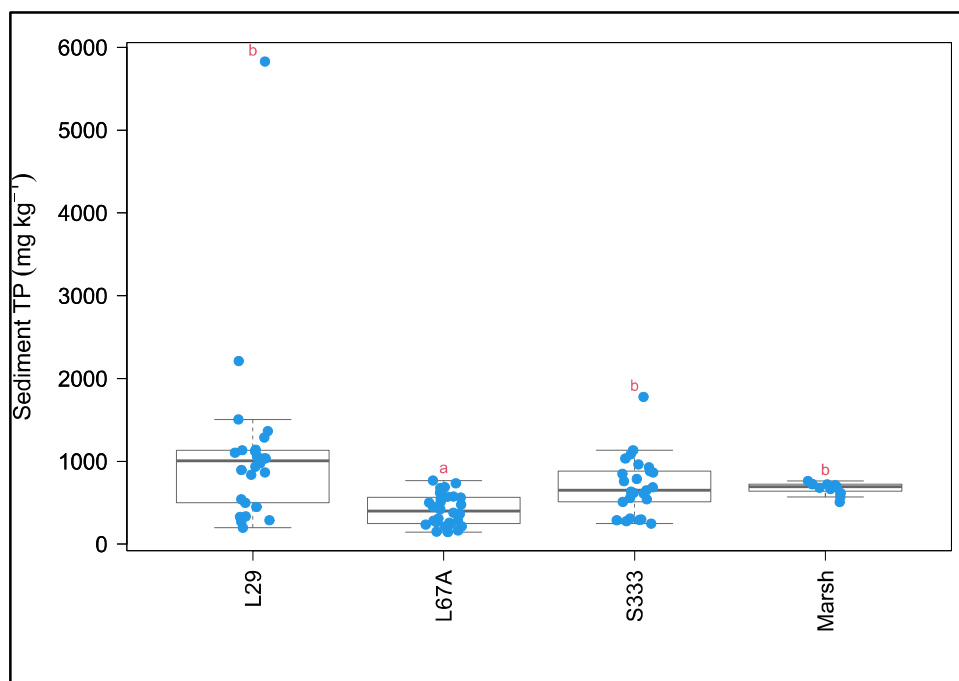
Figure 14. Sediment TP concentrations across the four compartments. Differences in letters above boxes indicates statistically significant differences between compartments.

Surface water cross-sectional sampling for TP and PP in front of S333 had varied vertical gradients over the seven sampling events (**Figure 15a**). Significant interactions among TP, distance from the southwest pole, and height from the canal floor were observed for sample events on April 14 and May 26 (data not shown). There were also significant relationships between height from canal bed and TP concentrations (Kruskal-Wallis, p < 0.05) for sample events April 14, May 5, May 26, and June 16 (**Figure 16**). For the seven sampling events, TP concentrations in these cross-sections were two to four times greater than 8 μg/L, which is the protective inflow target, throughout the water column. Like TP, particulate phosphorus (PP) concentrations increased with depth (**Figure 15b**). Some of the higher PP concentrations were observed during the March 5 (median = 25 μg/L; IQP = 22, 29 μg/L), March 26 (median = 29 μg/L; IQP = 24, 32 μg/L), and June 27 (median = 29 μg/L; IQP = 27, 32 μg/L) sampling events.
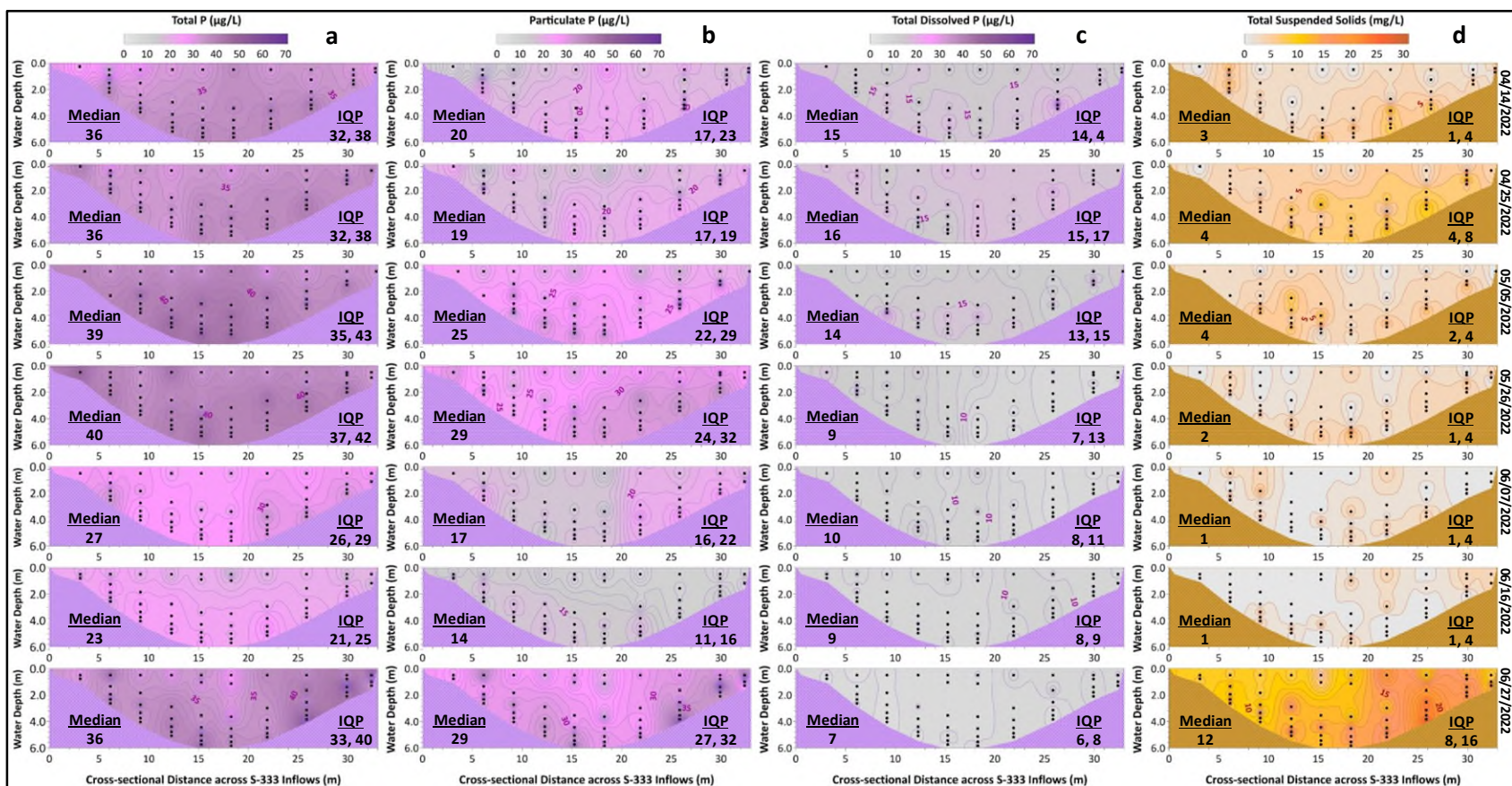
Figure 15. Cross-plot representations of the cross-sectional sampling in front of structure S333 for (a) TP, (b) PP, (c) TDP, and (d) TSS across the 7 surface water sampling events. (Note: IQP – Interquartile Percentiles.)
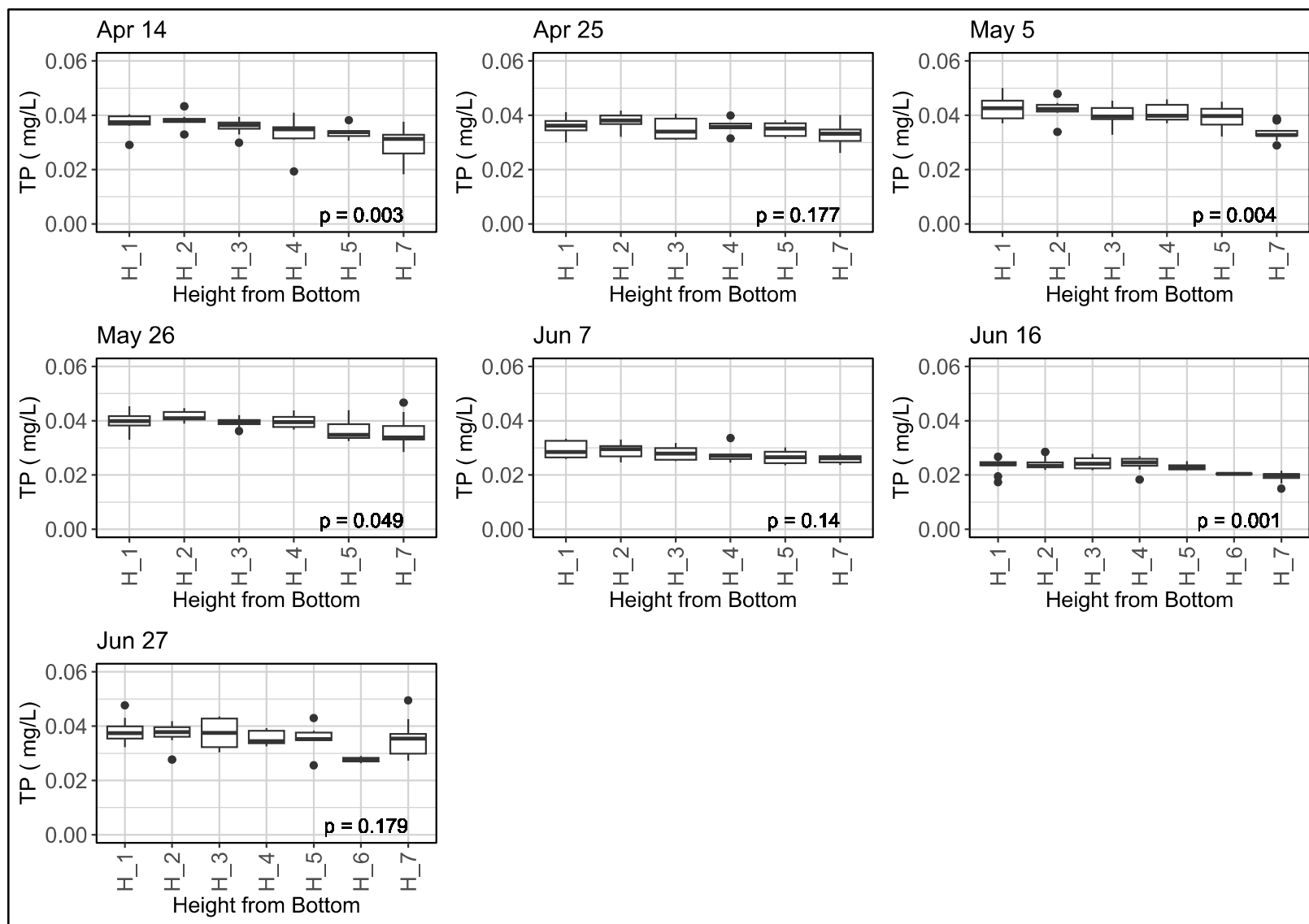
Figure 16. Boxplots of TP concentrations in milligrams per liter (mg/L) with height from canal floor. H1 represents 30 cm from the canal floor while H7 represent 50 cm from the canal surface. P-values are from the Kruskal-Wallis statistical test.

TDP at the cross-section in front of S333 had generally lower concentration (**Figure 15c**) as S333 stage and flows increased among the sampling events (**Table 1**). Median TDP concentrations among sample dates ranged from 7 µg/L (IQP = 6, 8 µg/L; June 27) up to 16 µg/L (IQP = 15, 17 µg/L; April 25). Only June 16 had a significant interaction with p-value = 0.099 among TDP, distance from the southwest pole, and height from the canal floor. There was also a significant relationship between height from canal floor and TDP concentrations (Kruskal-Wallis, $p < 0.05$) for the April 14 sample event (**Figure 17**).

Table 1. Mean flows in the L29 and L67A canals and at
the S333 structure gate during 7 water sampling events.

Date	S333 Gate Data [a]			Flow (cfs)	Flow (cfs) ADCP Measurements (QRev) [b,c]			Remarks for L29 Flow
	Gate Opening (ft)	Head Stage (ft)	Tail Stage (ft)	S333 DBHYDRO	S333	L67A	L29	
April 14, 2022	8.20	7.55	7.52	283.1	366.7	389.1	-30.2	flowing east towards S333
April 25, 2022	8.20	7.28	7.26	194.6	209.9	259.6	-16.6	flowing east towards S333
May 5, 2022	8.18	7.27	7.25	233.6	228.1	229.8	-97.0	flowing east towards S333
May 26, 2022	2.40	7.63	7.02	327.7	307.1	410.3	-1.4	flowing east towards S333
June 7, 2022	3.21	8.53	7.77	488.4	454.3	577.8	142.6	flowing west towards S12C&D
June 16, 2022	3.80	8.86	8.01	614.9	562.1	830.5	260.6	flowing west towards S12C&D
June 27, 2022	5.00	8.95	8.27	719.6	670.9	1614.0	823.9	flowing west towards S12C&D

a. S333 DBHYDRO flows, gate openings, and head and tail water stages are average for the duration of ADCP measurement taken in front of S333.

b. ADCP measurements at the S333 gate, and in the L67A and L29 canals were at ~1,500 ft upstream and they were not taken simultaneously but in a sequential order.

c. ADCP data processing software from the United States Geological Survey, which can be found at the following link: https://hydroacoustics.usgs.gov/movingboat/QRev.shtml.

TSS concentrations in the cross-section in front of S333 had significant decreasing concentrations with height from the canal floor for five of the seven sampling events (**Figure 18**). Median TSS concentration for all the profiles in the cross-section were highest during the June 27 (median = 12 mg/L, IQP = 8, 16 mg/L) sampling event and lowest for the June 7 and 16 events (median = 1 mg/L, IQP = 1, 4 mg/L; **Figure 15d**).
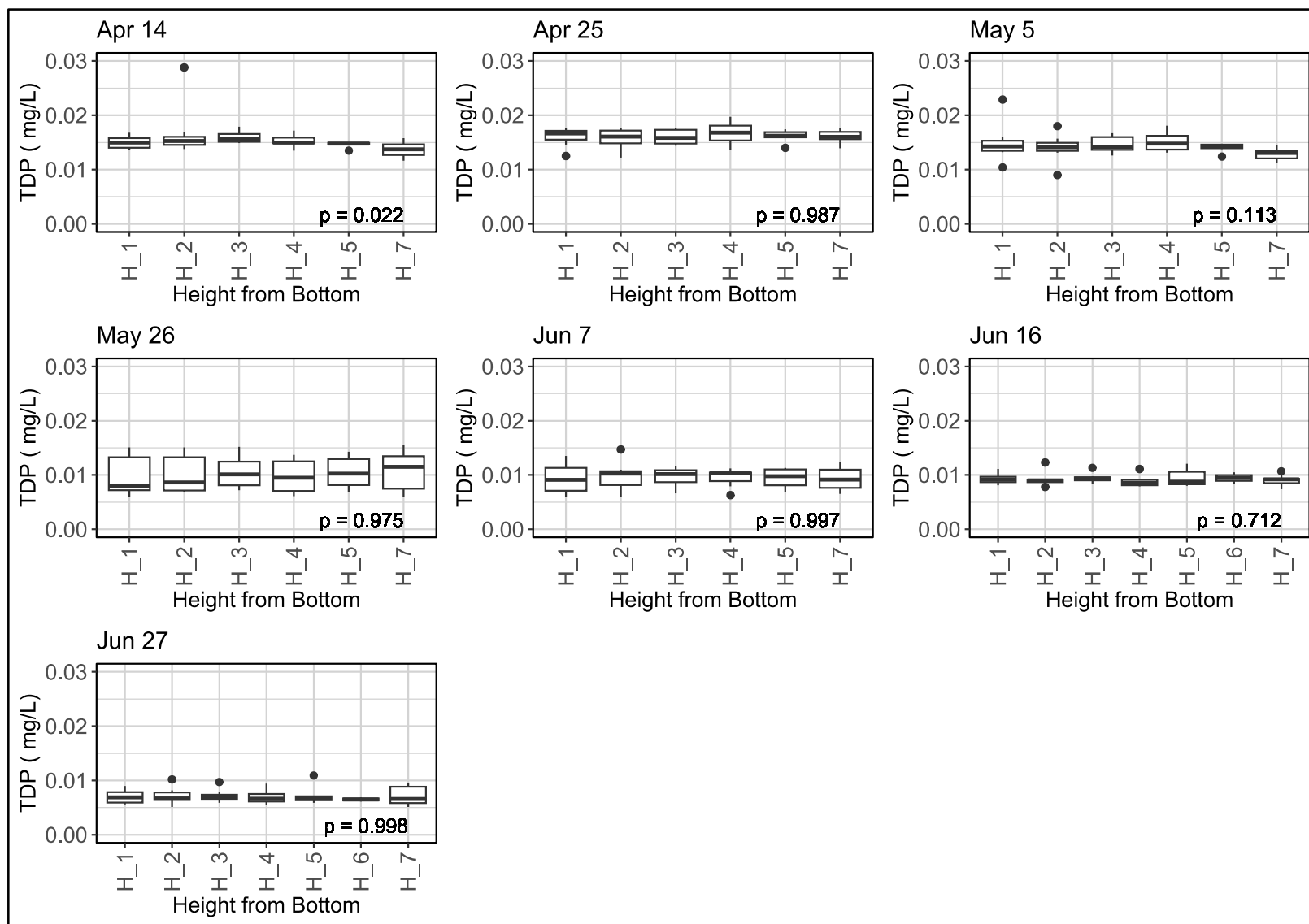
Figure 17. Boxplots of TDP concentrations with height from canal floor. H1 represents 30 cm from the canal floor while H7 represent 50 cm from the canal surface. P-values are from the Kruskal-Wallis statistical test.
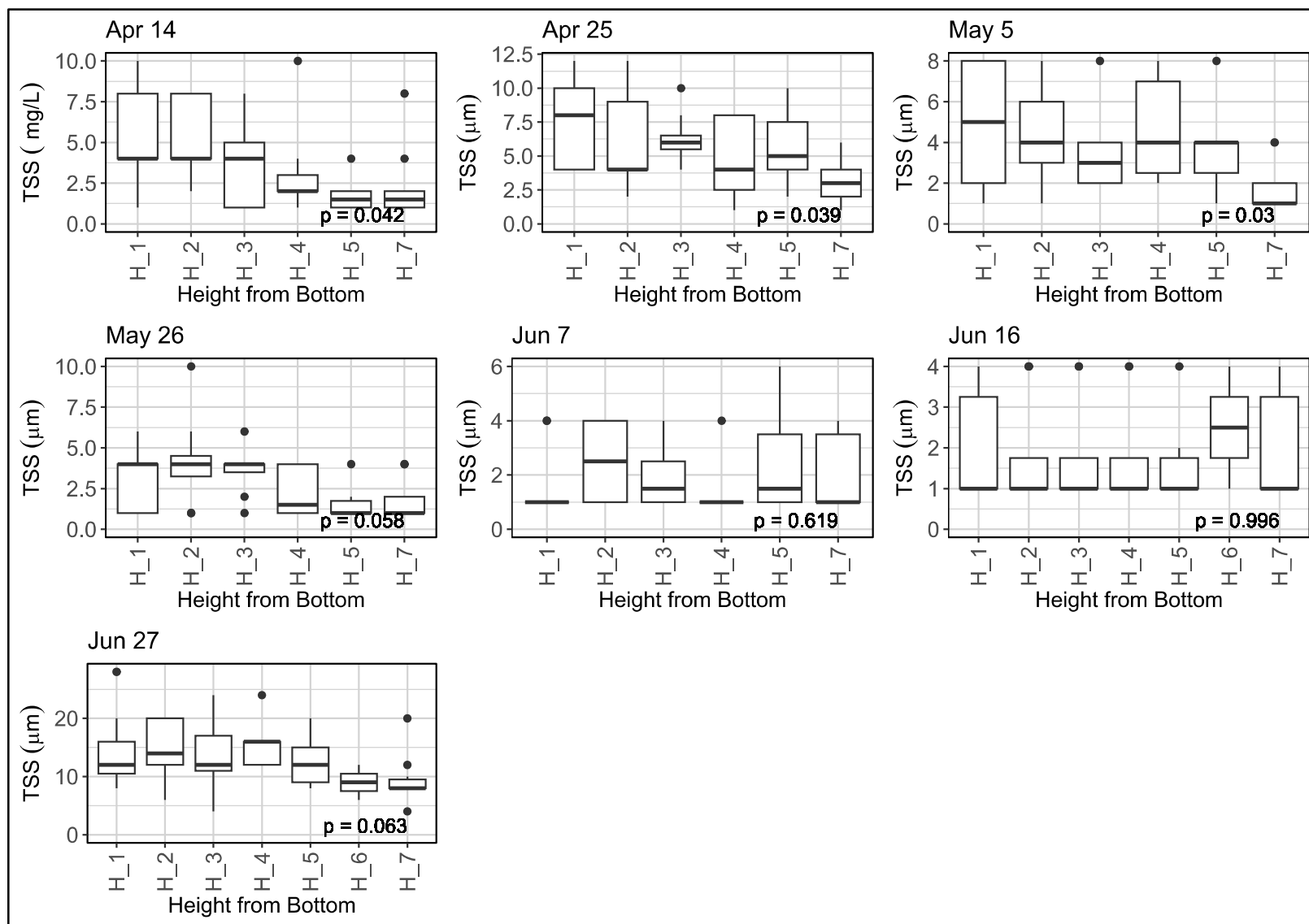
Figure 18. Boxplots of TSS concentrations with height from canal floor. H1 represents 30 cm from the canal floor while H7 represent 50 cm from the canal surface. P-values are from the Kruskal-Wallis statistical test.

Total Entrainable Sediment Volume

Total entrainable sediment volume in the top 5 cm of sediment across the three compartments was about 864 m^3 (**Figure 19**). Compartments L67A, L29, and S333 had about 352, 290, and 222 m^3 of entrainable sediment, respectively. L67A canal compartment median sediment mass per core was 25 kilograms per square meter (kg/m^2) (IQP = 19, 30 kg/m^2); median for L29 compartment was 8 kg/m^2 (IQP = 5, 25 kg/m^2); and S333 compartment median was 8 kg/m^2 (IQP = 4, 27 kg/m^2).
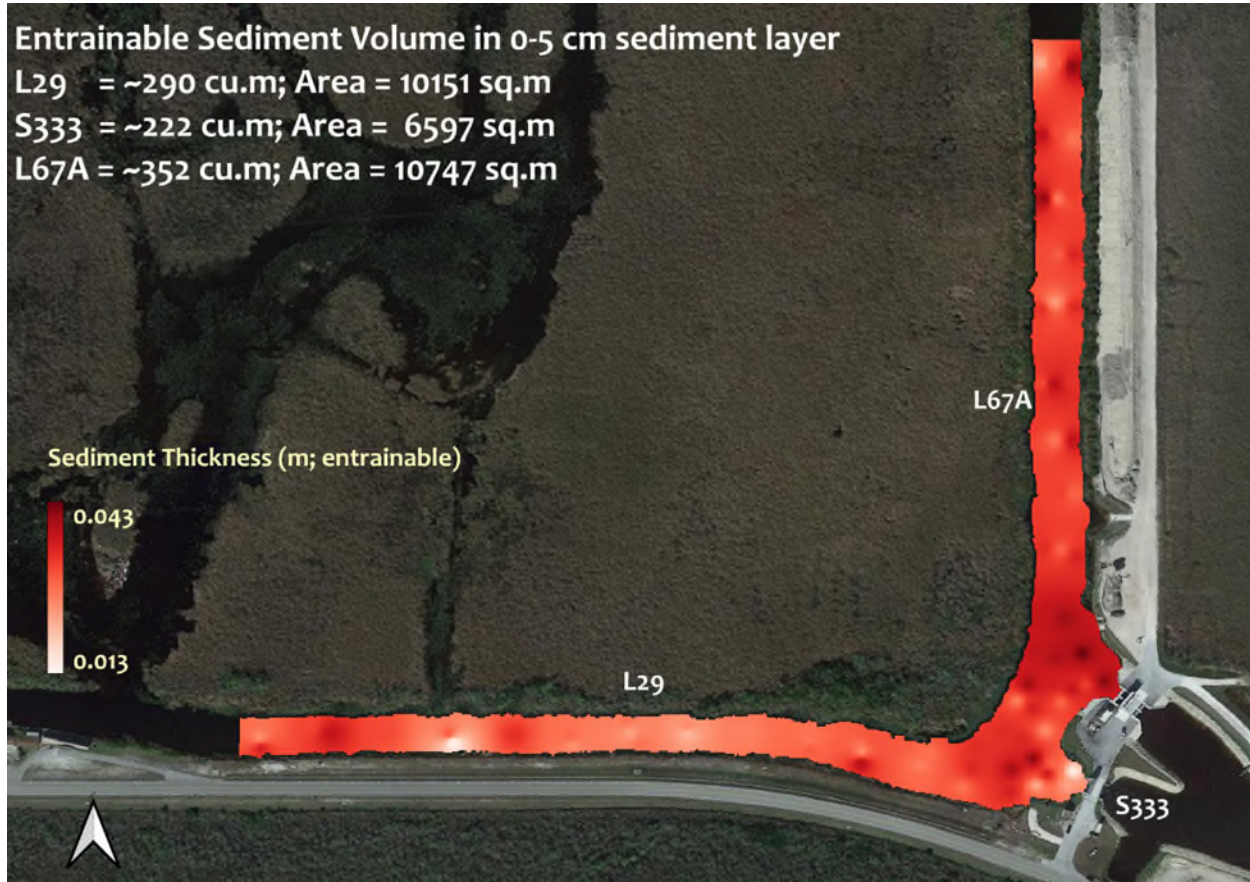
Figure 19. Entrainable sediment volume in L29 canal, S333 structure, and L67A canal compartments.

Entrainable Total Phosphorus Mass

Mass of the entrainable TP in the top 5 cm of sediment across all compartments was about 351 kg for the 27,635 m^2 (**Figure 20**). Compartments L67A, L29, and S333 had about 100, 203, and 48 kg of entrainable TP, respectively. Median L67A compartment TP mass per core was 9 grams per square meter (g/m^2) (IQP = 6, 12 g/m^2); L29 compartment median was 6 g/m^2 (IQP = 5, 11 g/m^2); and S333 compartment median TP mass was 7 g/m^2 (IQP = 4, 10 g/m^2).
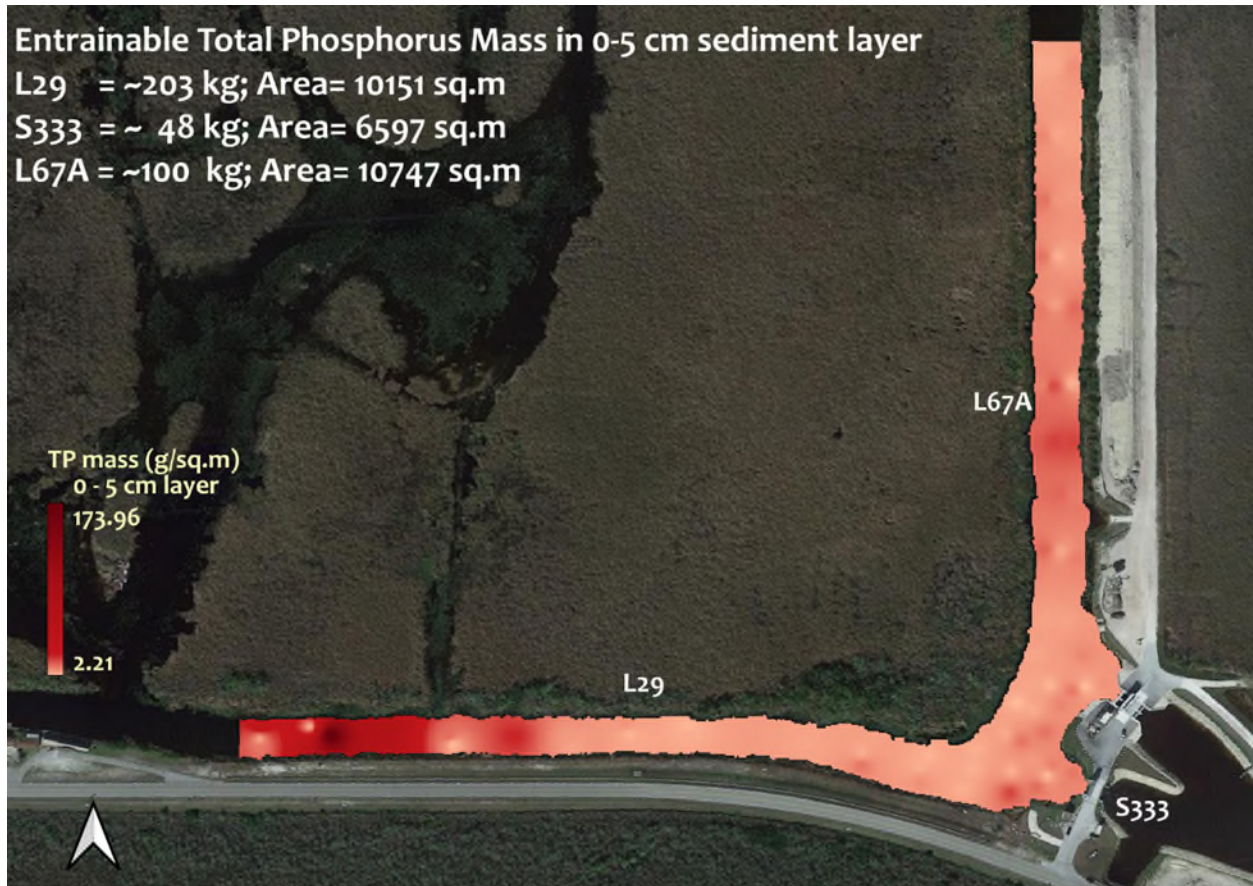
Figure 20. Entrainable TP mass in L29 canal, S333 structure, and L67A canal compartments.

Canal Flow Profiles

Based on ADCP data for the seven water sampling events, flows (**Table 1**) at S333 ranged from ~210 through 670 cfs and flows in L67A canal ranged from ~230 through 1,614 cfs. In L29, both eastward and westward flows were observed. Flows east (toward S333 structure) ranged from ~1 through 97 cfs and west (toward S12D) ranged from ~142 through 824 cfs. Eastward flow in L29 occurred when L67A flow was similar to flow through S333. Westward flow in L29 occurred when L67A flows exceeded S333 controlled discharges and the S12s were open. S333 flows from DBHYDRO and ADCP measurements (QRev) were not significantly different (Kruskal-Wallis; p = 0.423).

Cross-sectional flows were mostly similar on both sides from the center of the L67A and L29 canals (data not shown). However, variable fluxes were observed for the S333 cross-section on all sampling events. A single S333 transects collected on June 27 (**Figure 21a**) shows the volume of water passing through the northern half was not similar to the volume passing through the southern half of the cross-section's subsections. About ~75 % of flows at S333 occurred on June 27 in the southern half of the canal (**Figure 21a**). Other sampling dates had varying patterns.

The vertical velocity profiles among the three compartments reveal a unique pattern for flows at the S333 structure (**Figure 21b-d**). The L67A (**Figure 21c**) and L29 (**Figure 21d**) canals compartments had higher flows in the upper middle half of the canals. In contrast and at S333 structure (**Figure 21b**), higher flows occurred towards the bottom of canal, influenced by S333 lift gate (**Figure 2**), which forces water to pass through the bottom of the canal.
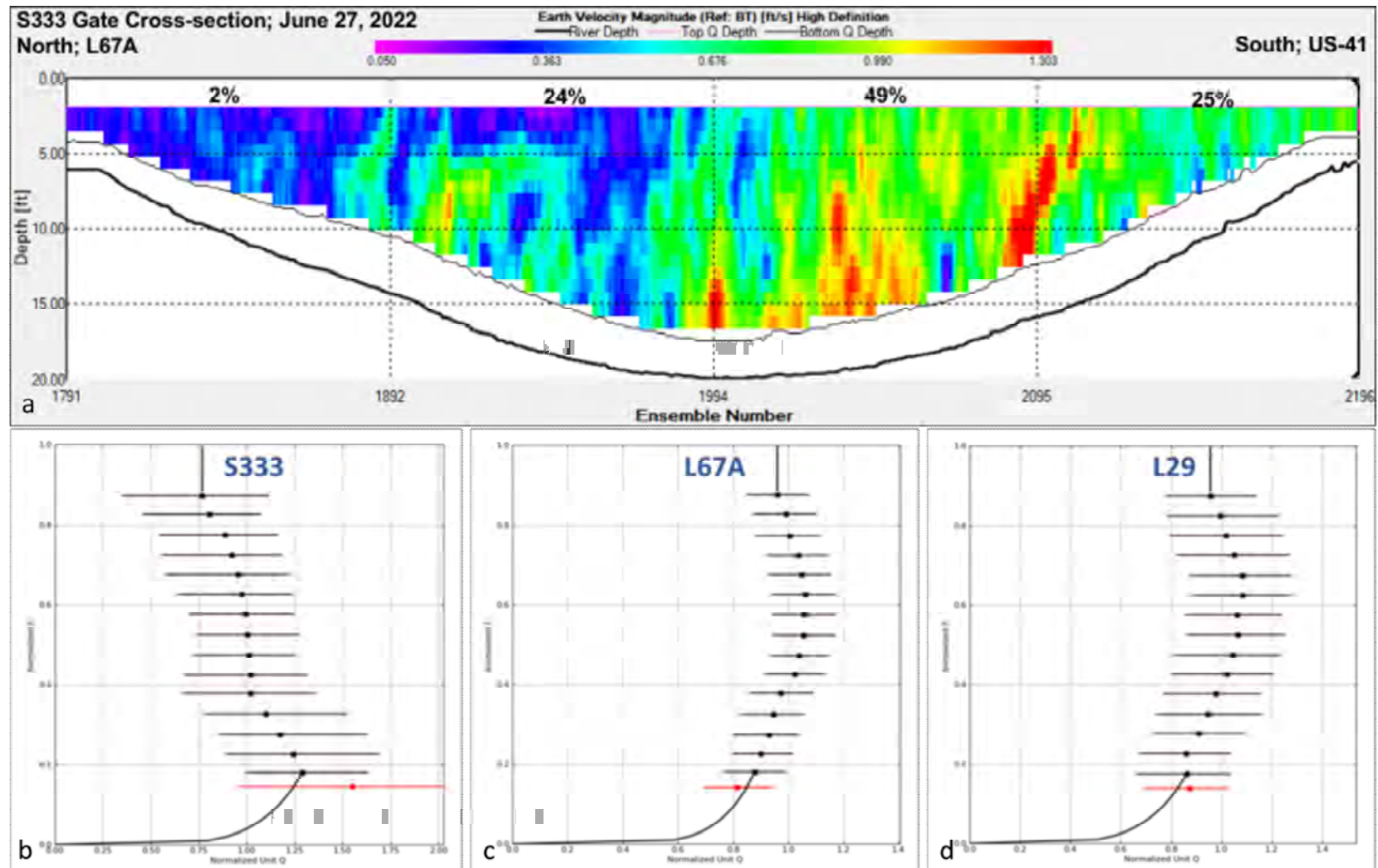
Figure 21. (a) ADCP estimated flows for June 27 at ~23 m in front of the S333 gate for a single horizontal transect. Numbers in percent show the percent of flow passing through each quarter marked by dotted lines (subsections). ADCP estimated normalized unit width flow for June 27 at (b) ~23 m in front of S333 gate and at ~457 m upstream in the (c) L67A and (d) L29 canals.

Flow Direction

In the L29 canal, ADCP observed data showed eastward flows towards S333 were limited to < 100 cfs and westward flows up to < 825 cfs towards S12C and D were observed during the period from April through June 2022 (**Table 1**). Westward flows in the L29 canal were sourced from L67A canal as these flows were in excess of S333 controlled-discharge capacity. Negative values for TCM water flow speed shows westward flows in L29 canal (**Figure 22**) at the TCM location. The L29 canal predominantly flows westwards towards S12C and D and draws water from the L67A canal when S12C and D gates are discharging.
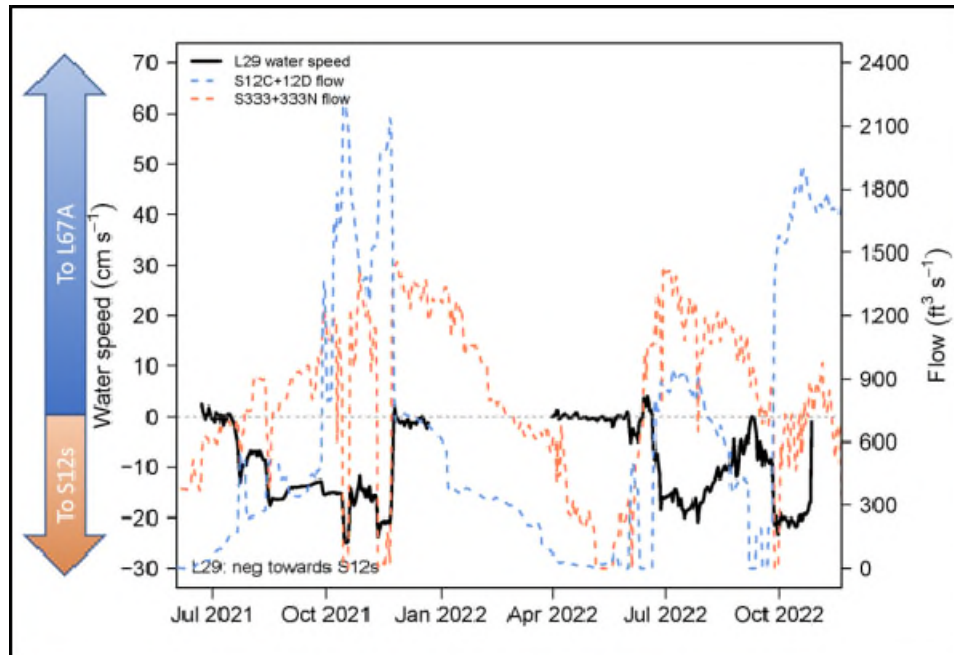
Figure 22. TCM speed and direction located at ~305 m upstream of S333 in the center of the L29 canal and flows through S333+S333N and S12C+S12D.

Discussion

Based on this sediment characterization study, there are a little more than 8,000 m^3 of sediments accumulated across the three examined compartments (L67A, L29, and S333). These sediments contain about 537 kg of TP in the top 5-cm layer. Median sediment TP concentrations across the compartments range from 400 to ~1,000 mg/kg. These TP levels in sediments are generally indicative of enrichment in sensitive Everglades marsh ecosystems (Qian et.al. 2004), such as the downstream Park. Hydrodynamic modeling conducted for this study suggests that canal flow velocities (> 1.5 cm/s) are high enough to entrain much of these sediments, particularly at relatively low S333 headwater stages (< 9 ft NGVD29) and low to moderate flow rates (390 to 1,600 cfs) observed in the L67A compartment during the sediment study.

Ninety-eight percent (98%) of sediment TP levels across the canal compartments are in apparently bound forms suggesting if dredging is implemented and turbulence happens, P will not be easily released to the water column in a biologically active form to ENP (**Figure 13b**). Removal of these sediments has a high potential to take the associated TP out of the canal bed, reducing TP from entrained sediments and nutrient loading into ENP.

Marsh sediments had higher d_{50} levels compared to canals (**Figure 12**) with an associated lower entrainment potential than the canals sediments. Total P concentrations in the marsh sediments were similar to the distribution of TP concentrations in the S333 compartment sediments, but not significantly different from TP concentration in the L29 compartment sediments. Sediment BD in the S333 compartment was lowest near the marsh boundary (< 0.5 grams per cubic centimeter [g cm^3]; **Figure 9**), with higher organic matter (**Figure 10**) content and thicker sediments deposits (**Figure 7**) than in the S333 bay. The marsh relative higher d_{50} indicates for the same levels of flows in marsh and canals, marsh mineral sediments would be relatively less susceptible to entrainment and transport. Similarities observed in BD, organic matter, and TP concentrations in sediments from the marsh and in the S333 compartment might be explained by canal embankment and marsh-edge exchange in the northwest corner of the S333 bay during the high stage wet period. Based on the hydrodynamic modeled velocities for the three water sampling campaigns, L67A and S333 compartment velocities were high enough to entrain TP rich sediments. During the June 27 event, velocities reached erosional levels (> 9 cm/s for particles less than 1,000 μm; **Figure 23**).

Based on the three sediments sampling campaigns coupled with the corresponding hydrodynamic modeling, flow velocities in the S333 bay were considerably higher than the minimum entrainment threshold (Figure 14-19 in Zeng et al. 2023). Sediments in the S333 bay were in the fine sand (125 to 250 μm; **Figure 24**) particle size distribution with a d_{50} particle size (**Figure 12**) generally smaller than 200 μm; particles this size are vulnerable to entrainment at velocities > 1.5 centimeters per second (cm/s). Over the seven water sampling events, discharges through S333 ranged from ~210 through ~720 cfs (**Table 1**). These discharges had water velocity variations across the gate horizontally and vertically (**Figure 21**). Variable velocities have different energy levels that can entrain multiple particle sizes and keep them suspended in the water column. Higher velocities at the canal bed in front of the S333 gate (**Figure 21b**) generally exhibit higher potential to entrain sediments from the canal bed than the velocities observed further upstream through each of the evaluated sampling events. Velocities in the S333 bay during these three modeled field sampling campaigns ranged between 9 to 30 cm/s. There was no pattern of d_{50} distribution with height in water column observed at S333 sampling cross-section. However, a clear pattern of decreasing TP (**Figure 16**) with height from canal bed indicates sediment entrainment potential from the canal bed, which may be due to higher water velocities towards the canal bed (**Figure 21a** and **b**).

Total suspended solid concentrations (**Figure 15d**) in the S333 cross-section during the relatively low stage conditions exhibited increasing concentrations with depth (**Figure 18**) similar to those observed with the surface water TP concentrations (**Figure 15a** and **16**). Interestingly, among the seven sampling events, the June 27 sampling event had the highest median TSS concentration across the cross-section profiles, 3 to 12 times higher than the other events. June 27 flow rates coming down the L67A canal and going through the gate were also the highest of the sampling events. Based on the hydrodynamic modeling, velocities in the S333 bay were substantially higher during the June 27 sampling event than the preceding sampling events, suggesting once velocities exceed 24 cm/s, the entire canal cross-section becomes relatively turbid through sediment resuspension.

Locally, sediments are transported toward the S333 structure as bedload movement associated with velocities in the L67A canal. These sediments get entrained into the water column near the S333 gate where velocities are higher towards the canal bed in relation to gate configuration (**Figure 2**). Sediment TP levels were the highest in the L29 canal followed by S333 and then the L67A canal (**Figure 14**). Flow directionality monitoring indicated that the L67A canal contributes substantial amounts of water to the L29 canal (**Table 1**). TCM continuous records (**Figure 22**) also supports the observation that waters from the L67A canal flows into the L29 canal when S12C and D gates are open.
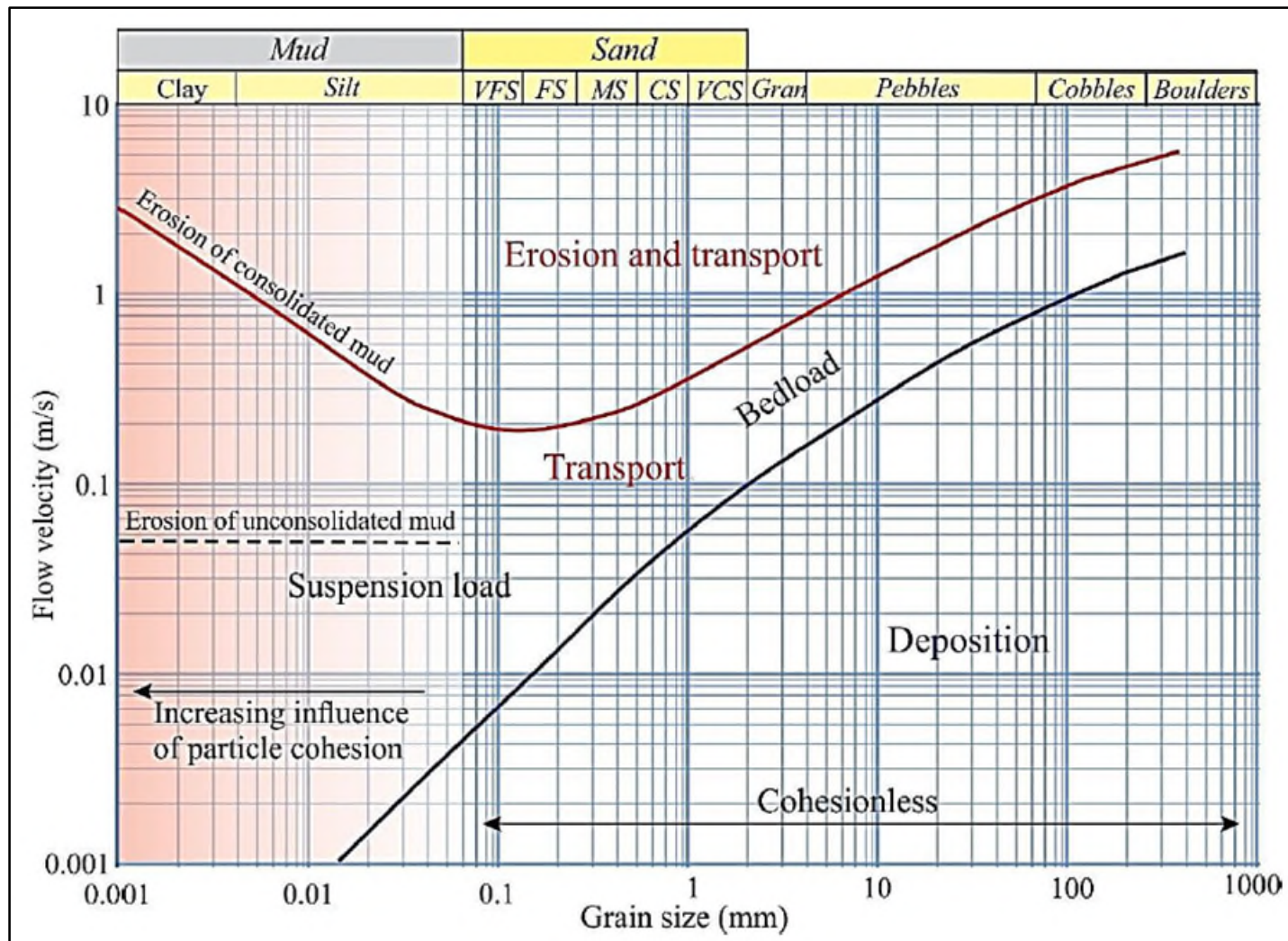
Figure 23. Nomogram of sediment grain (particle) size and velocities characterizing sediment entrainment and deposition potentials. (Note: m/s – meters per second.)
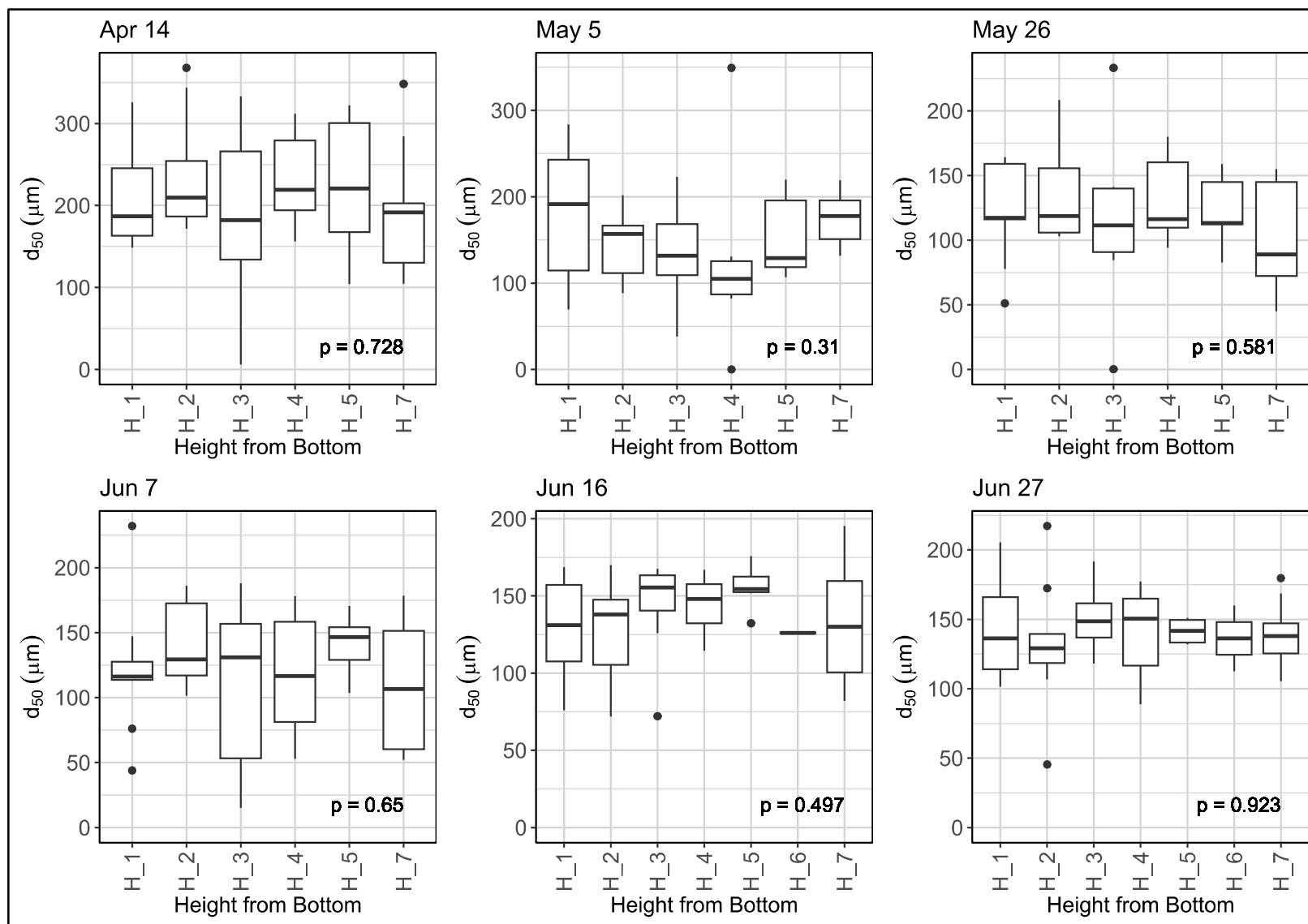
Figure 24. Box plot showing size and variations of d_{50} sediment particles in water samples with height (H) from the canal bed. (Note: H_1 = 30, H_2 = 60, H3 = 100, H_4 = 160, H_5 = 250, and H_6 = 500 cm from canal bed, and H_7 = 50-cm depth from canal water surface.)

2.0 HYDRODYNAMIC MODELING STUDY

As a complement to the sediment and TP transport studies conducted by ENP, this hydrodynamic study presented a three-dimensional Computational Fluid Dynamics (CFD) model of the local area around the S-333/S33N complex to analyze the pertinent hydrodynamic features that can potentially induce sediment and TP transport through the structures. More specifically, Phase I was designed to evaluate the local velocity fields under low- and high-water depths at the S-333/S33N complex and within immediate proximity of the canals and marsh areas around the structures and assess engineering measures to reduce flow velocity to below the value critical to suspending and transporting nutrient-rich materials. Evaluation of the engineering measures was conducted bearing in mind the geotechnical and environmental issues, construction constraints, and impacts on structure operations. The complete hydrodynamic study report is provided in Attachment 2, including the S-333 Working Group's comments on the report and responses provided by the SFWMD.

Methods

The hydrodynamic model domain extended up to 1,800 ft upstream of S-333 along the L-67A and L-29 canals. A two-dimensional Hydrologic Engineering Center River Analysis System (HEC-RAS) and three-dimensional Ansys Fluent CFD models were developed and used to simulate flow dynamics (velocities near bed, at the surface, and across the canals) for low, normal, and high flow conditions. Land surface elevations from existing digital terrain model (DTM) and bathymetric survey of the canals were used to develop the model geometry. Both low- and high-water depths at the S-333/S33N complex under existing and anticipated (future) conditions were investigated. Discharge close to the design flow of S-333 (1,350 cfs) was considered as normal flow (based on the Tamiami Trail flow formula), while 750 cfs was considered low flow. Flows much lower than this are not expected to discharge much sediment transport through the structures. S-333N design flow (1,150 cfs) combined with that of S-333 design flow (1,350 cfs) was assumed as high-flow (potential future Central Everglades Planning Project [CEPP] operation). When headwater stages are lower than the marsh elevation, the predominant discharge is the canal flow only. Canal-marsh interaction was considered wherever applicable (such as, high-stage scenarios).

Results

Sediment transport is a complex phenomenon that depends on physical factors such as particle size, slope of sediment bed, grain shape, and packing density of sediment bed, as well as flow conditions such as flow depth and velocity. This study adopted combining numerical simulations and a well-known empirical formula to indirectly evaluate the potential of sediment movement. Sediment samples collected in the L-67A and L-29 canals and surrounding marsh region by the ENP team during April–June 2022 revealed larger median sediment sizes (d_{50} – 0.20 to 0.45 mm) in the marsh region. Sediments in the canals were smaller (d_{50} – 0.13 to 0.20 mm) relative to the marsh. Plugging these sediment sizes in an empirical formula from literature yields a critical incipient velocity of 0.23 ft/s for the canals and 0.34 ft/s for the marsh region; meaning sediments will be in motion under a near bed velocity above these thresholds. Modeling results indicated that moderately high flows (1,000 to 1,500 cfs range) under low-stage (7.5 ft NGVD29) would cause sediment movement in the canals and therefore, potential undesirable TP concentrations. The near bed velocities in the marsh were less than its critical velocity for high-stage conditions. Erosive velocities were also observed in the L-67A canal from modeling of the field flow conditions, particularly when high flows occurred.

Several engineering measures for preliminary conceptual modeling were identified, of which the most promising included (1) creating sediment traps just upstream of S-333 and S-333N to reduce in-canal velocities and allow accumulation of bedload sediments, and (2) installing low-sill weirs before S-333 and

S-333N to reduce potential for resuspended sediments from flushing to the downstream. Low-sill weirs were found to reduce the canal velocities locally (**Figure 25**). In addition, they can trap near-bed sediments preventing them from being flushed to the downstream and thereby potentially reducing the likelihood of elevated TP occurrences. Results also showed the sediment traps can significantly reduce approaching flow velocities by 25 to 50% in the canals upstream of the spillways for some of the most concerning conditions (low stages–low flow and low stages–medium flow) and could promote sediment deposition (**Figure 26**). The extent and dimension of the sediment traps can be optimized using CFD modeling in subsequent phases. As the engineering measures were geared towards reducing flow velocities in the marsh and canals, not the discharge itself, the sediment traps or low-sill weirs are not expected to impact flows to the ENP. This should, however, be confirmed by backwater analysis to ascertain no negative impacts to flood control.
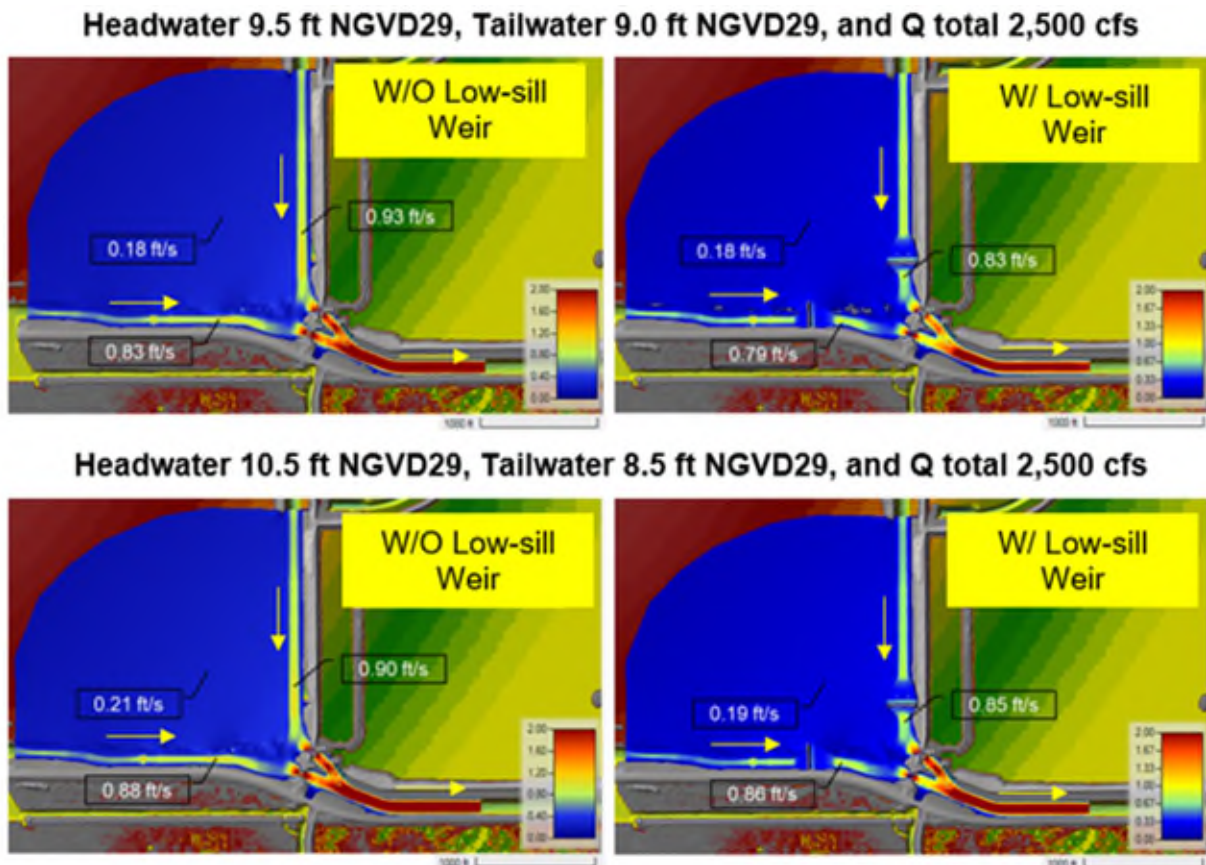
Figure 25. Test of concept without (W/O) and with (W/) low-sill weirs in canals. (Note: Q – flow.)
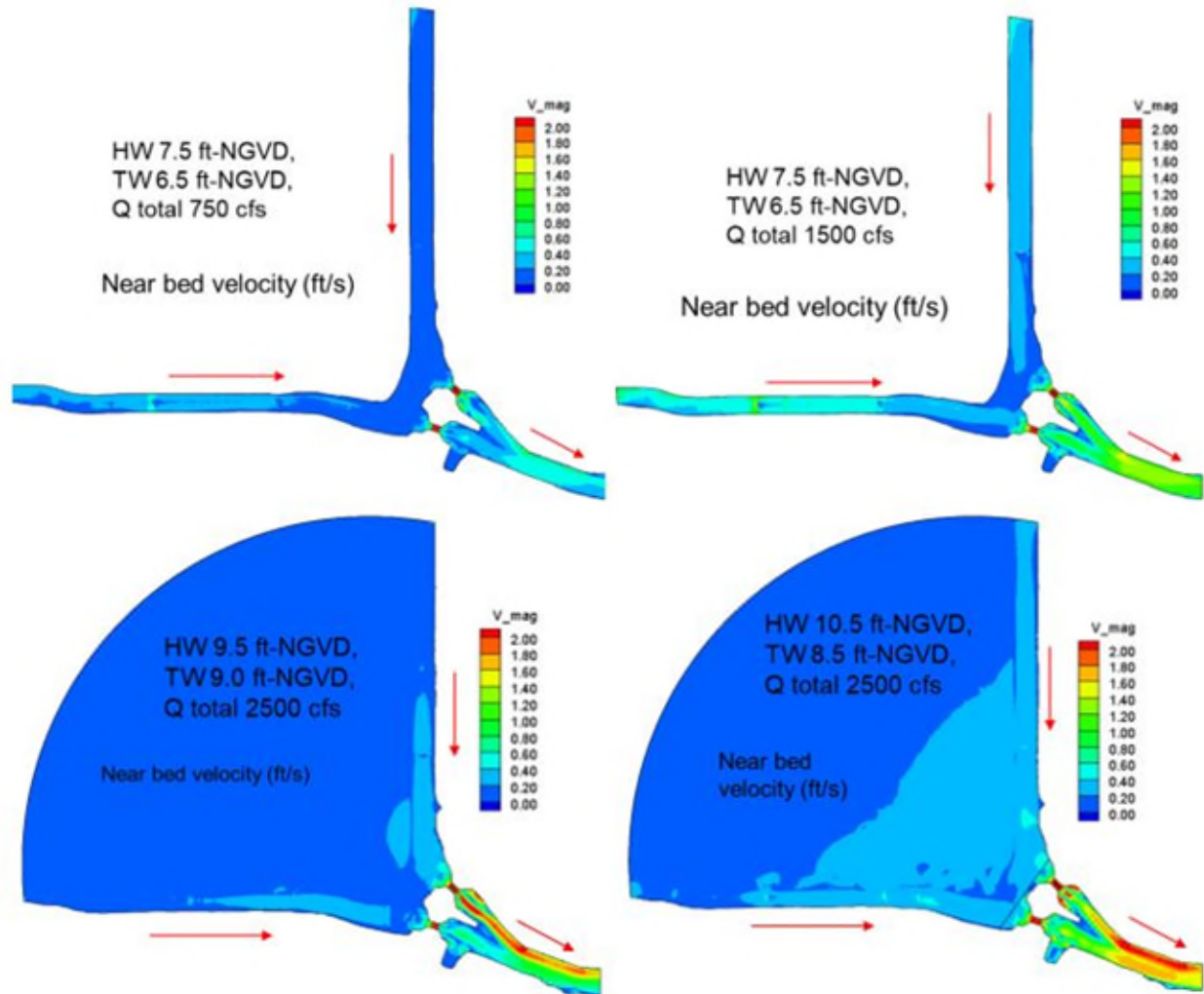
Figure 26. CFD modeling test of concept with sediment traps in canals.

Discussion

The sediment sampling in Phase I was limited to about 1,500 ft upstream of S-333/S-333N which showed on average predominantly sandy soils (d_{50} close to very fine to fine sand). Interpretation of the critical velocity in the canals and marsh were based on sediment size (d_{50}) data provided by ENP. Having said that, the Everglades is generally a system dominated by organic soils and floc materials with low particle density. Consequently, the critical velocity for certain type of entrained sediments (e.g., floc, cohesive sediment, etc.) could be lower. The current study focused on the transport of non-cohesive sediments that can realistically be assessed and potentially be trapped to reduce sediment transport through the S333/S33N complex.

3.0 PHASE I STUDIES SYNTHESIS

The sediment characterization study combined with the hydrodynamic modeling has provided some insight into potential entrainable (mobilized) sediments with high TP levels. Estimates of entrainable sediments were calculated based on sediment particle sizes below 200 μm in the sediment cores, coupled with sediment entrainment velocities determined in the hydrodynamic modeling.

Results show that a load of 100 kg of TP (entrainable) is available in the L67A compartment canal bed (top 5-cm layer) and if it instantaneously (a highly conservative scenario) mixes with overlaying canal water section (64,482 m^3), it will increase the background concentration by ~1,551 μg/L. In reality, this potential TP load would be gradually released over time when the entrainment velocity threshold is exceeded. Removing the sediments with the associated TP load from the canal system would likely prevent this load from increasing the surface water TP concentration for a period of time until new upstream sediments (sources not yet well understood) can transport into and through the canal, which restarts the cycle of bedload transport, erosion processes, and sediment accumulation.

Relative to the L29 compartment, the L67A compartment has a greater potential for contributing TP to the water column at the S333 structure. The L67A compartment has thinner sediment deposits and higher entrainable sediments with increasing TP mass closer to the S333 compartment. Further, based on the three sediments sampling campaigns coupled with the corresponding hydrodynamic modeling, the L67A compartment had higher modeled velocities than the L29 compartment with flows mainly heading towards the S333 compartment. Sediment organic matter and TP concentrations in the S333 bay near the marsh do suggest there is a potential for canal and marsh exchange contributing to the water quality at S333. Given 98% of the TP stored in the L29 compartment was apparently bound and flows were generally westwards towards S12C and D, L29 canal sediments and canal surface waters are likely not a dominant driver of the observed high TP levels at S333. Any engineering solution to improve S333 water quality should be first targeting the L67A canal and S333 compartments.

PART II: RECOMMENDED SOLUTIONS AND PHASE II STUDIES

Informed by the Phase I sediment and hydrodynamic studies, the recommended solution for immediate implementation include canal maintenance dredging and installation of low-sill weirs in both the L-67A and L-29 canals, implemented in 3 sequential steps, as described below. A monitoring and assessment program is recommended to monitor the effectiveness of this recommended solution for optimization and to inform future actions. In addition, because the recommended solution targets TP from consolidated sediment, a feasibility study on the potential use of innovative technologies to help address elevated TP levels from the flocculent material is being recommended. And finally, advancing the Phase I studies to Phase II to further evaluate regional nutrient transport and better understand nutrient origins and dynamics in the general system, is recommended. Longer-term recommendations are also presented for consideration.

1.0 RECOMMENDED SOLUTION

The S333 Working Group identified the minimal acceptable solution for consideration. Based on the results presented from the Phase I studies, a solution at the S333/S33N complex intake bay and lower reach of the L-67A should be prioritized and implemented, at a minimum, in Step I. Impacts following implementation should be comprehensively monitored and assessed for approximately 1 year, after which the monitoring plan will be revisited and scaled down. At that point, if warranted, it is recommended to move forward with Step II, which includes the upper reach of the L-67A canal up to

1,500 ft upstream of S333. The impacts following implementation should be monitored and assessed for another year. At that point, if warranted, it is recommended to move forward with Step III, which includes the upper reach of the L-29 canal up to 1,500 ft upstream of S333. The phased implementation approach was identified to afford incorporation of new information for each successive increment while balancing other considerations for implementation schedule and implementation cost. For planning purposes, the steps are defined below and depicted in **Figure 27**; however, the information collected from the monitoring and assessment plan following implementation of Step I will inform future work and Steps II and III may be refined.
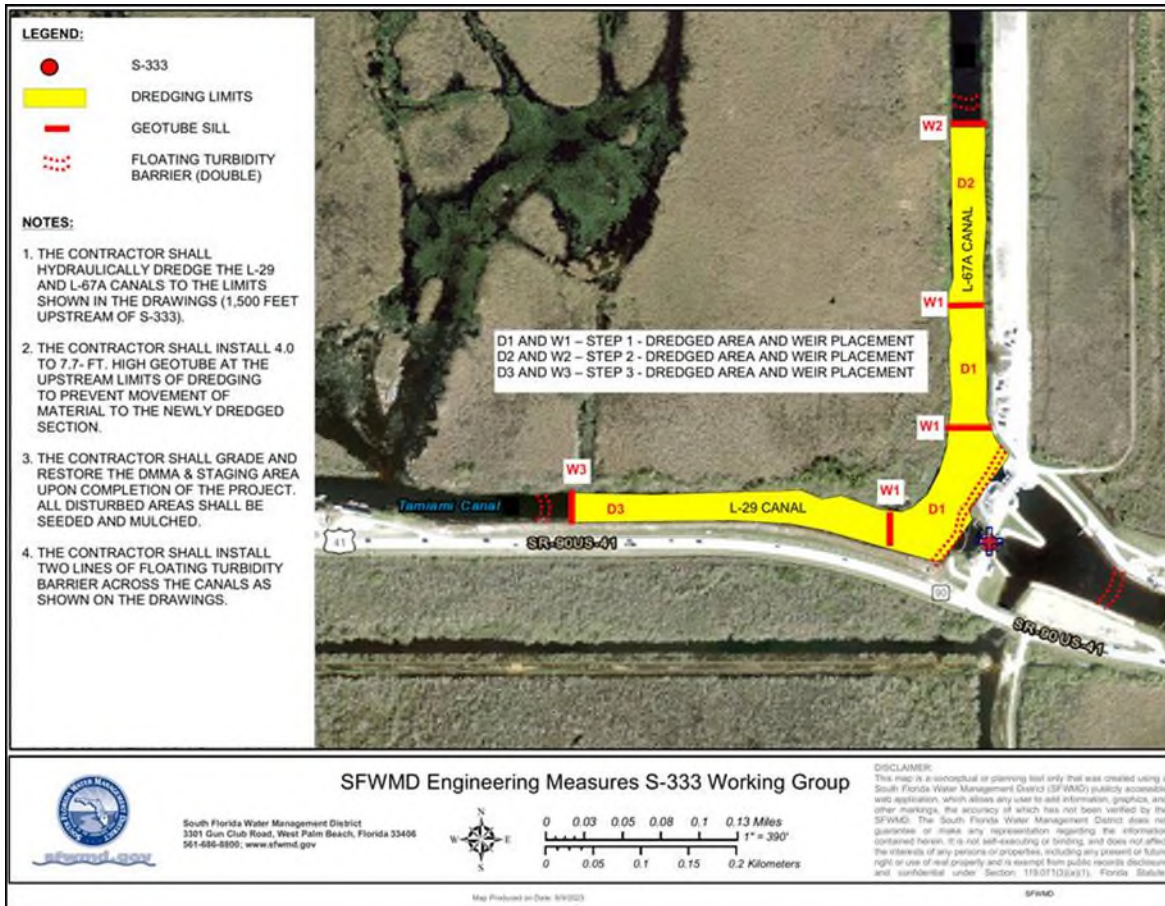
Figure 27. The recommended solution, which is to be implemented in three sequential steps.

Step descriptions are as follows:

- **Step I:** Canal maintenance dredging at the S333 intake bay, along the L-67A Canal up to 750 ft upstream of S333, and along the L29 Canal up to 350 ft upstream of S333. Install three low sill weirs with two located at the terminus of the dredged area in the L-29 and L-67A canals, and one in the L-67A canal just upstream of the S333 structure. Step I Estimated Cost: $1,489,479.

- **Step II:** Canal maintenance dredging along the L-67A canal from 750 to 1500 ft upstream of S333. Install one low sill weir at the terminus of the dredged area in the L-67A canal. Step II Estimated Cost: $573,669.

- **Step III:** Canal maintenance dredging along the L-29 canal from 350 to 1,500 ft upstream of S333. Install one low sill weir at the terminus of the dredged area in the L-29 canal. Step III Estimated Cost: $1,378,044.

Alternative recommendation options are presented in Attachment 3 for consideration. For, example, there may be cost and time savings by dredging the full 1,500 ft upstream of S333 along the L-67A and L-29 canals if this work was completed all at once rather than breaking it out in steps (i.e., cost and time associated with mobilization and monitoring for each step). Furthermore, a larger extent of canal maintenance dredging may provide additional opportunities to establish a larger baseline to better understand the movement and settling of sediments in the canal reaches, and better identify the mass balance of sediments and nutrients in the L-67A and L-29 canals, and at the S333/S33N complex. The cost estimate provided for each step includes planning, permitting, design, and construction, and does not include the cost for monitoring and assessment. The cost associated with monitoring and assessment is presented in the following section.

Canal Maintenance Dredging

Canal maintenance dredging in both the L-67A and L-29 canals has the potential to reduce sediment scour and PP-laden sediment transport. The goal of the project is to remove sediment containing PP from the bottom of the L-67A and L-29 canals returning these canals to their originally constructed cross-section profile. It is anticipated that removing the particulate matter will mitigate the resuspension of sediment material contributing to the majority of the increased TP peaks at the S-333/S33N complex. It is acknowledged that as a result of the maintenance dredging, there will be a period of time that sediments will be disturbed and resuspended in the water column. Mitigation measures will be developed during the scope of work and permitting process and implemented to minimize this disturbance and sediment transport.

All hydraulically dredged material, regardless of the executed segment option, shall be processed through a hydrocyclone separating the sediments from the water. The effluent water will be treated and the sediments temporarily deposited within the canal right-of-way (exact location will be determined during the permitting process), tested for potential contaminants, and disposed of properly. The overall effectiveness of the maintenance dredging in the L-67A and L-29 canals will be evaluated over time through the implementation of a monitoring plan and assessment plan that will determine sediment accretion rates and locations, and correlated water quality improvement to inform future maintenance dredging frequency.

Canal Maintenance Dredging Design and Construction Activities and Durations

Canal maintenance dredging will be implemented in steps as described above, however, the pre-construction activities will be completed at one time in Step I. This approach will allow for some time savings if and when we get to Steps II and III. The identified durations below for design, permitting, and construction are standard industry durations and could be reduced and fast tracked by establishing priorities and additional resources.

Step I

This step includes the following activities:

- Pre-Maintenance Dredging Survey (Step I, Step II, and Step III) – 45 days
- Pre-Maintenance Geotechnical Testing (Step I, Step II, and Step III) – 45 days
- Project Plans and Specifications (Step I, Step II, and Step III) – 60 days

- FDEP State 404 General Permit for Maintenance per 62-331.210, Florida Administrative Code (Step I, Step II, and Step III) – 60 days
- FDEP exemption per 403.813(1)f, Florida Statutes (Step I, Step II, and Step III) – 30 days (to be completed in parallel with the FDEP State 404 General Permit)
- USACE Section 408 not required for maintenance dredging; however, this determination will be made following development of the detailed scope of work – 30 days (to be completed in parallel with the FDEP State 404 General Permit)
- Dredging Contract Solicitation/Construction (Step I, Step II, and Step III) – 60 days
- Maintenance Dredging (Step I only) – 90 days
- Post-Maintenance Dredging Survey (Step I only) – 45 days

Total project duration for Step I is 405 days.

Step II

This step includes the following activities:

- Pre-Maintenance Dredging Survey (Step II only) –   45 days
- Maintenance Dredging – (Step II only) 90 days
- Post-Maintenance Dredging Survey – (Step II only) 45 days

Total project duration for Step II is 180 days.

Step III

This step includes the following activities:

- Pre-Maintenance Dredging Survey (Step III only) – 45 days
- Maintenance Dredging (Step III only) – 90 days
- Post-Maintenance Dredging Survey (Step III only) – 45 days

Total project duration for Step III is 180 days.

Low-Sill Weir Pilot Test

Low-sill weir installation in both the L-67A and L-29 canals has the potential to reduce near bed velocities and PP-laden sediment transport. The goal of the project is to facilitate the settling and restricting movement of sediments containing PP in the L-67A and L-29 canals' water columns through the implementation of a pilot test. In this application, a temporary removable low-sill weir (GeoTube) will be placed and tested along the bottom of a canal's cross-section to control localized water flow energy and reduce the velocity of water as it passes over the sill near the canal bottom. Reducing the water velocity with a low-sill weir would promote the settling of PP in the form of sediment preventing some TP transport through the S-333/S-333N complex. The overall effectiveness of installing low-sill weirs in the L-67A and L-29 canal will be evaluated over time through the implementation of a monitoring and assessment plan that will determine sediment accretion rates and locations, and correlated water quality improvement. The placement of the low-sill weirs (GeoTubes) in **Figure 27** and Attachment 3 are approximate, subject to minor field adjustments, and range from 4 to 7.5 feet high. Exact locations and height will be determined during design and permitting. A cross-section showing a typical installation of a low-sill weir (GeoTube) on the bottom of the L-67A canal or L-29 canal is provided in **Figure 28**.
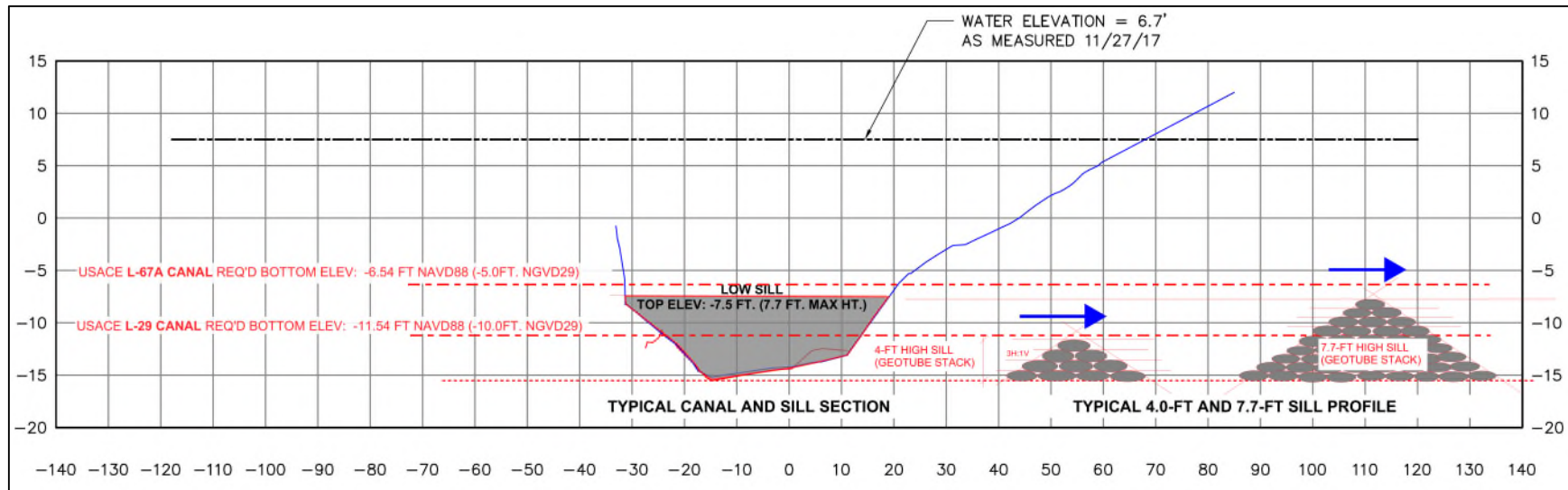
Figure 28. Typical canal cross-section and profile showing the low-sill weir (GeoTubes).

Low-Sill Weir Design and Construction Activities and Durations

Low-sill weirs will be implemented in steps as described above; however, the pre-construction activities will be completed at one time in Step I. This approach will allow for some time savings, if and when we get to Steps II and III. The identified durations below for design, permitting, and construction are standard industry durations and could be reduced and fast tracked by establishing priorities and additional resources.

Step I

This step includes the following activities:

- Project Plans and Specifications (Step I, Step II, and Step III) – 60 days
- Permitting (Step I, Step II, and Step III) – 270 days
  - FDEP State 404 – 120 days
  - FDEP General Permit – 30 days (to be completed in parallel with the FDEP State 404 General Permit)
  - USACE Section 408 – 90 to 270 days
- Low-Sill Weir Contract Solicitation/Construction (Step I, Step II, and Step III) – 60 days
- Low-Sill Weir Installation (Step I) – 60 days

Total project duration of Step I is 450 days.

Step II

This step includes the following activity:

- Low-Sill Weir Installation (Step II) – 60 days

Total project duration of Step II is 60 days.

Step III

This step includes the following activity:

- Low-Sill Weir Installation (Step III) – 60 days

Total project duration of Step III is 60 days

2.0 MONITORING AND ASSESSMENT PLAN

Upon completion of the EMOs, a monitoring and assessment plan will be implemented to determine sediment accretion rates and develop a mass balance within the L-67A and L-29 canals. Sediment samples taken will be tested for TP and inorganic content. The water column will be sampled and tested for both TP and TDP. In addition to these sediment and water column sampling parameters, upstream and downstream canal flow measurements and various TSS analytical methods (for example, laser analysis of particle size distribution) will be used in the water column to collect and analyze suspended solids data. Most of the data collection will be obtained every other week (subject to a meaningful change in hydrologic conditions from the previous week) for the first year and used with other routine compliance data that is collected at the same interval in correlating TP transport and respondent water quality improvement.

The following monitoring and assessment plan assumes full implementation of the 1,500 feet of canal maintenance dredging and installation of all three low-sill weirs (GeoTubes), in both the L-67A and L-29

canals upstream of the S-333/333N complex. In the event lesser implementation options are executed, the monitoring and assessment plan parameters and locations will be refined, adjusted, and reduced accordingly.

After completion of each annual monitoring and assessment period, information gained will be used to optimize and identify the monitoring parameters and frequencies for the upcoming year. Although it is anticipated that the monitoring and assessment plan will be annually improved and costs reduced, for budgeting purposes, it is assumed that the following parameters and sampling frequencies will take place each year for a five-year period. Information gained and assessed from the monitoring plan will be used to help inform future actions to further reduce monitoring requirements, TP concentrations at the S333/S333N complex if needed and establish a reasonable routine maintenance interval for future maintenance dredging rates.

Upon approval, the monitoring and assessment plan described below may be adjusted and revised as needed, and a detailed monitoring plan will be developed detailing the methodology, sampling protocol, locations, measuring devices, and measurement accuracy requirements.

Monitoring Parameters and Frequencies

The following summarizes the monitoring parameters and sampling frequency in the L-67A and L-29 canals for the first year of the monitoring and assessment plan. For planning purposes, this summary assumes full implementation of the 1,500 feet of canal maintenance dredging and installation of all low-sill weirs (GeoTubes) in both the canals upstream of the S-333/S33N complex.

1. Individual sediment sampling for P constituents at 250-foot intervals within the center and each canal bottom edge of the dredged canal segments every two weeks.

2. Three low-sill weir individual sediment samples for P constituents at 50-foot intervals up to and including 150 feet upstream of the low-sill weirs (GeoTubes) within the center of the canal and each canal bottom edge every two weeks.

3. Within the S333 and S333N bays, collect the vertical profiles during low and higher stages. The frequency of sampling shall be greater during the low stage periods (every 2 weeks) and lower during the high stage periods (monthly).

4. A multi-beam bathymetric survey of the dredged sections of the L-67A and L-29 canals, including a centerline survey and appropriate number of cross-sections, referenced to the North American Vertical Datum of 88 (NAVD88), every two weeks. The frequency of these surveys can be significantly reduced if significant changes in bed topography is not detected.

5. All sediment depth maintenance dredging and low-sill weir (GeoTube) material at the identified intervals in Items 1 and 2 above tested for TP and inorganic content every two weeks.

6. TP and TDP in the water column at the locations and intervals identified in Items 1, 2, and 3 above by utilizing a sampling protocol that follows best practices to collect enough samples to estimate the sediment flux in the canal for water stages and flows representative of high-, medium-, and low-flow conditions.

7. Low-level (< 1 mg/L) TSS in the water column at the locations and intervals identified in Items 1 and 2 above by utilizing a sampling protocol that follows best practices to collect enough samples to estimate the sediment flux in the canal for water stages and flows representative of high-, medium-, and low-flow conditions.

8. Two PVC sediment tube traps oriented vertically, located 100 feet upstream and 100 feet downstream of each of the three low-sill weirs (GeoTubes) collected every six weeks and analyzed for TP and inorganic content.

9. Sequential measurements of canal mean flow and velocity distributions at fixed locations and across select canal cross-sections upstream of the S-333/333N complex as needed to characterize the mean flow and flow velocity distributions for low-, medium-, and high-flow conditions concurrent with sediment and water column sampling to estimate the sediment flux. This will enable the team to develop sediment ratings (sediment discharges versus flow rate) to help appropriately size a sediment trap and assess its efficacy in the event this engineering solution is recommended in the future.

10. Measurements of critical velocity and or shear stress for incipient sediment motion in both the L-67A and L-29 canals, including the vertical profiles. These critical velocities and shear stresses would be used in interpreting past and future hydrodynamic simulations.

11. Continuous monitoring utilizing a TCM to determine flow direction.

12. Develop an updated local hydraulic model using information and data gained from the data collected in previous 11 items above. After the model is developed, apply it to further support existing infrastructure refinements (if required) and help define future potential EMOs. Upon approval, a detailed scope of work will be developed in the near term to further define the modeling scope, activities, and schedule. It is anticipated this work will be completed with internal resources rather than external contractual services. A detailed probable cost estimated for the hydraulic modeling will be developed and defined when the modeling scope of work is developed.

Monitoring and Assessment Plan Duration

Monitoring and assessment plan implementation is expected to be adaptively managed, adjusted annually, and executed over a 5-year period for data collection and assessment. After each year and the end of the monitoring term, information gained will be used to determine if further monitoring and assessment should be conducted and if there is a need to implement additional considerations to improve water quality. For budgeting purposes, it is assumed that the following parameters and sampling frequencies will take place each year for a 5-year period.

Monitoring and Assessment Plan Probable Cost Estimates

The following monitoring and assessment cost estimates assume full implementation of the 1,500 feet of canal maintenance dredging and installation of all low-sill weirs (GeoTubes), in both the L-67A and L-29 canals for five years:

- Maintenance Dredging and Low Sill Sediment Depths by Multi-Beam Bathymetric Survey – $520,000 per year for 5 years, total $2.6 million

- Surface Water and Sediment Sample Collection - $725,000 per year for 5 years, total $3,625,000 million

- Surface Water and Sediment Sample Laboratory Analyses – $460,000 per year for 5 years, total $2.3 million

- Sequential Canal Flow Measurements – $240,000 per year for 5 years, total $1.2 million

- Continuous Flow Monitoring via the TCM - $25,000 per year for 5 years, total $125,000

- Monitoring Data Assessment – $250,000 per year for 5 years, total $1.25 million

The monitoring and assessment plan total cost estimate is $2.22 million per year for 5 years for a grand total of $11.1 million.

3.0 INNOVATIVE TECHNOLOGIES FEASIBILITY STUDY

FDEP has an Innovative Technology Grant Program that evaluates and implements innovative technologies and short-term solutions to combat nutrient enrichment. The use of innovative technologies in both L-67A and L-29 canals has the potential to reduce PP and TDP concentrations in the water column. The goal of the program is to evaluate the feasibility and identify potential innovative technologies to increase nutrient removal efficiency by procuring an engineering and consulting firm to provide technical services. The technical services for this feasibility study will include conducting a literature review of existing pertinent studies and technologies, reviewing existing compliance water quality characteristics, and evaluating treatment technologies suitable for use in the headwaters of the S-333/S-333N complex. The engineering and consulting firm would assist in identifying cost-effective innovative technology options to reduce P nutrients by conducting an alternatives analysis. The alternatives analysis will consider technology cost-benefits, application trade-offs, appropriateness, and availability. The results of the feasibility study would help inform what types of technologies are suitable and available for use, future testing requirements prior to implementation if any, design considerations, and planning-level cost estimates.

Innovative Technologies Feasibility Study Activities and Durations

Activities and their duration for the feasibility study are as follows:

- Develop Feasibility Scope of Work – 120 days
- Procure Engineering and Consulting Firm – 60 days
- Conduct Feasibility Study – 450 days

The total project duration is 630 days. Estimated cost of contractual services is $1,050,000.

4.0 PHASE II STUDY RECOMMENDATIONS

Advancing the Phase I studies to Phase II to further evaluate regional nutrient transport and better understand nutrient origins and dynamics in the general system is recommended. The following study components are being recommended with Phase II. If approved to advance the studies to Phase II, the scope, schedule, and budget for the studies will need to be developed by the S333 Working Group.

Hydrodynamic Modeling

Concurrent with the monitoring and assessment plan for the EMOs it is recommended to develop and apply a regional hydrodynamic model to evaluate regional flow dynamics that will assist in improving our understanding of nutrients transport processes. Specifically, a phase 2 hydrodynamic study that extends the study area to a large portion of WCA3A and encompasses the interaction between the S12s and S333/S333N complex should be initiated, and will focus on the flow interaction between the WCA-3A marsh and L-67A and L-29 canals. This phase 2 study would require an extensive topographic survey (and possibly vegetation survey) in L67A, L29, and the marsh. The modeling scenarios may be enhanced considering stage and flow conditions to match the field conditions more closely. Use of a regional hydrodynamic model that encompasses the on-going infrastructure changes along the L-67A canal, would be a useful planning tool to help identify whether additional management measures to reduce elevated TP levels at the S-333/333N complex that originate regionally could prove useful. Use of sediment transport modeling tools may also provide additional understanding of the flow and sediment dynamics.

Evaluation of the S333 bay through enhanced modeling of flow vectors and streamlines (example provided in **Figure 29**) near the canal bed in response to gate operations would benefit the assessment of TP dynamics. Sediment transport modeling of these dynamics would also be useful in informing how bedload and associated TP are being entrained to support findings from the sediment characterization study.
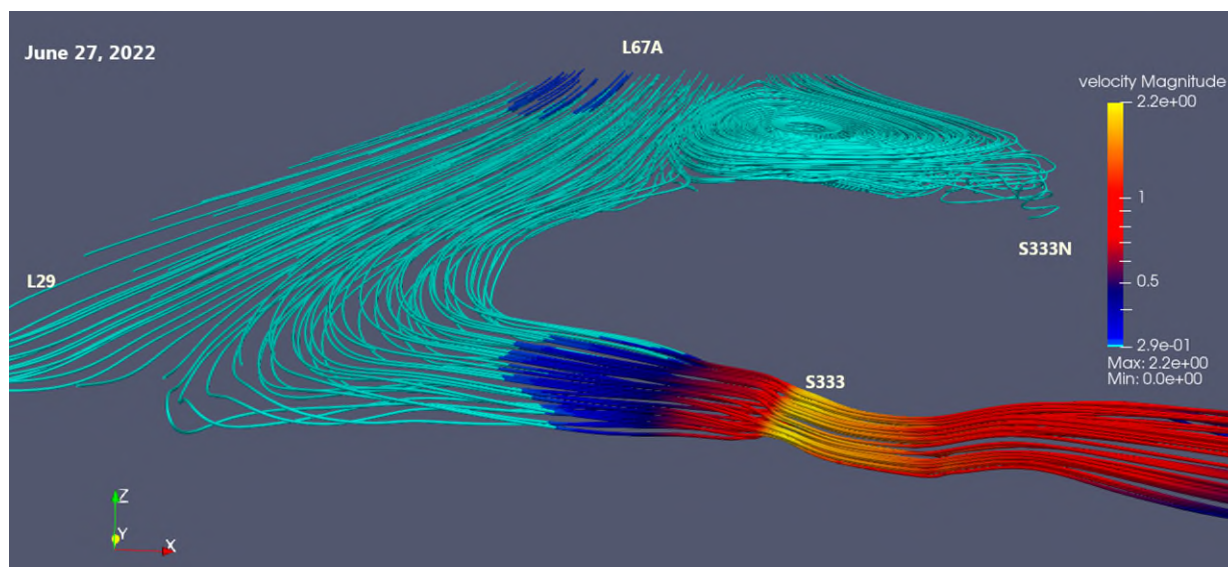
Figure 29. Stream tracing of flows from the L67A canal demonstrating flow directionality and variation in velocity magnitude at the S333 gate for June 27, 2022, CFD simulation.

Sediment Study

Upon completion of the monitoring and assessment plan for the EMOs, it is recommended that additional sediment studies be conducted. This is to allow for additional data and information to be collected during the monitoring and assessment plan to inform a Phase II sediment study.

The Phase I sediment study focused on non-cohesive sediments transport and the concept of managing canal bedload, but flocculent materials in the canal were not addressed; therefore, it is recommended we address this in Phase II. Floc is unconsolidated material in suspension above the canal bed and may be a contributor to peak TP concentrations. Given these flocculent materials tend to be lighter than sediments, these typically have a lower energy threshold required for entrainment and dispersion. Floc transport and dispersion in the water column could also contribute to high TP values observed at S333 (**Figure 30**).

Methods should be included for monitoring floc transport from L67A and canal-marsh interface. Erosion along the S333 compartment at the marsh embankment should also be monitored. Marsh and canal water exchange and the timing of hydrological disconnection should be investigated and quantified to establish a clear understanding of marsh and canal water connection and contribution to S333.

Finally, the initial study included a preliminary physicochemical investigation of the sediment sources accumulated at the S333 structure. This study would benefit from refinement. Expanding the spatial resolution and incorporating replicates should be considered as well as a thorough review of the methodologies and sampling parameters.
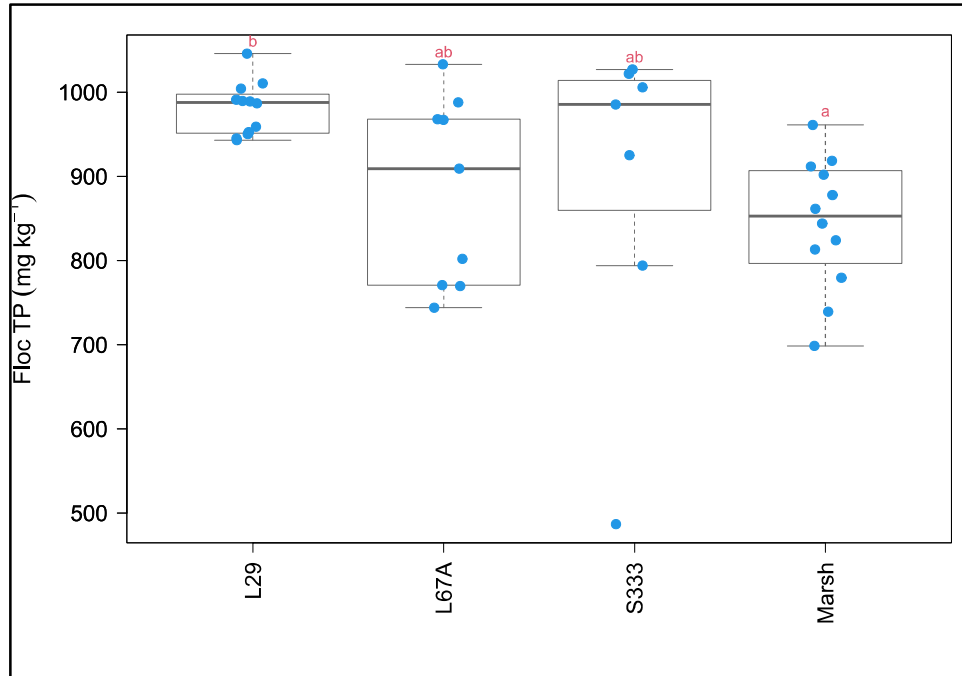
Figure 30. Floc TP concentrations across the four compartments.
Differences in letters above boxes indicates significant differences between compartments.

5.0 LONGER-TERM CONSIDERATIONS AND RECOMMENDATIONS

This section identifies an initial list of additional longer-term considerations recognized by the S333 Working Group; however, final consensus is still needed. These considerations include both structural and non-structural modifications to the system, that if needed after implementing the above-mentioned recommendations, could potentially be used longer term to reduce elevated TP transport through the S333/S333N complex. These considerations are identified as potential management measures (excluding CEPP) that should be further investigated in detail or could be implemented in the event the recommendations in this plan do not achieve nutrient reduction goals. CEPP, an independent federal action, will be tracked by the S333 Working Group as both structural and operational modifications to the system will directly influence the quality, quantity, timing, and distribution of flows to the L-67A and L-29 canals and the S-333/333N complex.

Sediment Trap

The recently completed CFD Study (July 2023) that investigated potential causes and effects of elevated TP concentrations identified the use of a sediment trap just upstream of S-333/S-333N complex to reduce near bed velocities. A sediment trap in this location indicated potential in reducing sediment transport during low to moderate flow periods. As such, the the S333 Working Group identified the use of a sediment trap upstream of the S333/S33N complex as a potential future engineering consideration that could be implemented pending the performance and outcome of implementing the previously recommended maintenance dredging and low-sill weir installation.

Marsh Short Circuiting

Anthropogenic inputs of TP into the WCA3A marsh are potentially being returned to the surrounding canal in areas where there are direct deep open water channel connections between the marsh and L-67A and

L-29 canals. Installation of vegetation buffers in deep open water connections or channels could reduce velocities and sediment transport in the marsh. Impact on potential reduction in TP transport from the deep-water marsh connections into the canals needs further investigation and is identified as a future consideration requiring additional examination in subsequent implementation phases.

Innovative Technologies

The Innovative Technologies Feasibility Study recommended above will identify cost-effective innovative technology options to reduce P nutrients in the flocculent material on which the recommended engineering solution is expected to have minimal impact. The innovative technology options identified in this study should be tested for implementation that is scalable and cost-effective to reduce P.

Implementation of the Central Everglades Planning Project (CEPP)

CEPP as authorized by the United States Congress includes several project features to restore flows to the central Everglades and will be tracked by the S333 Working Group. CEPP is already being implemented independent of the S333 Working Group and includes both structural and operational modifications to the system that will directly influence the quality, quantity, timing, and distribution of flows to the L-67A and L-29 canals and the S-333/333N complex. Of particular interest identified by the S333 Working Group, are the CEPP South project features (**Figure 31**) that include spoil mound removal and modification of operations to better mimic a natural delivery of water through the system in response to rainfall. Section 6.0 of the *Central Everglades Planning Project Final Integrated Project Implementation Report and Environmental Impact Statement* (USACE and SFWMD 2014) includes details on project features including spoil mound removal activities and can be accessed at the following link: https://www.saj.usace.army.mil/Portals/44/docs/Environmental/CEPP/01_CEPP%20Final%20PIR-EIS%20Main%20Report.pdf.

With application of the Decomp Physical Model (DPM) recommendations and CEPP adaptive management, refinements could be made to the CEPP South project designs to reduce TP to the S333/S333N complex and to WCA3B.

The CEPP South features are identified as Project 14S in the *Integrated Delivery Schedule 2022 Update* (USACE 2022) and are currently scheduled for completion on or before 2031. A complete list of the CEPP features (Project 14), including the CEPP South features (Project 14S), can be found online with project implementation schedules and planning level funding requirements at the following link: https://www.saj.usace.army.mil/Missions/Environmental/Ecosystem-Restoration/Integrated-Delivery-Schedule/.
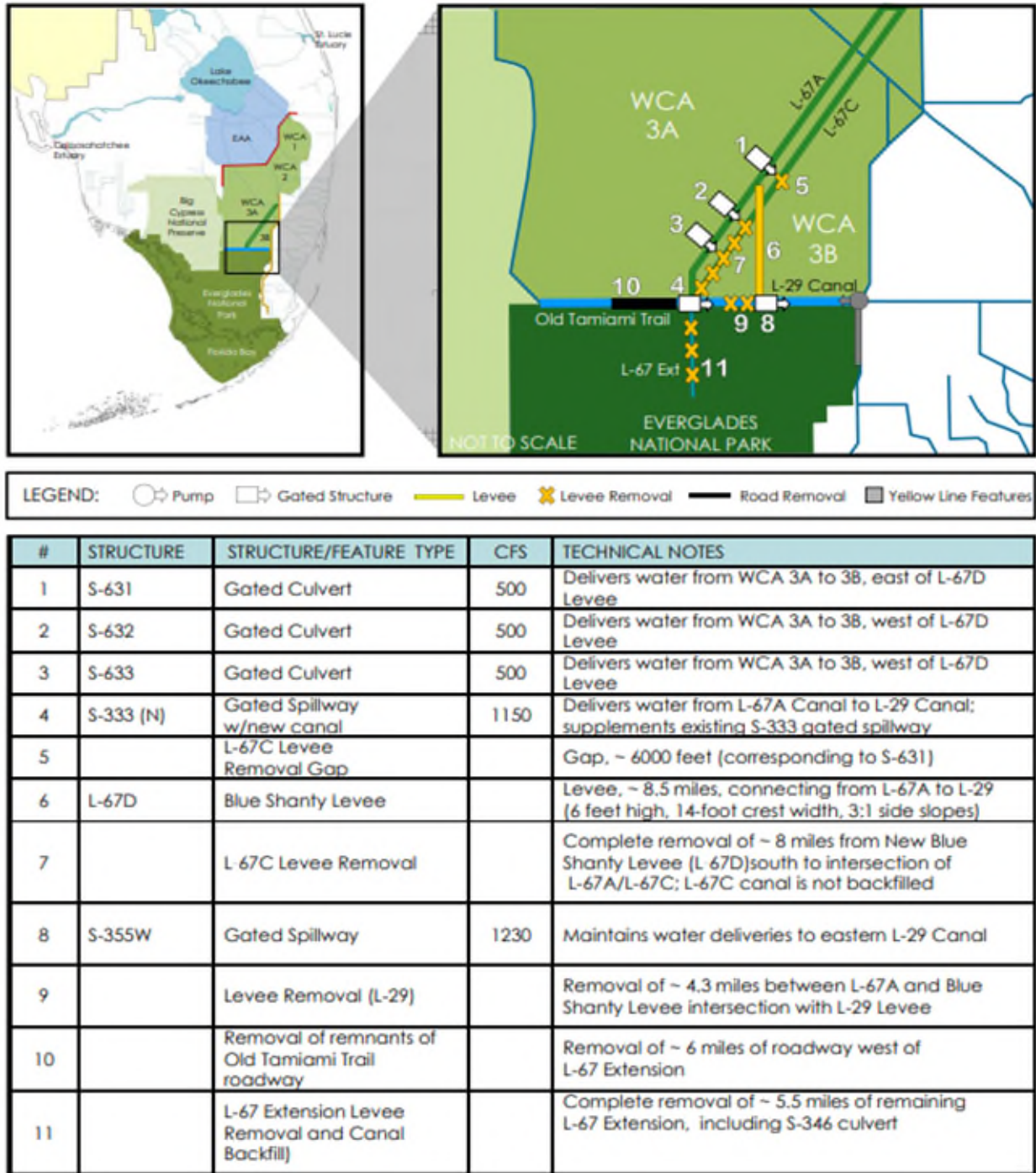
Figure 31. CEPP South southern distribution, conveyance features, and location.

#	STRUCTURE	STRUCTURE/FEATURE TYPE	CFS	TECHNICAL NOTES
1	S-631	Gated Culvert	500	Delivers water from WCA 3A to 3B, east of L-67D Levee
2	S-632	Gated Culvert	500	Delivers water from WCA 3A to 3B, west of L-67D Levee
3	S-633	Gated Culvert	500	Delivers water from WCA 3A to 3B, west of L-67D Levee
4	S-333 (N)	Gated Spillway w/new canal	1150	Delivers water from L-67A Canal to L-29 Canal; supplements existing S-333 gated spillway
5		L-67C Levee Removal Gap		Gap, ~ 6000 feet (corresponding to S-631)
6	L-67D	Blue Shanty Levee		Levee, ~ 8.5 miles, connecting from L-67A to L-29 (6 feet high, 14-foot crest width, 3:1 side slopes)
7		L 67C Levee Removal		Complete removal of ~ 8 miles from New Blue Shanty Levee (L 67D)south to intersection of L-67A/L-67C; L-67C canal is not backfilled
8	S-355W	Gated Spillway	1230	Maintains water deliveries to eastern L-29 Canal
9		Levee Removal (L-29)		Removal of ~ 4.3 miles between L-67A and Blue Shanty Levee intersection with L-29 Levee
10		Removal of remnants of Old Tamiami Trail roadway		Removal of ~ 6 miles of roadway west of L-67 Extension
11		L-67 Extension Levee Removal and Canal Backfill)		Complete removal of ~ 5.5 miles of remaining L-67 Extension, including S-346 culvert

REFERENCES

Ahn H, James T. 2001. Variability, uncertainty, and sensitivity of phosphorus deposition load estimates in south Florida. Water, Air, and Soil Pollution, 126:37-51.

Baird RB, Eaton AD, Rice EW. 2017. Standard Methods for the Examination of Water and Wastewater, 23rd Edition. APHA, Washington, DC.

Hjulstrom F, 1935. Studies of morphological activity of rivers as illustrated by the River Fyris. Bulletin of the Geological Institute University of Uppsala, 25:221-527.

Irick D, Li YC, Inglett PW, Harris WG , Gu B, Ross MS, Wright AL, Migliacio KW. 2013. Characteristics of soil phosphorus in tree island hardwood hammocks of the Florida Everglades. Soil Science Society of America Journal, 77(3):1048-1056.

Li Y, Qiu Y, Zeghbroeck JV, Shinde D, Surratt D. 2023. Sediment phosphorus profile, sources, types, and characterization in L67A and L29 canals upstream of S333 structures. University of Florida, Boca Raton, FL.

Noguchi K, Abel RS, Marmolejo-Ramos F, Konietschke F. 2020. Nonparametric multiple comparisons. Behavior Research Methods, 52:489-502.

Qian SS, Pan Y, King RS. 2004. Soil total phosphorus threshold in the Everglades: a Bayesain changepoint analysis for multinomial response data. Ecological Indicators, 4:29-37

Solórzano L, Sharp JH. 1980. Determination of total dissolved phosphorus and particulate phosphorus in natural waters. Limnology and Oceanography, 25: 754-758.

Sotolongo Lopez M, Hudson L, Xue SK. 2023. Chapter 3: Water Quality in the Everglades Protection Area. In: 2023 South Florida Environmental Report – Volume I, South Florida Water Management District, West Palm Beach, FL. Available at https://apps.sfwmd.gov/sfwmd/SFER/2023_sfer_final/v1/chapters/v1_ch3.pdf.

SFWMD. 2021. Initial recommendations – S333 Working Group. South Florida Water Management District, West Palm Beach, FL.

Surratt D, Shinde D, Aumen N. 2012. Recent cattail expansion and possible relationships to water management: Changes in Upper Taylor Slough (Everglades National Park, Florida, USA). Environmental Management, 49:720-733, DOI 10.1007/s00267-011-9798-x.

USACE. 2020. Appendix C: COP Adaptive Management and Monitoring Plan. In: Final environmental impact statement Combined Operational Plan, Broward, Miami-Dade, Monroe Counties, Florida. United States Army Corps of Engineers, Jacksonville, FL.

USACE. 2022. Integrated delivery schedule 2022 update. 2022. United States Army Corps of Engineers, Jacksonville, FL.

USACE, SFWMD. 2014. Central Everglades Planning Project final integrated project implementation report and environmental impact statement. United States Army Corps of Engineers, Jacksonville, FL, and South Florida Water Management District, West Palm Beach, FL. Revised December 2014.

USEPA. 1982. Methods for chemical analysis of water and wastes. EPA 600/4-79-020, United States Environmental Protect Agency, United States Government Print Office, Washington, DC.

Xue SK. 2023. Appendix 3-5: Water Year 2022 and Five-Year (Water Years 2018–2022) Annual Flows and Total Phosphorus Loads and Concentrations by Structure and Area. In: 2023 South Florida

Environmental Report – Volume I, South Florida Water Management District, West Palm Beach, FL. Available at https://apps.sfwmd.gov/sfwmd/SFER/2023_sfer_final/v1/appendices/v1_app3-5.pdf.

Zhang H, Kovar JL. 2009. Fractionation of soil phosphorus. Methods of Phosphorus Analysis for Soils, Sediments, Residuals, and Waters, 2:50-60.

Zeng J, Rakib Z, Ansar M, Wilsnack M. 2023. Computational fluid dynamics (CFD) study in support of investigation of elevated total phosphorus concentrations in discharges through S333 and S333N spillways. South Florida Water Management District, West Palm Beach, FL.

ATTACHMENT 1: SEDIMENT STUDY REPORTS AND S333 WORKING GROUP COMMENTS AND RESPONSES MATRIX

CONTENTS

SECTION 1: SEDIMENT PHOSPHORUS PROFILE, SOURCES, TYPES, AND CHARACTERIZATION IN L67A AND L29 CANALS UPSTREAM OF S333 STRUCTURES

FINAL REPORT

Sediment Phosphorus Profile, Sources, Types, and Characterization in L67A and
L29 Canals Upstream of S333 Structures

Principal Investigator
University of Florida
Yuncong Li

Co-Investigators
University of Florida
Yuheng Qiu, Joris Van Zeghbroeck
Haimanote Bayabil, Young Gu Her

Agreement Technical Representatives
South Florida Natural Resources Center
Everglades National Park
Dilip Shinde and Donatto Surratt

Submitted

June 2023

TABLE OF CONTENTS

EXECUTIVE SUMMARY

The objective of this study was to understand sources of phosphorus (P) in floc and sediment which influenced water quality delivered through S333 to the Everglades National Park (ENP). The findings of this study can be used to inform strategies for mitigating P sources delivered to S333.

Sampling was conducted at 15 sites near the S333 structure, including L29 canal, S333 structure, L67A canal, Miami canal, and adjacent marsh areas. Floc and surface sediment samples (0-5 cm) were collected for chemical analysis to examine P transport near the S333 structure. Total phosphorus (TP) analysis revealed that L29 canal samples had the highest TP concentration in floc and sediments, followed by Miami canal samples. Located downstream of Miami and L67A canals, L29 canal receives P from upstream L67A and Miami canals and the Water Conservation Area 3A (WCA3A) watershed. Additionally, the relatively low and stagnated flows in the L29 canal when S12C&D are not flowing allow for easy settling and accumulating P transported from upstream sources. Miami canal samples also showed high TP levels (floc and sediments), intercepting water from agricultural and ranch watersheds upstream. However, the dynamic conditions in Miami canal may make it difficult for P to settle, resulting in lower TP levels than L29 canal. Cluster analysis used as a tool to explore hidden linkages and similarities indicated that Miami and L67A canals may potentially contribute to the observed TP pool at S333. Miami canal water gets in the WCA3A marsh and is also routed to L67A canal, eventually reaching S333.

The study also estimated the potential sediment P load in the canal and adjacent marsh, which may contribute to observed TP peaks at S333. Samples from 40 floc (28 canal and 12 marsh samples) and 91 sediments (79 canal and 12 marsh samples) were collected for physical and chemical analysis. The TP mass per unit area of the sediment top 5 cm layer (sediment going forward) in each canal compartment was 0.031 kg m^{-2} for L29, 0.012 kg m^{-2} for S333, and 0.014 kg m^{-2} for L67A. The TP concentrations in sediment decreased from west to east in L29 canal and increased from north to south in L67A canal. S333 area sediment samples generally exhibited high TP concentrations relative to areas close to the S333 gate, which showed low TP concentrations. Bulk density (BD) analysis revealed a decrease in sediment BD from west to east in L29 canal. S333 sediment samples had low BD overall, except for samples near the S333 gate with high BD. Sediment samples from L67A canal had higher BD compared to L29 and S333 samples. The marsh region adjacent to L29 and L67A canals in WCA3A northeast corner, showed a sediment TP mass of 0.004 kg m^{-2} in top 5 cm sediment layer. All 12 marsh sediment samples exhibited similar levels of TP concentrations.

Laser particle analysis of canal bed sediments showed a median particle size of approximately 143 μm (sd=51) in the S333 upstream area. This falls in the fine sand category. In floc samples median particle size was ~567 μm (sd=114), which can be characterized as coarse sand size particles. These sediment and floc particles may be susceptible to entrainment when subjected to their threshold velocity at and above canal bed surface. Cross sectional flow measurements showed both vertical and horizontal water flux variations across the S333 gate. Higher flow velocities at the canal bed in front of the gate were observed, which indicated the potential for sediment and floc entrainment. TP measurements done on cross-sectional water sampling at S333 showed a clear pattern of decreasing TP with height from the canal bed, indicating a possibility of sediment entrainment from the canal bed, which may be due to higher water fluxes observed towards the bed of canal.

In conclusion, this study provides insights into the potential sources and pathways of P transport to S333 in the canal system. The Miami and L67A canals play a role in transporting nutrients to S333, either directly or may be through the marsh. It is recommended to validate and refine these findings through further research and monitoring efforts and targeted P reduction measures should be explored based on the identified sources and transport pathways.

1. Introduction

1.1. Background

The Federal Government sued the State of Florida in 1988 for alleged violations of State water quality standards due to concerns with the deterioration of the Everglades from increased eutrophication. The lawsuit was settled in 1991 and a Consent Decree was executed in 1992. The State of Florida adopted the Everglades Forever Act in 1994, which established a TP geometric mean limit of 10 µg L^{-1} for the Everglades Protection Area—the water conservation areas and ENP. The Consent Decree requires achievement of long-term P concentration limits for discharges into Shark River Slough (SRS) within the ENP and the limits have a long-term target of 8 µg L^{-1}. The annual flow-weighted mean TP concentration flowing into SRS is computed using flows and concentrations from the S12(A-D) and S333 structures (Fig. 1.1). An exceedance of the concentration limits occurs if the water year (Oct-Sep) flow weighted mean TP concentrations exceeds the flow-based limit (United States v. SFWMD et al. 1988).
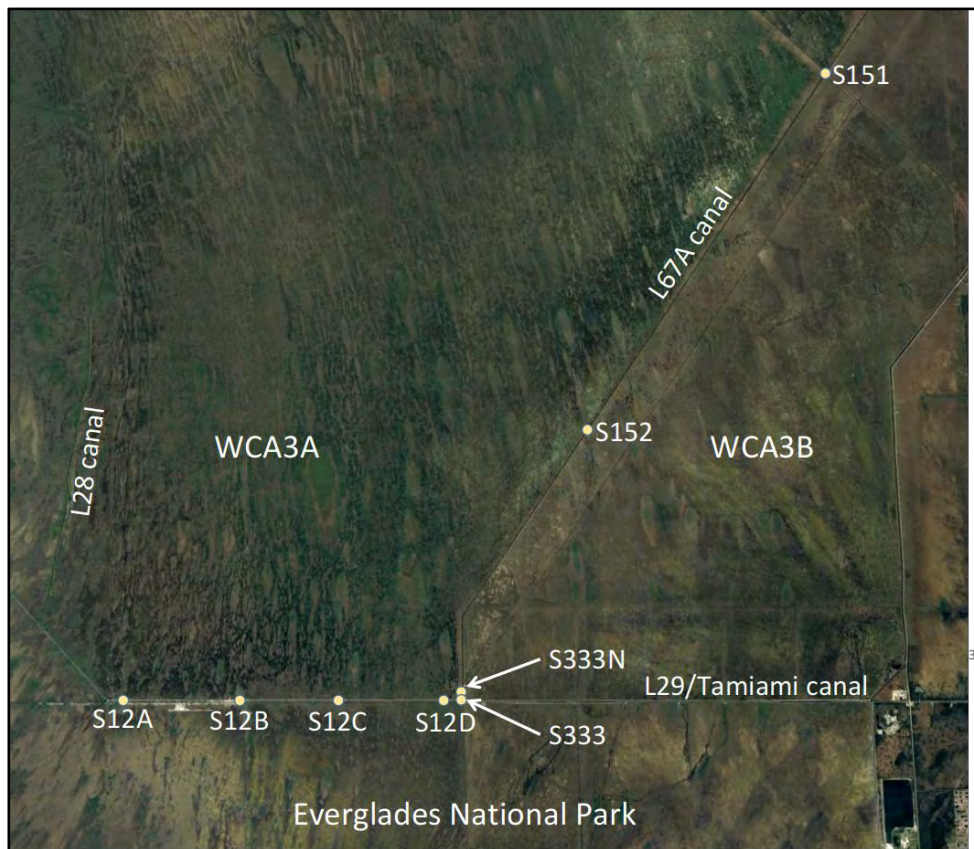
Figure 1.1. Location of discharge structures (S12A-D, S333, and S333N-operational since 2020) on L29 canal (aka, Tamiami canal) delivering water into Shark River Slough, ENP.

Hydrologically, WCA3A and the Everglades Agricultural Areas (EAA) are the major sources of water delivered to SRS. Runoff from the EAA is treated for P removal through a series of Stormwater Treatment Areas and then collected in several canals to be delivered through the Everglades. Miami canal captures a fraction of this water, directs it to the L67A canal, and then down to five control structures that release these waters into SRS. The Miami canal diverts a fraction of these flows to WCA3A (Fig. 1.2). Historically (prior to 2015), a relatively small fraction of that water was delivered to Northeast Shark River Slough (NESRS) through the S333

structure. Coincident with recent operational changes, captured in the Combined Operations Plan, there has been a considerable increase in the total flow distribution for SRS to NESRS and there have been cyclically elevated TP concentrations observed at S333.
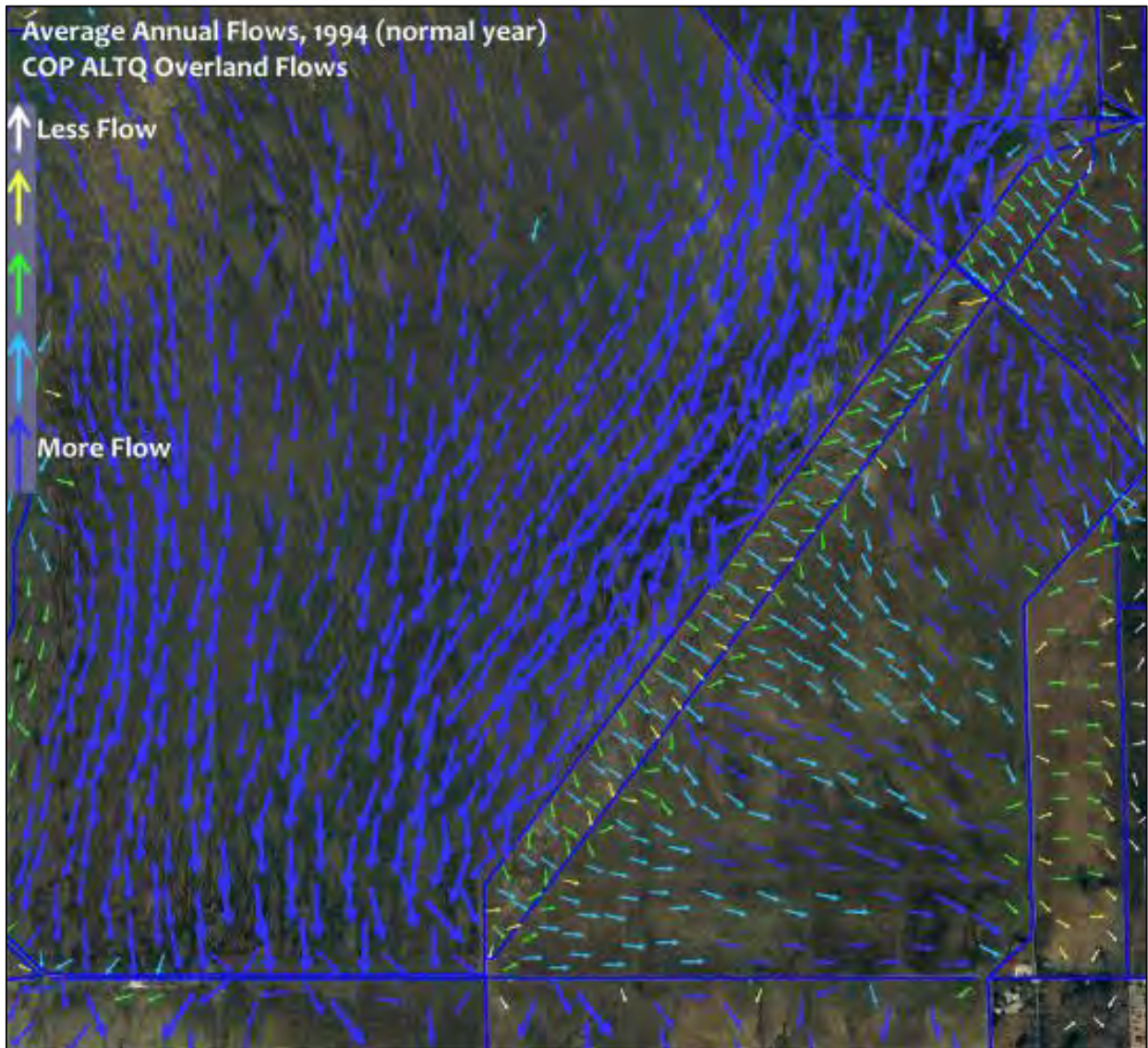
Figure 1.2. Subregional overland flows simulated by Regional Simulation Model for AltQ Combined operational Plan. Average annual overland flow vectors are shown for 1994 considered as normal year.

Fig. 1.3 shows elevated TP peaks at S333 in comparison with S152 and S151 (Fig. 1.1) in L67A canal. The TP peaks at S152 are lower than S151 likely associated with exchanges of marsh water between these two locations (Fig. 1.2). However, this water exchange mechanism, diluting the canal waters as it travels from S152 to S333, is not visible from Fig. 1.3. Understanding the possible mechanisms leading to elevated TP concentrations at S333 is thus essential.
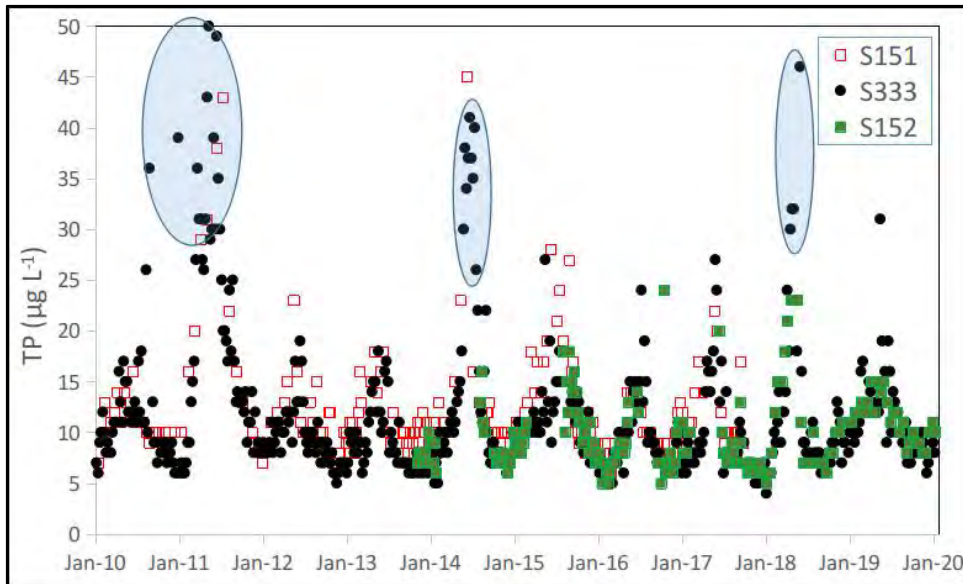
Figure 1.3. TP concentration of grab samples at S333 and in L67A canal at S151 and S152 monitoring locations (Fig. 1.1). L67A canal is a major source of water to S333 gated structure delivering water into Shark River Slough, ENP.

Sediments in canals L67A and L29 are suspected of contributing to increased TP peaks at S333 in relation to source waters monitored at S152 and S12D structures (Fig. 1.1). The sediment pool near or in front of S333 is susceptible to scour and entrainment due to the lift gate design (Fig. 1.4) and hydrodynamics (Fig. 1.5), which may result in variable flux across the gate and over the canal depth.
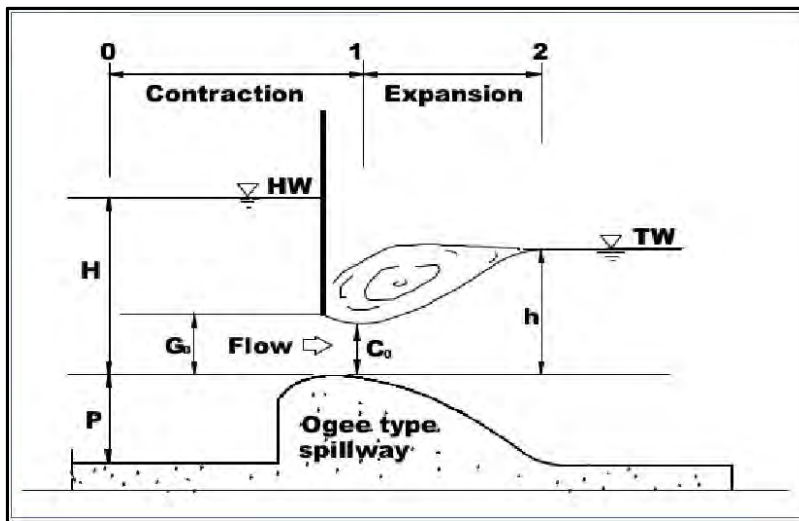
Figure 1.4. S333 gated structure design. Spillway with a lift-gate resting on it 3 ft from canal floor.
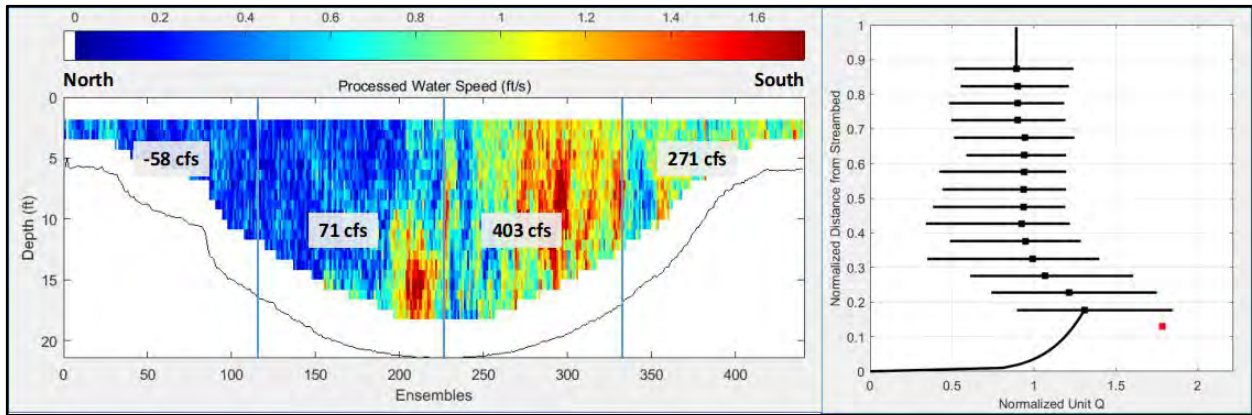
Figure 1.5. Water flows across the L29 canal upstream of S333 gate (Acoustic Doppler Current Profiler data Aug 27, 2018, NPS). Higher flows are observed midway to the southern end and towards the bottom of the canal. The gate opening is above 3 ft (sill height) from the canal bottom over the spillway (Fig. 1.4).

Observed TP concentrations at different stations in vicinity of S333 have > 90 % contribution from particulate phosphorous (PP) and less from soluble reactive phosphorus (SRP) (Figs. 1.6 & 1.7).
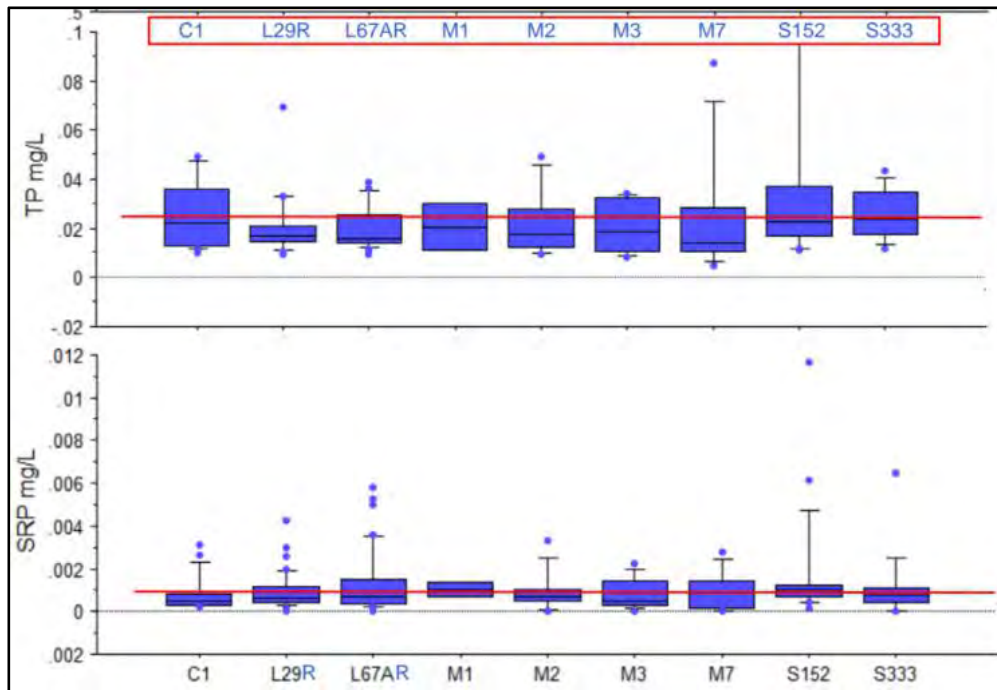
Figure 1.6. Boxplots for TP and SRP at different location in canal and marsh. Whiskers at 95th and 5th percentiles; box from 25th to 75th percentile; horizontal red line passing through S333 median value is for comparison. Figure taken and adapted from Briceno et al. 2019.

9

Figure 1.7. Location of different stations shown in Fig. 1.6. Station names starting with letter 'M' indicate marsh locations within 100 ft of canal. Figures taken and adapted from Briceno et al. 2019.

Identifying conditions or locations (surrounding S333) that may worsen TP levels in the L67A and L29 canals and at S333 is essential for determining effective solutions aimed at mitigating the nutrient loading concerns. The purpose of this investigation is to identify conditions or sources contributing to elevated TP at S333 (Fig. 1.3) and differentiating them by potential sources: (a) local effects and conditions at S333; (b) conditions upstream of S333, either within the L67A canal or along the L29 canal; and (c) conditions in adjacent marshes interacting with source waters in L67A and L29 canals.

1.2. Hypotheses and objectives

The working hypotheses are-

- During relatively low flows and low water levels (dry season; Dec-Apr), sediments accumulate in front of S333 due to settlement and roll-over effects. At the onset of wet seasons, when flows are increased but stages in the canals are low, this pool of sediments is susceptible to the elevated energy in the flow column, which brings these sediments into suspension to contribute to increased TP peaks. This pool of sediments may get flushed downstream within ~3-4 week period of continuous flow, after which the TP peaks tend to recede.
- There is variable water flux across the L29 canal (Fig. 1.5) just upstream of S333 due to gate design (Fig. 1.4), which may lead to the development of variable flux and turbulence, which can scour the canal floor to entrain TP loaded sediments and floc in the water column contributing to TP peaks. These sediment rich peaks are then transported through S333 and settle in the downstream L29 canal or get introduced into the ENP marsh.

Resource managers seek to reduce or eliminate high TP concentrations in discharge waters as much of the waters discharged from S333 gates ends up in northeast Shark Slough.

Specific objectives for this project include:

(1) Characterizing P in floc and sediments from canals and adjacent marsh at subregional and local scales that may contribute to TP peaks at S333,

10

(2) Estimating the TP load of sediments from canals and adjacent marsh at the local scale, and

(3) Determining particle size distribution in floc, sediments and waters flowing through S333.

2. Methods

2.1. Sampling

The sampling was done in two phases to meet Objectives 1 and 2 over different but overlapping areas (see Figs. 2.1 & 2.2). The sample collection methods were similar in both phases. For analyses presented in this research sampling locations were grouped into five compartments based on the geographical landscape within the sampling area (Fig. 2.1). Of the 15 sampling sites, the distribution was as follows: 1) two were in the L29 canal; 2) three in the S333 structure; 3) three in the L67A canal; 4) two in the Miami canal; and 5) five in the marsh.

2.1.1. Sampling area

Phase-1 (Subregional-scale study): The map in Fig. 2.1 shows the region where samples were collected. This sampling occurred during January of the year 2022. This study has a total of 15 sampling sites, of which five were marsh sites and ten were canal sites (Fig. 2.1). One floc and one sediment (0-5 cm) sample were collected from each site. The five marsh sampling sites were labeled M-1, M-2, M-4, M-5, and M-6. The ten canal sites include two L29 sites (L29-1 and L29-2), two Miami sites (Miami-1 and Miami-2), three L67A sites (L67-1, L67-2, and L67-3) and three sites located in front of S333 (S333-1, S333-2, and S333-3) (Fig. 2.1).

Figure 2.1. Locations of sampling event in January 2022 including five marsh sampling sites (M-1, M-2, M-4, M-5, and M-6) and ten canal sites [L29 sites (L29-1 and L29-2) and Miami sites (Miami-1 and Miami-2), and L67A sites (L67-1, L67-2, and L67-3)], and S333 structure sites (S333-1, S333-2, and S333-3).

Phase-2 (Local-scale study): The map in Fig. 2.2 shows the region where samples were collected in close proximity to S333 in L29, L67A, and WCA3A adjacent marsh. This sampling occurred during April and May in the canal, and September in the marsh of the year 2022. Additionally, sediment core samples (5-10 cm) were collected in May, however, these samples were not used in this report due to the objectives of this study. Marsh sampling was delayed and could not be done simultaneously due to low water depths in marsh, which made air-boat access to a priori sampling site impossible. Helicopter access to these sites was also not feasible because of the danger associated with vegetation height. For the sampling event of April to September 2022, a total of 91 sampling sites were selected, including 12 sites in marsh, 10 transects in L67A canal, 12 transects in L29 canal, and 8 transects near S333 (Fig. 2.2). For each transect in canals, three sites (middle of the canal, two-thirds from the middle of canal) were sampled for sediments and only middle canal location was sampled for floc samples. Sampling sites which were very close to the canal bank did not have enough sediment for sampling.
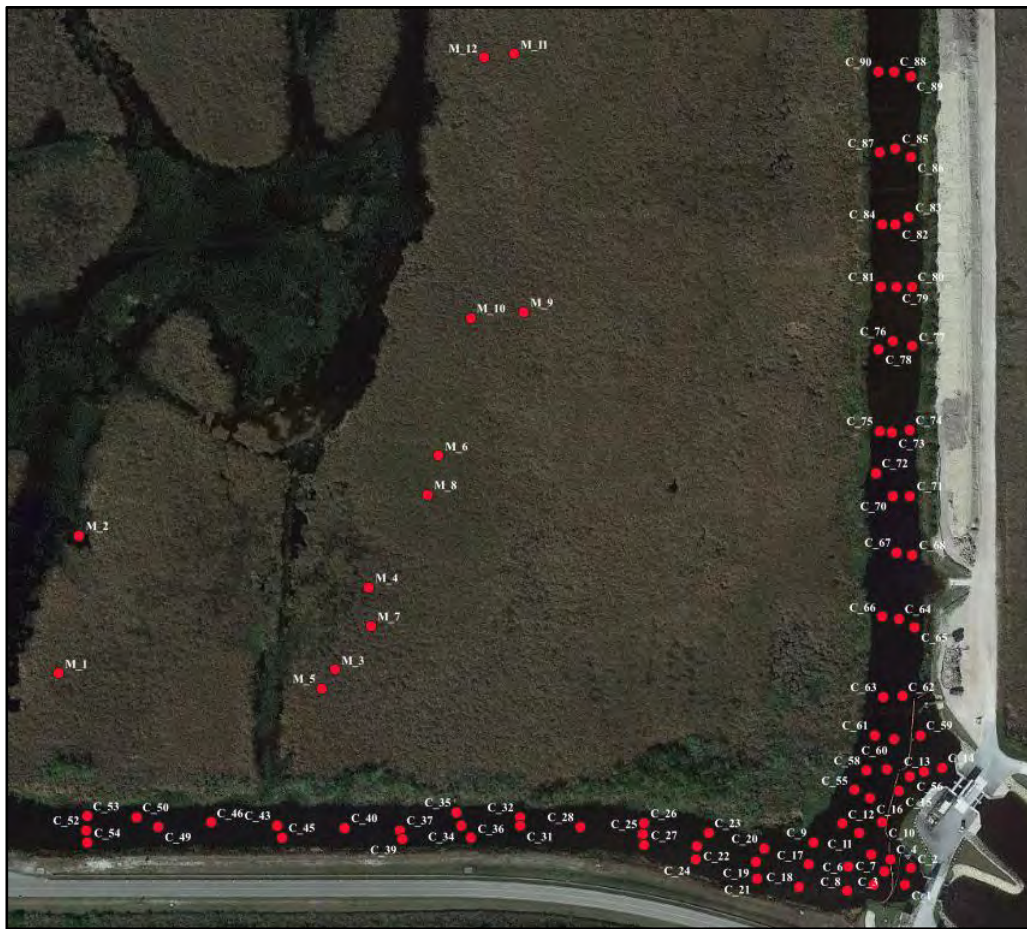
Figure 2.2. Locations of sampling event in April 2022 include 12 sites in marsh, 10 transects in L67A canal, 12 transects in L29 canal, and 8 transects near S333.

2.1.2. Sampling instruments

The materials needed for collecting floc and sediment samples in the wetland and canal systems are the same with the exception of extension rods used in canal sampling and an 80 L backpack needed for floc collection in the wetlands (Fig. 2.3). The collection materials selected for this study were chosen for their light weight, durability, and ease of use in both canal and wetland systems.
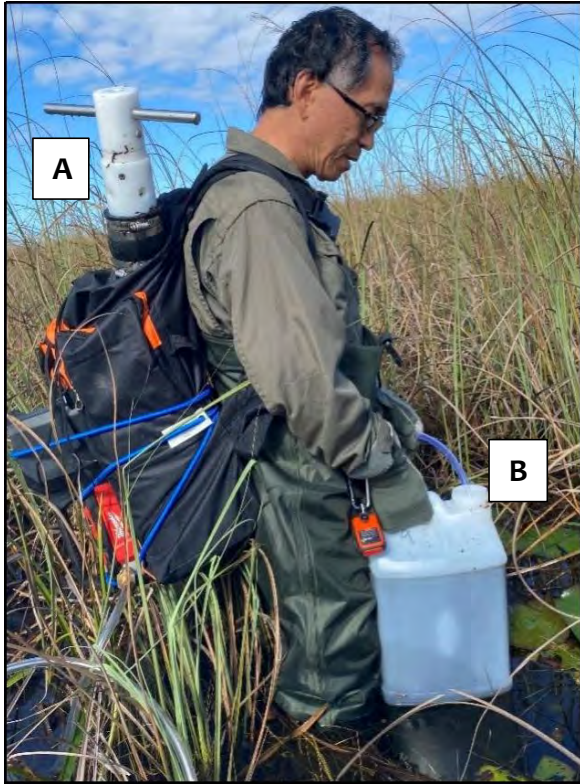
Figure 2.3. A floc sample collection backpack. A) A wetland core sample stored in the backpack. B) A 2-gallon container used for floc collection.

The canal sampling materials consisted of a Universal Corer, extension rod, polycarbonate cores, and a 5-gallon bucket. The Universal Corer contains a Universal Core Head which attaches to the polycarbonate corer barrel and creates a quasi-vacuum seal holding the sediment core in place as it is extracted from the wetland or canal (Fig. 2.4). Once extracted, the cores were capped and stored. Canal depth in this study was less than 10 m and it had higher currents than a wetland or lake system, an aluminum extension rod was selected for the collection of canal sediment cores. The extension rod gives the sampler more control while lowering the core through the water column and increases the precision of the sampling. Being physically connected to the core also increases the dexterity and allows the sampler to feel when they have hit the bedrock or if no sediment is present. In the wetland systems of most of the Everglades, the water is shallower and does not require as long an extension rod. The use of a 1 m extension rod is enough to collect core samples in the wetlands. Other than the length of the extension rod, all the materials needed for sample collection are the same.
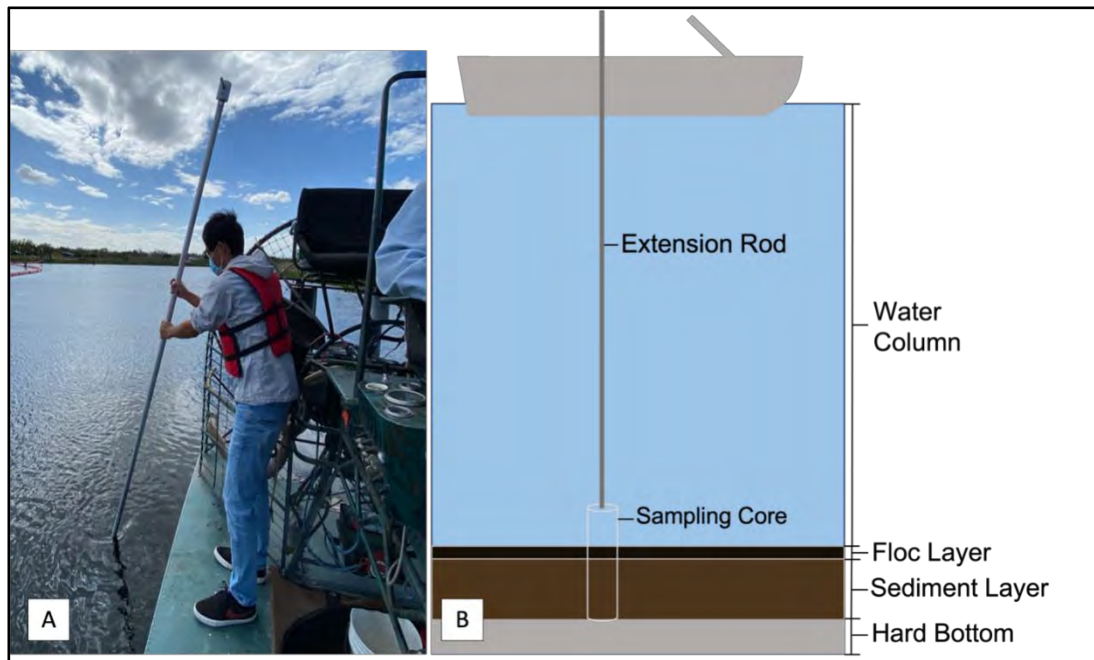
Figure 2.4. Collecting core samples in a canal system. A) A core sample being collected in the field. B) A diagram of the core sampling below the water surface.

The floc sampling for the canal and wetland systems contains the same base materials with a telescopic pole for the canals and a floc collection backpack (FCB) used for the wetlands. The base materials for floc collection consist of a M18 transfer pump, tygon tubing, and two-gallon collection jugs.

For the canal floc sampling, a 30 ft telescopic pole was outfitted with a plastic meshed enclosure on the sampling end (Fig. 2.5). Tygon tubing was then zip tied to the bottom portion of the extension pole and threaded through a hole in the top of the meshed base. The plastic plate helps the sampler feel when they reach the bottom of the canal reducing the amount of disturbed sediment, which could potentially result in sediment being collected instead of floc. The plastic plate (a test tube holder) was screwed onto the threading on the telescopic pole and was covered with a mesh and the tygon tube was then inserted into the plastic plate and was suspended 2 cm above the base. The mesh ensures that the tube does not get clogged with large debris such as seed pods (Fig. 2.5). Additionally, having the end of the tygon tube suspended 2 cm above the base suspends it in the floc layer maximizing the amount of floc collected. If the tygon tube is too close to the canal sediment, it is more likely to get clogged, and if it is too far away, then it will collect a sample with a lower concentration of floc. For the areas sampled in this study, 2 cm was the ideal height. However, based on the floc layer thickness, the height may vary. The other end of the tubing was attached to the M18 transfer pump, and a 2-gallon container was used to collect the sample.
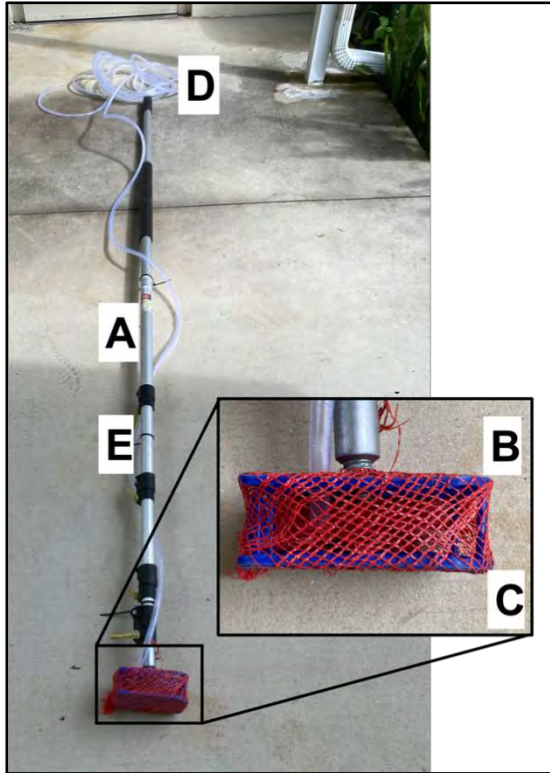
Figure 2.5. Canal floc sampling pole created from a telescopic pole (A), test tube holder (B), plastic mesh (C), tygon tubing (D), and zip ties (E).

In the wetland system, a hands-free device named the Floc Collection Backpack (FCB), was created to carry the pump and any collected core samples allowing the sampler to move more freely through the wetland to the sampling location and increasing the ease of floc collection (Fig. 2.6). The Floc Collection Backpack (FCB) was created by inserting a 7-gallon waste bin into an 80 L backpack and securing the pump and tygon tubing to the outside through the use of 36" bungee cords. The recycle bin is inserted directly into the main pocket of the backpack providing extra structure, which allows the pump to be strapped to the outside of the backpack. Additionally, this allows for collected core samples or other materials to be stored in the backpack while floc samples are being collected. The pump can then be attached by wrapping three 36" bungee cords around the pump and the backpack holding it securely in place. Lastly, the tygon tubing is attached to the pump and can be slid into the bungee straps on each side of the pack keeping them secure and readily available for the sampler. In addition to the backpack, a 2-gallon jug was used to collect the floc samples (Fig. 2.3).

Figure 2.6. The materials needed to create a floc collection backpack for floc collection in a wetland system.

2.1.3. Sampling procedures

2.1.3.1. Canal sampling

Once in location, the universal core head was screwed onto the extension rods and lowered into the canal (Fig. 2.4). The core was pushed into the sediment as deep as possible and slowly extracted. After removing from the water column, the core was capped and removed from the sampling pole. The pole was kept as vertical as possible to ensure no disturbance to the core. The new core was taken if it was evidencing the sediment was overflowed or dropped during the extraction. The collected cores were stored vertically in a large cooler until transported back to the lab. Once in the lab, all cores were stored vertically in a cooler room at 4 °C until they were processed.

Floc samples were collected using the canal floc sampling pole (Fig. 2.5). The pole was extended to the depth of the canal. The tygon tubing on the pole was then connected to the M18 pump, which had a second tygon tube going to the 2-gallon collection jug. Prior to the collection of each floc sample the pole was lowered 1-2 m into the canal and the pump was turned on to run at least 2 gallons through the system to flush the line. The canal floc sampling pole was slowly lowered into the canal until the base of the canal was felt. Once the base of the canal was reached a second person turned on the pump and filled the 2-gallon jug with the floc sample. The water would be dark brown if floc was present on the bottom of the canal. Once the water began to turn brown, then the sample was collected. Once the sample was collected, the pole was raised and flushed again with water.

2.1.3.2. Wetland sampling

Wetland systems tend to have shallower water levels and do not require as long of an extension pole for sediment sampling. Depending on the depth of the water in the wetland, researchers used the 1.2 m extension pole or no extension pole and can attach the T-head directly to the coring head. The core was pushed down into the sediment to the depth of the core. Once extracted, the core was capped and stored vertically in the FCB or in a 5-gallon bucket. In some

areas, the floc layer exceeded the length of the core, and the extension pole was needed to reach the sediment layer.

The floc samples were collected using the FCB and were best done with two people working together (Fig. 2.6). One person would hold the 2-gallon collection jug and the outgoing tube from the pump. The second person turned on the pump and collected the sample. Prior to collection, the pump was turned on and flushed with 2 gallons of water from the sampling site. The floc layer was typically seen through the water but can also be felt by hand. The tube was inserted into the middle of the floc layer. The end of the tube is prone to clogging with larger plant material and may need to be cleared a few times during floc collection, which was done by hand. After sampling, the line was flushed again.

2.1.3.3. Cross-sectional water sampling

Water samples were collected in front (~23 m) of S333 on a horizontal transect across vertical transects to form a cross-section (Fig. 2.7) at seven water sampling events (Apr 14, Apr 25, May 05, May 26, Jun 07, Jun 16, and Jun 27 of 2022). Water samples were analyzed for particle size distribution, TP, total suspended solids (TSS), and total dissolved phosphorus (TDP). The horizontal transect across S333 was established by tying a rope to two wooden posts on the north and south canal banks. The water samples were collected using the telescopic sampling pole and M18 pump. The pole was marked at heights of 30, 60, 100, 160, 250, and 500 cm from the bottom end, with tygon tubing attached at each marked height. Each tygon tubing was connected to the inlet of the pump during collection, and the outlet went to a 1 L collection bottle. Once the pole was extended to the canal bed, the pump was turned on to flush the line prior to each sample collection. The samples were collected at heights of 30, 60, 100, 160, 250, and 500 cm from the canal bed. Additionally, one sample from the water surface was taken at 50 cm depth for every vertical transect in the same manner by using an aluminum rod with a tygon tubing attached to it at 50 cm depth. Not all sampling depths were feasible for sample collection at all vertical transects, especially towards the canal banks due to the reduction in the height of water (see Fig. 2.7).
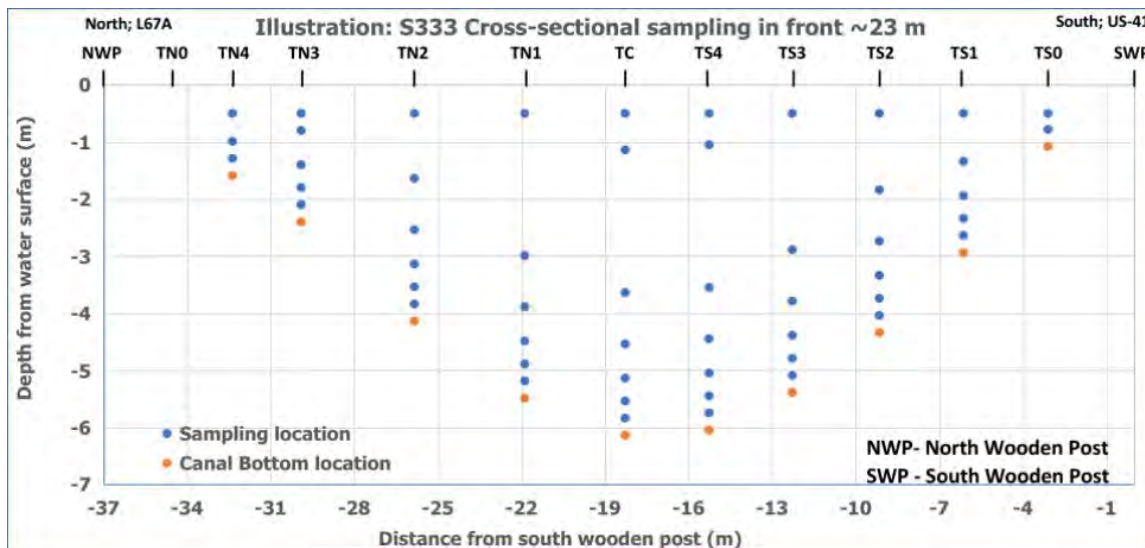
Figure 2.7. Illustration of water sample collection on seven sampling events from April through June 2022 ~23 m in front of S333. (SWP- towards US-41, NWP- towards L67A, TC- Central vertical transect, TS- Southern vertical transects, TN- Northern vertical transects).

2.1.3.4. Canal flow measurements

Flow measurements were taken during seven water sampling events (Apr 14, Apr 25, May 05, May 26, Jun 07, Jun 16, and Jun 27 of 2022) at ~457 m upstream of S333 across the L29 and L67A canals. Flows were also measured across the canal ~23 m in front of the S333 gate. The flow measurements were done by Acoustic Doppler Current Profiler from Teledyne RD Instruments using Model-Workhorse running at 1200 KHz frequency following manufacturer's operation manual. Analysis of acoustic data was conducted by using Teledyne RD Instruments WinRiver II software (https://hydroacoustics.usgs.gov/movingboat/WinRiverII.shtml) and also by QRev USGS software (https://hydroacoustics.usgs.gov/movingboat/QRev.shtml) for comparison. USGS QRev site mentions differences may occur in the computation of discharges as compared to WinRiver because- "Default QRev settings may result in discharge computations different from WinRiverII and RiverSurveyor Live. Potential differences in discharge are due to QRev data filters, interpolation algorithms, and computations that may differ from manufacturer software".

2.1.3.5. Sampling storage and processing

Sediment samples collected from the canal and wetlands were processed the same way. After collection, the samples were stored at 4 °C until processing. Cores were then sectioned at desired intervals (5 and 10 cm), oven dried at 60 °C, and stored until future analysis (Reddy & DeLaune, 2008). Floc samples were stored at 4 °C until they were processed. The floc samples were stored for 1-2 weeks, depending on the floc particle size and density, until processing to allow floc to settle to the bottom of the sampling container. The top portion of the sample (water) was then poured off and the settled floc sample was transferred to a wide based container and oven dried at 70 °C until dry (~3-5 days). The samples were then bagged and stored until analysis. The 2-gallon containers yielded 0.4-0.6 gallons of floc sample from the wetlands.

2.2. Chemical and Physical Analytical Methods

Table 2.1. List of physical and chemical analyses performed in Phase-1 and Phase-2 samples

Sample	Particle size (Sieving)	Particle size (Laser)	BD	TP	P fractionation	P sorption	IC	OM	Metals	Minerals	Isotopes
Phase-1 (Subregional-scale study)											
Floc		√		√		√	√	√	√	√	√
Sediment	√	√	√	√		√	√	√	√	√	√
Phase-2 (Local-scale study)											
Floc		√		√	√		√	√			
Sediment	√	√	√	√	√		√	√			

	Particle size (Laser)	TP	TDP	TOC	TSS
Water	√	√	√	√	√

BD: bulk density, TP: total phosphorus, P: Phosphorus, IC: inorganic carbon, OM: organic matter, TDP: total dissolved phosphorus, TOC: total organic carbon, and TSS: total suspended solids.

2.2.1. Total phosphorus

The soil TP concentration was determined following a modified EPA 365.3 colorimetric method (USEPA, 1982). The soil samples were dried in the oven at 60 °C for a week and sieved through

a 2-mm sieve. A 0.2 g of soil sample was weighed into a beaker and digested on a hotplate with 20 ml of 6 M hydrochloric acid (HCl) for approximately 3 to 4 hours (Anderson 1976; Belmont et al. 2009). The digested soil samples were then diluted to 50 ml by adding 2.25 ml 6 M HCl and 47.75 ml distilled deionized water. The diluted samples were shaken at 180 rpm for 2-5 minutes (New Brunswick Scientific, EDISON, NJ, USA) and were then filtered through Whatman 42 filter paper. All filtered aliquots were stored in the fridge at 4 °C and analyzed with a Beckman Coulter DU-64 UV-VIS spectrophotometer for TP concentration.

2.2.2. Phosphorus fractionation

The sequential fractionation procedure for phosphorus in floc and sediment involves a series of chemical extractions that partition TP into different forms or fractions. These fractions represent different pools of P with varying availability and potential for releasing P into the water. For this study, soil TP was differentiated into seven forms of P using a modified sequential fractionation procedure (Irick et al. 2013; Zhang and Kovar, 2009). These P fractions were extracted sequentially by different reagents as follows: Water-soluble P (H_2O), Exchangeable P (1 M NH_4Cl), Al-bound P (0.5 M NH_4F), Fe-bound P (0.1 M NaOH), Organic P (0.1 M NaOH + digestion), Ca-/Mg-bound P (0.5 M HCl),and Recalcitrant residual P (6 M HCl). Briefly, 0.5 g of soil sample was placed into a 50 ml centrifuge tube with 25 ml of each extraction solution to maintain a soil to solution ratio of 1:50 (g ml^{-3}). The tubes were shaken in a reciprocating shaker at 120 rpm for 1, 0.5, 4, 17, and 1 hour for DDI, NH_4Cl, NH_4F, NaOH, and HCl extractant, respectively. The sample solutions were then centrifuged at 2100 × g for 15 minutes, and the supernatant was filtered through Whatman 42 filter paper. All filtered supernatants were stored at 4 °C before analysis, and the P concentration was measured as described previously. Phosphorus measured in filtrates was soluble inorganic P (P_i). 0.1 g of $(NH_4)_2S_2O_8$ and 0.5 ml of 5 M H_2SO_4 were added to 12.5 ml of NaOH filtrates and were shaken at 180 rpm for 2 minutes. The sample solutions were autoclaved at 121 ºC and 20 psi for 30 minutes. The TP in the NaOH filtrates were determined colorimetrically as previously described. Organic P in the NaOH filtrates (NaOH-P_o) was determined as the difference between TP and P_i in the filtrates.

These P fractions can be divided into labile and non-labile categories based on availability and reactivity. Labile P refers to fractions (water-soluble P, Exchangeable P, and organic P) that can be easily released from floc and sediment into the water and are readily available to microbes. These fractions are influenced by short-term environmental conditions and management practices. Non-labile P, on the other hand, refers to fractions (Al/Fe-bound P, Ca/Mg-bound P, and residual P) that are tightly binding to soil minerals, organic matter, or other forms of chemical complexes, are resistant to immediate release and less available or inaccessible to microbes.

2.2.3. Phosphorus sorption

Phosphorus adsorption isotherms were determined according to the procedure of Zhou and Li (2001). One gram of soil sample was weighed into a 50 mL centrifuge tube. A 10 mL aliquot of 0.05M KCl solution containing 10, 50, 100, 200, and 400 mg L^{-1} P was added to each soil sample, respectively. All soil samples with added P standard were shaken at 100-120 rpm for 24 hours and then centrifuged at 1800 × g for 15 minutes. The supernatant was filtered through Whatman 42 filter paper. The P concentration in the filtered supernatant was measured as described previously (Wang and Li 2010). The total amount of sediment sorbed P (S, mg kg^{-1}) was calculated as the sum of measured P sorbed (S$'$, mg kg^{-1}) and the initial sorbed P in the sediment (S$_0$, mg kg^{-1}) (Belmont et al. 2009):

$$S = S' + S_0 \qquad \text{[1]}$$

The value of S_0 was evaluated by fitting the data into least-square linear fit of S' measured at low equilibrium concentrations (C):

$$S' = K'C - S_0 \qquad \text{[2]}$$

Where K' refers to the linear sorption coefficient (L kg^{-1}), also known as buffer capacity. The equilibrium phosphorus concentration (EPC$_0$) is net zero sorption means neither adsorption nor desorption occur ($S' = 0$):

$$EPC_0 = \frac{S_0}{K'} \qquad \text{[3]}$$

The soil adsorption capacity was evaluated by fitting the data into Freundlich and Langmuir isotherms:

Freundlich isotherm:

$$S = K_f \times C^N \qquad \text{[4]}$$

$$\log S = \log K_f + N \log C \qquad \text{[5]}$$

Where K_f is the Freundlich constant, and index N is the measure of intensity (Singh 2015). By plotting the linear Freundlich isotherm (Eq. 5), the slope is intensity N, and the intercept is log K_f. Both K_f and N are empirical constant with N < 1 (Zhou and Li, 2001).

Langmuir isotherm:

$$\frac{C}{S} = \frac{1}{kS_{max}} + \frac{C}{S_{max}} \qquad \text{[6]}$$

Where k is Langmuir sorption coefficient related to sorption energy, and S_{max} (mg kg^{-1}) is the maximum phosphorus sorption capacity of soil samples.

2.2.4. Bulk density, organic matter, and inorganic carbon

The BD of each 5 cm sediment layer was calculated by dividing the mass of sediment layer by its volume:

$$BD = \frac{M}{\pi \times r^2 \times h} \qquad \text{[7]}$$

Where M is the mass of 5 cm sediment (g), π is a mathematical constant that describes the ratio of the circumference of a circle to its diameter, r is the inner radius of sediment core (cm), and h is the height of each sediment layer (5 cm).

The soil OM content was measured by the loss-of-ignition (LOI) method (Salehi et al. 2011). Soil OM starts to ignite at 200 ^{o}C and is completely depleted at 550 ^{o}C (Santisteban et al. 2004). In this study, soil samples were dried in the oven at 60 ^{o}C for a week and sieved through a 2-mm sieve. Weighed 0.2 g of soil sample into a beaker and combusted at 250 ^{o}C and 550 ^{o}C for 30 minutes and 4 hours in a muffle furnace, respectively. The soil samples were cooled down at ambient temperature overnight and weighed again after combustion. The soil organic matter percentage from LOI method (SOM$_{LOI}$) was calculated as:

$$SOM_{LOI} = \frac{(\text{soil mass before combustion}+\text{beaker mass}) - (\text{soil mass after combustion}+\text{beaker mass})}{\text{soil mass before combustion}} \times 100 \qquad \text{[8]}$$

The pressure-calcimeter method described by Wang et al. (2011) was employed to determine the inorganic carbons present in floc and sediments. This method relies on the pressure generated by releasing carbon dioxide from floc and sediment samples when bicarbonate or carbonate in the sample reacts with 1 M HCl. Briefly, a sample (0.2 g) was placed in an Erlenmeyer flask that was connected to a manometer. The vial with 5 ml HCl was suspended inside the Erlenmeyer flask. Before initiating the reaction, the solution levels on both sides of the manometer were equalized to establish equal pressure inside and outside the manometer. The system was kept enclosed, and the HCl was released to initiate the reaction with the sediment sample. As a result of the reaction, a pressure was generated, which could be read from the manometer. The change in solution levels on either side of the manometer indicated the increase or decrease in pressure driven by the CO_2 released from the reaction vessel. The pressure measured was proportional to the quantity of CO_2 produced from the sample. A linear correlation between the quantity of $CaCO_3$ and the volume of CO_2 was established using a series of reagent $CaCO_3$ with varying quantities (0.05, 0.1, 0.2, 0.3, and 0.4 g) for calibration.

2.2.5. Particle size distribution

2.2.5.1. Mechanical sieving

Dried floc and sediment samples were finely ground using mortar and pestle and were sifted by passing through 2 mm and 0.053 mm sieves. Samples were separated into three fractions: 1) gravel that cannot pass through 2 mm sieve; 2) sand that can pass through 2 mm sieve but cannot pass through 0.053 mm sieve; and 3) silt that can pass 0.053 mm sieve. Each fraction of sediment soil samples was stored in a labeled plastic bag for further analysis. Gravel, sand, silt, and clay defined by USDA are used here to describe particle size distribution in an operational sense (solely based on size).

2.2.5.2. Laser diffraction

The particle size distributions in water, floc, or sediments were determined using the laser diffraction method, as described by the manual of LS 13 320 Laser Diffraction Particle Size Analyzer (www.beckmancoulter.com). In this method, a Laser Diffraction Particle Size Analyzer (LS 13 320, Beckman Coulter, Brea, CA) was used. Briefly, either 125 ml of water or 5 ml of dried floc and sediment samples (< 1 mm) were loaded into the liquid or dry powder module of the analyzer. Prior to each measurement, an auto-alignment adjustment was performed to ensure accurate calibration. For each water sample, the measurement duration was set at 60 seconds, while for floc and sediment samples, the duration ranged from 90 to 120 seconds. It is worth noting that despite an extensive literature review, a standard method for measuring floc or sediment particle size with a laser could not be found. For this study, dried samples were used, as oven- or air-dried samples have been widely accepted as a standard procedure for traditional soil particle size distribution measurements. However, floc materials are highly organic and non-fractal. Oven-drying the floc materials might lead to permanent changes in their physical properties and potentially influence the measurement results.

2.2.6. Metal analysis

For metal analysis, EPA method 3050B was used and total recoverable metals in sediments and flocs were analyzed. Briefly, each sample (~ 0.5 g) was digested with 5 ml of concentrated nitric acid at 95±5 °C on a hot block for one hour. After the samples cooled off, 1 ml of 30 % H_2O_2 was added, and the samples were placed back on the hot block and digested for 20 additional minutes. After the second heating, the samples were cooled to room temperature and diluted to a

50 mL volume with distilled water. After centrifugation (5000 rpm for 5 min), samples were further diluted if necessary, and analyzed for 23 metals including 6 non-trace metals (Al, Fe, Mg, Na, K, Mn), and 17 trace metals (Cr, Co, Cu, Zn, Se, Cd, Ba, As, B, Li, Be, Ag, Pb, Ni, Mo, Sb, Hg) using an inductively coupled plasma-mass spectrometry (ICP-MS, Perkin Elmer, Wellesley, MA). It is worth noting that the EPA 3050B method for this study used very strong acid digestion that can effectively dissolve almost all elements that could become environmentally available. However, the method is not specifically designed to digest aluminosilicates, which may result in underestimating total Al and Si in samples.

2.2.7. Isotope analysis

2.2.7.1. Nitrogen isotopes in floc and sediment bulk raw samples

All isotope analyses were conducted by Stable Isotope Mass Spec Lab at Department of Geological Sciences, University of Florida. Nitrogen isotopes in floc and sediment bulk raw samples were analyzed using a Thermo Electron DeltaV Advantage isotope ratio mass spectrometer, which was coupled with a ConFlo II interface connected to a Carlo Erba NA 1500 CNHS Elemental Analyzer. The samples were dried and pre-loaded into tin capsules where they were placed in a 50-position automated Zero Blank sample carousel on a Carlo Erba NA1500 CNS elemental analyzer.

The loaded samples were combusted in a quartz column at 1000 °C in an oxygen-rich atmosphere. The resulting sample gas was then carried by a helium (He) stream and passed through a hot reduction column (650 °C) containing elemental copper to remove oxygen. After passing through a chemical trap (magnesium perchlorate) to eliminate water, the gas stream was directed through a 0.7-meter gas chromatography (GC) column set at 125 °C to separate nitrogen (N_2) from carbon dioxide (CO_2). The sample gas was further directed into a ConFlo II interface and introduced into the inlet of a Thermo Electron Delta V Advantage isotope ratio mass spectrometer operating in continuous flow mode. The measurement of the sample gas was performed relative to laboratory reference N_2 and CO_2 gases. Nitrogen isotopic results were expressed in standard delta notation relative to atmospheric air (AIR).

2.2.7.2. Carbon isotopes of organic fraction of sample – samples were measured on acidified material (carbonate removed)

Carbon isotopes of the organic fraction in the samples were analyzed after acidification to remove carbonates. The acidification process involved soaking the samples in 1 M HCl overnight in 15 ml centrifuge tubes. Afterward, the tubes were spun down, and the acid was decanted. Fresh acid was added, and the samples were stirred using a vortex mixer and left to sit overnight. This process was repeated, with subsequent acid removal and replacement with fresh acid. The samples were allowed to sit overnight again. They were then spun down, and deionized water was added. The samples were stirred and spun before removing the water. This rinsing step was performed two more times. Finally, the samples were freeze-dried.

The same analytical method used for nitrogen isotopes was employed for carbon isotopes. The samples were loaded into tin capsules and placed in a 50-position automated Zero Blank sample carousel on a Carlo Erba NA1500 CNS elemental analyzer. Following combustion in a quartz column at 1000 °C in an oxygen-rich atmosphere, the resulting sample gas was transported using a helium (He) carrier stream. The gas stream passed through a hot reduction column (650 °C) containing elemental copper to eliminate oxygen. Then, the effluent stream was directed through a chemical trap (magnesium perchlorate) to remove water. A 0.7-meter gas chromatography (GC)

column set at 125 °C was used to separate nitrogen (N_2) from carbon dioxide (CO_2).

The sample gas was subsequently directed into a ConFlo II interface and introduced into the inlet of a Thermo Electron Delta V Advantage isotope ratio mass spectrometer operating in continuous flow mode. The measurement of the sample gas was performed relative to laboratory reference N_2 and CO_2 gases. Carbon isotopic results were reported using standard delta notation relative to VPDB (Vienna PeeDee Belemnite).

2.2.7.3. Oxygen isotopes of organic fraction of sample – samples were measured on acidified material (carbonate removed)

Oxygen isotopes of the organic fraction in the samples were measured after decarbonation following the approach described in the carbon isotope analysis section above. The measurement was performed using a Thermo Electron DeltaV Plus isotope ratio mass spectrometer, coupled with a ConFlo IV interface connected to a high-temperature conversion elemental analyzer (TCEA).

After decarbonation, the samples were loaded into silver capsules and placed into the Zero Blank autosampler. The samples were then subjected to high temperatures in an oven at 1400 °C to decompose the organic matter into gases. The oxygen from the sample combined with excess carbon in the tube, resulting in the formation of carbon monoxide (CO). To separate CO from other gases, a gas chromatography (GC) column set at 90 °C was utilized. The CO gas was transferred with a helium carrier gas to a ConFlo IV interface and then passed to the isotope ratio mass spectrometer (IRMS) for isotopic analysis. The Thermo Electron DeltaV Plus IRMS system performed the measurement and analysis of the oxygen isotopes in the CO gas. Oxygen isotopic results were reported using standard delta notation relative to VSMOW-SLAP (Vienna Standard Mean Ocean Water – Standard Light Antarctic Precipitation).

2.2.8. Mineralogical characterization

Mineralogical characterizations were conducted by Research Service Centers (RSC), Herbert Wertheim College of Engineering, University of Florida. Mineral identification and quantification of floc and sediment samples were performed using an X-ray diffraction (XRD) diffractometer (Empyrean, Malvern Panalytical, Malvern, UK) equipped with a Beta-filter Nickel filter, an RTMS detector, and operating at an accelerating voltage of 45 kV and a filament current of 40 mA. The measurements were conducted within the 2θ range of 18°–80° and the X-ray Wavelengths were Kα1 (Å): 1.540598 and Kα2 (Å): 1.544426.

Samples with standard added were prepared with a ratio of 15 % standard and 85 % sample, although acceptable ratios ranging from 10 % to 20 % were also employed. The actual weight ratios were entered into the processing software. For data processing, the HighScore+ 3.0 software was utilized, employing the ICDD PDF4+ database for peak matching and phase matching. A list of phases obtained from similar samples was saved and applied to subsequent samples to expedite the search for phases. Only unmatched peaks were examined for additional phase matching. HighScore+ Reitveld refinement was employed to fit the diffraction pattern, and the weight percentage of the standard Al_2O_3 phase was provided as input to enable the software to calculate the amorphous content within the sample. Semi-automatic refinement mode was used after an initial automatic fit, with parameters adjusted as necessary to optimize the goodness of fit. The generated report file includes information on the tool conditions, selected slits, and scan parameters utilized. The parameters remained constant throughout all scans.

2.3. Spatial and Statistical Data Analysis

2.3.1. Spatial analysis

The Quantum Geographic Information System (QGIS) software (version 3.30.2) was used to generate maps for sampling sites and results presented of this study. We determined TP mass present in 5 cm core depths for one square meter areas at sample collection points. For these sampling points, TP mass was interpolated for the desired area in the canal and the marsh using inverse distance squared weighting (IDW) tool and a grid size of one square meter. The summation of mass over this area provided total TP mass present in 5 cm depth. As IDW does not provide prediction standard errors they are not reported.

2.3.2. Normalization

Data normalization is often used to remove interference and improve data integrity. In this study, OM was collected among different compartments (e.g., different canals, unique marsh areas) with different levels of OM. To make TP more comparable among compartments, we normalize floc and sediment TP concentration by dividing by percent OM (Domagalski et al. 2007, Gan et al. 2020, Michelsen 1992). This approach standardizes the data and eliminates effects of varying levels of OM content.

2.3.3. Statistical analysis

Statistical analyses were conducted by a rank-based nonparametric multiple contrast test procedure (mctp) using "nparcomp" package via the "mctp" function (Noguchi et al. 2020). As a recently developed analysis method, mctp was able to control the possibility of type I errors appropriately (Noguchi et al. 2020). Significant differences for the mctp test were indicated by different letters among compartments. The Phase-1 (Subregional-scale study) sample size for statistical testing is small. Power maybe low to detect all significant differences.

Hierarchical cluster analysis was used for performing exploratory data analysis. With this approach, elements with higher similarity were grouped into the same clusters by building binary merge trees, starting from the single element, and merging iteratively until reaching the tree root that contains all the elements (Nielsen 2016). R programming language (version 4.1.1) and "factoextra" package (Kassambara 2016) were used for this analysis. Three indicator groups were used in this study (Fig. 2.8). Group 1 was all indicators combined from the subsequent groups, group 2 was conventional indicators including IC, TP, OM, and non-trace metals, and group 3 was geochemical indicators such as trace metal, clay minerals, and isotopes (Fig. 2.8).

Regardless of the overarching five compartments used for the subregional-scale portion of this study, given the potential for the marsh and canals to be contributing sources to the S333, we target these three general compartments for delineating clusters in the cluster analyses.
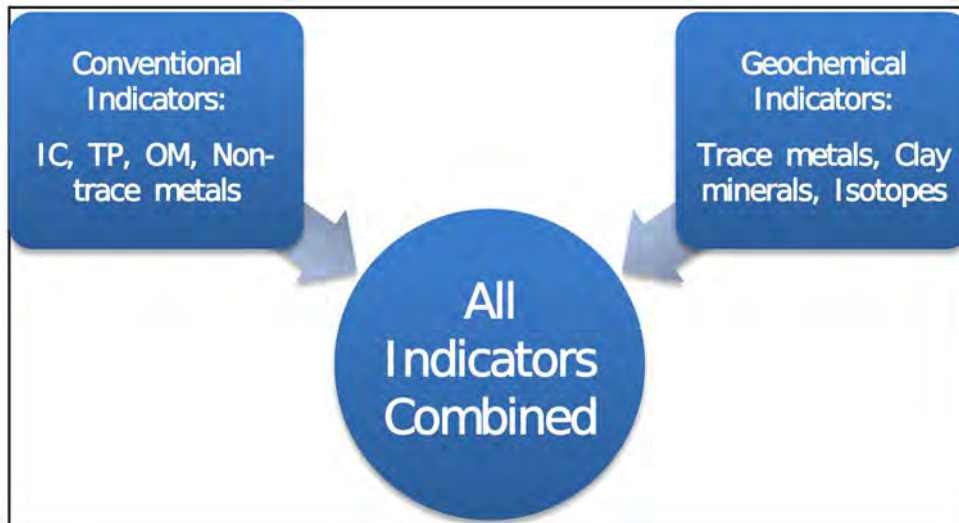
Figure 2.8. Three groups of indicators for the hierarchical cluster analysis.

3. Results

3.1. Phase-1 (Subregional-scale study) (Fig. 2.1)

3.1.1. Total phosphorus spatial distribution

As an implicative part of the process to help characterize the source of P in sediment, floc and sediment samples were collected and the TP concentration were analyzed. Floc and sediment samples from L29 canal had the highest TP concentration (Figs. 3.1 & 3.2), approximately 4000 mg kg^{-1} and 2000 mg kg^{-1}, respectively. TP concentrations of floc and sediment samples collected from the Miami canal were the second highest, approximately 1300 mg kg^{-1} and 900 mg kg^{-1}, respectively. Floc samples from L67A and S333 showed similar levels of TP concentration at ~1000 mg kg^{-1}, while the marsh samples exhibited lower TP concentration at ~600 mg kg^{-1}. In terms of sediment samples, L67A, S333, and marsh samples showed similar TP levels at ~500 mg kg^{-1} (Figs. 3.3 & 3.6).
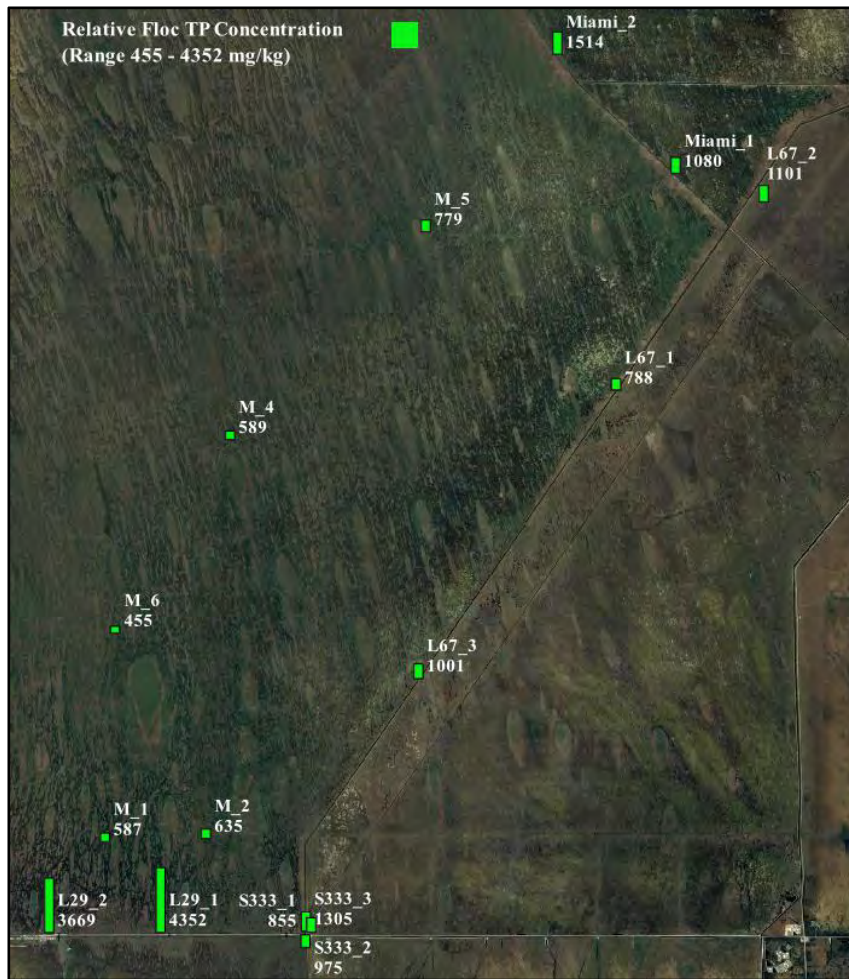
Figure 3.1. Total P concentrations (green bars) in floc collected from near S333 structure (S333-1, S333-2, S333-3), three canals- L29 (L29-1 and L29-2), L67A (L67-1, L67-2, L67-3), and Miami canal (Miami-1, Miami-2), and adjacent marsh (M-1, M-2, M-4, M-5, M-6). The height of each bar represents TP concentration (a number next of the bar, mg kg^{-1}) from the sampling location.
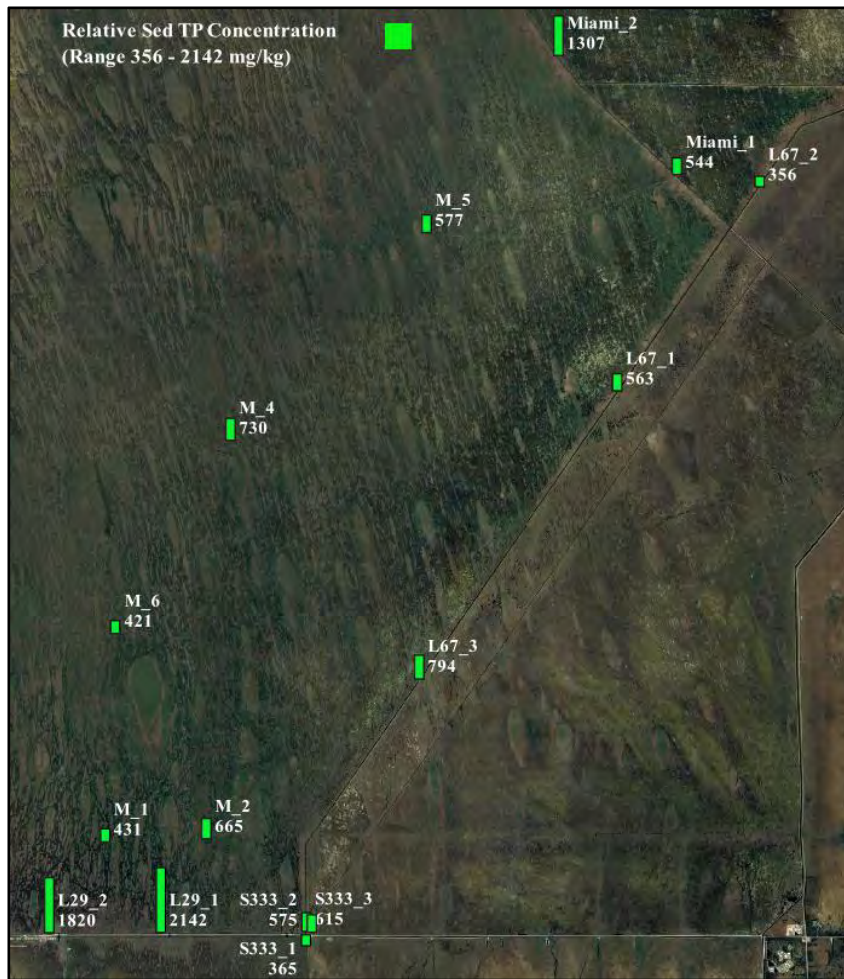
Figure 3.2. Total P concentrations (green bars) of sediment collected from near S333 structure (S333-1, S333-2, S333-3), three canals- L29 (L29-1 and L29-2), L67A (L67-1, L67-2, L67-3), and Miami canal (Miami-1, Miami-2), and adjacent marsh (M-1, M-2, M-4, M-5, M-6). The height of each bar represents TP concentration (a number next of the bar, mg kg^{-1}) from the sampling location.

3.1.2. Total phosphorus, organic matter, and inorganic carbon

Based on the geographical landscape within the sampling area that showed in the maps (Figs. 3.1 & 3.2), 15 sampling sites were grouped into five compartments: 1) L29 canal, 2) S333 structure, 3) L67A canal, 4) Miami canal, and 5) Marsh. The TP concentration found in L29 floc sample was significantly higher than that in marsh samples. S333, L67A, and Miami floc samples showed similar TP levels and they were neither significantly different from L29 samples nor marsh samples (Fig. 3.3). No significant differences were observed among the floc samples from different sampling locations in terms of organic matter content (Fig. 3.4). The order of inorganic carbon in floc samples is L67A > S333 > Miami > L29 > Marsh (Fig. 3.5).
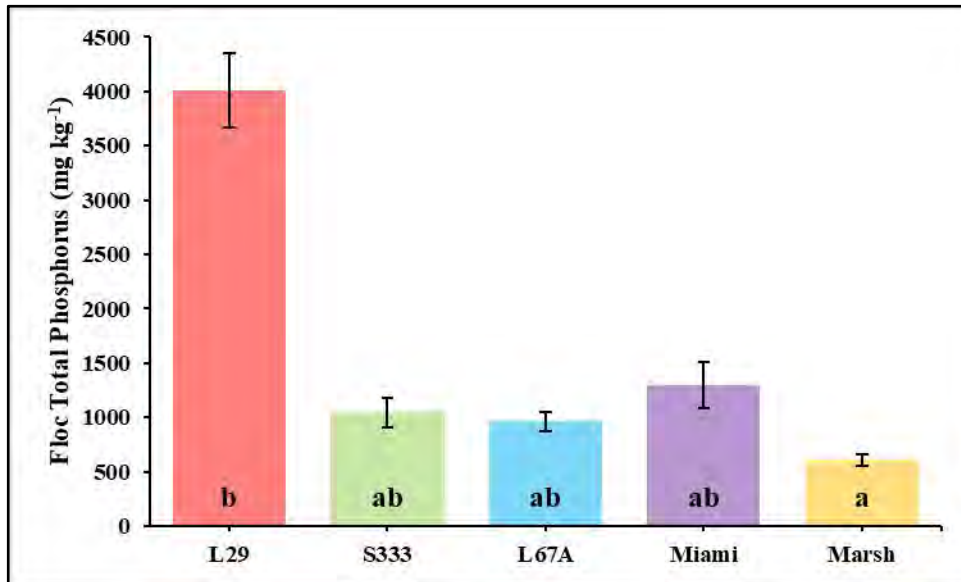
Figure 3.3. Mean concentrations of TP in floc samples collected near S333 structure (S333), three canals (L29, L67A, and Miami canal), and adjacent marsh (Marsh). Error bars represent the standard errors of the mean. Letters (a, b, ab) indicate the significant differences among different sampling locations.
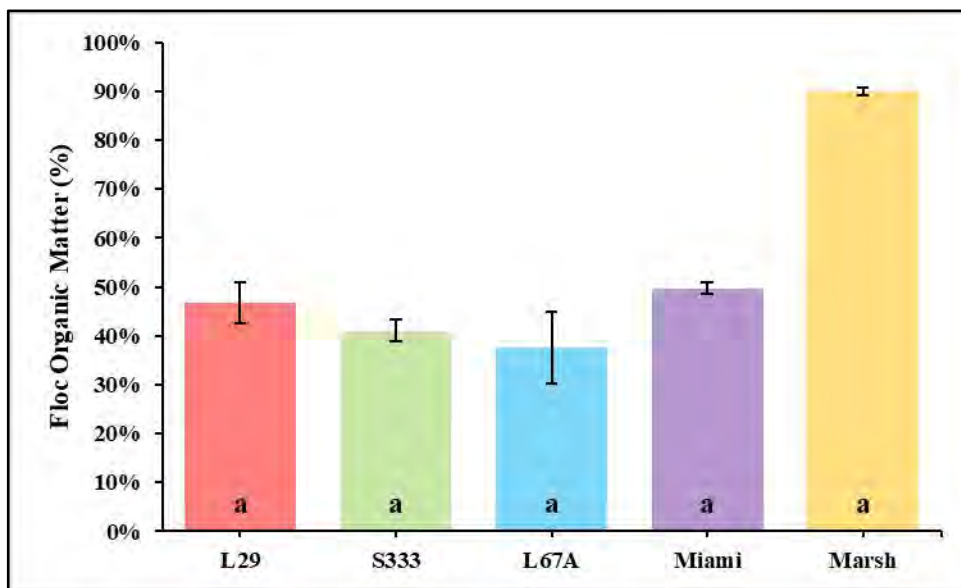
Figure 3.4. Mean concentrations of OM in floc samples collected near S333 structure (S333), three canals (L29, L67A, and Miami canal), and adjacent marsh (Marsh). Error bars represent the standard errors of the mean. Letters (a) indicate no significant differences were observed among different sampling locations.
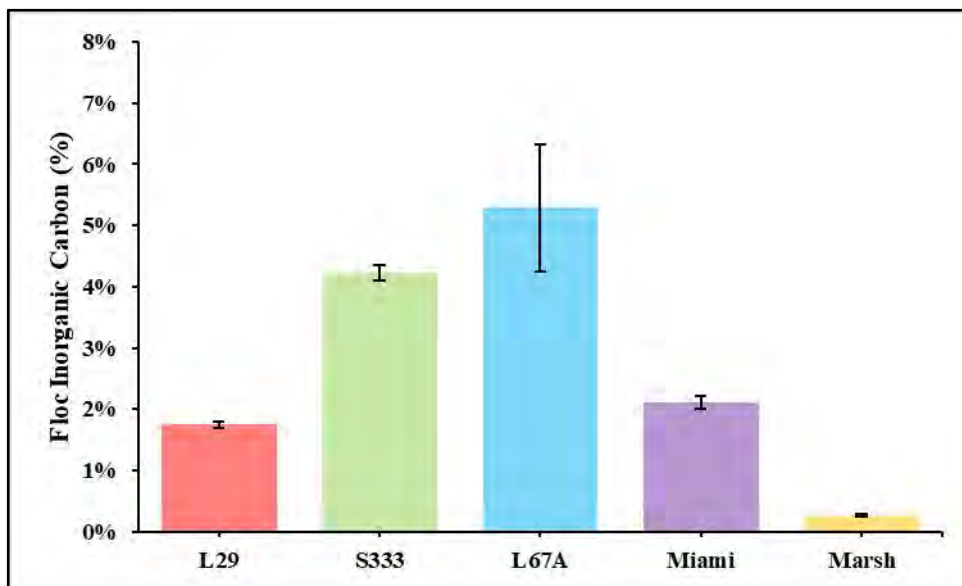
Figure 3.5. Mean concentrations of inorganic carbon in floc samples collected near S333 structure (S333), three canals (L29, L67A, and Miami canal), and adjacent marsh (Marsh). Error bars represent the standard errors of the mean.

The TP concentration of sediment samples did not show any significant difference among sampling sites (Fig. 3.6). The OM of sediment samples followed a pattern of Marsh ≈ Miami > L29 > L67A, and S333 samples were not significantly different with any of them (Fig. 3.7). L67A sediment samples showed significantly higher inorganic carbon than marsh samples. L29, S333, and Miami sediment samples showed similar inorganic carbon levels and they were neither significantly different from L67A samples nor marsh samples (Fig. 3.8).
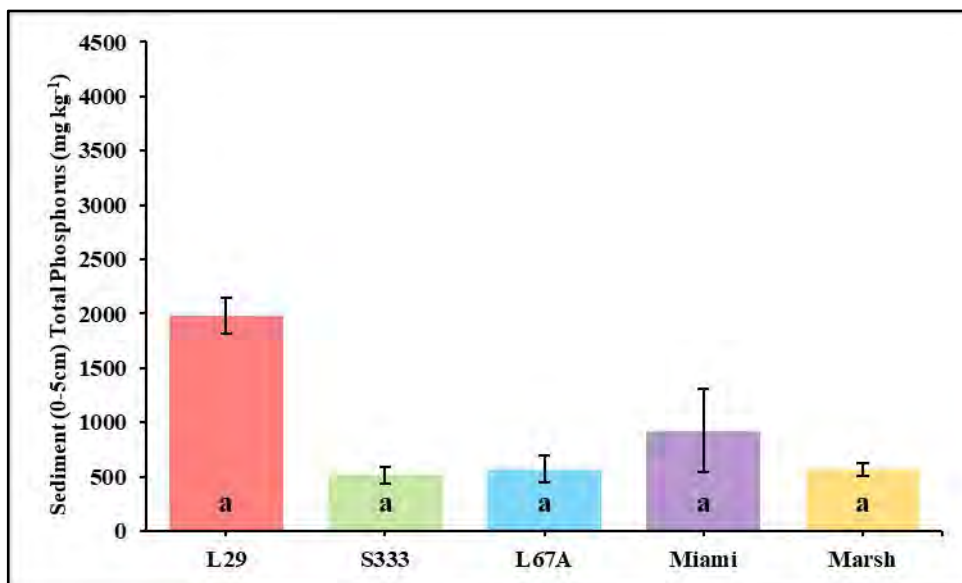
Figure 3.6. Mean concentrations of TP in sediment (0-5cm) samples collected near S333 structure (S333), three canals (L29, L67A, and Miami canal), and adjacent marsh (Marsh). Error bars represent the standard errors of the mean. Letters (a) indicate no significant differences were observed among different sampling locations.
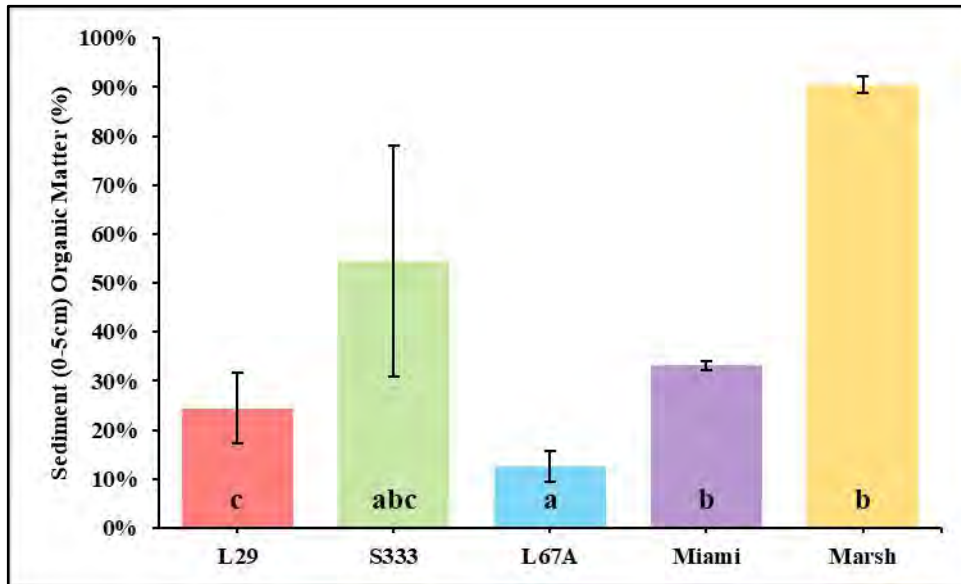
Figure 3.7. Mean concentrations of OM in sediment (0-5 cm) samples collected near S333 structure (S333), three canals (L29, L67A, and Miami canal), and adjacent marsh (Marsh). Error bars represent the standard errors of the mean. Letters (a, b, c, abc) indicate the significant differences among different sampling locations.
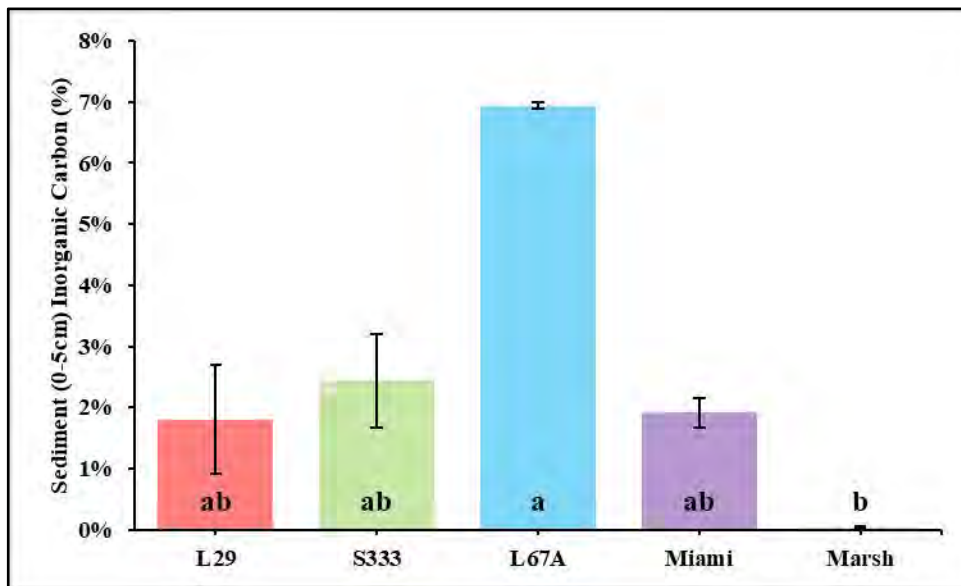
Figure 3.8. Mean concentrations of inorganic carbon in sediment (0-5 cm) samples collected near S333 structure (S333), three canals (L29, L67A, and Miami canal), and adjacent marsh (Marsh). Error bars represent the standard errors of the mean. Letters (a, b, ab) indicate the significant differences among different sampling locations.

3.1.3. Normalized total phosphorus

The OM normalized TP concentration of floc samples showed that L29 samples were significantly higher than marsh samples. S333, L67A, Miami samples showed similar levels and were not significantly different with L29 and marsh samples (Fig. 3.9). L67A sediment samples showed significantly higher organic matter normalized TP levels than Miami samples. L29, S333, and marsh samples were at the same level and did not show significant difference with L67A and

Miami samples (Fig. 3.10). No significant differences were detected among sediment samples from different sampling sites in terms of BD normalized TP (Fig. 3.11).
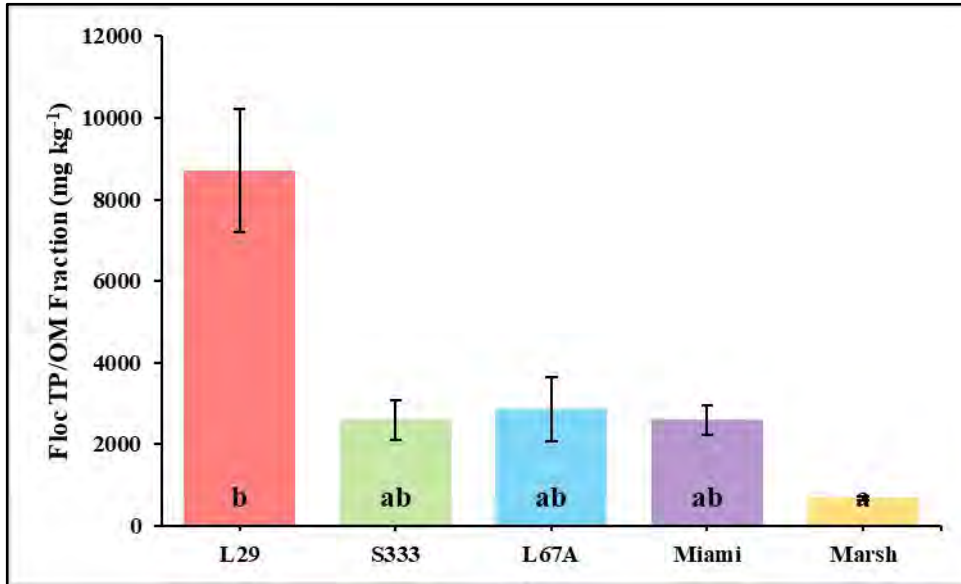
Figure 3.9. Mean normalized TP concentration by OM in floc samples collected near S333 structure (S333), three canals (L29, L67A, and Miami canal), and adjacent marsh (Marsh). Error bars represent the standard errors of the mean. Letters (a, b, ab) indicate the significant differences among different sampling locations.
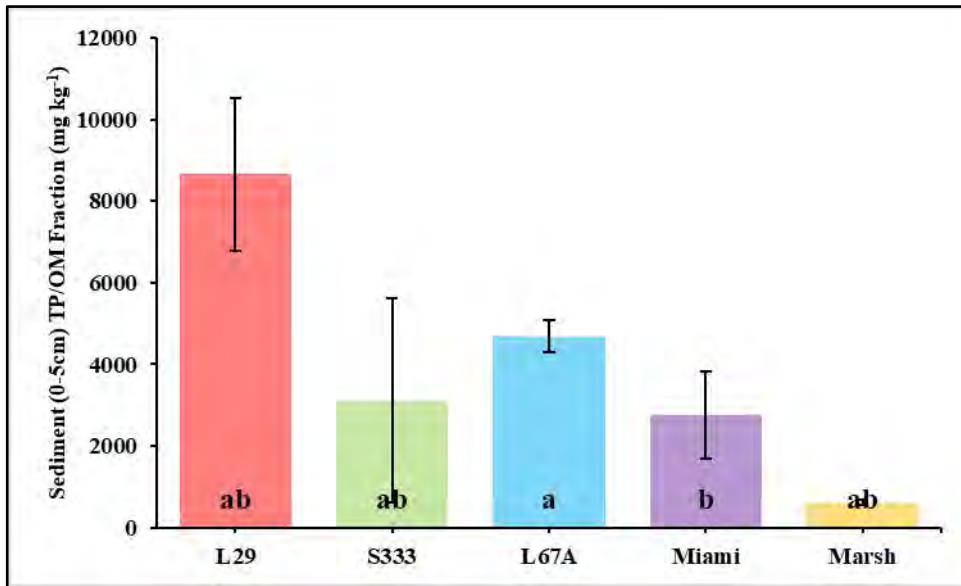
Figure 3.10. Mean normalized TP concentration by OM in sediment (0-5 cm) samples collected near S333 structure (S333), three canals (L29, L67A, and Miami canal), and adjacent marsh (Marsh). Error bars represent the standard errors of the mean. Letters (a, b, ab) indicate the significant differences among different sampling locations.
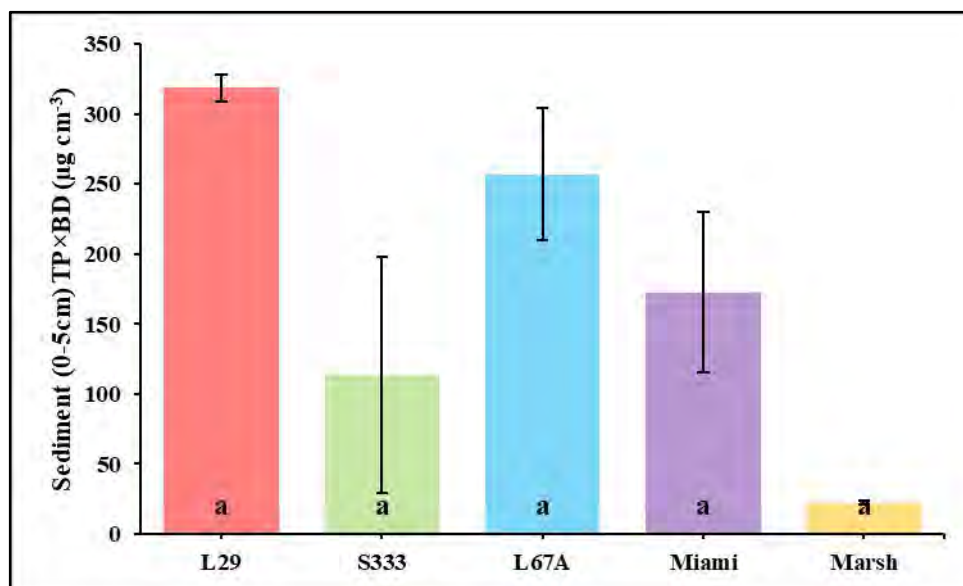
Figure 3.11. Mean normalized TP concentration by BD in sediment (0-5 cm) samples collected near S333 structure (S333), three canals (L29, L67A, and Miami canal), and adjacent marsh (Marsh). Error bars represent the standard errors of the mean. Letters (a) indicate no significant differences were observed among different sampling locations.

3.1.4. Phosphorus sorption

Table 3.1. Linear, Freundlich, and Langmuir sorption parameters for floc and sediments (0-5 cm) collected from canals (L29, L67A, Miami, and S333) and Marsh (M).

Sample	Linear[1]		Freundlich		Langmuir	
	EPC_0 (mg L^{-1})	S_0 (mg kg^{-1})	K_f (ml g^{-1})	N	S_{max} (mg kg^{-1})	K (L kg^{-1})
L29						
L29_1 Floc	1.05	162	401	0.41	2543	0.14
L29_2 Floc	0.92	154	344	0.49	2704	0.13
L29_1 Sediment	2.46	170	317	0.36	1918	0.11
L29_2 Sediment	9.45	168	173	0.38	1432	0.04
S333						
S333_1 Floc	1.98	154	289	0.42	2179	0.10
S333_2 Floc	1.66	155	296	0.43	2231	0.10
S333_3 Floc	2.51	162	302	0.41	2317	0.08
S333_2 Sediment	1.96	136	305	0.43	2456	0.08
S333_3 Sediment	14.72	111	96	0.36	626	0.09
L67						
L67A_1 Floc	8.04	137	155	0.43	1843	0.03
L67A_1 Sediment	20.89	110	89	0.34	516	0.12
L67A_2 Sediment	22.85	102	82	0.36	738	0.02
Miami						
Miami_2 Floc	2.37	75	89	0.64	2402	0.02
Miami_1 Sediment	52.82	130	53	0.40	432	0.06
Miami_2 Sediment	6.79	58	49	0.52	910	0.02
Marsh						

M_1 Floc	1.76	130	242	0.47	2122	0.09
M_2 Floc	0.08	94	520	0.43	2437	0.37
M_4 Floc	1.62	181	368	0.42	2076	0.21
M_5 Floc	15.86	238	5.25	1.09	476	-0.01
M_6 Floc	1.94	183	365	0.39	2076	0.16

[1]The data for least-square linear fitting to estimate S_0 included only three standard solutions (10, 50, and 100 mg L^{-1} P).

Table 3.2. Mean equilibrium phosphorus concentrations at zero net phosphorus sorption (EPC_0) and mean total sorption capabilities ($TSC = S_0 + S_{max}$) in flocs and sediments (0-5 cm) collected from canals (L29, L67A, Miami, and S333) and Marsh (M).

Sites	Floc		Sediment	
	EPC_0 (mg L^{-1})	TSC (mg kg^{-1})	EPC_0 (mg L^{-1})	TSC (mg kg^{-1})
L29	0.99	2781	5.95	1844
S333	2.05	2399	8.34	1665
L67A	8.04	1980	21.87	733
Miami	2.37	2477	29.81	765
Marsh	4.25	2002	NA[1]	NA

[1]Analysis not conducted due to lack of enough sample.

The floc obtained from five different sampling locations exhibited similar TSC levels, ranging from 1980 to 2781 mg kg^{-1} (Tab. 3.2). In terms of sediment, samples from L29 and S333 showed higher TSC levels compared to samples from L67A and Miami (Tab. 3.2). The floc displayed much higher TSC values compared to the sediment. This suggests that the floc plays a crucial role as a carrier in the transport of TP from one location to another. The floc showed different EPC_0 among five different sampling locations, ranging from 0.99 to 8.04 mg L^{-1} (Tab. 3.2). Sediment from L67A and Miami canal showed higher EPC_0 values compared to samples from L29 and S333. Also, sediment samples exhibited much higher EPC_0 values than floc (Tab. 3.2). The equilibrium P concentration at EPC_0 is defined as the concentration of P in a solution, where no net P sorption or desorption occurs. If P concentration is less than EPC_0, floc and sediment act as a source of P while canal water has P concentration higher than EPC_0, floc and sediment may act as sinks of P. The S_0 and EPC_0 may be overestimated using high initial P concentration (10, 50, and 100 mg L^{-1}).

3.1.5. Metals

Table 3.3. Mean concentrations (mg kg^{-1}) and standard deviations of 17 trace metals in floc and sediment 0-5 cm samples collected near S333 structure (S333), L29 canal (L29), L67A canal (L67A), and Miami canal (Miami), and adjacent Marsh (Marsh).

Sites	Cr	Co	Cu	Zn	Se	Cd	Ba	As	B	Li	Be	Ag	Pb	Ni	Mo	Sb	Hg
							Floc										
L29	31.22±4.79	6.77±1.12	65.60±10.13	84.71±19.96	0.28±0.30	0.66±0.08	133.82±9.84	2.08±0.66	0.73±0.45	80.95±12.04	0.87±0.09	0.99±0.09	5.59±0.50	5.05±0.85	0.38±0.19	0.35±0.35	0.11±0.01
S333	17.76±6.36	5.54±2.00	53.06±6.43	85.09±28.65	0.18±0.25	0.43±0.10	113.73±17.70	1.40±0.59	0.56±0.08	42.42±11.89	0.66±0.23	0.53±0.62	2.46±0.46	4.92±0.79	0.28±0.05	0.24±0.04	0.07±0.01
L67A	12.50±1.56	6.56±2.85	41.82±10.97	79.30±8.44	0.15±0.17	0.30±0.07	45.46±23.29	0.91±0.18	0.40±0.07	29.20±8.27	0.32±0.18	0.51±0.06	1.85±1.22	3.76±0.71	0.17±0.06	0.09±0.03	0.10±0.06
Miami	14.57±0.46	6.16±0.53	43.43±19.78	80.87±13.53	0.08±0.03	0.44±0.02	51.35±3.74	0.78±0.06	0.41±0.01	22.96±0.85	0.36±0.01	0.55±0.03	1.49±0.19	3.65±0.08	0.22±0.06	0.11±0.02	0.13±0.01
Marsh	2.07±0.41	2.90±0.54	14.22±2.51	96.23±18.45	0.13±0.14	0.13±0.04	100.37±37.30	1.08±0.75	0.13±0.01	2.01±0.81	0.06±0.02	0.94±0.94	0.69±0.23	2.89±0.36	0.20±0.07	0.09±0.03	0.06±0.02
							Sediment										
L29	40.61±20.23	7.58±4.83	37.96±19.91	19.93±5.30	0.46±0.09	0.77±0.49	158.27±9.80	1.77±0.22	1.71±0.45	109.01±72.80	1.28±0.82	0.08±0.06	11.46±8.37	4.93±3.25	0.36±0.21	0.22±0.13	0.09±0.01
S333	10.45±3.03	3.85±0.96	26.19±11.83	64.96±50.61	0.98±1.12	0.24±0.02	151.76±10.96	2.29±1.79	0.33±0.06	18.27±3.94	0.52±0.23	0.50±0.40	2.01±0.24	2.58±0.05	0.27±0.19	0.08±0.03	0.08±0.03
L67A	13.73±3.79	2.72±0.78	10.58±1.87	6.32±1.72	0.19±0.11	0.22±0.05	108.86±23.14	1.02±0.46	5.42±3.87	31.26±5.24	0.55±0.10	0.28±0.37	2.08±0.99	2.70±0.18	0.21±0.12	0.16±0.09	0.03±0.01
Miami	31.79±20.06	15.96±16.05	37.30±20.83	55.56±16.20	4.74±3.06	1.01±0.79	245.58±92.08	1.87±0.95	1.25±0.03	43.06±22.05	1.56±0.52	1.26±0.49	3.66±1.58	6.00±1.48	0.62±0.08	0.22±0.06	0.07±0.03
Marsh	4.38±4.76	6.14±7.65	15.42±4.13	88.14±26.55	0.22±0.12	0.22±0.08	88.46±17.02	1.08±0.26	0.28±0.26	8.09±13.31	0.20±0.25	0.70±0.25	1.61±0.64	3.94±2.14	0.30±0.09	0.08±0.02	0.08±0.03

Table 3.4. Mean concentrations (mg kg^{-1}) and standard deviations of 6 non-trace metals in floc and sediment 0-5 cm samples collected near S333 structure (S333), L29 canal (L29), L67A canal (L67A), and Miami canal (Miami), and adjacent Marsh (Marsh).

Sites	Mn	Fe	K	Mg	Na	Al
			Floc			
L29	29.09±3.78	26047.50±3416.03	2917.50±64.35	2841.50±430.63	1618.50±163.34	30239.00±1476.44
S333	44.99±12.41	26682.33±11361.83	3626.33±806.08	4900.67±1788.69	2308.67±424.56	21699.67±5725.53
L67A	32.54±4.30	16456.00±8054.44	3248.00±390.59	2870.33±968.21	3498.00±3119.11	11454.00±6150.21
Miami	74.44±28.86	18196.00±825.90	3411.00±11.31	2623.00±295.57	2782.50±491.44	11482.00±1574.02

Site					
Marsh	82.96±46.68	21562.00±11419.61	1198.00±214.33	2319.40±735.04	3116.60±558.43	2507.00±324.90

Sediment					
L29	17.84±2.62	28415.50±12129.00	3454.00±55.15	3665.50±1700.59	686.00±284.26	49979.00±30655.91
S333	34.44±8.60	30133.00±19200.09	3865.33±2426.87	5698.33±3403.30	1927.33±756.34	13225.33±3121.35
L67A	22.53±6.15	14652.67±8410.86	2503.00±687.71	4024.67±1328.78	717.00±235.27	18972.67±4778.87
Miami	63.19±10.03	52536.50±27956.88	7496.00±3317.75	10711.00±6286.18	2489.50±1348.45	43186.00±28059.41
Marsh	41.17±25.26	14213.80±5345.38	1272.20±500.88	2369.20±386.96	1856.80±344.55	6373.40±7125.27

Table 3.5. Comparing mean concentrations (mg kg^{-1}) of metals in floc and sediment (0-5 cm) collected near S333 structure (S333), L29 canal (L29), L67A canal (L67A), and Miami canal (Miami), and adjacent marsh (Marsh) with background concentrations of metals in Florida soils, Florida sediments, and sediment (0-10 cm) collected from Everglades National Park (ENP), the coastal fringes of Biscayne National Park (BNP), and Big Cypress National Preserve.

Site	As	Ba	Co	Cr	Cu	Mn	Ni	Pb	Zn	Al	Fe
Florida soil[1]	1.3	30.7	-	15.9	6.1	48.8	13	11.2	8.4	-	-
Florida sediment[2]	1.6	53.2	-	23.3	4.7	-	5.6	6.3	14.2	10793	3953
Sediment of 50 sites in 2006[3]											
Mean	2.6	18.9	0.7	11.4	8.5	46.5	2.8	19.4	19.1	4555	6415
Sediment in ENP (2006-2007)[3]											
Mean	3.5	35.3	1	17.7	3.8	76.6	3.7	23.1	14.4	6777	10138
Minimum	0.8	5.8	0.2	0.3	0.3	12.3	0.5	1	1	213	971
Maximum	10.8	83.9	3.5	154.6	22.2	233.6	18.5	377.3	204.8	47238	46150
Floc											
L29	2.1	133.8	6.8	31.2	65.6	29.1	5.1	5.6	84.7	30239	26048
S333	1.4	113.7	5.5	17.8	53.1	45.0	4.9	2.5	85.1	21700	26682
L67A	0.9	45.5	6.6	12.5	41.8	32.5	3.8	1.9	79.3	11454	16456
Miami	0.8	51.4	6.2	14.6	43.4	74.4	3.7	1.5	80.9	11482	18196
Marsh	1.1	100.4	2.9	2.1	14.2	83.0	2.9	0.7	96.2	2507	21562
Sediment											

L29	1.8	158.3	7.6	40.6	38.0	17.8	4.9	11.5	19.9	49979	28416
S333	2.3	151.8	3.9	10.5	26.2	34.4	2.6	2.0	65.0	13225	30133
L67A	1.0	108.9	2.7	13.7	10.6	22.5	2.7	2.1	6.3	18973	14653
Miami	1.9	245.6	16.0	31.8	37.3	63.2	6.0	3.7	55.6	43186	52537
Marsh	1.1	88.5	6.1	4.4	15.4	41.2	3.9	1.6	88.1	6373	14214

[1]Chen et al. 1999; [2]Carvalho et al. 2002; [3]Castro et al. 2013

Concentrations of 17 trace and six non-trace metals in floc and sediment are presented in Tabs 3.3 and 3.4. The presence of these metals in floc and sediment can originate from both natural processes and human activities, including geological processes, atmospheric deposition, agricultural activities, and urbanization.

Among the measured trace metals, Ba exhibited the highest mean concentration (88.95 mg kg^{-1} in floc and 150.59 mg kg^{-1} in sediment), while Hg showed the lowest mean concentration (0.09 mg kg^{-1} in floc and 0.07 mg kg^{-1} in sediment). For floc samples, among the five sampling locations, L29, Miami, and S333 had the highest concentrations for 15, 1, and 1 out of 17 trace metals, respectively. Conversely, Marsh, L67A, and Miami had the lowest concentrations for 11, 4, and 2 out of 17 trace metals, respectively. Regarding sediment, L29, Miami, and S333 had the highest concentrations for 8, 7, and 2 out of 17 trace metals, respectively, while L67A, Marsh, and S333 had the lowest concentrations for 9, 7, and 1 out of 17 trace metals, respectively. S333 exhibited the highest concentration of Zn in both floc and sediment and the lowest concentration of Sb in sediment.

Cadmium (Cd) is a commonly found trace metal in P fertilizers (Bracher et al., 2021) and has been used as a reliable tracer for identifying the source of fertilizer-derived P in wetland sediments. We detected Cd in all samples, with concentrations ranging from 0.13-0.66 mg kg^{-1} in floc and 0.22-1.01 mg kg^{-1} in sediment. Similar results were reported by Duan (2012) for average concentrations of metals in sediment (0.004-1.07 mg kg^{-1}) and floc (0.01-0.78 mg kg^{-1}) in the Everglades. These values are relatively higher than the average crustal abundance of Cd (~0.1-0.5 mg kg^{-1}). Jiao et al. (2015) reported significant accumulation of Cd, along with other trace metals such as As, Cr, Cu, Ni, Pb, Se, and Zn, in river sediments exposed to long-term agricultural practices. The order of Cd concentrations among the five sampling locations is L29 > Miami > S333 > L67A > Marsh in floc, and Miami > L29 > S333 > L67A ≈ Marsh in sediment.

In addition, we compared our data with background concentrations of these metals in Florida soils, Florida sediments, and sediment (0-10 cm) collected from Everglades National Park (ENP), the coastal fringes of Biscayne National Park (BNP), and Big Cypress National Preserve (Tab. 3.5). Based on these comparisons, enrichments were found for Ba, Co, Cu, Zn, Al, and Fe in floc and sediment from all locations, except for Zn in the sediment of L67A and Al in the sediment of marsh.

3.1.6. Minerals

Table 3.6. Mean percentage and standard deviations of 12 minerals in floc and sediment (0-5 cm) collected near S333 structure (S333), L29 canal (L29), L67A canal (L67A), and Miami canal (Miami), and adjacent marsh (Marsh).

Sites	Calcite	Quartz	Aragonite	Iron Sulfide	Hematite	Illite	Palygorskite	Kaolinite	Ca oxide phosphate	Mg carbonate	Na Al Fe phosphate
					Floc						
L29	15.62±3.25	2.94±1.15	2.70±1.15	0.36±0.33	0.06±0.08	ND	ND	3.20±3.19	ND	0.12±0.17	ND
S333	37.52±1.92	1.42±0.49	2.79±0.50	0.77±0.04	ND	0.12±0.12	0.56±0.53	0.33±0.32	ND	0.08±0.13	ND
L67A	40.53±19.55	10.28±14.69	3.38±0.23	0.80±0.16	ND	0.04±0.07	0.41±0.43	0.76±0.09	0.04±0.07	0.25±0.25	ND
Miami	14.46±0.69	18.65±3.82	2.23±0.88	0.79±0.06	ND	0.13±0.18	0.54±0.07	0.66±0.24	ND	0.30±0.42	ND
Marsh	1.51±0.92	0.14±0.05	0.12±0.17	ND	ND	0.10±0.13	0.12±0.17	0.28±0.06	ND	ND	ND
					Sediment						
L29	13.74±8.24	27.59±32.36	0.43±0.60	0.36±0.18	ND	0.12±0.17	0.29±0.41	3.56±4.36	ND	0.06±0.08	ND
S333	9.52±3.53	6.86±10.43	1.05±0.79	0.37±0.24	0.04±0.07	ND±ND	1.14±1.87	0.08±0.14	ND	0.21±0.25	ND
L67A	33.27±3.62	21.28±15.77	4.43±0.27	0.49±0.45	ND	ND±ND	0.45±0.51	0.32±0.30	ND	0.49±0.21	ND
Miami	8.85±1.72	25.32±7.52	1.51±1.10	0.48±0.17	0.06±0.08	0.06±0.08	0.85±0.01	0.49±0.69	ND	0.30±0.08	0.06±0.08
Marsh	0.24±0.09	1.37±2.75	0.13±0.19	ND	ND	0.07±0.10	0.24±0.23	1.00±1.74	ND	0.05±0.07	ND

ND: Not Detected
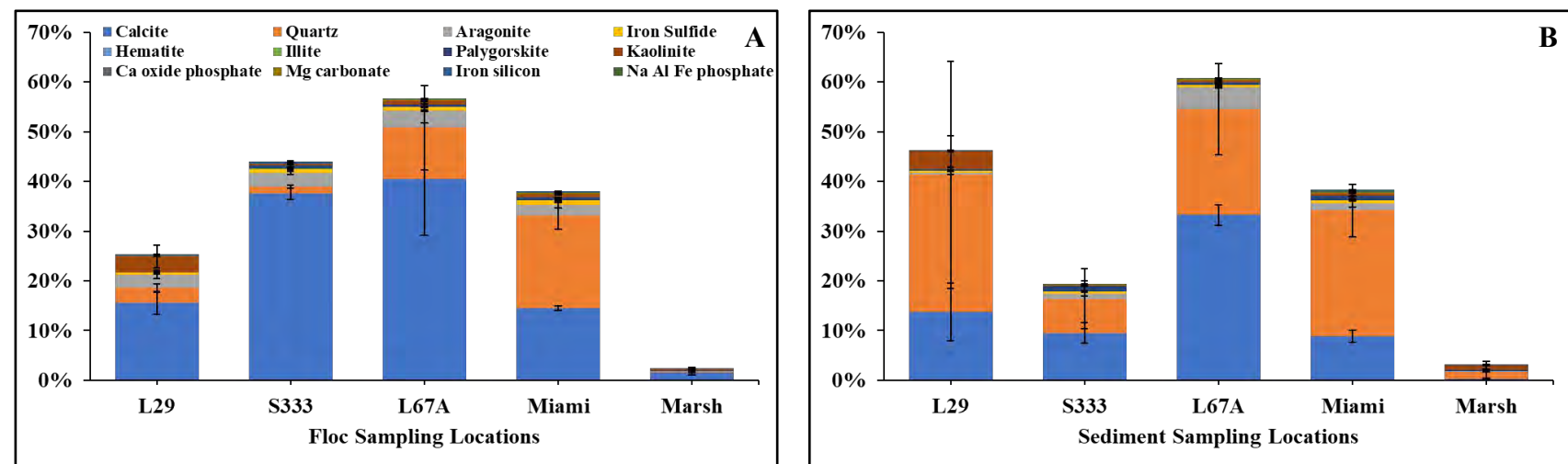
Figure 3.12. Mean percentage of 12 minerals in floc (A) and sediment 0-5 cm (B) samples collected S333 structure (S333), three canals (L29, L67A, and Miami canal), and adjacent marsh (Marsh). Error bars represent the standard errors of the mean.

Minerals detected in floc and sediment samples were shown in Tab. 3.6 and Fig. 3.12. Three carbonate minerals, calcite, aragonite, and magnesium (Mg) carbonate were detected in floc and sediment samples from all sampling locations, except Mg-carbonate was not detected in floc from the marsh. Calcite, which is the dominant mineral in the Everglades, was found in all samples due to the ideal calcium-pH-carbonate conditions for calcite formation in the ecosystem. The order of calcite contents among the locations was L67A >

S333 > L29 > Miami > Marsh for both floc and sediment. L67A had the highest calcite content, while the Marsh had the lowest. The source of calcite could not be differentiated by XRD analysis, but it could potentially originate from periphyton in the marsh or from fragments of limestone or shell (Irick et al. 2012). The stable isotope analysis of inorganic carbon has been suggested for fingerprinting the origin of carbonate (Dotsika et al. 2018).

Aragonite, another calcium carbonate mineral with a different crystal structure from calcite, was also detected in all samples. Although less common than calcite, aragonite was found in soils in the south Everglades and is formed through biological processes on limestone bedrock (Judy et al. 2021). The percentage order of aragonite among the locations was similar to that of calcite but at lower concentrations. Magnesium Carbonate ($MgCO_3$) is a carbonate mineral that occurs naturally as a mineral magnesite. Concentrations of Mg carbonate in these samples are much lower than calcite and aragonite. Mg carbonate was not detected in floc from the Marsh, likely due to the lower magnesium concentrations in the Marsh floc compared to other locations. Other locations with low percentages of Mg carbonate were floc from S333 and sediment from L29 and the Marsh.
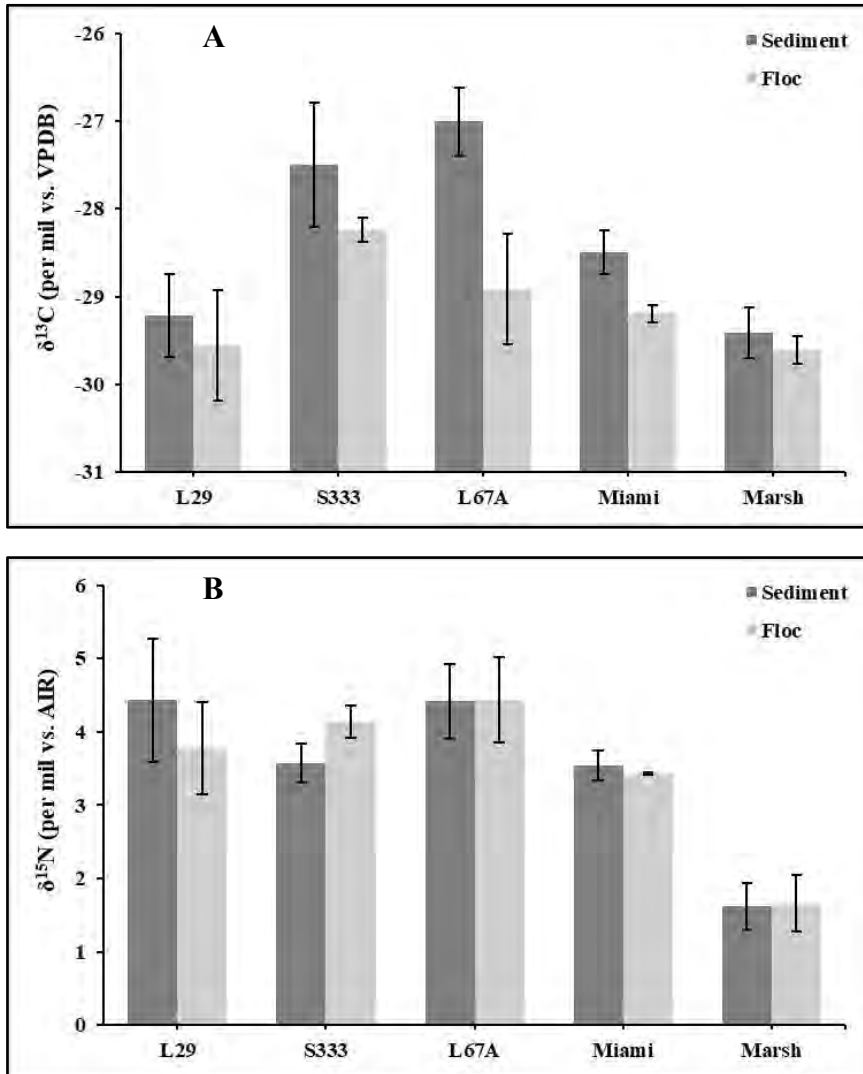
Quartz, a mineral composed of silicon dioxide (SiO_2), was the second most abundant mineral found in the samples. The origin of quartz in the Everglades is not well understood since the primary geological formations in the area are limestone and organic matter. Quartz possibly is carried by runoff water from external sources into the Everglades. The content of quartz in both floc and sediment was lower in the Marsh and S333 compared to other locations. Iron sulfide or pyrite (FeS_2) was found in floc and sediment samples from all locations except the Marsh. The conditions of pH and Eh in the marsh may not favor the formation of pyrite. Floc had a higher percentage of pyrite than sediment, which may be attributed to higher Eh values or sulfur content in the floc. Agricultural sulfur has been suggested to contribute to sulfur reactions, including methylation, in the Everglades.
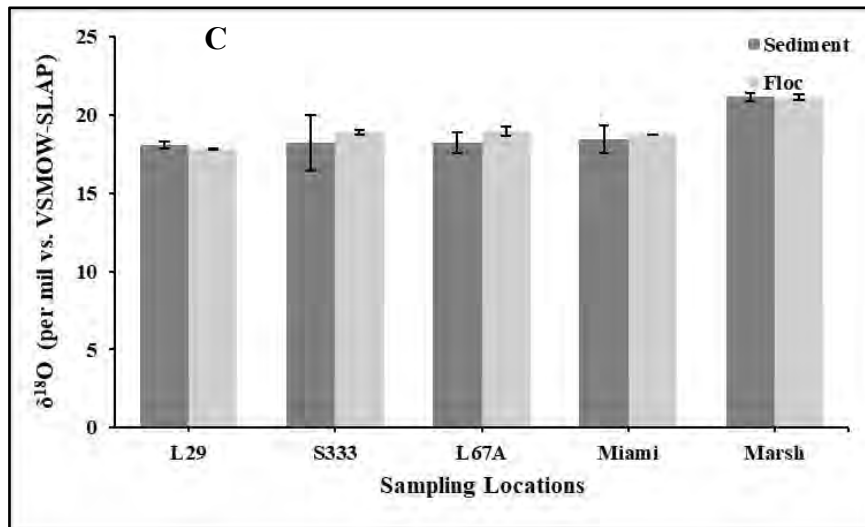
A trace amount of hematite, an iron oxide mineral (Fe_2O_3), was found in floc from L29 and sediment from S333 and Miami, indicating the connectivity among these locations. On the contrary, Illite, a clay mineral was not detected in floc from L29 and sediment from S333. The presence of palygorskite, a clay mineral, has been used to indicate sediment erosion and transportation through the Kissimmee River-Lake Okeechobee watershed (Sawyer et al. 1988). The data showed an accumulation of palygorskite at S333 compared to other locations. The presence of kaolinite, another clay mineral, indicates the transport of floc and sediment from upstream sources. Kaolinite is commonly found in soils derived from weathered rocks rich in aluminum silicates. The highest kaolinite content was found in floc from L29, while sediment from S333 had the lowest kaolinite content. This difference could be attributed to slower water movement at L29, favoring the settling of clay particles, while the structure of floc at S333 may prevent settling.

Two phosphorus-associated minerals, calcium oxide phosphate (Ca oxide phosphate) and sodium aluminum iron phosphate (Na Al Fe phosphate), were detected in the samples. It is surprising to note that Ca oxide phosphate was only detected in the floc from L67A, while Na Al Fe phosphate was only found in the sediment from Miami. No Ca oxide phosphate was detected in other samples, suggesting that the calcium phosphate detected here may not originate from a source like bone fragments. Apatite, a calcium oxide phosphate mineral, has been identified as the source of high phosphorus in sediments originating from bone fragments (Irick et al., 2012). Normal XRD analysis might not be able to reveal apatite and Zhang et al. (2014) used the high-

density (N2.7 SG) XRD and detected apatite in carbonate-free silt which had high total P (2257-4090 mg kg^{-1}) (Zhang et al. 2014). Ca-P-rich particles were often found under SEM-EDS, but they were not abundant enough for XRD detection (W. Harris, personal communication). By modifying measurement setting such as scanning with low-angle range (at least 2-60 degrees 2 theta), we might identify expansible phyllosilicates like smectites and dolomite. Additionally, it should be noted that the detection and quantification of minerals below 0.5-1 % using XRD may not yield accurate results.

3.1.7. Isotopes

Figure 3.13. Mean permillage of δ^{13}C isotope (A), δ^{15}N (B), and δ^{18}O (C) in floc and sediment 0-5 cm samples collected S333 structure (S333), three canals (L29, L67A, and Miami canal), and adjacent marsh (Marsh). Error bars represent the standard errors of the mean.

The average δ^{13}C were -29.10‰ in floc and -28.33‰ in sediment which fall within the δ^{13}C value ranges of −22 to −34‰ for organic matter produced by C3 plants (Wang et al. 2014). The δ^{13}C values for floc and sediment samples showed similar ranges across the five sampling locations, ranging from −28.24 to −29.61‰ in floc and from −27.01 to −29.41‰ in sediment. The ordering of δ^{13}C values was S333 > L67A > Miami > L29 > Marsh in floc samples, and L67A > S333 > Miami > L29 > Marsh in sediment samples (Fig. 3.13A). The relatively high δ^{13}C values in floc and sediment from S333 and L67A compared to L29, Miami, and Marsh suggest a greater contribution of C4 plants such as sugarcane (−11 ± 1‰), sugarcane-cultivated histosol (−25.37‰), or other organic biomass such as fish (−19.2 to −31.5‰) to the organic biomass source in these sampling sites (Wang et al., 2014).

The average δ^{15}N values were 3.49‰ in floc and 3.52‰ in sediment, which are similar to the δ^{15}N values reported for C3 plants (3.27‰) and lower than those for C4 plants (5.55‰) in C4 herbaceous plants (Liu et al., 2022; Wright and Inglett, 2009). These values also fall within the range of δ^{15}N values in prairie soils (2.98-3.86‰) reported by Liu et al. (2022) and Wright and Inglett (2009). Compared to sediment, the slightly lower δ^{15}N values in floc indicate recent deposition of organic matter, while higher δ^{15}N values in sediment represent older, more humified organic matter (Novak et al., 1999). The ordering of δ^{15}N values was L67A > S333 > L29 > Miami > Marsh in floc samples, and L29 > L67A > S333 > Miami > Marsh in sediment samples (Fig. 3.13B). Both floc and sediment from the Marsh had the lowest δ^{15}N values, which were less than half of the values from the Miami canal, the site with the second lowest δ^{15}N values for both floc and sediment samples. The low δ^{15}N values in the Marsh may be attributed to low growth rate of marsh plants and less isotope fractionation during N uptake, while the low δ^{15}N values in the Miami canal may indicate the input of fresh organic biomass from upstream sources (Inglett and Reddy, 2006). In contrast to marsh signatures which are indicative of primary producer sources, animal activity could be one of sources for canal sediment/floc particles and canal fauna may be included for potential management actions.

The average and range of δ^{18}O values were 19.50‰ (range: 17.88-21.15‰) in floc and 19.22‰ (range: 18.09-21.16‰) in sediment. Water samples collected from the EAA and WCAs showed

$\delta^{18}O$ values ranging from 20 to 25.5‰ (Li et al., 2011). The ordering of $\delta^{18}O$ values was Marsh > L67A > S333 > Miami > L29 in floc samples, and Marsh > Miami > S333 > L67A > L29 in sediment samples (Fig. 3.13C). While the Marsh had the highest $\delta^{18}O$ values and L29 had the lowest $\delta^{18}O$ values, the other three sites (Miami, L67A, and S333) had similar $\delta^{18}O$ values, indicating a similar oxygen source.

The relatively lower $\delta13C$ values in floc compared to sediment suggest that floc represents fresh deposited organic matter and sediment is more enriched in $\delta13C$ by loss of light isotope ($\delta12C$) with mineralization during longer time burial. S333 exhibited similar $\delta13C$, $\delta15N$, and $\delta18O$ values to Miami and/or L67A, indicating its potential impact from these canals.
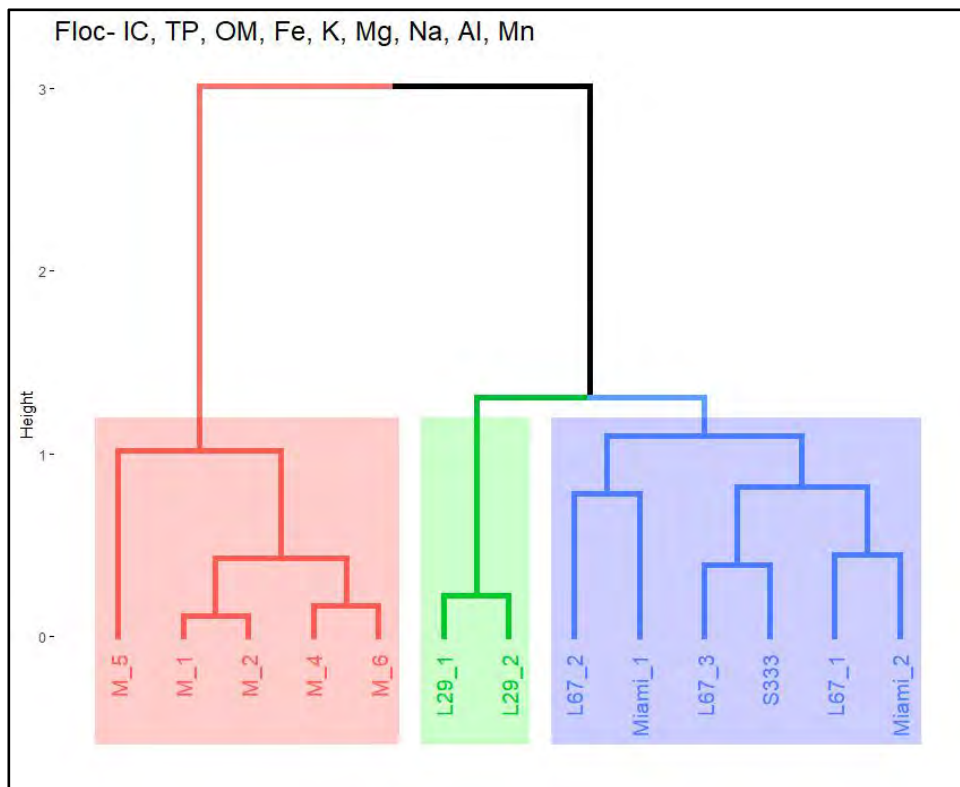
3.1.8. Cluster analysis

Marsh samples clustered and canal samples separated into two clusters. For floc samples, all indicators and conventional indicators (i.e., IC, TP, OM, and non-trace metals, Fig. 2.8) gave the same pattern of cluster: 1) Marsh samples were cluster 1; 2) L29 samples were cluster 2; and 3) L67A, Miami, and S333 samples were cluster 3 (Figs. 3.14 & 3.15). The geochemical indicators (i.e., Trace metal, clay minerals, and isotopes, Fig. 2.8) gave a different pattern of clusters: 1) Marsh samples still formed one cluster – cluster 1; 2) L67-1, L67-2, and Miami samples were cluster 2; and 3) L29, L67-3, and S333 samples were cluster 3 (Fig. 3.16).
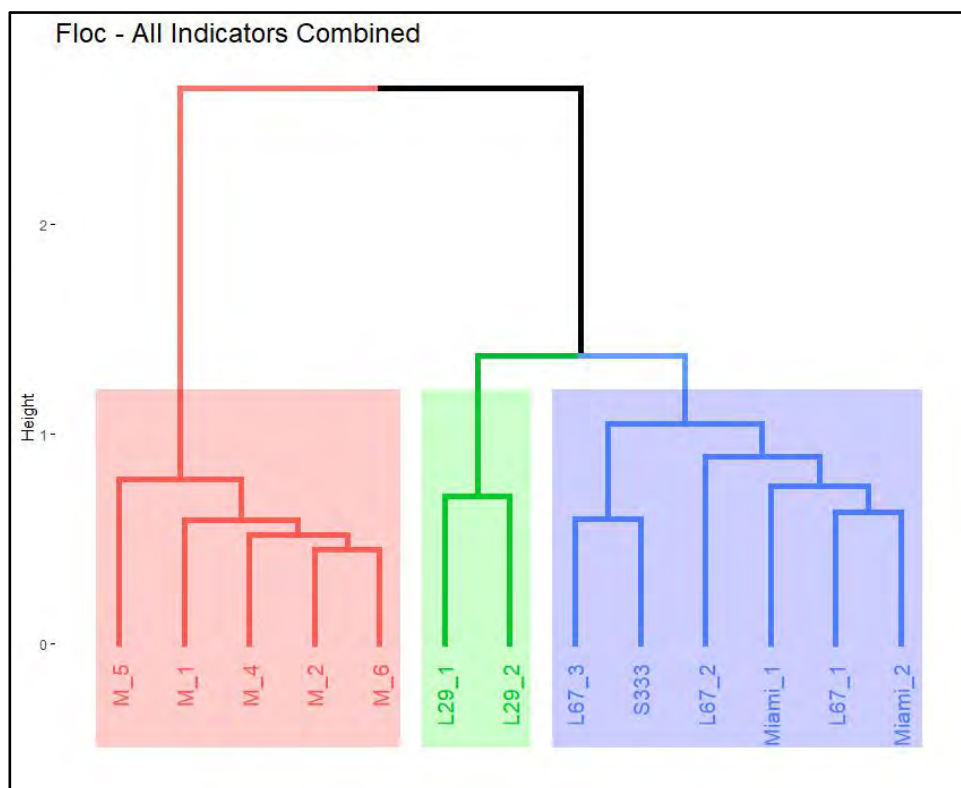
Figure 3.14. Cluster analysis for floc samples of L29, L67A, Miami canal, adjacent marsh, and S333 structure with all indicators combined.

Figure 3.15. Cluster analysis for floc samples of L29, L67A, Miami canal, adjacent marsh, and S333 structure with IC, TP, OM, and non-trace metals.

Figure 3.16. Cluster analysis for floc samples of L29, L67A, Miami canal, adjacent marsh, and S333 structure with trace metals, clay minerals, and isotopes.

For sediments, cluster analyses result for all indicators were: 1) Marsh samples were cluster 1; 2) Miami and S333 samples were cluster 2); and 3) L29 and L67A samples were cluster 3 (Fig. 3.17). The conventional indicators showed a slightly different pattern of cluster: 1) Marsh and S333 samples were cluster 1; 2) Miami samples were cluster 2; and 3) L29 and L67A samples were cluster 3 (Fig. 3.18). The geochemical indicators showed another combination of clusters: 1) Marsh samples were cluster 1; 2) L67A samples were cluster 2; and 3) L29, Miami, and S333 samples were cluster 3 (Fig. 3.19).
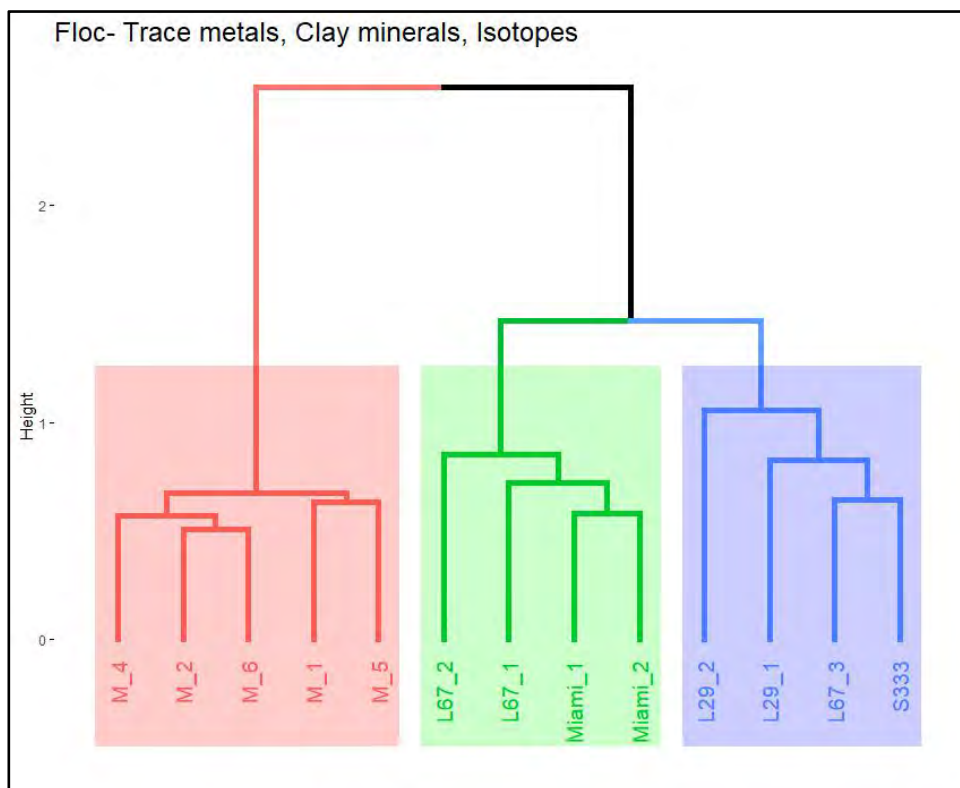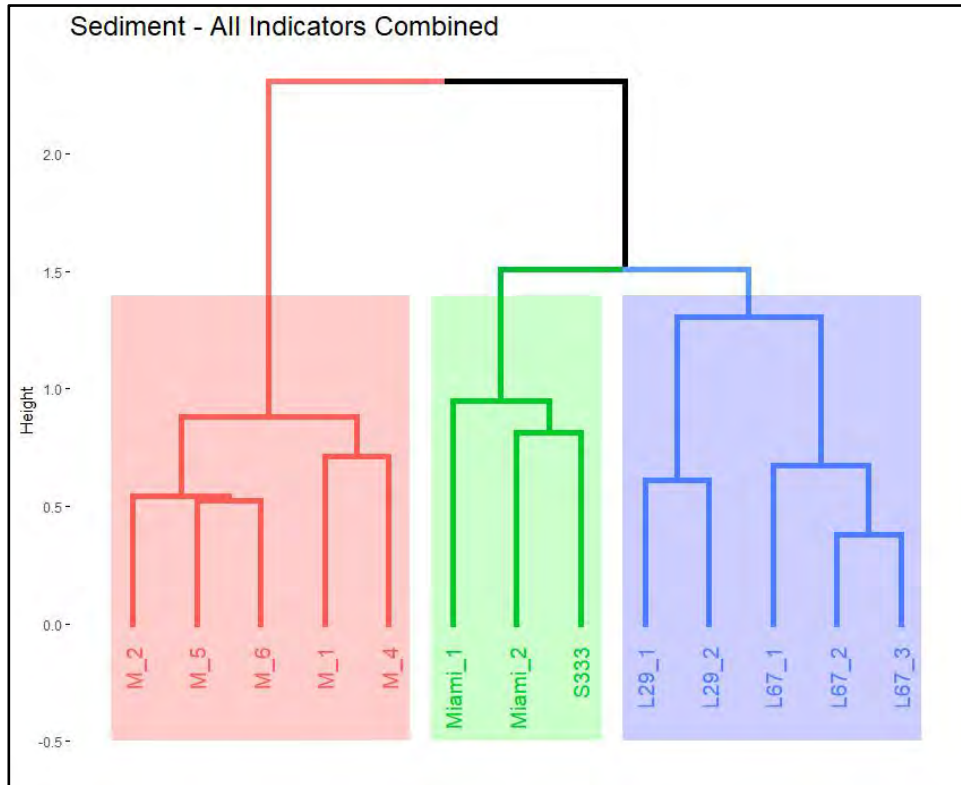

Figure 3.17. Cluster analysis for sediment 0-5 cm samples of L29, L67A, Miami canal, adjacent marsh, and S333 structure with all indicators combined.

Figure 3.18. Cluster analysis for sediment 0-5 cm samples of L29, L67A, Miami canal, adjacent marsh, and S333 structure with IC, TP, OM, BD, and non-trace metals.
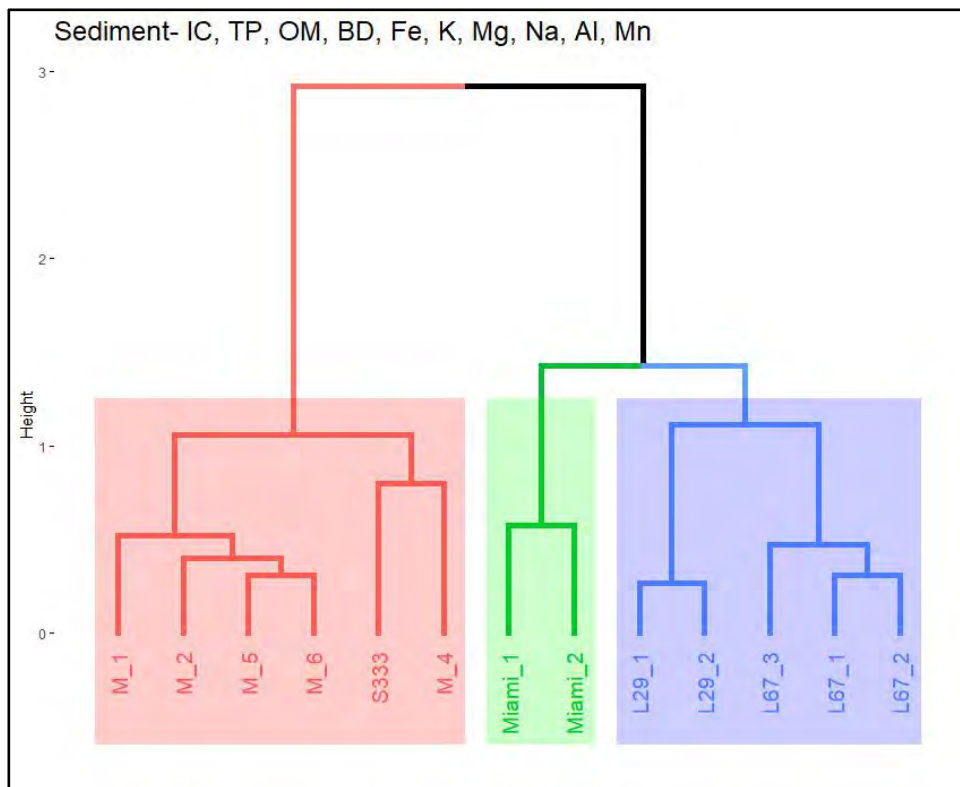

Figure 3.19. Cluster analysis for sediment 0-5 cm samples of L29, L67A, Miami canal, adjacent marsh, and S333 structure with trace metals, clay minerals, and isotopes.
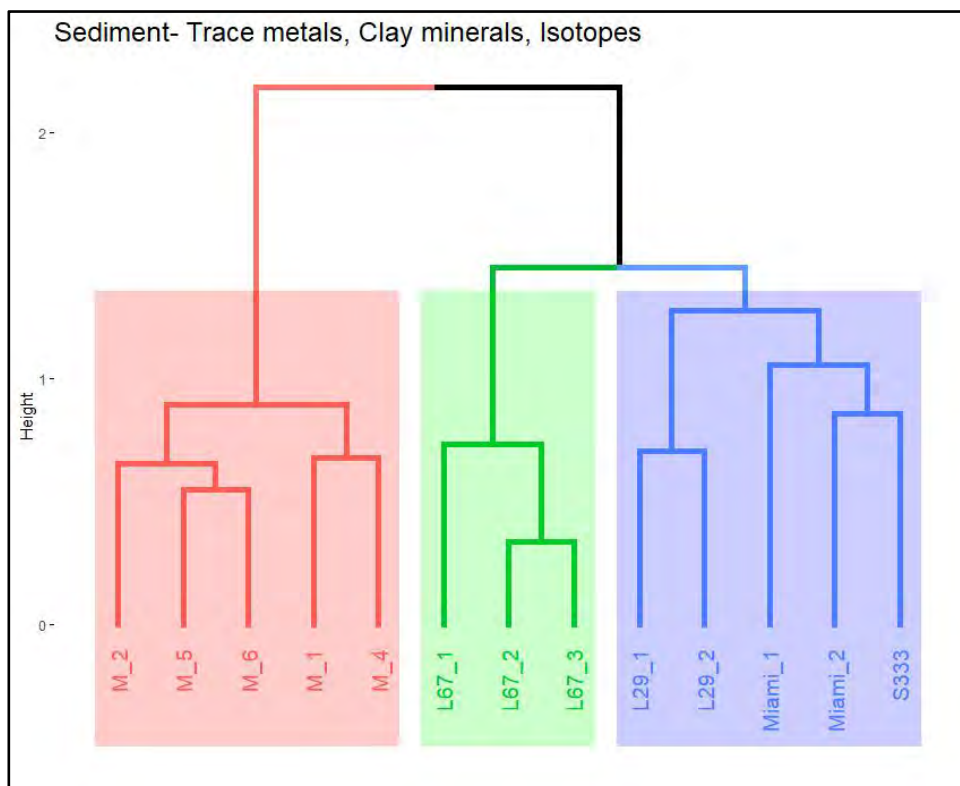
3.2. Phase-2 (Local-scale study) (Fig. 2.2)

3.2.1. Total phosphorus mass in sediment

For assessing TP mass near the S333, the canal sampling area was divided into three compartments with L29 at 9,978 m^2, S333 6,555 m^2, and L67A at 10,677 m^2 (Fig. 3.20). Total P mass in 0-5 cm top layer of sediments ranged from 77 kg in front of S333 to 307 kg in area for L29. The sediment TP mass decreased from west to east in L29 canal and increased from north to south in L67A canal. The S333 area sediment typically showed lower TP mass near the S333 gate and higher near the marsh (Fig. 3.21).

The BD of sediment samples in L29 decreased from west to east (Fig. 3.22). Different from sediment TP mass, S333 sediment BD was relatively lower near the marsh and higher near the structure. L67A sediment samples tend to have higher BD than L29 and S333 samples (Fig. 3.22). Based on the power model fit, BD of sediment is highly correlated with counterpart OM content (Fig. 3.23). TP mass was found to be similar in the 12-marsh sediment samples (Fig. 3.24).
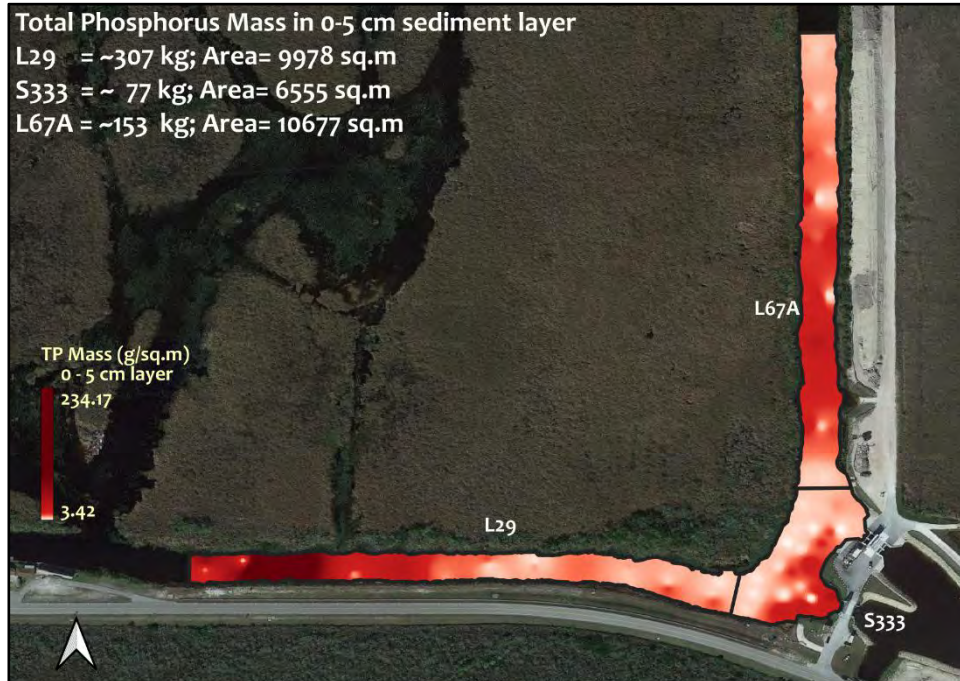
Figure 3.20. Total P mass heat map of sediment surface (0-5cm) near S333 structure, L29 and L67A canals.
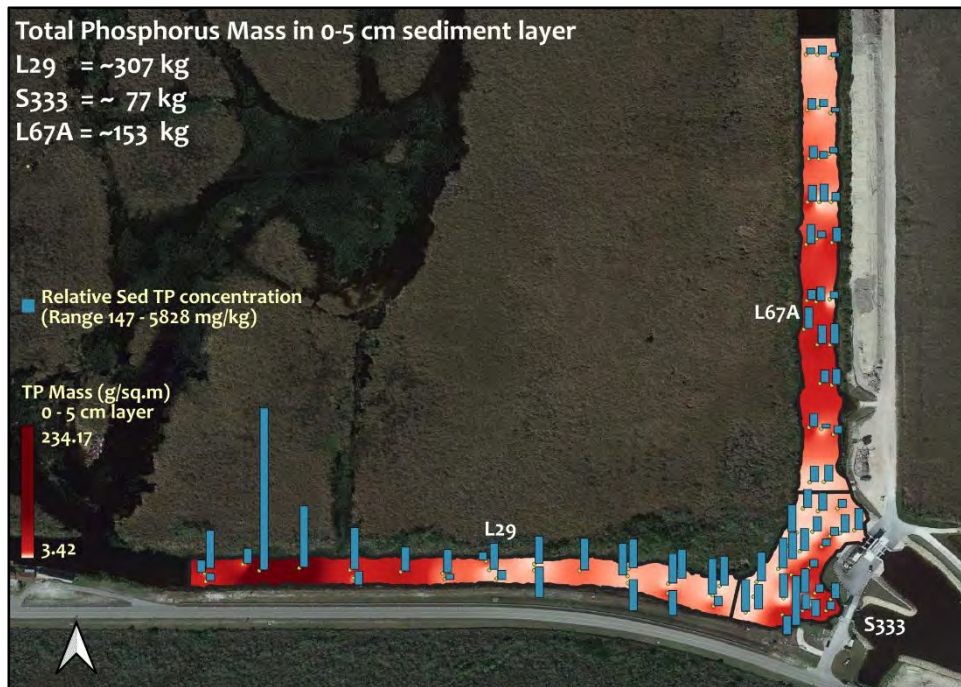
Figure 3.21. Total P concentration barplot of sediment surface (0-5cm) near S333 structure, L29 and L67A canals. The height of each bar represents relative TP concentration from the sampling location.
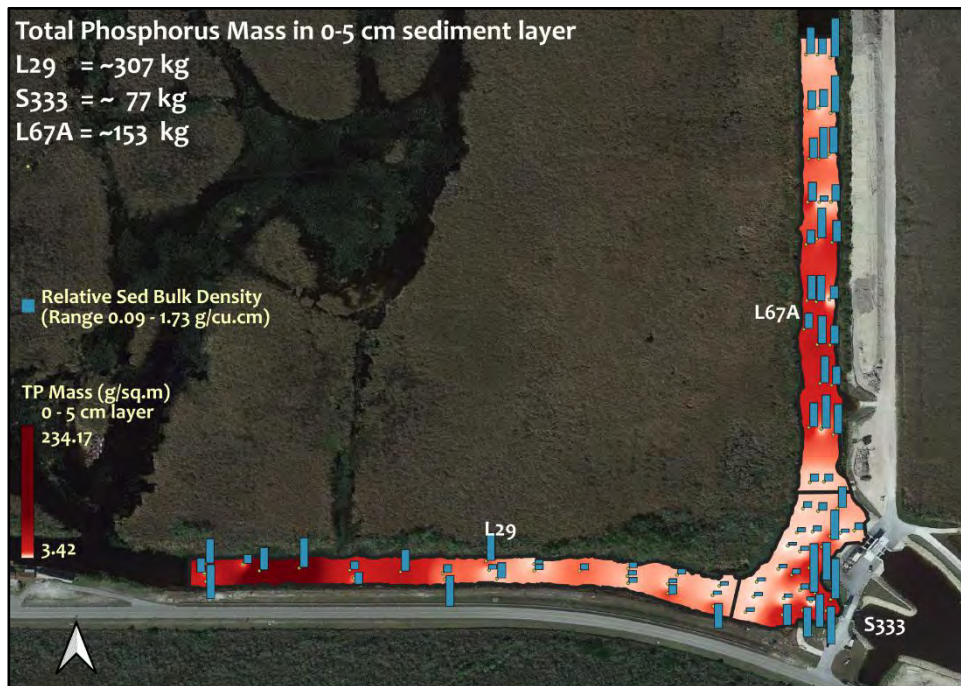
Figure 3.22. Bulk density barplot of sediment surface (0-5cm) near S333 structure, L29 and L67A canals. The height of each bar represents relative BD from the sampling location.
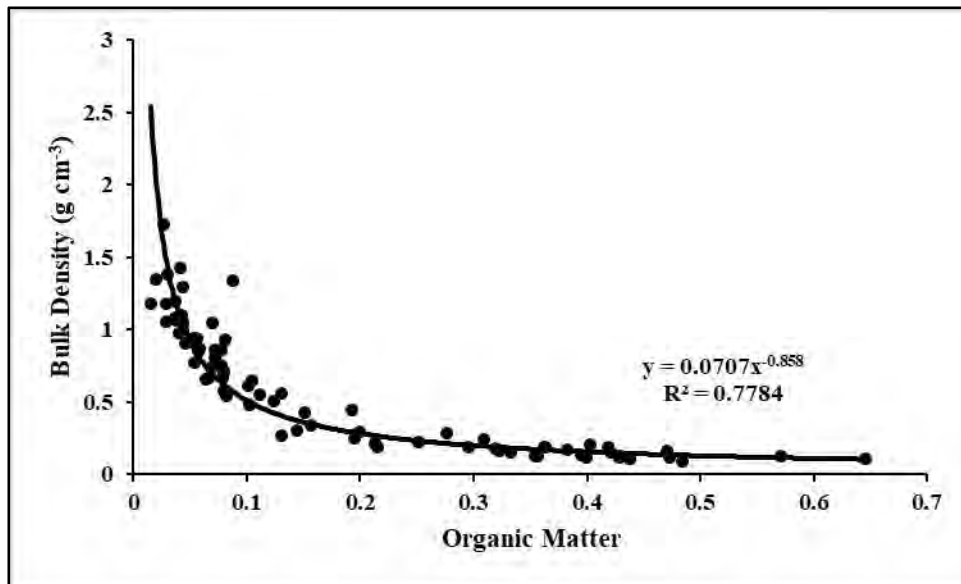
Figure 3.23. Bulk density and OM scatterplot of sediment surface (0-5 cm) near S333 structure, L29 and L67A canals.
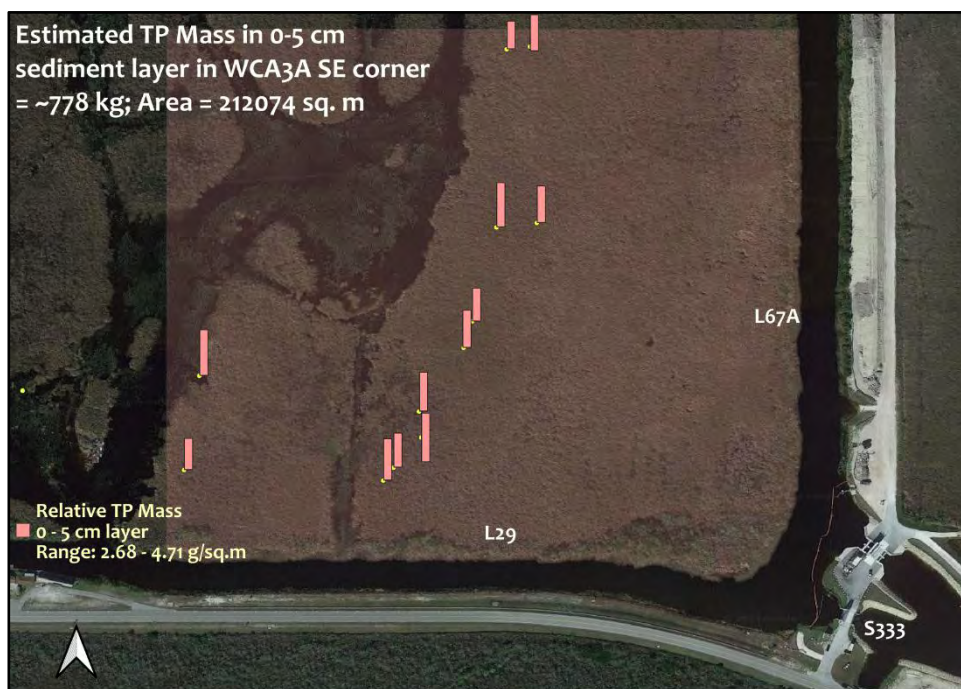
Figure 3.24. Total P concentration barplot of sediment surface (0-5 cm) at adjacent marsh near S333 structure, L29 and L67A canals. The square shaded represents marshland used for estimation. The height of each bar represents relative TP concentration from the sampling location.

3.2.2. Phosphorus fractionation in floc and sediments

The TP present in floc and sediment samples was further differentiated into seven forms by P fractionation analysis: 1) water-soluble P, 2) exchangeable P, 3) Al-bound P, 4) Fe-bound P, 5) Organic P, 6) Ca/Mg-bound P, and 7) residual P. Floc samples showed similar levels of TP among different locations which were ~900 mg kg^{-1} (Fig. 3.25A). Also, floc canal samples (L29,

L67A, and S333) showed similar patterns of P forms. Residual and Ca/Mg-bound P were the major P forms, with a good amount of Al-bound P, while water-soluble P and exchangeable P were barely present (Fig. 3.25C). Floc marsh samples exhibited a different pattern. Al-bound P was the major P form, with a substantial amount of residual P and a fairly good amount of Ca/Mg-bound P, water-soluble P, and exchangeable P (Fig. 3.25C).
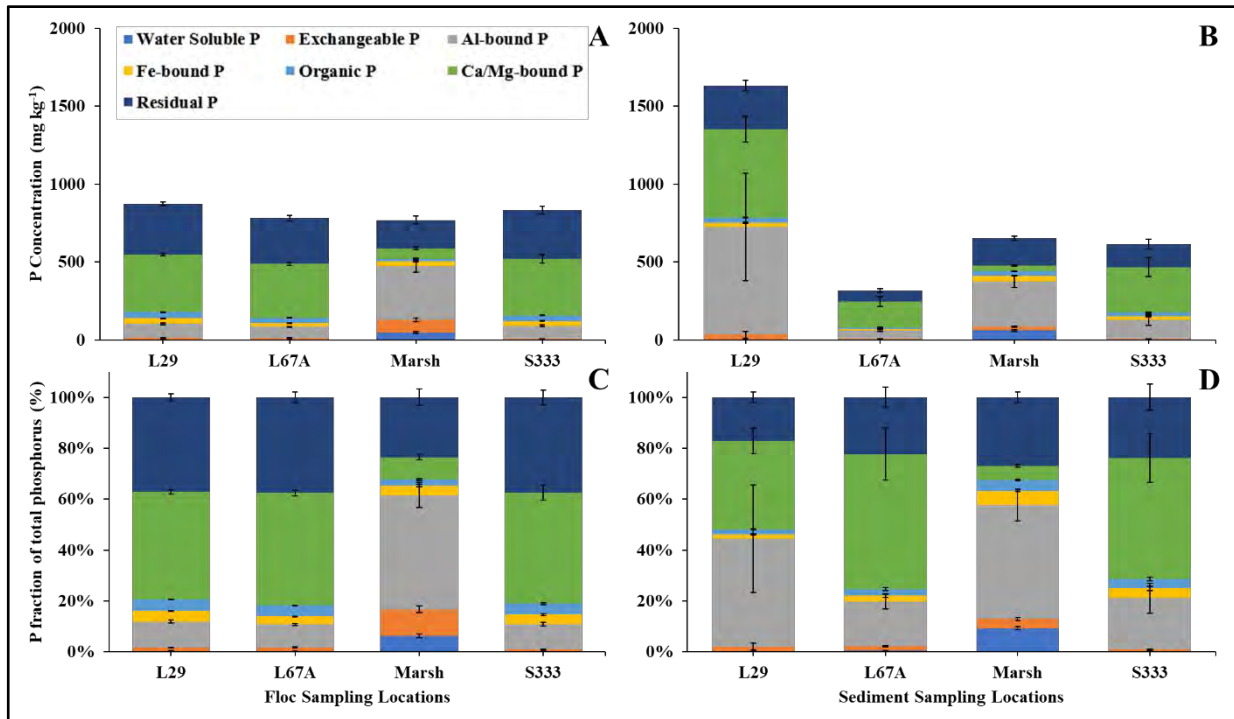
Figure 3.25. Distribution of various forms of P expressed as concentrations in flocs (A) and sediments (B) and percentage of the TP in flocs (C) and sediments (D). Vertical bars represent standard errors of the means.

The TP concentration in sediment samples followed an order of L29 > Marsh > S333 > L67A (Fig. 3.25B). The P forms present in the sediment were similar to floc. Residual P, Ca/Mg-bound P, and Al-bound P were also the major P forms present in the sediment canal samples (L29, L67A, and S333), with little water-soluble and exchangeable P were present (Fig. 3.25D). The majority of P in sediment marsh samples was present as Al-bound P and residual P, and a modest amount of Ca/Mg-bound P, Fe-bound P, water-soluble P, and exchangeable P were also present (Fig. 3.25D).

Sequential fractionation separated the soil P into labile and nonlabile pools (Zhang and Kovar, 2009). Labile P, including water-soluble and exchangeable P, refers to the fraction of P that plants could readily uptake and, therefore, is more available to contribute soluble reactive P in water. Soil inorganic P can form recalcitrant ionic complexes with Al and Fe (Al/Fe-bound nonlabile P) as well as precipitate with Ca (Ca-bound nonlabile P). The lability of Al/Fe/Ca-bound P depends on the soil redox potential and soil pH. Al and Fe-bound P could be released once the soil was fully saturated under reduced conditions. Mineral complexes with Al- and Fe-bound P, such as kaolinite, illite, palygorskite, iron sulfide, hematite and can become soluble only in strong alkaline or low redox potential condition. Ca/Mg-bound P which is bounded by calcium and magnesium minerals such as calcite, Ca oxide phosphate, Mg carbonate, and aragonite can be released under certain conditions, such as lowering pH in floc or sediment

(Grenon et al. 2021). The majority of soil organic P was nonlabile, however, some small molecules could be hydrolyzed by extracellular phosphate enzymes and producing inorganic P for plant uptake (Grenon et al. 2021). Residual P in P fractionation refers to the fraction of nonlabile P that remains tightly bound and strongly fixed in floc and sediment and is relatively unavailable for plant uptake or microbial activity. Compared to other fractions, residual P possesses less harm to the environment, especially to water quality.

3.3. Cross-sectional water sampling and flow measurements

3.3.1. Flows in L29 and L67A canal and at S333

Based on ADCP data for the seven sampling events, flows (Qrev estimates) at S333 ranged from ~210 through 670 cfs and in L67A canal ranged from ~230 through 1614 cfs (Tab. 3.7). In L29, both eastward and westward flows were observed. Flows towards east (S333) ranged from ~1 through 97 cfs and towards west (S12D) ranged from ~142 through 824 cfs. Flows east in L29 occurred when flow from the L67A was similar to flow through S333. Flows west in L29 occurred when L67A flows exceeded S333 controlled discharges and the S12s were open.

Flow estimates were similar for both software during May and June events but differed in April for L29 and L67A canals. S333 flows from DBHYDRO and ADCP measurement (QRev) were not significantly different.

Table 3.7. Mean flows in L29 and L67A canal and at S333 gate at seven water sampling events.

Date	[1]S333 Gate data			Flow (cfs)	[2]Flow (cfs) ADCP measurements						Remarks for L29 Flow
	Gate opening (ft)	Head Stage (ft)	Tail Stage (ft)	S333 DBHYDRO	S333 [3]WinRiver	S333 [4]QRev	L67A WinRiver	L67A QRev	L29 WinRiver	L29 QRev	
Apr-14, 2022	8.20	7.55	7.52	283.09	360.70	366.74	401.61	389.10	-50.65	-30.24	flowing east
Apr-25, 2022	8.20	7.28	7.26	194.59	205.83	209.92	269.81	259.59	-32.77	-16.60	flowing east
May-05, 2022	8.18	7.27	7.25	233.63	228.09	228.08	229.88	229.84	-97.02	-97.02	flowing east
May-26, 2022	2.40	7.63	7.02	327.72	309.07	307.13	410.33	410.32	-1.44	-1.44	flowing east
Jun-07, 2022	3.21	8.53	7.77	488.36	454.31	454.31	577.84	577.84	142.58	142.58	flowing west
Jun-16, 2022	3.80	8.86	8.01	614.90	562.15	562.11	830.46	830.45	260.62	260.62	flowing west
Jun-27, 2022	5.00	8.95	8.27	719.64	670.86	670.85	1612.67	1613.95	817.53	823.91	flowing west

[1]S333 DBHYDRO flows, gate openings, and head and tail water stages are average for the duration of ADCP measurement taken in front of S333.
[2]ADCP measurements at S333 gate, and L67A and L29 canals were at ~1500ft upstream and they were not taken simultaneously but in a sequential order.
[3]ADCP data processing software from Teledyne RD Instruments WinRiver II (https://hydroacoustics.usgs.gov/movingboat/WinRiverII.shtml)
[4]ADCP data processing software from USGS (https://hydroacoustics.usgs.gov/movingboat/QRev.shtml)

Cross-sectional flows were mostly similar on both sides from the center of canal in L67A and L29 (data not shown). However, variable fluxes were observed for the S333 cross-section on all sampling events. Example plots (Fig. 3.26) of variable fluxes for single S333 transects collected on April 14 and June 27 shows volume of water passing through northern half was not similar to volume passing through the southern half of the cross-sections subsections.
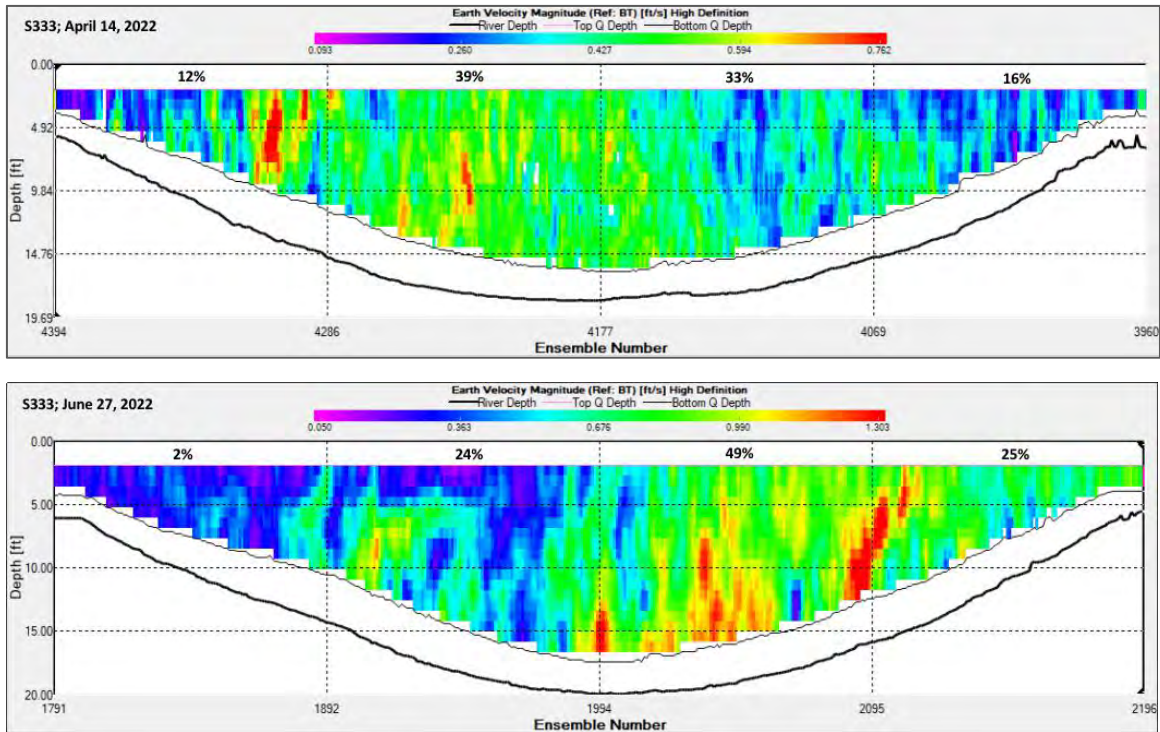
Figure 3.26. ADCP estimated flows (WinRiver-II) for April 14 (top) and June 27 (bottom) at ~23 m in front of S333 gate for a single horizontal transect. Numbers in percent show the percent of flow passing through each quarter marked by dotted lines (subsections).

Based on cross-sectionally normalized flows through normalized canal depth collected on April 14 and June 27, observed flows towards the bed of canal are higher (Fig. 3.27). June 27 shows higher flows towards the canal bed compared to April 14 consistent with higher discharge through S333 (Tab. 3.7).
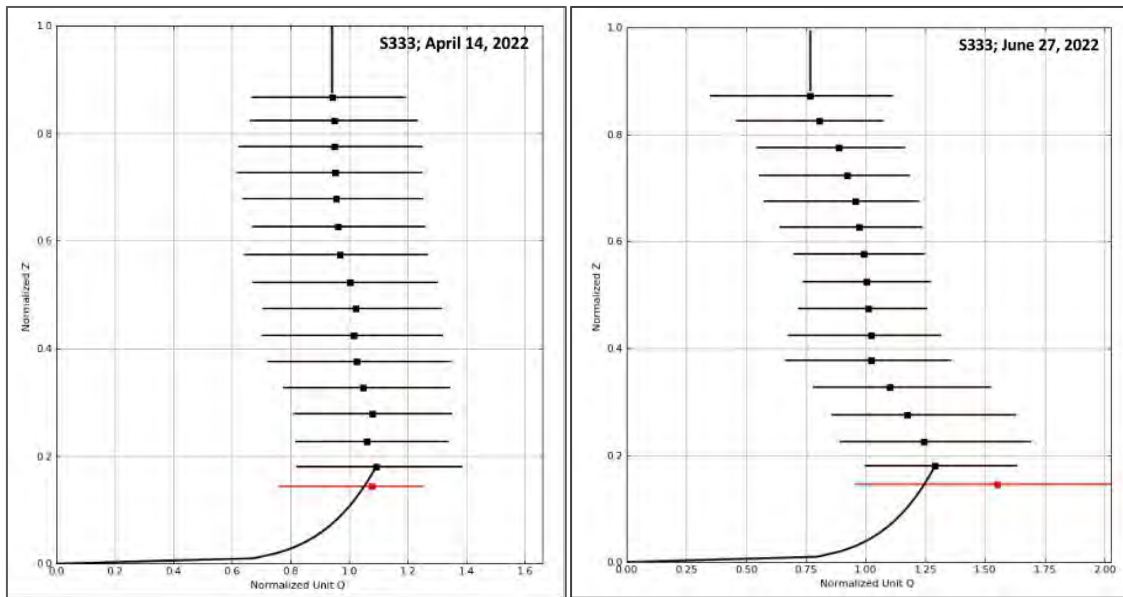
Figure 3.27. Horizontally integrated ADCP data estimated flows (QRev) for April 14 (left) and June 27 (right) at ~23 m in front of S333. The depth and flows are normalized to unit depth and

width, respectively.

3.3.2. Sediment particle size and phosphorus concentration

No clear relationship between d_{50} (median particle size in sample) and other parameters (e.g, TP, TSS, or PP) is visible from these scatter plots in Fig. 3.28 at S333. TP and PP have similar patterns over different water sampling events, however no similarity in pattern of magnitude and variations is observed during events between d_{50} and TSS or with TP and PP concentrations at S333 (Fig. 3.29). When TP variations at S333 are examined with depth, significant differences are observed on Apr 14, May 5, May 26, and June 16 samplings (Fig. 3.30). Corresponding d_{50} values on these sampling dates (Fig. 3.31) do not show significant differences.

Sediment and floc d_{50} size magnitude varies among the compartments (Marsh, in front of S333, and in the L67A and L29 canals; Fig. 3.32). The magnitude of d_{50} in floc was larger than in sediments. d_{50} particle size in floc did not differ significantly among these areas. However, based on the mctp statistical test, d_{50} particle size in sediments differed significantly among areas. Marsh was significantly different from all other areas and also had the largest d_{50}. L29 was significantly different from L67A, but neither differ significantly from S333.
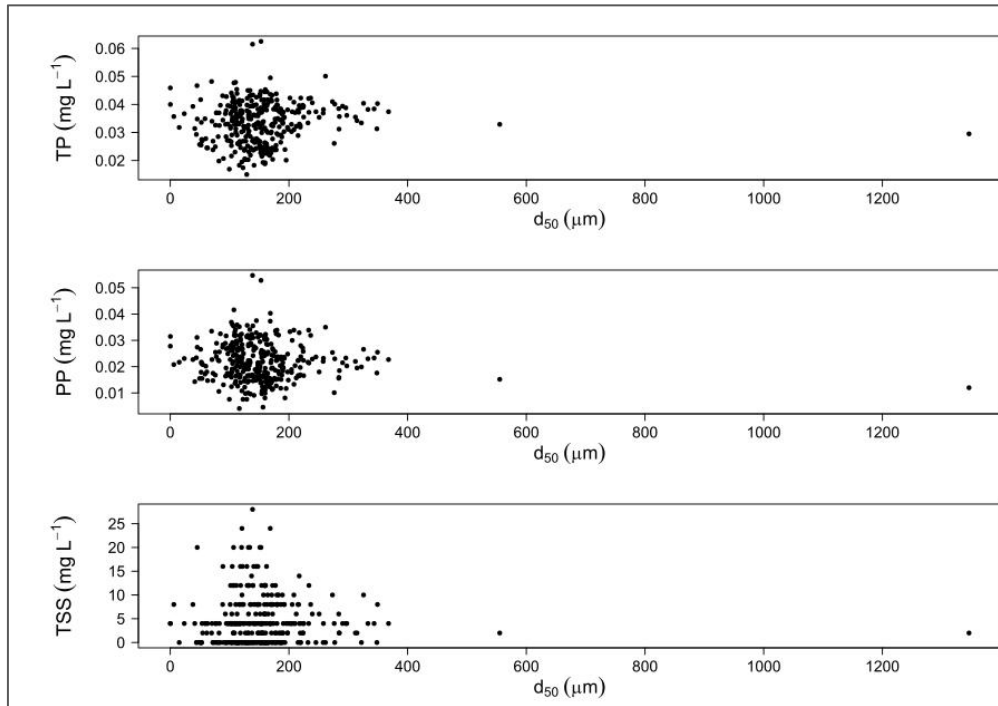
Figure 3.28. Scatter plot of d_{50} sediment particles size and TSS, PP, and TP concentrations in water samples at different sampling events.
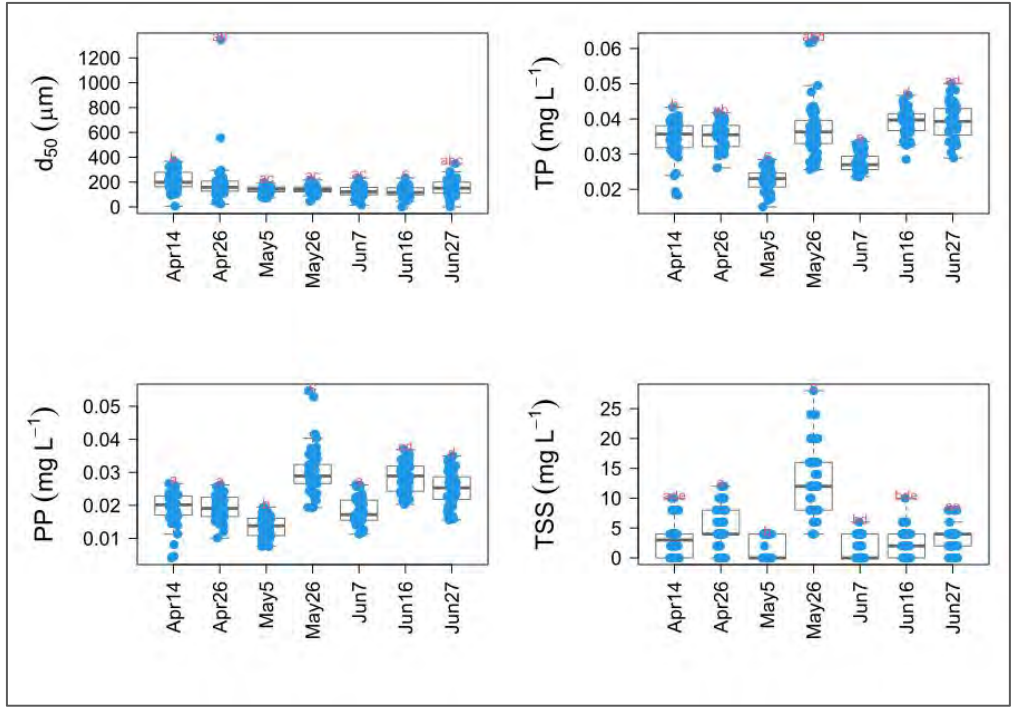
Figure 3.29. Box plot showing magnitude and variations of d_{50} sediment particles size and TSS, PP, and TP concentrations in water samples at different sampling events.
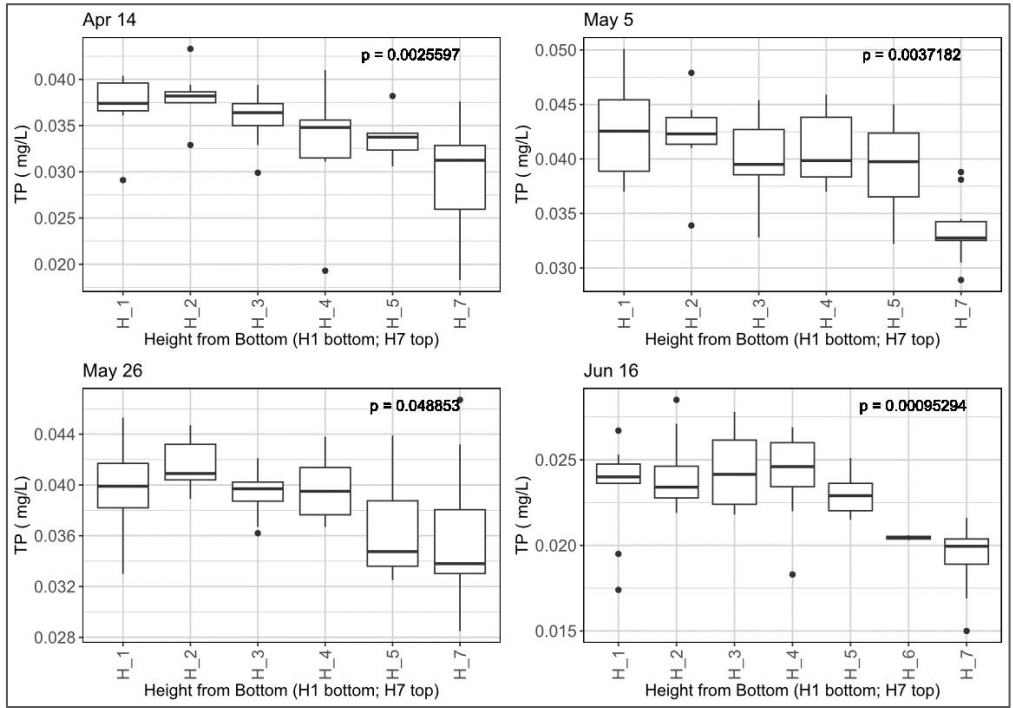
Figure 3.30. Box plot showing magnitude and variations of TP in water samples with height from canal bed. (H_1=30, H_2=60, H3=100, H_4=160, H_5=250, and H_6=500 cms from canal bed, and H_7=50 cms depth from canal water surface)

52
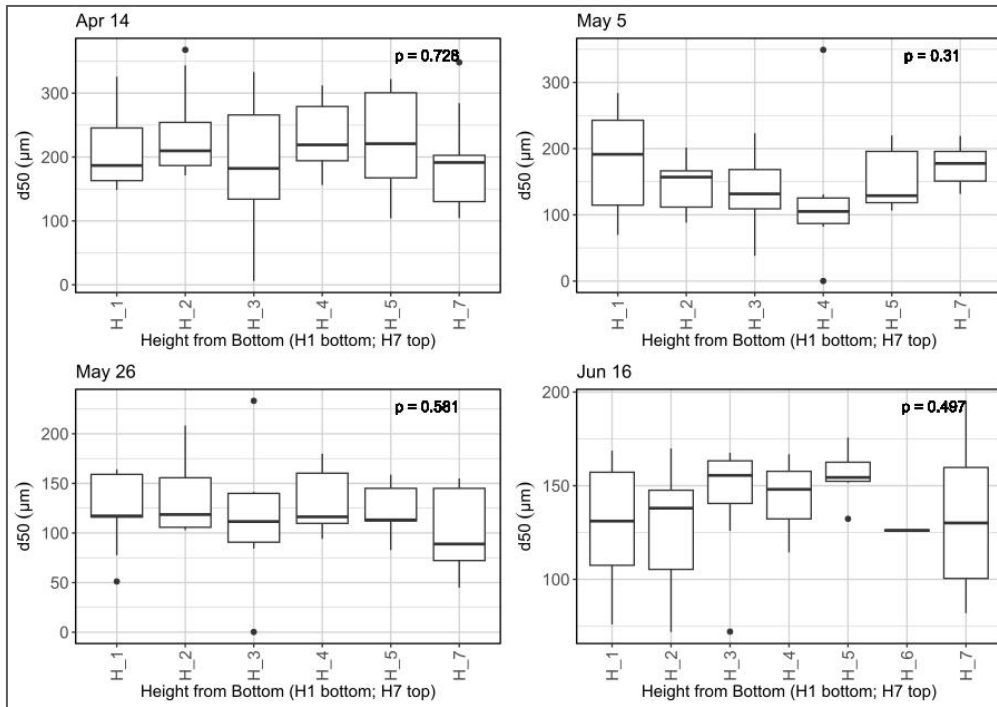
Figure 3.31. Box plot showing size and variations of d_{50} sediment particles in water samples with height from canal bed. (H_1=30, H_2=60, H3=100, H_4=160, H_5=250, and H_6=500 cm from canal bed, and H_7=50 cm depth from canal water surface)
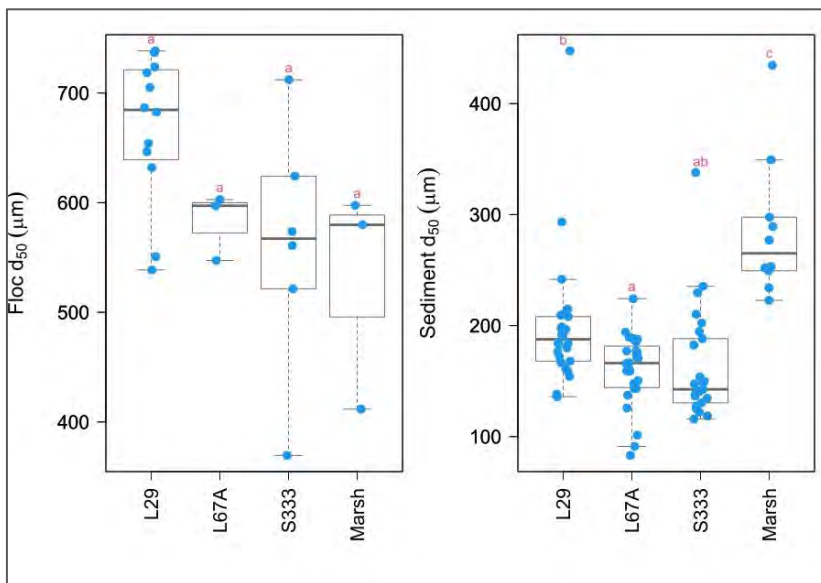
Figure 3.32. Box plot showing size and variations of d_{50} sediment particles in floc (left) and sediment (right) samples in different canal sections, area in front of S333, and adjacent WCA3A marsh area. Refer Fig. 3.20 for canal areas and sampling sites (Fig. 2.2) grouped together within these area.

53

4. Discussion

During different water sampling events variable discharges were observed through S333 ranging from ~210 through 670 cfs (Tab. 3.7; QRev column). These discharges showed water flux variations across the gate horizontally and vertically (Figs. 3.26 & 3.27). Variable fluxes have different energy levels which have potential to entrain multiple particle sizes and keep them afloat in water column. Higher flow velocities at the canal bed in front of the gate (Fig. 3.27) have a potential to entrain sediments from the canal bed. Median d_{50} in the S333 upstream area for sediments was ~143 μm (sd=51) and for floc was ~567 μm (sd=114), which can be characterized as fine sand (125 - 250 μm) and coarse sand size particles, respectively and may be susceptible to entrainment, if subjected to their threshold velocity at and above canal bed surface. However, a more thorough analysis is needed to examine flow vectors and streamlines near the canal bed as influenced by gate openings and discharge magnitudes to evaluate potential of sediment and floc entrainment and associated TP contribution to water quality at the S333.

For water samples taken during different sampling events, median d_{50} appeared to be around ~200 μm and below (fine sand category; Fig. 3.31). This indicates the canal bed may be a potential source of particles in water samples besides upstream sources. For the sampling events shown in Fig. 3.31 no particular pattern of d_{50} distribution with height in water column was observed at S333 sampling transect. However, a clear pattern of decreasing TP (Fig. 3.30) with height from canal bed indicated a possibility of sediment entrainment from canal bed, which may be due to higher water fluxes towards the bed of canal (Fig. 3.27).

Marsh sediments had higher d_{50} levels compared to canals and lower floc d_{50} levels compared to canals (Fig. 3.32). This indicates for the same levels of flows in marsh and canals, marsh sediments would be relatively less susceptible to entrainment and transport.

Cadmium, a commonly found trace metal in fertilizers was detected at all locations in floc and sediments. The order of concentrations among the five sampling locations was L29 > Miami > S333 > L67A > Marsh in floc, and Miami > L29 > S333 > L67A ≈ Marsh in sediments. Higher concentrations in both floc and sediments in canals indicates a linkage to upstream water sources.

Sorption analysis showed floc samples had higher sorption capacity than sediments and lower equilibrium concentration than sediments at all canal locations. Floc already being in suspension have a lower energy threshold required for transport compared to sediments. Floc transport from upstream water sources thus could be related to high TP values observed at S333. Phosphorus concentrations obtained from cross-sectional sampling were consistently lower than EPC_0 (Equilibrium P Concentration for Zero Net P sorption) for both floc and sediment samples collected at S333. This finding strongly suggests that floc and sediment act as sources of phosphorus, contributing to the phosphorus levels in the canal water.

The presence of clay minerals, kaolinite, illite, or palygorskite in both floc and sediment indicates the transportation of these clay minerals with water from upstream sources. The trace amount of hematite and the absence of illite in floc from L29 and sediment from S333 and Miami suggest connectivity among these locations. Similar to the Marsh, S333 exhibits low quartz content in both floc and sediment, as well as low Mg carbonate in floc. The presence and distribution of minerals in sediment can have an indirect influence on phosphorus transport and retention. Certain minerals, such as iron- and aluminum-rich clays, have a strong affinity for phosphorus adsorption. Sediments with higher mineral content, particularly those rich in these specific clay minerals, can act as sinks for phosphorus by effectively trapping and immobilizing

it. The composition of minerals in sediment can impact the availability and mobility of phosphorus, thereby influencing its transport and potential release in the water column.

Using cluster analysis as a tool to explore hidden linkages and similarities, floc sample results suggest that the P found in S333 may originate from L67-3 site. Indicators showed L67A and S333 samples belonged to the same cluster (Figs. 3.14-3.16). Considering the water flow paths in this region (Fig. 1.2), it is possible that the Miami canal also contributes to nutrients in L67A, as all indicators and conventional indicators indicated they were in the same cluster (Figs. 3.14 & 3.15). Geochemical indicators in the floc samples suggest that the nutrients in L67-3 site could flow to the L29 canal, as L29 sites were clustered with L67-3 and S333 (Fig. 3.16).

Similarly, sediment sample analyses show the Miami canal and S333 were within the same cluster when considering all indicators and geochemical indicators (Figs. 3.17 & 3.19), suggesting that the Miami canal could be a potential source for P in S333. Conventional indicators in sediment demonstrated that the Marsh samples had a higher similarity to S333 samples (Fig. 3.18). Geochemical indicators also suggest that the nutrients found in S333 could possibly be transported to L29 (Fig. 3.19), although this transport was not observed when considering all indicators and conventional indicators (Figs. 3.17 & 3.18). Data collected by ENP using TCM supports the observation that waters from L67A flow to L29 canal when S12C & D gates are open.

Based on the results of the cluster analysis for floc and sediment samples, it appears that the Miami and central L67A canals are a probable source of P in S333 on a subregional scale. The P may be directly transported from the Miami canal to the L67A or flow into the local WCA3A marsh and/or routed to L67A canal and then downstream to S333. On a local scale, sediments are transported towards the S333 as bedload movement and saltation may be occurring. These sediments get entrained into water column near the gate where fluxes are higher towards the canal bed due to gate configuration (Fig. 3.27).

These findings shed light on the potential sources and pathways of P transport to S333 in the canal system. They emphasize the significance of the Miami and central L67A canals in supplying nutrients to S333, either directly or through the marsh. These findings have important implications for understanding P dynamics and can guide management strategies aimed at reducing P loads in the canal system. It is recommended to further validate and refine these observations through additional research and monitoring efforts. Additionally, targeted P reduction measures can be developed based on the identified sources and transport pathways.

5. Conclusion

This study offers valuable insights into the potential sources and pathways of P transport to S333 in the canal system. Approximately 537 kg P is present in the 0-5 cm top sediment layer in 27,210 m^2 area located 1,500 ft upstream of S333 gate in the L67A and L29 canals. Approximately >90 % of this P is in a bound form (non-labile) with the sediment metrics which is not readily exchangeable with water.

Investigations of flows to study the influence of gate structure revealed some insight on sediment entrainment. Cross section flows in front of S333 revealed variable fluxes. Additionally, higher flows were observed towards the canal bed. Higher TP levels were observed towards the canal bed as compared to surface TP levels, which may have been influenced by variable fluxes in the cross section. The Miami and L67A canals appear to play a crucial role in supplying nutrients to S333, either directly or through WCA3A marsh.

Further research and monitoring efforts are recommended to validate and refine these findings. Additionally, the identified sources and transport pathways can inform the development of targeted P reduction measures. Understanding P dynamics is essential for mitigating the impact of P on water quality in the canal system and protecting the Everglades National Park.

6. Literature cited

Anderson, J. M., 1976. An ignition method for determination of total phosphorus in lake sediments. Water Research 10:329-331.

Belmont, M. A., J. R. White, and K. R. Reddy. 2009. Phosphorus sorption and potential phosphorus storage in sediments of Lake Istokpoga and the upper chain of lakes, Florida, USA. Journal of environmental quality, 38(3): 987-996.

Bracher, C., E. Frossard, M. Bigalke, M. Imseng, J. Mayer, and M. Wiggenhauser. 2021. Tracing the fate of phosphorus fertilizer derived cadmium in soil-fertilizer-wheat systems using enriched stable isotope labeling. Environmental Pollution, 287.

Briceño, H., P. Gardinali, and R. Garcia. 2019. Mechanisms and conditions responsible for elevated TP levels in surface water discharges to Shark River Slough within Everglades National Park. Final Report submitted by Florida International University to South Florida Natural Resources Center, Everglades National Park, Homestead, FL, November 2019.

Carvalho A., S. J. Schropp, G. Sloan, T. P. Biernacki, and T. L. Seal. 2002. Development of an interpretive tool for assessment of metal enrichment. In Florida freshwater Sediment. Report C2001-022. Florida Department of Environmental protection, Tallahassee, Florida. https://floridadep.gov/sites/default/files/Development-DWRM-Metals-Tool_2.pdf.

Castro, J. E., A. M. Fernandez, V. Gonzalez-Caccia, and P. R. Gardinali. 2013. Concentration of trace metals in sediments and soils from protected lands in south Florida: background levels and risk evaluation. Environ Monit Assess 185, 6311–6332. https://doi.org/10.1007/s10661-012-3027-9

Chen, M., L. W. Ma, W. G. Harris, and G. Willie. 1999. Baseline concentrations of 15 trace elements in Florida surface soils. Journal of Environmental Quality, 28(4): 1173–1181.

Domagalski, J., C. Lin, Y. Luo, J. Kang, S. Wang, L. R. Brown, and M. D. Munn. 2007. Eutrophication study at the Panjiakou-Daheiting Reservoir system, northern Hebei Province, People's Republic of China: Chlorophyll-a model and sources of phosphorus and nitrogen. Agricultural water management, 94(1-3): 43-53.

Dotsika, E., D. Kyropoulou, V. Christaras, and G. Diamantopoulos. 2018. $\delta^{13}C$ and $\delta^{18}O$ Stable Isotope Analysis Applied to Detect Technological Variations and Weathering Processes of Ancient Lime and Hydraulic Mortars. Geosciences, 8, 339. https://doi.org/10.3390/geosciences8090339

Duan, Z. 2012. The Distribution of Toxic and Essential Metals in the Florida Everglades. Thesis, DOI: 10.25148/etd.FI12080608

Gan, H., I. Schoning, P. Schall, C. Ammer, and M. Schrump. 2020. Soil organic matter mineralization as driven by nutrient stoichiometry in soils under differently managed forest stands. Frontiers in Forests and Global Change, 3, https://doi.org/10.3389/ffgc.2020.00099

Grenon, G., B. Singh, A. De Sena, C. A. Madramootoo, C. von Sperber, M. K. Goyal, and T. Zhang. 2021. Phosphorus fate, transport and management on subsurface drained agricultural organic soils: a review. Environ. Res. Lett. 16 013004.

Inglett, P. W., and K. R. Reddy. 2006. Investigating the use of macrophyte stable C and N

isotopic ratios as indicators of wetland eutrophication: patterns in the P-affected Everglades. Limnology and Oceanography, 51(5): 2380–2387.

Irick, D. L., Y. C. Li, P. W. Inglett, W. G. Harris, B. Gu, M. S. Ross, A. L. Wright, and K. W. Migliacio. 2013. Characteristics of soil phosphorus in tree island hardwood hammocks of the Florida Everglades. Soil Science Society of America Journal 77(3):1048-1056.

Jiao, W., W. Ouyang, F. Hao, and C. Lin. 2015. Anthropogenic impact on diffuse trace metal accumulation in river sediments from agricultural reclamation areas with geochemical and isotopic approaches. Science of the Total Environment, 536, 609–615. https://doi.org/10.1016/j.scitotenv.2015.07.118

Judy, J. D., W. Harris, G. M. Hettiarachchi, A. C. Buchanan, and K. R. Reddy. 2021. Mineralogy of particulate inputs and P-speciation and mineralogy of recently accreted soils within Everglades stormwater treatment wetlands. Science of The Total Environment, 781. https://doi.org/10.1016/j.scitotenv.2021.146740

Kassambara, A. 2016. Factoextra: extract and visualize the results of multivariate data analyses. R package version, 1.

Li, X., Y. Wang, J. Stern, and B. Gu. 2011. Isotopic evidence for the source and fate of phosphorus in Everglades wetland ecosystems. Applied Geochemistry, 26, 688-695.

Liu, X., Y. Li, Y. Zhang, Q. Su, T. Feng, and Y. Song. 2022. [15]N Natural Abundance of C3 and C4 Herbaceous Plants and Its Response to Climatic Factors along an Agro-Pastoral Zone of Northern China. Plants (Basel), 11(24): 3526. doi: 10.3390/plants11243526

Michelsen, T. C. 1992. Organic carbon normalization of sediment data. Technical Information Memorandum. Publication No. 05-09-050. Available at: https://apps.ecology.wa.gov/publications/documents/0509050.pdf. Last accessed: June 7, 2023

Nielsen, F. 2016. Hierarchical clustering. Introduction to HPC with MPI for Data Science, 195-211.

Noguchi, K., R. S. Abel, F. Marmolejo-Ramos, and F. Konietschke. 2020. Nonparametric multiple comparisons. Behavior Research Methods, 52:489-502.

Novak, M., F. Buzek, and M. Adamova. 1999. Vertical trends in $\delta^{13}C$, $\delta^{15}N$, and $\delta^{34}S$ ratios in bulk Sphagnum peat. Soil Biology and Biochemistry, 31, 1343–1346.

Reddy, K. R., and R. D. DeLaune. Biogeochemistry of wetlands: science and applications. CRC press, 2008.

Reddy, K. R., Y. Wang, W. F. DeBusk, M. M. Fisher, and S. Newman. 1998. Forms of soil phosphorus in selected hydrologic units of the Florida Everglades. Soil Science Society of America Journal 62(4): 1134-1147.

Salehi, M. H., O. H. Beni, H. B. Harchegani, I. E. Borujeni, and H. R. Motaghian. 2011. Refining soil organic matter determination by loss-on-ignition. Pedosphere, 21(4): 473-482.

Santisteban, J. I., R. Mediavilla, E. Lopez-Pamo, C. J. Dabrio, M. B. R. Zapata, M. J. G. García, S. Castano, and P. E. Martínez-Alfaro. 2004. Loss on ignition: a qualitative or quantitative method for organic matter and carbonate mineral content in sediments? Journal of Paleolimnology, 32:287-299.

Sawyer, R. K., C. C. Wieland, and G. M. Griffin. 1988. The clay mineralogy of calcitic seat earth in the northern Everglades of Florida. Journal of Sedimentary Research, 58(1): 81–88. doi: https://doi.org/10.1306/212F8D1E-2B24-11D7-8648000102C1865D

Singh, A. K. 2015. Engineered nanoparticles: structure, properties and mechanisms of toxicity. Academic Press.

USEPA. 1982. Methods for chemical analysis of water and wastes. EPA 600/4-79-020. US. Gov. Print Office, Washington, DC.

USEPA, 1996. Acid Digestion of Sludges, Solids and Soils, USEPA 3050B, In SW-846 Pt 1. Office of Solid and Hazardous Wastes, USEPA, Cincinnati, OH.

Wang, Q., and Y. Li. 2010. Phosphorus adsorption and desorption behavior on sediments of different origins. Journal of Soils and Sediments, 10:1159-1173.

Wang, Q., Y. Li, and Y. Wang. 2011. Optimizing the weight loss-on-ignition methodology to quantify organic and carbonate carbon of sediments from diverse sources. Environmental monitoring and assessment, 174:241-257.

Wang, Y., B. Gu, M. Lee, S. Jiang, and Y. Xu. 2014. Isotopic evidence for anthropogenic impacts on aquatic food web dynamics and mercury cycling in a subtropical wetland ecosystem in the US. Science of the Total Environment, 487, 557-564. doi: 10.1016/j.scitotenv.2014.04.060

Wright, A. L., and P. W. Inglett. 2009. Soil Organic Carbon and Nitrogen and Distribution of Carbon-13 and Nitrogen-15 in Aggregates of Everglades Histosols. Soil Science Society of America Journal, 73, 427-433.

Zhang, H., and J. L. Kovar. 2009. Fractionation of soil phosphorus. Methods of phosphorus analysis for soils, sediments, residuals, and waters 2: 50-60.

Zhang, M., C. Li, Y. C. Li, and W. G. Harris. 2014. Phosphorus minerals and solubility in native and agricultural calcareous soils. Geoderma, 232-234, 164-171.

Zheng, Z., Y. Xu, J. Wang, Y. Li, and B. Gu. 2019. Environmental stress and eutrophication in freshwater wetlands: evidence from carbon and nitrogen stable isotopes in cattail (Typha domingensis Pers.). Ecol Process 8, 31. https://doi.org/10.1186/s13717-019-0186-4

Zhou, M., and Y. Li. 2001. Phosphorus-sorption characteristics of calcareous soils and limestone from the southern Everglades and adjacent farmlands. Soil Science Society of America Journal, 65(5):1404-1412.

SECTION 2: INVESTIGATE SEDIMENT AND FLOC TRANSPORT OF PHOSPHORUS AT S333 GATED STRUCTURE ON THE NORTHERN BOUNDARY OF EVERGLADES NATIONAL PARK

College of Arts, Sciences, and Education
Institute of Environment

Investigate sediment and floc transport of phosphorus at S333 gated structure on the northern boundary of Everglades National Park

Principal Investigators:

John Kominoski

Institute of Environment and Department of Biological Sciences

Florida International University

11200 SW 8th Street, Miami FL 33199

Email: jkominos@fiu.edu

Telephone: (305) 348-7117; Fax: (305) 348-4096

Key Personnel:

Julia Pope, Veronica Restrepo

Administrative Contact:
Robert Gutierrez, Pre-Award Director
Division of Sponsored Research
Florida International University
Miami, FL 33199
E-mail: gutierrr@fiu.edu
305-348-2494 (ph); 305-348-4117 (fax)

Project Dates: March 01, 2021 – February 28, 2023

This project final report is for work conducted during **April to June 2022** under **Task Agreement P20AC00440 (Modification - 01)**.

Background
The Central & South Florida (C&SF) Project resulted in an extensive network of canals, levees and impoundments and enhancements to preexisting canal systems to provide flood control and water supply in Florida. The Water Conservation Areas were completed in the 1960s, resulting in impoundment and loss of ecological connectivity throughout the central and southern Everglades. The creation of the L-29 Canal and Levee eliminated overland flow into Shark River Slough. Construction of the Tamiami Trail (U.S. 41) was completed in 1928. The purpose of this roadway was to connect the east and west coasts of Florida; however, this road also functioned as a significant ecological and hydrologic barrier between the northern and southern Everglades, separating the modern day Water Conservation Area (WCA-3) from Everglades National Park (ENP).

Unintended environmental consequences from the wide scale drainage and urbanization of the Everglades ensued. Alterations in the vegetation community were detected in the early 1900s. The surface elevation of the Everglades subsided, unnatural fire frequencies increased, and a significant loss of tree islands occurred throughout the Everglades. The ridge and slough habitat that once characterized much of the central and southern Everglades is now degraded or absent from its historic range. Wading bird abundances decreased more than 70% and historical nesting locations are thought to have shifted from estuarine habitats to freshwater marshes. Another significant, unintended consequence was water quality degradation and the spread of invasive species throughout the Everglades.

A restudy of the C&SF Project was authorized by the Water Resources Development Act of 1992 that resulted in the recommended Comprehensive Everglades Restoration Plan (CERP). The CERP consists of more than 60 projects intended to help restore defining features of the pre-drainage Everglades such as the natural hydroperiods and hydrologic patterns.

In 1989, the U. S. Congress passed the Everglades National Park Protection and Expansion Act. This Act authorized the expansion of 109,000 acres of land within modern-day northeast Shark River slough (NESRS) into ENP and structural modifications to the C&SF project to help restore the natural hydroperiods and hydropatterns within ENP. The modification of the C&SF structural features to restore NESRS was called the Modified Water Deliveries Project (MWD). The U.S. Army Corps of Engineers issued a General Design Memorandum (GDM) in 1992 to restore the hydrologic components of the Shark Slough basin. This original GDM assumed that the existing culverts under Tamiami Trail would pass enough water to help restore

hydroperiods and hydrologic patterns in NESRS when water stages in the L-29 canal were raised. However, review of the historical water level data and modeling data, indicated that the culverts were not adequate to pass the required flows to restore the natural hydrology of Shark River Slough.

The MWD Final Revised General Reevaluation Report/Second Supplemental Environmental Impact Statement (RGRR/SEIS) for the Tamiami Trail Modifications (U.S. Army Corps of Engineers, 2005) recommended construction of a 3-mile, 2 bridge alternative and alterations of a 10.7-mile stretch of the Tamiami Trail to allow for additional water deliveries to ENP. However, due to budgetary constraints, an additional reevaluation study was recommended and in 2008, the MWD to Everglades National Park Tamiami Trail Modifications Limited Reevaluation Report and Environmental Assessment (U.S. Army Corps of Engineers and U.S. Department of the Interior 2008) was completed. The preferred alternative of the reevaluation plan was a Tamiami Trail 1-mile (0.6 km) bridge, an additional 4.2 km of bridging, and road raising to allow for additional water deliveries to ENP (**Figure** 1). The sample collection for this task agreement assessed the combined effects of the MWD and the Combined Operations Plan (COP) (which began in August 2020) on the water column and suspended sediment chemistry during the onset of wet-season water management in the L-29, L-67, and the S333 gated structures.

Currently, NESRS receives water that passes through the S-333 and S-333N, two gated structures at the southern end of the L-67A canal. The S-333 and S-333N discharge into the L-29 Canal on the north side of Tamiami Trail. Water is then discharged to NESRS through a series of culverts and the Tamiami Trail bridges.

The purpose of this proposed task was to:

1. Explore relationships between water level (depth), current velocity, sediment and floc composition, and erosion and sedimentation processes at the onset of the wet season.

Project Phases and Design

This project was scheduled to begin in April 2020 but was delayed due to COVID-19. A trial of sampling method occurred on 30 April 2021 to coordinate field sampling logistics. Subsequent coordination meetings occurred in 2021 and 2022 among FIU, Univ. of Florida (UF), and ENP to establish the field and laboratory sampling procedures and methodological approaches. This report includes the results from the water chemistry samples collected from mid-April to mid-June 2022.

Work Schedule & Analyses

Sampling occurred approximately mid-Apr – mid-June at the onset of 2022 wet season followed by chemical analysis and reporting. Water samples were collected from $n = 9$ locations at three sites in the L-67 Canal and, $n = 3$ locations at 1 site in the L-29 Canal upstream of the S333 and S333N structures, and $n = $ ~40-60 locations at 1 site in front of S333 gate. Sampling occurred on 7 days from April-June 2022 (**Table 1**). Water samples were collected at three depths (0.5 m from canal bottom, mid-depth of canal, and 0.5 m from canal surface; **Figure 12**c) in L67A and L29 canals and cross-sectionally at varying depths at S333 gate (**Figure 13**a&c). Water samples were analyzed at FIU for total dissolved phosphorus (TDP), total phosphorus (TP), total organic carbon (TOC), and total suspended sediment (TSS).

Figure 1a shows that total phosphorus (TP) peaks at S333 coincide with low headwater stages at S333. Stage at the headwater of S333 below ~8.0 ft tend to be associated with elevated TP levels over 10 ppb (**Figure 1**b). Elevated TP at S333 appears to result from a combination of local and upstream processes and are temporally focused during the spring wet season transition. Upstream contributions are evident in the alignment of TP peaks at S333 with peaks at upstream stations along the L67 (S152 and S151; **Figure 2**a). TP levels at S152 are lower than at S151 (the farthest-upstream station) possibly due to exchanges with surrounding marshes as water moves down the L67 from S151 towards S152 and S333. However, by the time water reaches S333, local processes lead to elevated TP peaks, with levels exceeding those at S152. Source waters in L29 also appear to have relatively lower TP levels than are observed at S333 (comparison with S12D; **Figure 2**b). Local processes near S333 appear to be raising TP concentrations at S333 in excess of TP levels in source waters (L67A and L29 canals). These processes remain unexplained and merit exploration.
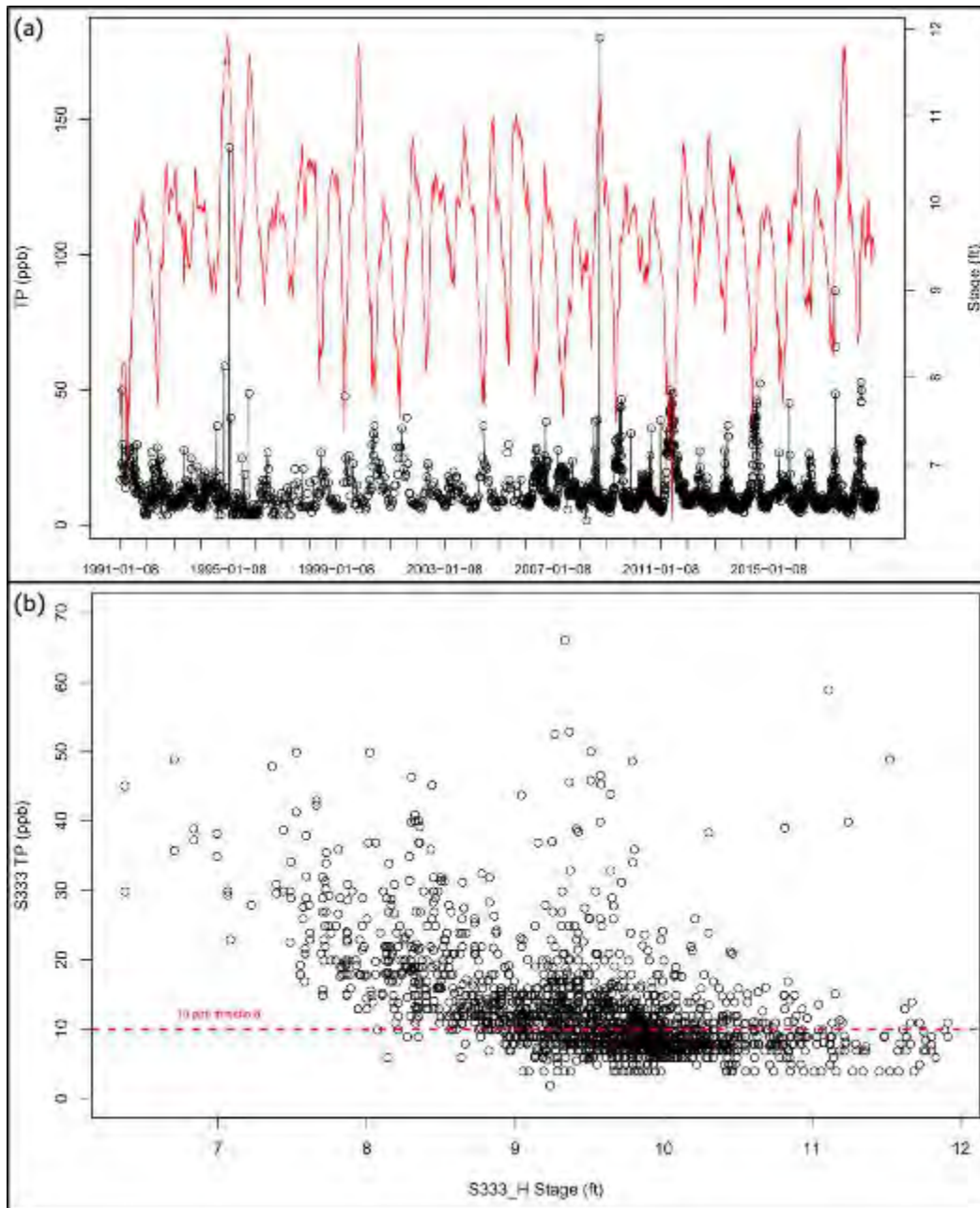
*Figure 1: (a)*Time series of water level (red line) and TP (black circle) for the period 1991-2018 at structure S333, *(b)* S333 head water stage and S333 TP concentrations for the period 1991-2018 (3 data points representing 140, 181, and 87 ppb are not shown).
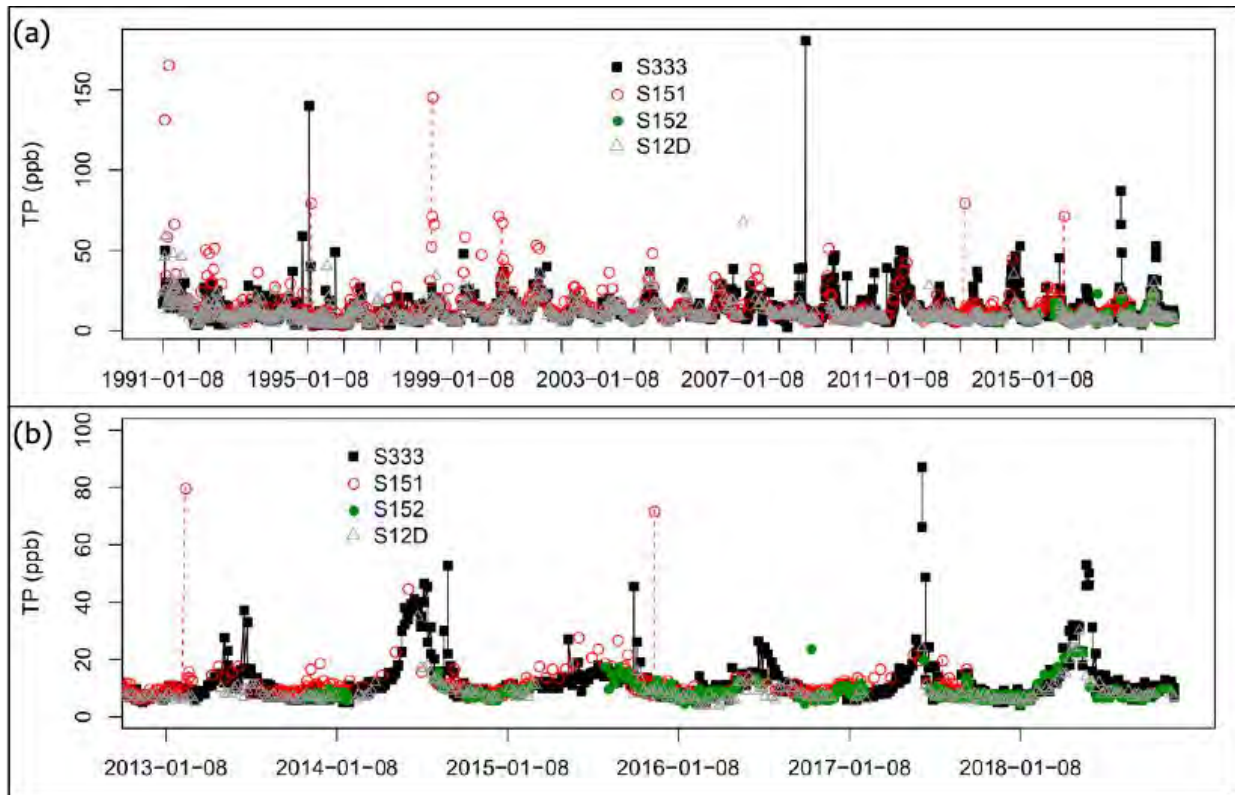
Figure 2: (a) Time series of TP concentrations at S151, S152, S12D and S333 for the period 1991-2018, *(b)* Time series of TP concentrations at S151, S152, S12D and S333 for the period 2013-2018.

Figure 3a shows time series plot of TP concentrations and turbidity at S333. Both time series show similar trends and **Figure 3**b shows a significant R^2 with p-value of 1.10e-49. Similar to Daroub et al. (2002) and Das et al. (2012) findings for the Everglades Agricultural Area, TP concentrations seem to be associated with turbidity at S333. This is an issue that requires examination at S333 of transport processes through S333 gated structure, its operation, and surroundings (canals L29 and L67A).
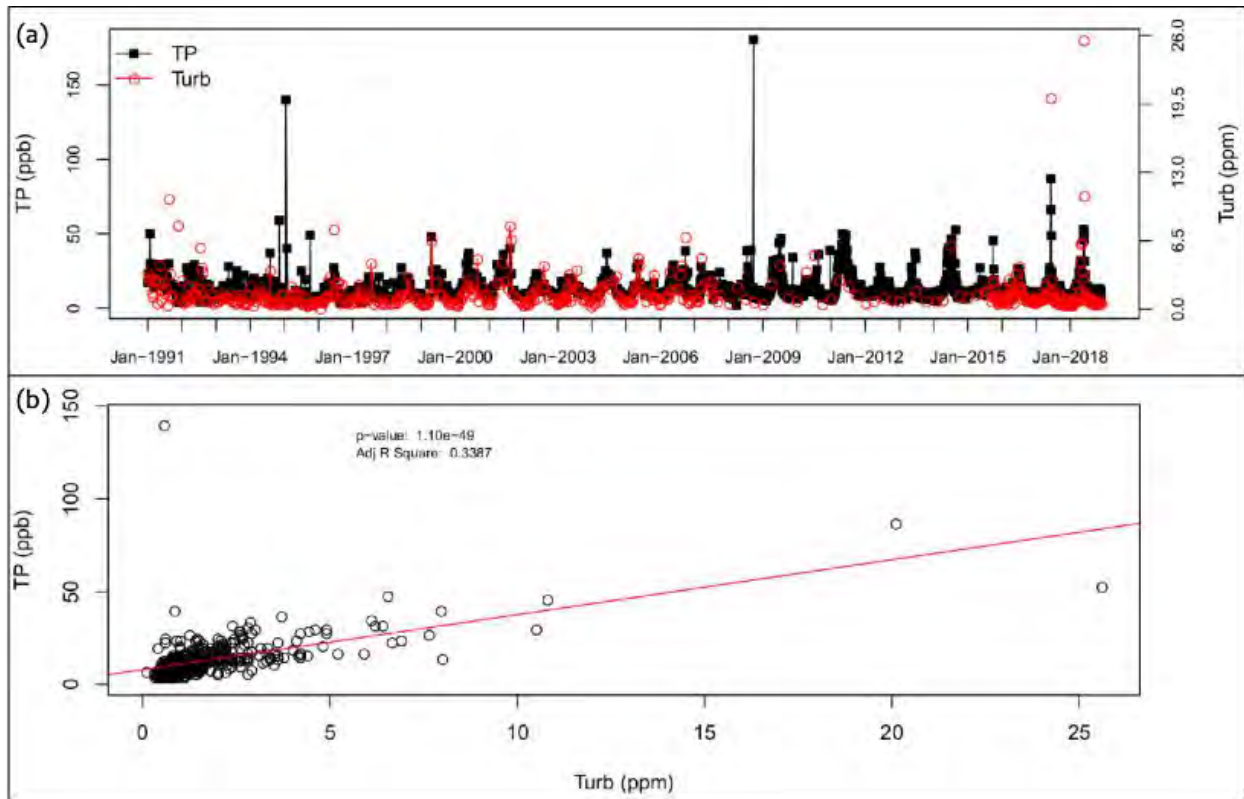
Figure 3: (a) *Time series of TP concentrations and turbidity at S333 for the period 1991-2018,* **(b)** *TP vs turbidity relationships at S333 for the period 1991-2018.*

Figure 4: *Locations of sediment core sampling (Briceño and Gardinali, 2018).*

Sediment samples were collected in L67A and L29 canals and at S333 (**Figure 4**; Briceño et al. 2019). The sediments in L29 are thicker and richer in organic content than upstream in L67, which are mostly carbonate sand (**Figure 5**). Total phosphorus

concentrations in upstream sediments ranged from 5.29 – 280.26 mg/kg (*n*=5) at L67A-R, 30.35 – 218.65 mg/kg (*n*=6) at L29R, and 13.87 – 224.33 mg/kg (*n*=5) at S333 taken at different times during 2016-17 (**Figure 4**; Briceño et al. 2019). And, the TP concentrations in upstream floc samples ranged from 96.48 – 296.25 mg/kg (*n*=4) at L67A-R, 214.74 – 534.33 mg/kg (*n*=4) at L29R, and 222.99 – 305.88 mg/kg (*n*=3) at S333 taken at different times during 2016-17 (**Figure 4**; Briceño et al. 2019). The range of TP values are highly variable. This requires more thorough investigation to get a correct estimate of TP load residing on the canal beds. The cause of TP enrichment near S333 is not clear yet, and thus requires additional sampling to be performed during this proposed project. This TP in sediments parallels a higher TP concentration in S333 waters mentioned above, suggesting that these sediments/floc in canal beds may contribute to elevate TP concentration at S333.

Figure 5: *Sediment cores (pictures) taken in L67A-R and L29R. The abundance of organic mud (black) in L29R contrasts with the thin layer on top of the core at L67A-R, which is mostly carbonate sand (Briceño and Gardinali, 2018).*

S333 Structure: The S333 structure is a reinforced concrete, gated spillway with vertical lift gate. The structure is located on L29 canal at the southeast corner of WCA-3A. **Figure 6**a shows a cross-section of gated structure at S333. Water is discharged downstream at the sill elevation through the area available when the gate is lifted open. Discharge rates depend on the difference between headwater, tailwater, gate lift (**Figure 6**a) and other factors.

The lift gate rests at sill elevation, 3.1 ft from the floor of the canal at S333. This reduces scouring of canal floor under the lift gate during discharge. Also, appears that elevated sill in spillway (**Figure 6**a) would trap and prevent heavier sediments and suspended material from moving through gate opening on the upstream side.
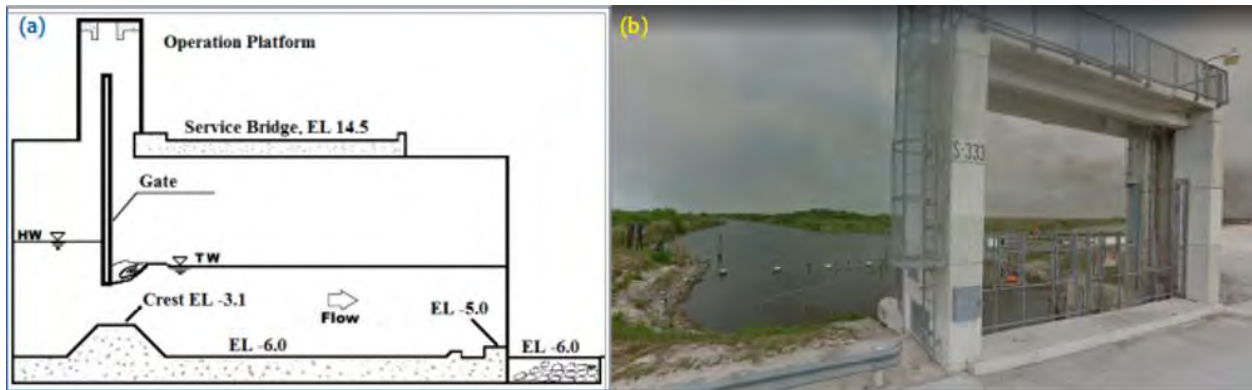
Figure 6: (a) Cross-section of controlled submerged flow type structure at S333 (SFWMD), (b) the physical structure at location (facing west).

Water Flows and TP at S333: Water discharges (flows) at S333 was governed by the WCA-3A Regulation Schedule that was based on the Everglades Restoration Transition Plan (ERTP) and transitioned to rules developed for the Combined Operations Plan (COP) after August 2020. COP is an integrated operational plan for two modifications of the C&SF project - known as MWD to ENP and the Canal C-111 South Dade projects. The Tamiami Trail Flow Formula is currently used to determine S-12s and S-333 target flows when the water levels are in Zones A and B of the regulation schedule. The Settlement Agreement/Consent Decree (1995) specified that interim and long-term TP concentration limits for discharges into ENP through Shark River Slough be met by October 1, 2003, and December 31, 2006, respectively (SFWMD 2018). Inflow concentrations of TP through S12A, S12B, S12C, S12D, S333, S355A, and S355B are compared to the interim and long-term limits at the end of each WY (October 1 through September 30; SFWMD 2018). The focus here is on TP concentration spikes at S333 and understanding flow dynamics around (in front of and immediately upstream) and through this structure that may explain the spikes of TP at the beginning of wet season (~April – June; **Figure 7**). These TP spikes may result in violation of consent decree and are a resource management challenge.
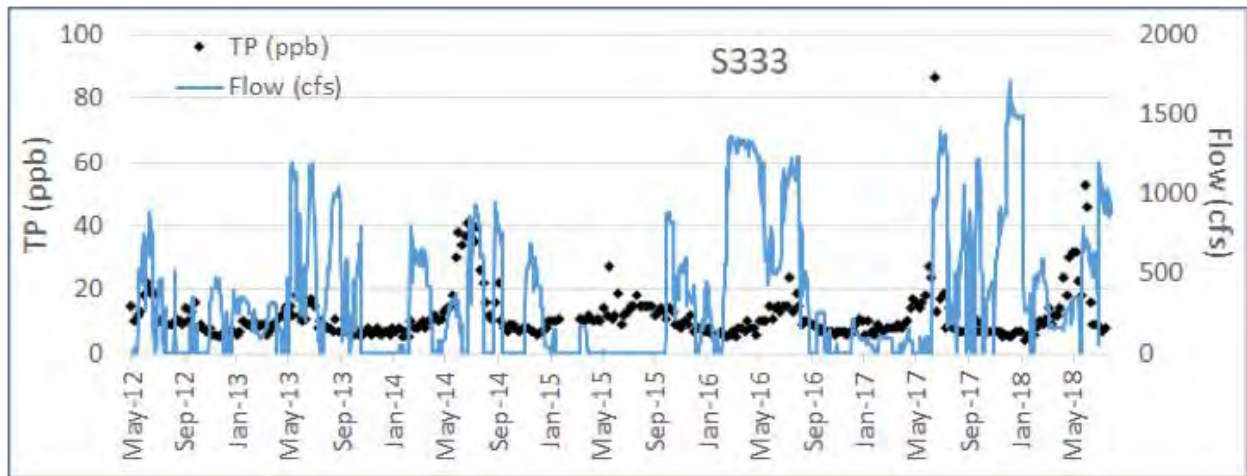
Figure 7: Flows through S333 coupled with TP concentrations at S333.

Figure 7 shows flows through S333 structure and TP concentrations sampled at a location (see **Figure 8**) upstream of the structure for the last seven years. Observed in **Figure 7** is a periodicity of high and low flows and TP concentrations, defining seasonal changes. High flow rates do not always coincide with high TP concentrations. In fact, there is no statistically significant relationship between TP and flow or turbidity and flow. Current measurements paired with water sampling and chemical analysis as proposed will bring some light to this apparent disconnect.

Water discharges at S333 are flow contributions from both L67A and L29 canals. The contribution from L29 varies and depends on S12s gate openings and stages in WCA-3A. Therefore, at times L67A may be contributing to discharges at both S333 and S12s gates at the same time. As such, flows at the juncture of L67A and L29 canals (**Figure 8**) are interesting in terms of interactions of the bio-physio-chemical energies of these two canals in the immediate vicinity of S333 upstream.

Figure 8: *Water quality sampling compliance site for consent decree at S333 (facing west).*

Water from two different directions (L67A: N→S and L29: W→E) merging at the S333 head waters, before passing through it, may create swirls (eddies) in the water column. The bend before S333 in L67A (**Figure 8**) would also contribute to the development of eddies in the water column even when L29 canal flow contribution is insignificant. An example of such flow dynamics is presented in **Figure 9**a from work of Gomez and Martinez (2014) which, though not exactly analogous to S333 bend in L67A, exhibits the physics of flow dynamics by a model of a real irrigation canal. In **Figure 10** ADCP measurement on immediate upstream of S333 near the bend in L67A towards S333 shows cross sectional water velocity from north to south end of canal similar to work of Gomez and Martinez (2014).
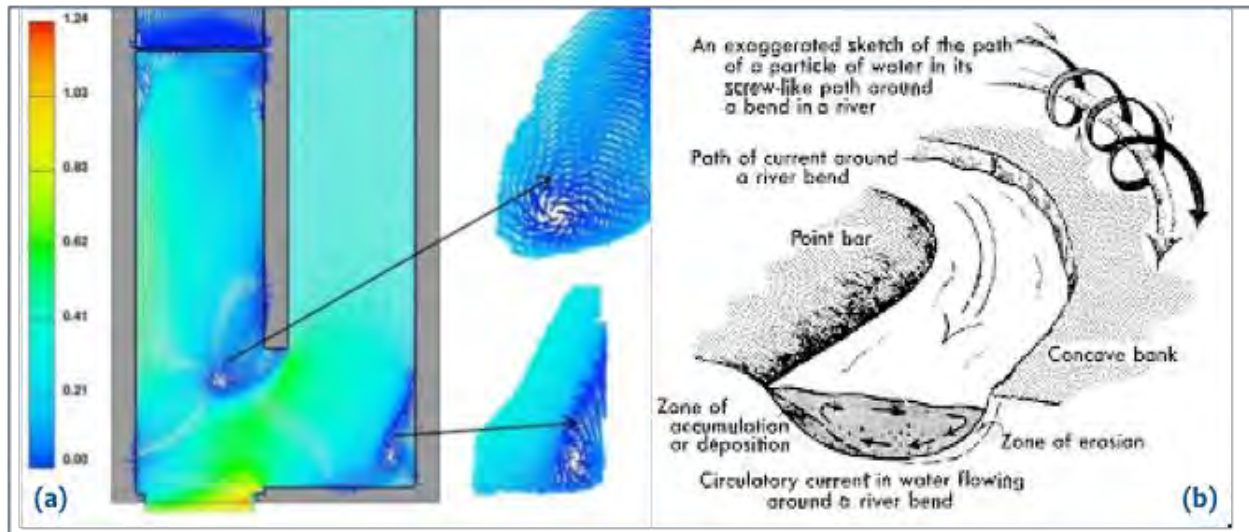
Figure 9: (a) Velocity vector in a plant cross section, in a half depth approximately (Valentin and Martínez-Gomariz 2014), (b) The effect of a curved channel on water flow (source: http://www.paleocurrents.com/castle_rock/docs/meandering_river.html#3).

Formation of such eddies (**Figure 9**a) near the bend and circulatory current (**Figure 9**b) create the local velocity fields required to suspend floc and lighter sediments (that may have been deposited during relatively static and low or no flow period) before water reaches the S333 gate. Also, note in **Figure 9**a that water flow is relatively static close to the bend edge and higher velocities are observed away from the bend in the curve. A similar condition can be envisaged at S333 on the bend in L67A (**Figure 8**) where the water quality sampling site is located (**Figure 10**: North end, low flows). **Figure 10** also shows higher velocity towards the south end away from the bend in L67A canal.
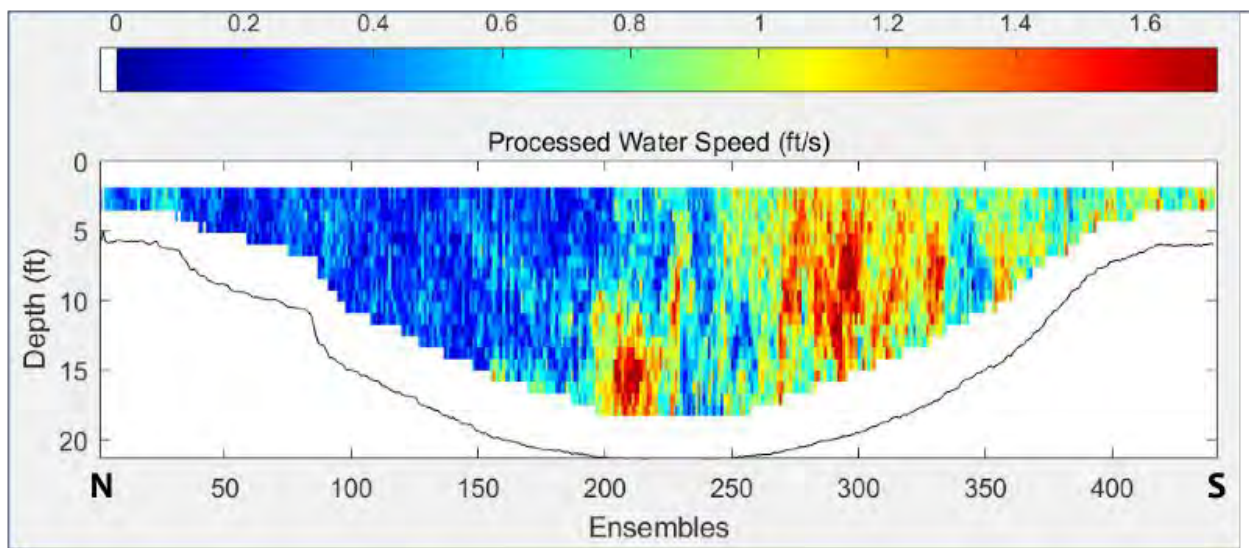
Figure 10: ADCP measurement immediately upstream of S333 showing cross sectional water velocity from north to south (ENP; Aug 27, 2018). Sampling site is located towards north end, within the low velocity, low energy blue area.

Figure 11 shows normalized profile of discharge immediately upstream of S333 estimated from ADCP measurements which shows higher flows towards the bottom of canal. This indicates possible scouring of canal floor reaches upstream of S333 before water flows through the gate. This (*Figure 10*) also indicates some vertical mixing of the water column may take place before water passes through the gate over the elevated sill (*Figure 6*a). It should be noted from **Figure 8** and **Figure 10** that the TP sampling site would fall in the zone of low flows just upstream of the structure (blue zone in **Figure 10** close to N end) and may not capture the true magnitude of TP concentration going through the S333 gate opening.
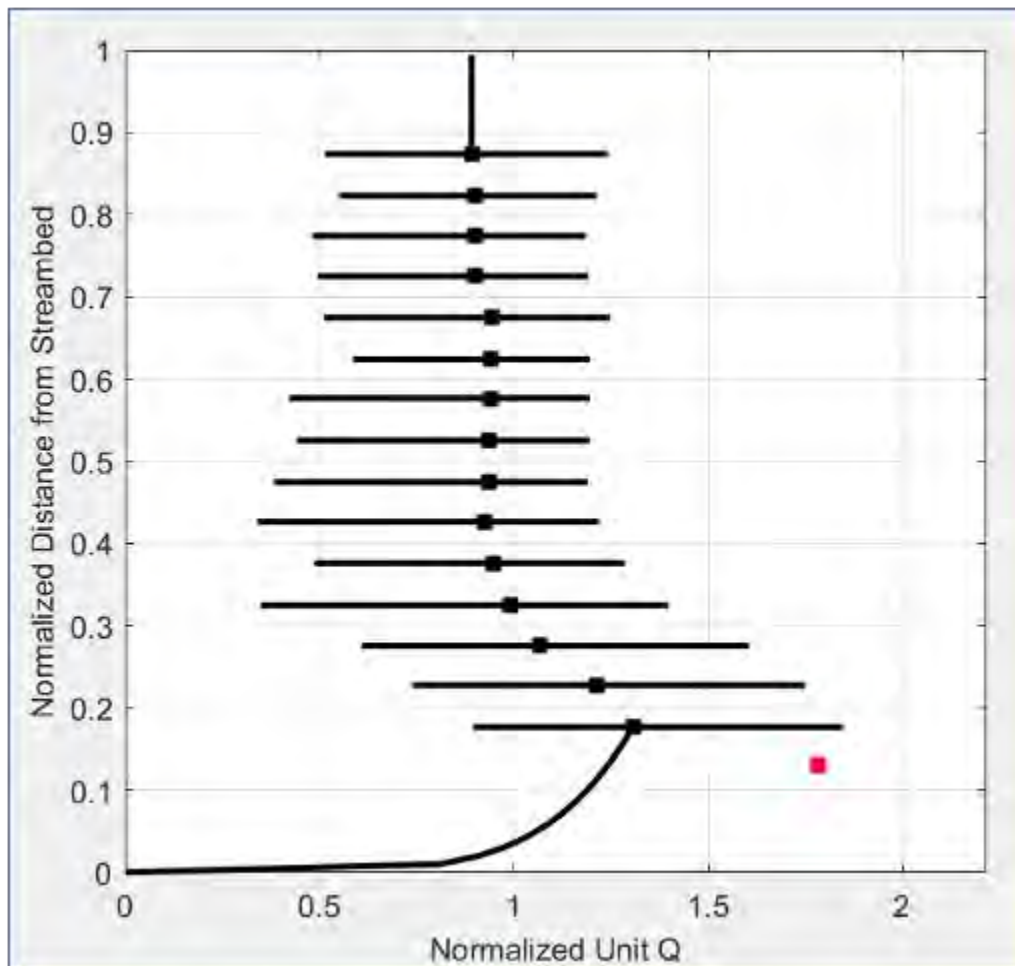
Figure 11: Profile of discharge measurement using ADCP data on immediate upstream of S333 (ENP; Aug 27, 2018). Normalized Q is unit-less as normalized by average Q (ft^3/s).

Task Objectives: Based on the preliminary analysis, description of possible flow dynamics in and around S333 structure, and physical characteristics of the current sampling location (**Figure 8**), a careful examination of water quality dynamics at the S333 structure is needed. We hypothesized that there is variable flux across the canal (**Figures 10** and **11**) just upstream of S333. This flux can lead to development of eddies and turbulence which suspend TP loaded sediments and floc in the water column. These dynamics can result in increased TP concentrations. The water loaded with these sediments can then be transported through S333 gate and may either settle in the downstream L29 canal or be introduced into the marsh in ENP, just downstream of the canal.

This task is related to the current ongoing project that monitors marsh response to rehydration in Northeastern Shark River Slough. The new tasks contribute to understand why TP concentrations increase during low stage conditions (**Figures 2a** & **7**). Resource managers seek to reduce or eliminate these seasonal events of high TP concentrations in turbid water as most of the waters discharged from S333 ends up in Northeast Shark River Slough.

Specific objectives for this task include:
1. Monitor TP at upstream (L29 and L67A) and in-front and near downstream location of S333 gate to investigate the contribution of L29 and L67A canals to the S333,
2. Design and monitor water quality across the S333 gate to investigate the influence of variable flux (**Figures 10** and **11**) in a 2-dimensional plane to capture the contribution of sediments and floc in TP concentrations.

Field work
Objective 1: Upstream/Downstream TP estimates in flows
Continuous water flow current velocity and direction were measured by ENP using Lowell TCM-1 tilt current meters (**Figure 12a**) at two locations ~1000 ft upstream on L29 and L67A (**Figure 12b**). The TCM-1 Tilt Current Meter measures current using the *drag-tilt principle*. Current meters were deployed for the duration of work collecting data every ten minutes. Upstream in L29 (~1500 ft) and L67A (~1500 ft, 1 mile [5280 ft], and 2 mile [10560 ft]) canal locations from S333 (**Figure 12b**) vertically depth stratified (3 depths; **Figure 13c**) at three locations across the canal water samples (9 samples for TDP, TP, TSS, TOC at each site) (canal center and sides; **Figure 12c**) and ADCP measurements (~1500 ft location) by ENP were collected to get an estimate of flow and TP contributions to S333 gate. This helped identify if similar TP intermediate increases in concentrations also occur in source waters to S333 at the same time and verify the possibility of a localized effect (floc and sediments) immediately upstream of the gate. In

addition, water samples were collected immediately downstream of the S333 (horizontally stratified over the gate width, ~4 samples) (**Figure 13c**). This upstream and downstream data collection were synchronized for the same 7-day events (**Table 1**) when detailed cross-sectional water quality sampling were collected at S333 (described below). A portion of water sample for laser particle analysis was shared with University of Florida.
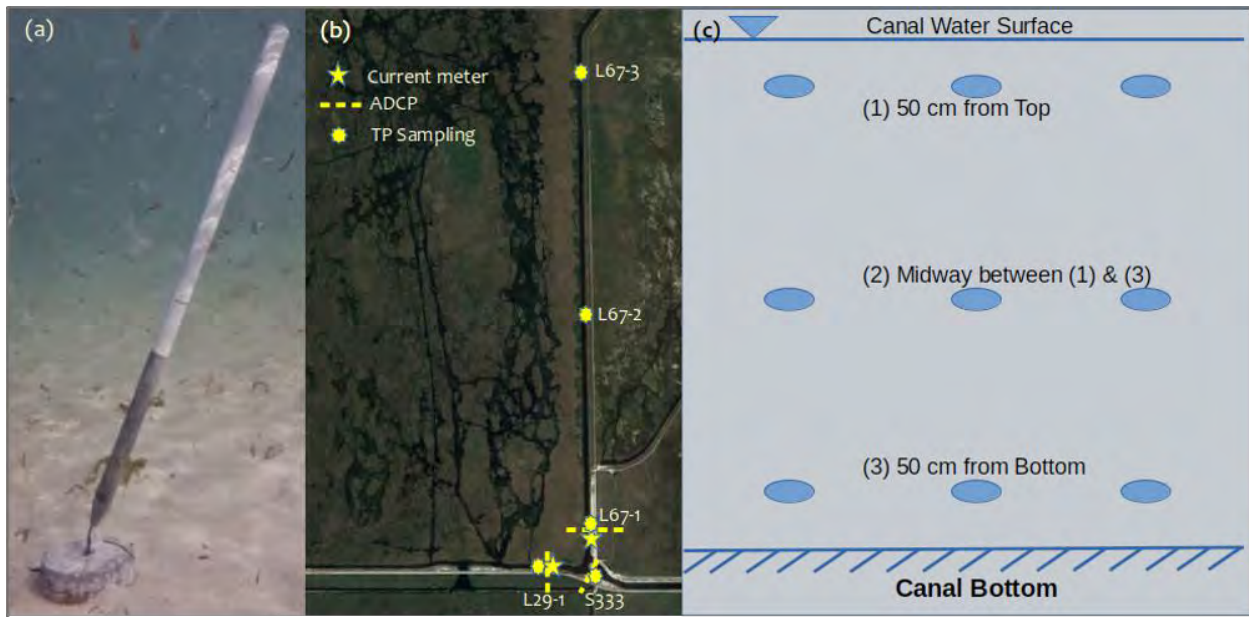
Figure 12: (a) *Lowell's Tilt Current Meter (TCM-1).* ***(b)*** *location of Current meter, (1000 ft) ADCP measurements and TP sampling. (1500 ft) L29-1 & L67-1 are 1500 ft (457.2 m) from S333, L67-2 & L67-3 are 1 mile (1609.34 m) and 2 mile (3218.69 m) from S333, respectively.* ***(c)*** *Illustration of canal transect water sampling. in L29 and L67A portion*

Objective 2: Cross-sectional canal water sampling
High-resolution sampling (~40-60 samples) along a cross-section of the L-29 canal provide valuable insights into wet-season TP concentration increases. This intensive sampling will document the magnitude of spatial (across the canal in front of S333) and temporal (over 7 days; **Table 1**) heterogeneity in sediment entrainment and TP concentrations, with the goal of capturing the rise and fall of TP concentrations near the start of the wet season (approximately mid-Apr- mid-June). It will also reveal the influence of variable flux (**Figures 10** & **11**) and possible scour and uplift of floc and sediments which may get transported through S333.

The sampling design illustration of an individual cross-section is shown in **Figure 13a** with collection of water samples (~40-60) along a grid weighted by anticipated current velocities from ADCP measurements. This water quality (TDP, TP, TSS, TOC) sampling were done as close (~75 ft) to the gate as possible (**Figure 13b**) depending on safety

and accessibility on upstream side at an interval of 10-11 days over the period when concentrations seasonally increase (~10 weeks, ~7 sampling events targeting the onset of the wet season; approximately Apr - Jun; **Table 1).** This sampling was carried out by UF and delivered to FIU. A portion of water sample for laser particle analysis was shared with UF. In addition, at the same time of water sample collection, ADCP measurement by ENP of cross-sectional velocities were taken close to the sampling transect to record the variable water fluxes across the sampling plane.

Methods
Water Sampling
Water grab samples were collected from surface and subsurface locations at all sites. Water grab samples were split into filtered and unfiltered subsamples according to the following protocol. Approximately 500 mL of surface water were collected along depth gradients in the water column (lower boundary floc/water interface, upper boundary water/air interface) at each location. Samples were collected from a boat using a peristaltic tubing pump and tubing deployed at known depths from the surface of the water. At each sampling location for a given site, a metal extension pole was lowered to 0.5-m from the bottom and 0.5-m from the surface of the canal. Samples were collected at recorded depths. Unfiltered samples were collected into bottles (rinsed 3 times with unfiltered water). Filtered samples were collected into bottles (rinsed 3 times with filtered water). We collected 60 mL samples for TDP, 125 mL for TP and TOC, and 250 mL for TSS.

A similar method was used by UF to collect water samples at various depths across the canal at the S333 gate (**Figure 13a**).

Water Analytical Methods as used in FIU Laboratories:
Samples were analyzed using standard analytical methods. Water were analyzed for total dissolved phosphorus (TDP) and total phosphorus (TP; USEPA method 365.1 following dry ashing according to Solorzano and Sharp 1980), Total organic C (TOC; US EPA 415.1) was determined on a Shimadzu TOC-VCSH. Total suspended sediment was measured following Baird et al. (2017).

Laboratory Quality Assurance / Quality Control (QA/QC):
Florida International University maintains strict Quality Assurance and Quality Control procedures. Calibration curves are analyzed and summarized at the beginning of all analytical runs according to method specification. Standards, either citrus or apple leaves, are digested or combusted for all TP and TN/TC analysis. All standards are accepted within the analytical range as defined by the National Bureau of Standards (NBS). Analytical duplicate samples are analyzed (10% of total samples) in all analysis runs. Acceptable duplicate analysis is ± 15% relative percent difference (RPD). Matrix

spikes are analyzed at 5% of total samples in all analytical runs and are accepted at ± 20% recovery. Additionally, analytical blanks are (5% of total samples) analyzed in all runs. Method Detection Limit (MDL) for TSS spiked samples (13 mg/L) and blanks (2 mg/L) were measured on 5% of total samples. A total of 552 of 618 TSS samples were at or below MDL, and 4 samples contained negative values that were below the MDL and therefore determined to be equivalent to zero. All QA/QC results are included with a combined data file. The Southeast Environmental Research Center within the Institute of Environment at FIU utilized Chain of Custody forms to ensure all samples and analysis are accounted for and tracked.
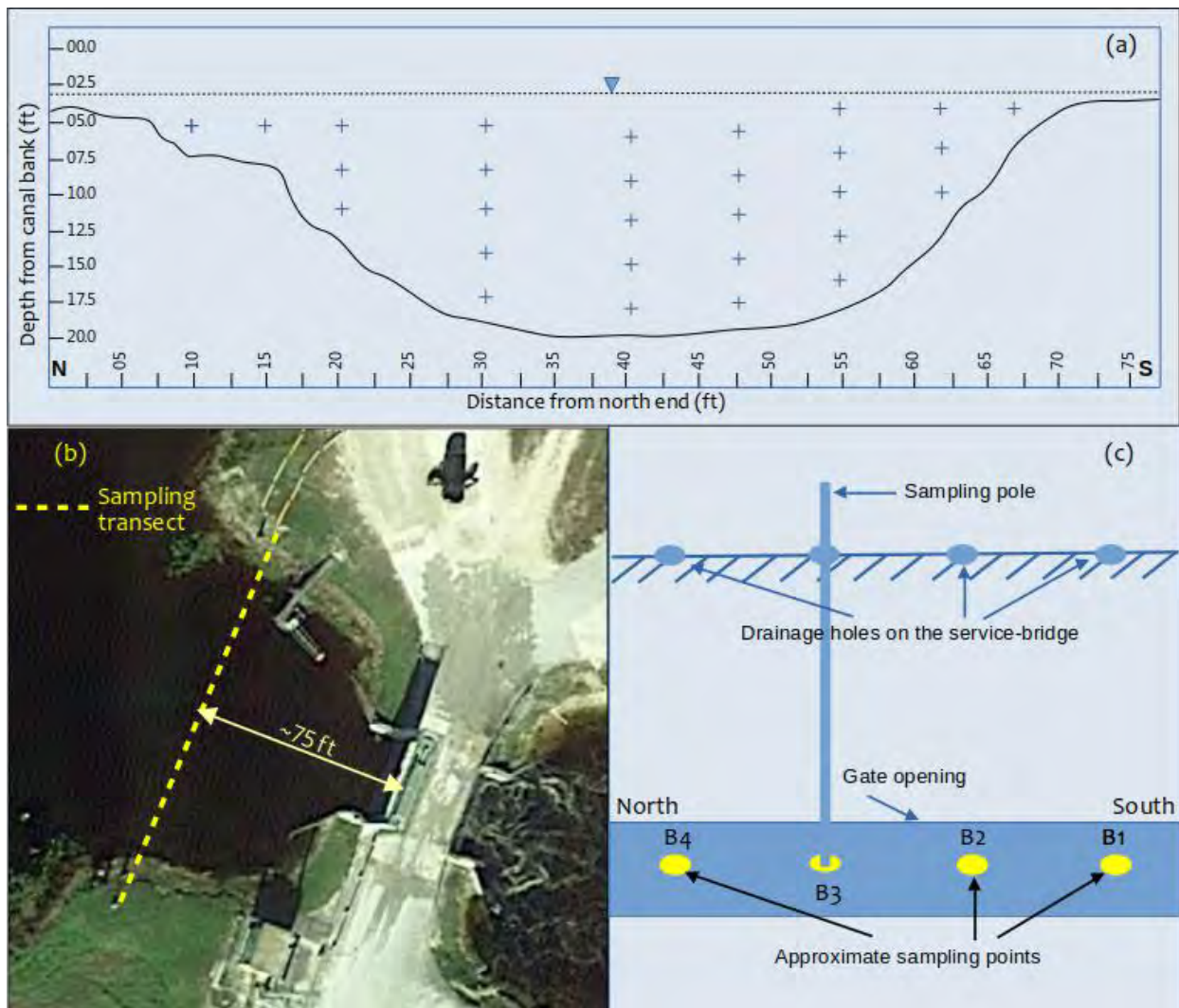
Figure 13: (a) Approximate depiction of 2-dimensional TP water sampling across the upstream at S333 gate ('+' indicates sampling points), (b) location of cross-sectional sampling transect near S333, (c) Illustration of downstream S333 gate water sampling from the service bridge at the gate opening. Univ. of Florida assisted with this sampling.

Table 1: *Sampling dates and existing flow conditions in L67A and L29 canals and at S333, S12D, and S12C gates.*

Sampling Date	Flow (cfs) NPS ADCP* measurement			Remarks for L29 Flow	Flow S12D (cfs) DBHYDRO	Flow S12C (cfs) DBHYDRO
	S333 gate	L67A (1500 ft)	L29 (1500 ft)			
14-Apr-22	366.74	389.10	-30.24	flowing east	18.5	0.0
25-Apr-22	209.92	259.59	-16.60	flowing east	10.3	0.0
5-May-22	228.08	229.84	-97.02	flowing east	7.0	0.37
26-May-22	307.13	410.32	-1.44	flowing east	0.0	0.0
7-Jun-22	454.31	577.84	142.58	flowing west	363.0	0.0
16-Jun-22	562.11	830.45	260.62	flowing west	0.0	0.0
27-Jun-22	670.85	1613.95	823.91	flowing west	558.0	315.0
*ADCP measurements at S333 gate, and L67A and L29 canals at ~1500 ft upstream were not taken simultaneously but in a sequential order.						

Data Analyses

We used linear fixed effects models to determine the main effects of site, depth of sample collection, and date as covariates on TDP, TP, TOC, and TSS. Due to the severity of non-normality in all variates, we used Kruskal-Wallis chi square non-parametric tests to compare differences among sites, depth, and dates. All analyses were conducted using the statistical software R v. 4.2.2 and RStudio v. 2022.12.0+353 (R Core Team 2022).

Results & Discussion

Water chemistry varied primarily by date across all sampling sites and depths. Water chemistry ranges were similar among sites with a few exceptions (**Figures 14A-D**), specifically L29-1 and L67-1 which contained exceedingly high values of TDP and TP (**Figures 14A-D)**.

Total Dissolved Phosphorus
Water TDP ranged from 4.9 to 37.3 µg L^{-1}, and TDP consistently declined across sites over time (**Figure 15A**, chi-squared = 527.45, *P* < 0.001). Water TDP did not change with water depth (chi-squared = 369.84, *P* = 0.105) within individual sites (no figure presented) or across all sites (chi-squared = 364.52, *P* = 0.145, **Figure 16A**). Water TDP was not related to TSS (**Figure 17A**).

Total Phosphorus
Water TP ranged from 14.3 to 299.5 µg L^{-1}, and TP generally increased with depth despite high variability (**Figure 16B**) and varied over time, but no significance was detected (date: chi-squared = 468.6, *P* = 0.369; depth: chi-squared = 475.7, *P* = 0.285, site: chi-squared = 477.5, *P* = 0.266). Water TP was not related to TSS (**Figure 17B**).
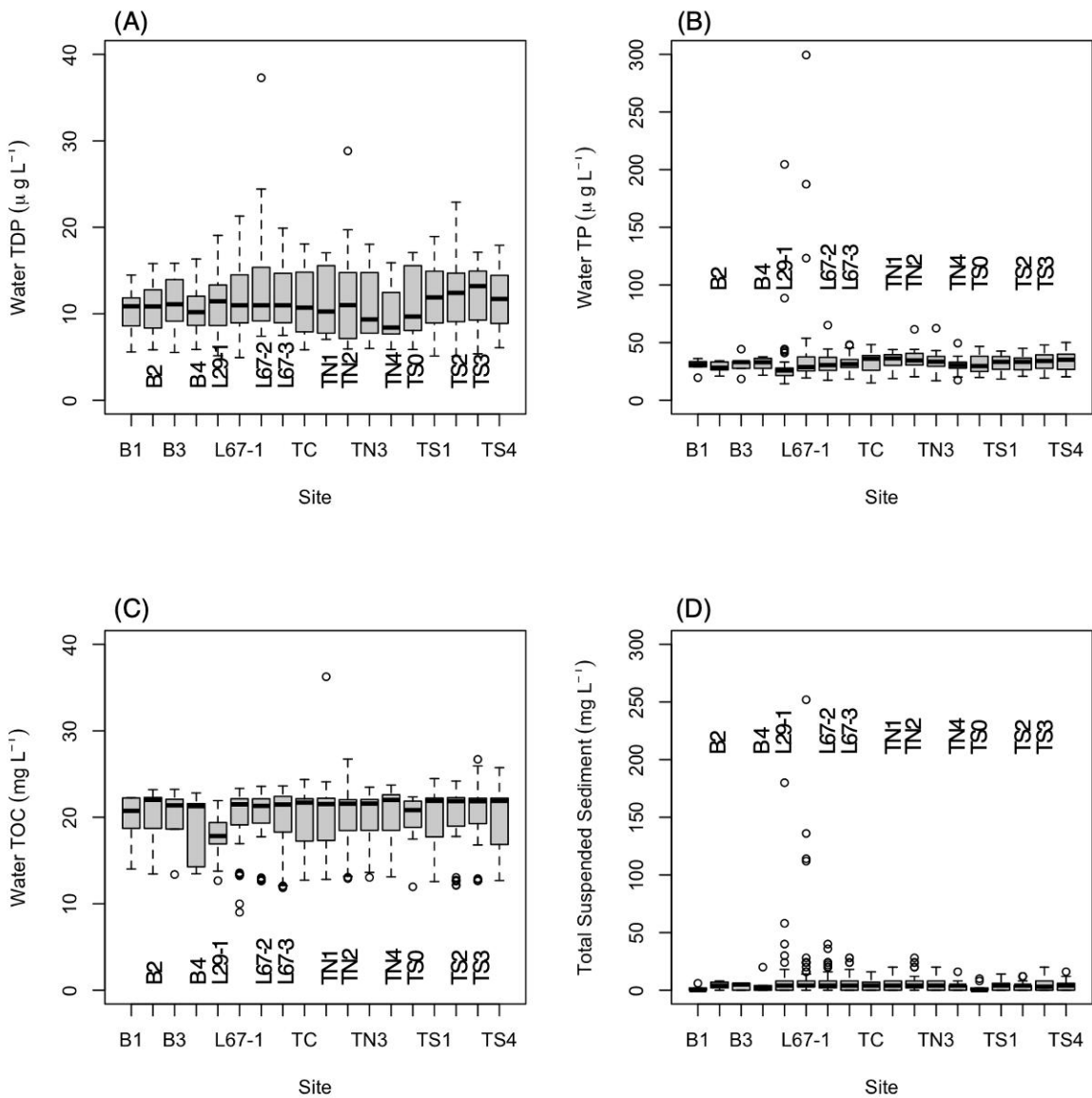
Total Organic Carbon
Water TOC ranged from 9.0 to 36.3 mg L^{-1}. Water TOC was consistently lowest at L29-1 and varied over time (date: chi-squared = 463.6, *P* = 0.017) and generally increased with depth despite high variability resulting in no significant depth and site trends (**Figure 16C**; (depth: chi-squared = 422.3, *P* = 0.222, site: chi-squared = 414.8, *P* = 0.260). Water TOC was not related to TSS (**Figure 17C**).

Total Suspended Sediments
Water TSS ranged from 0 to 252 mg L-1. Water TSS was similar among sites (site: chi-squared = 31, *P* = 0.101). High variability in TSS was observed over time and across depths (date: chi-squared = 151, *P* < 0.001; depth: chi-squared = 53, *P* < 0.001; **Figure 16D**).

Water TDP and TP concentrations do not follow the same responses to elevated flows in the L29 and L67 Canals; TDP declined over time during wet-season and TP were spatially and temporally variable. Comparing across all sites, mass ratios of TDP:TP were not related to TSS concentrations or water depth (**Figures 18A-B**). When analyzing transects immediately upstream of the S333 gate, we observed again no change in mass ratios of TDP:TP with depth but a decline with increasing TSS concentrations (**Figures 19A-B**). In summary, changes in water chemistry at these locations broadly occur during increased flows in the L29 and L67 Canals during the onset of the subtropical wet season. We observed temporal declines in TDP throughout the period of observation (**Figures 15A-E**) and no consistent site- or depth-specific patterns to these data. We detected episodic increases in TDP and TP concentrations at sites L29-1, L67-1, and L67-2 (**Figures 14A-B)**. Despite dates with high concentrations of TSS, TSS alone did not correspond to increases in TDP, TP, or TOC.

Figure 14: Water chemistry (A: total dissolved phosphorus, TDP; B: total phosphorus, TP; C: total organic carbon, TOC; D: total suspended sediment, TSS) across sites. Boxplots include median, upper and lower quartiles, and 95% confidence intervals of the range of values collected across all depths and dates at each sampling site.
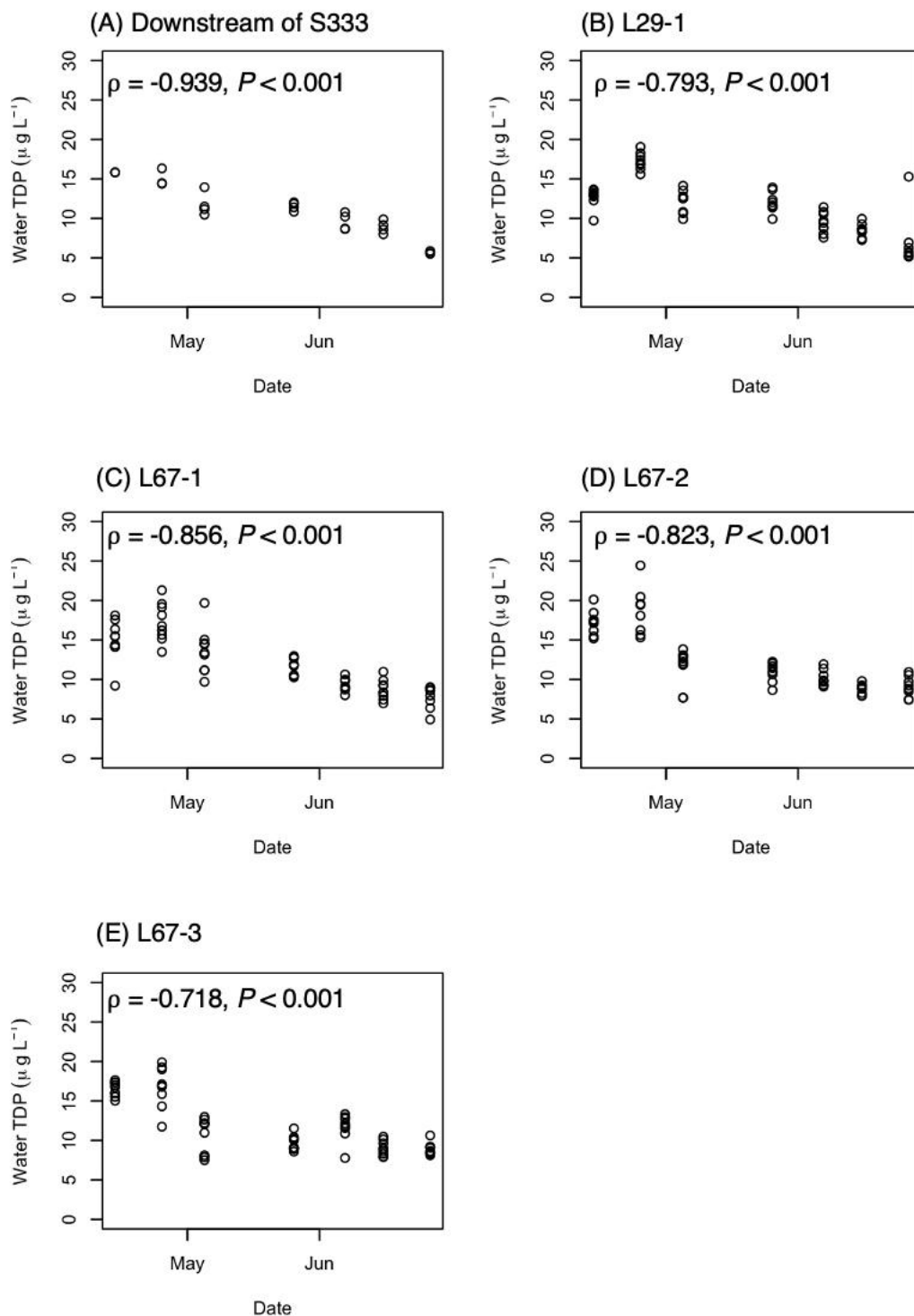
Figure 15: Example of changes in total dissolved phosphorus over time across downstream sites (A) B1-B4, and upstream sites (B) L29-1, (C) L67-1, (D) L67-2, (E) L67-3. Spearman's rho (ρ) and *P*-values provided for correlations.
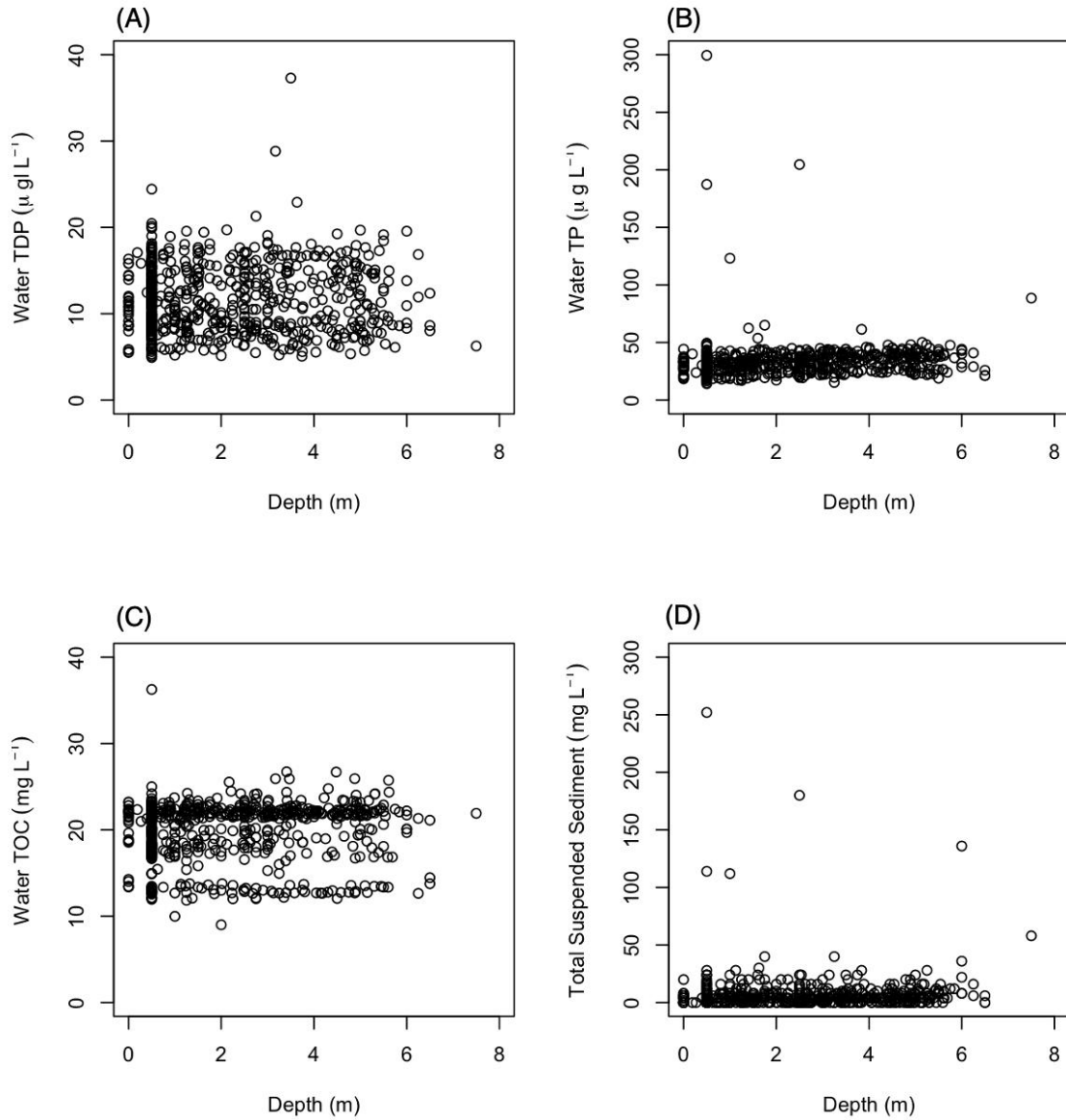
Figure 16: Water chemistry (A: total dissolved phosphorus, TDP; B: total phosphorus, TP; C: total organic carbon, TOC; D: total suspended sediment, TSS) at different water depths. Scatterplots include raw values collected across all sites and dates.
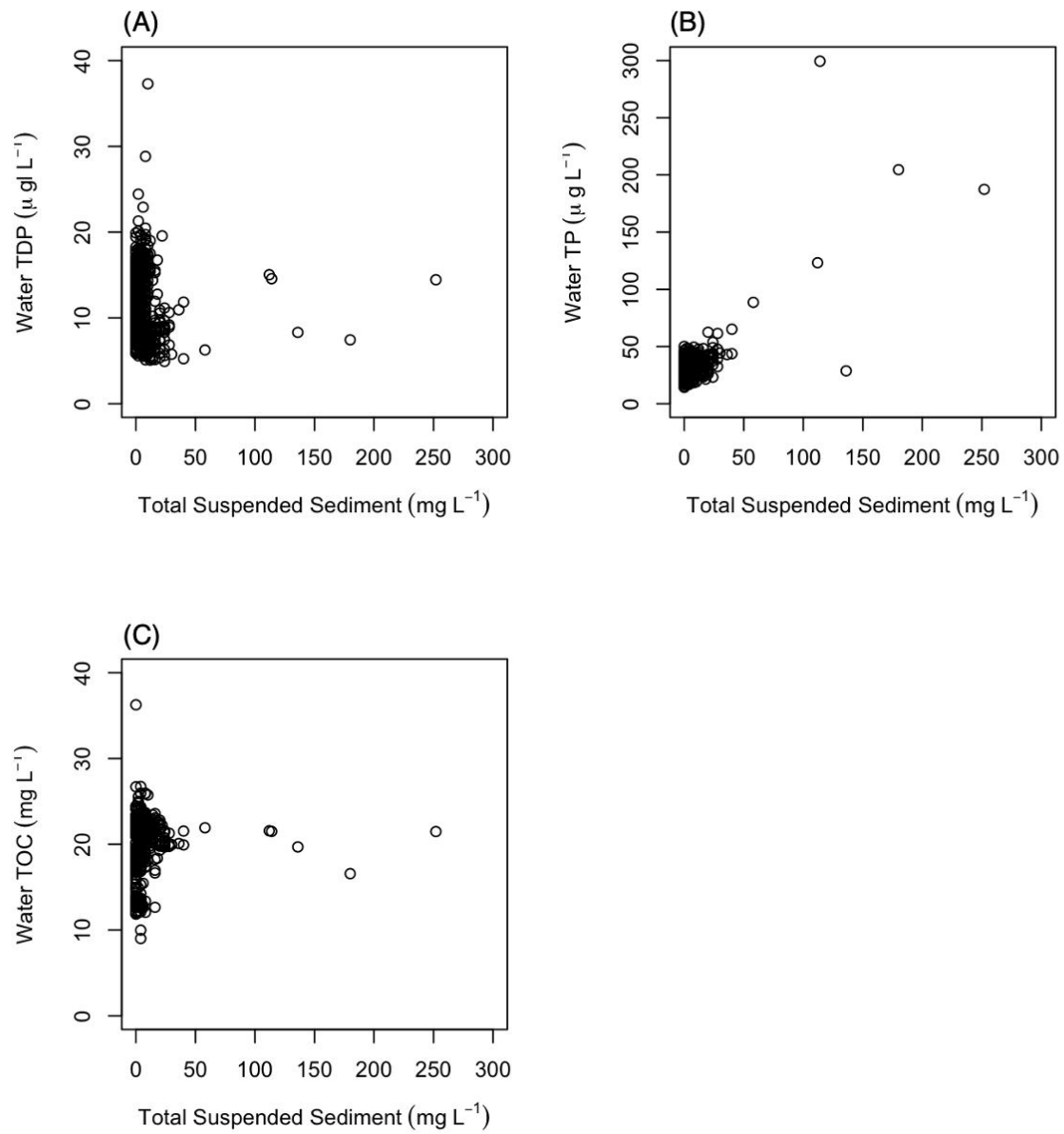
Figure 17: Comparisons of water chemistry (A: total dissolved phosphorus, TDP; B: total phosphorus, TP; C: total organic carbon, TOC) versus total suspended sediment, TSS. Scatterplots include raw values collected across all depths, sites, and dates.
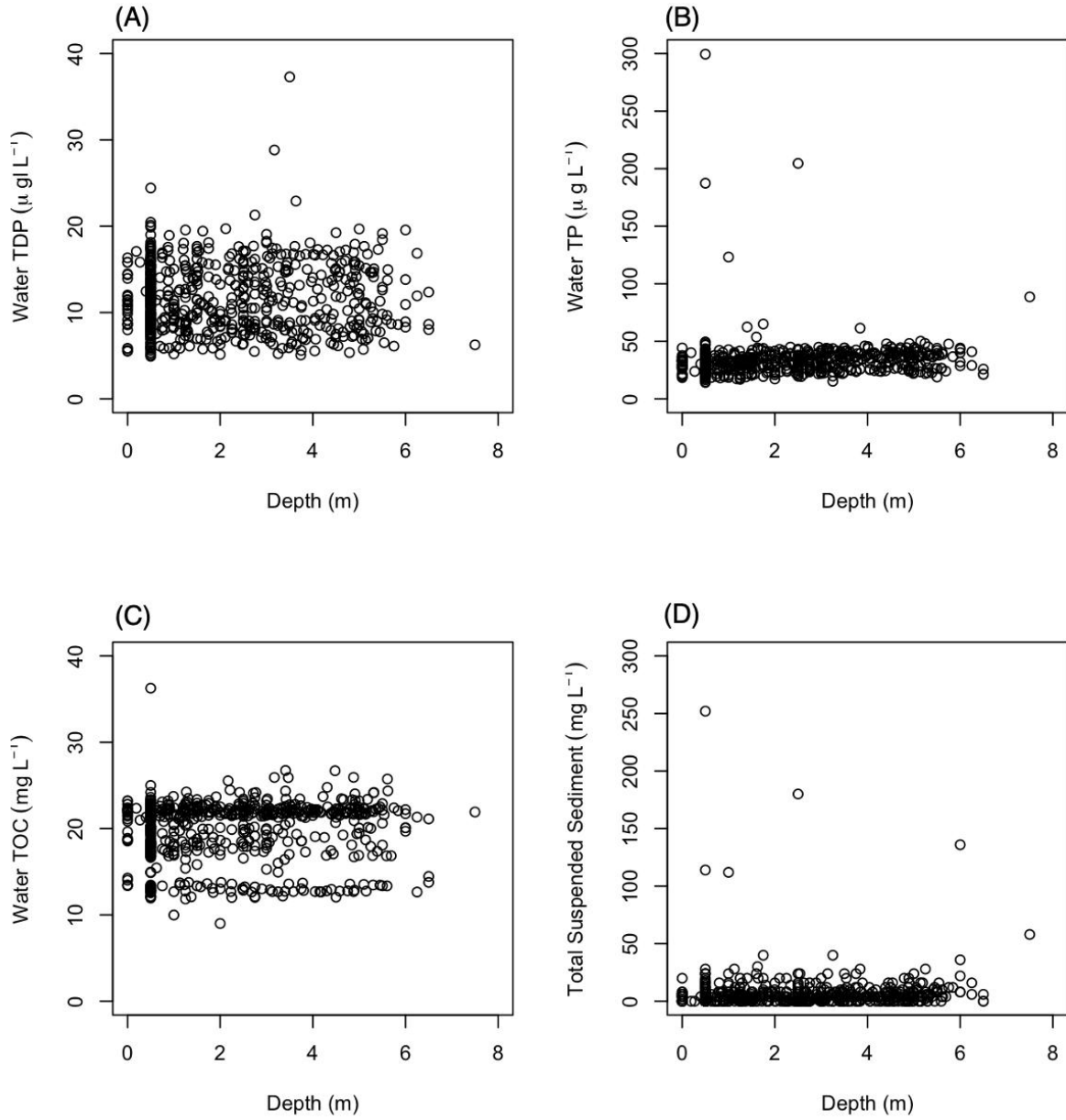
Figure 18: Comparisons of total dissolved phosphorus: total phosphorus mass ratios (TDP:TP) versus (A) total suspended sediment, TSS, and (B) depth. Scatterplots include raw values collected across all depths, sites, and dates.

(A) Upstream of S333 **(B) Upstream of S333**

ρ = -0.274, *P* < 0.001

ρ = -0.140, *P* < 0.01

TDP:TP

Total Suspended Sediment (mg L^{-1})
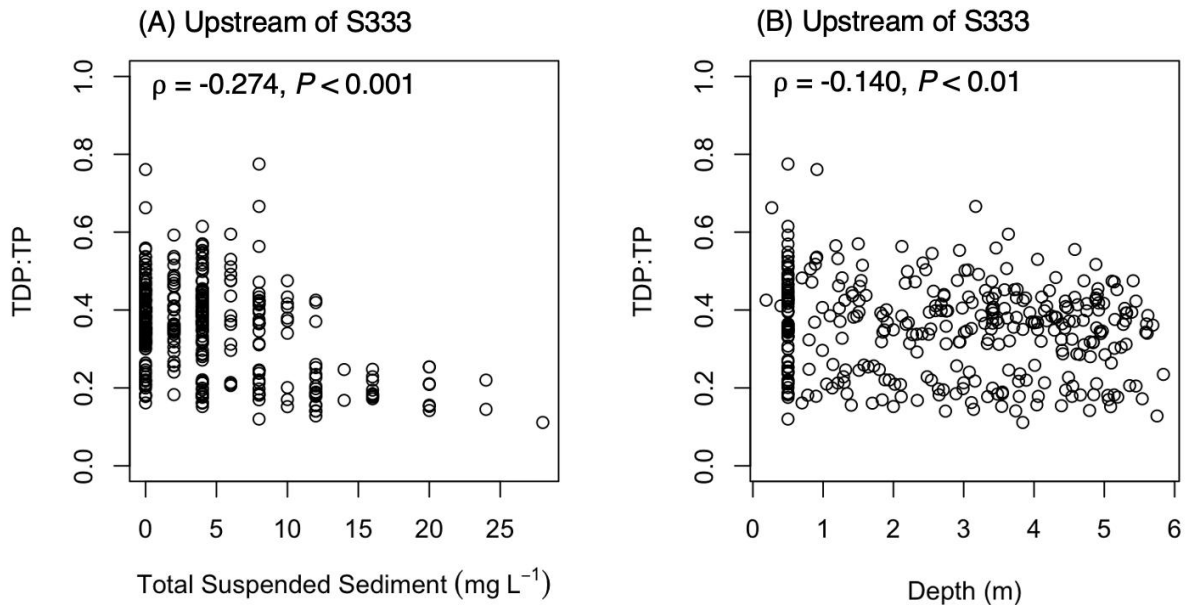
Depth (m)

Figure 19: Comparisons of total dissolved phosphorus: total phosphorus mass ratios (TDP:TP) versus (A) total suspended sediment, TSS, and (B) depth from transects immediately upstream of the S333 gate. Scatterplots include raw values collected across all depths and dates. Spearman's rho (ρ) and *P*-values provided for correlations.

Data Submittal

All data generated during execution of this project were submitted. All data collected during the project, associated metadata, and QA/QC reports were submitted to the ENP Agreements Technical Representative.

Acknowledgements: We thank ENP personnel Adam Karczynski and Amy Renshaw for providing previously collected ADCP data and Adam Karczynski for collecting ADCP data during this project. Sophia Hoffman, Rafael Travieso, and Liz Ortiz from FIU assisted with field sampling.

References

Baird, R. B., A. D. Eaton, and E. W. Rice. 2017. Standard Methods for the Examination of Water and Wastewater. APHA, Washington, DC, 23nd Edition.

Briceño, H., P. Gardinali, and R. Garcia. 2019. Mechanisms and Conditions responsible for elevated TP levels in   surface water discharges to Shark River Slough within Everglades National Park. Final Report 2019. Prepared by Florida International

University for South Florida Natural Resources Center, Everglades National Park Homestead, Florida.

Daroub, S.H., J.D. Stuck, T.A. Lang, and O.A. Diaz. 2002. Particulate Phosphorus in the Everglades Particulate Phosphorus in the Everglades Agricultural Area: II—Transport Mechanisms. SL198. Soil & Water Science Dpt. UFL. Gainesville. http://edis.ifas.ufl.edu.

Das, J., S.H. Daroub, J.H. Bhadha, T.A. Lang, O. Diaz, and W. Harris. 2012. Physicochemical assessment and phosphorus storage of canal sediments within the Everglades Agricultural Area, Florida. J. Soils Sediments (2012) 12:952–965.

R Core Team (2022). R: A language and environment for statistical computing. R Foundation for Statistical Computing, Vienna, Austria. URL https://www.R-project.org/.

SFWMD. 2018. DBHYDRO—South Florida Water Management District's Online database, http://www.sfwmd.gov/dbhydro, West Palm Beach.

SFWMD. 2018. Settlement Agreement Report, First Quarter, January – March 2018. Prepared for the Technical Oversight Committee July 12, 2018. Prepared by: Cheol Mo, Violeta Ciuca, and Jonathan P. Madden. Compliance Assessment and Reporting Section, Water Quality Bureau, SFWMD.

Gomez, M. and Martinez, E. (2014). 1D, 2D and 3D modeling PF A PAC-UPC laboratory canal bend. A: SimHydro International Conference. "SIMHYDRO 2014". Sophia Antipolis: 2014.

SECTION 3: ASV-HYDROACOUSTIC SEDIMENT PROFILING IN L67A AND L29 CANALS UPSTREAM OF S-333 AND S-333N GATED STRUCTURES FINAL PROJECT REPORT

ASV-Hydroacoustic sediment profiling in L67A and L29 canals upstream of S-333 and S-333N gated structures.

Final Project Report

(Submitted 8 March 2023)

(Task Agreement No. P21AC11341)

Camilo Roa, Ph.D. Principal Investigator

Email: croa@fiu.edu

Kevin M. Boswell, Ph.D. Co-Principal Investigator

Institute of Environment and Department of Biological Sciences,

Florida International University

11200 SW 8th Street, Miami FL 33199

Administrative Contact:

Regnier Jurado

Office of Research & Economic Development

Miami, FL 33199

E-mail: gutierrr@fiu.edu

Telephone: 305-348-2494; Fax: 305-348-4117

ABSTRACT:

The Central and South Florida Project resulted in an extensive network of canals, levees and impoundments and enhancements to preexisting canal systems to provide flood control and water supply in Florida. Sediments in canals L67A are suspected of contributing to increased total phosphorus (TP) peaks at the gate (S333 and S333N) that discharges into L29. Observed TP concentrations have over ~90% contribution from particulate phosphorus and less from soluble reactive phosphorus (Briceno et al. 2019). It is hypothesized that during period of relatively low flows (dry season) when water levels in the canal are relatively low and less connected to the marsh sediments accumulate in front of S333. At the onset of wet season, when flows increase, the elevated energy in flow column brings phosphorus loaded sediments in suspension which contribute to increased TP peaks that get flushed downstream within ~3-4 weeks period.

This project measured sediment thickness and bed-volume with Simrad EK80 echosounders and Kongsberg M3 multi-beam sonar along the L67A and L29 canals and near S333-S333N structure. Sediment estimates were done using backscatter from 38, 70 and 200 kHz transducers. Sediment thickness estimates were compared to core sample measurements, collected independently, and had an average error of 50%. Bathymetry of the survey area was also calculated.

1.   Introduction

The Central and South Florida Project resulted in an extensive network of canals, levees and impoundments and enhancements to preexisting canal systems to provide flood control and water supply in Florida (South Florida Water Management District, 1999). The Water Conservation Areas were completed in the 1960s, resulting in impoundment and loss of ecological connectivity throughout the central and southern Everglades. The creation of the L29 canal and levee critically limited overland flow into Shark River Slough through small culverts. Construction of the Tamiami Trail (US 41 highway) was completed in 1928 (Schellhammer, 2012). The purpose of this roadway was to connect the east and west coasts of Florida; however, this road also functioned as a significant ecological and hydrologic barrier between the northern and southern Everglades.
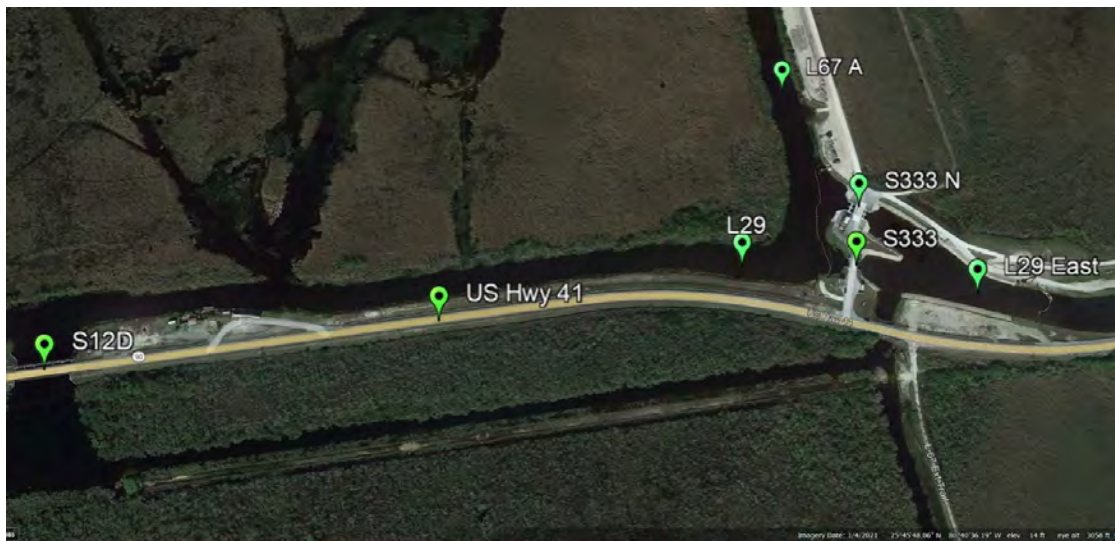

Figure 1. Two-gate structure (S333 and S333 N) at the intersection of canals L67A and L29.

Northeast Shark River Slough receives water that passes through the S333 complex. The complex is composed of a two-gate structure (S333 and S333 N gates) at the southern end of the L67A canal (**Figure 1**). The complex discharges into the L29 east canal. Water discharged through the complex enters Northeast Shark River Slough through a series of culverts and the 1-mile and 2.6-mile bridges on Tamiami Trail.

Sediments in L67A canal are suspected of contributing to increased total phosphorus (TP) peaks at S333 in relation to source waters monitored at other gated structures (S151 and S152) in the canal system (**Figure 2**). Observed TP concentrations have over ~90% contribution from particulate phosphorous and less from soluble reactive phosphorus (Briceno et al. 2019). It is hypothesized that during relatively low flows (dry season) sediments accumulate in front of S333. At the onset of wet season, when flows increase, the elevated energy in flow column entrains phosphorus loaded sediments which contribute to increased TP peaks that gets flushed downstream within ~3-4-week period.
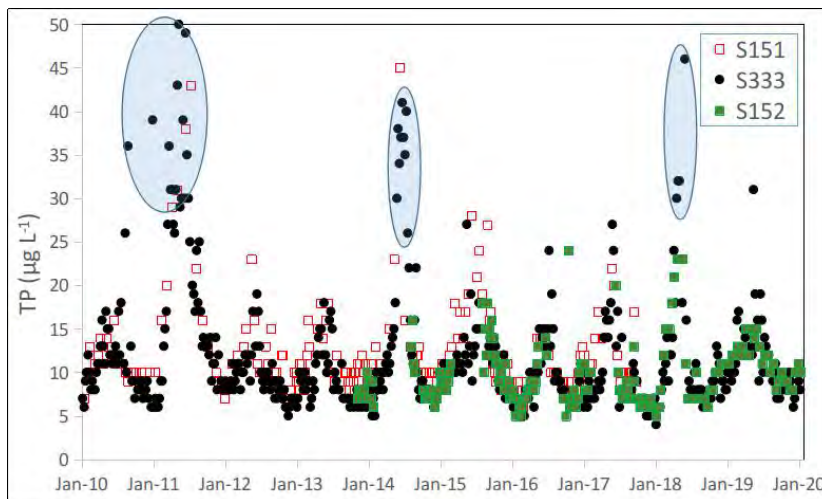
Figure 2. Total phosphorus grab sample concentration at S151, S152, and S333 monitoring locations. TP peaks at S333 are higher than S152 in L67A canal, a major source of waters to S333.

Acoustic configurations, using buried hydrophones, showed promising results on estimating sediment thickness (Hefner et al., 2009), but these configurations are typically applied on environments with depths greater than 10 m and up to several hundreds. They are usually not applicable on waters shallower than <5 m due to the limitation imposed by the near-field phenomena. They also require boats with large footprints.

Acoustic studies in shallow waters (<5 m) and relatively small sediment thickness (~1 m) are typically done with echosounders, to guide core sample methods (Anderson, 1950). Commercial echosounders, a kind of sonars where the acoustic beam is projected vertically downwards, have been proposed as tools for analyzing sediment composition and sediment thickness (Eleftherakis et al., 2012; Klusek et al., 2010; Komen et al., 2021). A combination of low frequency (~38 kHz) and high frequency (>200 kHz) echosounders is commonly used. Low frequency echosounders have greater sediment penetration but larger near-field, while high frequency echosounder have lower penetration but smaller near-field. The nearfield is the volume of area surrounding the echosounder transducer where the acoustic wave equation model breaks down; data collected within that volume tends to have a large error and is usually discarded (Parker-Stetter, 2009). In

3

addition, echosounders have a spatial resolution that affects their detection capabilities (Ehrenberg & Torkelson, 2000). The spatial resolution is the minimum distance two targets need to be separated for an echosounder to differentiate them; if the targets are closer, the echosounder would detect them as one. Studies that estimate sediment thickness are generally conducted at depths >5 m (Gaida et al., 2020), to avoid the near-field of low frequency echosounders, which is typically close to 5 m; and for sediment thicknesses close to 1 m (Anderson, 1950), to minimize the spatial resolution limitation.

The acoustic wave needs to penetrate through the entire sediment thickness to have an accurate estimate. There is a direct relationship between sediment penetration and the intensity of the acoustic wave, seen as power used by the acoustic device. Low frequency waves penetrate greater distances than high frequency ones, for the same equivalent intensity. Therefore, only low frequency echosounders can penetrate deep enough without using excessive power.

For commercial echosounders, only the 38 kHz is capable of enough penetration; non-commercial echosounders, either built in-house or modified from commercial ones, could penetrate more if they are designed around a lower frequency or have a larger power source, but they are not readily available, and their setups are often not reproducible.

The objective of this effort is to examine the feasibility of estimating the sediment thickness with commercial echosounders along the L67A and L29 canals and quantifying sediment bed-volume in these two canals near S333 and S333N structure (**Figure 3**). In addition, bathymetry of the study site will also be produced.

2.   Materials and methods

2.1. Study site
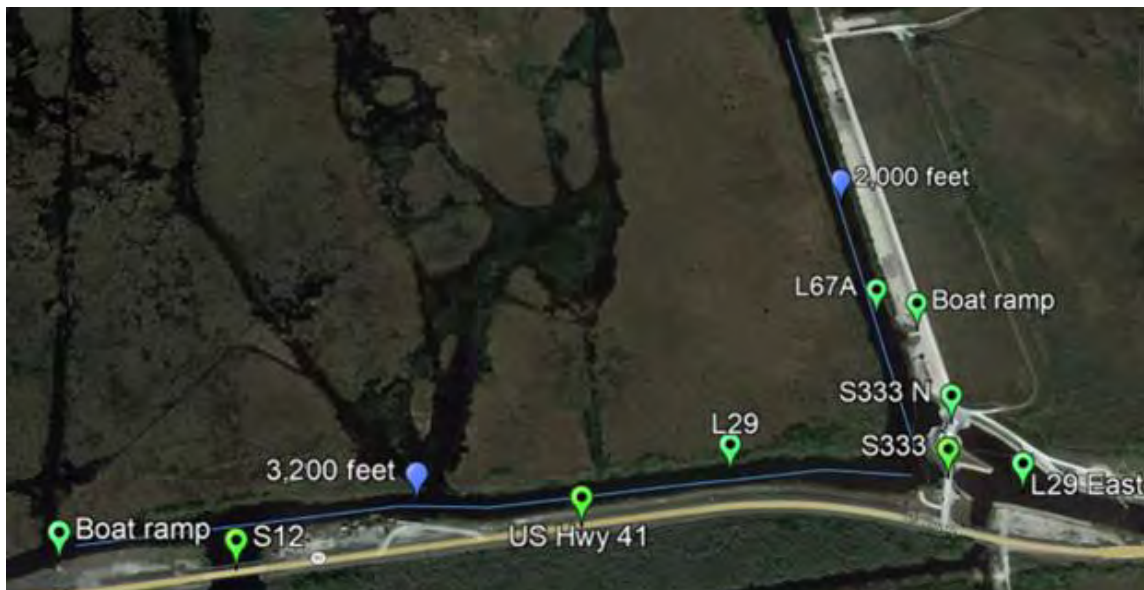
Figure 3. Survey area and distances from S333 in the canals L67A and L29.

The survey area consists of separate sections on the canals L67A and L29 of 2,000 ft (609.6 m) and 3,200 ft (975.36 m), respectively, with an average width of 100 ft (30.48 m). Two gates

4

(S333 and S333N) that regulate the discharge to L29 east canal are located at the intersection of L29 and L67A (lat: 25.762275, lon: -80.67449). Canal L67A flows north to south and L29 west (west of S333) can flow in both east and west direction depending on head gradients and gate openings (S333s and S12s gates). Access to the canals was possible by two ramps located north of gate S333 N and west of gate S12 (**Figure 3**). The survey area had a mean depth of 4 m which for this study is considered shallow waters.

Figure 4. Examples of different obstacles (piers, piles, and overgrown vegetation) that were present in the study site.

The acoustic survey was conducted on 04/06/2022, 04/07/2022 and 05/16/29022. There was no boat traffic observed during those days. Two crews were working at the same time: University of Florida core sampling crew and Florida International University acoustic sampling crew. Although the crews were working on different areas of the canals, sometimes they overlapped. The survey site had obstacles like piles, piers, and overgrown vegetation at the canal's sides, that were identified from satellite images and during field visits (**Figure 4**). The booms in front of the gates were removed during survey's days 04/06/2022 and 04/07/2022.

2.2. Hydroacoustic investigation

The acoustic survey was carried out using an autonomous surface vehicle (ASV; SeaRobotics). It automatically followed a programmed GPS trajectory; to guarantee sufficient coverage the ASV speed was kept at 4 knots (2 m/s). The vehicle was monitored from a station established near S333 structure. Obstacles like boats, pilons, or vegetation were avoided by temporarily taking remote control of the vehicle via radio frequency. Data were recorded on an internal hard drive and retrieved once the vehicle was recovered from the water. ASV's navigation system provided

time and GPS position to the on-board acoustic instrumentation. The average error of the ASV's GPS is less than 1 cm. All acoustic data were spatially and temporally synchronized at each deployment. Multiple deployments (04/06/2022, 04/07/2022, and 05/16/2022) were performed, guarantying redundant data.

2.2.1. Acoustic instrumentation
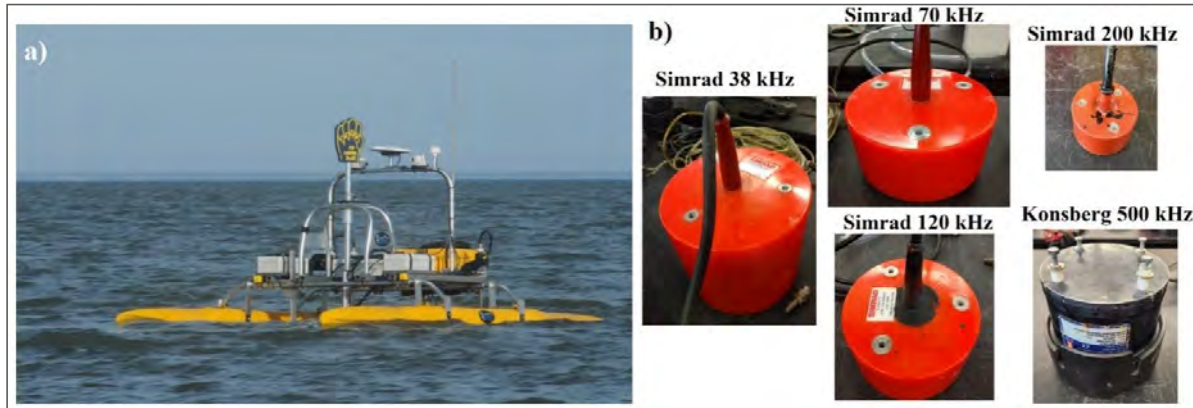
Figure 5. a) FIU's autonomous surface vehicles with **b)** acoustic instrumentation.

The ASV was instrumented with an echosounder (Simrad EK80) operating at 38, 70, 120, and 200 kHz, and a multi-beam sonar (Konsberg M3) operating at 500 kHz (**Figure 5**). The echosounder collected data to analyze the sediment thickness while the multi-beam collected data for a bathymetry map.

Echosounders have a transducer for each main (center) frequency they operate at. A characteristic single-beam pattern consists of a main lobe, where most of the acoustic energy is concentrated, and several side lobes. The beam is usually 5º to 15º wide. Multi-beam sonars, on the other hand, produce several lobes of similar form at once in a fan-shaped pattern. This setup allows for wider sound coverage, around 120º (Simmonds & MacLennan, 2005). Due to the more concentrated energy on the echosounder's beam, they were used for sediment penetration. Conversely, due to their wider coverage, the multi-beam sonar was used for bathymetry mapping (**Figure 6**).
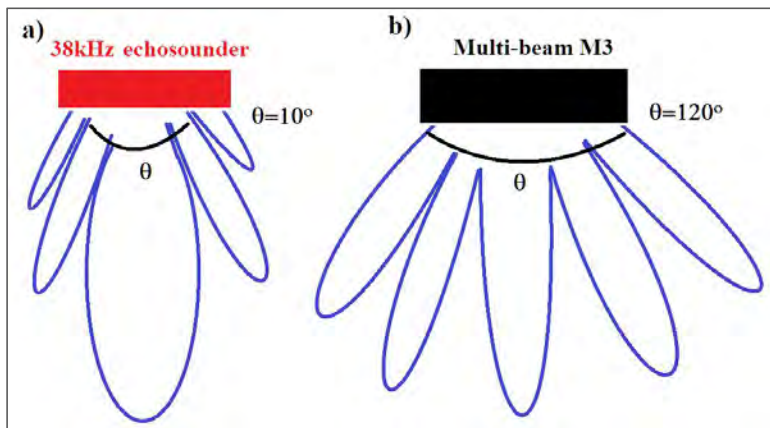
Figure 6. a) echosounder and **b)** multi-beam typical beam patterns.

When echosounders operate at a specific single frequency, it is commonly called continuous wave mode or CW. At CW there is usually a trade-off between spatial resolution and signal-to-noise ratio. However, some echosounders can also collect data at multiple frequencies; this is called FM slide or chirp. Multiple frequencies are compressed in time in a chirp and later detected in the echo by a match filter. The result is a narrow band of frequencies centered at the main frequency of the transducer. If several FM transducers of increasing main frequency are used together (38 kHz, 70kHz, 120kHz, and 200 kHz), a spectrum of frequencies from 38-200 kHz can be obtained. These data are called broadband data. Compared to CW mode, FM reduces the spatial resolution of a specific transducer without sacrificing its signal-to-noise ratio (Ehrenberg & Torkelson, 2000). For this study, both CW and FM modes were used, but only data collected at FM was used for the sediment estimates.

2.3. Survey transects
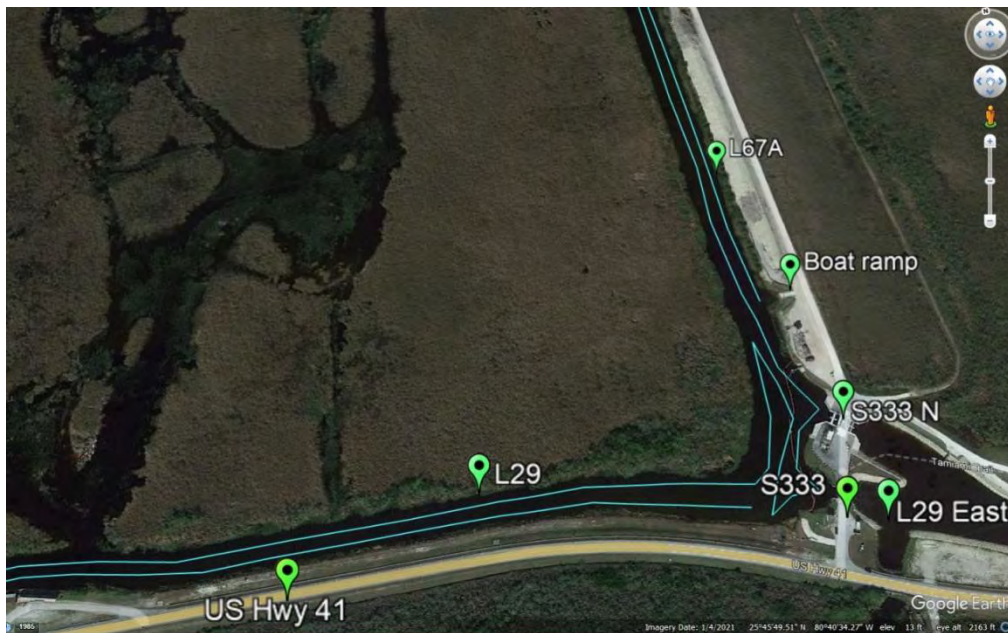
Figure 7. ASV transect representations (light blue lines) of the survey on canals L67A and L29.

Longitudinal transects were designed to cover the surveyed area (**Figure 7**). Transects were not drawn too close to the shores to prevent the vehicle from getting entangled in the overgrown vegetation. The insonified area on the canal's floor depends on the acoustic instrument. It can be assumed as cone with a projected circle on the floors, like a flashlight illuminating a wall. The projected circle's diameter (x) can be approximated by assuming a trigonometric relationship dependent on the transducer's depth and beam angle:
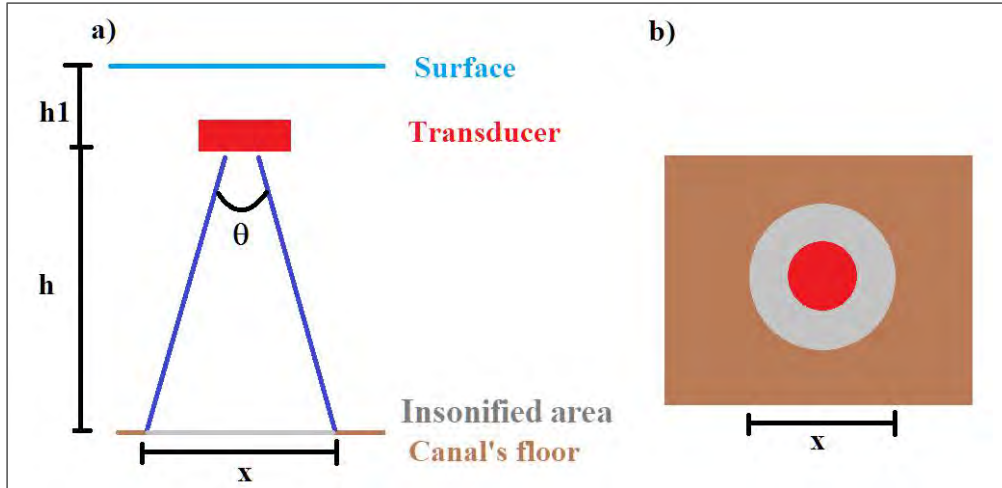
Figure 8. Depiction of insonified area equation, a) side view, b) top view.

$$x = 2(d - h1)\tan\left(\frac{\theta}{2}\right), d = h1 + h \qquad \text{Equation 1}$$

where d is the canal's depth, $h1$ is the transducer's depth (1 foot, ~30 cm), and θ is the beam angle (**Figure 8**). Considering an average width of the canal of 15 m ($w=15\ m$) and an average depth of 5m ($d=5\ m$), the insonified diameter of the projected circle for the multi-beam is 16.2 m ($x_{M3}=16.2\ m$), and for the 38 kHz echosounder is 0.82 m ($x_{EK80}=0.82\ m$) (**Figure 9**).
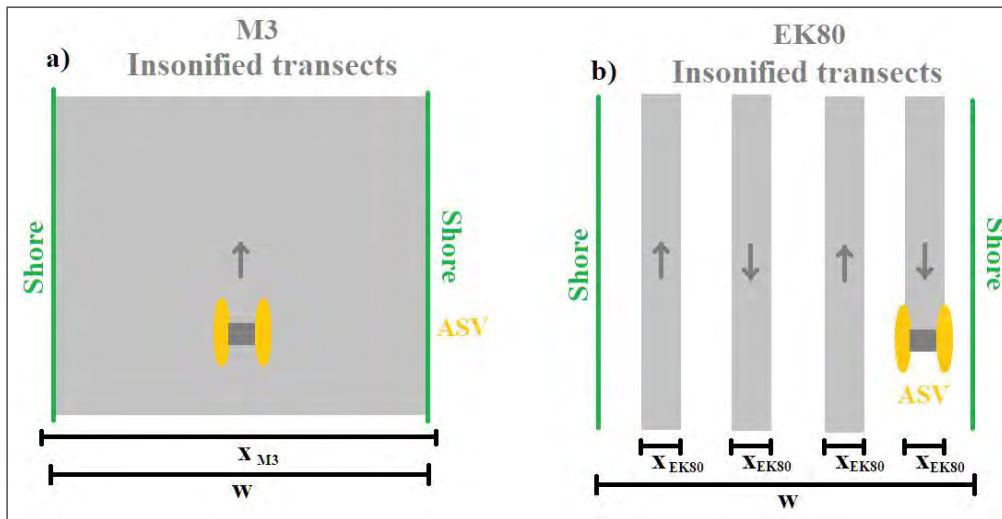
Figure 9. Top view of the approximation of the insonified area for **a)** multi-beam M3 and, **b)** echosounder EK80.

The multi-beam had a wide beam angle (120°) that allowed for a 100% insonification of the canal floor on just one transect. The echosounder had a much narrower beam angle (10^0, for 38 kHz); their total insonified area was approximately 33% of the canal floor. Considering that the 38 kHz frequency is the one with more penetration, the insonified area was calculated using it as reference.

8

The time taken to survey the entire area was approximately 6 hours per day. Deployment, calibration of the equipment, obstacle avoidance, and assessment of the data required 2 additional hours. All these processes were repeated on each survey day.

2.4. Data analysis

2.4.1. Canal sediment core samples

University of Florida provided 79 core sample sediment thickness, taken from the survey during April and May 2022. Core samples were used for ground truthing the acoustic estimates of sediment thickness. The core samples had a mean thickness of 30.04 cm, a maximum of 55.90 cm, a minimum of 8.50 cm, and standard deviation of 14.20 cm. Locations and thickness of core samples are presented in **Figure 10**. Error of core samples' GPS positions are less than 1.5 m. Thickness of most of the samples is between 40 and 50 cm (**Figure 11**).
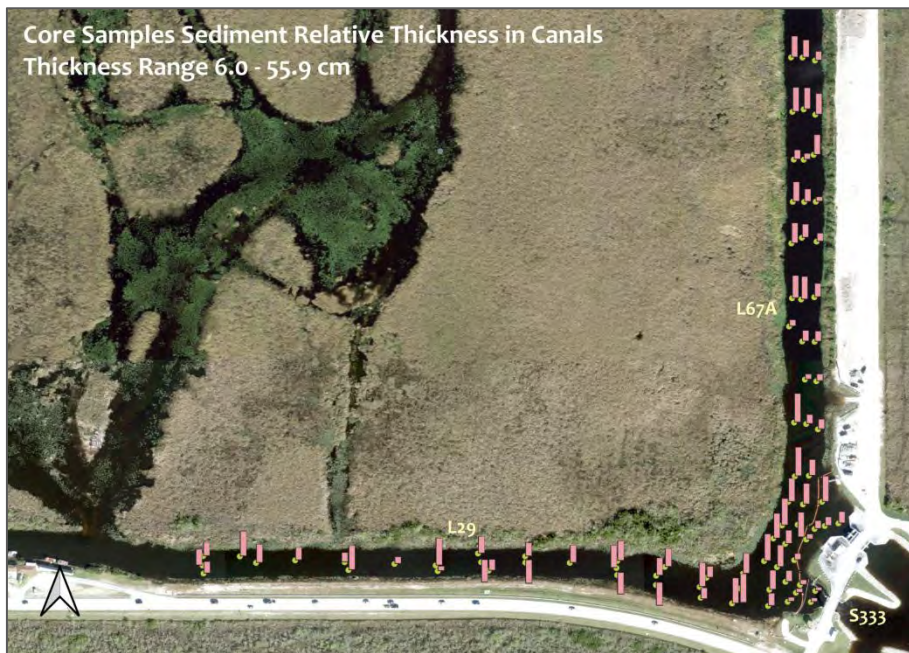
Figure 10. Sediment core locations and relative thickness (range: 6.0-55.9 cm) in canals L29 and L67A (data provided by University of Florida).
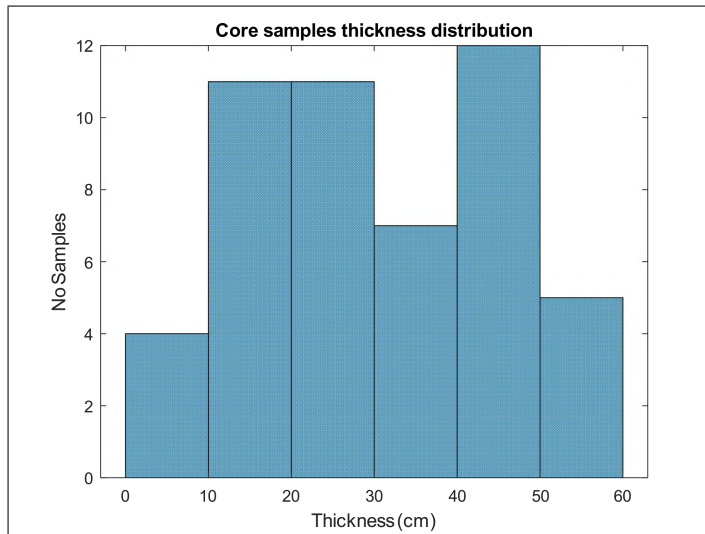
Figure 11. Histogram showing distribution of sediment core samples thickness.

2.4.2. *Canal bathymetry*

The bathymetry, obtained with the multi-beam sonar, was used to estimate the depth of the canal with a 2D horizontal resolution of 0.4 cm, a vertical resolution of 0.5 cm, and a minimum detectable depth of 40 cm. High-resolution bathymetric profiles of the canal were generated from the multi-beam sonar data using QPS's Qimera bathymetric analysis software. The resolution of the multi-beam sonar is very high. Most of the error, seen as outlier data points floating above the average bottom, was filtered out manually and by Qimera's algorithms.

2.4.3. *Canal sediment thickness estimation*

Echosounders collected volume backscatter data from the canal bottom, at frequencies of 38 kHz and 200 kHz, and normal incidence. With an estimated 1-3 dB/m attenuation for mud sediments (Stoll, 2016), the echosounder sediment penetration was expected to be greater than 1 meter (Mitchell, 1993). The backscatter data were used to model the sediment thickness at those edge frequencies (38 kHz and 200 kHz) to generate a vertical multilayer sediment profile. On day 05/16/2022, frequency transducer of 70 kHz was used as the high frequency edge due to malfunction on the 200 kHz.

Sound at 38 kHz penetrated down to the bedrock, while sound at 200 kHz was reflected at the water-sediment intersection layer. The spatial vertical difference between these two layers provided thickness estimates for sediment deposited across the canal floor (**Figure 12**).
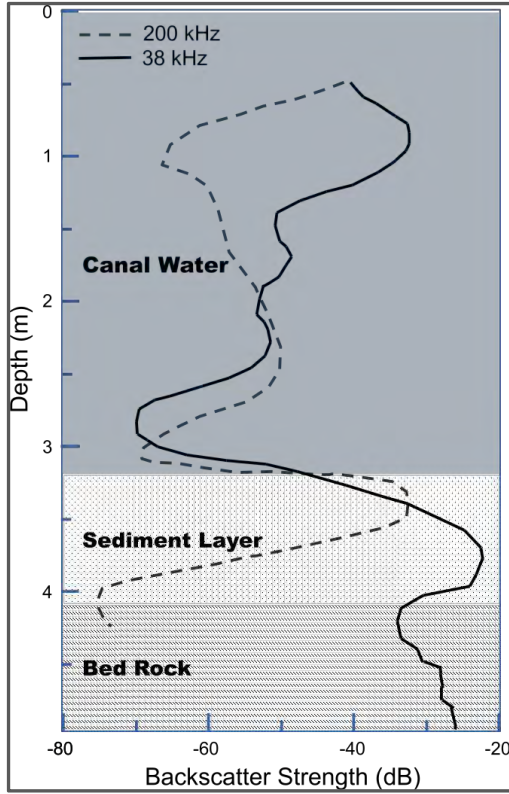
Figure 12. Conceptual illustration of echograms showing volume backscatter strength as function of depth from transducer face at 38 and 200 kHz.

The acoustic data were analyzed using acoustic processing software Echoview (Echoview, 2022). Acoustic data were presented by Echoview in the form of echograms (vertical cross-sections of the water column) and exported as CSV files.

The use of a 38 kHz transducer imposed a limitation on the minimum depth where reliable data could be collected. That minimum depth is given by the near field, which is the volume of water around the transducer where the acoustic equation model is not linear. Near-field distance is given in terms of distance from the transducer (Equation 2); most echosounders are designed to work outside the near field, as a rule of thumb, reliable data is obtained beyond twice the near-field distance. Near-field calculation were done base on the following equation (Rudstam & Sullivan, 2023)

$$R_{nf} = \frac{\left(\frac{2a}{100}\right)^2}{\lambda}, \quad a = \frac{1.6*100}{k\sin\left(\frac{\theta_{3db}}{2}\right)}, \quad k = \frac{2\pi}{\lambda} \qquad \text{Equation 2}$$

where λ is the wavelength, a is the active radius, and R_{nf} is the near-field distance.

For this project, the near-field distance was 0.42 m, on 04/06/2022 and 04/07/2022, and 1.36 m, on 05/16/2022; since the transducer was submerged 30 cm, the minimum depth then was 1.14 m and 3.0 m for the same days, respectively. On 05/16/2022 a 38 kHz transducer with a wider beam angle to improve insonified area was used, which explains the differences in the near-field distances. Acoustic samples shallower than the minimum depth were removed (1.9% approx.),

11

most of them on the shallower west side of the L29 canal. Sediment thickness estimations with negative values due to incorrect selection of the boundaries were ignored (10% of samples approx.). Estimations were done in Matlab. Two methodologies were used.

2.4.3.1. Data Processing Methodology 1 (Echoview)
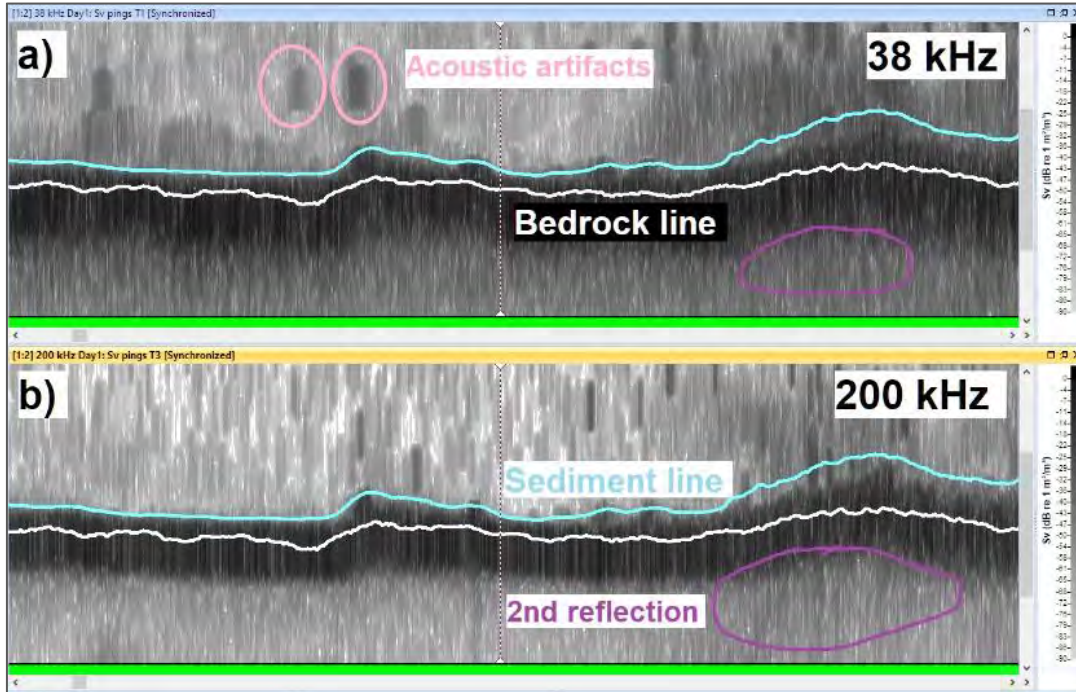
Figure 13. Echogram of acoustic data for **a)** 38 kHz transducer and **b)** 200 kHz transducer. Data was collected on 04/06/2022. White lines represent the sediment-rock boundary, called bedrock line, and detected by the 38 kHz transducer; and teal lines represent the water-sediment boundary, called sediment line, and detected by the 2000 kHz transducer. Some acoustic artifacts (possible vegetation, fish, bubbles, or debris) are circled in pink. Start of second reflection circled in purple.

Differences in the backscatter reflection corresponding to the water-sediment boundary, perceived at 70/200 kHz, and the sediment-bedrock boundary, perceived at 38 kHz, were identified by changes in the intensity of the volume backscattering strength (Sv). These boundaries are seen as a change in color from lighter to darker on the echogram of **Figure 13**, and are called sediment line and bedrock line, respectively. Acoustic data from second or third reflections, which are echoes that have bounced back and forth between the bottom and the water surface, were not used.
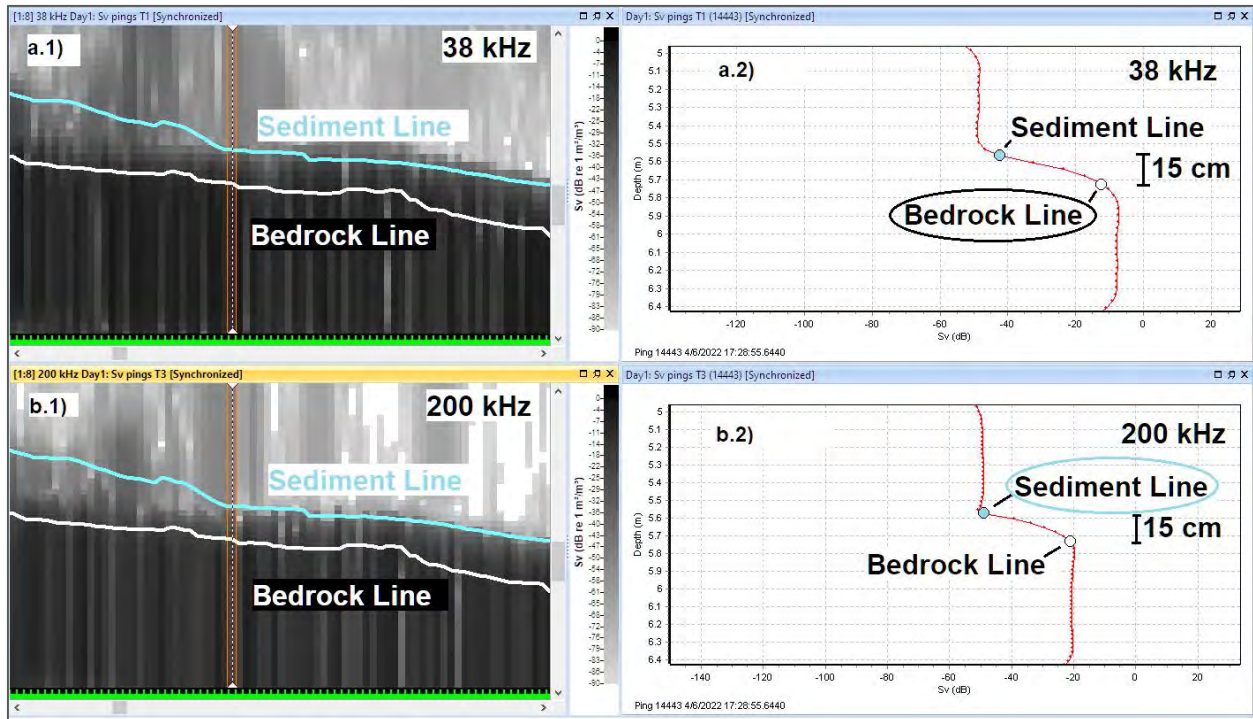
Figure 14. Echograms of **a.1)** 38 kHz and **b.1)** 200 kHz, and ping graphs of **a.2)** 38 kHz and **b.2)** 200 kHz at a specific GPS location (orange band on echograms). Sediment and bedrock lines were found using Echoview's "bottom detection algorithm". The vertical difference (sediment thickness) between sediment and bedrock lines was 15 cm approx. Core sample estimate at that location was 20 cm. Data from 04/06/2022.

Sediment and bedrock lines were calculated in Echoview by its "bottom detection algorithm" (Echoview, 2023). Both lines were exported as csv files, containing GPS coordinates and their associated depths. Matlab software was used to calculate the thickness of the sediment by taking the difference in depths at the same GPS position of the two lines extracted. The vertical difference between the two lines is the sediment thickness at that specific GPS coordinate.

Ping graphs are Sv vs. depth plots and help to recognize changes on backscattering strength (**Figure 14**). It was observed in Echoview, that the vertical difference (sediment thickness) between the sediment line, at 70/200 kHz, and the bedrock line, at 38 kHz, matched the core sediment thickness only at a few locations. For most core sample locations, the acoustic estimate was within 10 cm.

2.4.3.2. *Data Processing Methodology 2 (Matlab)*

To improve the sediment thickness estimation, a different methodology that detected the water-sediment and sediment-bedrock boundaries more accurately was developed. Backscatter data containing water-sediment and sediment-bedrock boundaries were exported from Echoview and processed in Matlab to find the sediment and bedrock lines. Typical values of bedrock backscattering strength range from 0 dB to -20 dB, while backscatter from sandy sediments range from -20 dB to -40 dB (Trzcinska et al., 2021). The peak closest to -20 dB and -40 dB, represented the transition between water and sediment and sediment and bedrock. We programmed an algorithm in Matlab that read all the pings and founds the closest peak to the

maximum value at 200 kHz, labeled sediment peak, and the closest peak to the maximum value at 38 kHz, labeled bedrock (**Figure 15**). The depth of all sediment peaks across pings represented the water-sediment boundary (sediment line, blue) and the one of all bedrock peaks, the sediment-bedrock boundary (bedrock line, red) (**Figure 16**). Sediment and bedrock lines were smoothed using an average filter with a window of 50 samples.
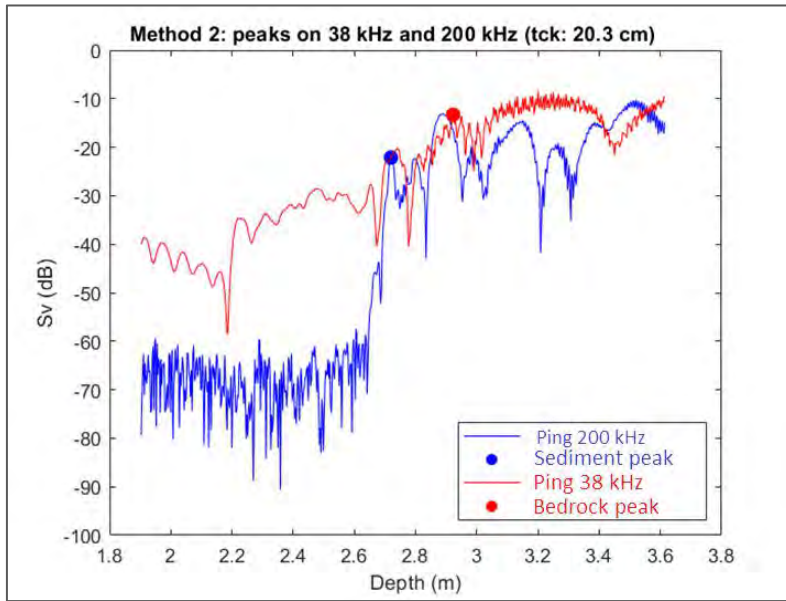
Figure 15. Individual ping at 200 kHz (blue), assumed to be water-sediment boundary and its sediment peak (blue dot); and ping at 38 kHz (red), assumed to be sediment-bottom boundary and its bedrock peak (red dot). Methodology 2. Sediment thickness was calculated as 20.3 cm for this sample.
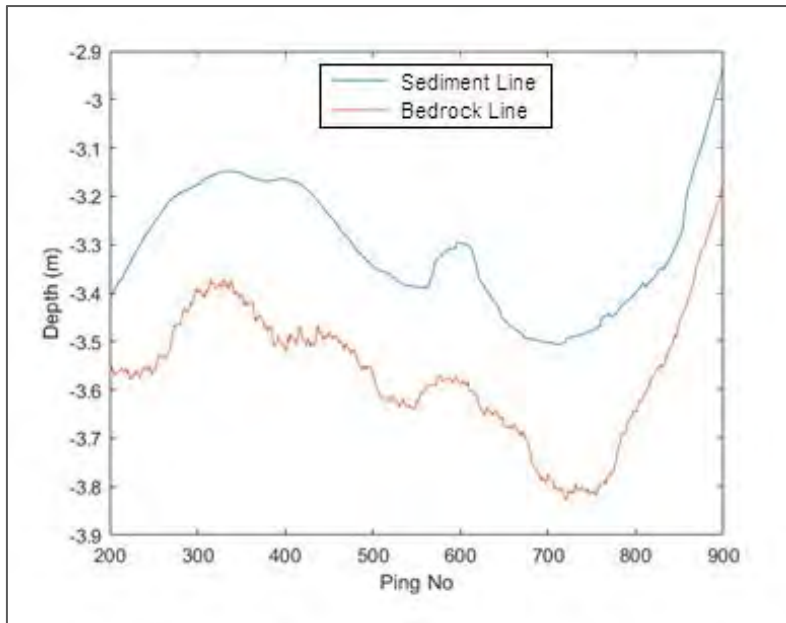
Figure 16. Example of sediment (blue) and bedrock (red) lines. Average filter was applied to smooth the lines.

2.4.3.3. Sediment thickness layer (extrapolation)

Point thickness estimates were extrapolated to a layer using inverse distance weighted (IDW) interpolation. The layer is bounded by the shores of the canal and represents the values of acoustic thickness estimation across the surveyed area.

2.4.3.4. Sediment thickness error estimation

The total error can mostly be attributed to the inadequate selection of the water-sediment boundary's depth and to the spatial resolution of the bandwidth system. Other sources of error like environmental or instrumental noise were negligible.

Water-sediment boundary's depth selection: Differentiating the water-sediment and sediment-bedrock boundaries and assigning a specific depth to them is difficult, since, from the acoustic point of view, they are more like transition areas of a few centimeters thick than clear lines. Other objects in the water column, like vegetation, or debris, are perceived as acoustic artifacts and can obscure the water-sediment boundary. Boundary's depth estimation relied on changes of the backscatter that could have up to 15 cm of uncertainty.

Spatial resolution: In addition, there is a *limitation on spatial resolution*, caused by the bandwidth of the acoustic system. The spatial resolution for a broadband system (FM mode) like the one used in the survey, is given by Equation 3 (Ehrenberg & Torkelson, 2000),

$$\Delta R = \frac{c\tau}{2}, \tau = \frac{1}{BW} \hspace{4cm} \text{Equation 3}$$

where ΔR is the spatial resolution, c is the velocity of speed in water (1500 m/s approx.), and BW is the bandwidth of the transducer (10 kHz for the 38 kHz transducer). If scatterers are separated less than ΔR their echoes will overlap, and they cannot be resolved as individual scatterers. The spatial resolution in this study was 7.54 cm. Measuring a continuous sediment thickness has then an intrinsic error related to the depth detection of the water-sediment and sediment-bedrock boundaries and is compound with the error due to acoustic artifacts. It is equivalent to rounding (quantizing) sediment thickness values into bins of 7.54 cm. Assuming a uniform distribution throughout the depth detections, the spatial resolution error was calculated as ±1.6 cm and represents between 8% and 10% of the overall error if calculated with Equation 4. This is the minimum error the system may have.

Total error: The total error was assessed as a percentage with respect to the core sample thickness for each location and as a mean square error, according to Equation 4 and Equation 5, respectively:

$$Error_{Total} = \frac{\sum_{i=1}^{n} \left(Tck_{EV,i} - Tck_{Cr,i}\right)/_{Tck_{Cr,i}}}{n} \hspace{2cm} \text{Equation 4}$$

$$MSE = \frac{\sum_{i=1}^{n} \left(Tck_{Cr,i} - Tck_{EV,i}\right)^2}{n} \hspace{3cm} \text{Equation 5}$$

where n is the total of compared locations, $Tck_{EV,i}$ is the sediment thickness of the *ith* acoustic location (from Echoview), and $Tck_{Cr,i}$ is the sediment thickness of the *ith* core sample. To account for the core samples' GPS error, only core samples that had at least one acoustic sample

within a 1.5 m radius were used when assessing the error (**Figure 17**). When more than one acoustic sample matched, the closest account sample to the core sample location was used. The number of core samples with a location matching acoustic sample was 61. The error was calculated using those 61 samples and their respective closest acoustic samples. Core samples are not necessarily a good substitute for ground truth since they have an intrinsic error themselves, error from Equation 4 and Equation 5 are presented as a guideline.
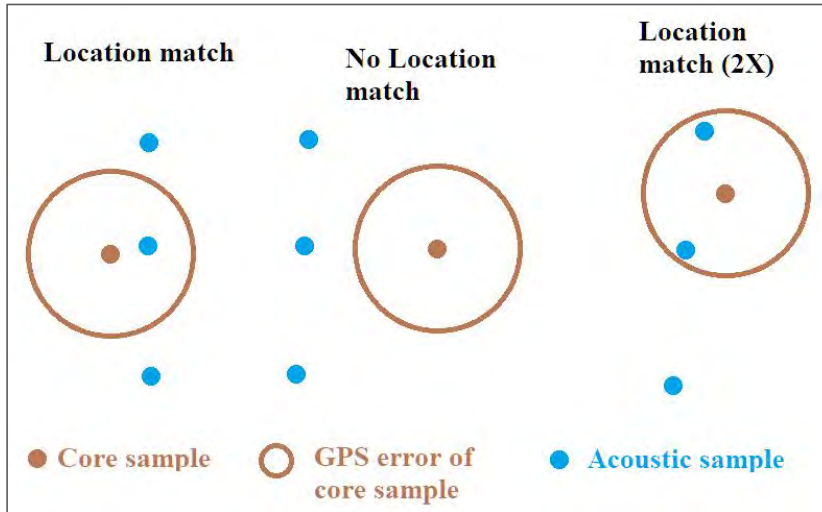
Figure 17. Location match between core samples and acoustic samples.

2.4.4. Bed-volume

Based on the estimated sediment thickness layer through kriging (QGIS Development Team, 2022a, 2022b), bed-volume is calculated using GRASS GIS 8.2.1 (Team, 2022) raster surface volume analysis. The volume limited in the *z* axis by the water-sediment and sediment-bedrock boundaries; and in the *x* and *y* axes by the shores of the canal (**Figure 18**).
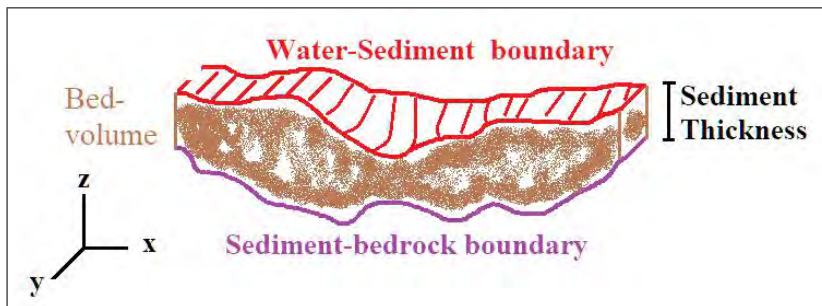
Figure 18. Illustration of cross-section bed-volume.

3. Results

3.1. Canal bathymetry

A bathymetry map of the survey area was generated **(Figure 19)**. Approximately 648,000 acoustic samples were gathered. The canals are deeper north of the S333N gate and shallower on the west end of canal L29.

16

Figure 19. Bathymetry of the survey Area. Data collected on 05/16/2022.

April's bathymetry has more data in front of gate S333, but not as much at the S12D gate on the west end of L29 canal. May's bathymetry has more data at the S12D gate in the west end of the L29 canal and partial data in front of gate S333. 130,000 bathymetry samples were collected in April and 630,000 were collected in May. The difference is due to a more detailed survey of area 2, close to the S333 gates, and of area 3, close to the S12 gate.

Table 1 provides summary of canal depth values in the area surveyed. Averages in **Table 1** are over all the samples of that specific section of the canals. Minimum depth is limited by the proximity of the vehicle to the shores. There was a 20 cm difference in the mean depth from April and May due to changes in water level.

Table 1. Minimum, maximum, mean, median and standard deviation of depth values in canals L67A and L29, for data collected in April 2022 (04/06/2022-04/07/2022) and May 2022 (05/16/2022).

Date	Area	Min (m)	Max (m)	Mean (m)	Median (m)	Std (m)
04/06/22-04/07/22	All	0.46	6.57	4.01	4.32	1.23
	1	0.46	6.57	3.98	4.20	1.27
	2	0.52	6.35	4.05	4.48	1.10
	3	0.46	6.39	4.02	4.35	1.23
5/16/2022	All	0.15	6.11	3.85	4.18	1.18
	1	0.24	5.93	3.69	3.65	1.34
	2	0.30	6.09	3.82	4.15	1.10
	3	0.15	6.11	3.96	4.30	1.06

3.2. Canal sediment thickness

Sediment thickness was interpolated using inverse distance weighted method in SAGA GIS software (Conrad et al. 2015) over the surveyed area, from sediment cores and acoustic data, shown in **Figure 20**. Error between the estimated sediment thickness and the sediment core sample thickness, for the 61 location-matching samples, is presented in **Table 2**.

Figure 20. Inverse distance weighted (IDW) interpolation estimate of sediment profile thickness and bed sediment volume estimate; **(a)** from sediment core data (provided by University of Florida) and **(b)** from the ASV surveyed area on dates 04/06/2022, 04/07/2022, and 05/16/2022.

Table 2. Statistics of thickness and error estimates for core and acoustic samples.

	Sediment Thickness					Error		Total No. of samples
	Min (cm)	Max (cm)	Mean (cm)	Median (cm)	Std. dev. (cm)	Percent (%)	MSE (cm)	
Core	8.5	55.9	30.0	25.8	14.2	NA	NA	79
Echoview Method 1	0.0	60	27.7	24.7	13.2	56.6	3.2	117,199
Matlab Method 2	0.0	60.0	22.0	21.6	14.1	67.9	4.63	147,191

A Wilcoxon-Mann-Whitney rank sum test (using 5% significance level) determined that there is a significant difference between the medians of methodology 1 and 2 (*p=0*) and there is a significant difference between the medians of methodology 2 and the core samples (*p=0.0038*).; but there is not a significant difference between the medians of methodology 1 and the core samples (*p=0.8*). Methodology 1 is closer to the core sample distribution, and it has a lower error.

Acoustic methods have greater maximum estimates than core samples; conversely, minimum acoustic estimates are smaller than core samples. The differences are probably due to a combination of factors like the larger number of acoustic samplings, the wider cover area, the intrinsic error of the acoustic instrumentation, and the minimum thickness a core sampler can sample. It is evident that acoustic methods collect several orders of magnitude more samples than core sampling methods which allows for a more detailed representation of the sediment profile.

3.3. Sediment bed-volume

The bed sediment volume was calculated on interpolated thickness estimates shown in **Figure 20** using QGIS software (QGIS Development Team, 2022). Raster surface volume analysis was used for volume estimates. For the acoustic sediment thickness data, the sediment bed volume was estimated 6,320 cu m. Following the same method, for the core sediment thickness data, the bed volume estimate was 8,447 cu m. Thus, sediment bed volume in canal section (**Figure 20**) based on acoustic method estimate was ~75% of sediment core-based estimate.

4. DISCUSSION

4.1. Canal bathymetry

On the first day (04/06/2022) once instruments were calibrated, and the area was free of obstacles, the data collection took around 6 hours. The process was more efficient on the subsequent days.

Data processing (QPS Qimera) takes significant time to deliver a product that is clean and understandable. Despite the automation tools provided in the software, a large amount of human effort was required. The bathymetry had an error that was seen as small peaks on the canal bottom, especially on the shallower west side of L29 canal. The error was removed manually. Considering the overlapping in pings and the redundancy of the data, the bathymetry is accurate. Electrical instrumentation noise was minimum, as well as ambient noise.

4.2. Canal sediment thickness

Considering that the method used for acoustic sediment thickness estimation was highly experimental, errors around 50% are not unusual (approximately ±15 cm), but do not provide high confidence in thickness estimates. Other acoustic methods that analyze depth estimates among the frequencies that we used, find errors > 7 cm for coarse sediments (sand with shells), and > 32 cm for fine sediments (sandy mud) (Gaida et al., 2020). Most of the overall error is due to inaccurate boundary location estimates.

For environments like the Everglade's canals, with shallow waters (<5 m) and very different values of sediment deposition within meters from each other, acoustic sediment estimation could work as a supporting methodology for ball-park estimation of sediment thickness but not as a high-resolution mapping method (Anderson et al., 2013). Due to the large number of acoustic samples that can be taken, that methodology provides a wide-area estimate, while core sampling provides a more precise, on-point measurement. The two acoustic methods used in this study provided similar results.

4.2.1. Methodology limitation

The near-field limitation removed approximately 1.9% of acoustic samples and was more affected by the shallower waters on the west side of L29 canal. The near-field limitation could represent an issue in areas with depths < 3m, but for most of the canal it was not a factor.

 On the other hand, error due to the spatial resolution limitation contributed to 1/5 of the overall error; unfortunately, for sediment profiling on narrow, shallow canals, there are not many other acoustic options. The error due to the limitations of the instruments was expected when using commercial echosounders.

The rest of the error is due to boundary detection, smoothing, and data processing. Differentiating the water-sediment and sediment-bottom boundaries was not accurate enough. Assigning a specific depth to the boundaries, based on echograms or ping graphs is difficult, since they are more like transition areas of few centimeters thickness than clear lines. In addition, the algorithms did not always choose the boundary correctly due to interferences by other objects in the water column such as vegetation, debris, acoustic artifacts, etc.

Finally, the number of core samples used for ground truthing might not have been enough for a reliable error estimation, especially in an environment where the sediment thickness varies so much at short distances.

4.2.2. *Hydroacoustic method improvements*

Improvements to the equipment and acoustic setup are difficult. The 38 kHz transducer was chosen to detect the bedrock layer because of its penetration power, but the trade-off was a lower resolution and a higher near-field, compared to higher frequencies. Higher frequencies have the potential for better resolution and reduced near-field error but would not penetrate enough to reach the bedrock layer. High frequency transducers were operated at maximum power, increasing their power is not possible with the current instrumentation.

However, improvements on the boundary's depth estimations could reduce the error and enhance the capacity of it. The methodologies could benefit from a better filtering-out of artifacts in the echograms which would improve the boundary location estimates. This time-consuming process must be done manually and would require more time than the one allocated to this project.

In addition, closer transects for the collection of backscatter data would also improve resolution and core sample location matching. It would require more survey days (10-15 days) and would increase the project's timetable.

Finally, a larger number of core samples (100+) and a better geographic alignment (within less than 1 m) between them and the acoustic samples will improve the error estimation. It would also allow for the implementation of more sophisticated boundary detection by using the core samples as ground truth for training machine learning algorithms. Such methods were not possible in this project due to the low number of location-matching core samples. For future projects, the core sampling team could collect more samples with more accurate GPS locations, which acoustic surveyors could add to its survey transects.

5. Conclusions

Bathymetry estimation using acoustic capable ASVs is very efficient, providing accurate results in relatively short times. Bathymetry constraints regarding number of transects and vehicle's speed are much more relaxed than the ones required for backscatter data collection. Processing of bathymetric acoustic data took several weeks since modern software is still not able to remove all the noise and the process had to be done manually. Overall, usage of ASVs in the Everglades' canals for bathymetry data collection is recommended.

Acoustic sediment profiling is possible with some limitations. There is an intrinsic error due to the frequencies and instrumentation used. The methodology can be improved by adopting more sophisticated algorithms for bottom detection and better ground truthing. Commercial broadband echosounders as means to estimate sediment thickness remain a supporting methodology for more traditional methods like core sampling, especially in shallow waters (< 5 m) with relatively low sediment bedload, like the L29 and L67A canals. Nevertheless, the use of acoustic capable ASVs is efficient in its data collection, and errors of 56% are encouraging for future endeavors.

References

Anderson, M. A., Conkle, J. L., Pacheco, P., & Gan, J. (2013). Use of hydroacoustic measurements to characterize bottom sediments and guide sampling and remediation of organic contaminants in lake sediments. *Science of The Total Environment*, *458-460*, 117-124. https://doi.org/https://doi.org/10.1016/j.scitotenv.2013.04.009

Anderson, V. C. (1950). Sound Scattering from a Fluid Sphere. *The Journal of the Acoustical Society of America*, *22*(4), 426-431. https://doi.org/10.1121/1.1906621

Conrad, O., Bechtel, B., Bock, M., Dietrich, H., Fischer, E., Gerlitz, L., Wehberg, J., Wichmann, V., and Böhner, J. (2015): System for Automated Geoscientific Analyses (SAGA) v.8.5.0. https://doi.org/10.5194/gmdd-8-2271-2015

Echoview. (2022). *Line Picking algorithms*. Retrieved 09/13 from https://support.echoview.com/WebHelp/Reference/Algorithms/Line_picking_algorithm.htm#Best_bottom_candidate

Echoview. (2023). *Multibeam bottom detection algorithm*. https://support.echoview.com/WebHelp/Reference/Algorithms/Multibeam_bottom_detection_algorithm.htm

Ehrenberg, J. E., & Torkelson, T. C. (2000). FM slide (chirp) signals: a technique for significantly improving the signal-to-noise performance in hydroacoustic assessment systems. *Fisheries Research*, *47*(2), 193-199. https://doi.org/https://doi.org/10.1016/S0165-7836(00)00169-7

Eleftherakis, D., Amiri-Simkooei, A., Snellen, M., & Simons, D. G. (2012). Improving riverbed sediment classification using backscatter and depth residual features of multi-beam echo-sounder systems. *The Journal of the Acoustical Society of America*, *131*(5), 3710-3725. https://doi.org/10.1121/1.3699206

Gaida, T. C., Mohammadloo, T. H., Snellen, M., & Simons, D. G. (2020). Mapping the Seabed and Shallow Subsurface with Multi-Frequency Multibeam Echosounders. *Remote Sensing*, *12*(1). https://doi.org/10.3390/rs12010052

Hefner, B., Jackson, D. R., Williams, K., & Thorsos, E. (2009). Mid- to High-Frequency Acoustic Penetration and Propagation Measurements in a Sandy Sediment. *Oceanic Engineering, IEEE Journal of*, *34*, 372-387. https://doi.org/10.1109/JOE.2009.2028410

Klusek, Z., Majewski, P., Dragan, A., & Psuty, I. (2010). Preliminary investigations on implementation of technology of broadband signals for marine biology and sediments recognition.

Komen, D., Neilsen, T., Mortenson, D., Acree, M., Knobles, D., Badiey, M., & Hodgkiss, W. (2021). Seabed type and source parameters predictions using ship spectrograms in convolutional neural networks. *The Journal of the Acoustical Society of America*, *149*, 1198-1210. https://doi.org/10.1121/10.0003502

Mitchell, N. C. (1993). A model for attenuation of backscatter due to sediment accumulations and its application to determine sediment thicknesses with GLORIA sidescan sonar. *Journal of Geophysical Research*, *98*, 22477-22493.

Parker-Stetter, S. L. R. L. G. S. P. J. W. D. M. (2009). Standard operating procedures for fisheries acoustic surveys in the Great Lakes [Technical Report].

QGIS Development Team. (2022). *GIS Geographic Information System*. In (Version 3.22.16) http://qgis.osgeo.org

Rudstam, L., & Sullivan, P. (2023). *Acoustics Unpacked*. Cornell University. Retrieved 01/18/2023 from http://www2.dnr.cornell.edu/acoustics/Examples/NearfieldDistance/NearfieldDistance.html

Schellhammer, M. (2012). Florida's Paradox Of Progress: An Examination Of The Origins, Construction, And Impact Of The Tamiami Trail.

Simmonds, J., & MacLennan, D. (2005). Chapter 3: Acoustic Instruments. In B. P. Ltd (Ed.), *Fisheries Acoustics: Theory and Practice* (2 ed., pp. 70-126). https://doi.org/https://doi.org/10.1002/9780470995303.ch3

South Florida Water Management District. (1999). *Central and Southern Florida Project Comprehensive Review Study - Final Integrated Feasibility Report and Programmatic Environmental Impact Statement*. https://www.sfwmd.gov/document/central-and-southern-florida-project-comprehensive-review-study-final-integrated

Stoll, R. D. (2016). *Sediment Acoustics*. Peninsula Publishing.

Team, G. D. (2022). *Geographic Resources Analysis Support System (GRASS) Software*. In (Version 8.2) Open Source Geospatial Foundation. https://grass.osgeo.org

Trzcinska, K., Tegowski, J., Pocwiardowski, P., Janowski, L., Zdroik, J., Kruss, A., . . . Schneider von Deimling, J. (2021). Measurement of Seafloor Acoustic Backscatter Angular Dependence at 150 kHz Using a Multibeam Echosounder. *Remote Sensing*, *13*(23). https://doi.org/10.3390/rs13234771

SECTION 4: EVALUATION OF DRIVERS OF S333 WATER QUALITY DYNAMICS PRESENTATION (62-SLIDE-DECK)

Evaluation of drivers of S333 water quality dynamics

Donatto Surratt & Dilip Shinde
Everglades National Park
South Florida Natural Resources Center

1

Introduction

- **Concern**: Peaks in TP concentrations during low water levels are contributing to exceedances of the long-term limit for Shark River Slough and potentially resulting in undesirable nutrient loading

- NPS hypothesized that during low flows or stagnant canal conditions combined with low stages in the canal, sediments accumulate in front of S333 due to settlement and roll-over processes. S333 lift gate at times promotes variable flux and turbulence, which may scour the canal floor to entrain sediments and floc contributing to TP peaks

- NPS invested in this sediment characterization study to provide insights on sediment physio-chemical properties for informing engineering solutions to resolve the TP peaks

- Several studies were formulated working with FIU and the University of Florida to perform the necessary research

- The initial study was designed to quantify and characterize the sediments at S333 and upstream in the L67A and L29 canals to provide insight into the types of sediments and forms of P that are contributing to the peaks

- A secondary subregional scale exploratory investigation was deemed necessary to assess sources of sediments and floc contributing to the water quality conditions at S333

Introduction

- Physicochemical properties of surface water, flocculant material (floc), and sediments were evaluated to assess local and subregional influences on S333 for these hypotheses:
  - Acoustic methods can be used to estimate sediment volume available in canals
  - Flow conditions result in transport or settlement of floc and sediments
  - Sediment and floc particle size distribution can provide insight into potential for entrainment into the water column
  - Flow directionality can be used to evaluate the influence of L29 on chemical signatures at S333
  - Collection of subregional physio-chemical data can be used to delineate drivers of water quality dynamics at S333

3

Introduction

- To address these hypotheses several major objectives are discussed at local and subregional scales
  - Local
    - Estimating mass of sediments near S333
    - Characterizing sediment particle size for canal and marsh locations
    - Evaluating potential for sediment entrainment at the headwater of S333
  - Subregional
    - Exploratory assessment of sources and potential transport pathways of sediments and floc

4

Specific Local Objectives

- Evaluate water quality cross-sectionally at the headwater of S333
  - Understand canal water depth relationship with water quality (TP, TDP, TOC, and TSS) and potential for sediment entrainment
  - Understand L67A flow influence on sediment transport through entrainment and roll-over (saltation effects) to accumulate in the vicinity of S333
- Evaluate water quality along vertical profiles in L67A and L29 canals
- Evaluate floc and sediment physico-chemical characteristics in front of S333, 1500 ft upstream along L67A and L29, and in the WCA3A marsh near S333
  - Assess TP, IOC, and OM spatial distribution in floc – similarities and differences
  - Estimate Bulk Density, TP, OM, and particle size spatial distribution in 0-5 cm sediment cores – similarities and differences
  - Quantify bound and exchangeable TP fractions
- Tilt Current Meter and ADCP based flow dynamics in L67A, at S333, and in L29

5

Specific Subregional Objectives

- Evaluate physio-chemical properties of floc and sediments at Miami, L67A, and L29 canals, S333, and in the marsh
  - Understand spatial distribution of TP, OM, Bulk Density, d_{50} particle size – similarities and differences
  - Understand spatial distribution of metals, isotopes, and clay mineral, sorption/desorption – similarities and differences
- Evaluate relationships between floc and sediments

6

Methods

National Park Service

South Florida Natural Resources Center

Methods – abbreviated

Sampling Events and Observed Hydrological Configuration

1 S333 DBHYDRO flows, gate openings, and head and tail water stages are average for the duration of ADCP measurement taken in front of S333.
2 ADCP measurements at S333 gate, and L67A and L29 canals were at ~1500ft upstream and they were not taken simultaneously but in a sequential order.
3 ADCP data processing software from Teledyne RD Instruments WinRiver II (https://hydroacoustics.usgs.gov/movingboat/WinRiverII.shtml)
4 ADCP data processing software from USGS (https://hydroacoustics.usgs.gov/movingboat/QRev.shtml)

Date	[1]S333 Gate data			Flow (cfs)	[2]Flow (cfs) ADCP measurements						Remarks for L29 Flow
	Gate opening (ft)	Head Stage (ft)	Tail Stage (ft)	S333 DBHYDRO	S333 [3]WinRiver	S333 [4]QRev	L67A WinRiver	L67A QRev	L29 WinRiver	L29 QRev	
Apr-14, 2022	8.20	7.55	7.52	283.09	360.70	366.74	401.61	389.10	-50.65	-30.24	East
Apr-25, 2022	8.20	7.28	7.26	194.59	205.83	209.92	269.81	259.59	-32.77	-16.60	East
May-05, 2022	8.18	7.27	7.25	233.63	228.09	228.08	229.88	229.84	-97.02	-97.02	East
May-26, 2022	2.40	7.63	7.02	327.72	309.07	307.13	410.33	410.32	-1.44	-1.44	East
Jun-07, 2022	3.21	8.53	7.77	488.36	454.31	454.31	577.84	577.84	142.58	142.58	West
Jun-16, 2022	3.80	8.86	8.01	614.90	562.15	562.11	830.46	830.45	260.62	260.62	West
Jun-27, 2022	5.00	8.95	8.27	719.64	670.86	670.85	1612.67	1613.95	817.53	823.91	West

8

Methods – abbreviated

- Sample locations
  - Local monitoring: S333, L67A, L29, and Marsh
  - Canal water cross-sections: 9 to 10 vertical transects
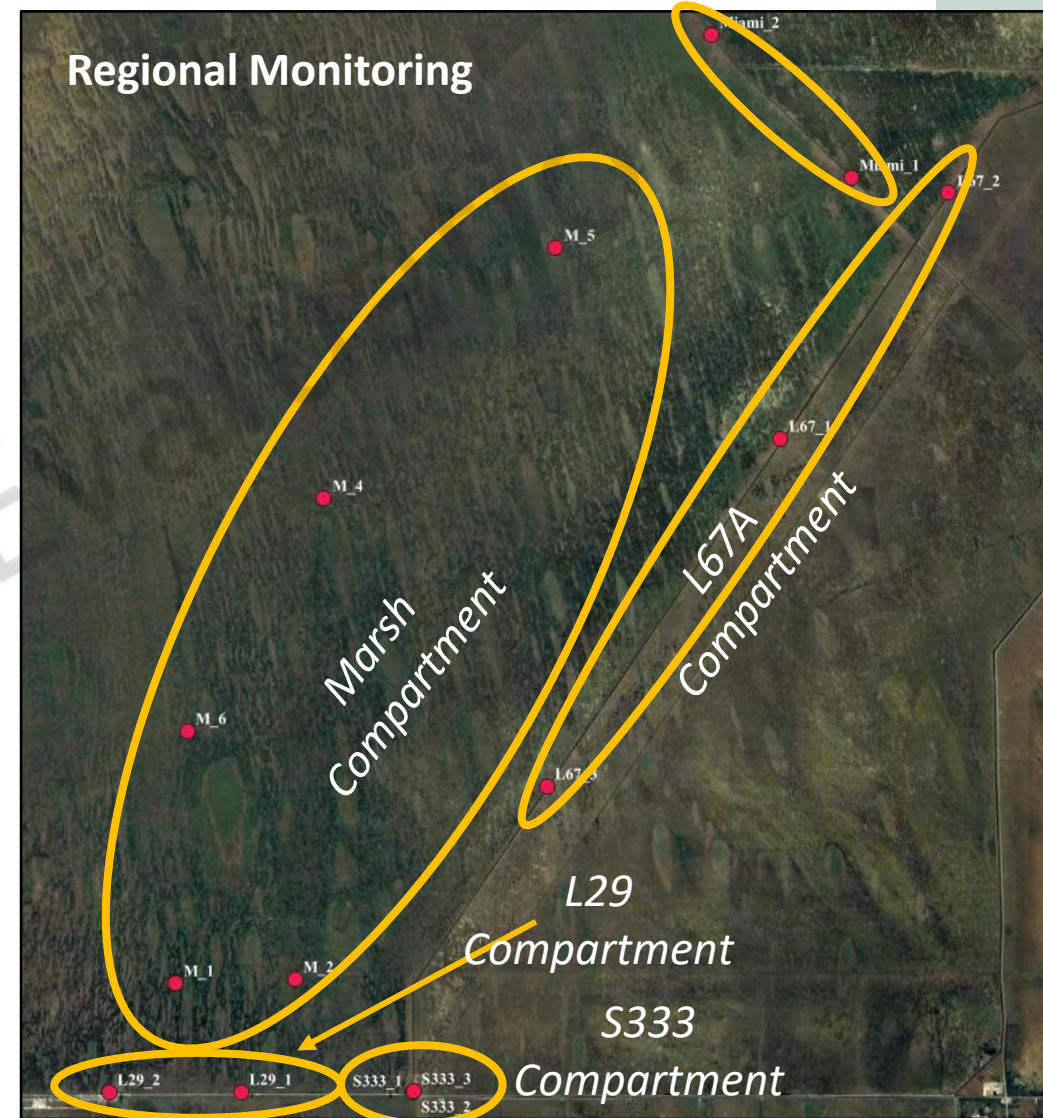

9
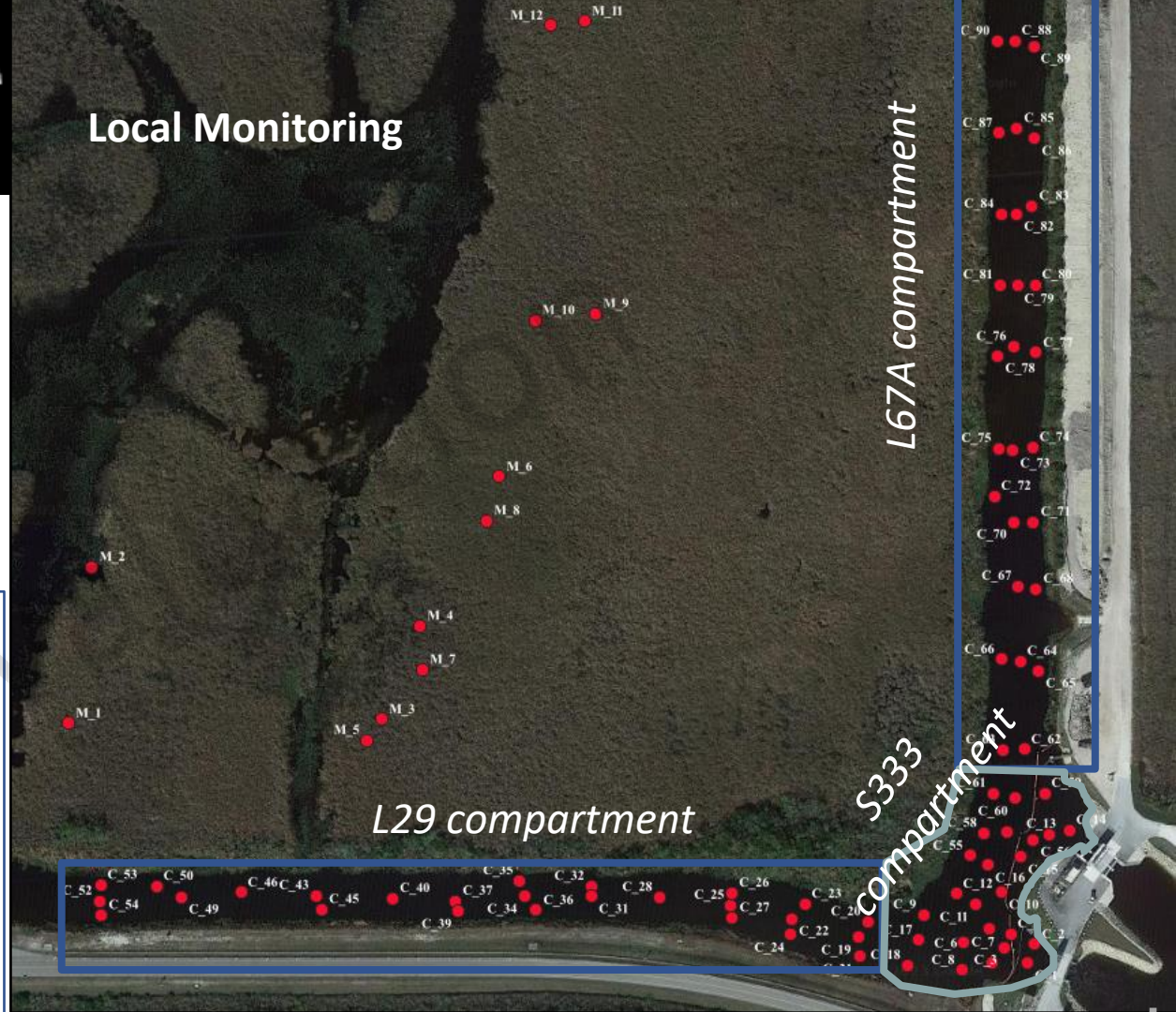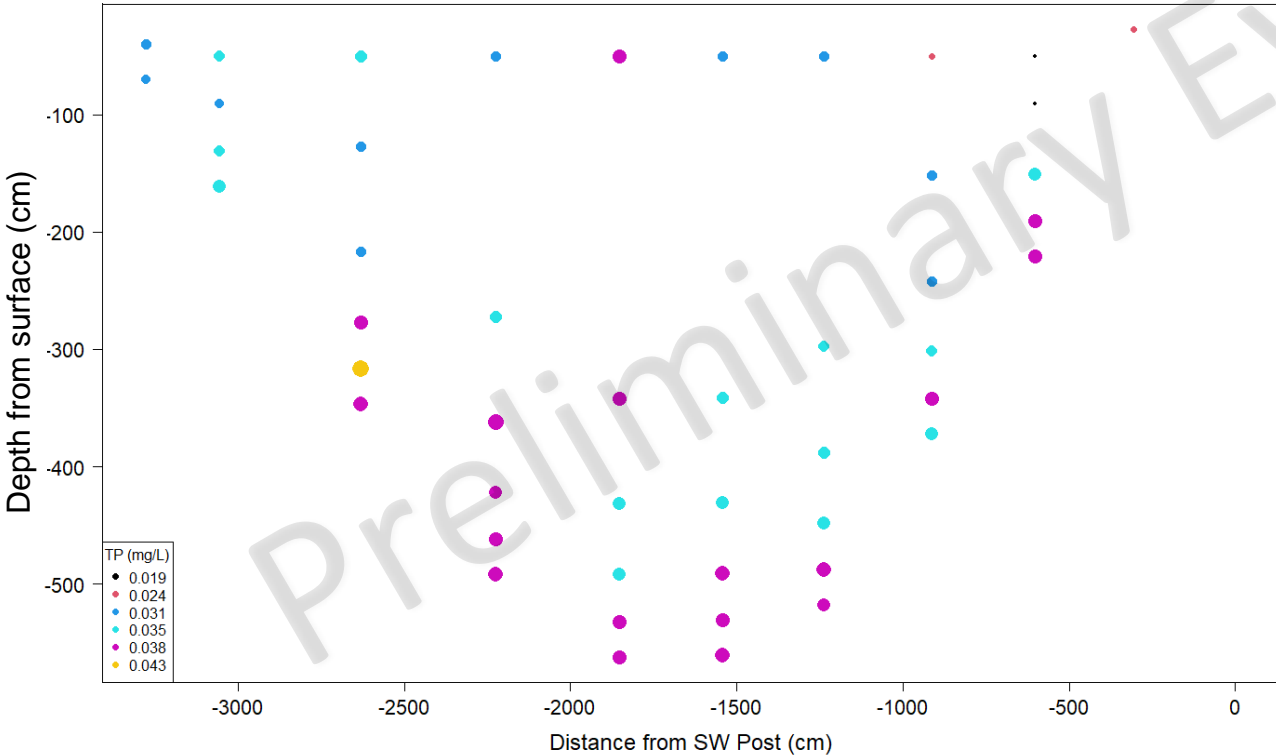
Methods – abbreviated

- Sample locations
  - Subregional monitoring
    - 5 compartments:
      - Miami canal: 2 locations
      - L67A canal: 3 locations
      - L29 canal: 2 locations
      - S333: 3 locations
      - Marsh: 5 locations

Methods – abbreviated

- Physio-chemical analytical approaches
  - TP, phosphorus fractions, P adsorption / desorption
  - Bulk density
  - Organic matter
  - Inorganic carbon
  - Clay minerology
  - Metals (trace and heavy)
  - Isotopes (δ13C, δ15N, δ18O)

Methods – abbreviated

- Statistical analyses**
  - Spatial – Inverse Distance Weighting
  - TP normalization
  - Differences among compartments - Nonparametric multiple contrast test and simultaneous confidence intervals (mctp in the nparcomp R package)
  - Differences within compartments– Kruskal Wallis nonparametric test
  - Effect size – Permutation Multivariate Analysis of Variance (module adonis2 in the R vegan package)
  - Correlations – Kendall tau nonparametric test
  - Dimensionality reduction – Principal Components analysis
  - Cluster analysis – Hierarchical cluster analysis using the R factoextra package using a three clusters discrimination with the anticipated compartments being marsh, canal, and the receptor compartment S333

  Being an exploratory investigation, the subregional sample sizes were small. Statistical tests applied to these small sample sizes have lower power to detect differences and effects. As such, for this portion of the study there is a potential some differences and effects were not detected.
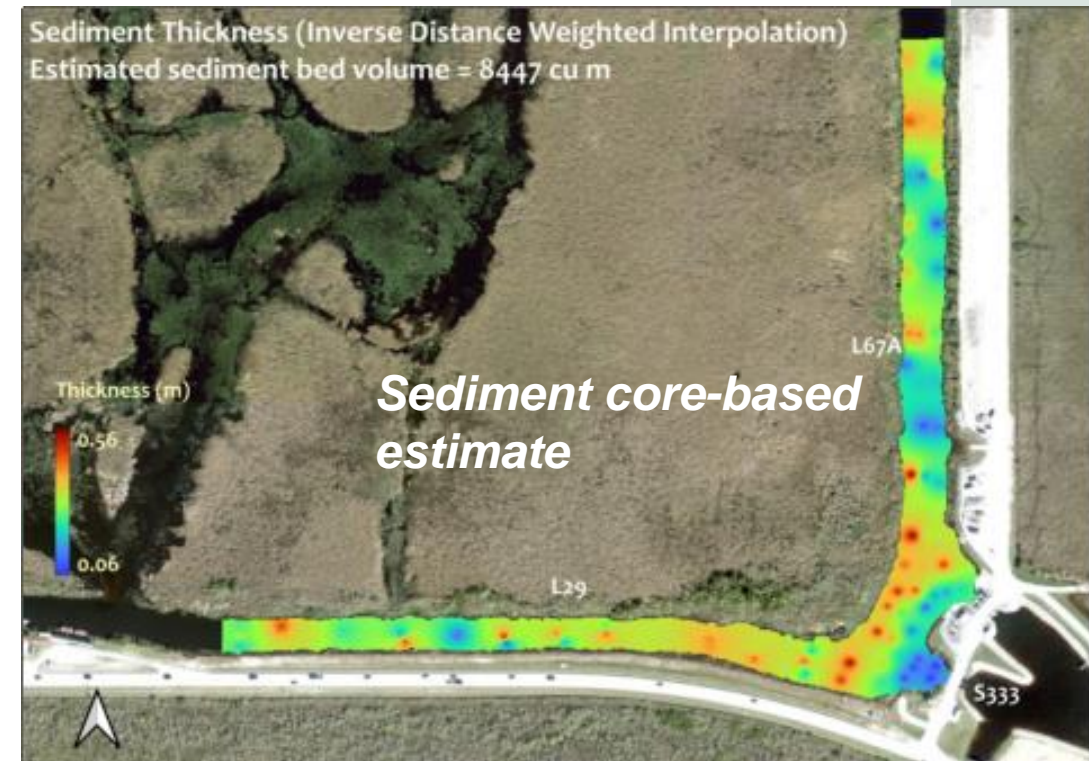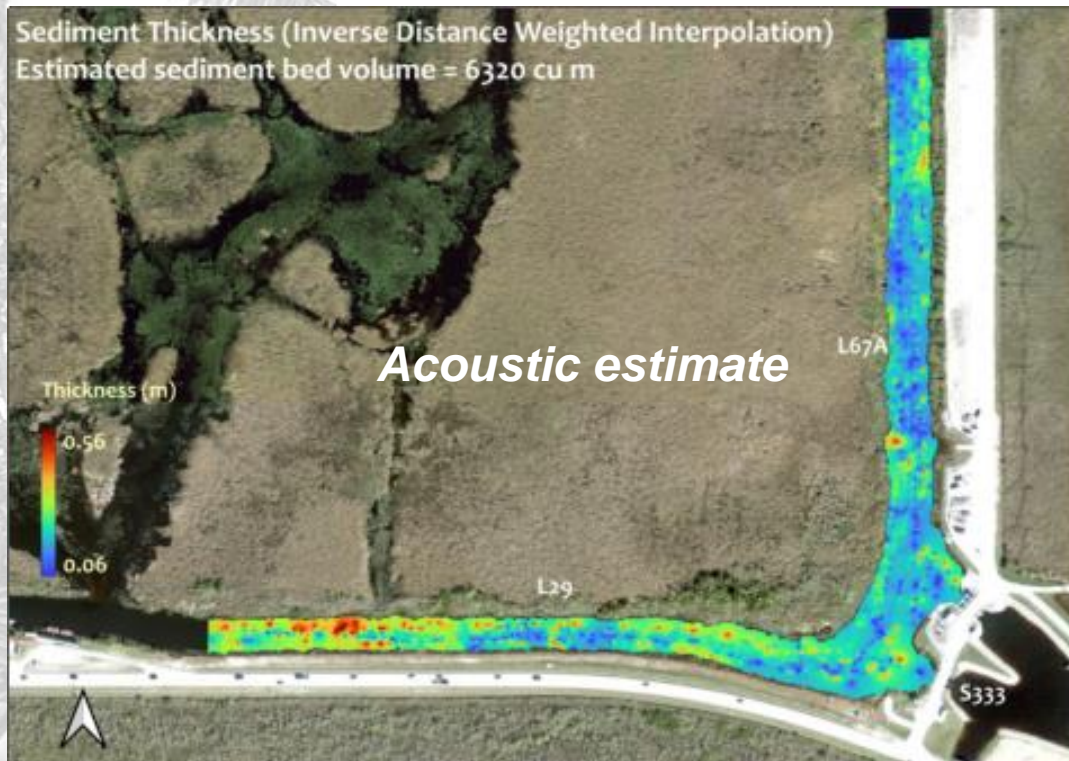
- Hydrology
  - Flows and directions in the L67A and L29 were determined using ADCP and Tilt Current Meters

12

Local Results:
Sediment Volume and TP Mass

National Park Service

South Florida Natural Resources Center

Results

- Sediment Volume
    - 6,320 m^3 based on interpolated acoustic sampling
    - 8,447 m^3 based on interpolated sediment core thickness

14

Results

- ## Sediment Volume
  - The acoustic sediment thickness estimation did not provide high confidence due to associated error (~57 - 68 %)
  - For environments like the Everglades canals, with shallow waters (<5 m) and very different values of sediment deposition within meters from each other, acoustic sediment estimation could work as a supporting methodology for a ball-park estimation of sediment thickness but not as a high-resolution mapping method
  - Core samples provide greater accuracy at the sampling point, but less spatial coverage

Results

- Canal sediment TP mass in top 5 cm layer
  - L29:   307 kg
  - S333:   77 kg
  - L67A: 153 kg

- These sediments were characterized by greater than 95% bound phosphorus

Total Phosphorus Mass in 0-5 cm sediment layer
L29   = ~307 kg
S333 = ~ 77 kg
L67A = ~153 kg

Relative Sed TP concentration
(Range 147 - 5828 mg/kg)

TP Mass (g/sq.m)
0 - 5 cm layer
234.17

3.42

L67A

L29
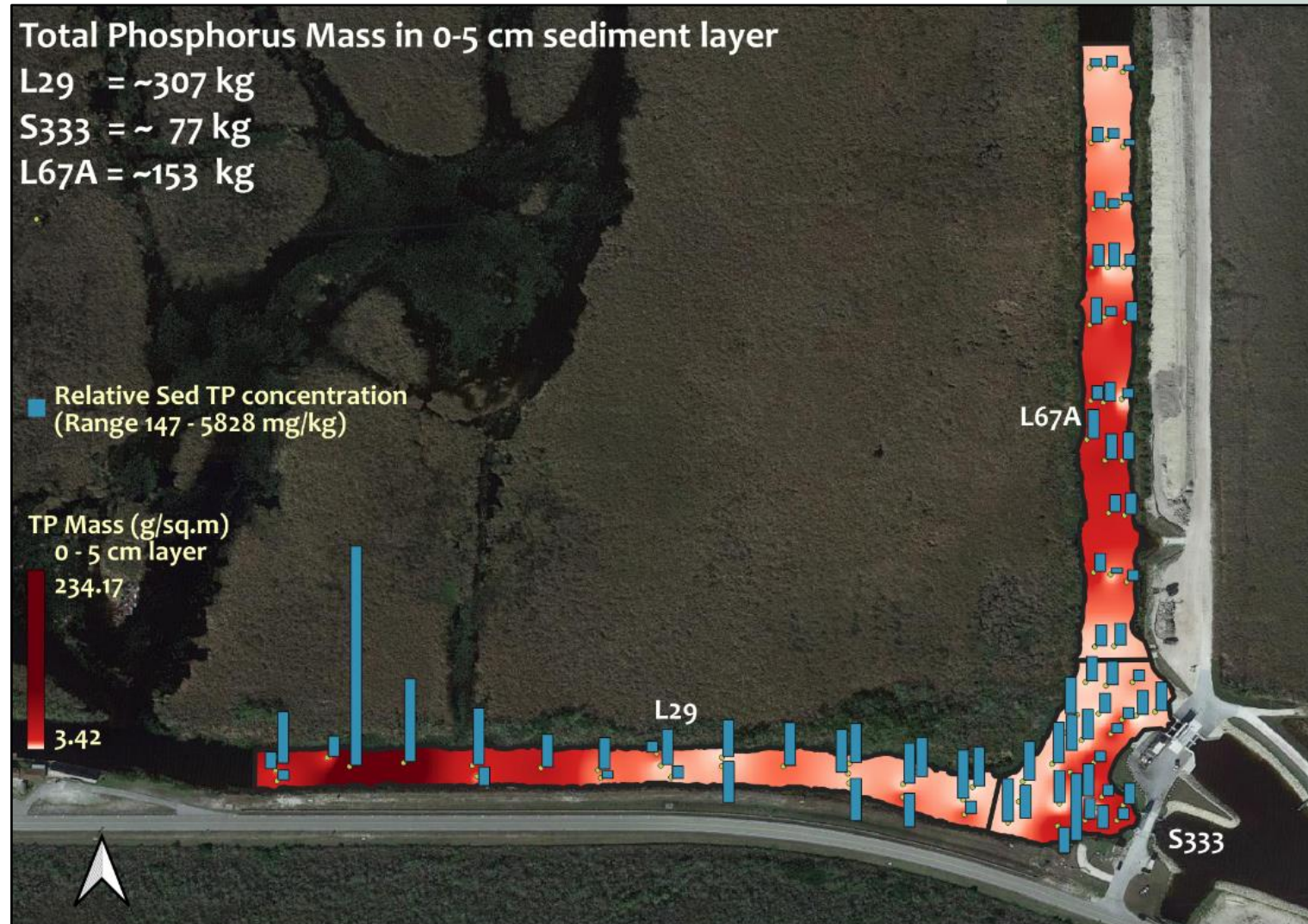
S333

Local Results:
S333 Canal Cross-section

National Park Service

17

South Florida Natural Resources Center

Results - Local
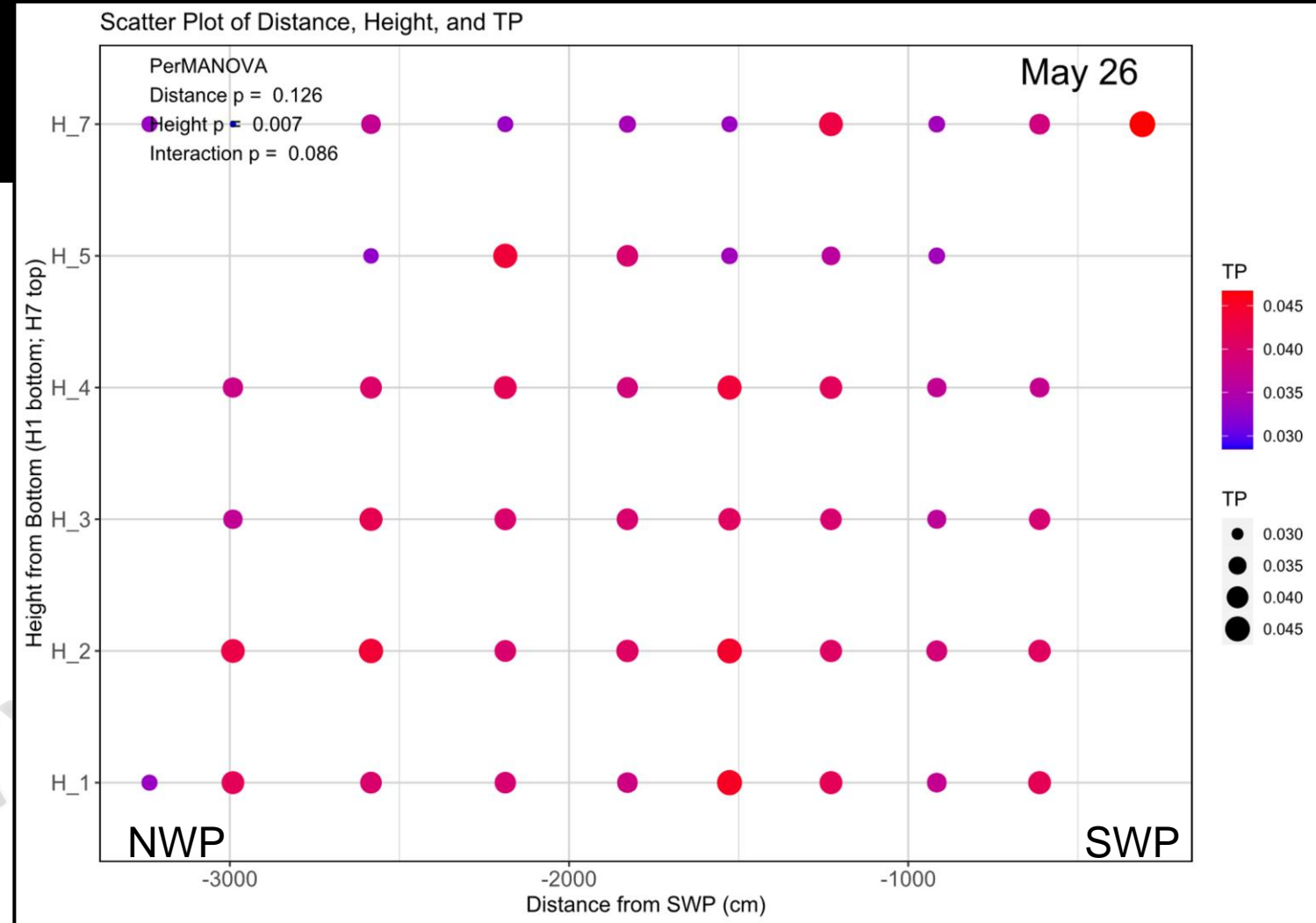
Cross-section

- Sample events with significant interaction action effects for TP relative to Distance from the SWP and Height from canal bottom

Sample Event Date	Variable	R2	F	pvalue
Apr 14	Distance	0.0594	4.9303	0.024
	Height	0.3050	5.0655	0.001
	Interaction	0.2022	3.3577	0.02
May 26	Distance	0.0388	2.7442	0.114
	Height	0.2731	3.8626	0.005
	Interaction	0.1649	2.3331	0.053

Permutation Multivariate Analysis of Variance

TP was the only parameter with significant interaction effects

Scatter Plot of Distance, Height, and TP

PerMANOVA
Distance p = 0.126
Height p = 0.007
Interaction p = 0.086

May 26

NWP   SWP

H1 = 30 cm; H2 = 60 cm; H3 = 100; H4 = 160 cm; H5 = 250 cm; H6 = 500 cm from canal bottom, H7 = 50 cm from water surface

Among the seven sampling events, only Apr 14 and May 26 indicated TP interaction effects with height and distance, they both also had significant depth effects on TP with higher TP being observed near the canal bottom
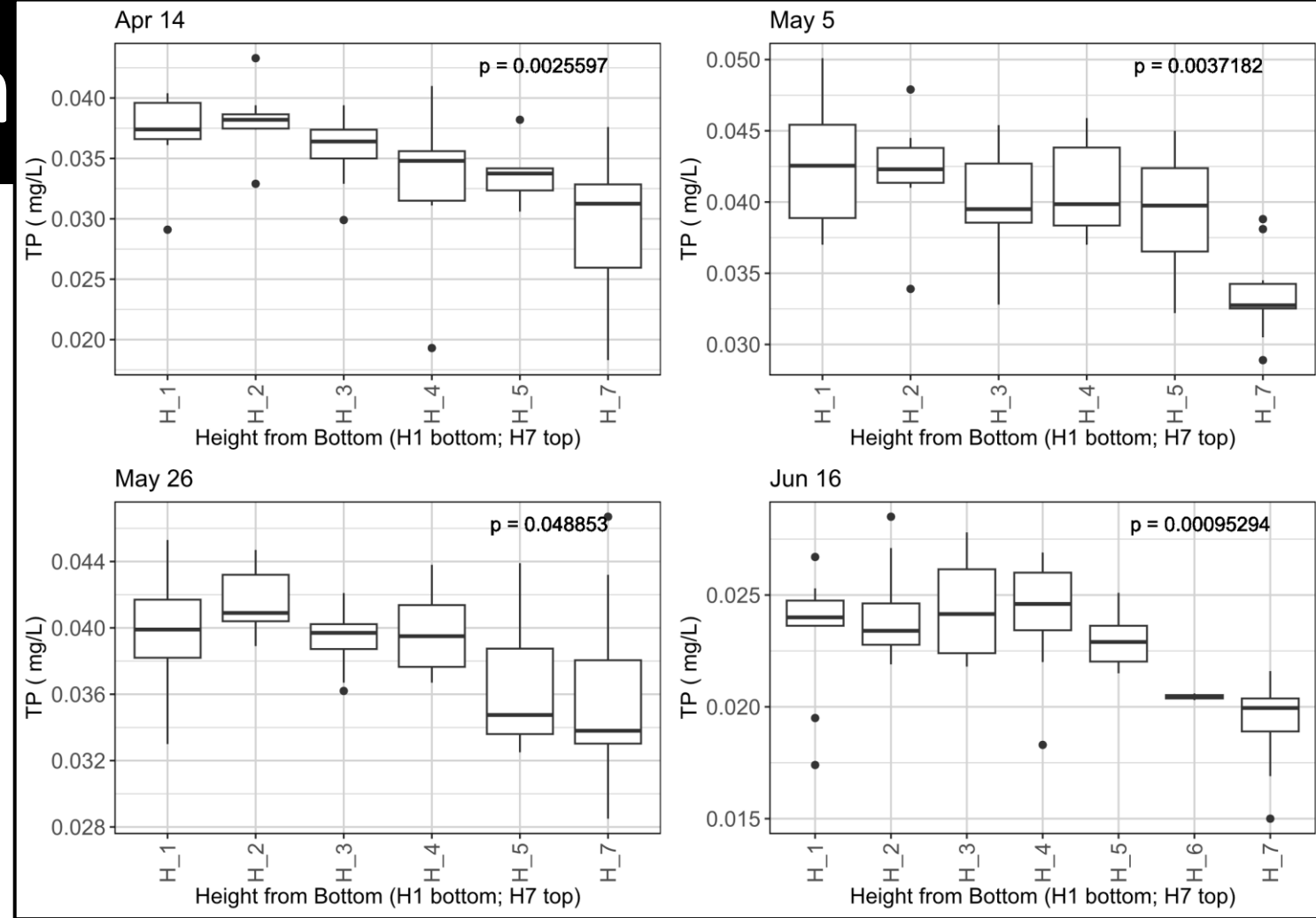
18

Results – Cross-section

Water depth effects

- Significant Kruskal-Wallis results for TP by Height from canal bottom

Event Date	X^2	pvalue
Apr 14	18.279	0.003
May 5	17.506	0.004
May 26	11.081	0.050
Jun 16	22.585	0.001

When considering depth effects alone (Kruskal Wallis) Apr 14, May 5, May 26, and Jun 16 had higher TP concentrations near the canal bottom
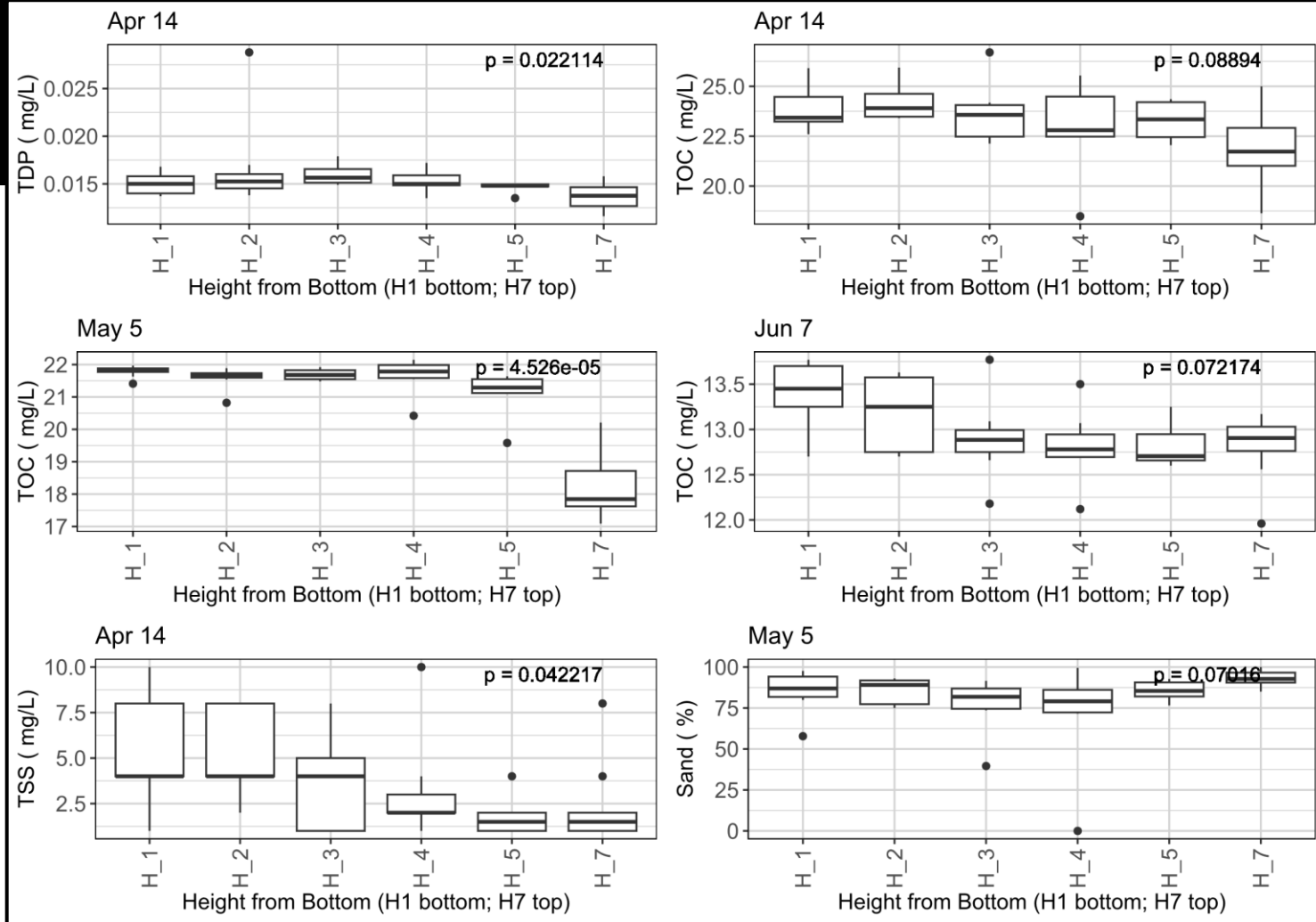

H1 = 30 cm; H2 = 60 cm; H3 = 100; H4 = 160 cm; H5 = 250 cm; H6 = 500 cm from canal bottom, H7 = 50 cm from water surface

Water depth effects

- Significant Kruskal-Wallis results for other water quality parameters by Height from canal bottom

Parameter	Event Date	X^2	pvalue
TDP	Apr 14	13.139	0.022
TOC	Apr 14	9.553	0.089
TOC	May 5	27.515	<0.001
TOC	Jun 7	10.110	0.072
TSS	Apr 14	11.506	0.042
Sand (50-2000 μm)	May 5	10.185	0.070

H1 = 30 cm; H2 = 60 cm; H3 = 100; H4 = 160 cm; H5 = 250 cm; H6 = 500 cm from canal bottom, H7 = 50 cm from water surface

- Apr 14 had depth effects for TDP, TOC, TSS with higher levels near the canal bottom

- May 5 had depth effects for TOC and Sand (50-2000 mm particle size), TOC had higher levels near the canal bottom
- Jun 7 had depth effects for TOC

20

Normalized Unit Q effects
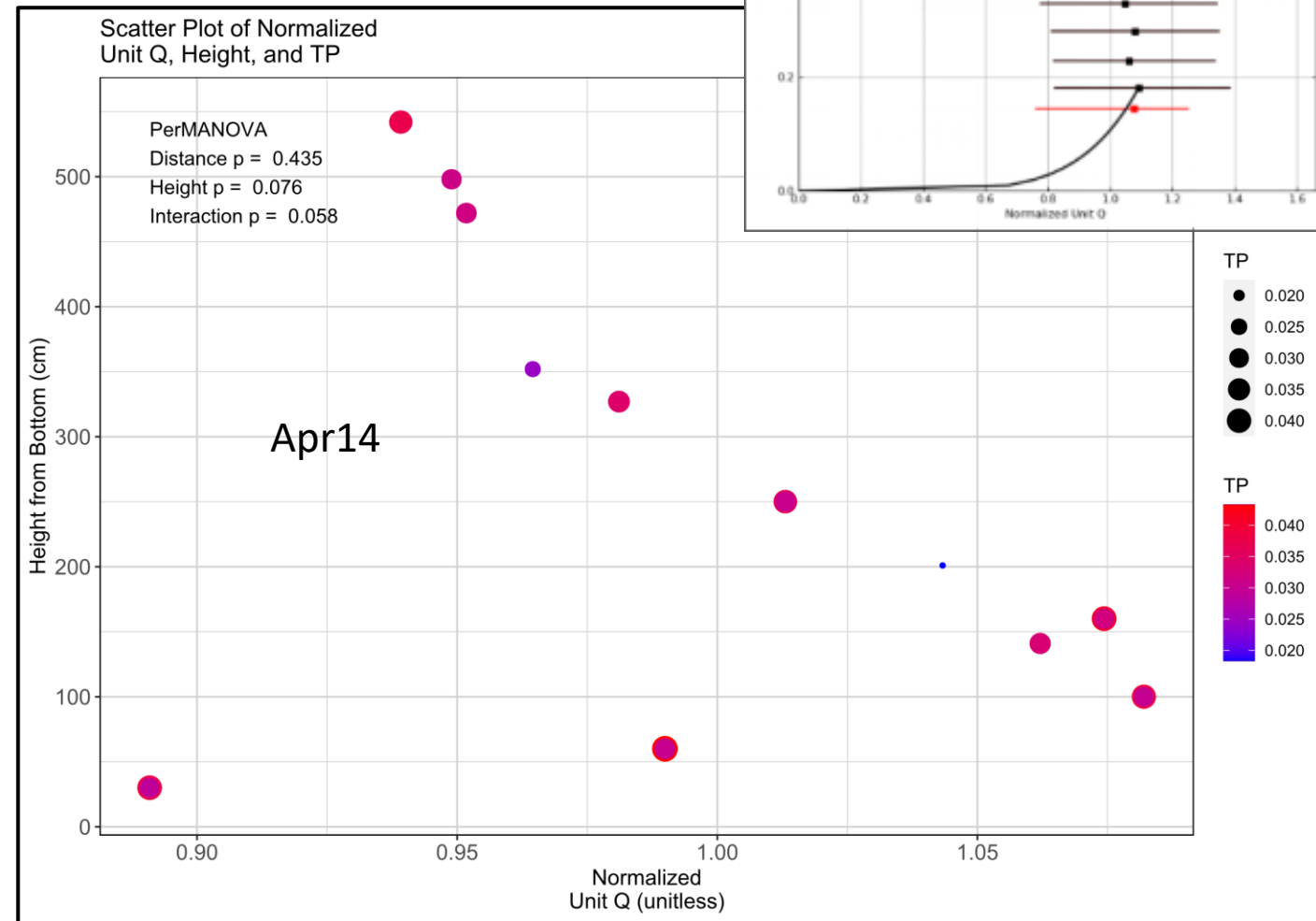
Sample Event Date	Variable	R2	F	pvalue
Apr 14 – TP	Normalized Unit Q	0.0113	0.5863	0.435
	Height	0.0634	3.2824	0.076
	Interaction	0.0748	3.8699	0.058
Apr 25 – d_{50}	Normalized Unit Q	0.0485	2.5535	0.057
	Height	0.0684	3.6017	0.029
	Interaction	0.0854	4.4986	0.01

Permutation Multivariate Analysis of Variance

- TP and d_{50} were the only parameters with significant interaction effects
- Apr 14 for TP and Apr 25 for d_{50} had interaction effects with normalized unit flow and height

21

S333- higher flows towards the bottom

Scatter Plot of Normalized Unit Q, Height, and TP

PerMANOVA
Distance p = 0.435
Height p = 0.076
Interaction p = 0.058

Apr14

Normalized Unit Q effects

Significant Kruskal-Wallis results for TP by Normalized Unit Q

Event Date	X^2	pvalue
May 26 – TP	22.601	0.031
Jun 16 – TP	20.726	0.055
May 5 –TOC	28.138	0.009
Apr 14 - Silt	19.480	0.078
Jun 16 – Silt	18.945	0.090
Jun 16 – Sand	21.525	0.043
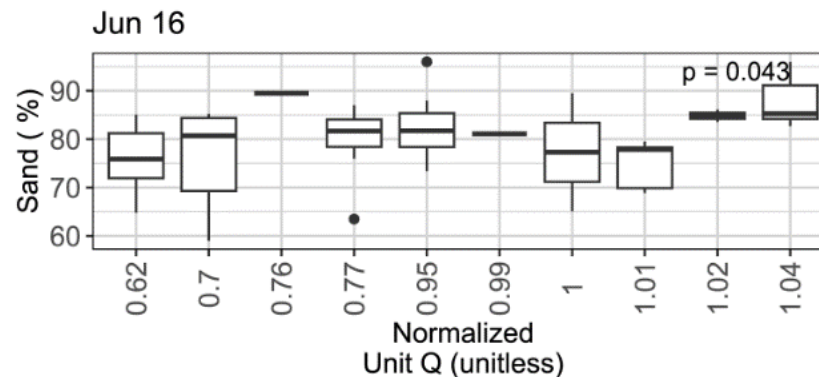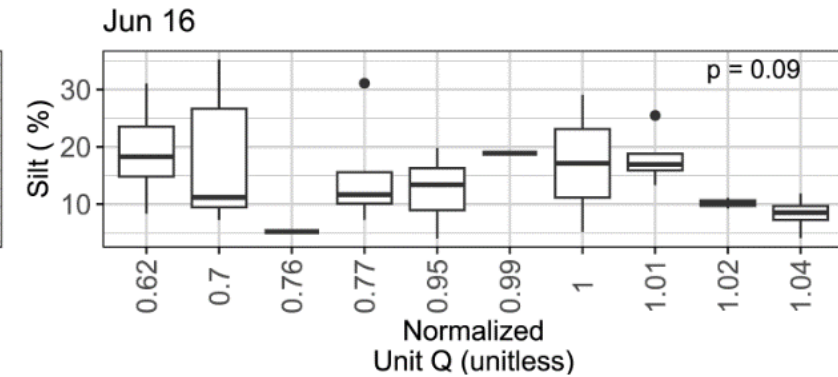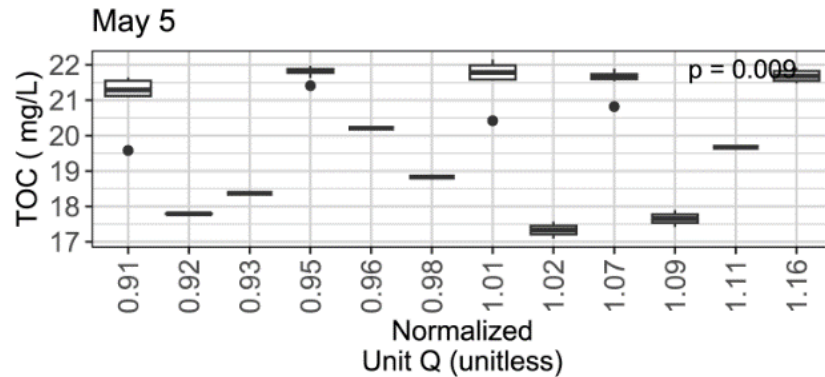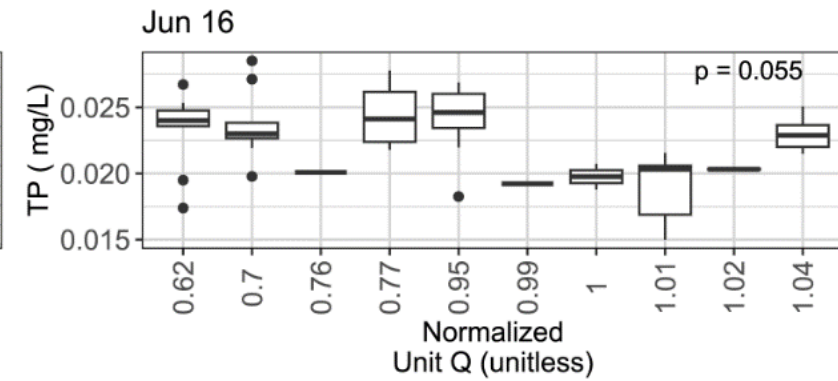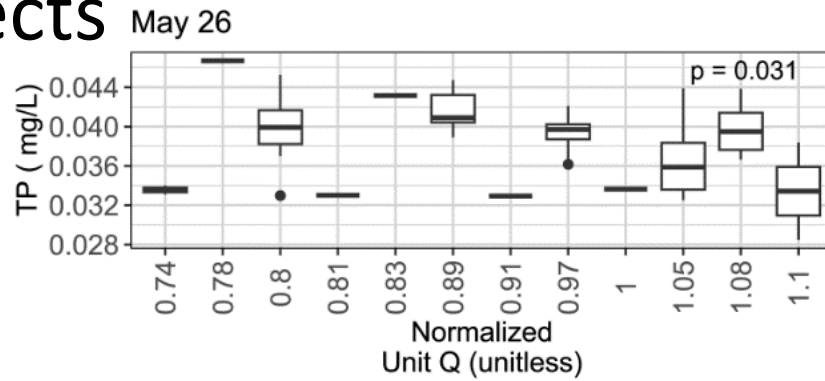
Interpreting these results is difficult as vertical flow profiles represent a median across the canal instead of at the individual vertical transect

Another means of evaluating flow influence on water quality parameters needs further investigations

22

Cross-section

Discussion

Combined these results suggest that water depth, gate operations (lift from bottom), and variable fluxes contributed to increased TP during some of the events

Local Results:
Floc and Sediments

d$_{50}$ median laser particle size
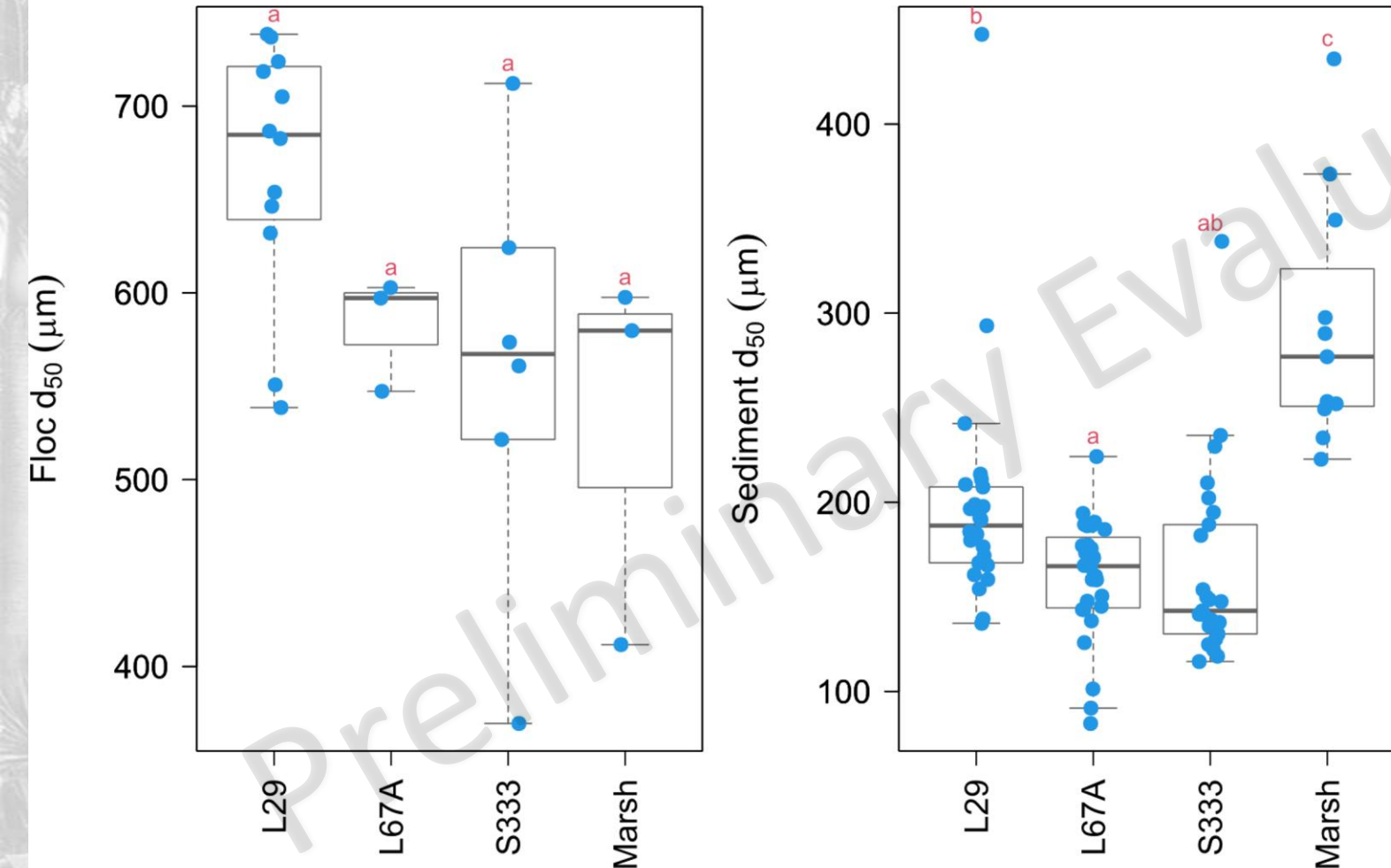
- **Floc**: No statistical differences were observed among compartments (*most sampling compartments had small sample sizes)

- **Sediments**: Marsh was highest; S333 was similar to L67A and L29

- **Entrainment Potential**: Nomograph suggests particle size < 730 μm can be suspended at flow velocities > 0.32 ft s^{-1}

25

Total Phosphorus
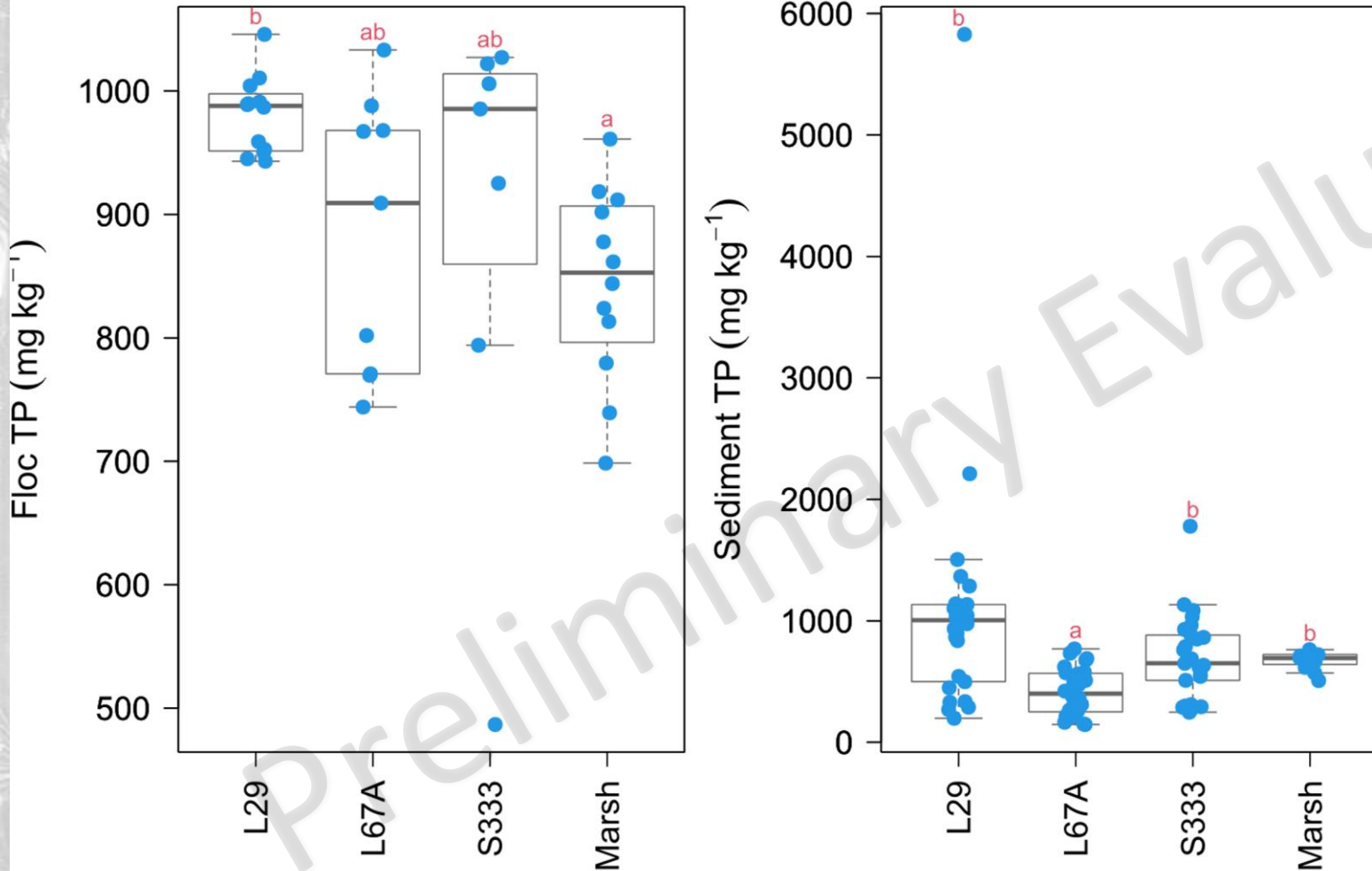
- **Floc**: Marsh TP was lower than L29; S333 was similar to all compartments
- **Sediments**: S333 similar to L29 and Marsh; L67A lower than all compartments

Organic Matter

- **Floc**: Marsh was higher than all compartments; S333 was similar to L67A and lower than L29

- **Sediments**: Marsh was higher than all compartments; S333 was similar to L29 and L67A

27
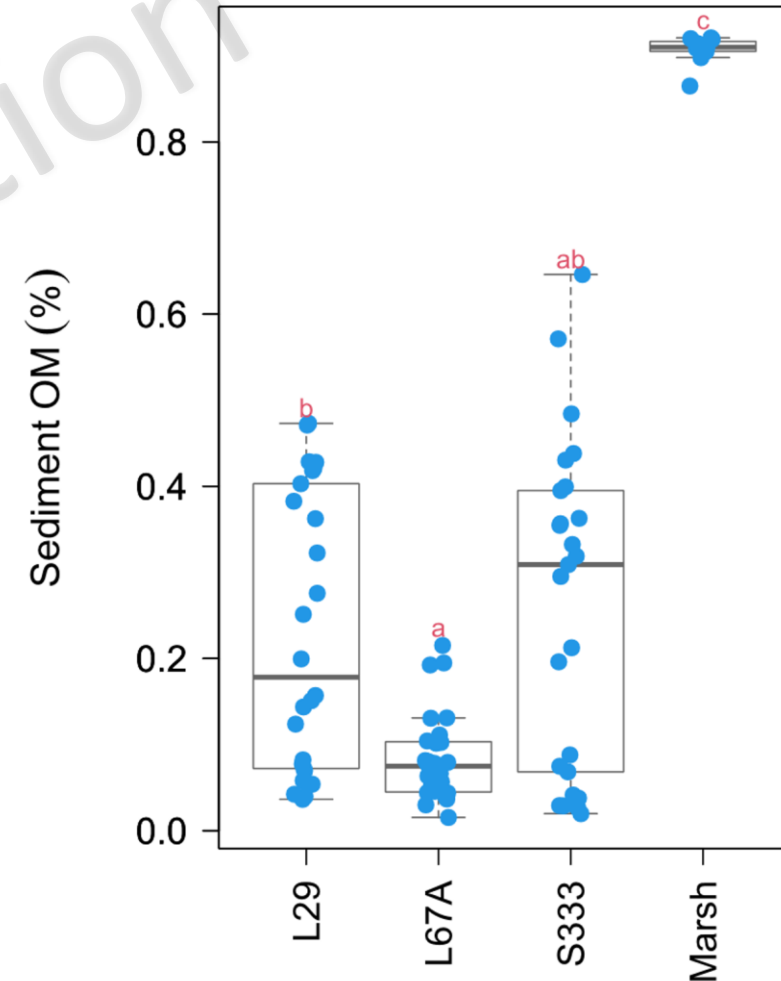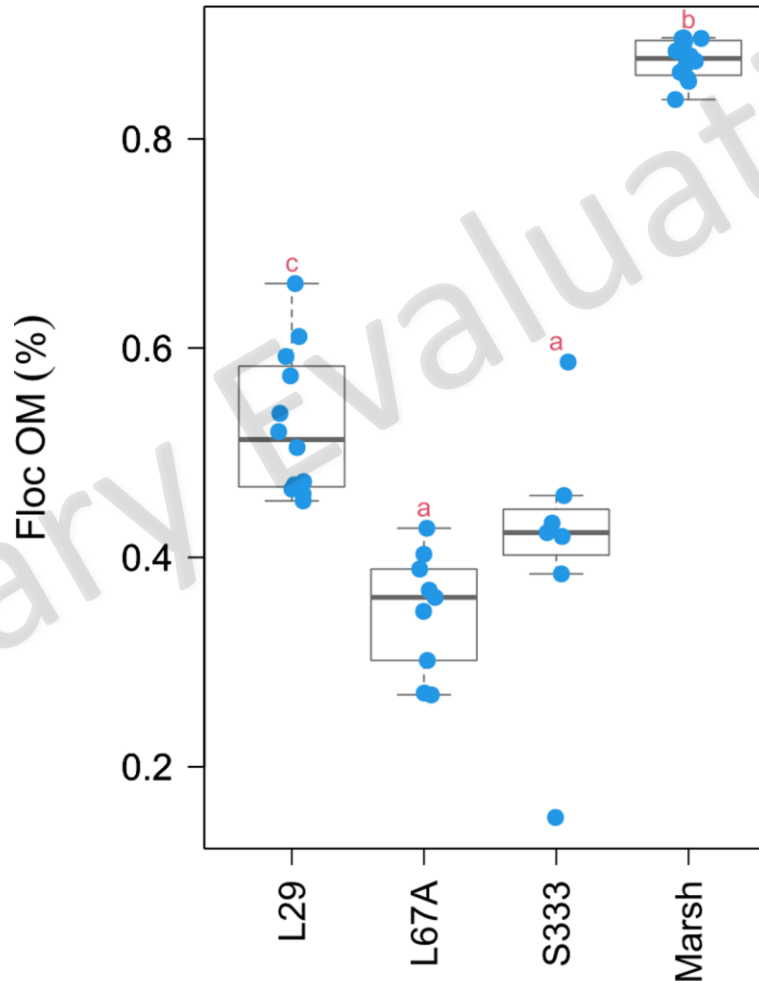
OM% Normalized Total Phosphorus
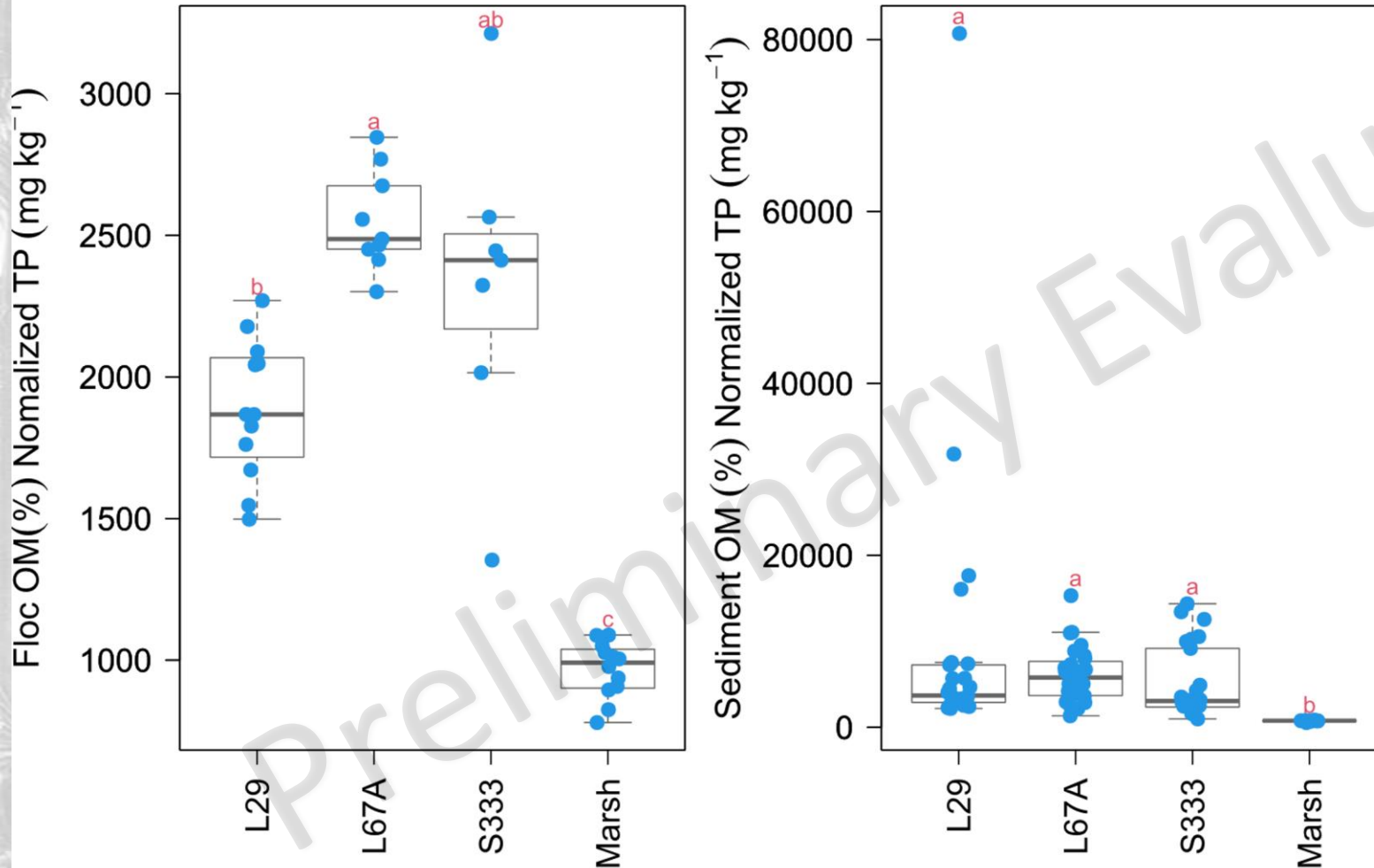
- **Floc**: Marsh was lower than all compartments; S333 was similar to L29 and L67A

- **Sediment**: Marsh was lower than all compartments; S333 was similar to L29 and L67A

28

Organic Phosphorus

- **Floc**: Marsh had the lowest levels; S333 was similar to both canal compartments
- **Sediments**: S333 was similar to all compartments
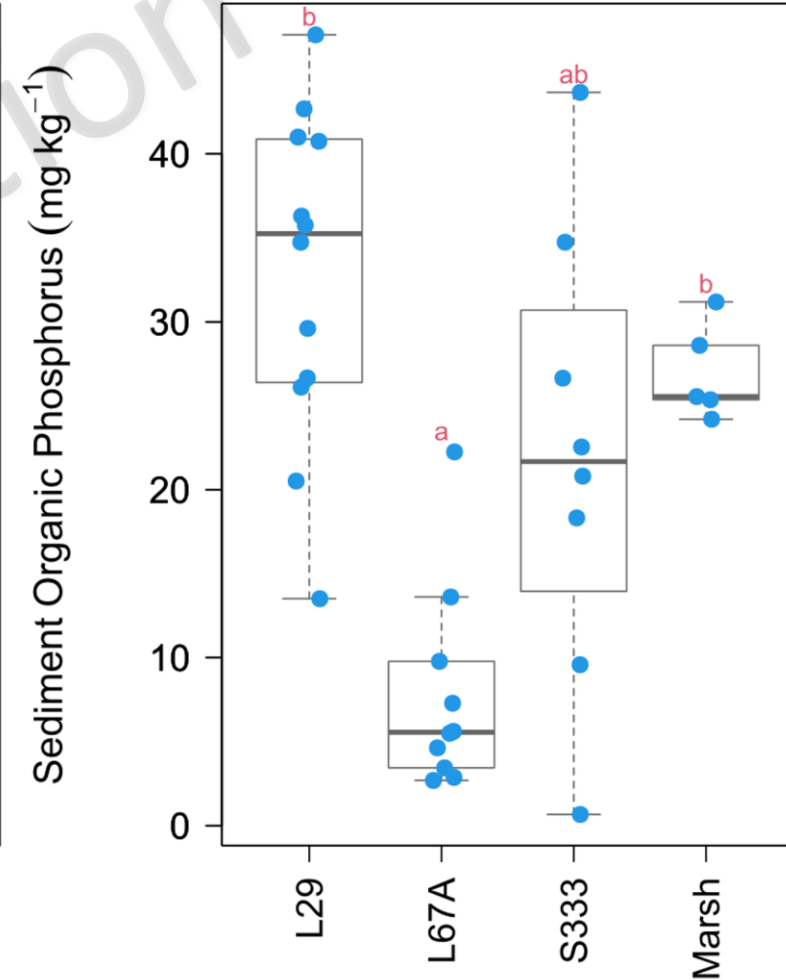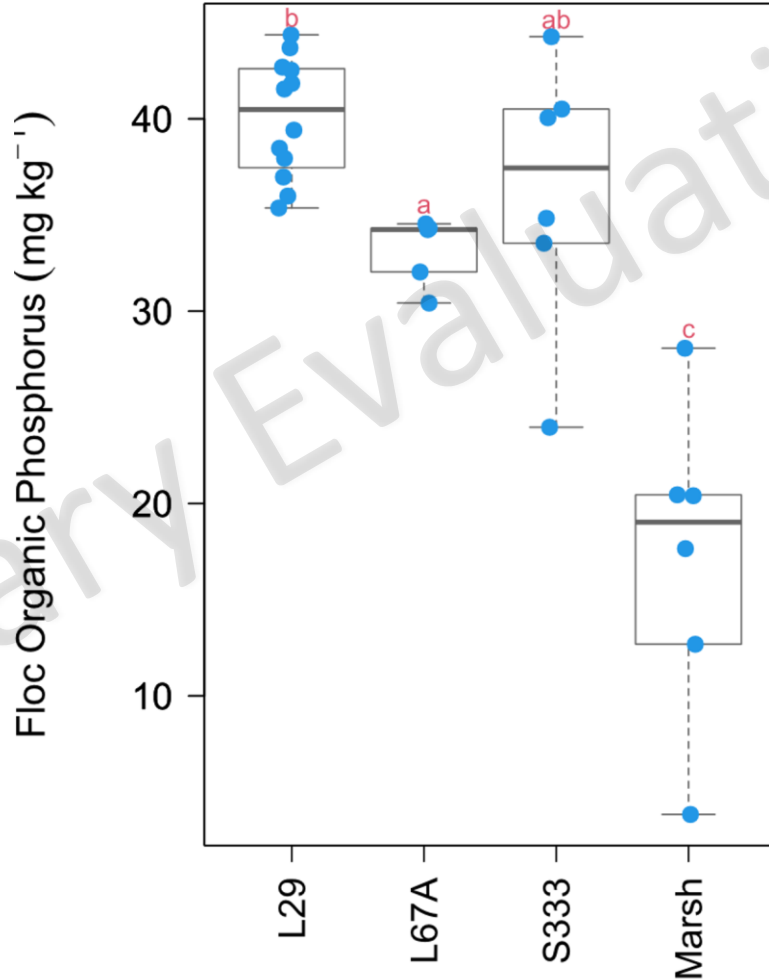
Inorganic Carbon
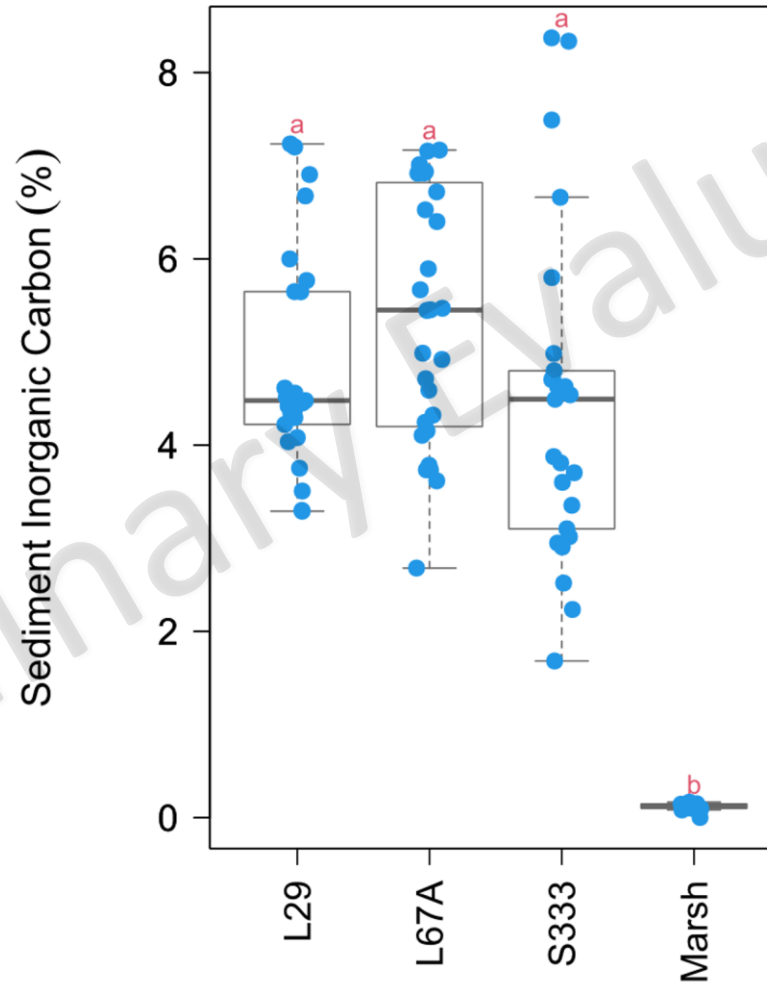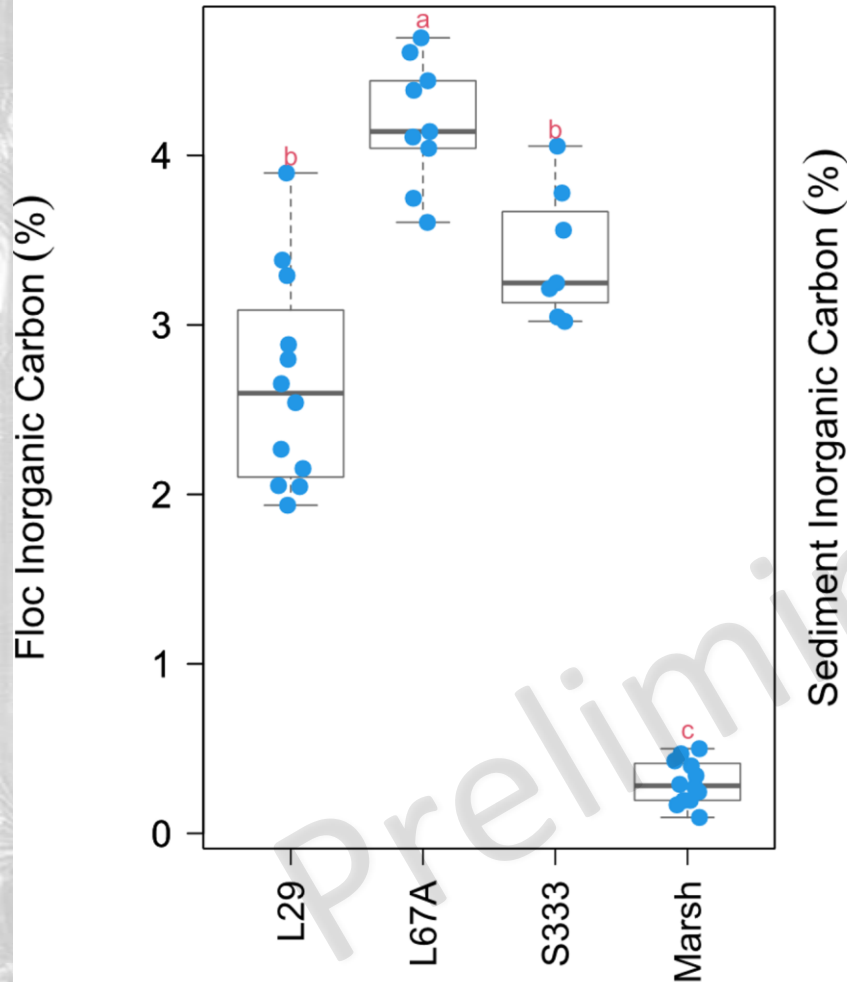
- **Floc**: Marsh was lower than all compartments; S333 was similar to L29; all values are low
- **Sediments**: Marsh was lower than all compartments; S333 was similar to L29 and L67A

30

*Available Phosphorus
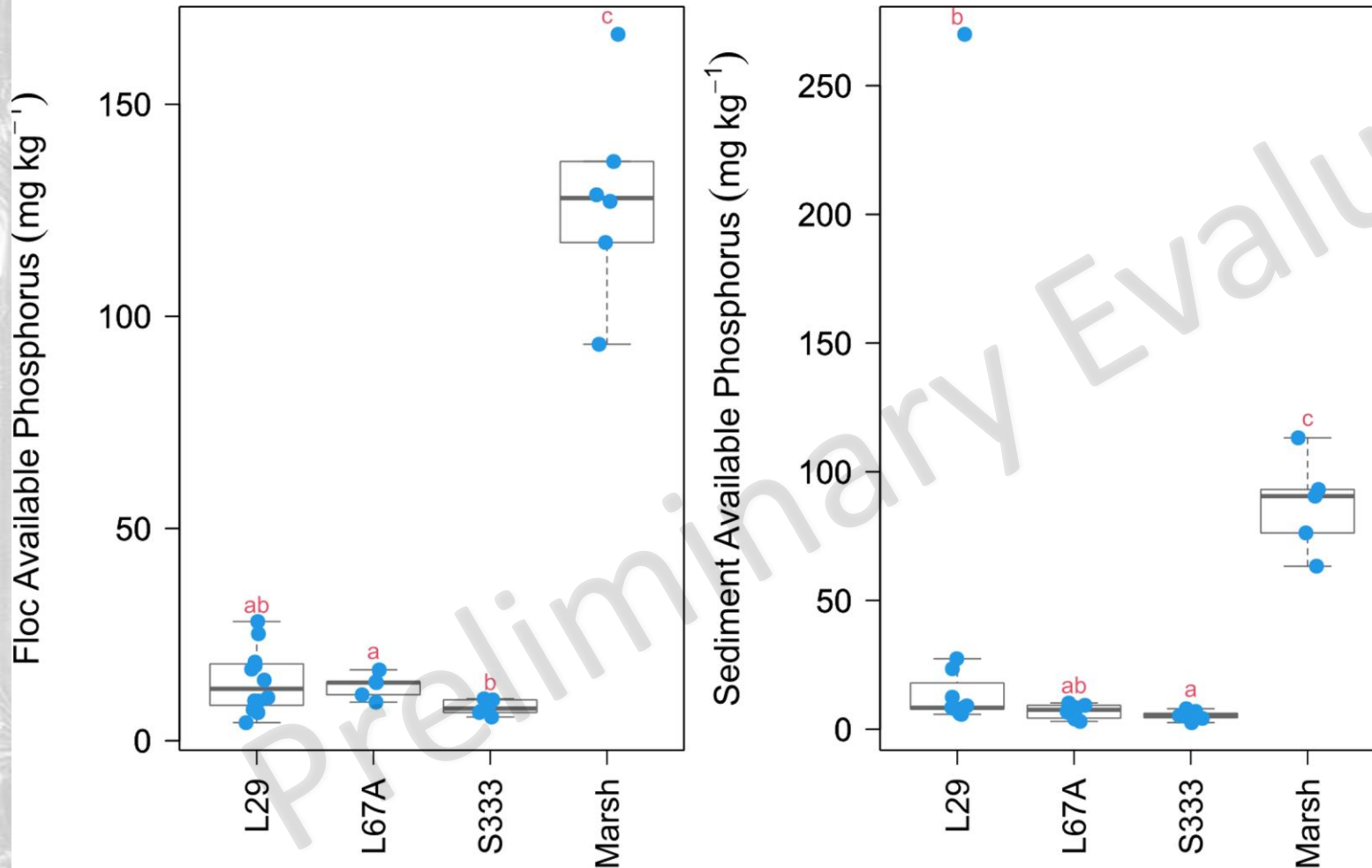
- **Floc**: Marsh had the highest value of the compartments; S333 was similar to L29
- **Sediments**: Marsh was highest; S333 was similar to L67A

*Available Phosphorus- extractable by distilled deionized water & 1 M NH_4Cl

31

*Bound Phosphorus

- **Floc**: Marsh had the lowest levels; S333 was similar to both canal compartments
- **Sediments**: S333 was similar to all compartments
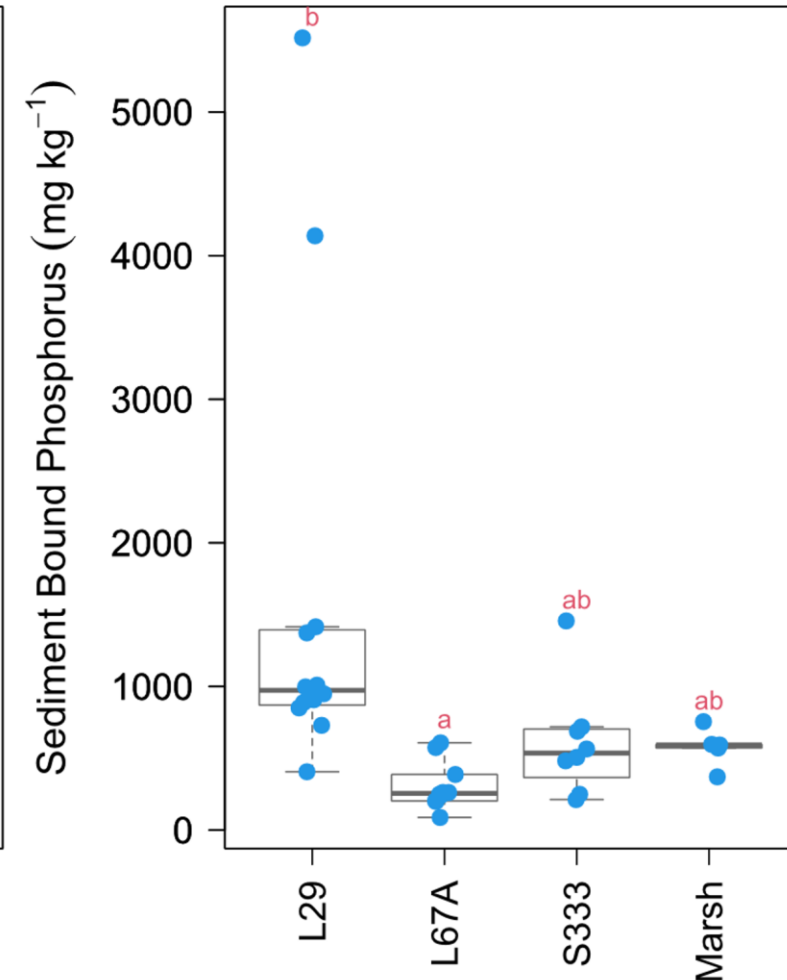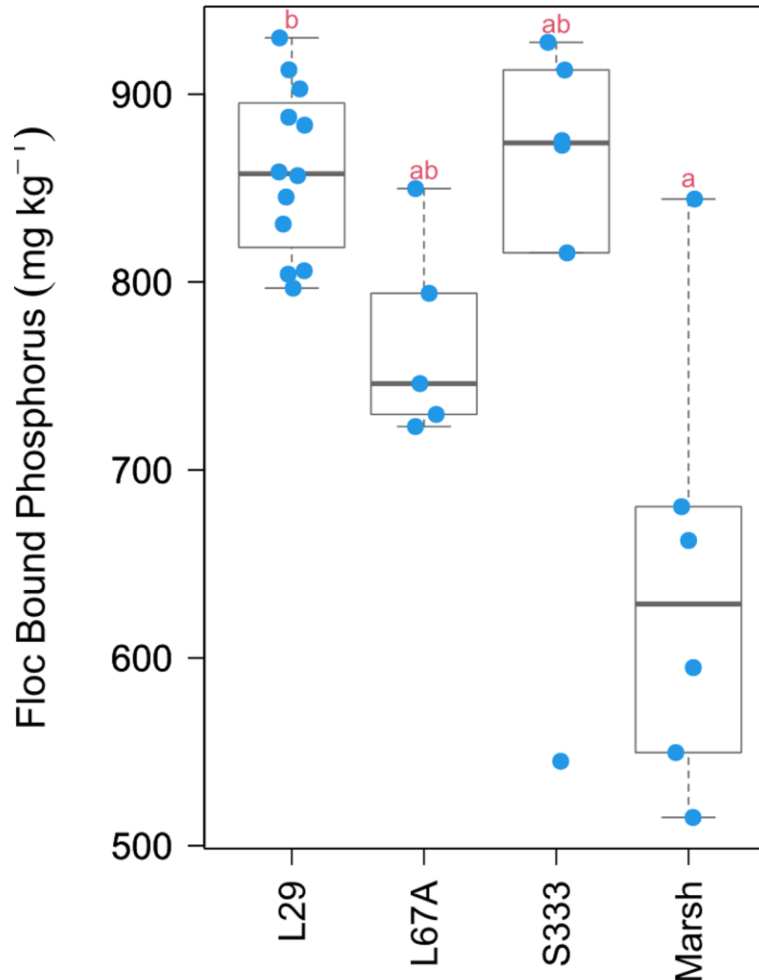
Al-bound P and Fe-bound P, organically-bound P, Ca- or Mg-bound P, and recalcitrant P

32

Principal Components Analysis

- **Floc**: Marsh samples were characterized by high organic matter and low inorganic carbon (IOC), while L29 was characterized by higher TP and larger particle sizes, L67A and S333 were characterized by higher IOC

33

Principal Components Analysis

- **Sediments**: Marsh samples were characterized by high OM and low IOC, L29 was characterized by higher d_{50} and TP for most locations

34
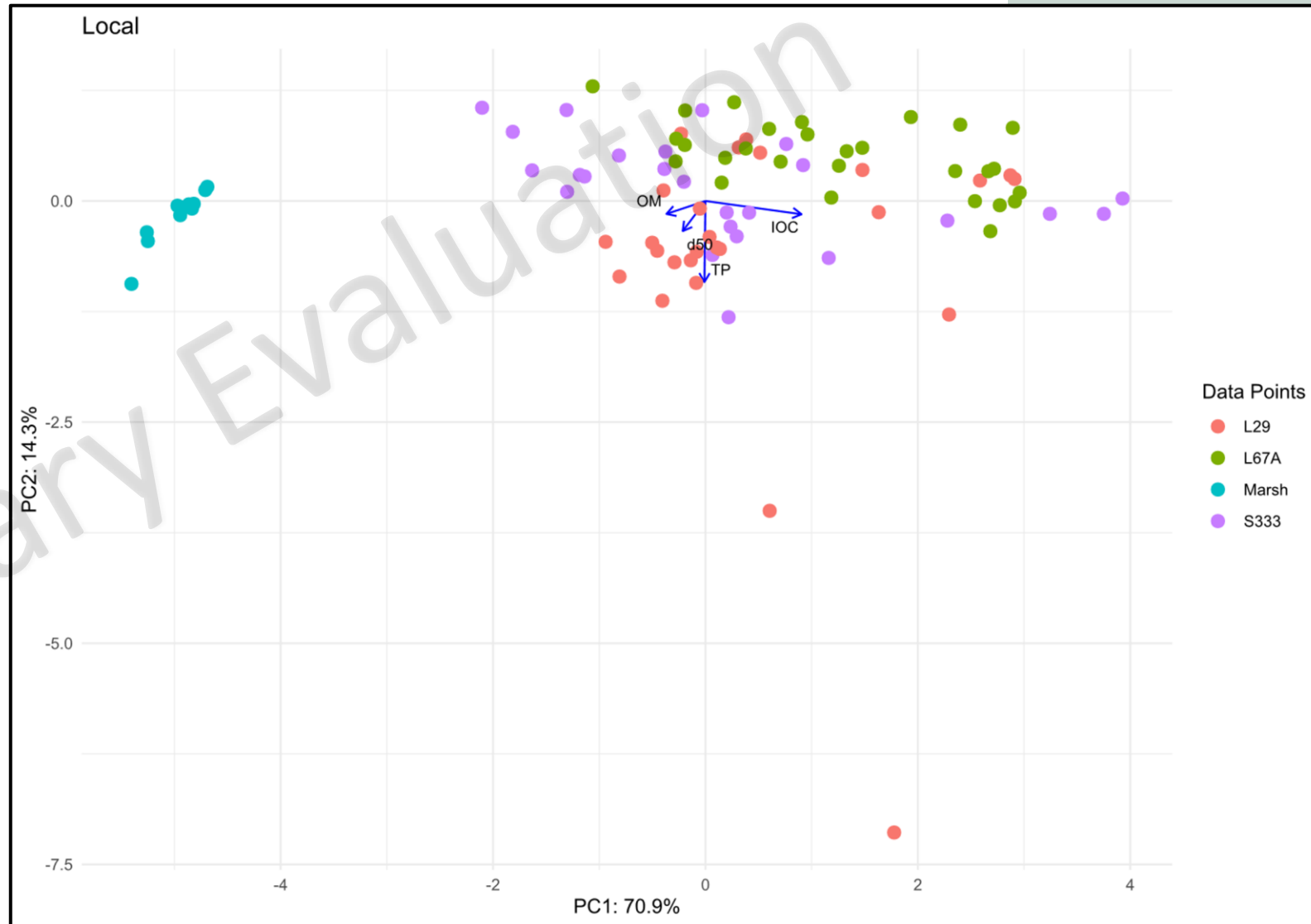
Local Results:
Flow Directionality

National Park Service

South Florida Natural Resources Center

Results – Flows at a local scale

- Flow directions in L29 canal is mostly west
- Flows east (S333) occurred at minimum rates (<100 cfs) when L67A flows were similar to S333 and S12s flows are very low
- When L67A flows exceed S333, the remainder moved west (S12s) in L29
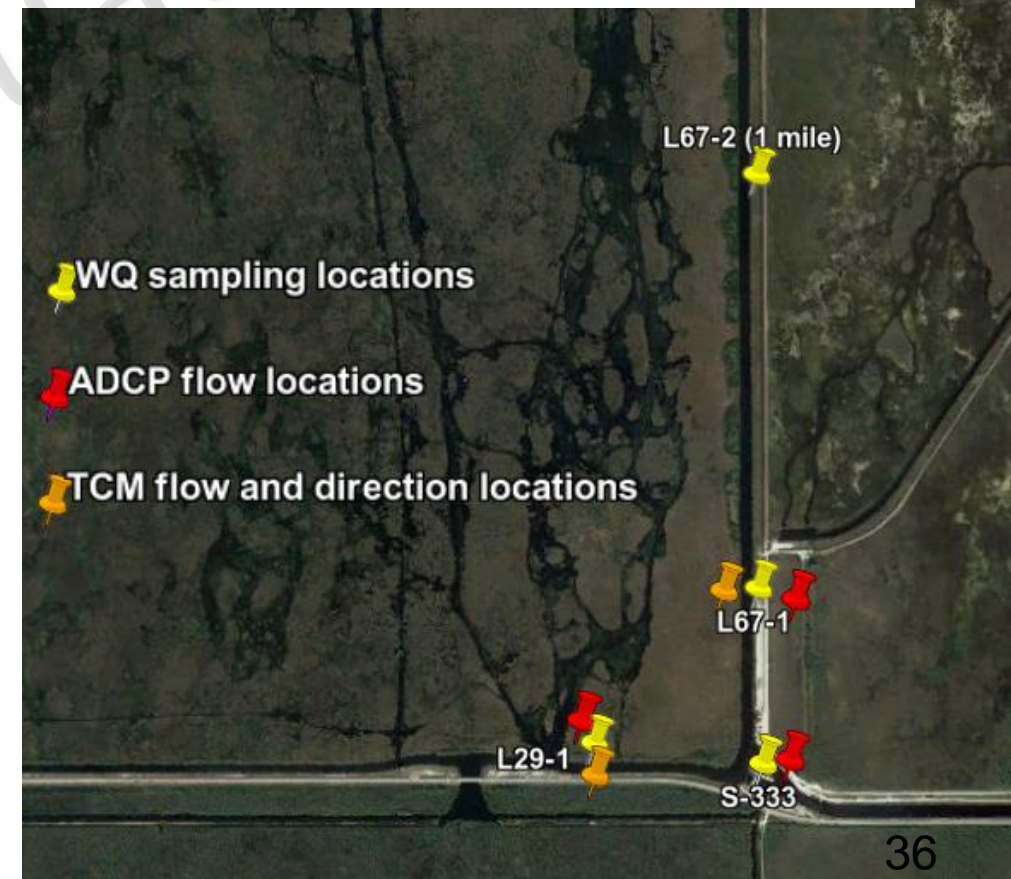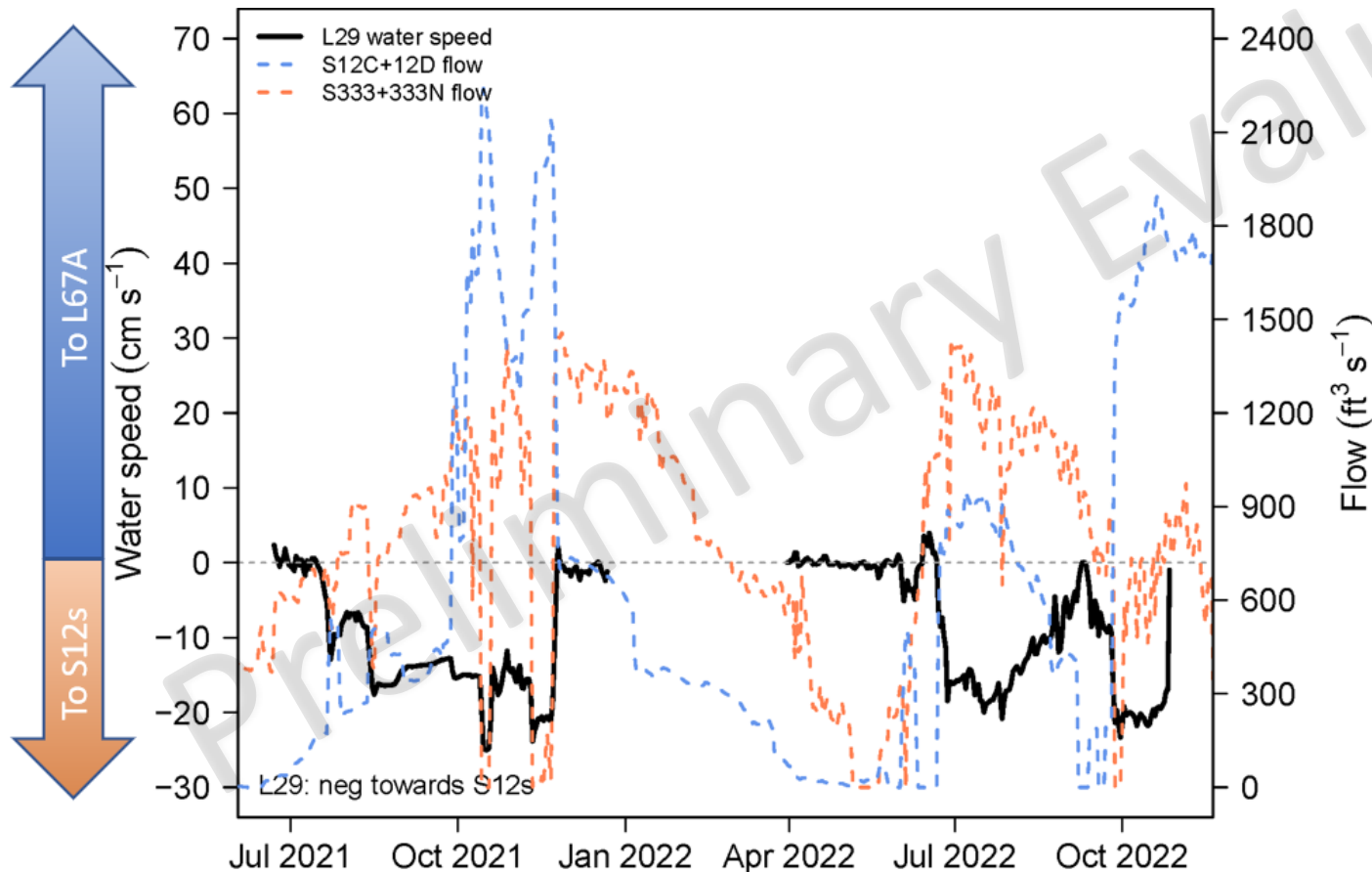
Floc and Sediments

- Given floc and sediments within the canal compartments are characterized by low OM, moderate particle sizes, and highly bound P, removal of these materials has a potential to reduce P loading to S333

- Consideration of engineering solutions for the S333 should focus on L67A as a major contributor and potentially the marsh as little flow from the L29 canal appears to be reaching the S333 structures

Subregional Results:
Floc and Sediments

d_{50} median laser particle size
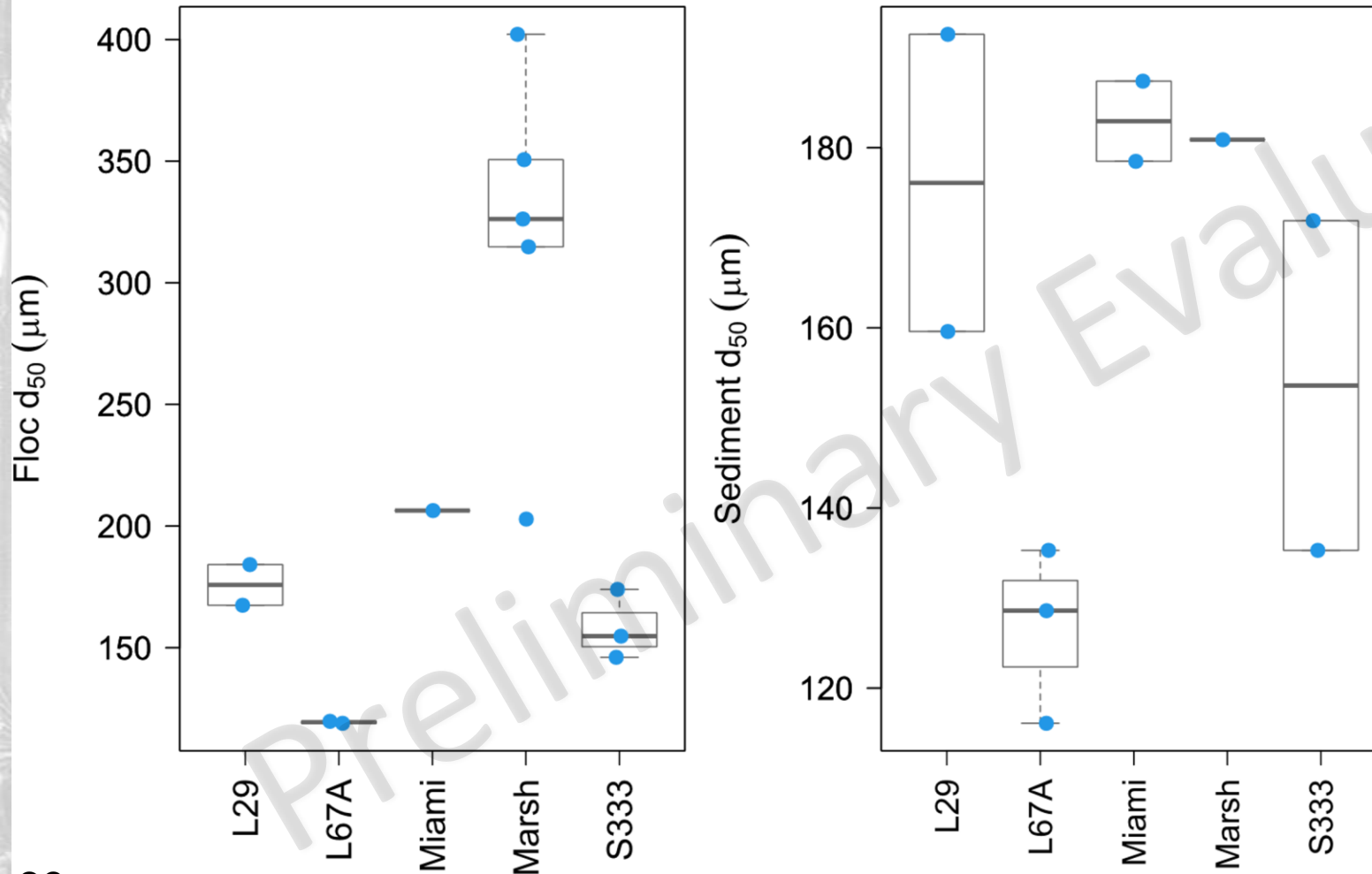
- **Floc**: S333 median was ~150 μm, while marsh was ~320 μm
- **Sediments**: S333 was less than 180 μm

The subregional scale sample size for statistical testing is sufficiently small. Power maybe low to detect all significant differences

Total Phosphorus

- **Floc**: L29 was higher than Marsh; S333 was similar to all compartments
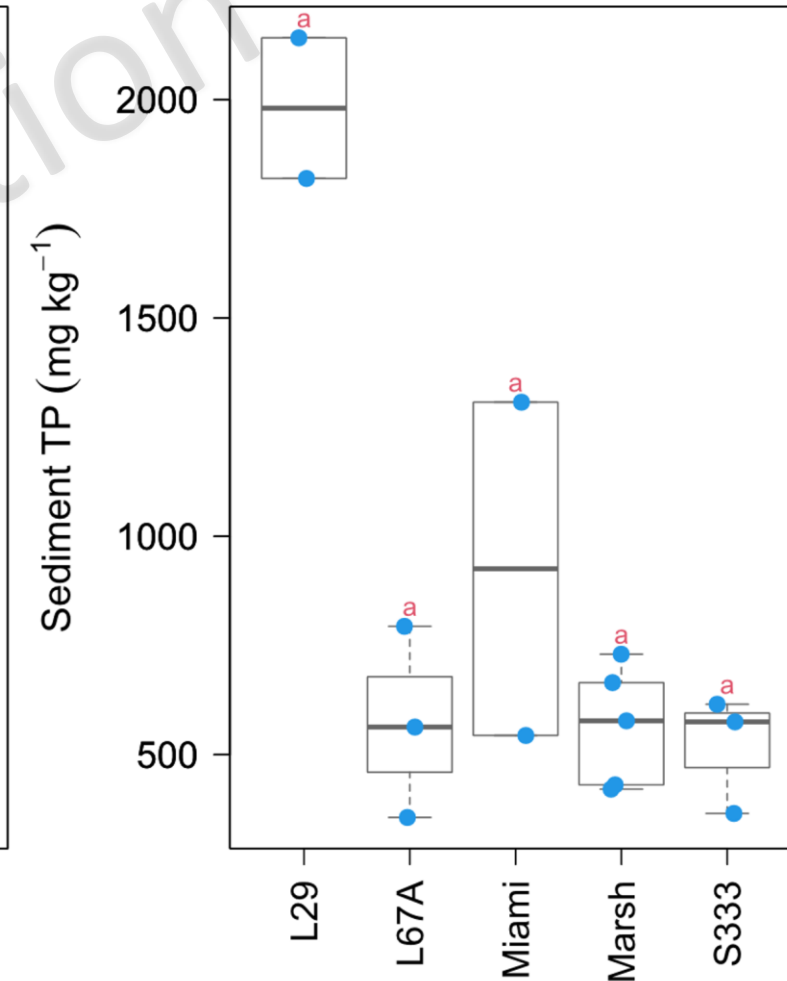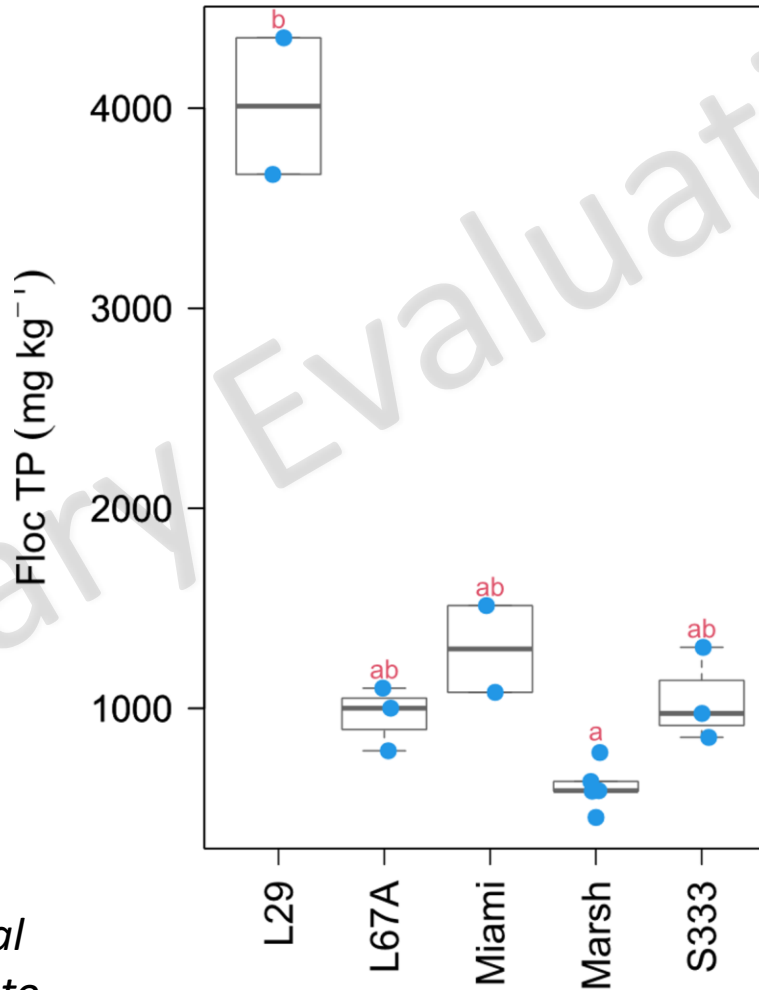
- **Sediments**: S333 was similar to all compartments

The subregional scale sample size for statistical testing is sufficiently small. Power maybe low to detect all significant differences

40

Organic Matter

- **Floc**: S333 was similar to all compartments
- **Sediments**: S333 was similar to all compartments

The subregional scale sample size for statistical testing is sufficiently small. Power maybe low to detect all significant differences

41
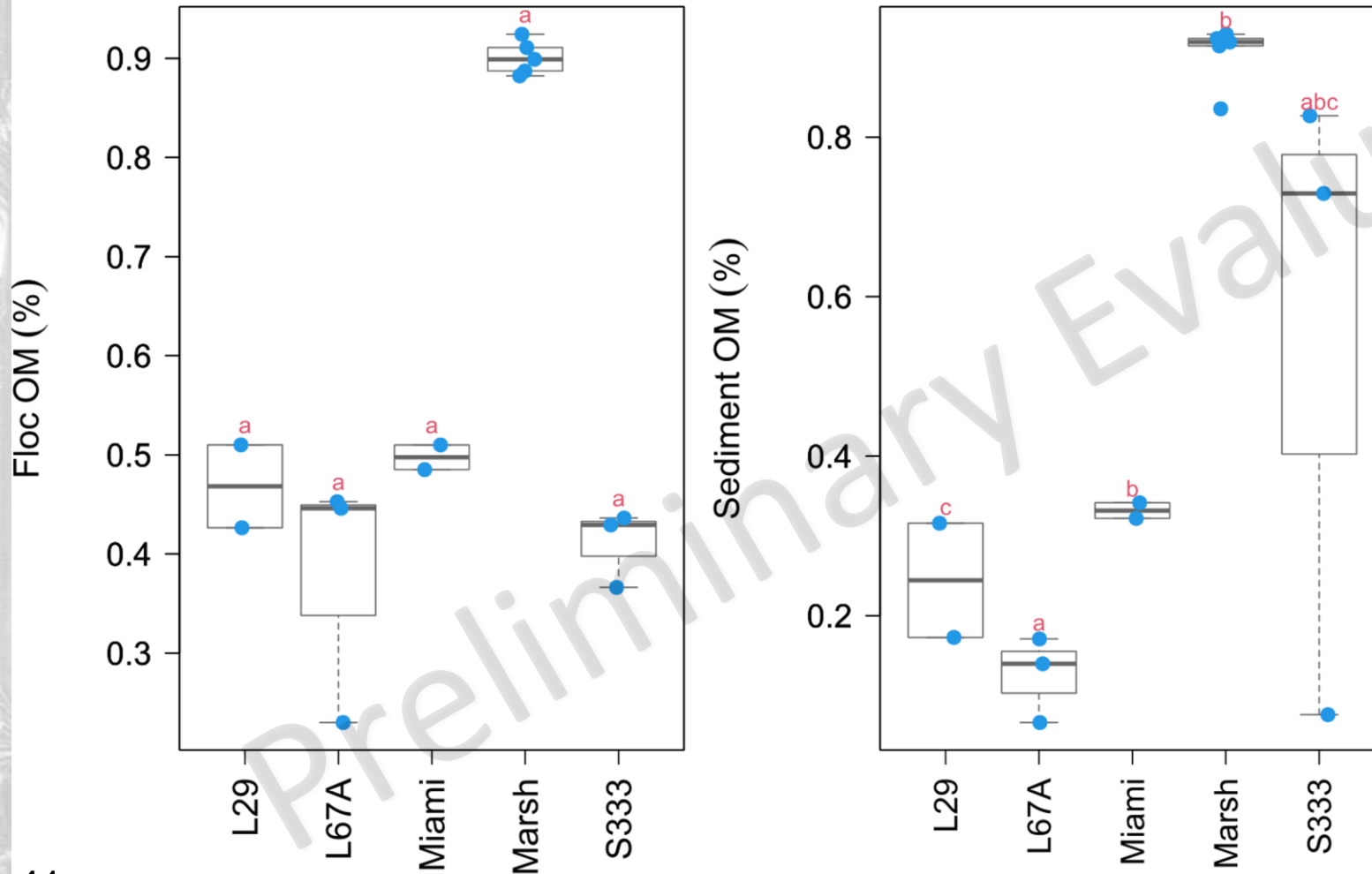
OM% Normalized Total Phosphorus

- **Floc**: S333 was similar to all compartments, while Marsh was lower than L29

- **Sediments**: S333 was similar to all compartments

The subregional scale sample size for statistical testing is sufficiently small. Power maybe low to detect all significant differences

42

Cobalt

- **Floc**: S333 was similar to all compartments
- **Sediments**: S333 was similar to all compartments

The subregional scale sample size for statistical testing is sufficiently small. Power maybe low to detect all significant differences

Zinc

- **Floc**: S333 was similar to all compartments
- **Sediments**: S333 was similar to all compartments

The subregional scale sample size for statistical testing is sufficiently small. Power maybe low to detect all significant differences

44

Iron

- **Floc**: S333 was similar to all compartments
- **Sediments**: S333 was similar to all compartments

The subregional scale sample size for statistical testing is sufficiently small. Power maybe low to detect all significant differences

45

Manganese

- **Floc**: S333 was similar to all compartments
- **Sediments**: S333 was similar to all compartments

The subregional scale sample size for statistical testing is sufficiently small. Power maybe low to detect all significant differences

46

Lead

- **Floc**: S333 was higher than Marsh, but similar to all other compartments
- **Sediments**: S333 was similar to all compartments

The subregional scale sample size for statistical testing is sufficiently small. Power maybe low to detect all significant differences

47

Nickel

- **Floc**: S333 was similar to all compartments
- **Sediments**: S333 was similar to all compartments
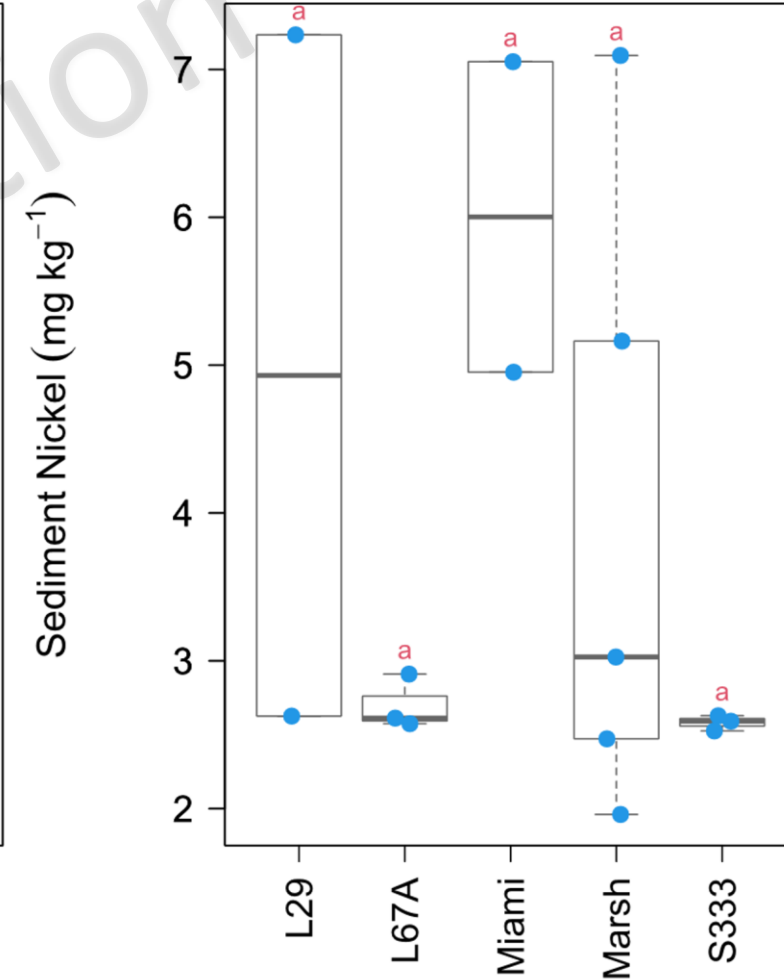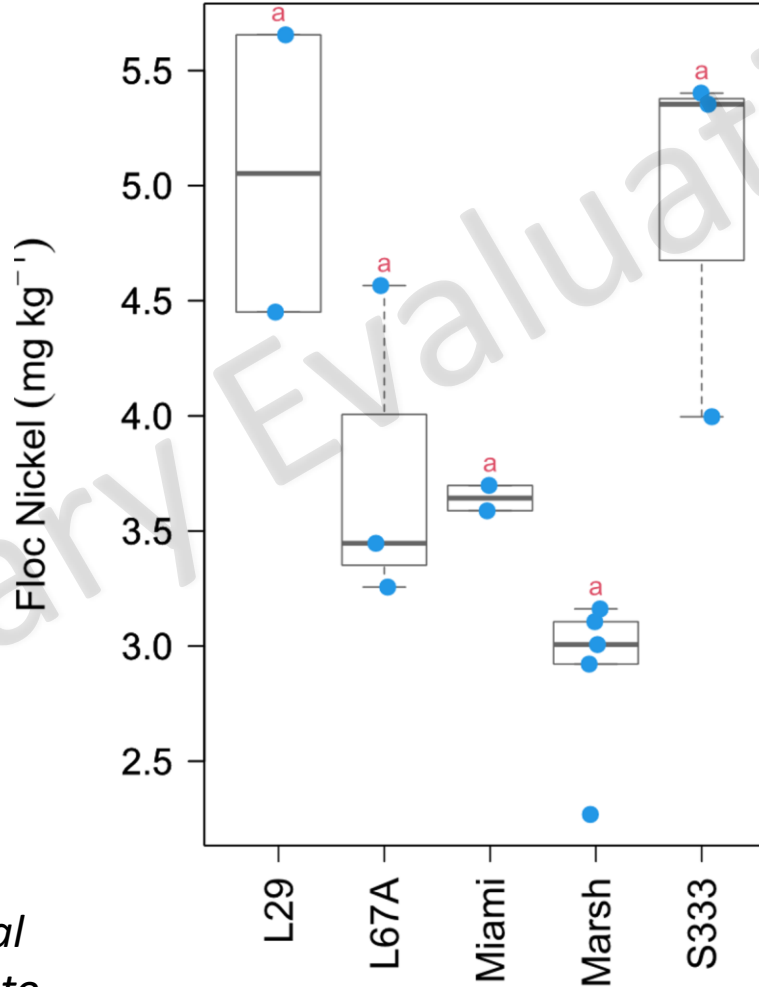
The subregional scale sample size for statistical testing is sufficiently small. Power maybe low to detect all significant differences

48

Cadmium

- **Floc**: S333 was similar to all compartments
- **Sediments**: S333 was similar to all compartments

The subregional scale sample size for statistical testing is sufficiently small. Power maybe low to detect all significant differences

49

Results – Floc and sediments at a subregional scale

$\delta13C$

- **Floc**: S333 was similar to all compartments
- **Sediments**: S333 was similar to all compartments

The subregional scale sample size for statistical testing is sufficiently small. Power maybe low to detect all significant differences

50

$\delta15N$

- **Floc**: S333 was similar to all compartments
- **Sediments**: S333 was similar to all compartments

The subregional scale sample size for statistical testing is sufficiently small. Power maybe low to detect all significant differences

51

δ18O

- **Floc**: S333 was similar to all compartments

- **Sediments**: S333 was similar to all compartments

The subregional scale sample size for statistical testing is sufficiently small. Power maybe low to detect all significant differences

52

Calcite

- **Floc**: S333 was similar to all compartments
- **Sediments**: S333 was similar to all compartments

The subregional scale sample size for statistical testing is sufficiently small. Power maybe low to detect all significant differences

53

Quartz

- **Floc**: S333 was lower than Miami, but similar to Marsh and L29 compartments
- **Sediments**: S333 was similar to all compartments
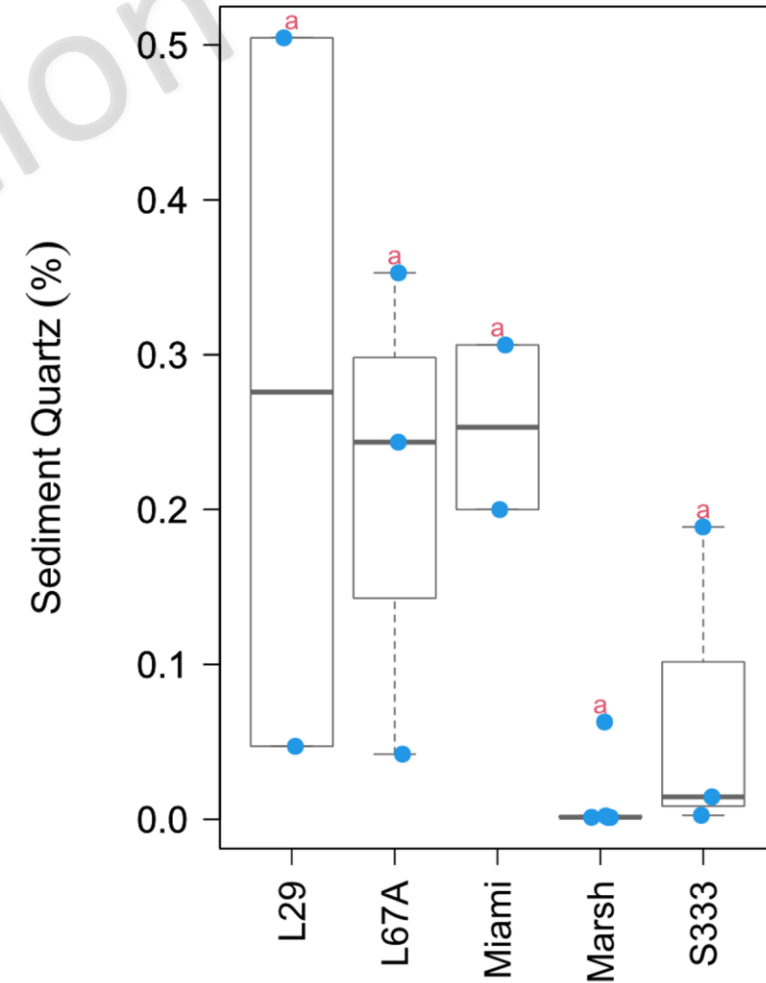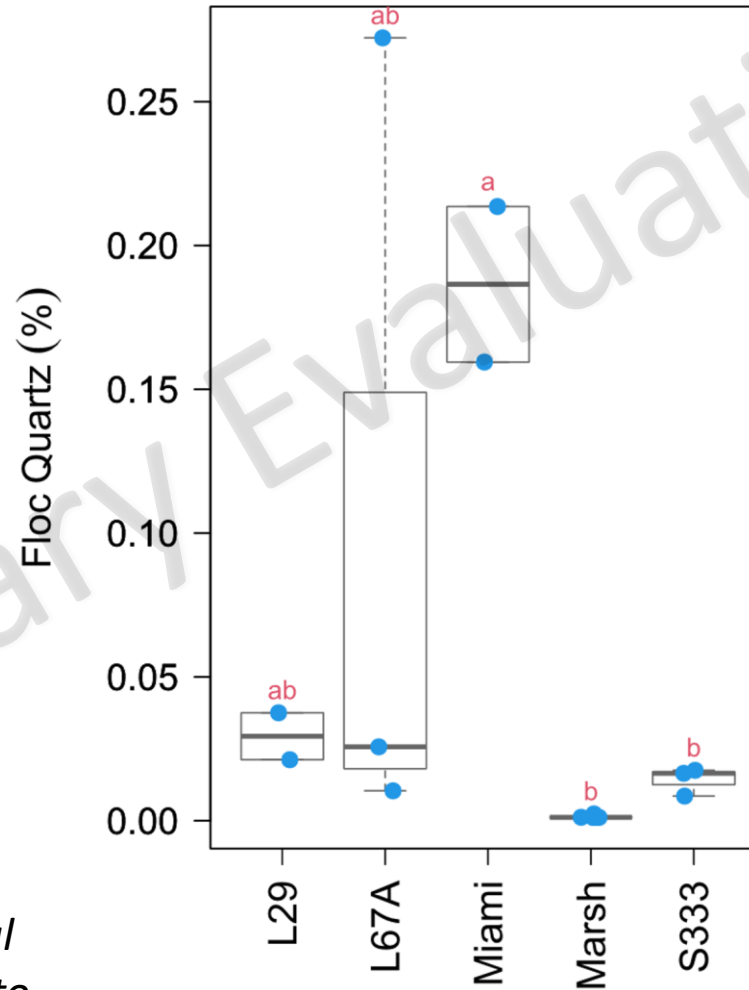
The subregional scale sample size for statistical testing is sufficiently small. Power maybe low to detect all significant differences

54

Clay minerals in floc

- Among the canal compartments, calcite dominates the clay mineral fractions followed by quartz
- S333 had very little quartz relative to the other canal locations
- Very little clay minerals were observed in the marsh

Clay minerals in floc

Legend:
- Calcite
- Quartz
- Aragonite
- Iron Sulfide
- Hematite
- Illite
- Palygorskite
- Kaolinite
- Ca oxide phosphate
- Mg carbonate
- Iron silicon
- Na Al Fe phosphate

Clay minerals in sediments
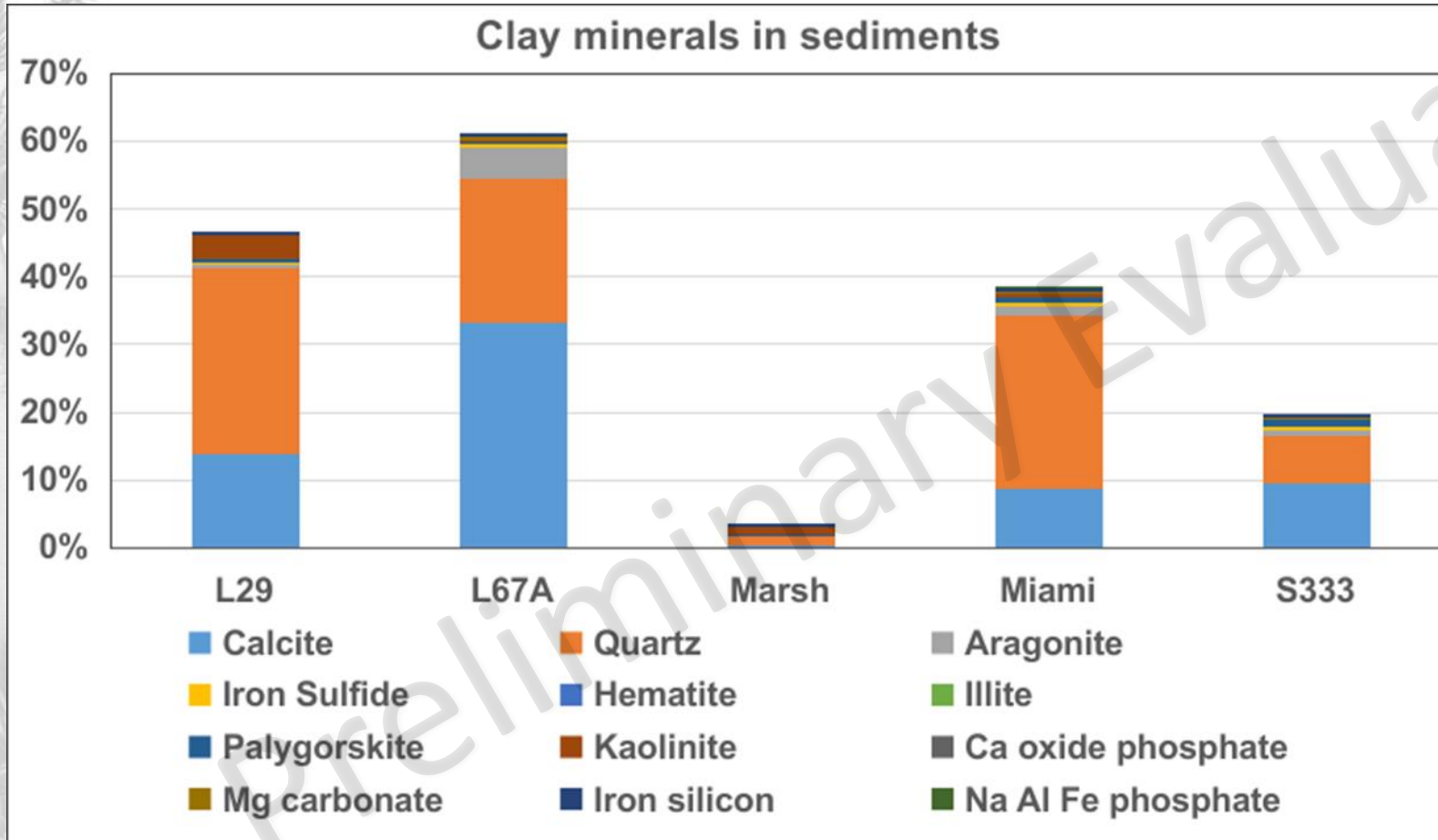
- Quartz percent of clay minerals was greater in the L29 and Miami canal followed by calcite
- Calcite dominated at L67A
- At S333, quartz and calcite were about equal
- Very little clay minerals were observed in the marsh

56

Principal Components Analysis for Floc

- Marsh was characterized by higher $\delta18O$ and OM*
- L29 was characterized by elevated TP*, Pb, and Cd
- S333 was characterized by higher $\delta15N$ and lower $\delta18O$
- Miami was characterized by higher quartz, calcite and cobalt

* Similar results than the local scale study

Regional for Floc

57
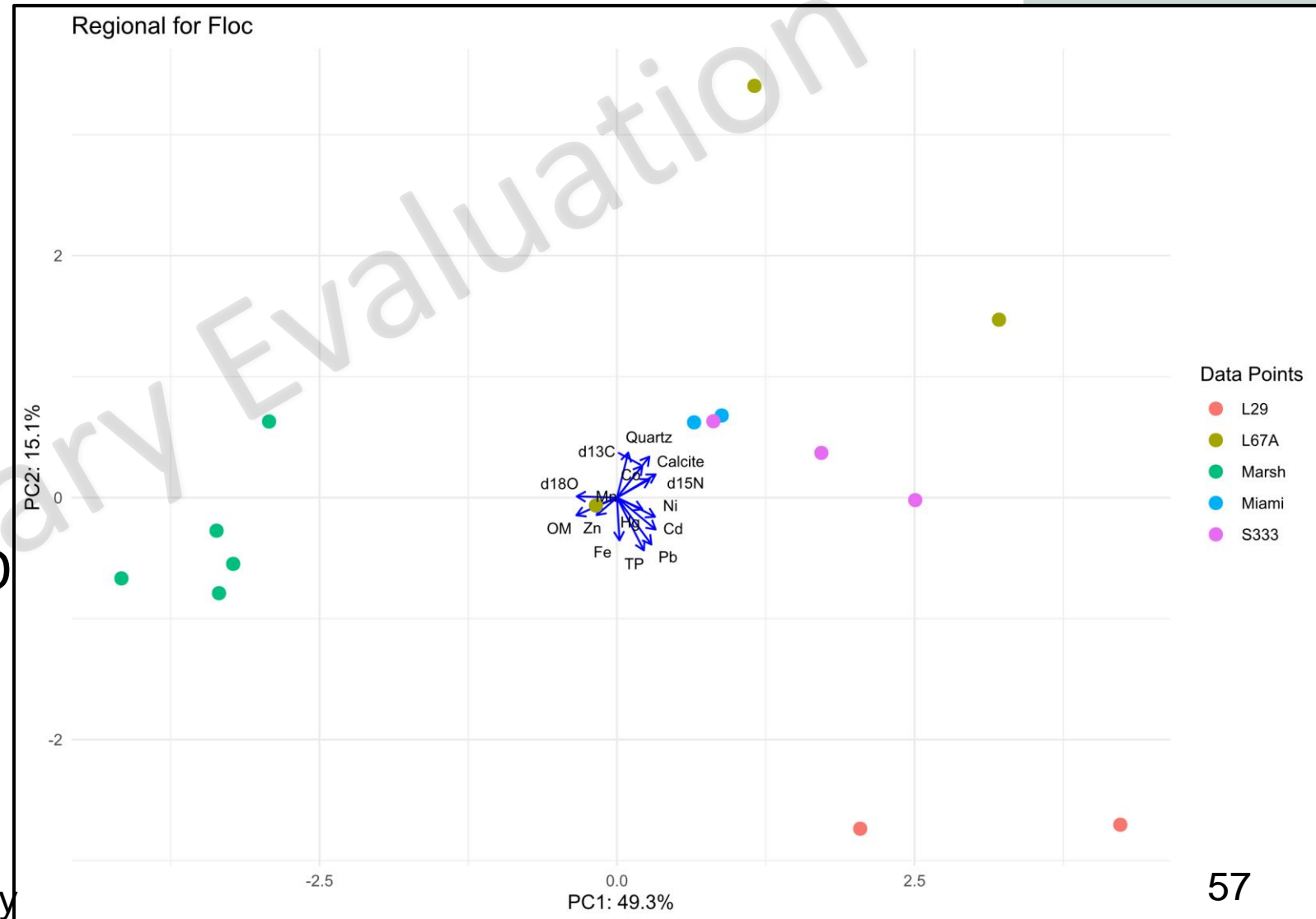
Principal Components Analysis for Sediments
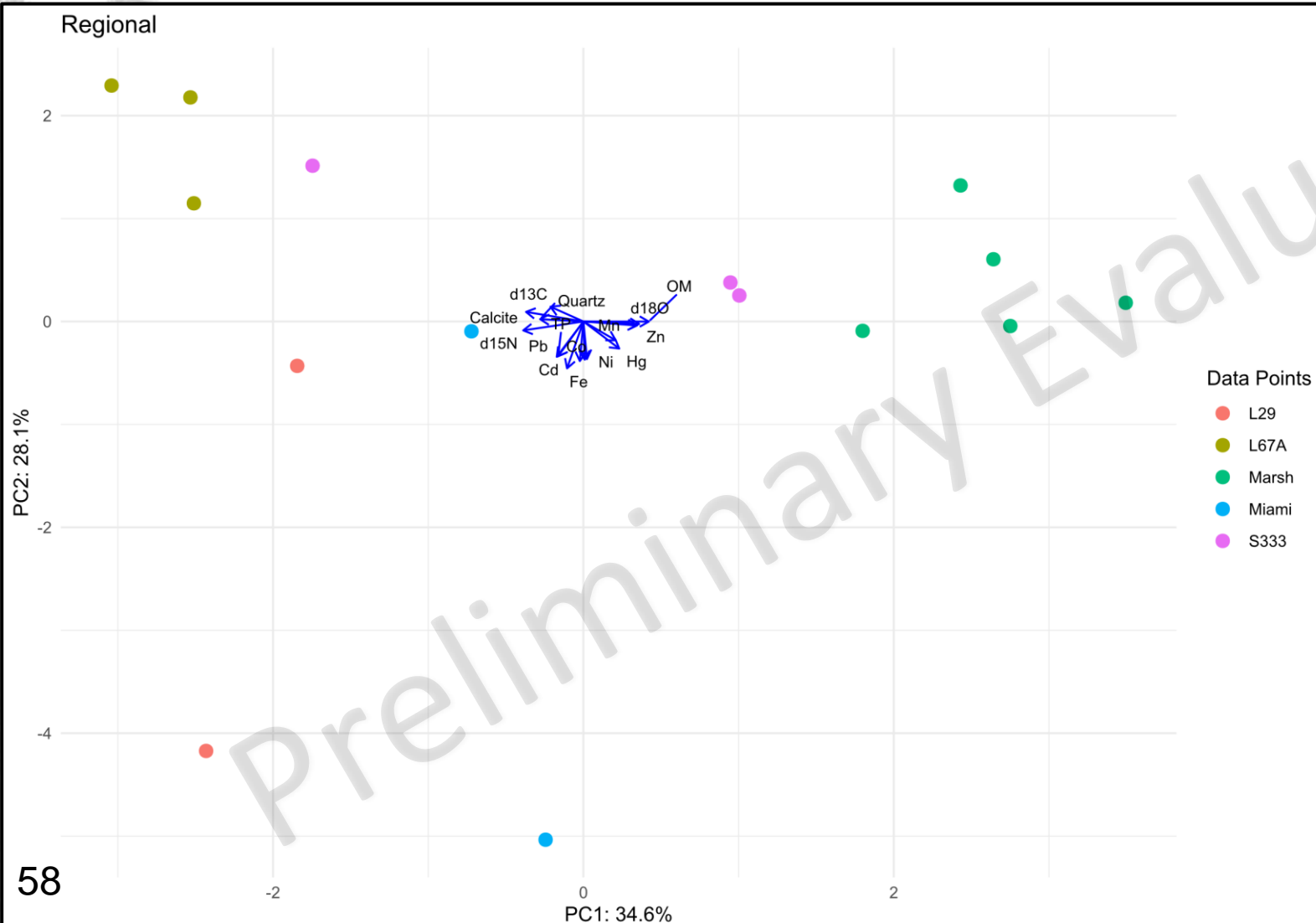
- Marsh was characterized by higher OM*, $\delta18O$, and Zn
- L67A was characterized by higher $\delta18C$ and calcite
- L29 and Miami were characterized by higher $\delta15N$ and cadmium

58

* Similar results than the local scale study

Hierarchal Cluster Analysis

- Cluster analysis based on all parameters (IOC, TP, OM, metals, clay minerals, and isotopes) for floc resulted in:
  - Marsh stations clustering
  - L29 clustering
  - S333, L67A, and Miami clustering

Floc - All data

Hierarchal Cluster Analysis

Sediment - All data
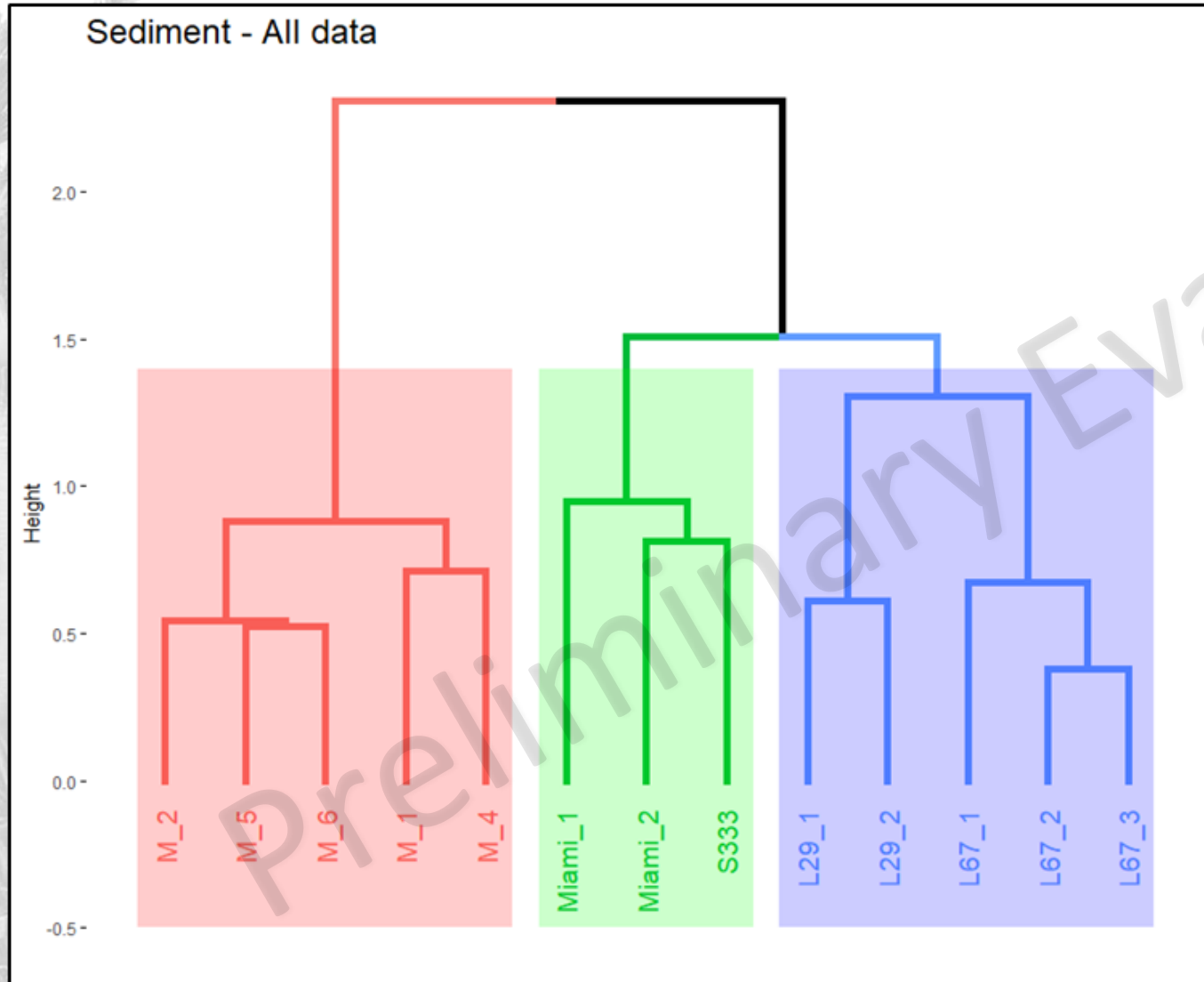
- Cluster analysis based on all parameters (IOC, TP, OM, metals, clay minerals, and isotopes) for sediments resulted in:
  - Marsh stations clustering,
  - L29 and L67A clustering,
  - S333 and Miami clustering

60

Hierarchal Cluster Analysis

- Cluster analysis based on all parameters (OM, herbicide associated metals, quartz and calcite clay minerals, and isotopes) for floc and sediments resulted in:
  - S333 sediment cluster with Marsh floc and sediment
  - S333 flocs are clustered with all canal floc and sediment

Floc and Sediment Hierarchical Clusters

61
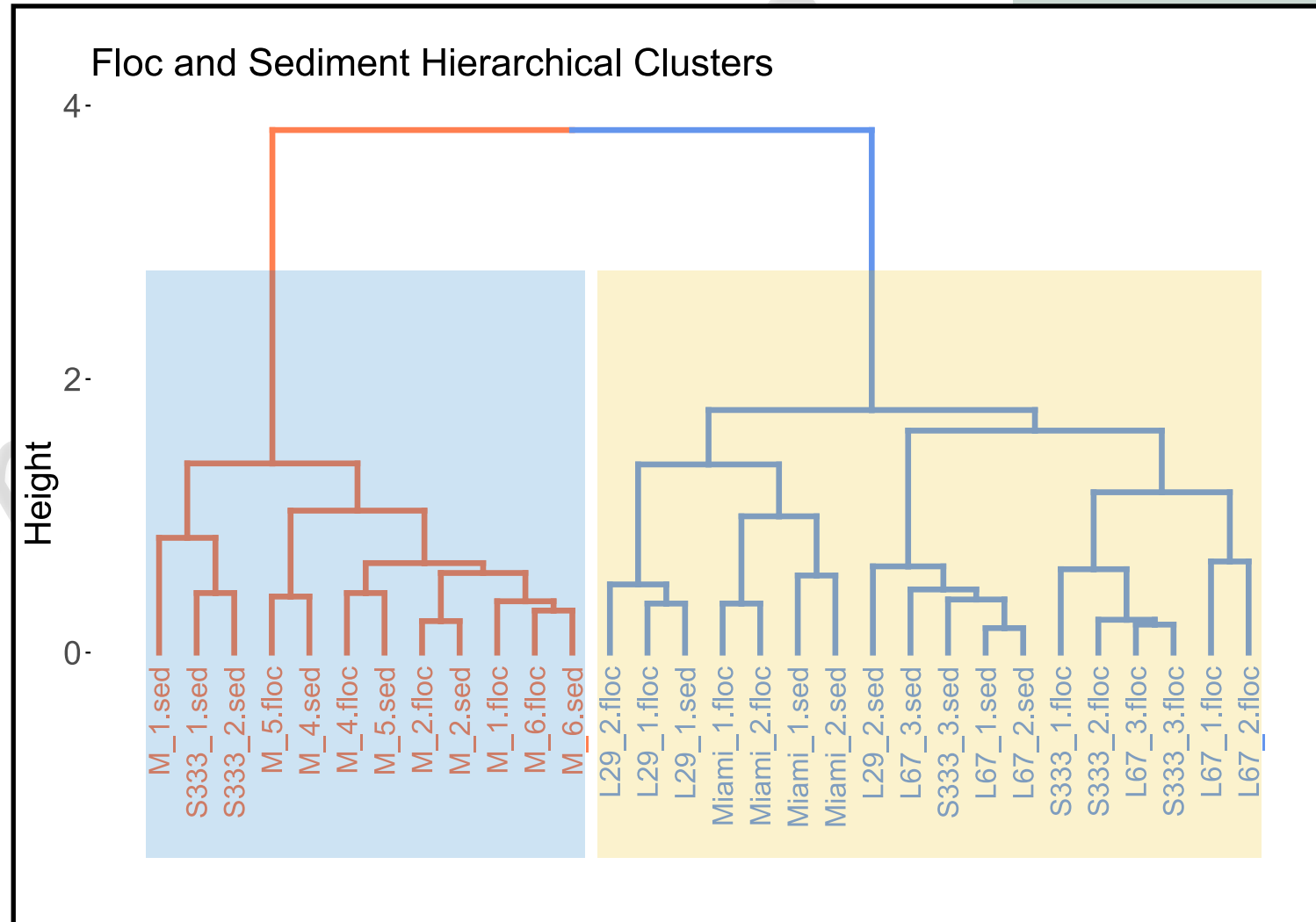
Discussion – Subregional scale

Floc and Sediments

- Based on the floc and sediment results at the subregional scale, S333 tended to have chemical and physical properties similar to contributing canals. Marsh locations might have minor contribution.

- Hydrologic analysis through Tilt Current Meters (TCM) situated in L67A and L29 indicated that flows down L67A can overwhelm the S333 gate-controlled discharge resulting in L67A flows moving west along the L29 canal. Further, there are very few observed conditions that resulted in flows from L29 east toward the L67A canal or S333, reducing the likelihood that L29 is a consistent source of nutrients to S333 structures.

SECTION 5: CONSOLIDATED COMMENTS AND RESPONSES

Commenter Name	Agency	Deliverable	Slide/Page Number	Comment/Question	Responses from ENP	Commenter Response
Seán Sculley	SFWMD ASB Chief	62-Slide-Deck	1	2nd bullet: define "roll-over processes.	It is the transport of sediments through the process of saltation.	No issues noted
Seán Sculley	SFWMD ASB Chief	62-Slide-Deck	1	4th bullet: what was SFWMD role in SOW development, data provision, and work product review?	SOWs of were shared with SFWMD to provide comments. Data and reports will be shared when finalized.	No issues noted
Seán Sculley	SFWMD ASB Chief	62-Slide-Deck	15	How was acoustic method error estimated?	$$Error_{Total} = \frac{\sum_{i=1}^{n} {(Tck_{EV,i} - Tck_{Cr,i})}/{Tck_{Cr,i}}}{n}$$ where n is the total of compared locations, TckEV,i is the sediment thickness of the ith acoustic location (from Echoview), and TckCr,i is the sediment thickness of the ith core sample.	
Seán Sculley	SFWMD ASB Chief	62-Slide-Deck	15	Is the interpolated sediment core thickness estimate of volume more accurate?	Yes, compared to acoustic method in this particular study.	No issues noted
Seán Sculley	SFWMD ASB Chief	62-Slide-Deck	5	1st bullet: "cross-sectionally", were samples taken horizontally (perpendicular to flow) in addition to varying depths?	Yes, this is referenced further down the presentation in slide 9. Wording has been revised.	No issues noted
Seán Sculley	SFWMD ASB Chief	62-Slide-Deck	9	locations where samples were taken are not identified on the graph	Locations were ~23 m in front of the gate and has been included.	No issues noted
Seán Sculley	SFWMD ASB Chief	62-Slide-Deck	15	FYI, SFWMD field station crews excavated 80-100K yd3 of sediment from STA-5/6 about 15 years ago with beneficial results. The reported sediment volume equates to about 11K yd3, an order of magnitude smaller. Sharing this if excavation of this sediment is being considered.	S333 working group will come up with recommendations in September and sediment removal may be considered. Thank you for sharing this information.	No issues noted
Seán Sculley	SFWMD ASB Chief	62-Slide-Deck	25	3rd bullet: is the 0.32 ft/s velocity relevant to observed velocities upstream of S333 when flowing?	Reviewing output from the SFWMD Hydrodynamic modeling suggest that at least Jun 16 and 27 had flow rates at this level based on observed conditions during the sampling events.	No issues noted
Colin Saunders	SFWMD	62-Slide-Deck	26-32	It is difficult to understand what the TP units really mean in these graphs. For instance, is "OM% normalized P" in units of mg-P per kg-total or mg-P per kg-OM? Guessing the latter, but needs clarifying. Same question for the other slides with graphs of different Phosphorus types (e.g., sediment available, floc bound, etc..)	Units are corrected for future presentations.	Comment Addressed
Colin Saunders	SFWMD	62-Slide-Deck	59-61	the "subregional" cluster analyses of floc and sediment chemistry, when done separately (slides 59,60), show canal floc/sediments cluster separately from the marsh. However, clustering of all sediment/floc data together (slide 61) shows some S333 samples clustering with Marsh M1. Need to clarify how and why this could be the case.	When adding more data and groups (the case for floc and sediment combined) the underlying data distribution can contain overlapping patterns which are revealed through the cluster analysis. When we combined them we were looking to understand if the sediment and floc locations would group which would have been inferred to mean they have some type of interaction, but as you see that was not strictly true.	Comment Addressed
Colin Saunders	SFWMD	62-Slide-Deck	61, 10, 12, 62	take home message from slide 61 is that S333 sediments & floc are primarily related to L67A sediments, although S333 sediments at sites S333-1 and -2 are primarily related to marsh sediments at M1 (farthest southwest, slide 10). It is unclear how marsh site M1 (farther west) clusters with S333 sediments, while M2 (east, nearer S333) does not. I wonder if the sediments/floc collected at M1 and M2 were in different habitats? If Marsh M2 is not a source (but M1 is), then the likely path from M1 to S333 is through L29. However, hydraulic data and modeling shows relatively little influence of L29 (west) on S333 sediments (slide 62). This apparent contradiction (and uncertainty) needs to be resolved. Could this be an artifact of low sample sizes (per slide 12) on the analysis?	This was an exploratory investigation, limited samples were taken so over interpreting is cautioned. Regardless, M1 is completely surrounded by a newtork of airboat trails (highly disturbed) while M2 was about 270 m to the closest airboat trail (relatively less distrubed).	The condition of marsh sites is helpful. The grouping of the sediments from the disturbed marsh site (M1), despite its hydrologic separation from the canal sites, contributes to a line of evidence that disturbance (e.g., oxidation through erosion into the water column, or faunal processing) may be a critical driver of canal sediment biogeochemistry. Further investigation is needed to determine to what extent canal sediment signatures are driven by 1) a local source of disturbed sediments (e.g., marshes along the canal edge, between spoil mounds?), 2) a more upstream source (e.g., STA or agriculture), or 3) local processing (i.e., all sediments entering the canal are rapidly oxdized/processed by fauna).

Commenter Name	Agency	Deliverable	Slide/Page Number	Comment/Question	Responses from ENP	Commenter Response
Colin Saunders	SFWMD	62-Slide-Deck	51, 52	Subregional data show the d15N signature and TP of the marsh sediments are substantially lower than those from canal sites (L29, S333, L67A). The magnitude of high TP (>>1000 mg/kg) and d15N from canal samples is consistent with particles sourced from higher trophic levels (invertebrates, fish, alligators), in contrast to marsh signatures which are indicative of primary producer sources. So animal activity could be a source of canal sediment/floc particles and a mechanism that concentrates sediment/floc TP. Should the role of canal fauna be evaluated for potential management actions? A related question (for minerology experts) - would calcite signatures also be related to different biological sources (ie., bone fragments; as opposed to CaCO3 generated by periphyton)?	1. Regarding the results for isotopes, the information is included in the final report and states that: "The average $\delta^{13}C$ were -29.10‰ in floc and -28.33‰ in sediment, which fall within the $\delta^{13}C$ value ranges of −22 to −34‰ for organic matter produced by C3 plants (Wang et al. 2014). The $\delta^{13}C$ values for floc and sediment samples showed similar ranges across the five sampling locations, ranging from −28.24 to −29.61‰ in floc and from −27.01 to −29.41‰ in sediment. The ordering of $\delta^{13}C$ values was S333 > L67A > Miami > L29 > marsh in floc samples, and L67A > S333 > Miami > L29 > marsh in sediment samples (Figure 1A). The relatively high $\delta^{13}C$ values in floc and sediment from S333 and L67A compared to L29, Miami, and marsh suggest a greater contribution of C4 plants such as sugarcane (−11 ± 1‰), sugarcane-cultivated histosol (−25.37‰), or other organic biomass such as fish (−19.2 to −31.5‰) to the organic biomass source in these sampling sites (Wang et al., 2014). The average $\delta^{15}N$ values were 3.49‰ in floc and 3.52‰ in sediment, which are similar to the $\delta^{15}N$ values reported for C3 plants (3.27‰) and lower than those for C4 plants (5.55‰) in C4 herbaceous plants (Liu et al., 2022; Wright and Inglett, 2009). These values also fall within the range of $\delta^{15}N$ values in prairie soils (2.98-3.86‰) reported by Liu et al. (2022) and Wright and Inglett (2009). Compared to sediment, the slightly lower $\delta^{15}N$ values in floc indicate recent deposition of organic matter, while higher $\delta^{15}N$ values in sediment represent older, more humified organic matter (Novak et al., 1999). The ordering of $\delta^{15}N$ values was L67A > S333 > L29 > Miami > marsh in floc samples, and L29 > L67A > S333 > Miami > marsh in sediment samples (Figure 1B). Both floc and sediment from the marsh had the lowest $\delta^{15}N$ values, which were less than half of the values from the Miami canal, the site with the second-lowest $\delta^{15}N$ values for both floc and sediment samples. The low $\delta^{15}N$ values in the marsh may be attributed to low growth rate of marsh plants and less isotope fractionation during N uptake, while the low $\delta^{15}N$ values in the Miami canal may indicate the input of fresh organic biomass from upstream sources (Inglett and Reddy, 2006). In contrast to marsh signatures which are indicative of primary producer sources, animal activity could be one of sources for canal sediment/floc particles and canal fauna may be included for potential management actions."	Given the wide range of potential source values of d13C (-11 to -34), versus the range of values in floc & sediments, I do not think d13C data are very informative about teasing out sources. My question was primarily aimed at identifying potential sources that could influence d15N - specifically whether agricultural sources or fauna-processing seemed likely to explain the range in d15N observed at different sites in the study. While it is helpful to state that relationships between age or fauna and increased d15N simply exist, it would be more helpful to show the quantitative relationships between those drivers and d15N. Perhaps a table summarizing d15N values in the literature in comparison to site-specific values would be more helpful. For instance, are canal d15N values more similar to the d15N of Everglades fish, lower trophic levels [invertebrates], higher trophic levels [birds], or agricultural sediments? Similarly, are the d15N of the marsh sites lower than all of the latter sources? Since Calcite is more concentrated in the canal sediments, and since the d15N of canal sediments are higher than those of the marsh, would they interpret these findings to infer that canal sediments have been chemically processed (either through decomposition or consumption by small or large fauna) compared to marsh sediments? Or would they interpret that canal sediments are simply produced from a different non-marsh source? The text provided from the report does not provide any insights to these questions.

Commenter Name	Agency	Deliverable	Slide/Page Number	Comment/Question	Responses from ENP	Commenter Response
					2. Regarding the calcite, the following information is included in the final report: "Three carbonate minerals, calcite, aragonite, and magnesium (Mg) carbonate were detected in floc and sediment samples from all sampling locations, except Mg-carbonate was not detected in floc from the marsh. Calcite, which is the dominant mineral in the Everglades, was found in all samples due to the ideal calcium-pH-carbonate conditions for calcite formation in the ecosystem. The order of calcite contents among the locations was L67A > S333 > L29 > Miami > marsh for both floc and sediment. L67A had the highest calcite content, while the marsh had the lowest. The source of calcite could not be differentiated by XRD analysis, but it could potentially originate from periphyton in the marsh or from fragments of limestone or shell (Irick et al. 2012). The stable isotope analysis of inorganic carbon has been suggested to fingerprint the origin of carbonate (Dotsika et al. (2018). Aragonite, another calcium carbonate mineral with a different crystal structure from calcite, was also detected in all samples. Although less common than calcite, aragonite was found in soils in the south Everglades and is formed through biological processes on limestone bedrock (Judy et al. 2021). The percentage order of aragonite among the locations was similar to that of calcite but at lower concentrations. Magnesium Carbonate (MgCO3), a carbonate mineral that occurs naturally as the mineral magnesite. The concentrations of Mg carbonate in these samples are much lower than calcite and aragonite. Mg carbonate was not detected in floc from the marsh, likely due to the lower magnesium concentrations in the marsh floc compared to other locations. Other locations with low percentages of Mg carbonate were floc from S333 and sediment from L29 and the marsh."	
Nenad Iricanin	SFWMD	62-Slide-Deck	27, 41, 50, 51,52	It appears that these slides have the wrong units. The OM slides (27 and 41) are presented as less than 1 on Y-Axis. This may have occurred because the original data (I assume it was provided in spreadsheet was formatted as % while the data was in decimal form (ratioed). The isotope data should have units of ‰ (per mille). Please check your results with the information provided by Qiu, Li, Shinde, and Surratt for the 2023 GEER conference.	The Y-axes for the OM will be updated and that will be correctly reflected in future presentations and reports. Stable isotopes units will be corrected in the final reporting.	No issues noted
Nenad Iricanin	SFWMD	62-Slide-Deck	30, 53, 55	I assume that the inorganic carbon is predominantly CO_3. Could an explanation be provided why inorganic C in floc (Slide 30) for L67A ranges from 0.01-4.8% while calcite ($CaCO3$) ranges from 0.2 to ~0.6% (Slide 53), and 40% on slide 55? All the carbonate mineral for floc (Slide 55) look to be around ~45% for L67A. These values do not match. There are contradictions.	The unit for calcite ($CaCO3$) is incorrect (Slide 53). It is not 0.2-0.6%, it is 0.2-0.6 or 20-60%. The inorganic C is calculated based on its proportional molar mass of calcite (12/100=0.12). The inorganic C in floc (Slide 30) for L67A ranges from 3.6-4.8%, which equals 30-40% calcite. The results match the 20-60% calcite in Slide 53 and 45% in Slide 55. Inorganic carbon also includes other carbonate minerals, aragonite, and magnesium (Mg) carbonate.	When the average calcite, aragonite and dolomite concentrations in sediments are converted to inorganic carbon and compared with the average value provided in Figure 3.8, there still appears to be an inconsistency with the mineral data for these minerals in Table 3.6 (no label for table in Li report, Page 35 and 36). For example, inorganic C for S333 averages ~2.5% as C. The sum of calcite and aragonite (based on means) is 10.6% as $CaCO_3$. That converts to 1.3% as inorganc C. The same inconsistency is observed for L67A where the inorganic C from Figure 3.8 is approximately 6.8% compared to 4.6% inorganic carbon for calcite and aragonite (~38% as $CaCO_3$)from Table 3.6. Contribution from dolomite for these two locations is <1%. Can you explain this difference?

Commenter Name	Agency	Deliverable	Slide/Page Number	Comment/Question	Responses from ENP	Commenter Response
Nenad Iricanin	SFWMD	62-Slide-Deck	26, 27, 29	Marsh floc TP is reported as ~700 to 950 ppm (Slide 26). Marsh OM is reported as (I assume) 83 to 90% or 83,000 to 90,000 ppm (Slide 27). Assuming that organic carbon is approximately 2.3 to 2.7 times lower than organic matter, The organic C content can be estimated at 33% to 36% (33,000 to 36,000 ppm) using a conversion of 2.5. A generalized molar ration of C:N:P in organic matter can be assumed as 106:16:1 or the molar ratio of C:P is 106:1 or 41:1 by weight. That would suggest that approximately 800 ppm to 900 ppm of P can be attributed to organic matter. How was the organic P content in floc determined for Slide 29? If I use a C:P ratio of 22 (by weight for freshwater detritus (Meybeck 1982), the expected P from organic matter is approximately 1500 to 1600 ppm based on the organic matter content.	The organic P content measured here was the organic P in the NaOH extractant solution only, not for the entire floc sample; therefore, it was low. The NaOH organic P fraction is generally attributed to humic and fulvic acid P (Irick et al. 2013). For our samples, most of the organic phosphorus which was not extracted by NaOH should be fractionated into residual P. While phosphorus fractionation is a valuable technique for understanding the different forms of phosphorus in a sample, there are limitations associated with chemical sequential fractionation technique. The method may not always provide a complete representation of all phosphorus fractions present in a sample. The sequential extraction approach used in this method is based on assumptions about the specific chemical forms of phosphorus, but in reality, phosphorus compounds can be complex and diverse. Therefore, there is a possibility that certain phosphorus fractions may not be fully captured or accurately quantified using this method.	As indicated in the response from Line 87, there appears to have been some analytical issues due to the centrifugation process where some sediment particles may have been lost with the supernatent. This raise concerns regarding fractionation analyses performed.
Nenad Iricanin	SFWMD	62-Slide-Deck	27, 29	The organic matter content for marsh sediments is ~90%. This value is corresponds to approximately to 36% or 36,000 ppm) organic C. Slide 29 shows the sediment organic P in the marsh to be 25 to 32 ppm. Using these data, the organic C to organic P ratio is 1,100:1 to 1,400:1 by weight (3,000:1 on a molar level). Can you explain this large ratio?	Please see the response above for row 16. We can consider labeling organic P extracted with this method as "NaOH extracted organic P instead of "organic P". We also can explain it as "a portion of organic P" or "active organic P".	See above comment
Nenad Iricanin	SFWMD	62-Slide-Deck	32	How was the bound P determined (analyzed). It is indicated that the P is bound by Al, Fe, Ca, Mg, etc. Were these parameters measured to determine if they were available in sufficient levels to bind the P?	These metals were measured for total concentrations, not available or active fractions. It cannot be determine if they were available in sufficient levels to bind the P for this study.	Actually metals were not analyzed for total content as the EPA method used only leaches metals from the sediments and does not perform a total digest for these metals, especially Al.
Nenad Iricanin	SFWMD	62-Slide-Deck	49	Considering that crustal abundance of Cd ranges from 110 to 115 ppb, can you explain why Cd levels in floc range from 100 to 700 ppb and in sediments from 200 to 1,600 ppb?	The following information is in the final report: "Cadmium (Cd) is also the most commonly found trace metal in the P fertilizer (Bracher et al., 2021) and Cd has been used as a reliable tracer for identifying the source of fertilizer-derived P in the wetland sediments. Cd was found in all samples and ranged from 0.13-0.66 mg kg-1 in floc and 0.22-1.01mg kg-1 in sediment. Similar results were reported by Duan (2012) reported average concentrations of metals in sediment (0.004-1.07 mg kg-1) and floc (0.01-0.78 mg kg-1) in Everglades. These values are relatively higher than the average crustal abundance of Cd (~0.1-0.5 mg kg-1). High accumulation of Cd, along with other trace metals including As, Cr, Cu, Ni, Pb, Se, and Zn have been detected in the river sediments which were exposed to long-term agricultural practices. The concentrations are found 1.23-1.71 times higher as compared to the local soil background level that obtained from natural forested and grassed areas (Jiao et al., 2015)."	See response in Line 132 regarding the discussion with Cd. No correlation between trace metal concentrations was performed to see which metals could potential be associated with each other.

Commenter Name	Agency	Deliverable	Slide/Page Number	Comment/Question	Responses from ENP	Commenter Response
Nenad Iricanin	SFWMD	62-Slide-Deck	43-49	Were the metal data compared with crustal abundance values to determine if enrichment existed at monitoring locations? Also, how were the sediment samples prepared for analysis and which methodology was used to analyze the samples (AAS, ICP-MS, ICP-AES, pXRF, etc.)? Were the sediments digested with just HNO_3 or were other acids used in the extraction of metals from sediments? Which grades of acids were used (reagent, instranalyzed,, trace metal, trace metal plus)? Was concentrated acid used or diluted?	1. In the report, Table 3.5 compares mean concentrations (mg kg-1) of metals in floc and sediment (0-5 cm) collected near S333 structure (S333), L29 canal (L29), L67A canal (L67A), and Miami canal (Miami), and adjacent marsh (Marsh) with background concentrations of metals in Florida soils, Florida sediments, and sediment (0-10 cm) collected from Everglades National Park (ENP), the coastal fringes of Biscayne National Park (BNP), and Big Cypress National Preserve. 2. The analytical method: "For metal analysis, EPA method 3050B was used and total recoverable metals in sediments and flocs were analyzed. Briefly, each sample (~ 0.5 g) was digested with 5ml of concentrated nitric acid at 95±5 °C on a hot block for one hour. After the samples cooled off, 1 ml of 30 % H2O2 was added and the samples were placed back on the hot block and digested for 20 additional minutes. After the second heating, the samples were cooled to room temperature and diluted to a 50 mL volume with distilled water. After filtration, samples were further diluted, if necessary, and analyzed for 23 metals including 6 non-trace metals (Al, Fe, Mg, Na, K, Mn), and 17 trace metals (Cr, Co, Cu, Zn, Se, Cd, Ba, As, B, Li, Be, Ag, Pb, Ni, Mo, Sb, Hg) using an inductively coupled plasma-mass spectrometry (ICP-MS, Perkin Elmer, Wellesley, MA)." 3. Please also see the answer for question #81 for more information regarding the method.	The report does not provide any references for crustal abundance of various metals discussed in the report. Where did the ~0.1 - 0.5 ppm for Cd come from? Are you sure that it is not 0.10 - 0.15 ppm? It is stated in one of the comments that trace metal samples were not filtered but centrifuged. The respons states the samples were filtered. Which is correct?
Nenad Iricanin	SFWMD	62-Slide-Deck	43-49	Presenting trace metal data as box plots is not very informative to understand source. I thought ratios of trace metals to Al or Fe would be used to normalize the trace metal data.	Ratios will be evaluated and incorporated for future evaluations.	No additional comment
Nenad Iricanin	SFWMD	62-Slide-Deck	53-54	The Y-Axis is not correct. See comment regarding Slides 27, 41, 50, 51,52 with respect with labeled Y-Axis. How was calcite determined? How was quartz determined?	The unit for calcite (CaCO3) is not correct (Slide 53) and will be corrected for future products. It is not 0.0-0.6%, it is 0.0-0.6, which is 0-60%. Methods: Mineral identification and quantification of floc and sediment samples were performed using an X-ray diffraction (XRD) diffractometer (Empyrean, Malvern Panalytical, Malvern, UK) equipped with a Beta-filter Nickel filter, an RTMS detector, and operating at an accelerating voltage of 45 kV and a filament current of 40 mA. The measurements were conducted within the 2θ range of 18°–80° and the X-ray Wavelengths were Kα1 (Å): 1.540598 and Kα2 (Å): 1.544426.	No additional comment

Commenter Name	Agency	Deliverable	Slide/Page Number	Comment/Question	Responses from ENP	Commenter Response
Sue Newman	SFWMD	62-Slide-Deck	5,11	Bound and exchangeable are operational definitions- pls note what chemicals were used for the different fractions, or provide reference to the method.	Please see the report, pages 18-19: 2.2.2. Phosphorus fractionation The sequential fractionation procedure for phosphorus in floc and sediment involves a series of chemical extractions that partition TP into different forms or fractions. These fractions represent different pools of P with varying availability and potential for releasing P into the water. For this study, soil TP was differentiated into seven forms of P using a modified sequential fractionation procedure (Irick et al. 2013; Zhang and Kovar, 2009). These P fractions were extracted sequentially by different reagents as follows: Water-soluble P (H2O), Exchangeable P (1 M NH4Cl), Al-bound P (0.5 M NH4F), Fe-bound P (0.1 M NaOH),Organic P (0.1 M NaOH + 19 digestion), Ca-/Mg-bound P (0.5 M HCl),and Recalcitrant residual P (6 M HCl). Briefly, 0.5 g of soil sample was placed into a 50 ml centrifuge tube with 25 ml of each extraction solution to maintain a soil to solution ratio of 1:50 (g ml-3). The tubes were shaken in a reciprocating shaker at 120 rpm for 1, 0.5, 4, 17, and 1 hour for DDI, NH4Cl, NH4F, NaOH, and HCl extractant,respectively. The sample solutions were then centrifuged at 2100 × g for 15 minutes, and the supernatant was filtered through Whatman 42 filter paper with 0.45μm membrane. All filtered supernatants were stored at 4 oC before analysis, and the P concentration was measured as described previously. Phosphorus measured in filtrates was soluble inorganic P (Pi). 0.1 g of (NH4)2S2O8 and 0.5 ml of 5 M H2SO4 were added to 12.5 ml of NaOH filtrates and were shaken at 180 rpm for 2 minutes. The sample solutions were autoclaved at 121 ºC and 20 psi for 30 minutes. The TP in the NaOH filtrates were determined colorimetrically as previously described. Organic P in the NaOH filtrates (NaOH-Po) was determined as the difference between TP and Pi in the filtrates. These P fractions can be divided into labile and non-labile categories based on availability and reactivity. Labile P refers to fractions (water-soluble P, Exchangeable P, and organic P) that can be easily released from floc and sediment into the water and are readily available to microbes. These fractions are influenced by short-term environmental conditions and management practices. Non-labile P, on the other hand, refers to fractions (Al/Fe-bound P, Ca/Mg-bound P, and residual P) that are tightly binding to soil minerals, organic matter, or other forms of chemical complexes, are resistant to immediate release and less available or inaccessible to microbes.	Comment addressed. Suggest additional basis for selection of drying samples, when the method they cite did not needs to be understood.
Sue Newman	SFWMD	62-Slide-Deck	9	I may be confused, but in earlier drafts, I thought it was one transect per canal, with 9-10 vertical profiles per canal transect? Pls clarify how many transects per canal.	Vertical transects will be changed to vertical profiles in future reporting. The report and metadata provide more details.	Comment addressed
Sue Newman	SFWMD	62-Slide-Deck	12	Pls clarifiy TP normalization	TP normalization for comparison across compartments assuming sediment and floc matrices are distinct, percent organic matter was used to normalize the TP concentrations. Units will be updated to mg P per kg OM in future products.	Comment addressed
Sue Newman	SFWMD	62-Slide-Deck	15	Acoustic error 57-68%- does this mean when compared to measured? Did you see a difference in acoustic sensitivity as a function of floc & sediment bulk density, such that we could understand under what conditions acoustic mapping would work better than others?	Error is based on acoustic estimations compared to measured core data. Good point on acoustic sensitivity. No, this was not done by FIU. We do not have capacity at NPS to analyze acoustic data.	Comment addressed by FIU- perhaps ask ENP if acoustic sensitivity can be captured?

Commenter Name	Agency	Deliverable	Slide/Page Number	Comment/Question	Responses from ENP	Commenter Response
Sue Newman	SFWMD	62-Slide-Deck	16,32	Pls specify what is meant by bound. The different operationally defined pools will have different extractabilities so while called say Ca- bound, it does not mean it will not be released under conditions that would destabilize them, e.g., acid dissolution of CaP, oxic/anoxic control of Fe compounds. Similarly, pls clarifiy why the recalcitrant pools and the Ca, Al etc bound pools are added together to collectively form a bound pool. GIven their availability/exchangeability differs, it is not intuitive to pool them. Recalcitrant P likely refllects the least readily available P	The bound indicates the pools with different extractabilities. Ca-P can be used instead of Ca-bound P for clarification. Recalcitrant, Ca, Al, etc. pools will be presented separately in the fractionation section of the report with updated figures and paragraphs.	Suggest use operational definitions, particularly as noted below, Al bound is not supported by other data collected.
Sue Newman	SFWMD	62-Slide-Deck	18	Permamova information on the scatter plot does not match that in the table…perhaps a different date? Also, based on flow, you see edge versus middle canal flow differences, would it make sense to group the distances into near edge, canal middle etc?	No seed was set for the test resulting in slightly different R2 and pvalues each run. A seed has been set and will be reported along with the results in future products.	Comment addressed
Sue Newman	SFWMD	62-Slide-Deck	20	Here significance noted at p values > 0.07. Pls specify what significance level is being used.	Significance level used is 0.1	Comment addressed
Sue Newman	SFWMD	62-Slide-Deck	21	Pls define normalized Q	The term "Normalized Unit Q" in QRev software refers to the discharge per unit width of the channel. By normalizing this value, QRev software provides a way to compare and analyze discharge measurements across different channel widths.	Comment addressed
Sue Newman	SFWMD	62-Slide-Deck	25	Entrainment is a function of mass and size. I believe you can use the LISST to also look at particle density/mass. Was any work done to look at mass of different size classes?	No, but it can be explored. However, the LISST website listed the following caveats (https://www.sequoiasci.com/article/converting-lisst-volume-concentration-to-mass-concentrations/): "Major problems arise when the density of the particles in suspension are not all the same. There are several reasons why this might be: 1. Flocculation. If particles flocculate their density decreases. The more they flocculate, the smaller the density. A floc with a diameter of a few hundred micro meters can easily have a density very close to that of water (1 g/cm3), because most of its volume *is* water. 2. Mixture of organic / inorganic particles. If the suspended particles are made up of a mixture of organic (e.g diatoms) and inorganic particles, then the densities will differ, as the organic particles tend to have (much) smaller densities than the mineral grains. 3. Different minerals. If the suspended particles in your sample are made of of minerals with varying densities, the same thing will happen."	Comment addressed
Sue Newman	SFWMD	62-Slide-Deck	28	Instead of doing OM corrected TP (not sure exactly what that is here), suggest that correct based on bulk density, such that have mass per unit volume, so can look at storage/density of P.	The issue is that there is no bulk density for floc so we would have multiple comparisons. Regardless, this will done for future products.	Comment addressed
Sue Newman	SFWMD	62-Slide-Deck	29	How is organic P determined?	Organically-bound P in the NaOH solution was determined as the difference between P dissolved in the NaOH solution and P dissolved in the persulfate digested solution.	Comment addressed
Sue Newman	SFWMD	62-Slide-Deck	39-61	Given small sample size, does it make sense to conduct statistical analyses due to low power- perhaps after just showing data, just use the clusters to group the data and then evaluate it for the different parameters of interest?	While this point was caveated in the presentation, it will be removed from the statistical analysis for future products.	Comment addressed
Dong Yoon Lee	SFWMD	62-Slide-Deck	8	Was the timing and number of observations (sampling) appropriate to capture marsh/canal impact on nutrient loading through S333(N) as initially proposed? (i.e., before, during, and after TP spike)	Water sampling was done from April through June (7 events) to capture the occurence of spikes in water. We believe this was sufficient for our objective.	

Commenter Name	Agency	Deliverable	Slide/Page Number	Comment/Question	Responses from ENP	Commenter Response
Dong Yoon Lee	SFWMD	62-Slide-Deck	12	Inverse Distance Weighting. Are parameters of IDW analysis calculated for each subregion (e.g., L29, L67, S333) or all together? In an L-shape region, the sampling location near the corner may have limited neighboring points. Other interpolation methods (kriging or spline-based) can model irregularly shaped regions and improve the accuracy of interpolation, especially near the corners	The IDW was applied to the entire region without sub-sections. Kriging relies on a set of underlying assumptions to provide accurate and reliable estimates. We do not think our data meets all these assumptions which are as follows: 1. Stationarity, 2. Second-order stationarity, 3. Gaussian distribution, 4. Linear relationship, 5. No measurement error, and 6. Homoscedasticity	
Dong Yoon Lee	SFWMD	62-Slide-Deck	14	Was the core sample validated with the acoustic survey? (vice versa) Any potential improvement on the acoustic survey with core samples? (i.e., calibration, adjustment)	The P.I. validated and did the error analysis using core data. More details are available in the report.	
Dong Yoon Lee	SFWMD	62-Slide-Deck	16	Please provide more detailed statistics (e.g., average, median, variability)	Mean=17.62, Median=10.70, Stdev=28.7 (Units=g/m2)	
Dong Yoon Lee	SFWMD	62-Slide-Deck	18	Please indicate which structure, S333 or S333N, is shown	The entire study is limited to S333. S333N was not included.	
Dong Yoon Lee	SFWMD	62-Slide-Deck	20	"Sand (50 – 2000 mm) particle size" Is this typo? Seem too big. Would smaller size fractionation be helpful to understand the impact of flow threshold on transport/deposition of different size groups?	Thank you, this was a typo and the units will be changed to micrometers	
Dong Yoon Lee	SFWMD	62-Slide-Deck	21	What is normalized uint Q? I guess discharge, but why normalized? It's difficult to interpret the statistical result	The term "Normalized Unit Q" in QRev software refers to the discharge per unit width of the channel. By normalizing this value, QRev software provides a way to compare and analyze discharge measurements across different channel widths.	
Dong Yoon Lee	SFWMD	62-Slide-Deck	36	Please mark the sampling points. Also, please provide L29 water speed (black line) from Jan to April 2022 (missing)	Sampling points are marked as TCM (orange pins)	
Nenad Iricanin	SFWMD	62-Slide-Deck	50, 52	Have you looked at the relationship between $\delta^{13}C$ and $\delta^{18}O$?	We have looked at them in the form of clusters and scatter plots, but not directly through correlations. This can be evaluated for future products.	No additional comment
Nenad Iricanin	SFWMD	62-Slide-Deck	26-32; 40-54	Box plots, as presented, are not very helpful to understand the characteristics of a particular core sample. It looks like box plots were generated using three or less samples. Please provide the full data set by core sample and sampling date to see the interrelationship between parameters.	All data were provided on the agreed upon date of Jul 1. The evaluation is now considering iron normalized metals.	No additional comment
Nenad Iricanin	SFWMD	62-Slide-Deck	General	How thick were the floc layers from sample to sample?	Floc thickness was estimated to be approximately 2-10 cm in canals and 5-20 cm in the marsh, respectively. To measure the depth of the floc layers, an underwater camera was obtained prior to sampling. Unfortunately, it was unable to obtain a clear visual for accurate measurements.	Based on the method for collecting floc, can the investigator be certain that no surficial sediments were mixed in with the floc layer? If not that should also be caveated in the report.
Nenad Iricanin	SFWMD	62-Slide-Deck	52	Are the sediment $\delta^{18}O$ results normalized to VPDB rather than VSMOW? I am no isotope expert but the $\delta^{18}O$ seem a bit high.	The description of the method provided by the Stable Isotope Mass Spec Lab is "Oxygen isotopic results were reported using standard delta notation relative to VSMOW-SLAP (Vienna Standard Mean Ocean Water – Standard Light Antarctic Precipitation)."	
Nenad Iricanin	SFWMD	62-Slide-Deck	55, 56	While Illite, Kaolinite and Palygorksite are clay minerals, not sure that the other minerals are clay minerals. By Mg carbonate do you mean Dolomite? Does iron sulfide refer to pyrite? What does iron silicon refer to? Ferrosilicon? What is Ca oxide phosphate? What is Na Al Fe phosphate? How were all these components determined?	Each mineral is defined in the final report	Don't agree
Nenad Iricanin	SFWMD	62-Slide-Deck	55	Using the floc organic matter data from GEER presentation (April 2023) and the "Clay Mineral" plot data, could an explanation be provided why there is a compositional deficit of ~ to 30% based on location?	The amount of total "Clay Mineral" was not equal to the whole inorganic matter present in the samples, and it is only a part of the inorganic matter.	What were the other inorganic fractions in the sediments?
Nenad Iricanin	SFWMD	62-Slide-Deck	56	A similar deficit is observed using the data from Slide 56 and estimating OMO from Slide 41	See response above.	See comment above

Commenter Name	Agency	Deliverable	Slide/Page Number	Comment/Question	Responses from ENP	Commenter Response
Nenad Iricanin	SFWMD	62-Slide-Deck	45	Where was the sample collected in the Miami Canal with 7% Fe in the sediments? Why is there a 3.3% difference in sediment Fe concentrations at S333? Two of the samples look to have similar Fe content.	1. Miami 2 (0-5cm sediment): 7.2% Fe 2. Three samples (S333-1, S333-2, S333-3) were collected from a depth of 0-5 cm in frontal area of two S333 structure (see figure below). This will be further evaluated in future products. Yellow markers represent sampled locations close to planned locations (circles)	It appears that one of the sediment samples is completely different from the other two
Nenad Iricanin	SFWMD	62-Slide-Deck	race metal s	In order to understand whether there is a similarity between trace metal concentrations in sediments, the metals need to referenced to a more stable component such as Al or Fe. While concentrations of a metal may vary within a group, their ratio to Al or Fe can provide information regarding the observed differences. Additional, the dominant sediment type can also provide information regarding the higher observed concentration. For example, metal concentrations tend to be lower in quartz and carbonate rich sediments and higher in clays and silts.	Excellent suggestion. Metals will be analyzed based on the suggestion for future products.	No additional comments
Nenad Iricanin	SFWMD	62-Slide-Deck	General	Providing meaningful comments with respect to sediment composition is difficult without context. Based on the information provided, it is impossible to determine which dots on the box plots correspond to each other across the slides. Additionally, it appears that the units and/or values on the axes are not correct, This does not instill confidence in trying to interpret and provide meaningful and constructive comments.	The unit for many analyses conducted was percent (%), it is easy to get mixed up sometimes. The units in the data submitted were double checked to ensure all units listed on the axes were correct.	No additional comments
Colin Saunders	SFWMD	62-Slide-Deck	19	Slide 19 consistently shows higher water TP in deeper canal waters and lower TP at the surface – across all dates spanning late dry to early wet season (Apr to June). Given that this is the time of year when canal stages are lower than marsh, and marsh water is entering the canal, do these profiles alter our current conceptual model that the marsh (or canal-marsh edge) is adding sediments to the canal which in turn increases canal water TP? Based on the latter model, wouldn't we expect higher TP at the surface if water entering the canal from the edge is increasing TP? Perhaps the vertical profiles would be different earlier in the dry season (Jan – Mar)? Alternatively, do the depth profiles of TP observed suggest sediments are settling (and concentrating) into deeper layers, even as the canal is flowing? Can we infer settling rates from these data?	This conceptualization is greatly appreciated.	Comments Addressed
Chelsea Qiu	SFWMD	62-Slide-Deck	25, 39	The d50 concept does not seem to apply to floc materials, which do not have a sphere shape like mineral particles.	The d50 value is actually a median which indicate the particle size as a cumulative percentage of values either above or below median values. Floc samples were processed in the same manner as sediment (oven drying, crushing, sieving).	Comment Addressed
Chelsea Qiu	SFWMD	62-Slide-Deck	26	The largest sediment TP data point for L29 seems to be an outlier. Statistical results will be different if the outlier is excluded.	It could be an outlier, but given the one time sampling nature for these data, it is difficult to justify removing data just because it stands out from other locations. Further, we know that there is great heterogenity in sediments across the system and we did not believe we made an error in the sample collection or chemical analysis. But you are correct, removing data would result in different statistical results.	Comment Addressed

Commenter Name	Agency	Deliverable	Slide/Page Number	Comment/Question	Responses from ENP	Commenter Response
Chelsea Qiu	SFWMD	62-Slide-Deck	25-32	General comments - The data, in general, exhibit different characteristics of floc and sediment between marsh and canal. One would wonder how the data are relevent to sediment sources.	One can infer that sediment sources at S333 are probably from upstream canal transport	This statement doesn't seem to be warranted by the data presented in the report for the following reasons.

1)The significant spatial variability of sediment in the marsh-canal system: Sediment variability is especially pronounced in the marsh, depending on sampling locations in the ridge slough system and flow conditions during sampling. It raises concerns about whether the number of samples in the marsh is sufficient to represent the marsh system.

2)The complexity of flow dynamics involved in floc and sediment transport: The response mentioned that "floc would be easily transported and entrained." Additionally, discharge and sediment from upstream structures mix with floc and sediment from the marsh in the WCA-3A internal lake in front of S151.

3)In-situ biogenic growth and decomposition: Organic sediment in the canal, particularly floc materials, can be biogenic or produced in situ by the decomposition of aquatic vegetation.

The researchers should be encouraged to clarify how this inference is made based on the data presented or if such inference about sediment sources should be explored further by future studies. |
Chelsea Qiu	SFWMD	62-Slide-Deck	55	Please clarify the particle sizes used for this analysis. Are calcite and quarts clay minerals?	Clay mineral is a misnormer that we have moved away from. Calcite is a carbonate mineral composed of calcium carbonate (CaCO3). Quartz, on the other hand, is a silicate mineral composed of silicon dioxide (SiO2). The samples were seived for 2 mm seive size.	Comment Addressed
Jose Guardiario	SFWMD	62-Slide-Deck	8	On the flow (cfs), what is the equivalent velocity (fps)	This can be provided.	
Jose Guardiario	SFWMD	62-Slide-Deck	9	Are there samples collected in areas without the dots? If so, indicate values. How are these intervals determined?	No, samples were collected in empty areas. The objective was to determine entrainment and its influence on TP from the canal bottom. For this reason intervals were set from canal bottom at 30, 60, 100, 160, 250, 500 cm, and 50 cm from water surface.	
Jose Guardiario	SFWMD	62-Slide-Deck	19-20	Provide velocities for each date	This can be provided.	
Jose Guardiario	SFWMD	62-Slide-Deck	26	Consider using a log normal graph and combining both floc and sediments	This sugestion will be considered and the team is looking forward to discussing its rationale at a later time.	
Jose Guardiario	SFWMD	62-Slide-Deck	33	On the statement "Floc: Marsh samples were characterized by high organic matter and low inorganic carbon (IOC), while L29 was characterized by higher TP and larger particle sizes", is this becauseof larger floc size?	This would require further evaluation. However, working with the district, the PCA analyses have been revised to include metal ratios. The results are now different. Thank you for this comment.	
Jose Guardiario	SFWMD	62-Slide-Deck	37	Which one shall the biggest impact? Floc or Sediments? Where in the water profile has the water quality sampling been made?	Floc would be easily transported and entrained. Further assessments are needed to examine model results- such as flow vectors and streamlines especially near the canal bend and in front of gate to get a clear picture of physical forces towards the bottom of canal on both floc and sediments. As regards to where water sampling in this project has been done- refer to slide 20 and response to your earlier comment.
In general, the compliance regular monitoring samples are collected at 50 cm depth from water surface from the edge of canal.	
Jose Guardiario	SFWMD	62-Slide-Deck	55-56	Not all clay size particles are clay minerals. Discriminate one from the other.	Agree. Changes will be made to clarify this in future products.	

Commenter Name	Agency	Deliverable	Slide/Page Number	Comment/Question	Responses from ENP	Commenter Response
Chelsea Qiu	SFWMD	UF-Li-Sediment-Floc-Characterization	18	"The top portion of the sample (water) was then poured off and the settled floc sample was transferred to a wide based container and oven dried at 70 °C until dry (~3-5 days). " 1.Drying out floc irreversibly changed its content and made the d50 size meaningless. This analysis method differs from the EPA REMAP study, which analyzed TP with the whole sample. 2.Filtering is needed to separate floc from water. No filter process is documented.	1.After an extensive literature review, we could not find a standard method for measuring floc or sediment particle size with a laser. An oven- or air-dried sample has been used as a standard procedure for traditional soil particle size distribution measurement. 2.We only wanted to collect floc (flocculent detrital material found at the surface water-sediment interface), not these solids in the water column.	The researchers failed to acknowledge the fundamental difference between floc materials, which are highly organic and non-fractal, and the general sediment, which are dominated by inorganic particles with "fractal dimension." Oven-drying the floc materials permanently changes their properties, partly due to the irreversible shrinking of the organic matter. Thus, the d50 obtained as such carries limited meaning or, at most, pertains only to the inorganic particles trapped in the flocs. Moreover, floc materials are fragile and loosely bound, lacking a fixed shape, and can break down easily during sampling and preparation. The researchers may want to acknowledge these difficulties to justify the need for further exploration in future studies.
Sue Newman	SFWMD	UF-Li Spreadsheet	sub-regional	Suggest size delineation definition into sand etc is not appropriate. For example, > .9 fraction (95-100?) of material in marsh sediment is in the sand fraction, however it has 93 % OM- instead, this would suggest that the sediment is organic, not sand in nature and thus would behave differently re: suspension and tranport	We appreciate this comment and would like to further discuss this topic.	Happy to discuss further.
Sue Newman	SFWMD	UF-LI Report	13	What is the diameter of the universal core tube and does the head have a serrated or sharp edge, such that it cuts through roots and minimizes compaction in wetland sites? Was compaction determined in any sites?	The inner and outer diameter of the universal core tube is 6.8cm and 7.1cm, respectively. Yes, the head has a sharp edge which allowed us to cut through the roots. There were few sites (mostly wetland sites) we had to try multiple times to get a nice core.	Comment addressed. Though suggest it would be helpful to define the degree of compaction that is acceptable in a "nice" core.
Sue Newman	SFWMD	UF-LI Report	16	The clearest floc data would be obtained via coring. Was a comparison with floc collected in sediment core versus that via pumping? Otherwise not sure how it is possible to account for the likely intermixing of water column and sediment into the floc matrix?	Good suggestion. Collection of floc and sediment at the same time with the core sampler was initially planned. This was not pursued due to the following concerns: 1) the volume was too small, and not enough sample for a series of analysis; 2) inserting the core would disturb surface sediment and affect real floc; 3) floc might overflow through the holes on the top of the core sampler; and 4) it was also hard to separate floc and sediment on canal sites.	These observations are helpful and we can use this knowledge in the future such that floc collection can be imporved, hopefully via coring, e.g., using larger diameter corer, and not pumping where it is not possible to observe the floc/sediment water interface, and sampling inherently mixes floc into the overlying water.
Sue Newman	SFWMD	UF-LI Report	16	"in some areas, floc layer exceeded the length of the core"…so floc discarded, how long was the core?	The length of the universal core tube was 60 cm. For some locations with sediment deep than 60 cm, we used an extended core tube of 120 cm long. Holes on the top of the sampling core allow floc to flow out if it is a thick floc layer.	Comment addressed.
Sue Newman	SFWMD	UF-LI Report	18	"stored until future analysis"- P speciation can change during storage, how long were the samples stored prior to analysis? Also, were all samples oven dried, which affects P fractionation- Irick et al 2013 specify nominally 0.5 g dry weight, here noted as 0.5 g. Oven dried not appropriate for aquatic/wetland sediments with high moisture content, high OM content, and subject to anaerobic/aerobic conditions.	At the beginning of the project, the research team engaged in a thorough discussion regarding the appropriate method for processing floc and sediment samples. Various options were carefully considered, including storing the samples while keeping them moist at 4 °C, air-drying, freeze drying, and oven-drying. An extensive literature review on processing wetland soil samples was conducted. Findings revealed that there is no universally accepted standard protocol, and each method has its advantages and disadvantages. Given the specific objectives of the study, analysis to be conducted, the number and volume of samples, as well as the availability of suitable facilities, it was ultimately opted to dry our samples in an oven with a low temperature.	Agreed- P fractionation can be quite problematic and lacking standardization means that if the same approaches are not used, then data cannot be directly compared. Suggest a path forward would be for studies to use methods that are consistently used in the Everglades and STAs-specifically the method of Ivanoff, D.B., K.R. Reddy, and S. Robinson. 1998. Chemical fractionation of organic phosphorus in histosols. Soil Sci. 163(1):36-45. To ensure data are directly comparable, suggest confirming with the RS group, whether they have any modifications to this method before implementation. Regardless of method, by drying the sediments, how they interact with chemicals during P fracttionation is fundamentally changed. For example, the key pools considered bioavailable/labile fractions, e.g., water extractable, in aquatic sediiments would include porewater, which would be lost when sediments are dried- hence prior comment for page 21.

Commenter Name	Agency	Deliverable	Slide/Page Number	Comment/Question	Responses from ENP	Commenter Response
Sue Newman	SFWMD	UF-LI Report	18	Similiarly, 1-2 week settling allows P to diffuse from floc into overlying water based on gradient?.	During sample collection, not only floc, but also water overlying floc layer (interface of sediment and water) was collected. During the sampling and transportation, floc and water samples were well mixed. The purpose of allowing settling is to obtain the actual floc material, rather than capturing solid particles suspended in the water column. Regarding the diffusion of phosphorus (P) from the floc into the overlying water, the process should be similar to what occurs in canals or wetlands.	Typically, when sampling and transporting soil and floc, mixing of floc and overlying water is minimized, to avoid any potential for exchange, I understand that with the pumping method this was not possible. Agreed diffusion would occur in canals and wetlands, however, the boundary conditions for diffusion would be different under static versus flowing conditions.
Sue Newman	SFWMD	UF-LI Report	19	Suggest this should be reworded to operational definitions unless there is strong evidence these pools are as stated..e.g, compare with Everglades mineralogical results, growth studies, etc	This suggestion is appreciated.	Thank you.
Sue Newman	SFWMD	UF-LI Report	19	Were isotherms conducted using oven dried samples?	Yes, the isotherms were conducted using oven-dried samples.	Prior Everglades wetland isotherm research has typically been conducted on field moist samples. Drying samples changes their properties, which in turn influences the sorption characteristics. Suggest any future studies should use field moist samples.
Sue Newman	SFWMD	UF-LI Report	18/19	what standards were used to check accuracy/precision of P measurements? E.g., peach leaves of known P content? In looking at the P fractionation data, the concentration of TP (mg/kg) should be close to (water soluble + Exch + Al bound + Fe Bound + Org bound + Ca/Mg bound + Residual). While the mean and median ratio of summed to total is 88 and 91, so a good match, the ratio ranges from 25 to 275, suggesting some pools are not be captured, or dilution/multiplication factors have made summation difficult	1.The peach leaves of known P content were used to check the accuracy/precision of P measurement, and the average extraction/recovery rate is ~95%. 2.Samples for P fractions were from local-scale study and have different TP as these samples from sub-regional study. The comparison of TP and P fractionation should be done only for local scale study. 3.Theoretically, the sum of TP fraction concentration should equal the TP concentration. In this study, 204 samples were analyzed for TP fractionation, of which 168 were within the recovery range of 70-130%. TP fractionation is a sequential process with seven extraction steps. Some soil particles of samples may get lost in the supernatant at any step even though samples were centrifuged at 2100 × g for 15 minutes. It is also why TP was analyzed separately and the sum of P fractions was not used.	Comment addressed.
Sue Newman	SFWMD	UF-LI Report	20	Assuming this is dry bulk density?	Yes, the bulk density was calculated based on the dry weight.	Comment addressed.
Sue Newman	SFWMD	UF-LI Report	21	Not sure I agree with this...how has this been documented? "These P fractions can be divided into labile and non-labile categories based on availability and reactivity. Labile P refers to fractions (water-soluble P, Exchangeable P, and organic P) that can be easily extracted- this would not be the same in samples that have been dried versus field moist. Floc and sediment typically exist in a hydrated state, thus drying and sieving with subsequent mechanical or laser diffraction would not accurately capture the size fractions- particularly for samples with a high organic matter content	This perspective is appreciated. The categorization of P fractions into labile and non-labile categories can indeed be subjective rather than precise. The intention is to convey that certain P fractions may exhibit higher bioavailability compared to others.	Comment re: size fractionation not addressed.
Sue Newman	SFWMD	UF-LI Report	25	Would be easier to display numbers for TP concentration on the map...hard to differentiate the scale.	Excellent suggestion.	Thank you.

Commenter Name	Agency	Deliverable	Slide/Page Number	Comment/Question	Responses from ENP	Commenter Response
Sue Newman	SFWMD	UF-LI Report	47	It does not appear to make sense the dominant P form is "Al bound P" in the Everglades, particularly the marsh, when looking at mineralogy the only Al associated P was only found in the sediment from Miami canal?	1. P fraction terms were adapted from standard methods used for P fractionation in the literature. It is correct to state that terms such as "Al bound P" or "Fe bound P" are not precise. It could probably be called "NaOH extracted P". 2. While phosphorus fractionation is a valuable technique for understanding the different forms of phosphorus in a sample, the method may not always provide a complete representation of all phosphorus fractions present in a sample. The sequential extraction approach used in this method is based on assumptions about the specific chemical forms of phosphorus, but in reality, phosphorus compounds can be complex and diverse. Therefore, there is a possibility that certain phosphorus fractions may not be fully captured or accurately quantified using this method.	Agree P fractionation is operational- hence comment above re: use operational definitions as stating things such as Al - Bound, particulary when there is other data available that negates the definition as Al-bound. Those not familiar with the caveats associated with the bound-definitions would find these inconsistencies confusing.
Sue Newman	SFWMD	UF-LI Report	50	the lack of relationship between particle size and other paramaters makes sense if sediment dried & sieved prior to analysis	This perspective is appreciated.	Comment addressed.
Nenad Iricanin	SFWMD	UF-LI Report	18	The report does not provide information on how the dried samples were treated prior to metal analyses. Sediments that are oven dried tend to aggregate and become hard. How were these sediments pulverized in preparation for their acidification?	The dried samples were pulverized and sieved through a 2-mm sieve.	This should be described in the report
Nenad Iricanin	SFWMD	UF-LI Report	21	What types of filters were used to remove the particles from the solution? Where they acid washed? Was a blank digestion also performed to ensure no contamination from acid or hyrogen peroxide? What grade of acid was used to digest the samples? What types of vessels were used in the digestion? Was a standard reference material used to determine what percent of the metals were leached from a known, certified sediment?	The solution was not filtered. No filter was used. The sample was centrifuged. Yes, there were method blanks. They were lower than PQLs. Trace metal grade acid was used. Plastic digestion tubes from Environmental Express for metals analysis. Yes, a soil CRM MESS-3 was used. The recoveries were within the specified ranges.	NRC MESS-3 marine sediment was used as a reference material. Could the results of the analyses of this reference material in conjunction with the sediment analyses be provided? Additionally, all QA/QC data for all analyses must be provided in a report such as this for reviewers to better understand the accuracy of the results. This response seems to contradict response for Line 20. Also, what were the detection limits for various analyses performed by the investigators?
Nenad Iricanin	SFWMD	UF-LI Report	21	EPA method 3050B may be an acceptable method to determine the leachable/recoverable metal concentration in sediments with respect biological ingestion of particles, however, it is not suitable in geochemically "finger-printing" the sediments and identifying similarities in metla content using metal to metal ratios. EPA method 3052 is more appropriate.	The description of the EPA 3050B method stated that "it is a very strong acid digestion that will dissolve almost all elements that could become environmentally available." We agree that the EPA 3050B method is not designed to digest aluminosilicates and is unsuitable for analyzing total Al and Si. Analysis of both elements is not included in this project's statement of work (SOW). As stated in the SOW of this project, "Trace metals: Based on Inductively Coupled Plasma Mass Spectrometry (ICP-MS) analysis, the multi-element fingerprinting method can be used for determining sources of water, sediment, and chemical elements in them", we are focused on trace metals. Al and other non-trace metals were included because it is a minimal extra cost to use ICP-MS for analyzing them. These additional analyses might provide helpful information along with trace metals.	It seems that the PI is agreeing that the EPA Method selected for trace metal "extraction" is not apporpriate for Al (as some of the Al, as well as some metals, are bound in a Al/Si matrix. The digestion used is not strong enough to break the Al/Si matrix. That raises the question as to the usability of Al and even the reporting of Al.
Nenad Iricanin	SFWMD	UF-LI Report	ons 3.1.5 and	Was a comparison made between the data determined analytically for inorganic carbon and trace metals, e.g., pressure-calcimeter and ICP-MS (Table 3.3) and those data determined using XRD? An example would be to compare inorganic carbon with Calcilte, Aragonite and dolomite to see if the carbon is balanced.	The comparison was not made for this report but can be done for future products.	No issues noted
Chelsea Qiu	SFWMD	UF-Li-Sediment-Floc-Characterization	General	The subregional-scale study should include sampling from three distinct layers: water, floc, and sediment. However, it appears that water column samples were missing and not collected.	Based on the objective of sub-regional investigation one time sampling event, surface water samples are too transient to provide sufficiently robust inputs with respect to the longer term intergrating matrices (floc and sediment).	Comment Addressed

Commenter Name	Agency	Deliverable	Slide/Page Number	Comment/Question	Responses from ENP	Commenter Response
Chelsea Qiu	SFWMD	UF-Li-Sediment-Floc-Characterization	General	Are the five marsh sites located in the ridge or slough? They can exhibit significantly different behaviors. Also, the study could have collected a few more samples around each site to capture the variability within each site.	Open areas were sampled. The subregional study was an ad-hoc exploratory study that our management provided additional funding for to get initial insight for understanding sources to S333. As such, the budget was very limited and allocated to the highest priority locations and matrices. If Phase II is approved, more spatial coverage will be pursued.	Comment Addressed
Colin Saunders	SFWMD	FIU-Kominoski-Sediment-Floc-Transport	pages 18-24	Additional visualizations would help elucidate the extent to which water TP and TSS covary and vary as a function of depth, site and within-canal location (e.g., west, central, east). To the extent possible (where dates & locations are approximately the same), I recommend overlaying velocity cross sections from the CFD study (Figures 4.1 (p.31) and 4.2 (p.33) of Zeng et al.) with water chemistry values. The velocity cross sections demonstrate some asymmetry in velocity in a given cross-section (e.g., see L29 cross sections in figure 4.1-higher velocities occurring on the west bank of the canal). Does this variability in velocity match with higher (or lower) TP, TSS, TDP:TP values for similar sampling locations within a given canal cross section? The overlays should tell us that. This seems important as substantial asymmetry in velocity upstream of S333 (Figure 10, p. 12) was suggested to explain why sediment erosion may be localized (i.e., not homogeneous) within the canal bed/banks.	Samples were collected in the east, west, and center portions of the canal and aligning them with ADCP profile is not possible.	I believe data can still be visualized side by side with ADCP data.
Nenad Iricanin	SFWMD	UF-Li-Sediment-Floc-Characterization	cel File, Local	Shouldn't the sum of TP fraction concentrations equal the total TP concentration?	1. Samples for P fractions were from local-scale study and have different TP as these samples from sub-regional study. The comparison of TP and P fractionation should be done only for local scale study. 2. Theoretically, the sum of TP fraction concentration should equal the TP concentration. In this study, 204 samples were analyzed for TP fractionation, of which 168 were within the recovery range of 70-130%. TP fractionation is a sequential process with seven extraction steps. Some soil particles of samples may get lost in the supernatant at any step even though samples were centrifuged at 2100 × g for 15 minutes. It is also why we analyzed TP separately and did not use the sum of P factions.	The PI responded that the fractionation recoveries for 82% of samples was 70-130%. This seems like a substantial lose in the extraction as well as a substantial contamination of the samples during analysis. The Principal indicated that partilces could have been lost in the supernatant even though samples were centrifuged. It seems as though the 2100 rpm may not have been a sufficient rotation velocity to assure that the particles settles to the bottom of the centrifuge tube. This raises the question if the same issues existed with trace metal analyses as these too were centrifuged.
Nenad Iricanin	SFWMD	UF-Li-Sediment-Floc-Characterization	General	Were values (that extend to the nth decimal place) properly rounded to significant figures before any statistical analyses were performed?	Values were analyzed as provided. Future evaluation of these data will consider significant digits.	
Sue Newman	SFWMD	FIU-Roa-Sediment-Profiling	13	The report notes that for method 2, acoustic backscatter ranges for bedrock and sandy sediments based on ocean floor studies were used. Are there any ranges for less dense more organic/mixed sediments that could be used? This might help refine the sediment/water boundary.	Good suggestion. The project has concluded and the PI is no longer funded for such additional work.	Comment addressed.
Colin Saunders	SFWMD	FIU-Kominoski-Sediment-Floc-Transport	12	Figure 14 (p.12) shows water chemistry from all sites, however, there is no mention in the report where the sites TN1-4 and TS0-4 are located or how they are associated with this study.	Fig. 12(b) p.15 shows all water sampling locations. Obj 2 p.15 mentions cross-sectional sampling at S333. Fig. 13(a) provides an illustration of water sampling at S333. While these do not show TN1-4 and TS0-4 locations, the metadata for this project provides complete information of S333 cross-sectional sampling and location of verticle transects.	
Colin Saunders	SFWMD	FIU-Kominoski-Sediment-Floc-Transport	19	"We detected episodic increases in TDP and TP concentrationsat sites L29-1, L67-1, and L67-2 (Figures 14A-B)." The graph only shows some apparent outliers in TDP and TP at these sites - but "episodic" increases suggests there is some pattern or driver of these values varying over time. Please clarify.	Based on the depth of the samples, they were collected slightly closer to the canal than in the sample collection design and may represent actual outlier. Your observation is appreciated.	
Luke Hudson	FDEP	FIU-Kominoski-Sediment-Floc-Transport	4	"Upstream contributions are evident" - I am not sure if that is positively demonstrated just by the visualization provided (Figure 2a).	S151 concentration peaks coincide with S333 concentration peaks and historically have been slighly greater than S333. This pattern continues until sampling was discontinued at S151.	Need to discuss conclusions being made regarding upstream sources

Commenter Name	Agency	Deliverable	Slide/Page Number	Comment/Question	Responses from ENP	Commenter Response
Luke Hudson	FDEP	FIU-Kominoski-Sediment-Floc-Transport	4	"Local processes lead to elevated TP peaks, with levels exceeding those at S152." - This suggests a local driver more than an upstream driver. There must be an alternate phosphorus source not accounted for by S152 data.	Contributions from upstream can be increased by local processes. This is one of the central tenets for evaluation in the overall S333 sediment characterization project.	
Luke Hudson	FDEP	FIU-Kominoski-Sediment-Floc-Transport	5	Figure 1b: A log scale on the y-axis could show the relationship between TP and S333HW stage more clearly.	This suggestion is appreciated.	
Luke Hudson	FDEP	FIU-Kominoski-Sediment-Floc-Transport	7	"The sediments in L29 are thicker and richer in organic content than upstream in L67, which are mostly carbonate sand" - This suggests a difference in soil/particulates in upstream and downstream sources.	Continuous flow in L67A transports lighter organic particles downstream which may end up depositing in L29.	
Luke Hudson	FDEP	FIU-Kominoski-Sediment-Floc-Transport	18	R (v. 4.2.2) was used to compute the Kruskal-Wallis chi square non-parametric tests. Which package/function was used to perform these tests?	The package used was the 'stats', using kruskal.test.	
IH	FDEP	62-Slide-Deck	General	We recommend that ENP should provide to the S333WG the draft reports and the data that was collected, including the QC methodology, lab and field methods. Better understanding will facilitate so that we could come up with joint conclusions and recommendations. At this moment, the scatter plots are real difficult to read, the scale on the plots are all mixed up (not consistent), some of the scatter plots measures from the bottom, some from the surface. I'm not sure that we can draw firm conclusions from what was provided as the results are difficult to interpolate.	Data and reports were shared on July 1.	
JT	FDEP	62-Slide-Deck	2	The third bullet mentions informing engineering solutions. Should this also include maintenance and operational solutions?	Engineering solutions may require maintenance.	Anything else from the studies to inform any of the 11 initial EMOs such as the operational solutions.
JT	FDEP	62-Slide-Deck	8	Please recognize that the data is only representative of the conditions at the time of study (April - June) and should not be used to interpret conditions for the rest of the year.	We focussed on investigating conditions just before and during the onset of wet season at local scale to identify conditions that may be contributing to the P peaks.	
MS	FDEP	62-Slide-Deck	8	Please include in the report flow charts for the entire period used in this study	Reports were shared on July 1.	
MS	FDEP	62-Slide-Deck	16	The section for sediment volume and TP mass shows high TP mass in the 0-5 cm of the layer in the L29 canal compared with L67A and S333. No conclusions were proposed through the report that use these results.	In the slide deck, no conclusions are made, only discussion points are provided. Conclusions will be drawn through synthesis report development.	
MS	FDEP	62-Slide-Deck	18	The Permutation Multivariate Analysis of Variance shows only one out of seven sampling events where distance and TP have interactions (no significant p value)	This slide shows two of those seven event had significant interaction effects for depth from canal bottom and distance from canal embankment. This is the point of this slide. Evaluation of height from the bottom are further investigated for effects in the following slide.	
IH	FDEP	62-Slide-Deck	19	Please consider using the same scale on the 4 plots. Also recommend showing db hydro period flow chart for S-333 to show sampling period and periods of no flow.	This will be considered for a synthesis report	
IH	FDEP	62-Slide-Deck	19	Please make a comparison of the May 5 vs May 26, 2022 samples for TP including the bottom sample. Keeping the structure close appears not to build up sediments in front of the structure and does not result in higher TP after opening the structure.	The provided plots show that concentrations decline towards the surface, but all are much higher than protective of Park resources.	Operations of the structures should be considered.
MS	FDEP	62-Slide-Deck	19	Interestingly no effect on TP concentrations in H1 (30cm to the bottom of the canal) was observed between May 5 to May 26 although S333 was closed from May 6 to around May 2O.	Depth has a significant effect for the four dates shown.	
MS	FDEP	62-Slide-Deck	29	The statement that Organic Phosphorus in the sediments at S333 is similar to all compartments is should not be written. Concentrations range is from more than 40 mg/kg to almost 0 mg/kg.	While the 0 in this comment is not consistent with the data, there are enough data to support the resulting test that was applied.	
MS	FDEP	62-Slide-Deck	36	The map shows three WQ sampling locations in L67, can you please provide the data collected in these three stations?	Data and reports were shared on July 1.	

Commenter Name	Agency	Deliverable	Slide/Page Number	Comment/Question	Responses from ENP	Commenter Response
JT	FDEP	62-Slide-Deck	37	The second bullet mentions informing engineering solutions. Should this also include maintenance and operational solutions?	Engineering solutions may require maintenance.	
Nenad Iricanin	SFWMD	FIU-Kominoski-Sediment-Floc-Transport	General	It appears that the S333 cores were all aggregated for the for the PCA and Cluster analyses while individual cores were used for the other locations. Based on correlation analysis, one of three S333 cores is distinctly different from the others and aggregation of all three cores may yieled erroneous conclusions.	For the PCA, the S333 are treated separately. In the clusters, which are reported in the slide deck (copied from the Li Report), the S333s were aggregated. Future evaluations will use individual cores.	No issues noted
Jose Guardiario	SFWMD	FIU-Kominoski-Sediment-Floc-Transport	4	On the statement, "by the time water reaches S333, local processes lead to elevated TP peaks, with levels exceeding those at S152". Could this phenomenon be caused by introduction of overland flow from the marsh?	This dynamic appears unlikely. Monitoring or modeling or a combination of both would inform the magnitude of overland flow. For the dynamic to occur, there is a dependence on whether there is enough energy to transport sediments. Thick vegetation near the marsh edges would do a lot of filtering. In general, water in the marsh has a range of concentration ~ 5-7 ppb.	
Jose Guardiario	SFWMD	FIU-Kominoski-Sediment-Floc-Transport	7	On the statement "he sediments in L29 are thicker and richer in organic content than upstream in L67, which are mostly carbonate sand". Flows through the S-12 structures west of S-12D have longer and frequent haitus.	There is more opportunity for sediments to be deposited in L29 compared to L67 which experiences higher flows.	
Jose Guardiario	SFWMD	FIU-Kominoski-Sediment-Floc-Transport	9	On the statement "elevated sill in spillway (Figure 6a) would trap and prevent heavier sediments and suspended material from moving through gate opening on the upstream side." With the amount of flow through the structure and the presence of a deep canal (elevation -12.0 ft NAVD88) upstream, the likelihood of trapping heavier sediments is unlikely unless it approaches rubble size.	We appreciate this perspective.	
jose Guardiario	SFWMD	FIU-Kominoski-Sediment-Floc-Transport	10	On teh statement "High flow rates do not always coincide with high TP concentrations. In fact, there is no statistically significant relationship between TP and flow or turbidity and flow." The SFWMD graph for 16 years indicate that spikes in TP occur when the water levels are low and corresponding flows are low to zero.	High TP during low stages are known. Fig. 1 p.5 shows that. Referenced SFWMD graph should be shared with us or please provide reference to the document.	
Jose Guardiario	SFWMD	FIU-Kominoski-Sediment-Floc-Transport	12	On the statement "Formation of such eddies (Figure 9a) near the bend and circulatory current (Figure 9b) create the local velocity fields required to suspend floc and lighter sediments (that may have been deposited during relatively static and low or no flow period) before water reaches the S333 gate. The SFWMD graph for 16 years indicate that spikes in TP occur when the water levels are low and corresponding flows are low to zero.	The PI is describing conditions that may have an influence on TP peaks. Referenced SFWMD graph should be shared with us or please provide reference to the document.	
Jose Guardiario	SFWMD	FIU-Kominoski-Sediment-Floc-Transport	14	On the sttement, "there is variable flux across the canal (Figures 10 and 11) just upstream of S333. This flux can lead to development of eddies and turbulence which suspend TP loaded sediments and floc in the water column." This may be true at high flows, but the spikes in TP occur when the water levels are low and corresponding flows are low to zero, as shown in the SFWMD graph for 16 years.	Even at low flows there is variable flux as our ADCP data shows. Referenced SFWMD graph should be shared with us or please provide reference to the document.	

Commenter Name	Agency	Deliverable	Slide/Page Number	Comment/Question	Responses from ENP	Commenter Response
Jose Guardiario	SFWMD	FIU-Kominoski-Sediment-Floc-Transport	14	On the statement, "The water loaded with these sediments can then be transported through S333 gate and may either settle in the downstream L29 canal or be introduced into the marsh in ENP, just downstream of the canal." Yes, there is settlement. However, water quality sampling needs to be conducted downstream of the bridges to verify TP concentrations.	This concept is beyond the scope of the present study.	
Jose Guardiario	SFWMD	FIU-Kominoski-Sediment-Floc-Transport	19	On the statement, "Despite dates with high concentrations of TSS, TSS alone did not correspond to increases in TDP, TP, or TOC". Does this mean that the TDP, TP and TOC are up in the upper elevations of the water column an dnot at the bottom where the sediments are?	Having grouped data across all events does not allow for the individual flow and stage configuration to be tested for these interactions.	
Jose Guardiario	SFWMD	FIU-Roa-Sediment-Profiling	2	On the statement, "Sediments in canals L67A are suspected of contributing to increased total phosphorus (TP) peaks at the gate (S333 and S333N) that discharges into L29. " This is contrary to the statement, "Despite dates with high concentrations of TSS, TSS alone did not correspond to increases in TDP, TP, or TOC." (Kominski, Investigate sediment and floc transport of phosphorus at S333 gated structure on the northern boundary of Everglades National Park, 2023, 19)	Roa report provides a hypothesis, while Kominoski's report attempts to evaluate the concept. Please see comment above on Kominoski's approach.	
Jose Guardiario	SFWMD	FIU-Roa-Sediment-Profiling	2	On the statement, "It is hypothesized that during period of relatively low flows (dry season) when water levels in the canal are relatively low and less connected to the marsh sediments accumulate in front of S333. " The marsh may be less connected but the flow velocity over the marsh may be high that it picks up floc. The spikes in TP occur when the water levels are low and corresponding flows are low to zero, as shown in the SFWMD graph for 16 years.	There is no monitoring data or modeling that shows marsh velocities are high during that part of the year. The existence of thick vegetation may act as filter to block floc. Referenced SFWMD graph should be shared with us or please provide reference to the document.	
Jose Guardiario	SFWMD	FIU-Roa-Sediment-Profiling	3	On the statement, "At the onset of wet season, when flows increase, the elevated energy in flow column entrains phosphorus loaded sediments which contribute to increased TP peaks that gets flushed downstream within ~3-4-week period." The spikes in TP occur when the water levels are low and corresponding flows are low to zero, as shown in the SFWMD graph for 16 years.	Referenced SFWMD graph should be shared with us or please provide reference to the document.	
Jose Guardiario	SFWMD	FIU-Roa-Sediment-Profiling	5	On 2.2. Hydroacoustic investigation, consider the use of EM 1110-2-1003 CECW-CE I CECW-ODHydrographic Surveying	The suggestion is appreciated, but the project has been concluded.	
Jose Guardiario	SFWMD	FIU-Roa-Sediment-Profiling	12	On Fiogure 13. the water-sediment boundary closely follows the sediment rock boundary. I would expect that where the excavated rock is deeper, the sediment is thicker. Where the rock excavation is shallower, the sediment is thinner.	Agreed.	
Jose Guardiario	SFWMD	FIU-Roa-Sediment-Profiling	18	On Figure 20, It is expected that the middle of the canal have thicker sediments compared to the sides. These figures show otherwise. I expect blue (thin) on the sides and red (thick) in the middle.	This expectation is noted.	

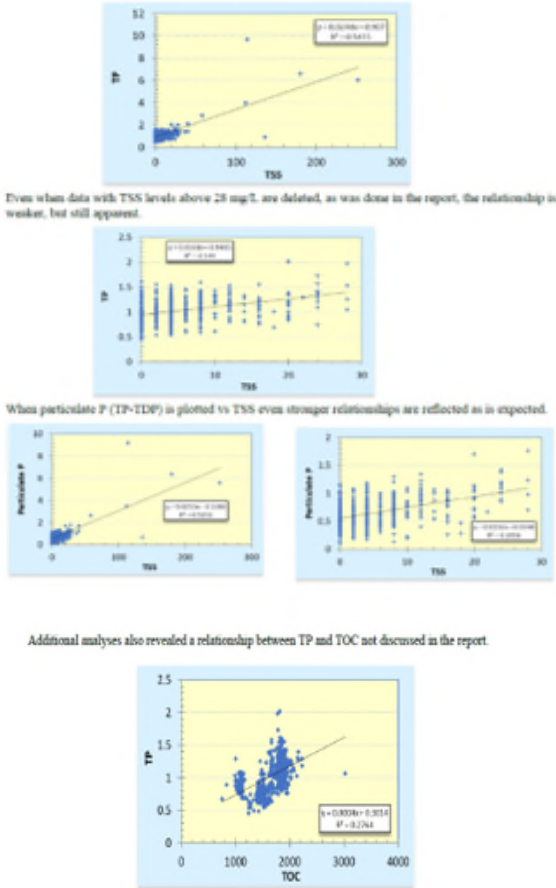| Commenter Name	Agency	Deliverable	Slide/Page Number	Comment/Question	Responses from ENP	Commenter Response
Jose Guardiario	SFWMD	UF-Li-Sediment-Floc-Characterization	4	On the statement, "Total phosphorus (TP) analysis revealed that L29 canal samples had the highest TP concentration in floc and sediments, followed by Miami canal samples." L29 structures have more frequent hiatus in flows, hence more likelihood of deposition	This comment is appreciated.	
Jose Guardiario	SFWMD	UF-Li-Sediment-Floc-Characterization	4	On the stetement, S333 sediment samples had low BD overall, except for samples near the S333 gate with high BD. " High BD near S33 indicate that the sediments are more sandy with less organics	Agreed	
Jose Guardiario	SFWMD	UF-Li-Sediment-Floc-Characterization	4	On the sttement, "In floc samples median particle size was ~567 μm (sd=114), which can be characterized as coarse sand size particles." We need to be careful on naming the floc as sand size. The low density (1.005gm/cm3) prevents settlement similar to 2.65 gm/cm3 sand	Agreed. "sand size" was specifically used here to not get confused with sand (2.65 gm/cm3).	
Jose Guardiario	SFWMD	UF-Li-Sediment-Floc-Characterization	4	On the statement, "TP measurements done on cross-sectional water sampling atS333 showed a clear pattern of decreasing TP with height from the canal bed, indicating a possibility of sediment entrainment from the canal bed, which may be due to higher water fluxes observed towards the bed of canal." Is this not contrary to the findings in Investigate sediment and floc transport of phosphorus at S333 gated structure on the northern boundary of Everglades National Park Principal Investigators, John Kominoski, 2003, 19. "Despite dates with high concentrations of TSS, TSS alone did not correspond to increases in TDP, TP, or TOC."	Kominoski pooled all the data together.Li's report provides a microscopic analysis at the S333 gate and we report that result.	
			8	On Figure 1.3, Indicate water levels and flow rates.	This can be only done at S333. The requested information on other locations is not collected.	
Jose Guardiario	SFWMD	UF-Li-Sediment-Floc-Characterization	8	ON Figure 1.4, Spillway with a lift-gate resting on it 3 ft from canal floor. This contrary to the actual survey of the canal which is 1t elevation -12.ft NAVD88	Fig. 1.4 is from SFWMD.	
Jose Guardiario	SFWMD	UF-Li-Sediment-Floc-Characterization	10	On Section 1.2. Hypotheses and objectives, During relatively low flows and low water levels (dry season; Dec-Apr), sediments accumulate in front of S333 due to settlement and roll-over effects. At the onset of wet seasons, when flows are increased but stages in the canals are low, this pool of sediments is susceptible to the elevated energy in the flow column, which brings these sediments into suspension to contribute to increased TP peaks. This may be true at high flows, but the spikes in TP occur when the water levels are low and corresponding flows are low to zero, as shown in the SFWMD graph for 16 years.	According to modeling, sediment bed transport can happen. When this reaches the zone near gate where cross-section gets smaller, velocities near the bed can increase to a threshold above which sediments can entrain. More investigations are needed. Referenced SFWMD graph should be shared with us or please provide reference to the document.	

Commenter Name	Agency	Deliverable	Slide/Page Number	Comment/Question	Responses from ENP	Commenter Response
Jose Guardiario	SFWMD	UF-Li-Sediment-Floc-Characterization	21	On 2.2.5.1. Mechanical sieving, "Samples were separated into three fractions: 1) gravel that cannot pass through 2 mm sieve; 2) sand that can pass through 2 mm sieve but cannot pass through 0.053 mm sieve; and 3) silt that can pass 0.053 mm sieve. " Can't the lighter floc fraction be separated from the heavier sediment fraction?	Floc and and sediment samples were collected separately and processed separately after drying.	
Nenad Iricanin	SFWMD	UF-Li-Sediment-Floc-Characterization	35	The paragraph starting with "Cadmium (Cd) is commonly" should be revised to indicate that the ranges discussed are location averages as opposed to raw data. The actual ranges for Cd in sediments and floc are 0.14-1.57 µg/g and 0.09-0.71 µg/g, respectively. Interstingly, there does not appear to be a realtionship between sediment Cd and P. Highest sediment Cd concentrations observed at Miami_2 and L29_1. For floc the highest Cd concentrations were observed at L29_1 and L29_2. Floc data does show a relationship with P. With the highest conentrations observed in the L29 which may also be affected by roadside runoff from US41. High sediment Cd at the Miami_2 station may also be afected by roadside runoff from I-75. How much influence on observed Cd concentrations does agricultural activity have over roadside runoff, fossil fuel combustion and aeolian deposition? What about airboat operations? Could they also contribute to high Cd levels? Also can an explanation be provide for the strong relationship between Pb and Cd?	This is being investigated further and may be incorporated.	Needs further discussion
Nenad Iricanin	SFWMD	UF-Li-Sediment-Floc-Characterization	35-36	Why are the sum of Fe containing minerals 2-9 times lower than sediment Fe content?	X-ray diffraction (XRD) diffractometer can only detect iron minerals in crystalline minerals, and most of the iron in our samples could be in noncrystalline forms, such as amorphous iron.	No issues noted
Nenad Iricanin	SFWMD	FIU-Kominoski-Sediment-Floc-Transport	Fig 17	It appears that the analytical method used for TSS is not appropriate for this study. 250 mL of water is not an appropriate volume to use to determine TSS values accurately for environmental samples. As a result, the data shows substantial PP (TP-TDP) when the method has not detected TSS. That raises the question of what type of filters were used and what were the pore sizes of the filters used. By definition, dissolved materials are those that pass through a 0.45 µ filter. If a larger pore size was used, the associated TDP are not really technically dissolved but filtered. When TSS = 0 mg/L, PP concentrations for all the stations (across all depths) range from 17 - 22 µg/L as geometric means. Further, no statistical difference was detected between PP for TSS=0 - TSS=10 mg/L, except for TSS=0 and TSS=8 mg/L. (p=0.006). This raises the question of the appropriateness of using 250 mL of water to determine TSS. Statistical test used: Steel-Dwass-Critchlow-Fligner all pairs comparisons	The PI indicated 0.7 micron filters were used for this analysis. In future work, the adequate amount of water sample will be used.	
Zubayed Rakib	SFWMD	FIU-Kominoski-Sediment-Floc-Transport	4	Test procedure indicates that water samples were collected at three depths (0.5 m from canal bottom, mid-depth of canal, and 0.5 m from canal surface) in L-29 and L-67A canals. Are the reported water quality parameter results average of these samples from three depths? Please clarify.	Results presented in Figures are not avarages	
Zubayed Rakib	SFWMD	FIU-Kominoski-Sediment-Floc-Transport	7	Is the conclusion "sediments in L-29 are thicker and richer in organic content than upstream in L-67, which are mostly carbonate sand (Figure 5)" only based on visual observation or data analysis?	PI is citing another study (Briceno et al. 2019) p.17 based on general observation. No statistical analysis was performed on the data.	

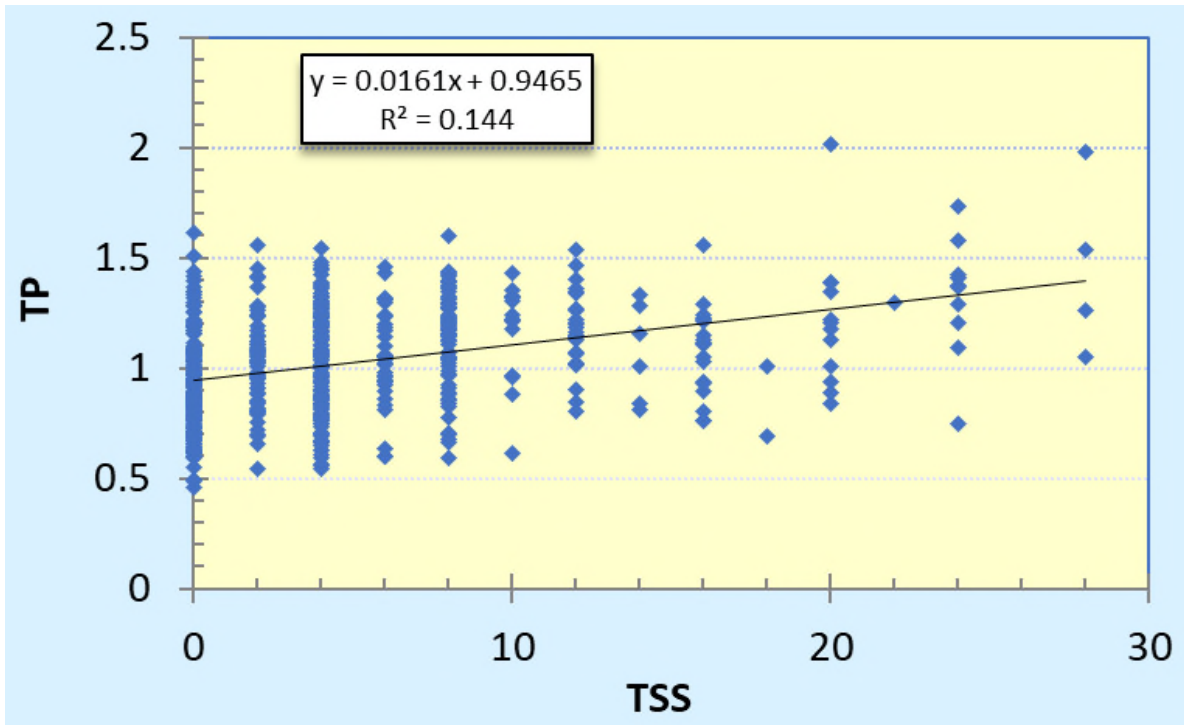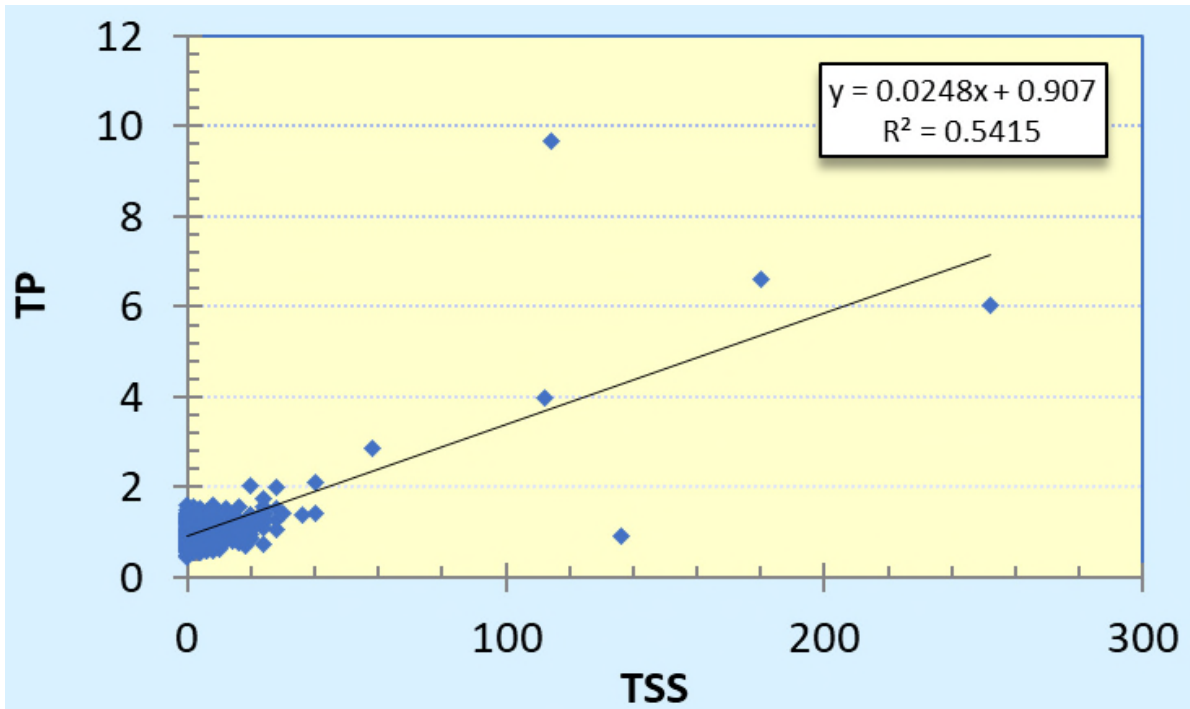| Commenter Name	Agency	Deliverable	Slide/Page Number	Comment/Question	Responses from ENP	Commenter Response
Zubayed Rakib	SFWMD	FIU-Kominoski-Sediment-Floc-Transport	9	What does the 'Zones A and B' of the regulation schedule refer to?	This is related to WATER CONTROL PLAN . More details are available at https://usace.contentdm.oclc.org/utils/getfile/collection/p16021coll7/id/15766 (Figure 7-7: WCA-3A Regulation Schedule) (p. 7-23 through 7-26)	
Zubayed Rakib	SFWMD	FIU-Kominoski-Sediment-Floc-Transport	19	"TSS alone did not correspond to increases in TDP, TP, or TOC." What does this imply in terms of elevated TP at S-333?	PI's interpretation is based on pooled data. More detailed look at the data is needed. Part of future analysis.	
Zubayed Rakib	SFWMD	UF-Li-Sediment-Floc-Characterization	General	The domain for Phase I sediment study is not clearly stated in the text. Consider delineating the domains for Phase I and II on the maps.	Its clearly stated in text- p.11 "Phase-1 (Subregional-scale study): The map in Fig. 2.1 shows the region where samples were collected." and p.12 "Phase-2 (Local-scale study): The map in Fig. 2.2 shows the region where samples were collected in close proximity to S333 in L29, L67A, and WCA3A adjacent marsh."	
Zubayed Rakib	SFWMD	UF-Li-Sediment-Floc-Characterization	12	2.The map in Fig. 2.2 for Phase-2 (local-scale study) appears to be analogous to the Phase I domain identified by the Working Group. Please clarify the inconsistency.	Phases of investigation in this report apply to PI's investigation only and are clearly defined. They do not relate to the Working Group phases.	
Zubayed Rakib	SFWMD	UF-Li-Sediment-Floc-Characterization	4	"The dynamic conditions in Miami Canal may make it difficult for P to settle, resulting in lower TP levels than L29 Canal". Does this imply that the elevated TP at S-333 is due to a far-field TP source issue from the Miami Canal?	Miami canal is a source of water at S333 but TP peaks may be formed by additional sources besides what is coming down from L67A.	
Zubayed Rakib	SFWMD	UF-Li-Sediment-Floc-Characterization	Section 3	Please present the particle size distribution (sieve analysis) chart (particle size versus % finer).	The data can be visualized in many ways. Raw data has been shared for independent analysis.	
Odi Villapando	SFWMD	UF-Li-Sediment-Floc-Characterization	9	Text made specific reference to particulate P contributing >90% to observed TP concentrations at different locations near S333 in Figure 1.6 where only SRP and TP are shown.	PI made that interpretaion based on visual comparison in Fig. 1.6 (Briceno et al. 2019)	
Odi Villapando	SFWMD	UF-Li-Sediment-Floc-Characterization	11	In the methods section under sampling, it would be helpful to specify the various physical and chemical analyses performed on Phase 1 and II samples, and also for clarity.	Table has been incorporated	
Odi Villapando	SFWMD	UF-Li-Sediment-Floc-Characterization	13	Were the floc and sediment collections conducted according to standard methods? With the bottom of the water column especially in the canals being not so visible to the naked eye, it is likely that the floc collector collected samples other than floc.	Prior to collecting samples for this project, we conducted a literature review on floc and sediment sampling from wetland and canals. There is no standard protocol for collecting floc and sediment and we developed a protocol which we feel fits the purpose of this project. For determining floc, we employed an underwater camera prior to sampling. Unfortunately, we were unable to obtain a clear visual for accurate measurements.	
Odi Villapando	SFWMD	UF-Li-Sediment-Floc-Characterization	18	Can you cite the method used in the wet acid digestion for TP? I believe the cited EPA method was for the colorimetric determination of P following digestion.	1.Anderson, J. M., 1976. An ignition method for determination of total phosphorus in lake sediments. Water Research 10:329-331. 2.Belmont, M.A., White, J., Reddy, K.R. 2009. Phosphorus Sorption and Potential Phosphorus Storage in Sediments of Lake Istokpoga and the Upper Chain of Lakes, Florida, USAJ. Environ. Qual. 38:987–996	
Odi Villapando	SFWMD	UF-Li-Sediment-Floc-Characterization	19	The range of initial P concentrations used in the isotherms (10-400 mg P/L) did not include solution P concentrations below <10 mg P/L needed to estimate S_o using least squares fit of S'. At low (<10 mg P/L) equilibrium concentrations C, the linear relationship between S' and C can be described by Equation 2.	Excellent observation. We only have 5 initial P concentration levels (10, 50, 100, 200, and 400 mg P/L) for the sorption study and we don't have low concentration below <10 mg P/L. Due to the limited sample amount, it only allows us to have 5 P concentration levels. We do agree using low initial P concentration is more appropriate for estimating So.	
Odi Villapando	SFWMD	UF-Li-Sediment-Floc-Characterization	21	Why run particle size analysis on floc samples that were dried and finely ground? Floc is unconsolidated and structureless. Should you have used wet sieving instead of dry sieving for samples with high concentrations of fine particles? On page 4 of the report, it was mentioned that floc had a median particle size much larger than canal bed sediments that would charaterize them as coarse sand sized particles. Is this possible?	1.After an extensive literature review, we could not find a standard method for measuring floc or sediment particle size with a laser. An oven- or air-dried sample has been used as a standard procedure for traditional soil particle size distribution measurement. 2. We like the suggestion and will measure floc samples without drying and grinding in the future study.	

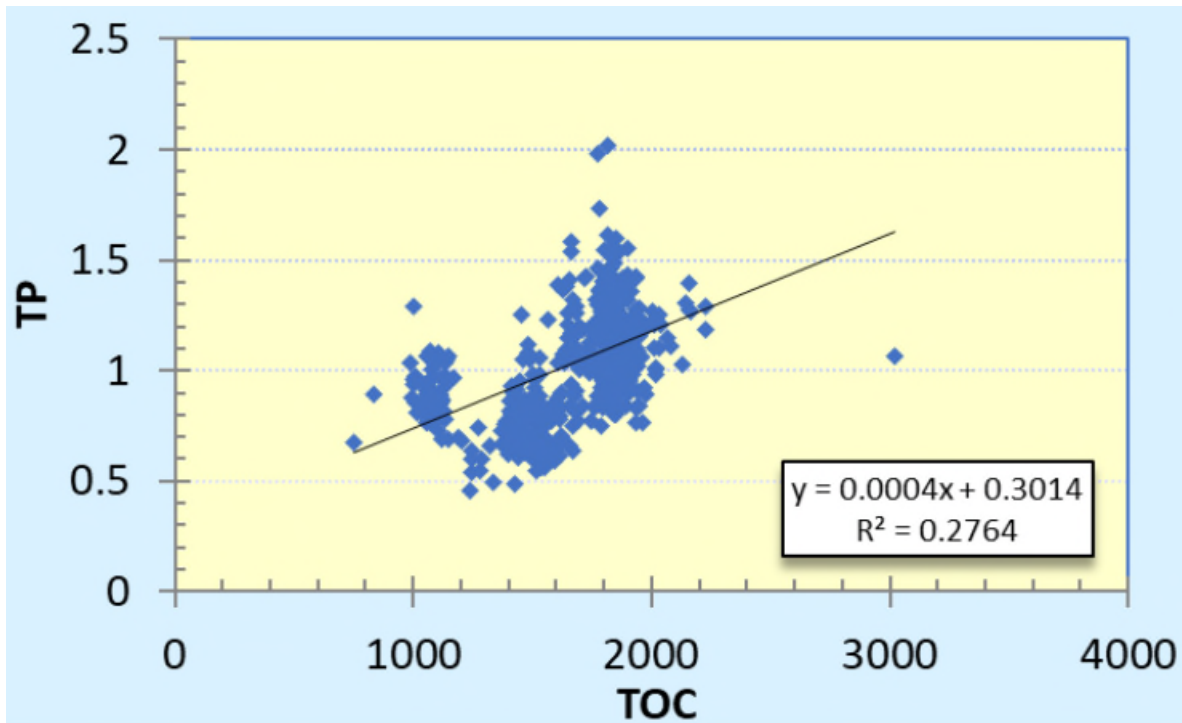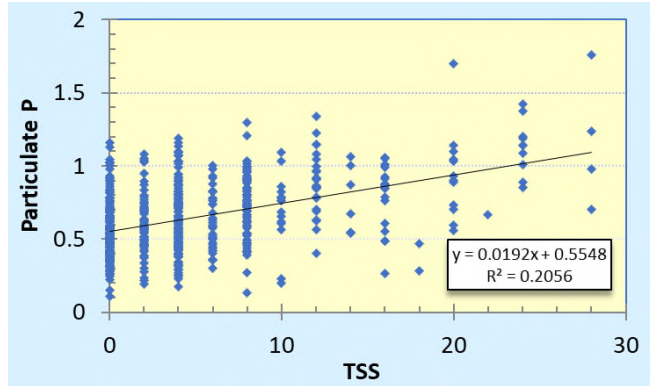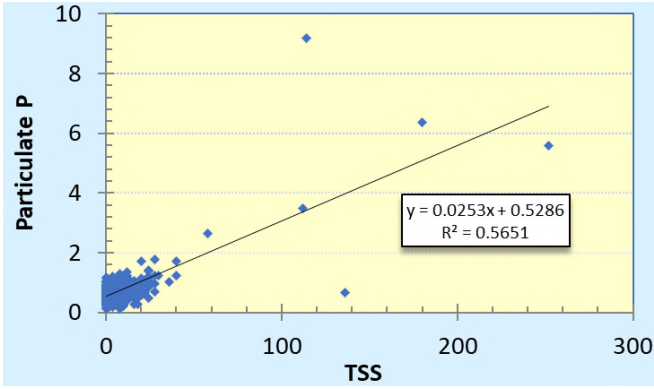| Commenter Name	Agency	Deliverable	Slide/Page Number	Comment/Question	Responses from ENP	Commenter Response
Odi Villapando	SFWMD	UF-Li-Sediment-Floc-Characterization	21	What was the purpose of isotope analysis? Was it to trace the origins of P in the canals and marsh?	We use isotopes as one of the indicators to help tracing the source of P in the canals and marsh, same as metals and minerals. Oxygen isotopic analysis of phosphate has been used for studying the source and degree of microbial cycling of phosphorus in various ecosystems. Li et al. (2011) used oxygen isotope to link phosphorus in canal to the anthropogenic P input. Carbon and nitrogen isotopes have been often used to identify sources of organic matters in sediments and soils (Wang et al., 2002). Li, X., Y. Wang, J. Stern, and B. Gu. 2011. Isotopic evidence for the source and fate of phosphorus in Everglades wetland ecosystems. Applied Geochemistry 26(5):688-695. Wang, Y., Y.P. Hsieh, W.M. Landing, Y.H. Choi, V. Salters, and D. Campbell. 2002. Chemical and carbon isotopic evidence for the source and fate of dissolved organic matter in the northern Everglades. Biogeochemistry, 61 (3) (2002), pp. 269-289.	
Odi Villapando	SFWMD	UF-Li-Sediment-Floc-Characterization	24	I don't think the number of samples was large enough to capture spatial variability of TP in the marsh and canals.	Agreed for Phase -1 samples. Phase-2 had lot more samples (40 floc and 91 sediment).	
Odi Villapando	SFWMD	UF-Li-Sediment-Floc-Characterization	27-30	The authors discussed the lack of statistically significant differences in the measured parameters among the three canals and adjacent marsh but failed to acknowledge that it was due to small number of samples.	The number of samples can impact statistical differences. Due to limited resources, we were unable to obtain a larger sample size for Phase 1.	
Odi Villapando	SFWMD	UF-Li-Sediment-Floc-Characterization	31	Many of the *EPCo* values for floc and sediments summarized in Tables 3.1 and 3.2 are unusually high and do not make practical sense. As alluded to earlier, the relationship between *S'* and *C* is linear at low (<10 mg P/L) equilibrium concentrations. Since *So* in this study was estimated using initial P concentrations of up to 100 mg P/L, *So* was likely overestimated, which led to erroneous calculation of *EPCo* using Equation 3.	As answered in comment #147, we agree that the relationship between S' and C is linear at low EPC (typically lower than 1 mg P/L). However, we only have 5 concentrations of P solutions (10, 50, 100, 200, and 400 mg P/L) for the sorption study due to insufficient sample mass. The estimated EPCo may not be overestimate using high initial P concentration. We will add a statement to that effect.	
Odi Villapando	SFWMD	UF-Li-Sediment-Floc-Characterization	32	The authors talked about EPCo and TSC values in the report but did not provide insights/explanation as to how these parameters relate to the function of floc and sediment as either a source of or a sink for P with changing TP concentrations of water in the canals and marsh. How did the TSC values compare with the respective TP content of floc and sediment in the canals and marsh?	The PI has revised the report and this evaluation may be considered in future reports.	
Odi Villapando	SFWMD	UF-Li-Sediment-Floc-Characterization	35	What standards (background concentrations) were used to compare the enrichments of the different metals in the floc?	In Table 3.5, we listed background concentrations of selected metals in Florida soil and Florida sediments, and sediment (0-10 cm) collected from Everglades National Park (ENP), the coastal fringes of Biscayne National Park (BNP), and Big Cypress National Preserve.	
Odi Villapando	SFWMD	UF-Li-Sediment-Floc-Characterization	36	Not all of the minerals depicted in Figure 3.12 are clay minerals. Illite, kaolinite and playgorskite are the only phyllosilicate minerals.	Agreed. The word "clay" was deleted from Figure 3.12 caption.	
Odi Villapando	SFWMD	UF-Li-Sediment-Floc-Characterization	47	How did the sums of the P fractions in floc and sediment compare to TP values obtained using wet acid digestion?	Theoretically, the sum of TP fraction concentration should equal the TP concentration. In this study, 204 samples were analyzed for TP fractionation, of which 168 were within the 70-130% recovery range. TP fractionation is a sequential process with seven extraction steps, and a small amount of soil particles may get lost in the supernatant at any step. It is also why we analyzed TP separately and did not use the sum of P factions.	

Commenter Name	Agency	Deliverable	Slide/Page Number	Comment/Question	Responses from ENP	Commenter Response
Odi Villapando	SFWMD	UF-Li-Sediment-Floc-Characterization	52	The statement that marsh sediments would be less susceptible to entrainment and transport given the same levels of flows in the marsh and canals, could this be due to the fact that marsh is thickly vegetated and the canals are not, and not so much because of differences in mean particle size?	Context of this statement is higher d50 of marsh sediment compared to canal sediments subjected to same levels of flow energy. Other factors such as vegetation also play a major role in reducing the impact of flow energy (mannings's roughness coefficient used in hydrologic models for vegetation presence). In general, marsh flow velocities are also far below the canal flow velocities.	
Odi Villapando	SFWMD	62-Slide-Deck	3	What specific flow condition (i.e., low, moderate, high) was hypothesized to promote transport or settling of floc and sediments?	This was an exploratory investigation, so no specific flow rates were hypothesized to promote transport or settling.	
Odi Villapando	SFWMD	62-Slide-Deck	16	Did the statement that 95% of TP in the canal sediments are bound come from the P fractionation study?	Yes	
Odi Villapando	SFWMD	62-Slide-Deck	25	Could the lack of statistically significant differences in particle size of floc in marsh and canals be due to small sample size? Looking at the boxplots, the median particle size for the floc in L29 is much larger than the rest.	Yes	
Odi Villapando	SFWMD	62-Slide-Deck	32	Were the values on the Y axis of both graphs obtained by subtracting water- and NH4Cl extractable P from the sum of all P fractions and not from the TP values obtained using wet acid digestion?	Yes	
Odi Villapando	SFWMD	62-Slide-Deck	39	Why are these results very different from particle size analysis done at a local scale?	Samples were collected in very different location between local and subregional.	
Odi Villapando	SFWMD	62-Slide-Deck	41	Floc-OM was actually much higher in the marsh than OM in other compartments but due to small sample size no significant differences could be detected. Similar case for sediment-OM.	Agreed.	
Odi Villapando	SFWMD	62-Slide-Deck	55-56	These are not all clay minerals. Only illite, kaolinite and palygorskite are; the rest are just minerals (i.e. oxides of iron, carbonates of calcium).	Agreed. Will be corrected in future reporting.	
Odi Villapando	SFWMD	62-Slide-Deck	62	While the results of floc and sediment analyses at a subregional scale show apparent differences among canals and marsh, the lack of statistically significant differences due to small sample size, puts limitations on how data should be interpreted.	This caveat is appreciated	
DEAR	FDEP	FIU-Kominoski-Sediment-Floc-Transport		Nearly a third of the TSS measurements collected during this study had a value of 0, but there was sufficient material present to conduct the particle size analysis. The TSS data should be verified or a more sensitive analytical technique should have been utilized.	TSS data has been verified. Analysis was done using 0.7 micron filter. Particle size analysis was also done on these samples, which also detects size lower than 0.7 micron.	
DEAR	FDEP	FIU-Kominoski-Sediment-Floc-Transport		All data associated with TSS measurements above 28 mg/L were omitted from analysis without any explanation or justification. Doing this also removed data with the highest TP levels, which were described as the focus of the study.	The PI has verified the TSS data and revised the report.	
DEAR	FDEP	FIU-Kominoski-Sediment-Floc-Transport		Because the evaluation of the existing data demonstrated typical "first flush" type phenomena, there should be a description of the flow conditions prior to the study to assure the "first flush" had not occurred prior to the study.	The sampling was timed to capture the rise & fall in peaks based on previous years data which does not happen over days. We were able to capture some part of this process. Future analysis will include the flow conditions over the period.	
DEAR	FDEP	FIU-Kominoski-Sediment-Floc-Transport		There was no analysis or discussion of the flow or the particle size data provided.	Particle size analysis on water samples was done by UF-Li in a different project. Future synthesis report will combine all data from different projects for such analysis.	

Commenter Name	Agency	Deliverable	Slide/Page Number	Comment/Question	Responses from ENP	Commenter Response
DEAR	FDEP	FIU-Kominoski-Sediment-Floc-Transport		Graphs of data collected during the study and subsequent conclusions based on these graphs are not consistent with the data set provided. While a couple of the errors are discussed in detail below, all the analyses and interpretation of the data should be redone and verified prior to accepting any of the conclusions. The graph Figure 17 B was provided in the report as evidence of the lack of relationship between TP and TSS. Because the majority of the TP is particulate P, the lack of any relationship is concerning. When the data provided was plotted to verify the report findings, the expected relationship is apparent and the conclusion that TP levels are not related to TSS levels is shown to be erroneous. Note that none of the total phosphorus or TOC concentrations were converted from µM to µg/L in the graphs below, but that should not change the shape of the relationships.Based on these findings, all the analyses and plots should be redone and verified prior to accepting any of the conclusions made in the report. Additionally, a more in depth analysis could potentially reveal other relevant relationships. See the end of the section for larger images Even when data with TSS levels above 28 mg/L are deleted, as was done in the report, the relationship is weaker, but still apparent. When particulate P (TP-TDP) is plotted vs TSS even stronger relationships are reflected as is expected. Additional analyses also revealed a relationship between TP and TOC not discussed in the report. 	The PI has reexamined and provided the revised report. Note that PI used non-parametric methods as the data was not normally distributed.	

Commenter Name	Agency	Deliverable	Slide/Page Number	Comment/Question	Responses from ENP	Commenter Response
DEAR	FDEP	FIU-Roa-Sediment-Profiling		This project used "highly experimental" hydroacoustic sediment profiling techniques to estimate sediment thicknesses in the L29 and L67 canals and the area around the S333 structure. While these methods were able to collect a large amount of sediment thickness data rather quickly, they exhibited large errors (>50 % error) in estimating the total sediment thickness. To further refine the estimates to reduce the error would require a great deal of human input and time. While these methods may prove useful in the future, they are still "highly experimental" and require more development prior to being relied on for accurate estimates of sediment thickness. Also, while they provide a course estimate of the sediment thickness, they do not consider the floc thickness in their estimates.	Floc is unconsolidated and highly transient. Any attempt to estimate its thickness using acoustic methods would be extremly difficult considering the results obtained for sediments. We agree with the comment on sediment thickness estimates using hydroacoustic method.	
DEAR	FDEP	UF-Li-Sediment-Floc-Characterization		Most of the conclusions made in this report appear to be based on the results of the cluster analyses performed using floc and sediment data collected at sites in the L29, L67, and Miami canals, the marsh north of L67, and at S333. While two of the three floc clusters did indicate that S333 was more similar to the L67 and Miami canal sites, the third cluster using floc trace metals, clay minerals, and isotopes showed the L29 canal sites in the same cluster with S333 and a single L67 site. The clusters analysis based on the sediment data provided mixed results with none of the L67 sites being in the same cluster as S333. One cluster showed S333 to be most similar to the Miami canal sites. The second cluster showed S333 to be clustered with the marsh sites with the L29 and L67 sites in the same cluster. The third cluster indicated that S333 was similar to the Miami and L29 canal sites. The conclusions made in the report seem to be focused on showing that the L67 and Miami canals are the primary contributors of the P reaching the S333. These results suggest that TP at S333 is probably more of a mixture of sources. During periods when floc transport is occurring, L67 may have a significant role in transporting P to the S333 structure. While during higher flows when sediment transport occurs, the L29 may be more of a prominent source with the L67 playing a lesser role. It is important to note that the cluster analyses do not reflect cause and effect relationships and only indicate relative similarities between groups of data.	The interpretation is appreciated. Also need to consider relative hydrologic connectivity of different comprartments representing diferent groups of data. Sampling sites in L29 were located west of S12C and S12B miles away in the west from S333. Out of seven water sampling event L29 contributed little flow to S333 (62-slide-deck#8). For a nearly continuous record of flow direction in L29 (62-slide-deck#36), L29 predominantly flowed towards west (S12s). Thus, it appears highly unlikely that L29 is a dominant source of sediments to S333.	
Nenad Iricanin	SFWMD	FIU-Kominoski-Sediment-Floc-Transport	Excel file	It appears that several sampling events had duplication of sampling at the 0.5 meter water depth. These sampling events are: L29-1 North on 4/14/2022, L29-1 North and L-67_1 West on 5/5/2022, L29-1 North and South on 5/26/2022, and L67-3 East on 6/27/2022. It is unclear whether these were data sets were field dups or were incorrectly identified as being sampled at 0.5 meters. If the additional data provided at these stations were field dups, they need to be correctly identifies. Could some clarification be provided?		

Enlarged figures from FDEP, DEAR comments:

$y = 0.0253x + 0.5286$
$R^2 = 0.5651$

$y = 0.0192x + 0.5548$
$R^2 = 0.2056$

$y = 0.0004x + 0.3014$
$R^2 = 0.2764$

ATTACHMENT 2: HYDRODYNAMIC STUDY REPORT AND S333 WORKING GROUP COMMENTS AND RESPONSES MATRIX

CONTENTS

SECTION 1: CFD STUDY IN SUPPORT OF INVESTIGATION OF HIGH TOTAL PHOSPHORUS (TP) CONCENTRATIONS IN DISCHARGES THROUGH S-333 AND S-333N SPILLWAYS

Computational Fluid Dynamics (CFD) Study in Support of Investigation of Elevated Total Phosphorous Concentrations in Discharges through S-333 and S-333N Spillways

July 2023

Jie Zeng, Zubayed Rakib, Matahel Ansar, and Mark Wilsnack
Applied Hydraulics Section
Hydrology and Hydraulics Bureau
South Florida Water Management District

TABLE OF CONTENTS

LIST OF FIGURES

LIST OF TABLES

ACRONYMS, ABBREVIATIONS, AND UNITS OF MEASUREMENT

2D	two-dimensional
3D	three-dimensional
μm	micrometer
ARE	Absolute Relative Error
ADCP	acoustic Doppler current profiler
CAD	computer aided design
CERP	Comprehensive Everglades Restoration Plan
CEPP	Central Everglades Planning Project
CFD	Computational Fluid Dynamics model
cfs	cubic foot per second, cubic feet per second
cm	centimeter(s)
D_{50}	Median sediment particle size
D_{100}	Maximum sediment particle size
DBHYDRO	South Florida Water Management District's environmental database
DTM	Digital Terrain Model
EAA	Everglades Agricultural Area
ENP	Everglades National Park
ft	foot, feet
ft/s	foot per second, feet per second
HEC-RAS	Hydraulic Engineering Center River Analysis System
m	meter(s)
m/s	meter(s) per second
mm	millimeter(s)
NAVD88	North American Vertical Datum of 1988
NGVD29	National Geodetic Vertical Datum of 1929
NPS	National Park Service
Q	Flow/Discharge
RANS	Reynold's Averaged Navier Stokes
SFWMD	South Florida Water Management District
TP	total phosphorus

USACE	United States Army Corps of Engineers
USBR	United States Bureau of Reclamation
V_mag	Velocity Magnitude
W/	with
W/O	without
WCA	water conservation area

1.0 INTRODUCTION

S-333 and recently constructed S-333N spillways are located at the intersection of the L-67A Canal and Section 3 of L-29 Canal in Miami-Dade County. These two structures control discharges from Water Conservation Area (WCA)-3A to Everglades National Park (ENP) as a part of Comprehensive Everglades Restoration Plan (CERP). Cyclic occurrences of high total phosphorus (TP) transport through the S-333/S-333N complex has long been of concern. Sediments in the L-67A and L-29 canals are suspected of contributing to increased TP peaks at the S-333 complex. Observed TP concentrations have over 90% contribution from particulate phosphorous (Briceño et al. 2019). It is hypothesized that when flow velocities are smaller during relatively low flows (dry season; December–April), sediments accumulate in front of S-333. At the wet season onset, when flows start to increase, the elevated energy in the water column brings the phosphorus loaded sediments in suspension, which contribute to increased TP peaks that gets flushed to the downstream.

Outcomes of previous investigations have added insight into this problem: (1) the stage-TP inverse relationship is region-wide and applicable to canals that are not directly connected to Lake Okeechobee or the Everglades Agricultural Area (EAA); (2) sediment core samples taken near the S-333 and S-333N complex in the L-67A and L-29 canals were very sandy, while fine and organic-rich material was found at a site west of the S-12D structure in the L-29 Canal; (3) TP spikes may be activated by hydraulic conditions that incite sediment resuspension, levee erosion, and peat erosion within the canal margins; and (4) fractionating the TP species found in canal floc and sediments suggest that TP spikes originate from bottom sediments, floc, and possibly peat soils in the marshes (Daroub et al. 2002, Li et al. 2011, Wang et al. 2011, Das et al. 2012, Briceño et al. 2019). Despite these findings, no clear answer exists as to where the elevated TP concentrations come from and what the transport mechanisms are through the S-333/S-333N complex.

Local field monitoring enhancements, hydrodynamic analyses, and sedimentation transport studies have recently been proposed to further investigate the problem. These studies will assess the mechanisms responsible for the transport of sediment particulates and TP within the portion of the water column that is highly influenced by near-bed velocity, water depth and other hydrodynamic features. The current study area focuses on the canal system near S-333/S-333N while encompassing the marsh and canals within southern WCA-3A. **Figure 1** shows the overall domain of the hydrodynamic analysis. Analysis of the local area around S-333/S-333N to determine the pertinent hydrodynamic features that incite sediment and TP transport through the structures is also indicated. This analysis will be carried out in Phase I (the focus of this report). Phase II, if approved, will include analysis of the upstream areas within WCA-3A.

Traditionally, a reduced-scale physical model would have been used for this type of study since it is the most reliable approach. Unfortunately, physical models can be prohibitively costly and time consuming. Consequently, instead of relying on the physical model, three-dimensional (3D) Computational Fluid Dynamics (CFD) has been used in Phase I to explore the hydrodynamic process that induce the transport of TP through S-333 and S-333N.

The purpose of three-dimensional CFD analysis was to examine the local velocity fields under low- and high-water depths at the S-333 complex and within immediate proximity of the canals and marsh areas around the structures. Engineering measures for reducing sediment and potentially reduce TP transport, such as sediment trap or low-sill weir, and marsh vegetation buffer were also evaluated.
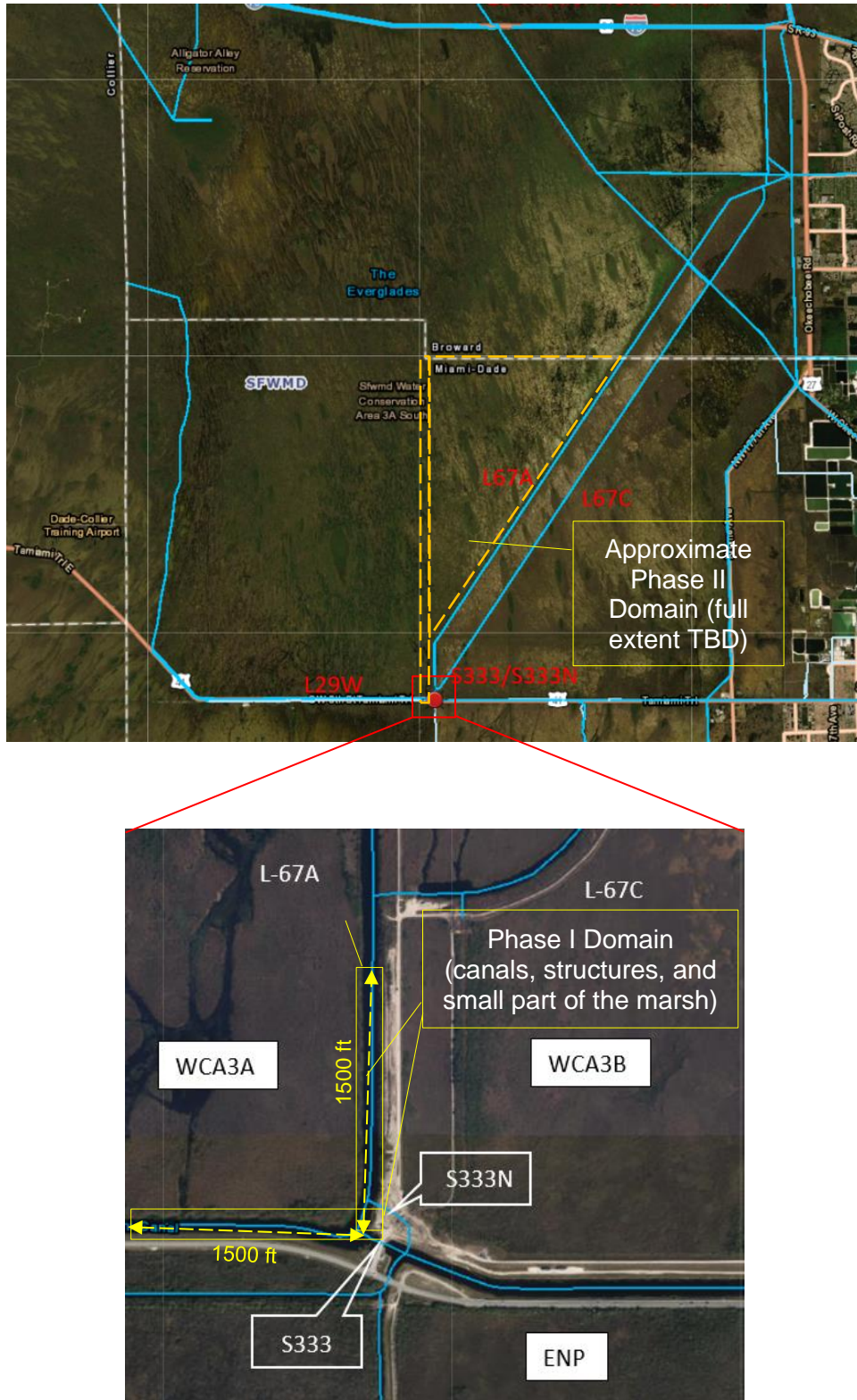
Figure 1. Location of study area with the top panel showing the overall domain for Phase II and the bottom panel showing the Phase I CFD Study Area. (Note: TBD – to be determined.)

2.0 OBJECTIVES

To study the hydrodynamics of flow along the canal system near S-333/S-333N and expand the effort to include the southern WCA-3A canals and marsh areas, the study was proposed to be carried out in two phases. The following sections discuss the phases.

Phase I

The first phase involved extending the existing 3D CFD model (Zeng et al. 2018) of the local area around S-333/S-333N to analyze the pertinent hydrodynamic features that incite sediment and TP transport through the structures. The extended model was also used to examine the effect of structural and operational measures on sediment transport. More specifically, Phase I was designed to answer the following:

1. What velocities can be expected near the S-333/S-333N complex under various conditions (historically observed and future Central Everglades Planning Project (CEPP) stage/flow conditions)?

2. What is the feasibility and impacts of installing a sediment trap or low-sill weir, or a vegetation buffer, upstream of the structures?

3. How can these alternatives be designed to reduce velocities below the values critical to suspending and transporting nutrient-rich materials?

4. Does the near bed velocity distribution indicate potential to reduce erosive potential of sediments (i.e., given consideration of National Park Service or NPS sediment study datasets) adjacent to the S-333 or S-333N intake basins with engineering and maintenance solutions, including but not limited to adding vegetation buffers in marsh adjacent to the L-67A and L-29 canals for reducing marsh velocities, creating sediment traps upstream of S-333/S-333N to reduce in-canal velocities and allow accumulation of bedload sediments, and/or installing low-sill weirs before S-333/S-333N spillways to reduce potential for resuspended sediments from flushing to the downstream?

To answer these questions, several model scenarios that encompass historic and future conditions were simulated. With the new S-333N Spillway in operation, the total design flow in L-29 Canal has increased. Consequently, investigation of only the historical conditions was not adequate. The analysis focused on evaluating historically observed and anticipated flow scenarios that could cause the highest near bed velocities at the S-333/S-333N complex. Different structural improvement alternatives were included to slow down sediment transport, such as a sediment trap, a low-sill weir, channel improvements such as widening and deepening, or a combination of these. Considering maintenance issues, only one sediment trap on each upstream canal was considered for initial examination. Near bed velocities were simulated with and without these structural improvements. Impacts to water surface profiles were also considered. Progressive understanding of the problem helped to adjust the selection of the types and locations of the structural alternatives that would prevent the elevated TP transport. Their evaluation was conducted bearing in mind the geotechnical and environmental issues, the construction constraints, and the impacts on structure operations. Detailed 3D flow fields were used to evaluate the efficiency of each or combination of the engineering measures to reduce sediment incipient motion.

No direct sediment transport modeling was considered in the statement of work. The approach in the statement of work adopted combining numerical simulations and empirical formula to indirectly evaluate the potential of sediment movement. For example, detailed 3D velocity field from CFD simulations can be compared with incipient velocity diagrams, charts, and nomograph from the United States Bureau of Reclamation (USBR) and United States Army Corps of Engineers (USACE) to connect flow velocities to sediment motion (USBR 1974, USACE 1991).

Ground water exchange is not considered in this modeling. The focus was on the surface water, and it is believed to be the major driving factor for sediment transport. In addition, impacts from rainfall were not considered.

Phase II

Pending results of Phase I and findings from the NPS sediment study, a Phase II hydrodynamic study may be carried out. It is subject to South Florida Water Management District (SFWMD) leadership's approval. Phase II work, if approved, will build upon Phase I and expand the modeling domain to include the upstream areas within WCA-3A. The objectives of the Phase II modeling study will be determined following review of the results from Phase I hydrodynamic and the NPS Phase I sediment studies. It should be noted hydrodynamic results in this report, as currently authorized, pertains only to Phase I.

3.0 CFD MODEL STUDY FOR PHASE I

Survey

A bathymetric survey was required prior to this phase of model study to obtain the detailed geometric properties of the L-67A and L-29 inflow canals along with the local marsh topography. The survey was carried out by SFWMD in-house staff. It extended the available survey at S-333 and S-333N by 1,800 feet (ft) upstream along the L-67A and L-29 canals. Land surface elevations were extracted from existing digital terrain model (DTM) from Miami Dade County and USACE that was put together by SFWMD geospatial staff.

Model Development

The CFD modeling in this study relied on solving the Reynolds Averaged Navier Stokes (RANS) equations. Commercial CFD software, ANSYS FLUENT, was used for the 3D near-field modeling of the S-333/S-333N complex.

The CFD model domain of the S-333/S-333N complex used in another study (Zeng et al. 2018) is shown in **Figure 2**. For this hydrodynamic study, the CFD model domain was extended to about 1,800 ft of the L-67A and L-29 inflow canals, and 700 ft of the L-29 Canal downstream of the structures. The computational domain included suitable inflow and outflow boundaries that can be characterized by quasi-uniform and quasi-steady flow conditions. The upstream boundary was situated 1,800 ft upstream from the structures to ensure that stages and flows at this location are not influenced by either structure operations or proposed structural improvements. The outlet boundary was located at 700 ft downstream of S-333/S-333N to avoid both fluctuations on the free surface induced by the hydraulic jump and large eddies near the canal walls. The headwater and tailwater elevations, treated as pressure inlet and outlet, were used for upstream and downstream boundary conditions. Desired flow through each structure was attained by controlling the gate

opening estimated using site-specific rating equations (Rakib et al. 2017). Flows in L-29 and L-67A are computed by the model based on hydraulic boundary conditions. Channel characteristics including layout, cross-sectional geometry, and distribution of the wall and bed surface roughness were based on the new survey/information.
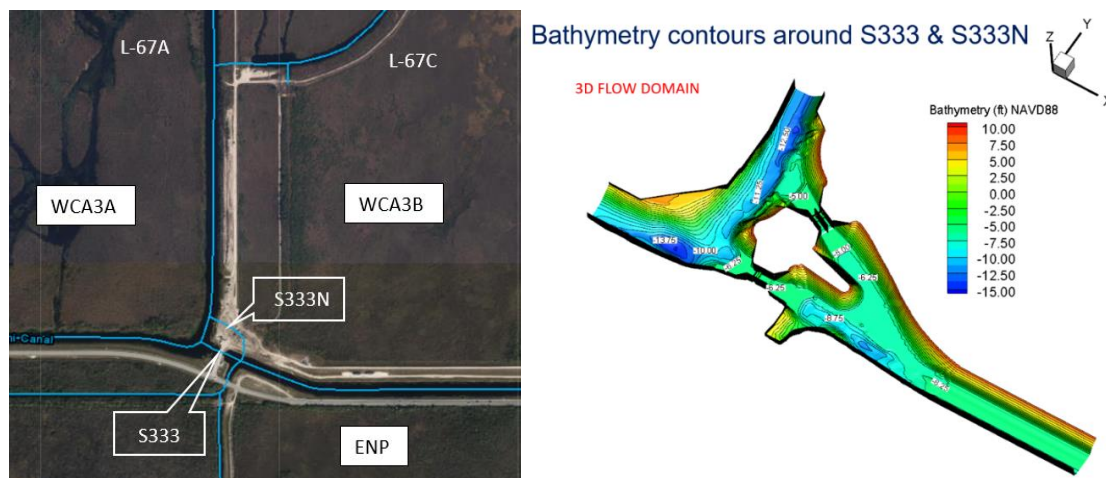
Figure 2. Simulation domain (left) and existing CFD Model for the S-333/S-333N complex (right). The CFD model shows the existing configuration from another project that was extended for this study. (Note: NAVD88 – North American Vertical Datum of 1988.)

The solid boundaries within the domain were represented by no-slip boundary conditions. Form roughness due to bed forms or geometry features of the structure was considered while configuring the computational mesh. The effects of turbulence on the simulated flow fields were accounted for using k-epsilon (k-ε) turbulence closure. After the numerical model setup, a mesh independence analysis was performed. For each steady-state simulation, the total mass flow rate through the gate (including water and air mass flux) was used as an indicator for model convergence. Model convergence was considered achieved when the fluctuations of the mass flow rate at the gate were less than 5% of the average value for the simulation period.

More details on CFD model setup are available in Zeng et al. (2017). The 3D model preparation and mesh generation tasks included (1) creating structure geometry using computer aided design (CAD) software or other software, and (2) importing the CAD model into the pre-processor and preparing the CFD 3D mesh for all alternatives considered. The various facets of CFD model setup and validation processes included (1) initial setup, (2) model validation, and (3) application of the validated CFD model to selected scenarios.

Model Validation

CFD has been rigorously validated based on several field and experimental data, both by SFWMD and other researchers (Savage and Johnson 2001, Ge et al. 2005, Kirkgoz et al. 2009, Dargahi 2006, Zeng et al. 2017, Pedersen et al. 2018). Calibration and validation of the CFD model is beyond the scope of this report. Having said that the CFD RANS model used was calibrated in numerous previous SFWMD studies. Some limited CFD model validation was done in Phase I making use of the stage-discharge-structure operation measurements taken at S-333N. **Table 1** shows the performance of the CFD model for S-333N.

Table 1. CFD model validation results at S-333N. [a]

Date	Headwater (ft NGVD29)	Tailwater (ft NGVD29)	Gate Opening (ft)	Q Measured (cfs)	CFD Results	
					Q CFD (cfs)	ARE [b]
02/02/2021	10.10	8.11	2.59	543.00	538.69	0.60%
02/02/2021	10.08	8.15	4.00	920.00	884.14	3.53%
03/25/2021	9.09	8.24	3.65	559.00	580.64	3.87%
02/02/2021	10.05	8.19	5.19	1243.00	1188.70	2.59%
					Average	**3.23%**

a. Key to abbreviations: ARE – Absolute Relative Error, CFD – Computational Fluid Dynamics model, cfs – cubic feet per second, ft – feet, NGVD29 – National Geodetic Vertical Datum of 1929, and Q – Flow.

b. ARE = absolute(Q measured – Q simulated)/Q measured

CFD Model Applications

The validated CFD models were first applied to evaluate both the existing and anticipated conditions without any improvements at the S-333 complex. Subsequently, the model was used to simulate the flow fields including the structural improvements. These model simulations are summarized as follows:

1. Simulation of existing flow condition, which included performing CFD simulations to investigate the hydrodynamics of the existing high and low flow conditions along the L-67A and L-29 inflow canals at the S-333/S-333N structures and in the L-29 Canal downstream. This served as a baseline scenario.

2. Simulating future conditions without improvements.

3. Evaluating proposed structural improvements.

A CFD model scenario involving backfill of the S-12E intake basin on the tailwater side of S-333 for the purpose of demonstrating whether it may enhance the flow and sediment transport characteristics downstream of S-333 (per recommendation from S-333 Working Group Evaluation Matrix) was also considered. However, past CFD runs (Zeng et al. 2018) of the S-333/S-333N complex indicated a dead hydrodynamic zone in this area. Consequently, it is not expected to have any significant impact on the flow field.

The CFD model simulation categories are described below.

Scenario 1: Low-Water Scenario, Existing Conditions

The low-stage scenario concentrated on hydrodynamics in the canal. To address the TP concern, the low-flow scenario was also considered. This set of model simulations considered flow in upstream canals when water levels are below the average marsh ground elevation (approximately 7.5 ft National Geodetic Vertical Datum of 1929 or NGVD29) and tested the feasibility of operating under low-stage conditions for low (750 cubic feet for second or cfs), normal (1,500 cfs) and high (2,000~2,500 cfs) flows to avoid any high shear stresses that flush the fine sediment and high nutrient materials from the marsh areas. Discharge close to the design flow

of S-333 (1,350 cfs) was considered as normal flow, while about half of it was taken as low-flow. The 750 cfs scenario was considered low in this study. Flows much lower than this is not expected to be a discharge of much sediment transport to the structures. S-333N design flow (1,150 cfs) combined with that of S-333 flow was assumed as high-flow condition. The low, normal, and high flows cover the existing and anticipated flow conditions including operation of the S-333N spillway. At about 7.5 ft NGVD29, the canal flow starts to meaningfully separate from the marsh flow. It is also a significant cutoff number in the regulation schedule of the WCA-3A. Water supply to the South Dade Conveyance System at S-333/S-333N for stages at 7.5 ft NGVD29 or lower must be made up by equivalent amount from upstream water bodies (such as, Lake Okeechobee). When headwater stages are lower than the marsh elevation, the predominant discharge is the canal only flow. Some limited flow from the marsh into the canals may possibly occur (mostly as groundwater). However, it is expected to be insignificant as far as sediment transport. To simplify model simulations, when water stages were lower than the marsh ground elevation, the CFD model setup considered in-canal flows only.

With upstream canal stages below 7.5 ft NGVD29 and downstream canal stage at about 6.5 ft NGVD29 (based on cyclic analysis of stages at S-333, see **Figures A-1** and **A-2** in **Appendix A**), the gate openings were calculated for different discharges based on the flow rating equation of each structure. The velocity field associated with each gate opening was analyzed to determine the potential for sediment resuspension and transport. The flow split between S-333 and S-333N was not necessarily even and depended on operating conditions.

Scenario 2: High-Water Scenario, Future Conditions

Canal-marsh interaction was considered in the high-stage scenario. The canals along with portions of the marsh were included in this scenario in Phase I. At higher stages, flows also tend to be higher. The intention of this scenario was to evaluate the hypothesis that high shear stresses occur in the marsh and whether problematic velocities exist under high-flows.

These simulations considered higher upstream water levels (9.5 ft and 10.5 ft NGVD29) and flow spilling from the marsh area into the canals. Based on the previous studies, this is a condition where high flow velocities could possibly occur (Zeng et al. 2018). The gates were regulated to pass total design flow of 2,500 cfs through the structures. The objective was to investigate the velocities in the canal, improve understanding of the flow velocities in the marsh, and evaluate the potential operational measures that can reduce these velocities.

Scenario 3: Structural Improvements

Scenario 3 evaluated the feasibility of implementing engineering measures to reduce flow velocities in the canals and marsh and avoid any undesirable sediment movement that can contribute to the elevated TP. Consequently, installing low-sill weirs and sediment traps across L-29 and S-67A upstream of the structures were considered. These scenarios are expected to reduce velocities in the canal. **Figure 3** shows a sketch indicating the probable sediment trap locations in the L-67A and L-29 canals. Including such engineering measures in the model attempted to provide flow field information to evaluate their benefit and efficiency in controlling sediment transport, as well as to support operational decisions. The engineering scenarios were examined for low-flow condition as well, to make sure the developed alternatives would work for low upstream stages (~7.5 ft NGVD29).

The most common operations occur at headwater stages between 7.5 ft NGVD29 and 9.5 ft NGVD29. The current operations determined by the Tamiami Trail flow formula typically has much reduced flows during dry conditions and flows of 2,500 cfs or even 1,500 cfs would likely not be delivered through the S-333 structure during the dry conditions (low-stages). Since operations of the S-333 complex is currently limited to 1,500 cfs (per FDEP permit and COP operations manual), flows up to 1,500 cfs can be described as the current condition scenarios, while flows up to 2,500 cfs was considered under potential future condition where operations may be changed under future operation plans to a maximum flow of 2,500 cfs once rest of the CEPP South system comes online (such as, with increased capacity at S-356E).

A scenario matrix for the CFD simulations is given in **Table 2**. Gate openings for the different scenarios were obtained from the flow rating equation of each structure (Rakib et al 2017, 2021). The flow split at S-333 and S-333N in **Table 2** are based on their design flow proportion. Please note that L-29 Canal in the results discussion section refers to the L-29 portion west of S-333. The L-29 section east of S-333 have been referred to as the S-333 downstream reach. For the CFD scenario modeling, it is assumed that the flow direction in L-67A is from north to south, while in L-29 is from west to east. Phase I focused on assessing velocities that induce sediment transport into S-333/S-333N and in the vicinity of these structures. As such, flow towards these structures in L-29 and L-67A were considered. There can be real-time occurrences when flow in L-29 moves from east to west. Modeling results of such field conditions are presented in Section 4.0.

Figure 3. Assumed sediment trap and low-sill weir upstream of S-333 and S-333N complex. Red line indicates the boundary of the sediment trap.

Table 2. Scenarios for simulations in Phase I.

Scenario	Headwater (ft NGVD29)	Tailwater (ft NGVD29)	Total Flow (cfs)	S-333 Flow (cfs) / Gate Opening (ft)	S-333N Flow (cfs) / Gate Opening (ft)	Potential Engineering Measures
1 (low-stage)	7.5	6.5	750	405 / 2.19	345 / 2.00	None
			1,500	810 / 4.21	690 / 3.74	
			2,000 [1]	1,080 / 5.53	920 / 4.91	
			2,500	1,350 / 6.83	1,150 / 6.07	
2 (high-stage)	9.5 [2]	9.0 [2]	2,500 [2]	1,350 / 9.12	1,150 / 8.11	None
	10.5 [3]	8.5 [3]	2,500 [3]	1,350 / 5.11	1,150 / 4.54	
3	7.5	6.5	750	405 / 2.19	345 / 2.00	Low-sill weir, sediment trap, and canal modifications
			1,500	810 / 4.21	690 / 3.74	
			2,500	1,350 / 6.83	1,150 / 6.07	
	9.5 [2]	9.0 [2]	2,500 [2]	1,350 / 9.12	1,150 / 8.11	
	10.5 [3]	8.5 [3]	2,500 [3]	1,350 / 5.11	1,150 / 4.54	

Notes: [1] likely future high-flow under low-stage, [2] indicates design stages and flow (likely future condition), [3] indicates high head differential for design flow (likely future extreme condition). Scenario 3 includes sub-scenarios due to the engineering measures that will be tested.

NGVD29 = North American Vertical Datum of 1988 (NAVD88) + 1.54 ft.

Model Results

The CFD modeling domain extends from the structures to about 1,850 ft and 2,000 ft into the L-67A and L-29 inflow canals, respectively, and 750 ft into the outflow L-29 Canal based on the survey data. **Figure 4** shows the bathymetric survey of the study area. On average, the canal bottom elevation is between -11 to -12.5 ft North American Vertical Datum of 1988 (NAVD88; -9.5 to -11 ft NGVD29) in L-67A, -12 to -14.5 ft NAVD88 (-10.5 to -13 ft NGVD29) in L-29 (west of S-333), and -6.5 to -8.5 ft NAVD88 (-5 to -7 ft NGVD29) in downstream L-29 (east of S-333). The average ground elevation in the marsh is 5.5~6 ft NAVD88 (7~7.5 ft NGVD29). The canal bed is relatively deeper just upstream of the spillway complex than at the upstream regions of L-67A and L-29 canals.
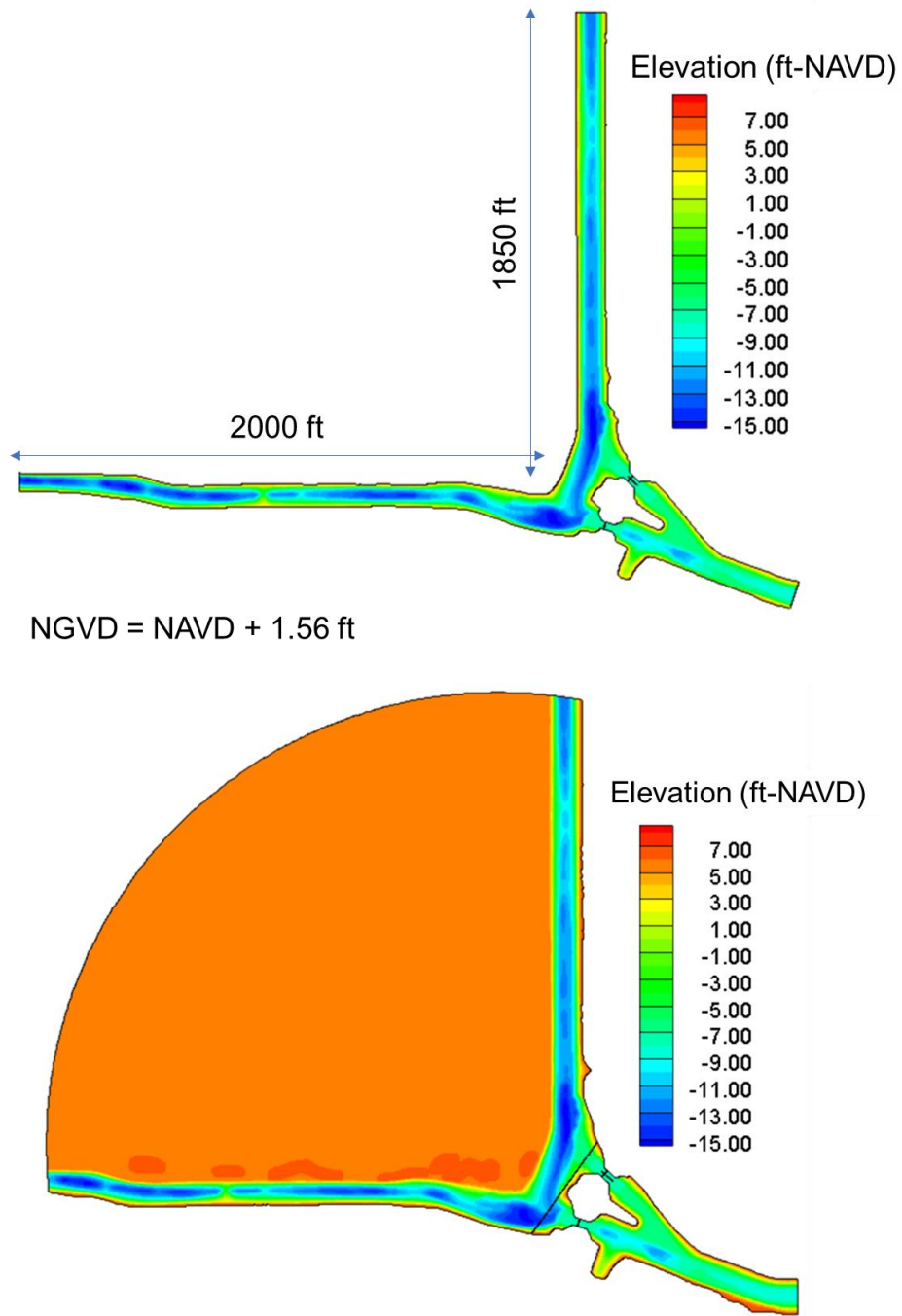
Figure 4. Bathymetry and topographic survey of the study area.

Low-Stage Scenario

The first set of CFD simulations concentrated on the low operation stage at S-333 and S-333N. These simulations considered in-canal flows only as water stage was lower than the marsh ground elevation. **Figure 5** shows the model results for headwater 7.5 ft NGVD29, tailwater 6.5 ft NGVD29 for a low-flow of 750 cfs (Note V_mag in the figure legend is the velocity magnitude in ft/s). Results indicated near bed velocities about 0.30 feet per second (ft/s) in L-67A and 0.25 ft/s in L-29 (west) away from the structures. Those velocities decreased to 0.05 to 0.10 ft/s just upstream of the structures due to deeper canal bed. At the downstream, near-bed velocities remained in the range of 0.25 to 0.35 ft/s in L-29 (east). Near the water surface level, velocities were about 0.35 ft/s and 0.25 ft/s in L-67A and L-29, respectively. Cross-sectional mean velocities were 0.34 ft/s and 0.25 ft/s in L-67A and L-29, respectively. The estimated Froude number of flows in the L-67A and L-29 canals were 0.013 and 0.022, respectively. Froude number (Fr) is the ratio of inertial and gravitational forces. It encompasses the effects of both flow depth and velocity and is used to characterize flow in open channels and closed conduits (Fr<1 subcritical flow, Fr= critical flow and Fr>1 supercritical flow). The approaching flow was distributed as expected without any large recirculating eddies. There are some flow nonuniformity across the channel, as is typical in a channel flow. Flow jets at the downstream merged uniformly and were evenly distributed in L-29. The 750 cfs scenario is a conservative case for low-flow conditions. Flows less than 750 cfs with same stages will generate lower velocity than above and is not expected to be of much sediment transport potential towards the structure.
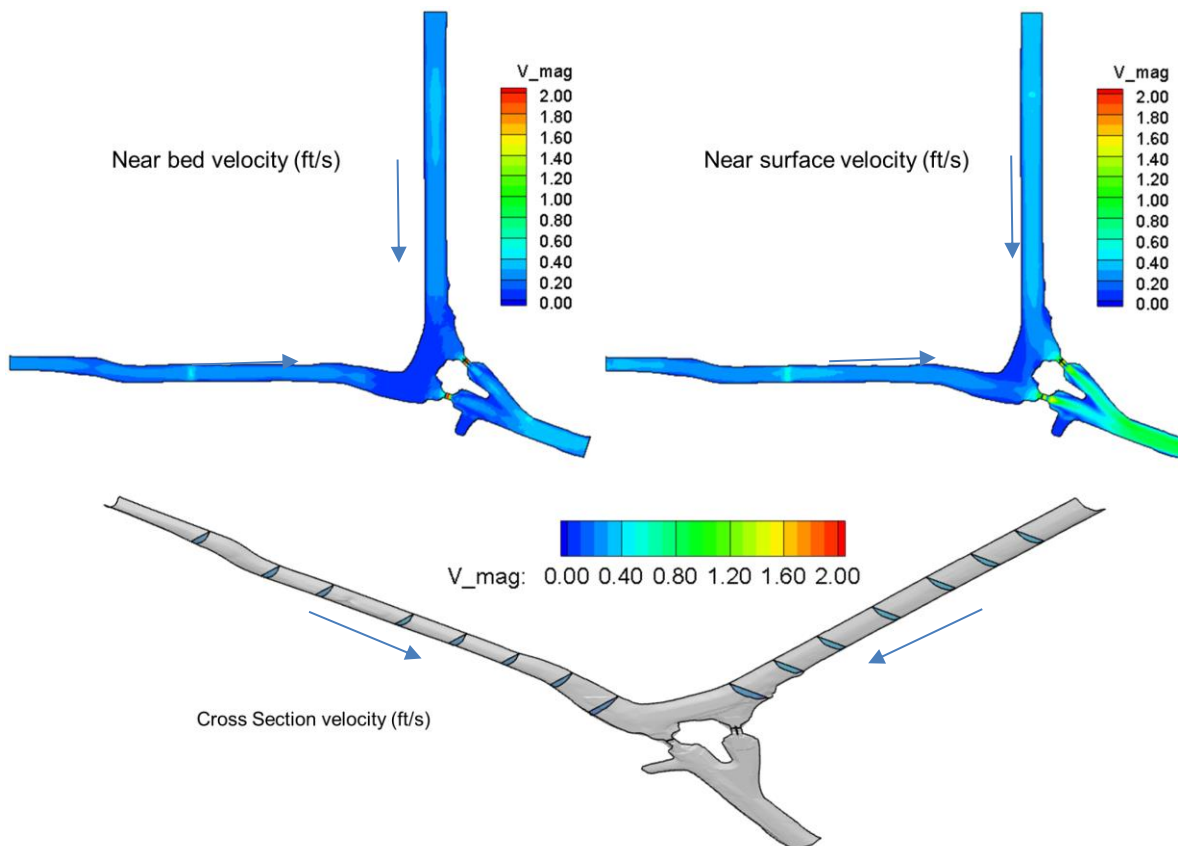
Figure 5. CFD simulation results for headwater 7.5 ft NGVD29, tailwater 6.5 ft NGVD29, and total flow 750 cfs.

The next simulation with headwater 7.5 ft NGVD29 and tailwater 6.5 ft NGVD29 at 1,500 cfs discharge represent normal flow condition. The model results are shown in **Figure 6**. As expected, with increasing flow, near bed and near surface velocities also increase. Away from the structures, the near bed velocities upstream in L-67A and L-29 (west) were 0.55 and 0.45 ft/s, respectively, which decreased to about 0.05 to 0.10 ft/s near the S-333/S-333N complex. Near bed velocities indicate velocity magnitudes at 10 to 15 cm from the canal bed. Near the water surface, velocities were about 0.65 and 0.50 ft/s in L-67A and L-29, respectively, while cross-sectional mean velocities were 0.63 and 0.48 ft/s in L-67A and L-29 (west of S-333). The Froude number of flows in the L-67A and L-29 canals were 0.026 and 0.045, respectively. The lower the flow velocity is, the lower will be the Fr. Potential of eddy formation appeared to be minimal based on the somewhat uniform approaching flow field.
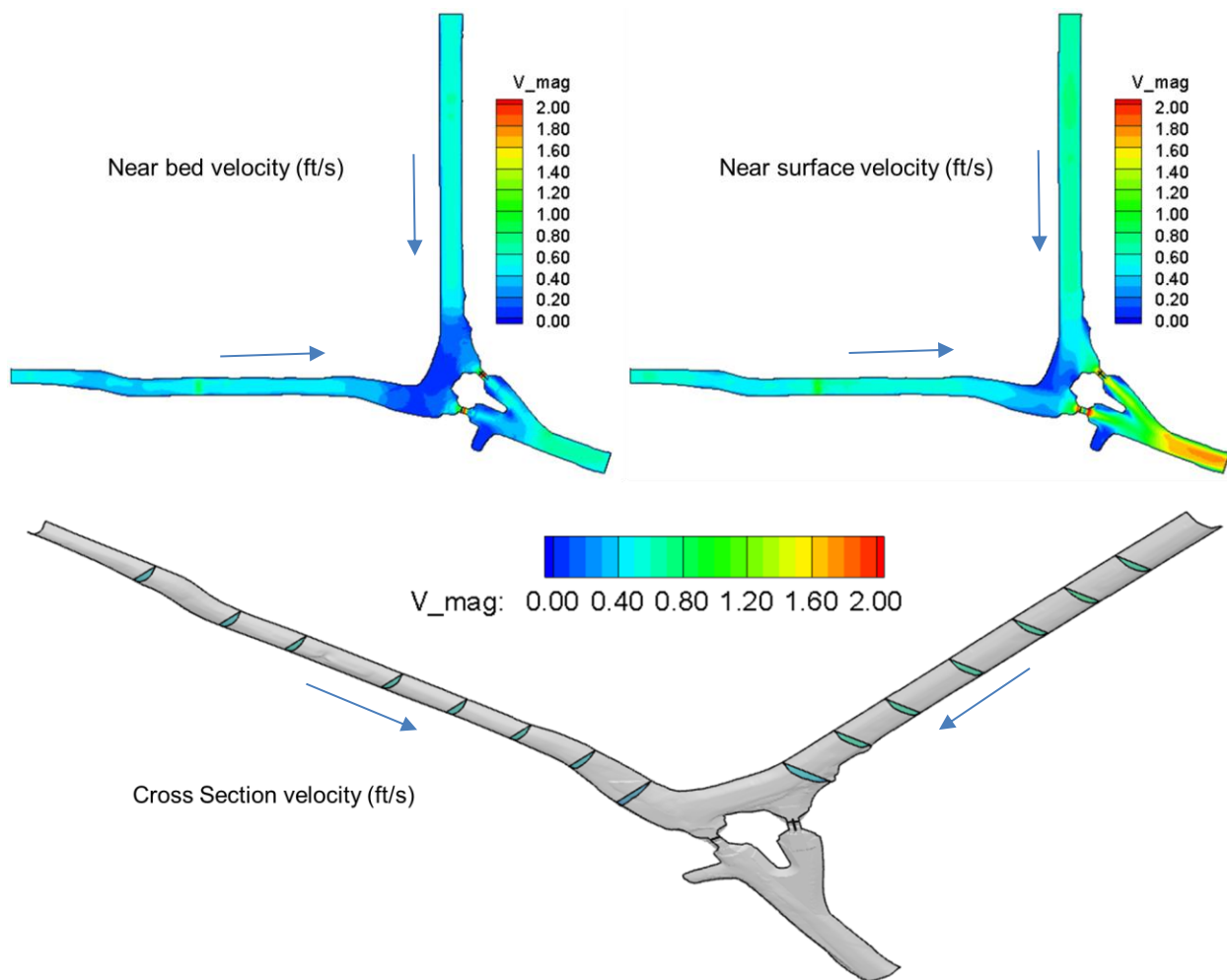
Figure 6. CFD simulation results for headwater 7.5 ft NGVD29, tailwater 6.5 ft NGVD29, and total flow 1,500 cfs.

Figure 7 shows the model results for headwater 7.5 ft NGVD29, tailwater 6.5 ft NGVD29 for a high flow of 2,000 cfs. The flow pattern is similar to previous scenarios but with larger near bed and surface level velocities. On average, near bed velocities in L-67A and L-29 (west) were 0.80 and 0.65 ft/s, respectively. They reduced to 0.10 to 0.15 ft/s just upstream of S-333 due to deeper canal bed resulting in larger cross-section area. Mean velocities were 0.92 and 0.77 ft/s in L-67A and L-29, respectively. The Froude number of flows in L-67A and L-29 canals were 0.035 and 0.060, respectively.
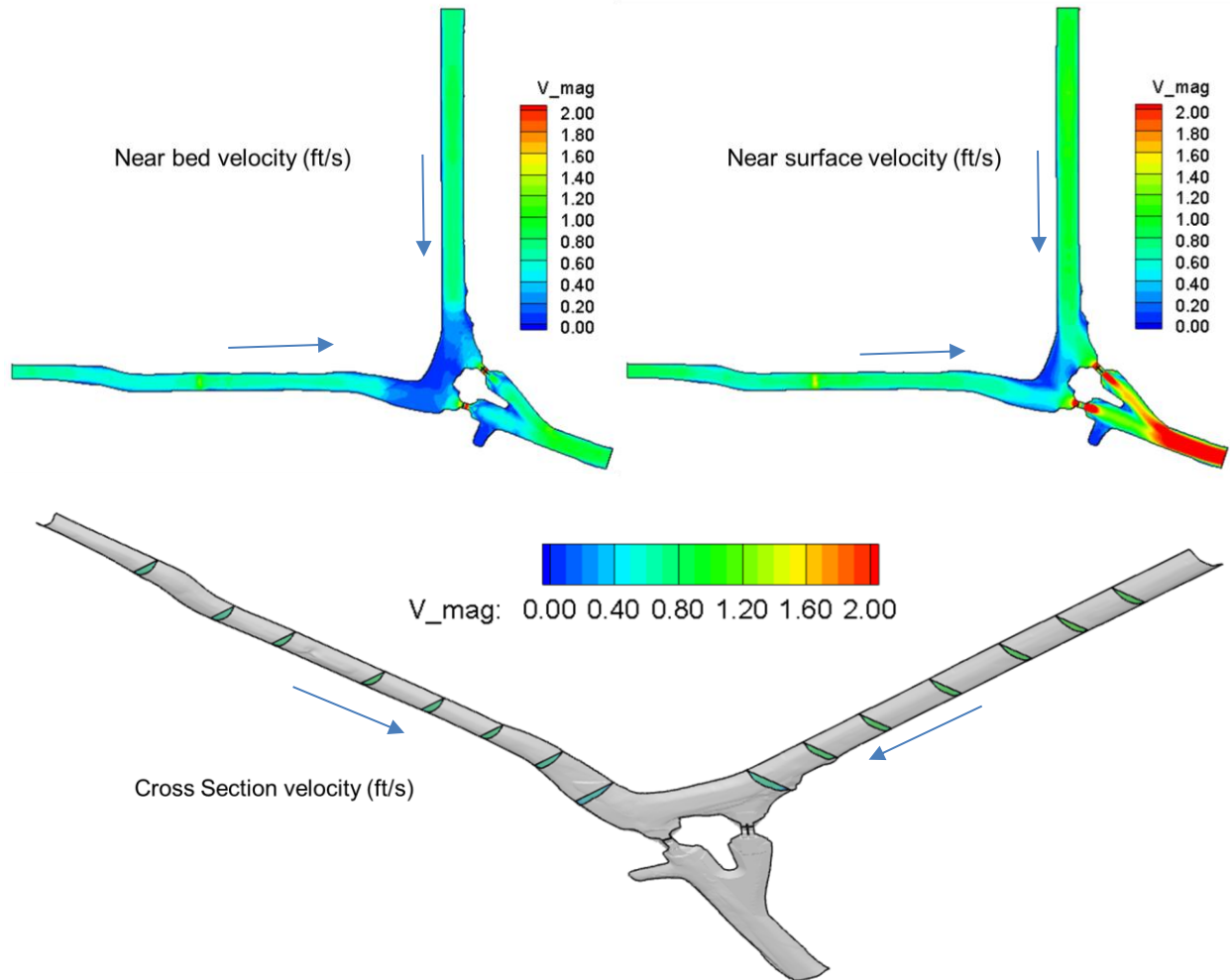
Figure 7. CFD simulation results for headwater 7.5 ft NGVD29, tailwater 6.5 ft NGVD29, and total flow 2,000 cfs.

Figure 8 shows the model results for headwater 7.5 ft NGVD29 and tailwater 6.5 ft NGVD29 at 2,500 cfs discharge, representative of high (design) flow condition. The average near bed velocities in L-67A and L-29 (west) were 0.95 and 0.75 ft/s, respectively. Near surface velocities were 1.15 and 0.95 ft/s in L-67A and L-29, respectively, while cross-sectional mean velocities were 1.12 and 0.93 ft/s in L-67A and L-29 (west) canals, respectively. Froude number of flows in L-67A and L-29 were approximately 0.043 and 0.075, respectively. For all scenarios, the S-12E culvert (just downstream of S-333) was considered closed and it did not have significant impact of the flow field. This zone acted as a dead zone with minimal flow circulation.

Figure 8. CFD simulation results for headwater 7.5 ft NGVD29, tailwater 6.5 ft NGVD29, and total flow 2,500 cfs.

High-Stage Scenario

The next set of CFD simulations considered high-flow high-stage operation at the S-333/S-333N complex. The purpose was to evaluate canal marsh interaction and whether erosive velocities occur in the marsh under these conditions. These simulations considered marsh-canal interaction. **Figure 9** displays CFD model results for the design condition of headwater 9.5 ft NGVD29 and tailwater 9.0 ft NGVD29 for a high-flow of 2,500 cfs. The near bed flow velocities in the marsh were about 0.10 to 0.15 ft/s, while near bed flow velocities in L-29 (west of S-333) and S-67A were 0.25 to 0.35 ft/s, respectively. Mean velocities were about 0.58 ft/s in L-67A and L-29 (west) canals.

Figure 10 shows the CFD model results for the design condition of headwater 10.5 ft NGVD29, tailwater 8.5 ft NGVD29 for a high-flow of 2,500 cfs. This scenario characterizes an extreme head differential situation, where high flow velocities could occur (Zeng et al. 2018). Results indicated average near bed velocities of 0.25 to 0.30 ft/s and 0.15 to 0.25 ft/s in L-67A and L-29, respectively. Near bed flow velocity in the marsh area was approximately 0.15 ft/s.
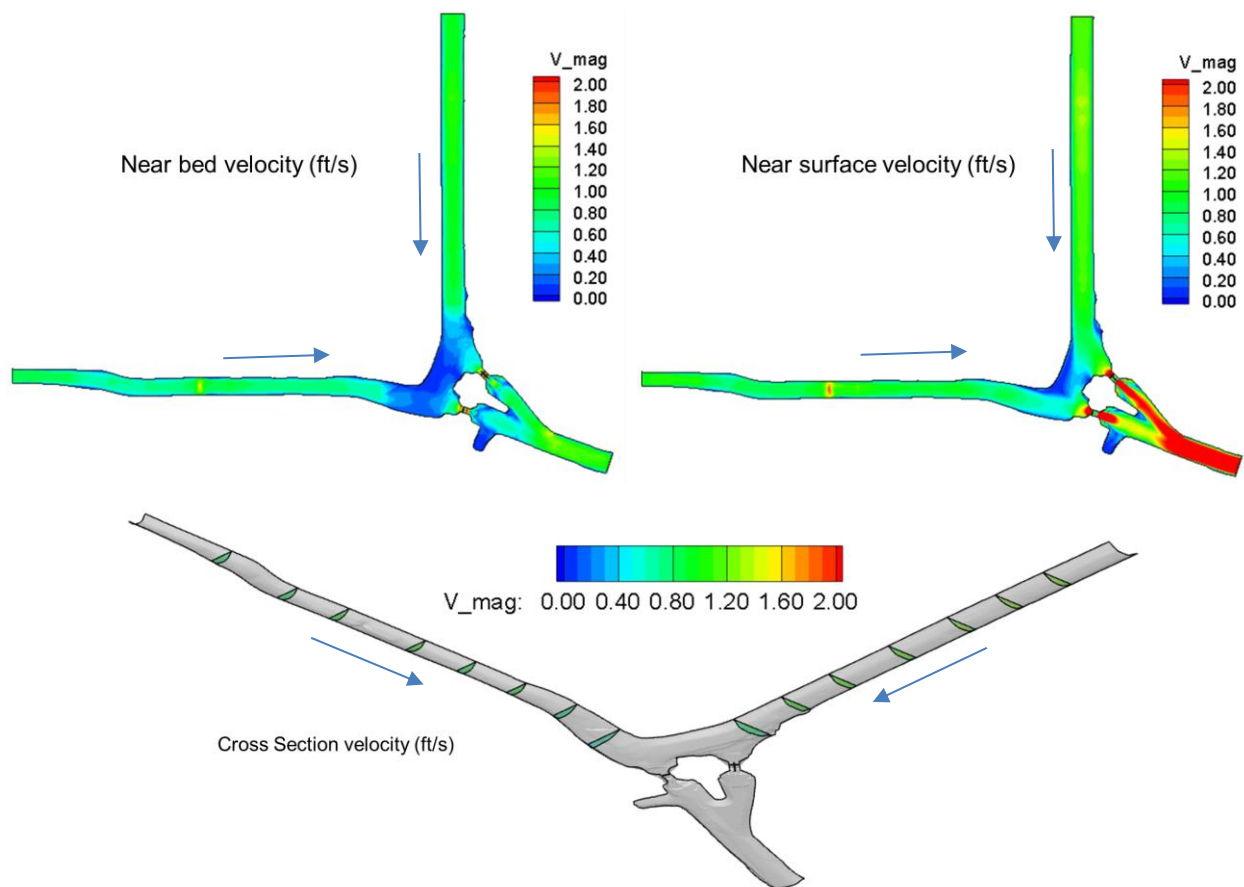

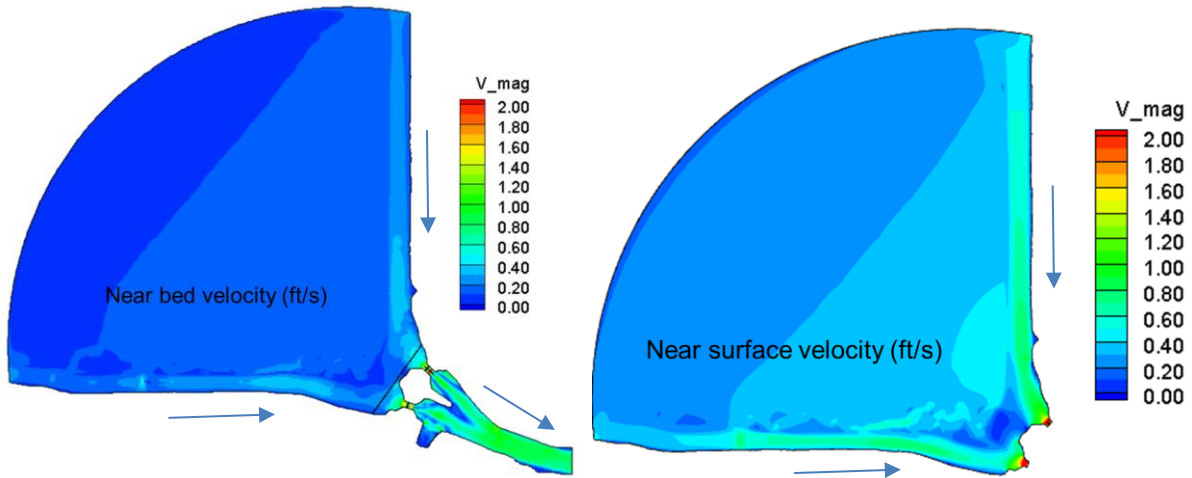**Figure 9.** CFD simulation results for headwater 9.5 ft NGVD29, tailwater 9.0 ft NGVD29, and total flow 2,500 cfs.

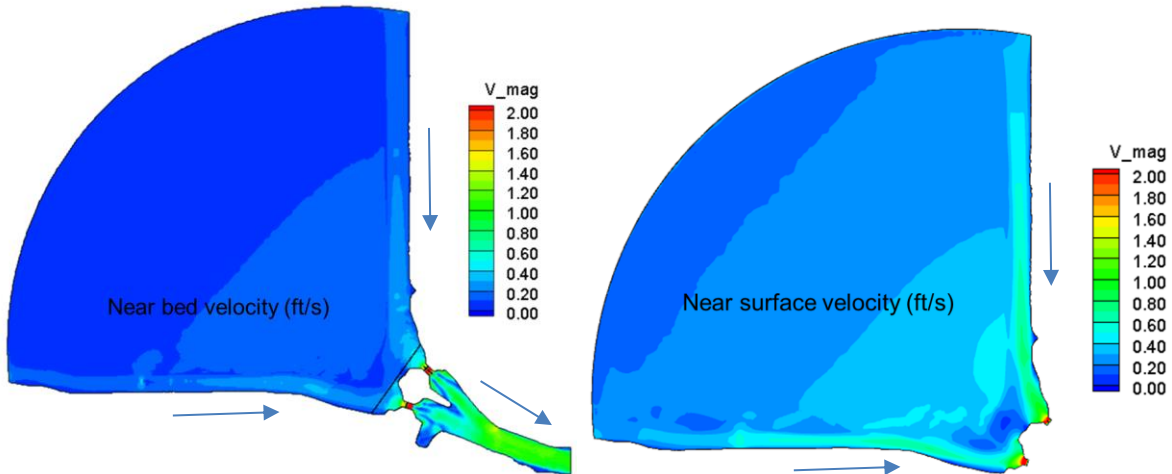**Figure 10.** CFD simulation results for headwater 10.5 ft NGVD29, tailwater 8.5 ft NGVD29, and total flow 2,500 cfs.

Results Discussion

Table 3 summarizes the flow velocities for low- and high-stage scenarios. These CFD model results were compared with existing literature on incipient motion of sandy sediment to infer the scouring potential at the S-333/S-333N complex.

Table 3. Simulations results for low- and high-stage scenarios.

Scenario	Headwater (ft NGVD29)	Tailwater (ft NGVD29)	Total Flow (cfs)	L-67A Canal Velocity (ft/s)			L-29 Canal Velocity (ft/s)		
				Near Bed	Mean	Near Surface	Near Bed	Mean	Near Surface
1 (Low Stage)	7.5	6.5	750	0.30	0.34	0.35	0.25	0.25	0.25
			1,500	0.55	0.63	0.65	0.45	0.48	0.50
			2,000	0.80	0.93	0.95	0.65	0.77	0.80
			2,500	0.95	1.12	1.15	0.75	0.93	0.95
2 (High Stage)	9.5	9.0	2,500	0.35	0.58	0.62	0.25	0.58	0.62
	10.5	8.5	2,500	0.30	0.57	0.60	0.20	0.56	0.62

Sediment transport is a complex phenomenon that depends on physical factors such as particle size, slope of sediment bed, grain shape, and packing density of sediment bed, as well as flow conditions such as flow depth and velocity. Mavis and Laushey (1948) developed the following equation for sediment at incipient motion:

$$V_b = K\sqrt{d_{mm}}$$

where, V_b is the bottom velocity, K is a constant (0.51 when V_b is in ft/s, 0.155 when V_b is in meters per second or m/s), and d_{mm} is the sediment size in millimeters (mm).

Another velocity approach to incipient motion by Hjulstrom (1935) has a detailed analysis of experimental data obtained from the movement of uniform particles (**Figure 11**). Hjulstrom's diagram is used to represent sediment entrainment or deposition based on flow velocities and sediment sizes. Hjulstrom's (1935) curves are based on average velocity and are most appropriate for flow depth of 1 meter or 3.28 ft. The position of the curves varies for different flow depths and different sediment characteristics. In another flume study, Stoeber (2005) obtained the critical incipient velocity of 0.88 ft/s (median sediment particle size, D_{50}) and 1.6 ft/s (maximum sediment particle size, D_{100}) for non-cohesive soil (for very fine sand) and 0.74 ft/s for cohesive soil (very fine silty clay).

Sediment samples were collected in the L-67A and L-29 canals and the surrounding marsh region by the NPS team during April through June 2022. The grain size analysis of the samples shed light on the nature and size of these sediment particles. The sediment D_{50} data are mapped in **Figure 12** (for overall Phase I flow domain) and **Figure 13** (zoomed in near the spillway complex). The larger and greener dots mean larger D_{50} values. Sites in the marsh have larger D_{50} values (0.20 to 0.45 mm) relative to the L-67A Canal near the marsh edge. Sediments in the canals also have smaller D_{50} (0.13 to 0.20 mm) relative to the marsh. The marsh edge within the S-333/S-333N complex has smaller D_{50}, which is consistent with where near bed velocities are less (deep blue

area in **Figures 5** through **8**) based on the hydrodynamic model results. The typical size of the sand particles in the canals is about 0.20 mm.
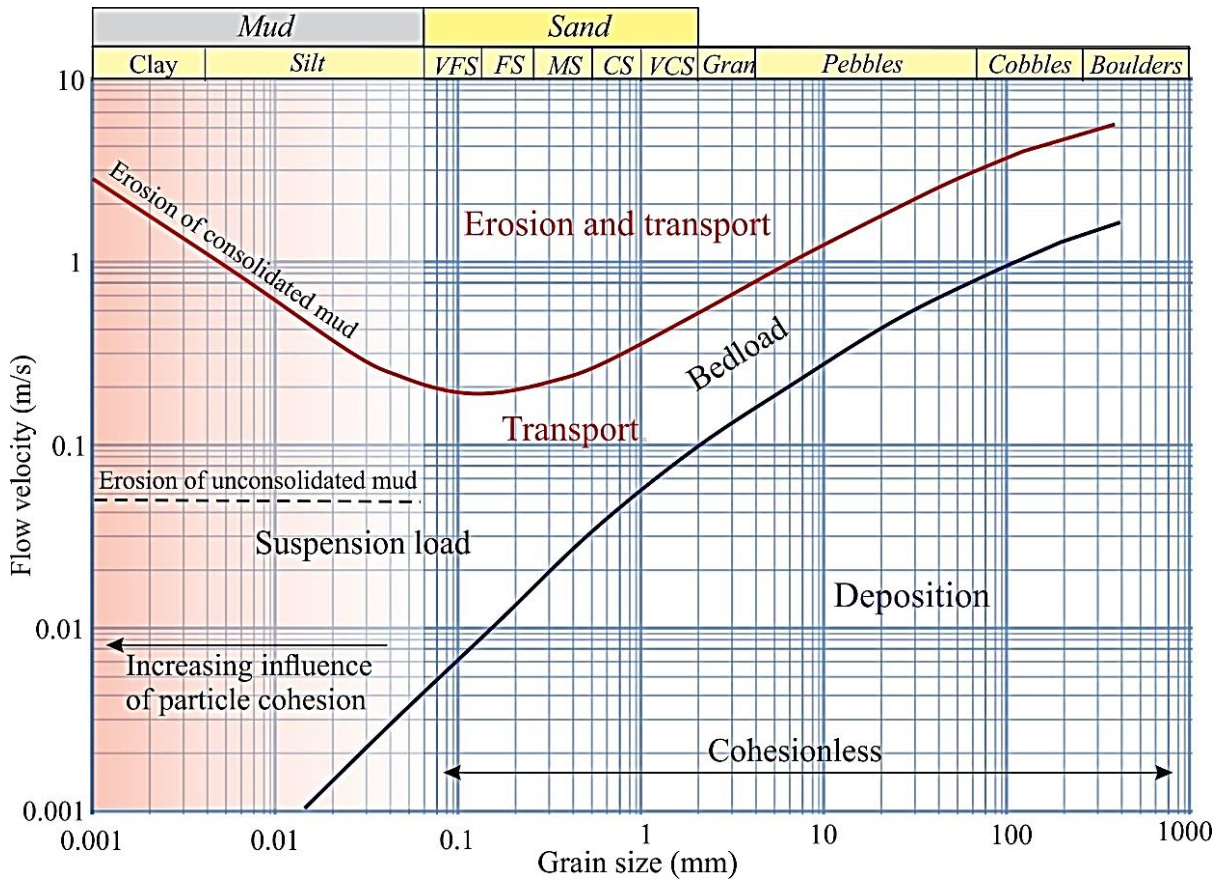
Figure 11. Hjulstrom's diagram with sediment entrainment or deposition based on flow velocities and sediment sizes. (Note: m s^{-1} – meters per second.)

Plugging the typical sand size in the canals (D_{50}=0.20 mm) in Mavis and Laushey's (1948) equation yields an incipient velocity of 0.23 ft/s, meaning a sediment having D_{50} about 0.20 mm will be in motion under a near bed velocity of 0.23 ft/s. The near bed velocities in the L-67A and L-29 canals (**Table 3**) for the high-stage high-flow condition (Scenario 2) are in the range 0.20 to 0.35 ft/s. There is less potential for sediment motion under these conditions. However, for the low-stage high-flow scenario (1,500 to 2,500 cfs), the near bed velocities are strong enough to transport the sandy sediment through the S-333/S-333N complex. These flow conditions are less likely to occur based on the typical operation of the S-333 and S-333N (**Figure A-3** in **Appendix A**). Nonetheless, modeling results indicate that high flows under low-stage would cause sediment movement and therefore, potential undesirable TP concentrations. Velocities under the low-stage and low-flow conditions does not appear to pose strong potential for sediment transport in the canals. In comparison, the sediment size in the marsh was larger (D_{50}=0.45 mm), which translates to an incipient velocity of 0.34 ft/s (Mavis and Laushey 1948). The near bed velocities in the marsh were less than this critical velocity for high-stage conditions, meaning there is less potential of sediment transport from the marsh into the canals during such hydraulic conditions.
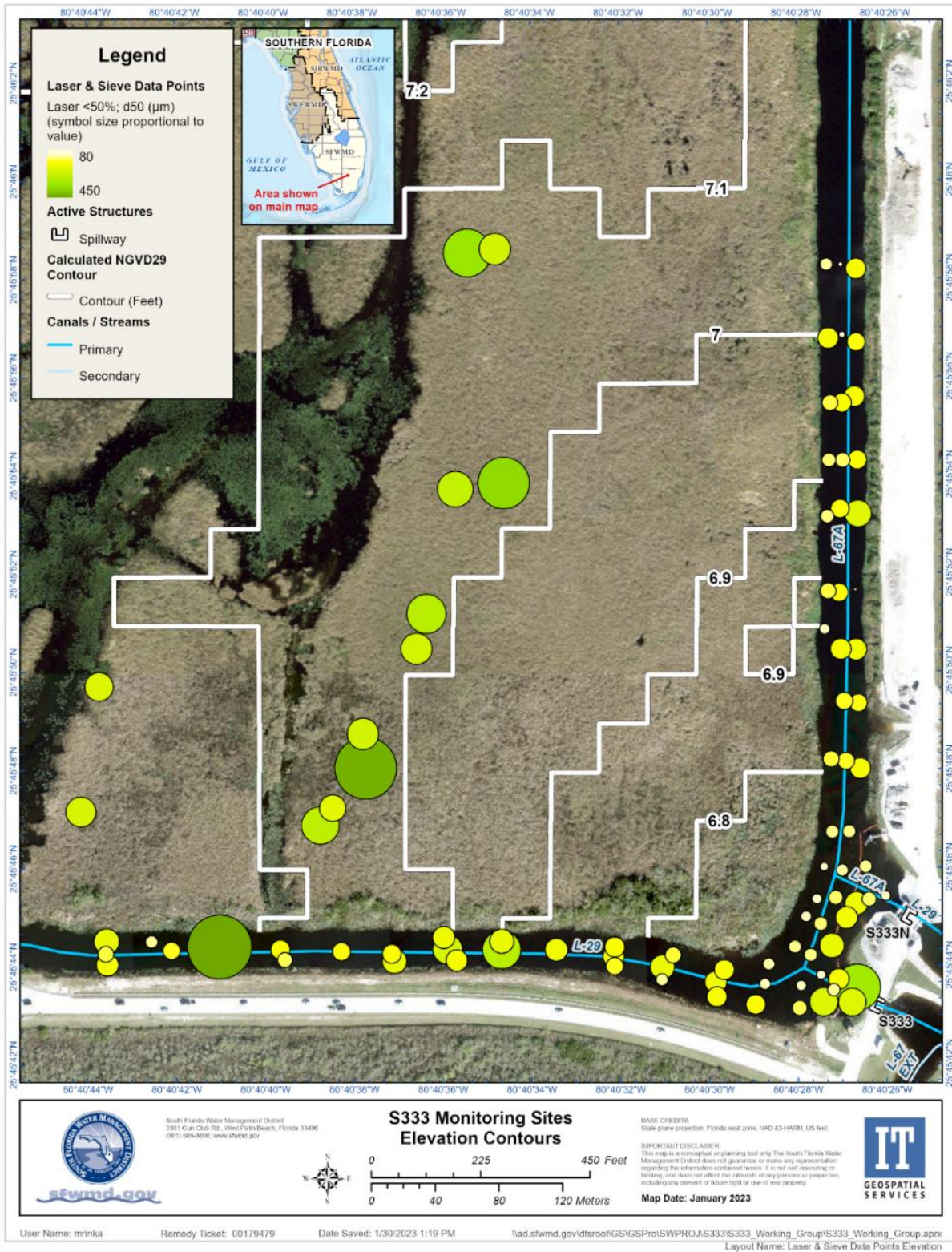
Figure 12. Sediment D_{50} size distribution in the model domain (Source: Data from NPS 2022). (Note: μm – micrometer)
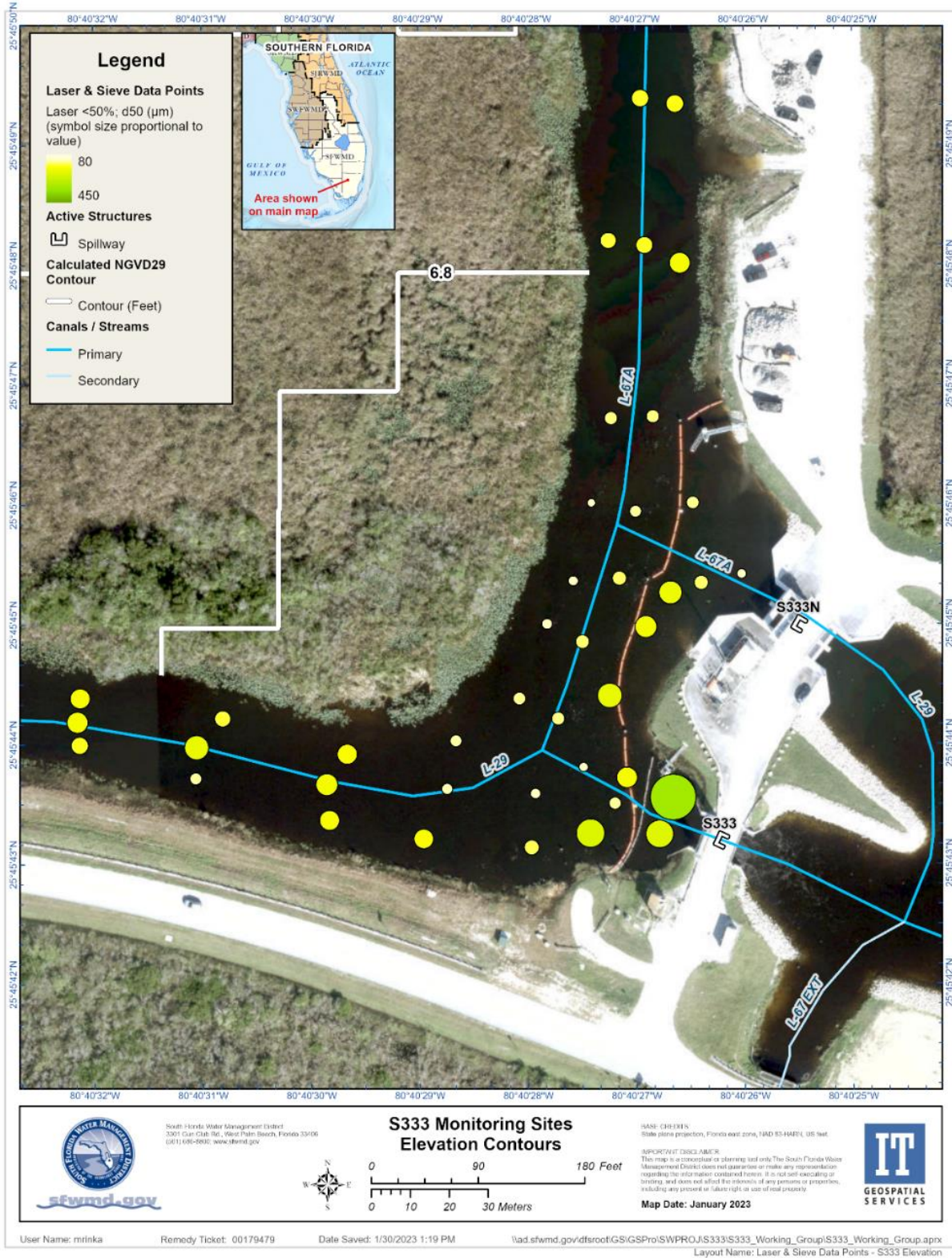
Figure 13. Sediment D$_{50}$ size distribution near S-333/S-333N (Source: Data from NPS 2022). (Note: µm – micrometer)

Hjulstrom's (1935) diagram indicates that sediments with D_{50} of 0.20 mm (average sediment size in study domain) may be transported as bedload under average velocity about 0.05 to 0.65 ft/s. The mean velocities in the L-67A and L-29 canals under low-stage low and medium flow conditions (750 to 1500 cfs) fall within this range. Similar is observed for the high-stage scenarios. Stoeber's (2005) experiments indicate a higher incipient motion limit for the non-cohesive fine sand. It is well understood that sediment transport is a complex hydraulic phenomenon that depends on physical and flow conditions. Hence, the criteria for sediment motion vary based on literature review. Conservatively speaking based on literature suggestion, the near bed velocities in canals should be limited to about 0.25 ft/s to avoid the adverse sediment transport concerns at S-333/S-333N (based on Mavis and Laushey 1948). This velocity may not be achievable under certain operations (see results in **Table 3**). Engineering scenarios (such as sediment trap and low-sill weirs) and operation strategies can be planned to limit sediment movement, so that they can be trapped upstream of the spillways and routinely removed from the canals.

4.0 CFD MODELING FOR FIELD CONDITIONS

The NPS team collected sediment and water samples in the study area during April through June 2022. The objective was to characterize the sediments in the marsh, canals and in water. The field conditions that existed on the sampling days are tabulated in **Table 4**. S-333 DBHYDRO (the SFWMD environmental database) flows, gate openings, and headwater and tailwater stages given in the table show average for the duration of the acoustic Doppler current profiler (ADCP) measurement taken in front of S-333. The ADCP measurements at S-333 gate, and at L-67A and L-29 about 1500 ft upstream from the structures were not taken simultaneously but in a sequential order. S-333N was closed during these data collection events.

The field flow conditions were simulated using CFD to obtain detailed hydraulics that can be linked with the respective sediment data to evaluate the potential of sediment transport. The boundary conditions at L-67A and L-29 were set using inlet discharge at the upstream, while the downstream boundary condition was set as non-gradient outflow boundary.

For the purpose of discussion, the sampling days during April and May 2022 were grouped as one category, as the flow in L-67A canal ranged between 260 and 410 cfs, while 210 to 367 cfs was discharged through S-333. There was minimal eastward flow in the L-29 Canal. For the sampling days in June 2022, flows in L-67A Canal were as high as 1,614 cfs, and there was westward flow in L-29 Canal. **Figures 14** through **19** illustrate the CFD model results for sampling date April 14, June 16, and June 27, 2022, respectively (Q in the figures in flow). The east and west in the cross-sections refer to right and left banks looking downstream of the canal. The 27-June 2022 event is an interesting scenario where there was more than 1,600 cfs flowing south along the L-67A Canal, of which 670 cfs was discharged through S-333 and the remaining 825 cfs was flowing westward. Local turbulence and erosive velocities were observed in L-67A, particularly when high flows exist. These velocities exceed the velocity range from Hjulstrom's (1935) chart under which the sediment would be transported as bedload. The engineering measures need to be designed to slow down these high erosive near bed velocities so that the sediments are not resuspended and flushed downstream but allow for deposition and/or bedload transport. This will provide the opportunity to trap the TP-containing sediments and remove them from the system.

Table 4. NPS field sampling conditions.

Date	Flow from DBHYDRO (cfs)	Gate Opening (ft)	Headwater Stage (ft NGVD29)	Tailwater Stage (ft NGVD29)	Flow from NPS ADCP Measurement (cfs)			Remarks for L-29 Flow	Flow S-12D from DBHYDRO (cfs)	Flow S-12C from DBHYDRO (cfs)
	S-333				S-333	L-67A (1,500 ft)	L-29 (1,500 ft)			
April 14, 2022	283.09	8.20	7.55	7.52	366.74	389.10	30.24	flowing east	18.5	0
April 25, 2022	194.59	8.20	7.28	7.26	209.92	259.59	16.60	flowing east	10.3	0
May 5, 2022	233.63	8.18	7.27	7.25	228.08	229.84	97.02	flowing east	7	0.37
May 26, 2022	327.72	2.40	7.63	7.02	307.13	410.32	1.44	flowing east	0	0
June 7, 2022	488.36	3.21	8.53	7.77	454.31	577.84	-142.58	flowing west	363	0
June 16, 2022	614.90	3.80	8.86	8.01	562.11	830.45	-260.62	flowing west	0	0
June 27, 2022	719.64	5.00	8.95	8.27	670.85	1613.95	-823.91	flowing west	558	315

Notes:

1. S-333 DBHYDRO flows, gate openings, and headwater and tail water stages in the table above are average for the duration of ADCP measurement taken in front of S-333.

2. ADCP measurements at the S-333 gate and L-67A and L-29 canals at about 1,500 ft upstream were not taken simultaneously but in a sequential order.

3. Information on S-12D and S-12C is provided for existing flow conditions on the day in the L-29 Canal.

Figure 14. Part 1: CFD model results for sediment sampling on April 14, 2022.
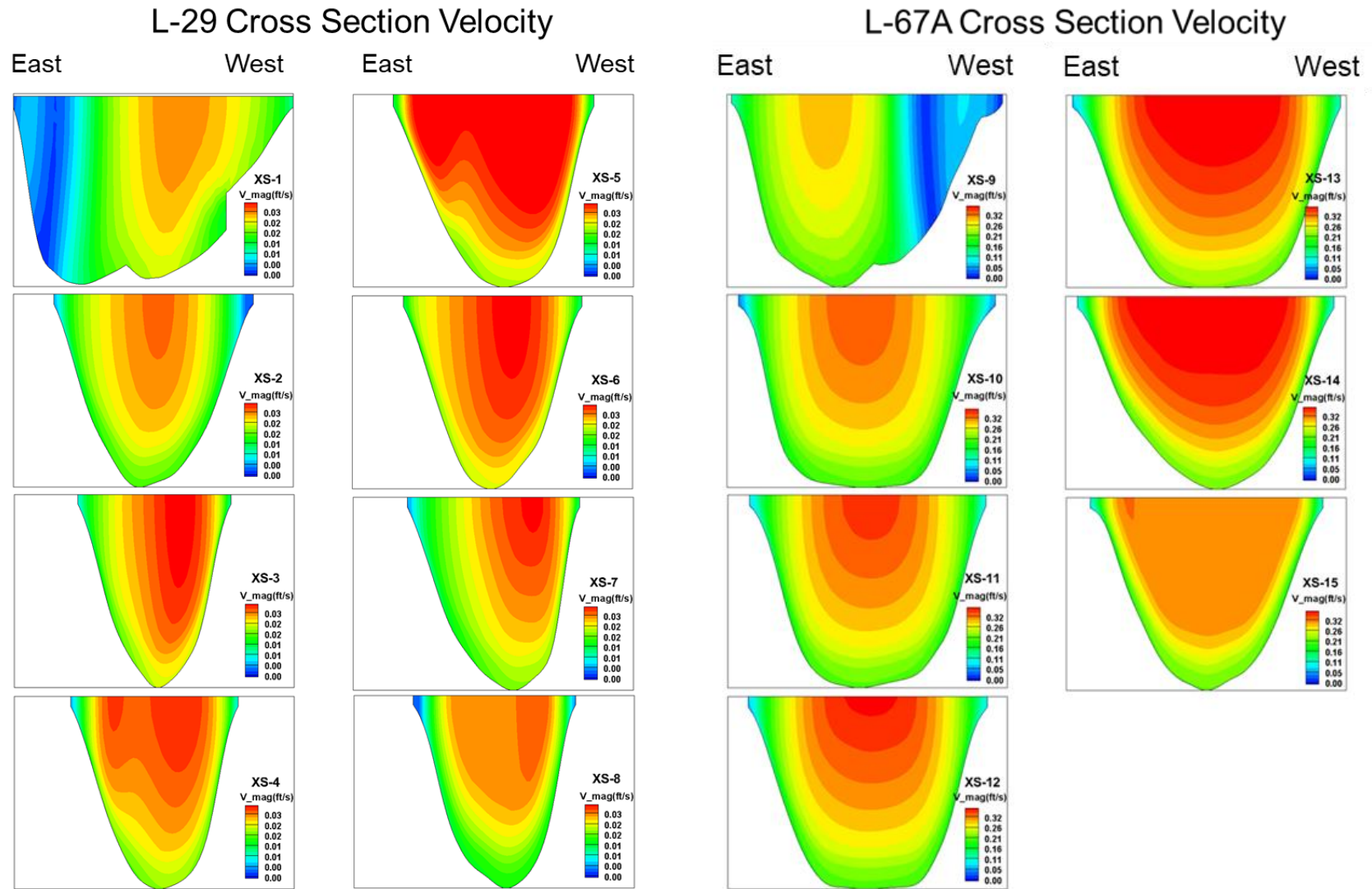
Figure 15. Part 2: CFD model results for sediment sampling on April 14, 2022.
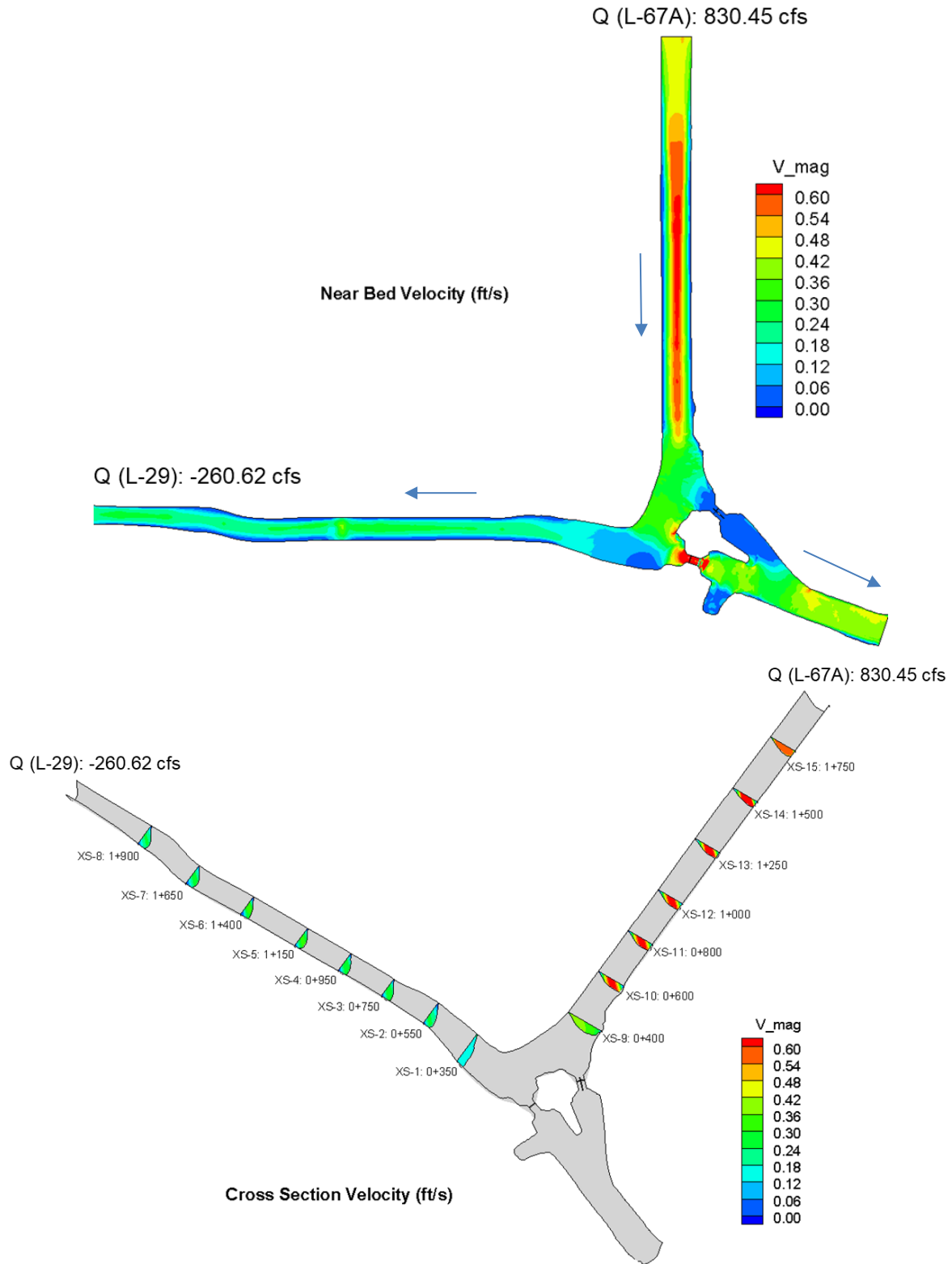
Figure 16. Part 1: CFD model results for sediment sampling on June 16, 2022.
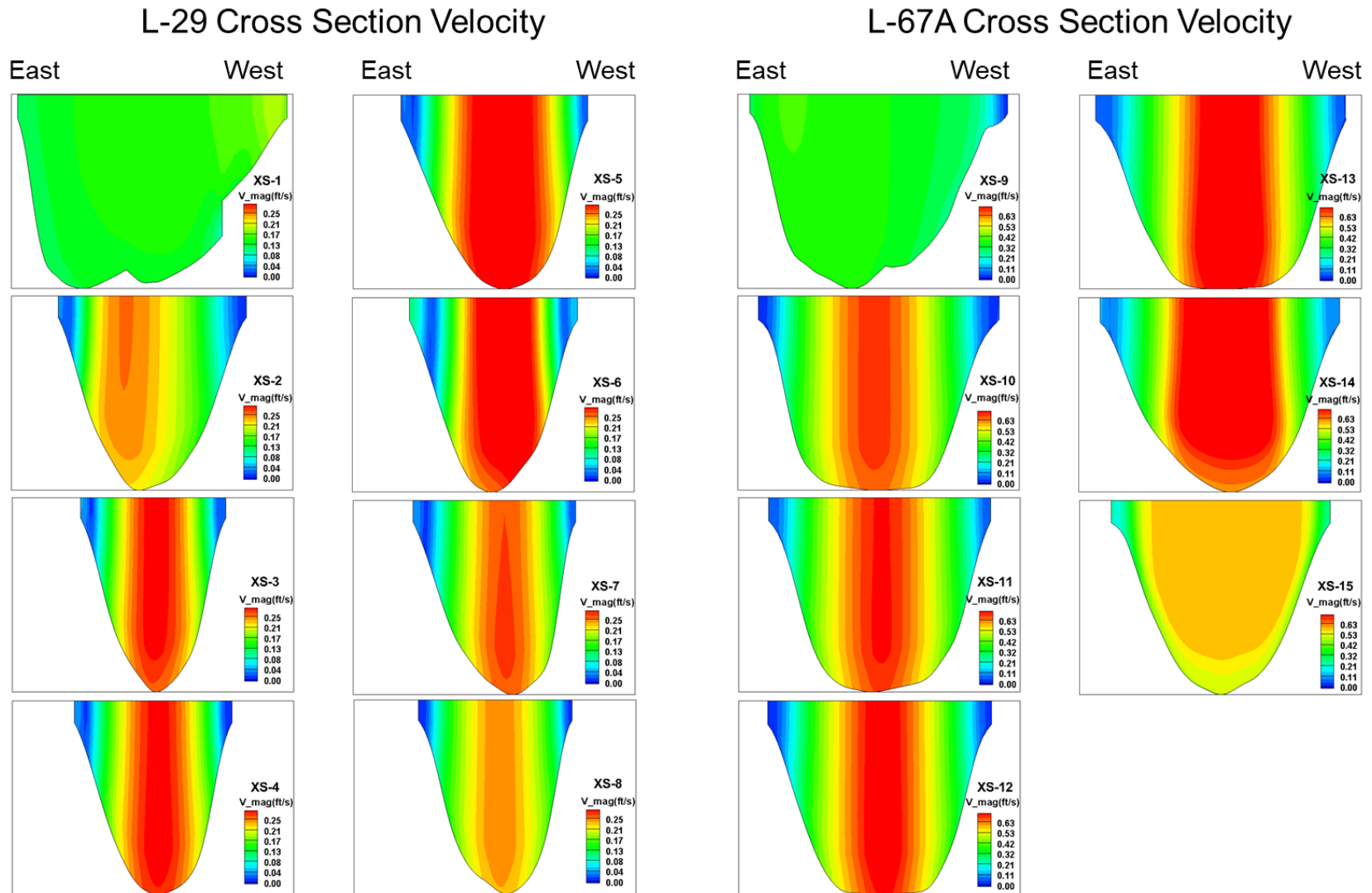
Figure 17. Part 2: CFD model results for sediment sampling on June 16, 2022.

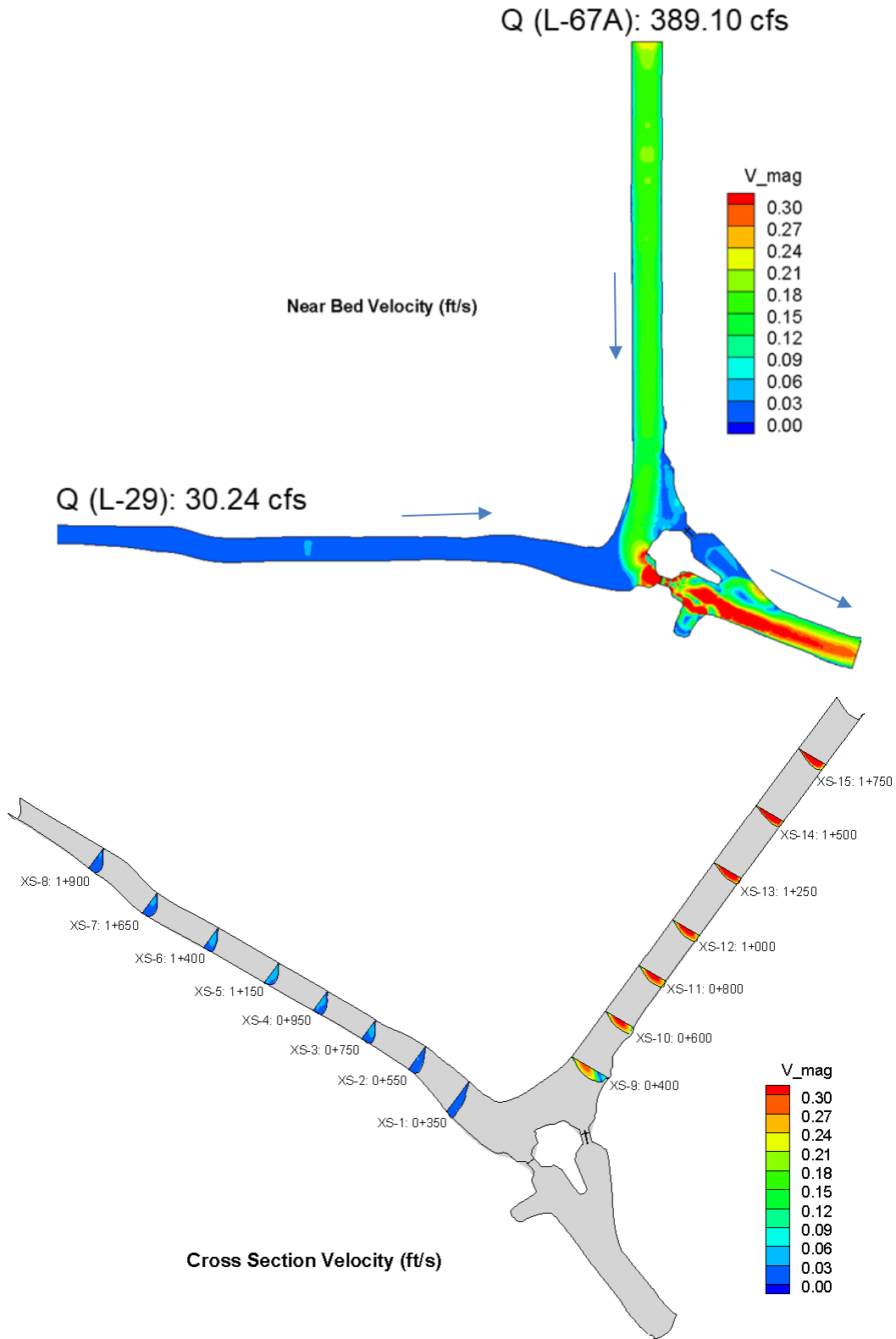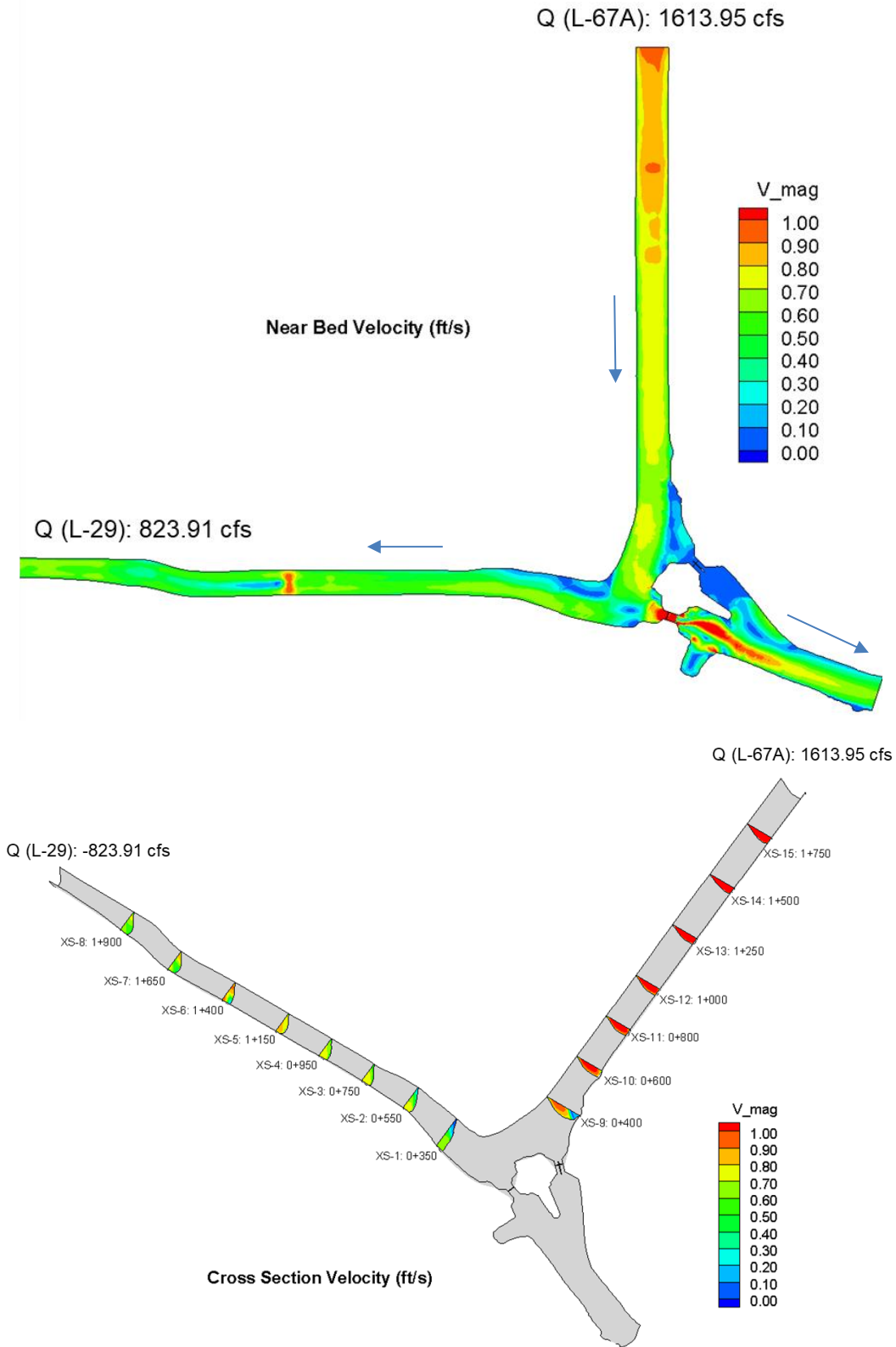**Figure 18.** Part 1: CFD model results for sediment sampling on June 27, 2022.
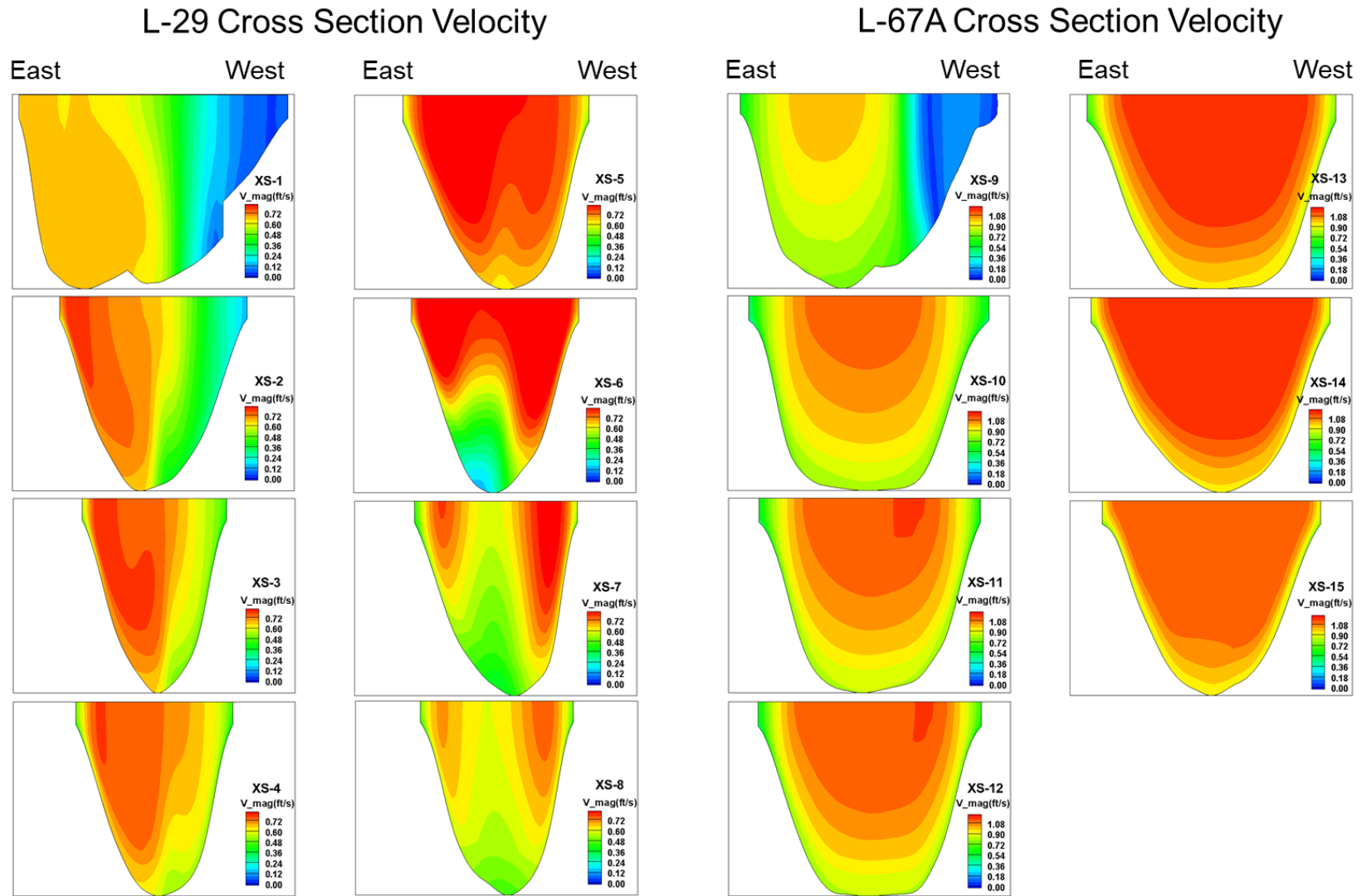
Figure 19. Part 2: CFD model results for sediment sampling on June 27, 2022.

Note: The W-shaped velocities in the middle of L-29 is due to a bump in the canal bottom that caused local disturbance.

5.0 HEC-RAS MODEL STUDY FOR PHASE I

Modeling Objective

The Hydrologic Engineering Center River Analysis System (HEC-RAS) modeling was used in conjunction with 3D CFD modeling for initial testing of engineering measures focused on slowing down flow velocities in L-29 and L-67A canals and surrounding marsh and consequently reduce the potential of sediment transport through the S-333/S-333N complex. HEC-RAS results are depth averaged and are only intended for primary proof of concepts before establishing additional CFD models. It was done as a reality check on CFD results and not rigorously developed for conceptual design purposes.

Model Development

HEC-RAS, Version 6.1 (September 2021) was used for analysis and mapping. The two-dimensional (2-D), unsteady flow module was used for the routing of flows through the model domain. The same bathymetric survey data used in the CFD model was applied to the HEC-RAS. Land surface elevations were extracted from existing DTM data for this area. The spatial location of the channel and marsh was georeferenced according to its proper location. Geometric features in the model were added utilizing the HEC-RAS Mapper feature or directly within the geometric data editor. A 2D flow area polygon was added to represent the boundary of the 2D area using the geometry editing tools in HEC-RAS Mapper. A computational mesh was created within the 2D flow area. The 2D mesh contained about 409,000 cells with average cell size of 13 sq. ft.

Figures 20 and **21** show the topography and simulation domain in the 2D HEC-RAS model. The manning's coefficients were defined based on the vegetation distribution in the model domain by adding spatially varying land use classification versus Manning's n value layer in RAS-Mapper (**Figure 22**). Canal and marsh flow resistance values were based on the vegetation resistance coefficients referred from literature and calibrated Environmental Fluid Dynamics Code (EFDC) model for Blue Shanty Flow Way project.

The upstream boundary line was set at the L-29 and L-67A canals and surrounding marsh about 2,000 ft upstream from the S-333/S333N complex, while the downstream boundary was located at 650 ft downstream of the complex. The upstream and downstream boundaries for each scenario were defined by stages identified in **Table 2**. Flows through S-333 and S-333N were set by flow hydrographs. In essence, this simulates a steady-flow system but using the unsteady flow computational engine.
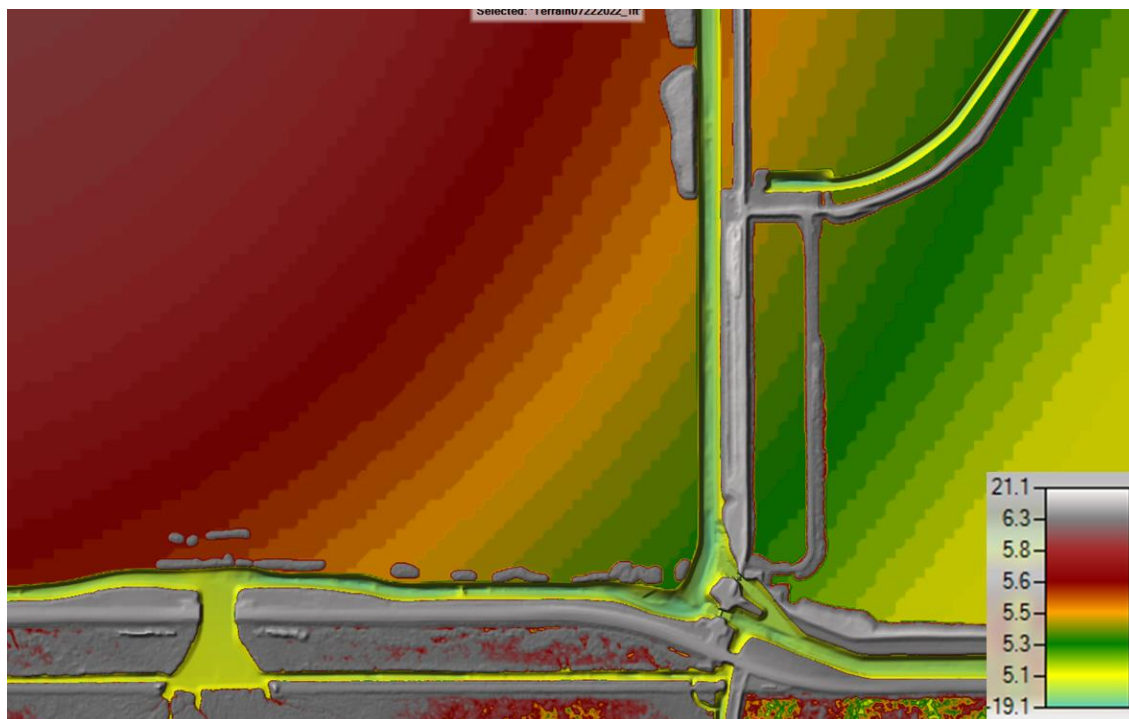
Figure 20. Topography of the 2D HEC-RAS model (elevation in ft NAVD88).
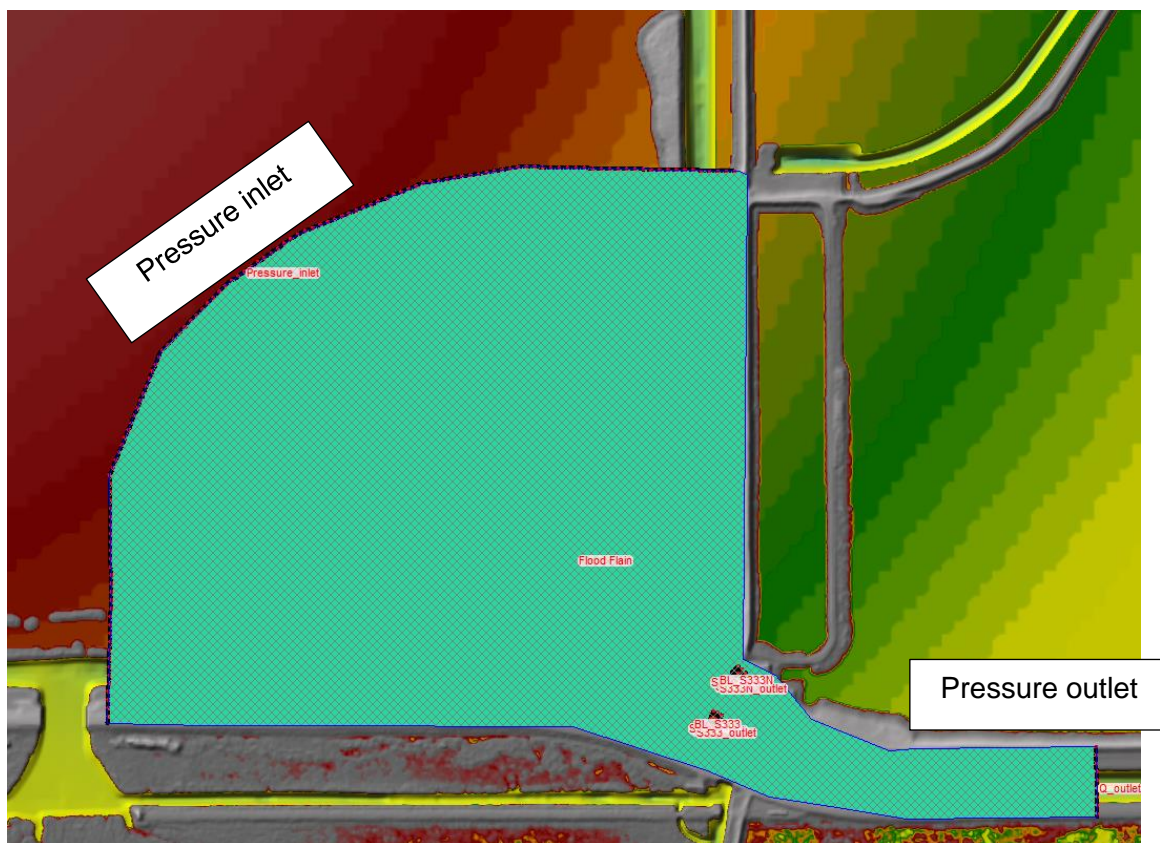
Figure 21. Model domain of the 2D HEC-RAS model.

ID	Name	/	ManningsN
1	Developed Land		0.07
2	Dry Prairie		0.1
3	Emergent Marsh		0.085
4	Mixed Shrubs		0.1
0	NoData		0.035
5	Open Water		0.035
6	Wet Prairie		0.2

Figure 22. Manning's roughness coefficients based on vegetation distribution.

Model Results

The same scenarios identified for Phase I (see **Table 2**) were simulated using HEC-RAS, that served as the baseline scenarios. The velocity fields for low-stage (Scenario 1) and high-stage (Scenario 2) conditions are shown in **Figures 23** and **24**, respectively.

2D HEC-RAS model results (depth averaged velocity) compared well with the CFD results (mean velocity). Overall, similar flow field patterns were observed in both models. Since, HEC-RAS model runs can be accomplished is less time compared to CFD simulations, they were used for initial testing of concepts for engineering measures. Engineering scenarios were identified by the SFWMD staff to be modeled that included adding vegetation buffer in the marsh adjacent to the L-67A and L-29 canals for reducing marsh velocities, creating sediment traps just upstream of S-333/S-333N to reduce in-canal velocities and allow accumulation of bedload sediments, and installing low-sill weirs before S-333/S-333N to reduce potential for resuspended sediments from flushing to the downstream.
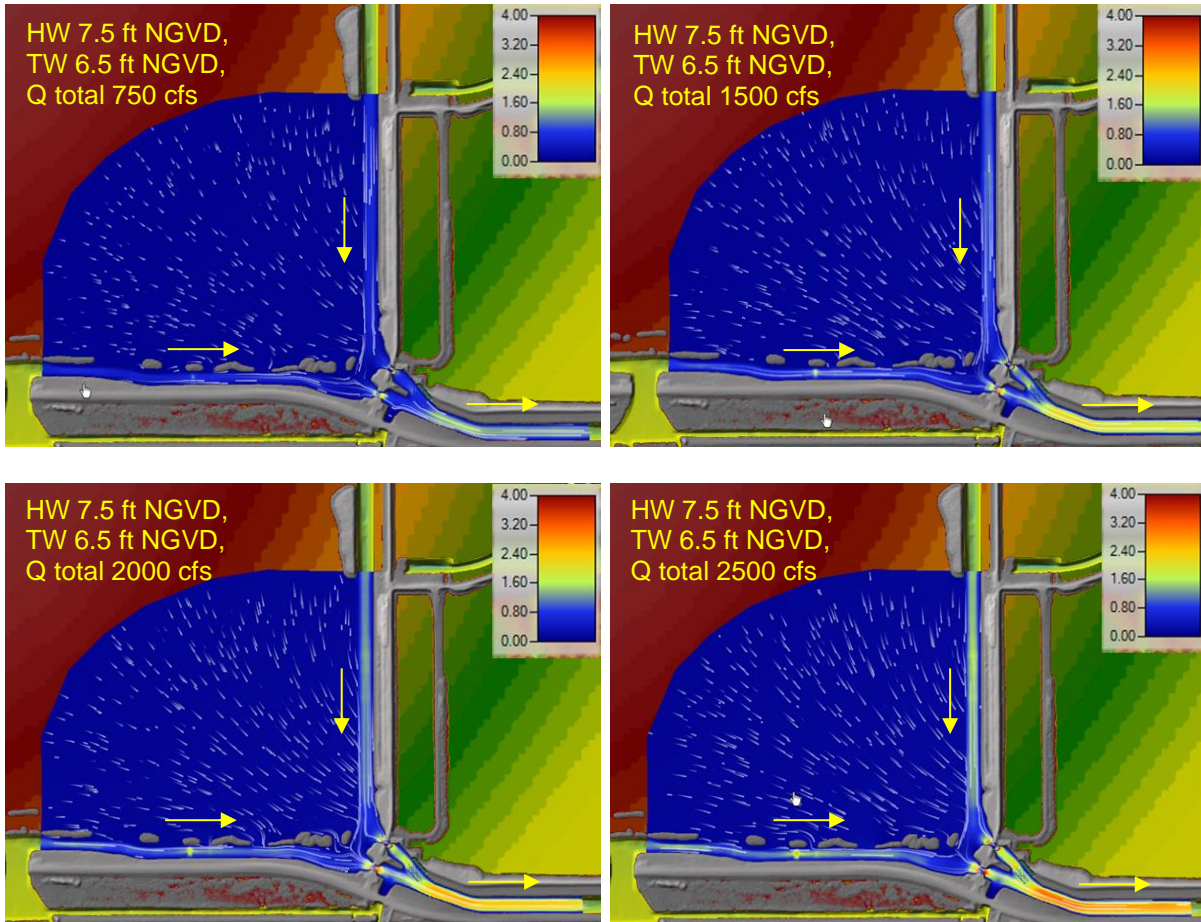
Figure 23. HEC-RAS results for low stage scenarios.
(Note: velocity field in ft/s, HW – headwater, Q – flow, and TW – tailwater.)
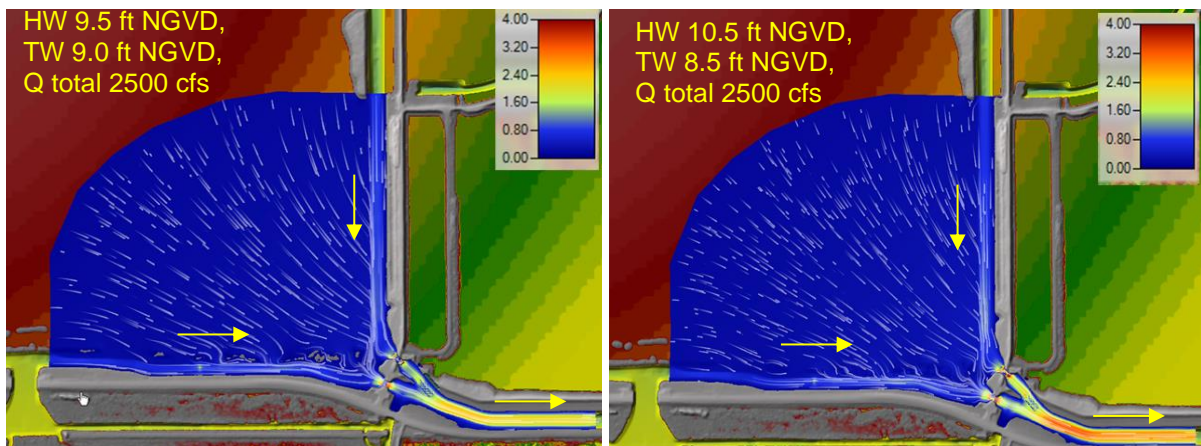
Figure 24. HEC-RAS results for high stage scenarios.
(Note: velocity field in ft/s, HW – headwater, Q – flow, and TW – tailwater.)

Two vegetation densities defined by artificial manning's roughness region were simulated for the vegetation buffer, indicated as vegetation 1 (low density, manning's n=0.6) and vegetation 2 (high density, n=1.2) in **Figures 25** and **26**. Deliberately high n-values were used to block marsh flow into the canals as a test of the concept. Results show the vegetation buffer can reduce flow velocities significantly in the marsh. It increased the velocity in the canals as the marsh becomes disconnected from canals due to the vegetation buffer and flows defined in the model boundary setup primarily moves through the canals. Lower marsh velocity implies less potential for sediment transport from marsh. There are some sediments mounds along the north bank of the L-29 Canal and the west bank of the L-67A Canal that can locally affect flow from the marsh into the canals. Sediment mounds on the west bank of the L-67A Canal were outside the modeling domain for Phase I.

To represent the low-sill weirs in HEC-RAS, canal bed elevation was raised at the sill location, modeled as a broad crested weir. They were placed across the canal (about 90 ft wide, thickness 6 ft, slope: 1:2.5, top elevation -7.5 ft NAVD88) at 500 ft upstream from the structures. The low-sill weirs were found to reduce the canal velocities slightly (**Figure 27**). Although this does not offer a significant improvement to the flow field, it can help trap sediments. Based on 3D CFD and 2D HEC-RAS results, relatively higher velocities were observed at the upstream regions of the canal. As there appears to be more potential for sediment transport from these portions, low-sill weirs can trap the resuspended sediments preventing it from being flushed to the downstream and thereby reducing the probability of elevated TP occurrences. The trapped sediments can routinely be removed from the canals. The low-sill weirs in canals coupled with a vegetation buffer around marsh can be more effective in reducing both marsh and canal velocities. Those results are illustrated in **Figure 28**.

The performance of sediment traps in the L-29 and L-67 Canals upstream of S-333 and S-333N were evaluated next. For conceptual testing, the canal bottom elevation was deepened to about -20 ft NAVD88 (-18.5 ft NGVD29) while maintaining the existing canal side slopes to create the sediment trap. The traps were extended to about 600 ft from the structures. A second sediment trap with larger excavation (cutting partly into the canals) was tested. The traps are shown in **Figure 29**.

HEC-RAS results show the sediment traps can significantly reduce flow velocities in the canals upstream of the spillways, which will allow for sediment deposition (**Figures 30** and **31**), for sediment of sizes greater than D_{50}. A larger sediment trap appears to be more effective by reducing the average velocities by as much as 65 to 70%. There can be environmental limitations on cutting partly into the canals. The extent and dimensions of the sediment traps can be optimized using CFD modeling in the next phase. Supplementary low-sill weirs just upstream of the spillways could prevent bedload movement from flushing to the downstream.
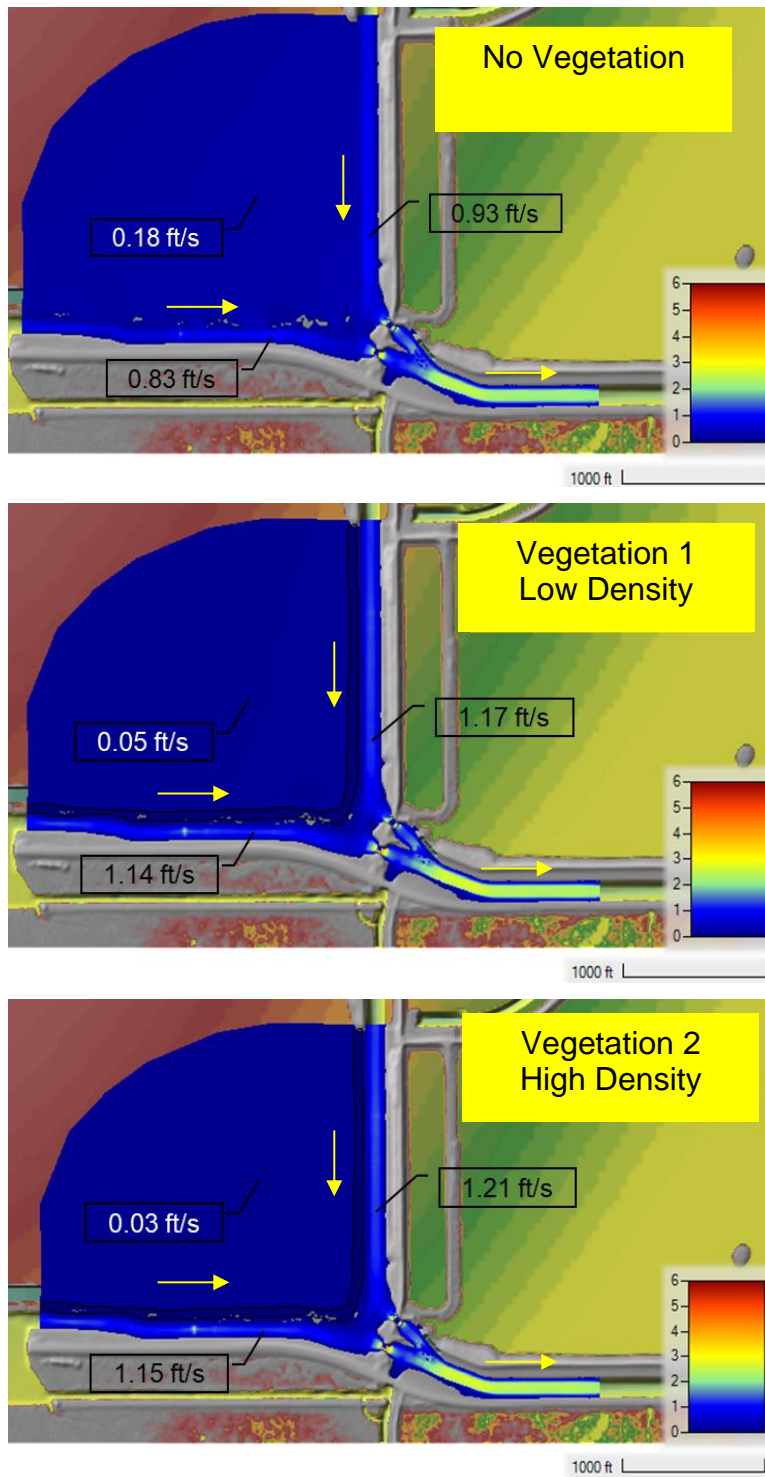
Figure 25. HEC-RAS 2D modeling test of concept with a vegetation buffer around the marsh, depth average velocity in ft/s, headwater at 9.5 ft NGVD29, tailwater at 9.0 ft NGVD29, and a total flow of 2,500 cfs.
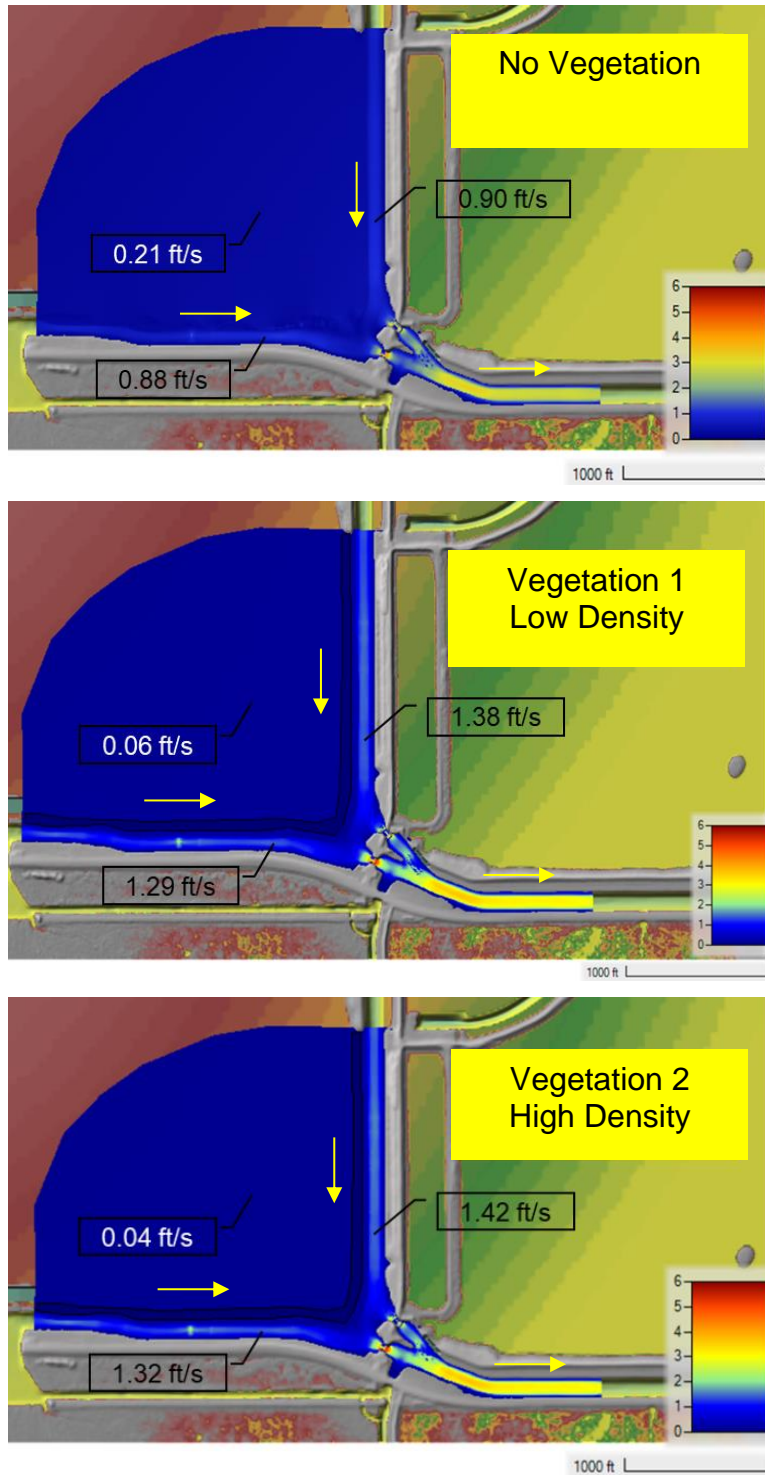
Figure 26. HEC-RAS 2D modeling test of concept with a vegetation buffer around the marsh, depth average velocity in ft/s, highwater of 10.5 ft NGVD29, tailwater 8.5 ft NGVD29, and total flow of 2,500 cfs.

Headwater 9.5 ft NGVD29, Tailwater 9.0 ft NGVD29, and Q total 2,500 cfs
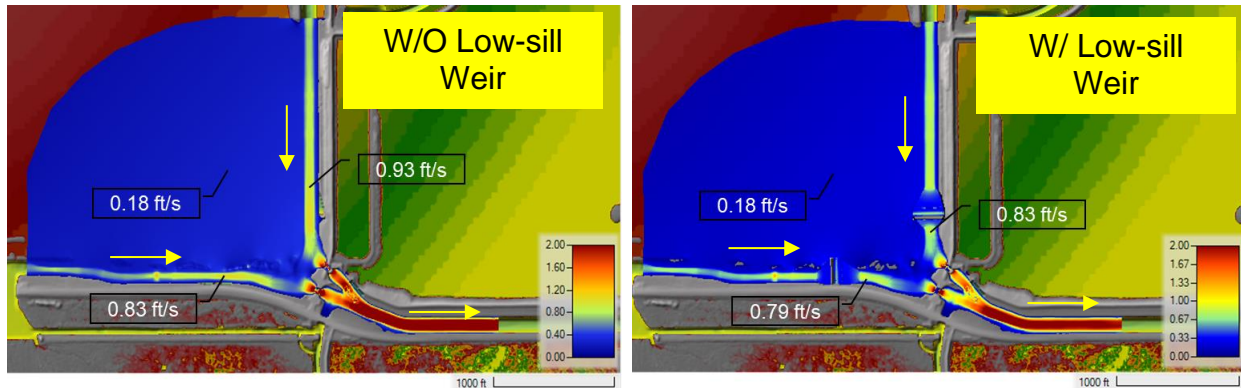
Headwater 10.5 ft NGVD29, Tailwater 8.5 ft NGVD29, and Q total 2,500 cfs
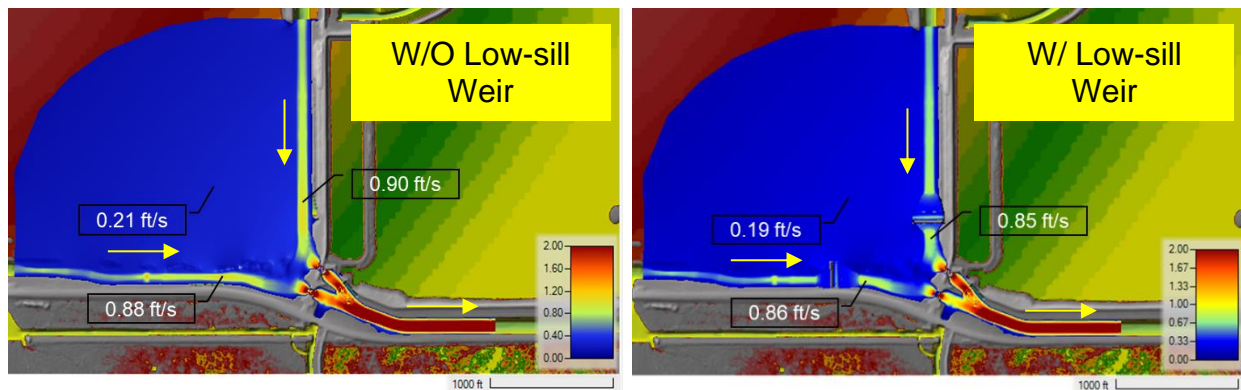
Figure 27. HEC-RAS 2D modeling test of concept without (W/O) and with (W/) low-sill weirs in canals with depth average velocity in ft/s.

Headwater 9.5 ft NGVD29, Tailwater 9.0 ft NGVD29, and Q total 2,500 cfs
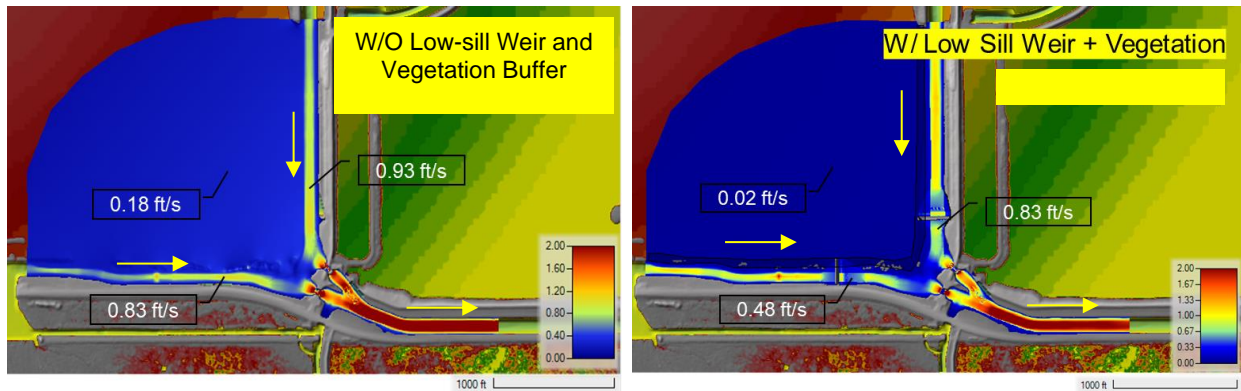
Headwater 10.5 ft NGVD29, Tailwater 8.5 ft NGVD29, and Q total 2,500 cfs
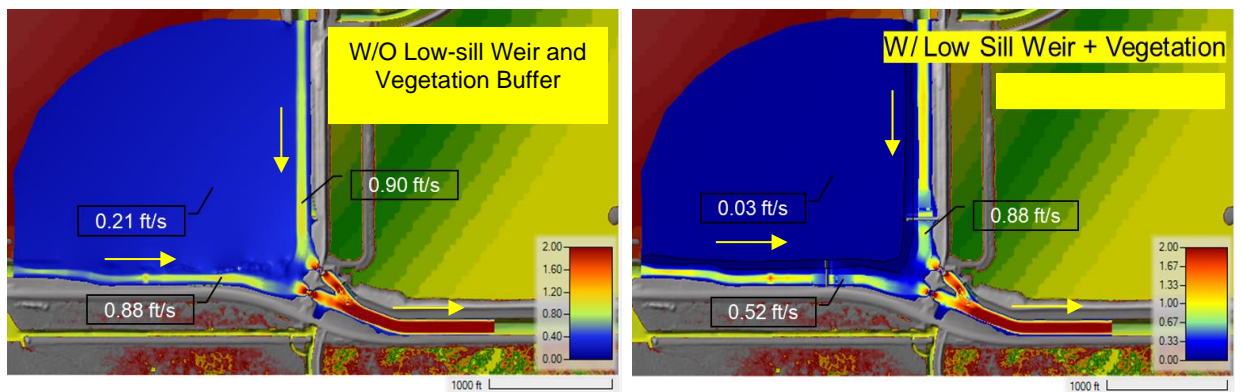
Figure 28. HEC-RAS 2D modeling test of concept without (W/O) and with (W/) a vegetation buffer around the marsh and low-sill weirs in canals with depth average velocity in ft/s.

Sediment Trap Option 1
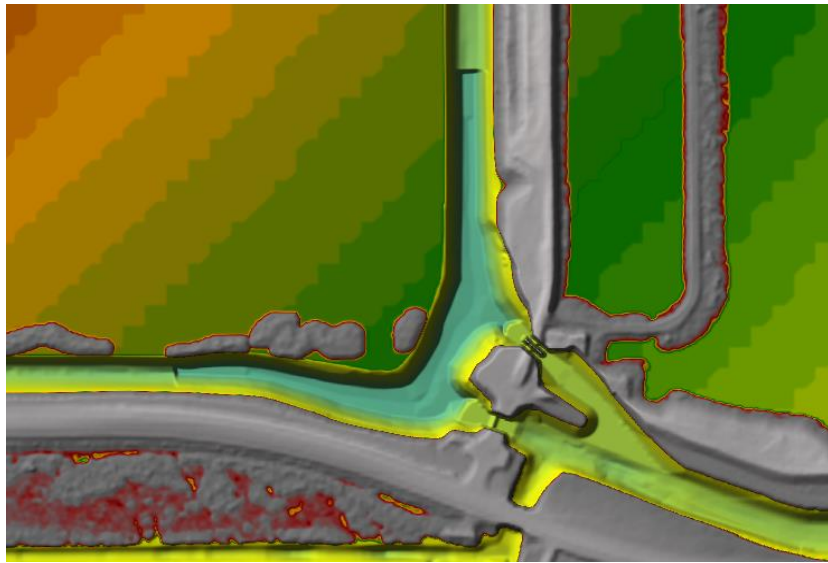
Sediment Trap Option 2: Larger Excavation (cutting into canals)
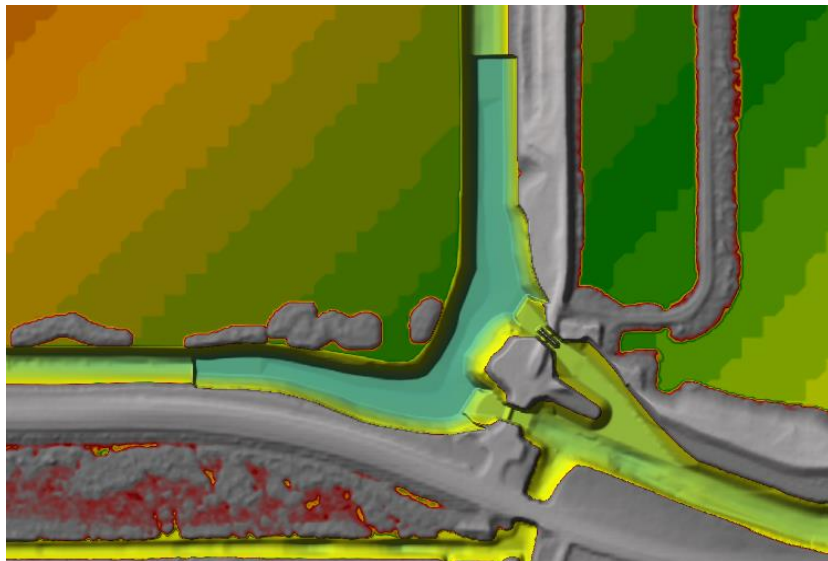
Figure 29. Conceptual sediment traps in canals for HEC-RAS model testing.
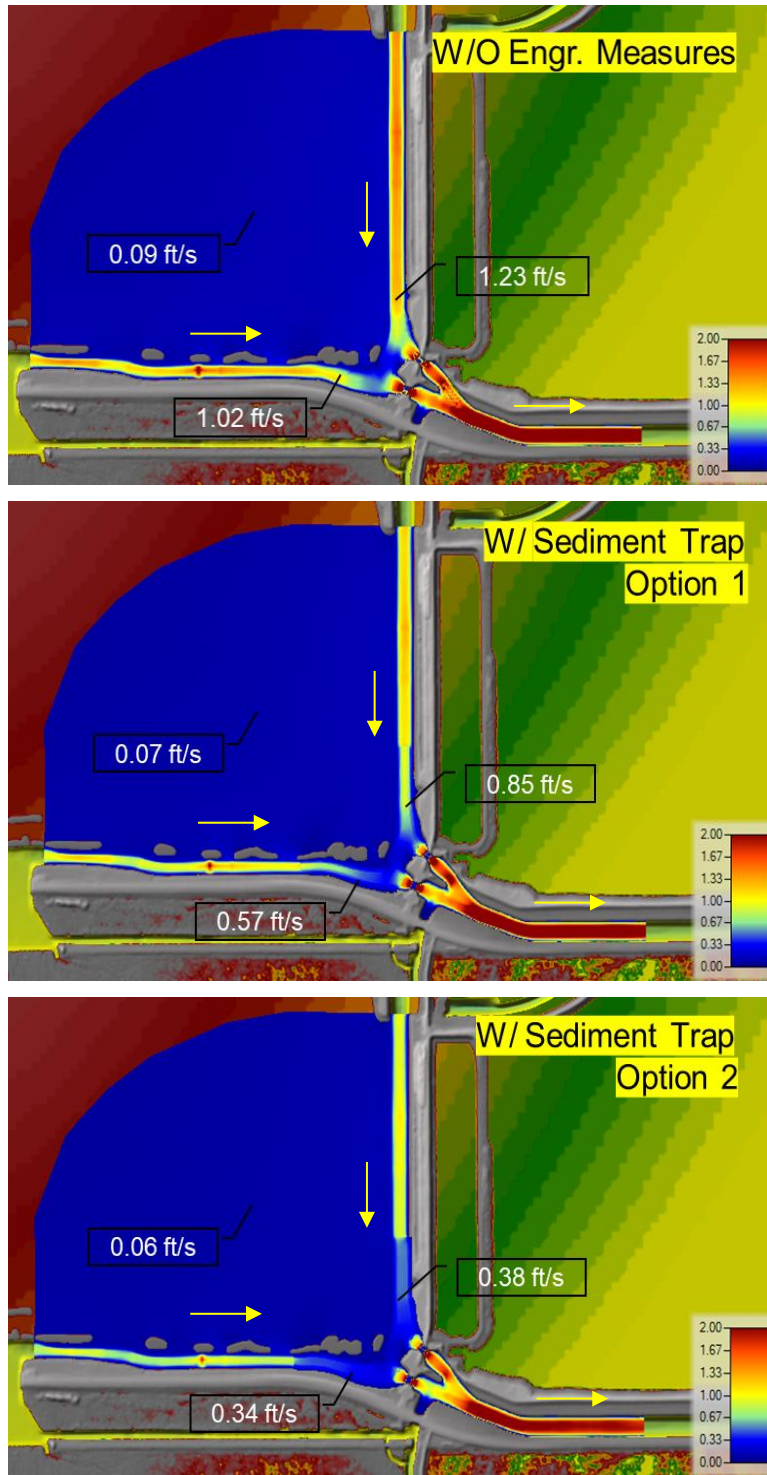
Figure 30. HEC-RAS 2D modeling test of concept without (W/O) and with (W/) sediment traps in canals, with depth average velocity in ft/s, headwater of 7.5 ft NGVD29, tailwater of 6.5 ft NGVD29, and total flow of 2,500 cfs.
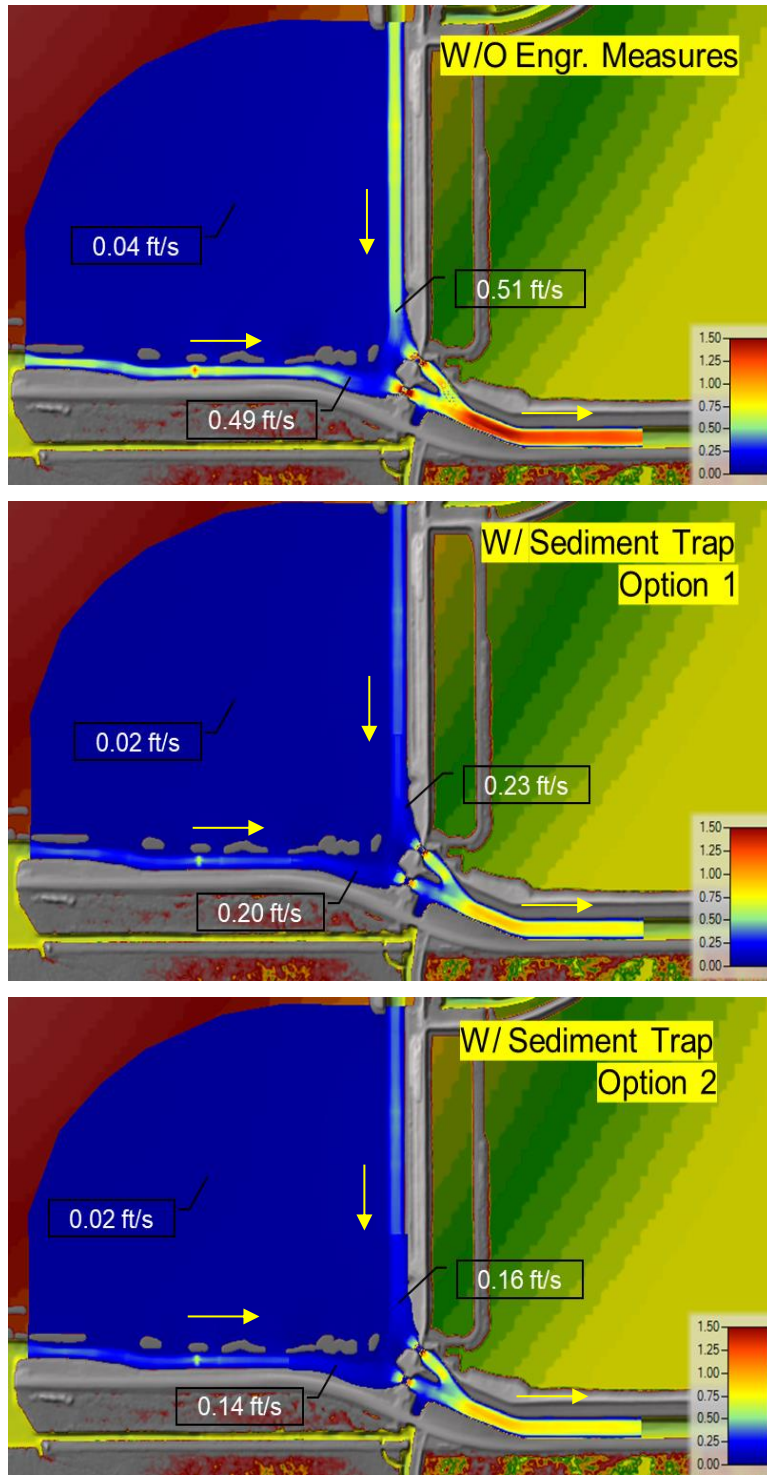
Figure 31. HEC-RAS 2D modeling test of concept without (W/O) and with (W/) sediment traps in canals with depth average velocity in ft/s, headwater of 7.5 ft NGVD29, tailwater of 6.5 ft NGVD29, and total flow of 750 cfs.

6.0 CFD MODELING FOR EVALUATING ENGINEERING METHODS

HEC-RAS modeling served as an initial test of concepts for potential engineering scenarios to attain the desirable flow field to reduce sediment transport at S-333/S-333N. Based on discussions with the S-333 Working Group, the engineering improvement of creating sediment traps upstream of the S-333/S-333N complex was further evaluated using 3D CFD. The CFD model geometry was modified to include the sediment trap and the mesh generation, and the simulation process was repeated for each scenario with the engineering measure. **Figure 32** illustrates the conceptual sediment trap from the 3D CFD geometry.

For these simulations, flow direction in L-29 was eastwards, and in L-67A was southwards. Flow split in L-29 and L-67A Canals were based on the respective design capacities at S-333 and S-333N (1,350 cfs at S-333, 1,150 cfs at S-333N). For example, for a 750 cfs total flow, the split in L-29 and L-67A was 405 cfs and 345 cfs, respectively.

The simulation results for low-stage cases (see **Table 2** earlier in the report) are illustrated in **Figures 33** to **36**, while the high-stage scenarios are shown in **Figures 37** and **38**. Generally, the sediment trap was able to reduce near bed velocities of the approaching flow in L-67A and L-29 due to increase in cross-section area. Flow at S-333 historically has been about 600-700 cfs when headwater is at or below 7.5 ft NGVD29 (**Figure A-3** in **Appendix A**). For such low-flow low-stage condition, the inclusion of the sediment trap decreased near bed velocities from 0.28 ft/s to 0.14 ft/s at the trap (by about 50%). For the low-stage high-flow condition (the more critical scenario), at the sediment trap, near bed velocities decreased from 0.76 ft/s to 0.58 ft/s, by about 25%. With higher discharges, the decrease in near bed velocities is not as large as low-flow scenarios due to the sudden drop in canal bed at the sediment trap. However, near surface velocity plots and cross-section velocities reveal an overall gradual slowdown of the flow jets. This is expected to promote deposition of sediment particles and prevent motion through the spillways. Vacuum dredging can be performed to remove these loose sediments from the canal bed. For high-stage high-flow conditions, the sediment trap does not seem to have a significant impact on the near bed velocity magnitudes. Comparing the velocity magnitudes with Hjulstrom's (1935) curves, inclusion of the sediment trap appears to have good potential to prevent sediment transport to the downstream for the most likely operation condition (low-stage low-flows).
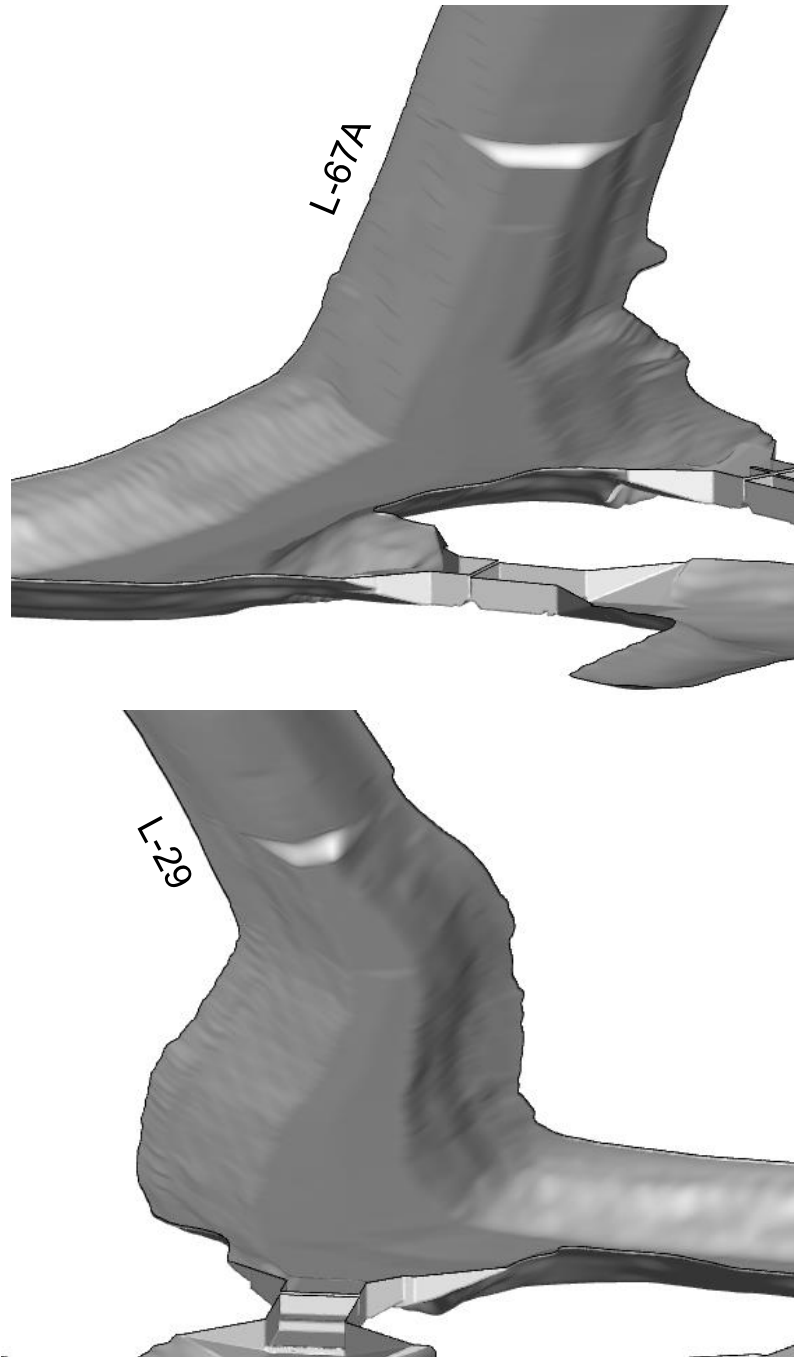
Figure 32. Conceptual three-dimensional sediment traps in L-29 and L-67A canals
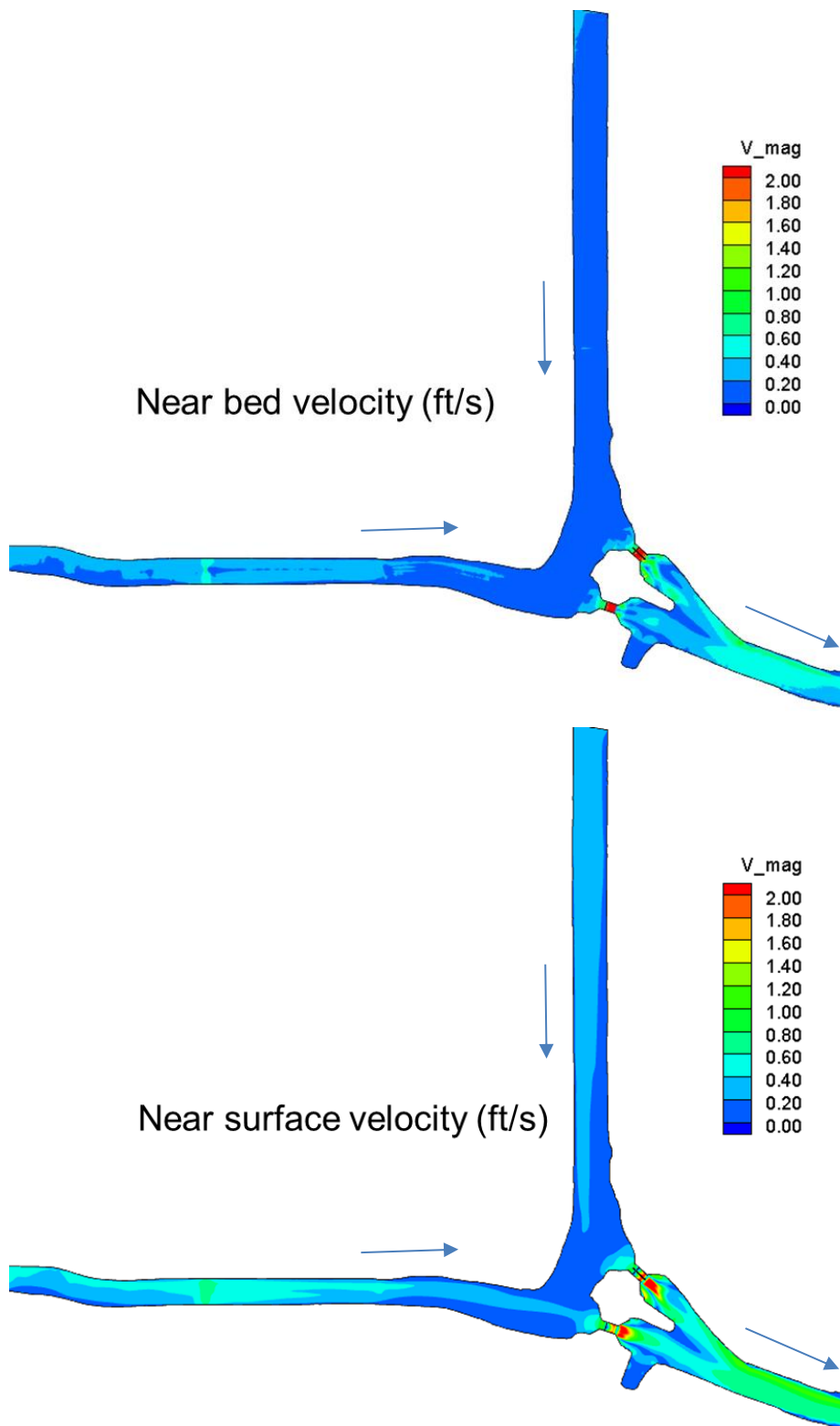
Figure 33. CFD modeling test of concept with sediment traps in canals,
headwater of 7.5 ft NGVD29, tailwater of 6.5 ft NGVD29, and total flow of 750 cfs.
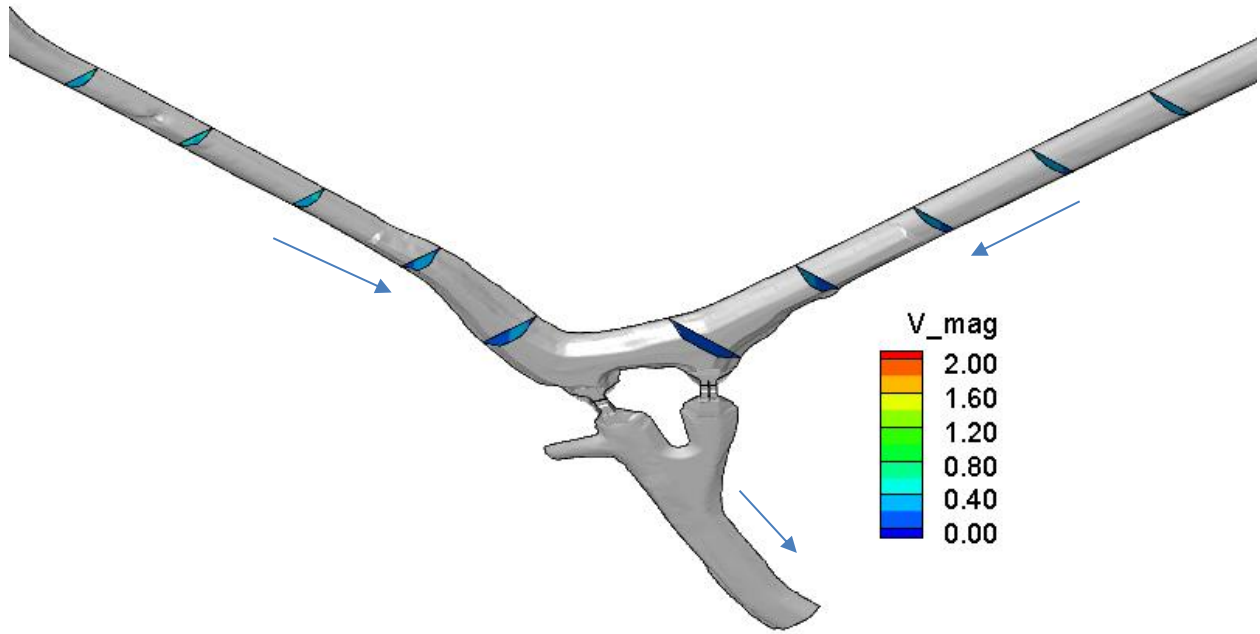
Figure 33. Continued.
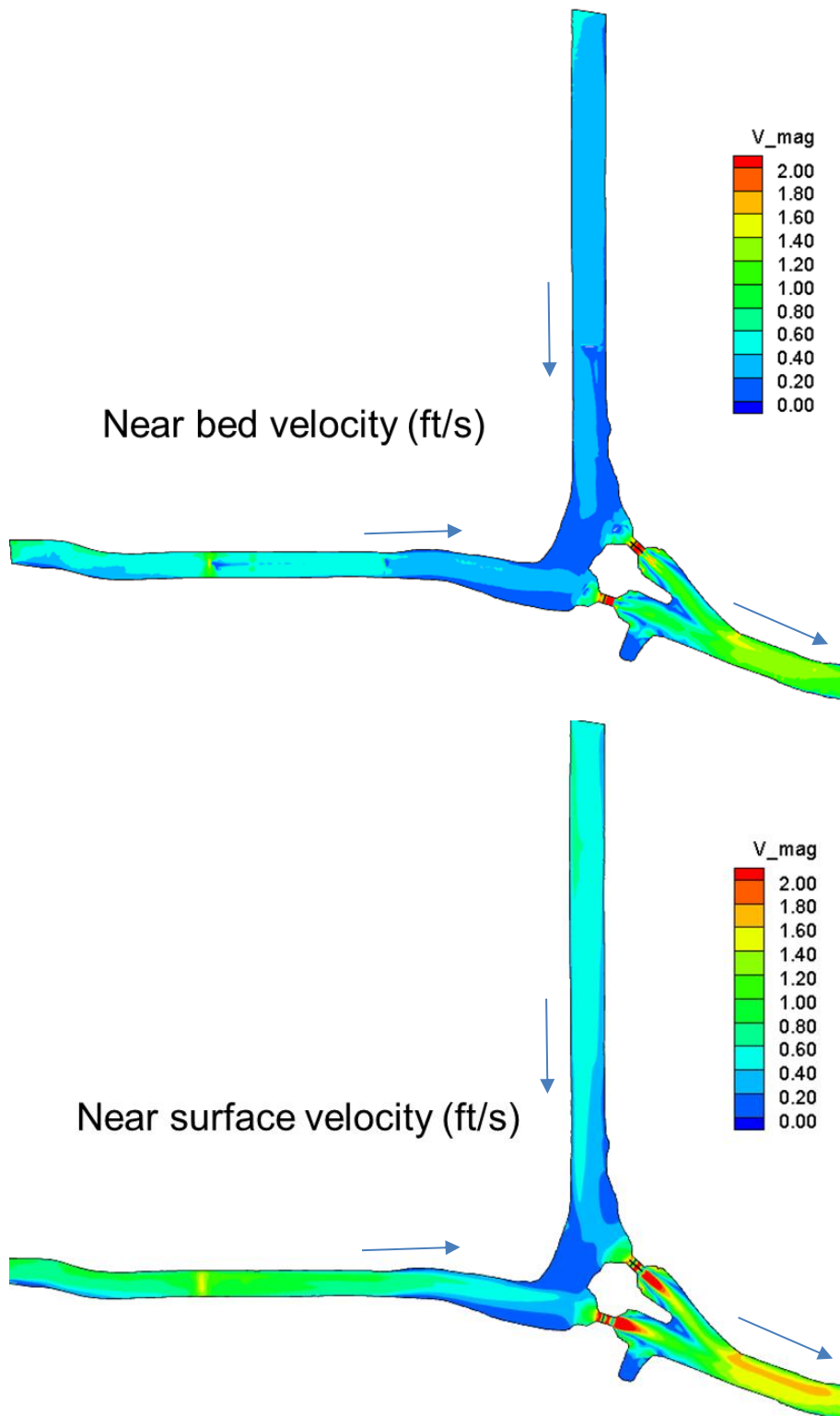
Figure 34. CFD modeling test of concept with sediment traps in canals, headwater of 7.5 ft NGVD29, tailwater of 6.5 ft NGVD29, and total flow of 1,500 cfs.
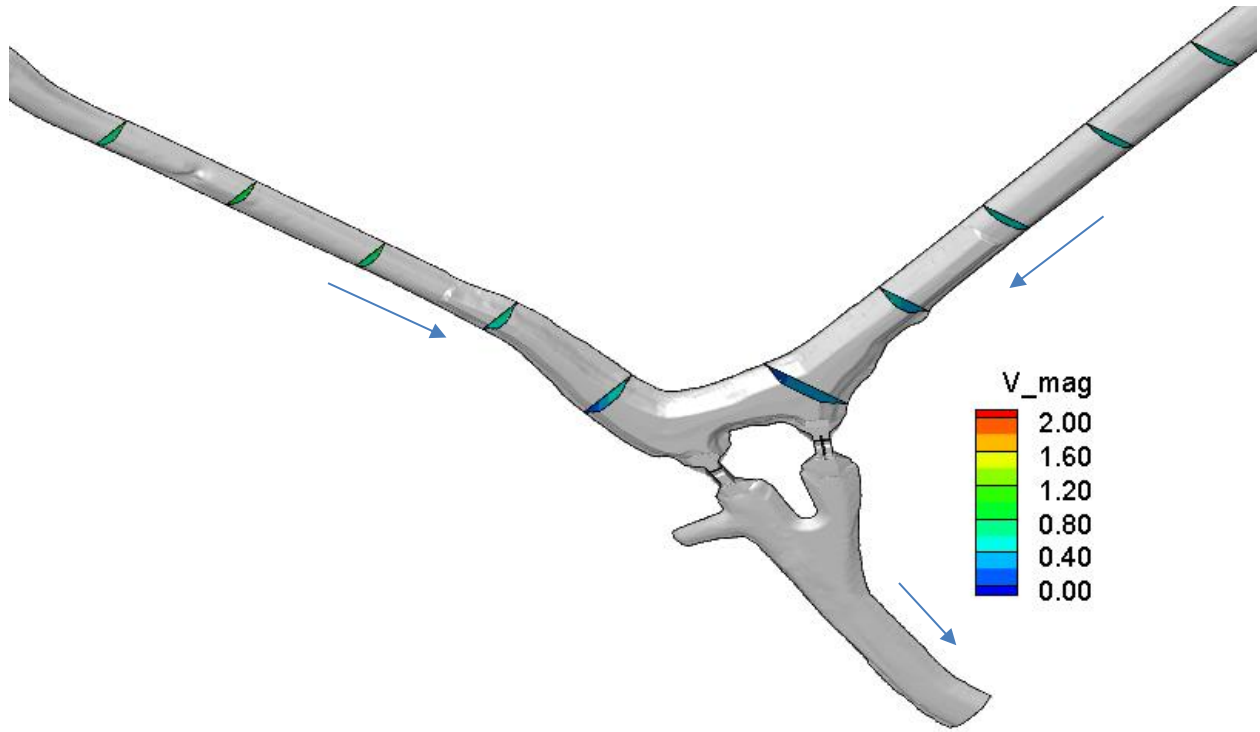
Figure 34. Continued.
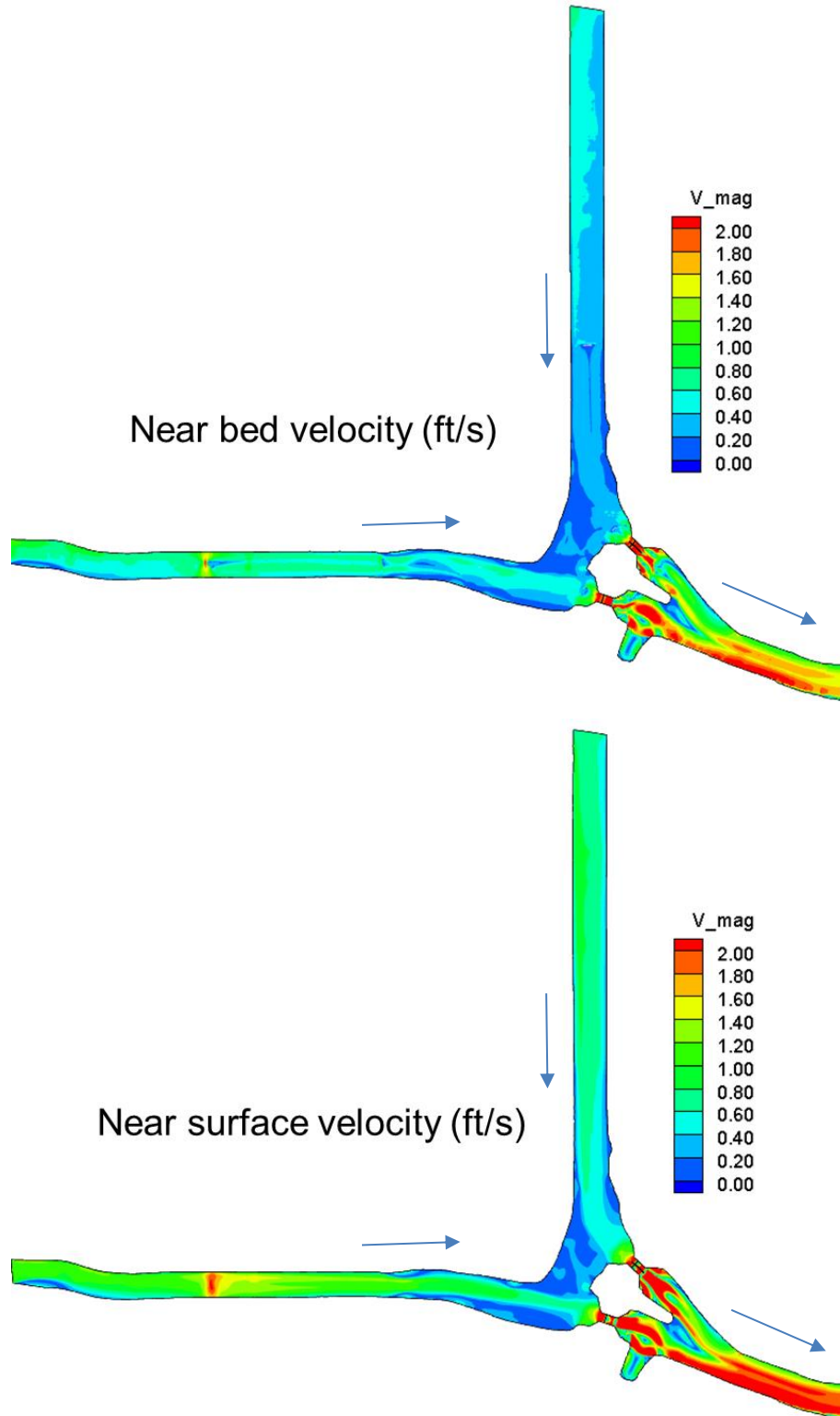
Figure 35. CFD modeling test of concept with sediment traps in canals, headwater of 7.5 ft NGVD29, tailwater of 6.5 ft NGVD29, and total flow of 2,000 cfs.
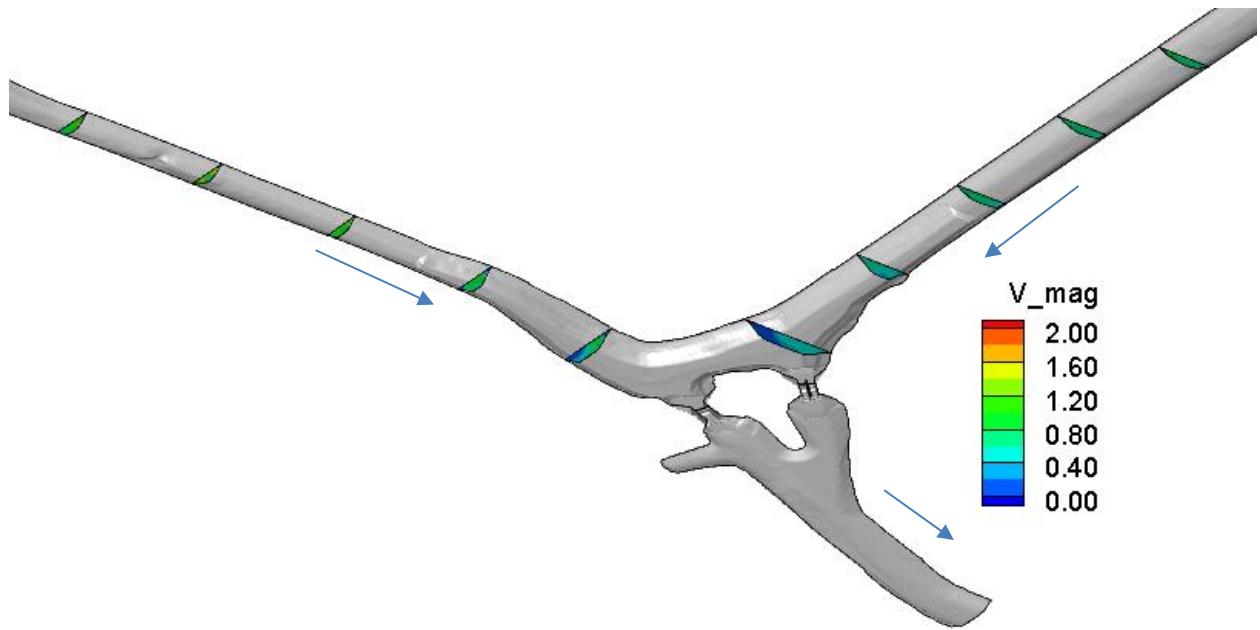
Figure 35. Continued.
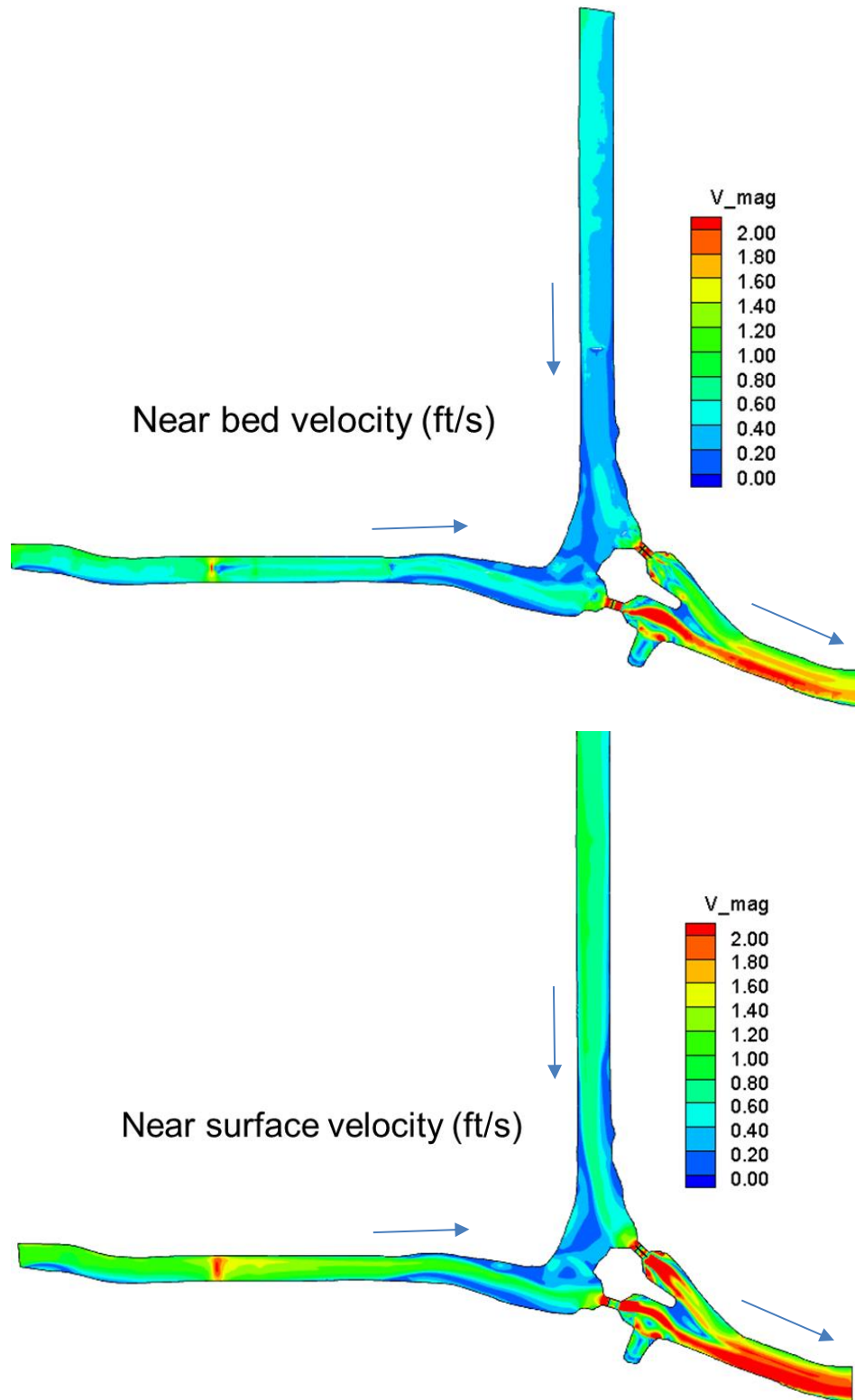
Figure 36. CFD modeling test of concept with sediment traps in canals, headwater of 7.5 ft NGVD29, tailwater of 6.5 ft NGVD29, and total flow of 2,500 cfs.
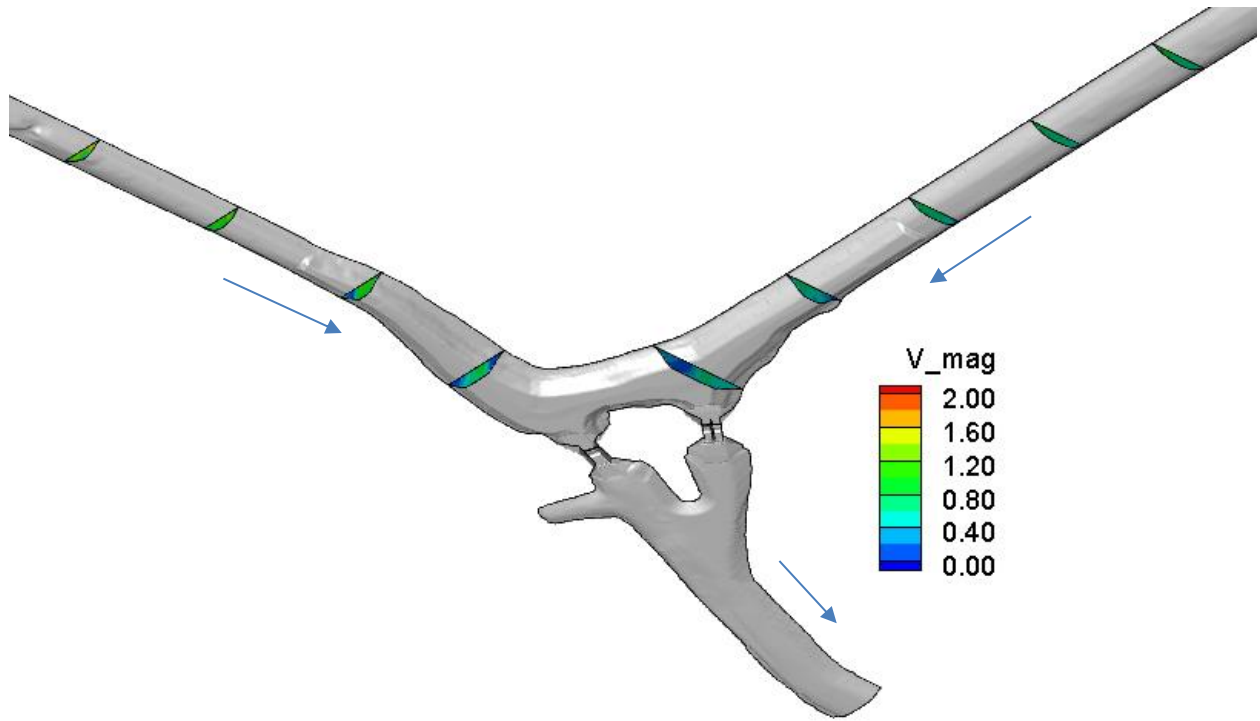
Figure 36. Continued.
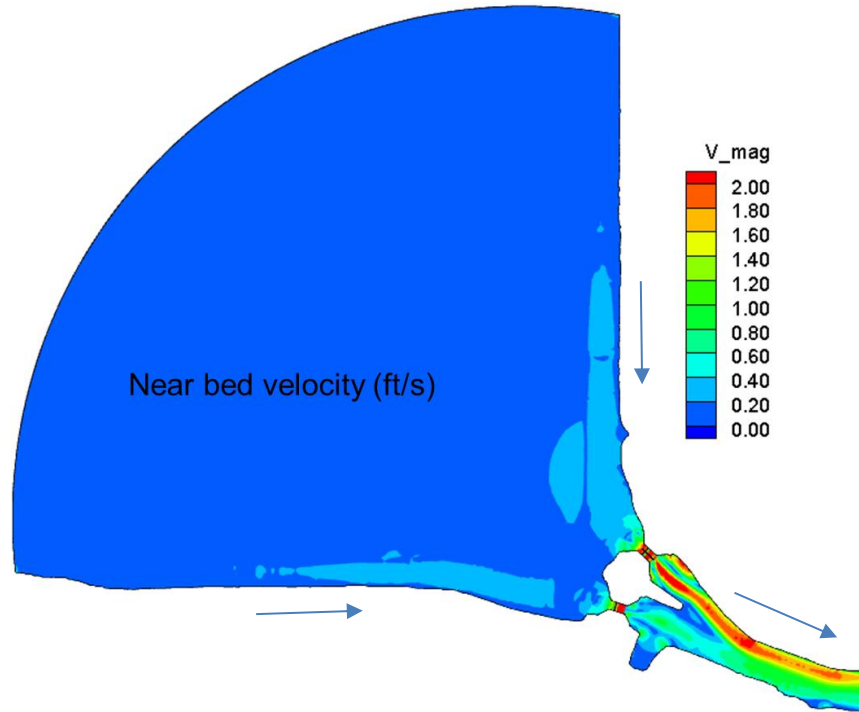
Figure 37. CFD modeling test of concept with sediment traps in canals,
headwater of 9.5 ft NGVD29, tailwater of 9.0 ft NGVD29, and total flow of 2,500 cfs.
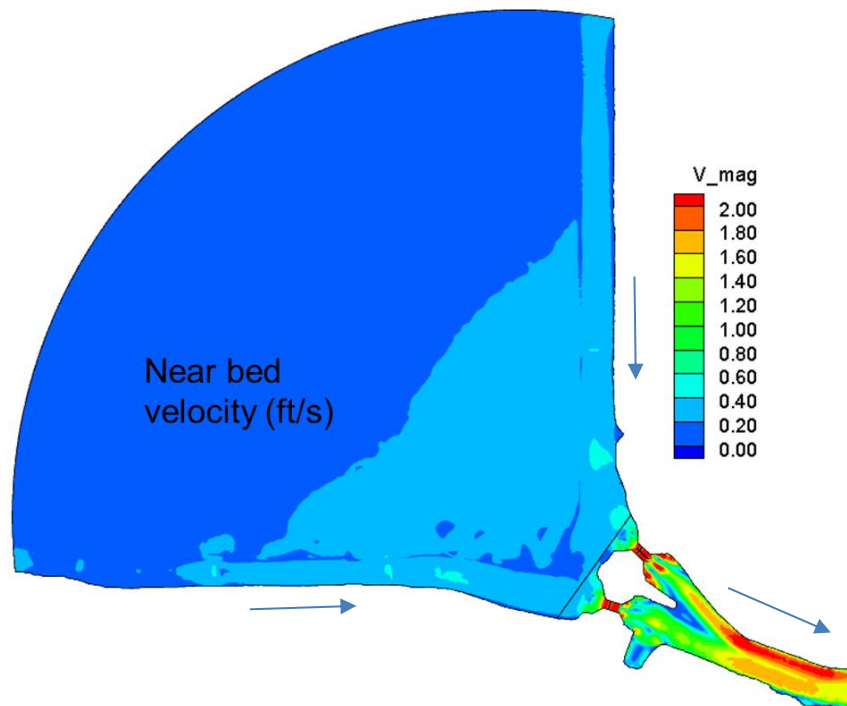
Figure 38. CFD modeling test of concept with sediment traps in canals,
headwater of 10.5 ft NGVD29, tailwater of 8.5 ft NGVD29, and total flow of 2,500 cfs.

7.0 CONCLUDING REMARKS

The objective of this project was to study the hydrodynamics of flow along the canal system near the S-333/S-333N complex and adjacent parts of the marsh area. The first phase, discussed in this report, involved 3D CFD modeling of the local area around the spillways to analyze the pertinent hydrodynamic features that incite sediment transport through the structures. The 3D CFD modeling was also used to examine the effects of structural measures on sediment transport. Additional 2D HEC-RAS simulations involving engineering measures to slow down flow velocity in marsh and canals were mainly used as an additional check to CFD simulations and were not intended to be as rigorous conceptual design simulation runs. Phase I study adopted combining well-known empirical formulae and numerical simulations to indirectly evaluate the potential of sediment movement. Concluding remarks on critical velocity criteria relied solely on CFD model results. The major findings are as follows:

1. A vegetation buffer along west bank of the L-67A Canal and north bank of the L-29 Canal (west of S-333) significantly reduce velocities in the marsh during high stages. Its impact on potential reduction in TP transport from the marsh into the canals needs further testing. In the subsequent phases, addition of vegetation buffers along marsh-canal edge as a potential for reducing velocities should consider the long-term biogeochemical effects of high sediment (and P) accumulation in these areas.

2. A sediment trap just upstream of S-333/S-333N complex reduces near bed velocity in the canals for some of the most concerning conditions (low stages–low flow and low stages–medium flow) and shows strong potential in reducing sediment transport from the canals into the S333/S333N complex.

3. A low-sill weir installed in both L-67A and L29 Canals shows limited potential in reducing near bed velocities and sediment transport. Future phases of the study (if any) should consider combining a low-sill weir with a refined sediment trap. As the engineering scenarios were geared towards reducing flow velocities in marsh and canals, not the discharge itself, the sediment trap or low-sill weir is not expected to impact flows to the ENP.

4. CFD simulated near bed and mean velocities combined with L-67A and L-29 canals sediment characteristics (D_{50}, collected by NPS), and well-known sediment-versus-incipient-velocities (velocities that move a sediment of particular size) charts were used to infer potential for sediment transport at S-333/S-333N. In future field sediment study (if any), it is highly suggested to measure actual incipient velocities in these canals to make more accurate interpretations of the CFD simulations. It is also suggested to develop sediment ratings (sediment discharges versus flow rate) to help appropriately size the sediment trap and assess its efficacy.

The critical near bed velocity for reducing non cohesive sediment transport in the canals were suggested conservatively based on literature data and empirical formulae (Hjulstrom 1935, Mavis and Laushey 1948, Stoeber 2005). The sediment sampling in Phase I was limited to the about 1500 ft upstream of S-333/S-333N which showed on average predominantly sandy soils (D_{50} close to very fine to fine sand). Interpretation of the critical velocity in the canals and marsh were based on the sediment size (D_{50}) data provided by the National Park Service (NPS, 2022). Having said that, the Everglades is generally a system dominated by organic soils and floc materials with low

particle density. Consequently, the critical velocity for certain type of entrained sediments (floc, cohesive sediment, etc.) could be lower. The current study focused on the transport of non-cohesive sediments that can realistically be assessed and potentially be trapped to reduce sediment transport through S333/S333N Complex. Assessment of transport of cohesive sediment that are typically transported as flocs in suspension or bedload is beyond the scope of the Phase I analysis.

8.0 LITERATURE CITED

Briceño, H., P. Gardinali, and R. Garcia. 2019. *Mechanisms and conditions responsible for elevated TP levels in surface water discharges to Shark River Slough within Everglades National Park, Final Report 2019*. Prepared by Florida International University for South Florida Natural Resources Center, Everglades National Park, Homestead, FL.

Dargahi, B. 2006. Experimental study and 3D numerical simulations for a free-overflow spillway. *Journal of Hydraulic Engineering* 132(9):899-907.

Daroub, S.H., J.D. Stuck, T.A. Lang, and O.A. Diaz. 2002. *Particulate phosphorus in the Everglades Agricultural Area: II—Transport Mechanisms*. SL198, Soil and Water Science Department, University of Florida, Gainsville, FL.

Das, J., S.H. Daroub, J.H. Bhadha, T.A. Lang, O. Diaz, and W. Harris. 2012. Physicochemical assessment and phosphorus storage of canal sediments within the Everglades Agricultural Area, Florida. *Journal of Soils and Sediments* 12:952-965.

Ge, L., S.O. Lee, F. Sotiropoulos, and T. Sturm. 2005. 3D unsteady RANS modeling of complex hydraulic engineering flows, II: Model validation and flow physics. *Journal of Hydraulic Engineering* 131(9):809-820.

Hjulstrom, F. 1935. The morphological activity of rivers as illustrated by river fyris. *Bulletin of the Geological Institute*, *Uppsala* 25:221-527.

Kirkgoz, M.S., M.S. Akoz, and A.A. Oner. 2009. Numerical modeling of flow over a chute spillway. *Journal of Hydraulic Research* 47(6):790-797.

Li, X., Y. Wang, J. Stern, and B. Gu. 2011. Isotopic evidence for the source and fate of phosphorus in Everglades wetland ecosystems. *Applied Geochemistry* 26(5):688-695.

Mavis, F., and L. Laushey. 1948. A reappraisal of the beginning of bed movement - competent velocity. *International Association for Hydraulic Research*, Second Meeting, Stockholm, Sweden.

Pedersen, Ø., G. Fleit, E. Pummer, B.P. Tullis, and N. Rüther. 2018. Reynolds-Averaged Navier-Stokes modeling of submerged ogee weirs. *Journal of Irrigation and Drainage Engineering* 144(1):04017059.

Rakib, Z., J. Li, and J. Zeng. 2017. *Flow Rating Improvement for Spillway S333 Technical Note*. South Florida Water Management District, West Palm Beach, FL.

Rakib, Z., J. Zeng, and T. Bhuiyan. 2021. *Flow Rating Development for Spillway S333N with CFD Technical Note*. South Florida Water Management District, West Palm Beach, FL.

Savage, B.M., and M.C. Johnson. 2001. Flow over ogee spillway: Physical and numerical model case study. *Journal of Hydraulic Engineering* 127(8):640-649.

Stoeber, M. 2005. *Minimum Velocities for the Suspension of Fine Sediment in the Green River Canal*. MS Thesis, All Graduate Plan B and Other Reports 810, Utah State University, Logan, UT.

USACE. 1991. *Hydraulic Design of Flood Control Channels*. Engineer Manual 1110-2-1601, United States Army Corps of Engineers, Washington , DC. July 1, 1991.

USBR. 1974. *Hydraulic Design of Stilling Basins and Energy Dissipators*. Engineering Monograph No. 25, United States Bureau of Reclamation, United States Department of the Interior, Washington, DC.

Wang, Q., Y.C. Li, and O. Ying. 2011. Phosphorus fractionation and distribution in sediments from wetlands and canals of a water conservation area in the Florida Everglades. *Water Resources Research* 47:1-11.

Zeng, J., M. Ansar, and Z. Rakib. 2018. Applications of CFD to S333N Spillway Design. In: Erdman Anthony, *Design Report S-333N Gated Structure*, submitted under Work Order 4600003017-WO13 to the South Florida Water Management District, West Palm Beach, FL .

Zeng, J., L.Q. Zhang, M. Ansar, E. Damisse, and J.A. Castro-Gonzalez. 2017. Applications of computational fluid dynamics to flow ratings at prototype spillways and weirs, I: Data generation and validation. *Journal of Irrigation and Drainage Engineering* 143(1):04016072.

APPENDIX A: CYCLIC ANALYSIS AND HISTORIC RECORDS
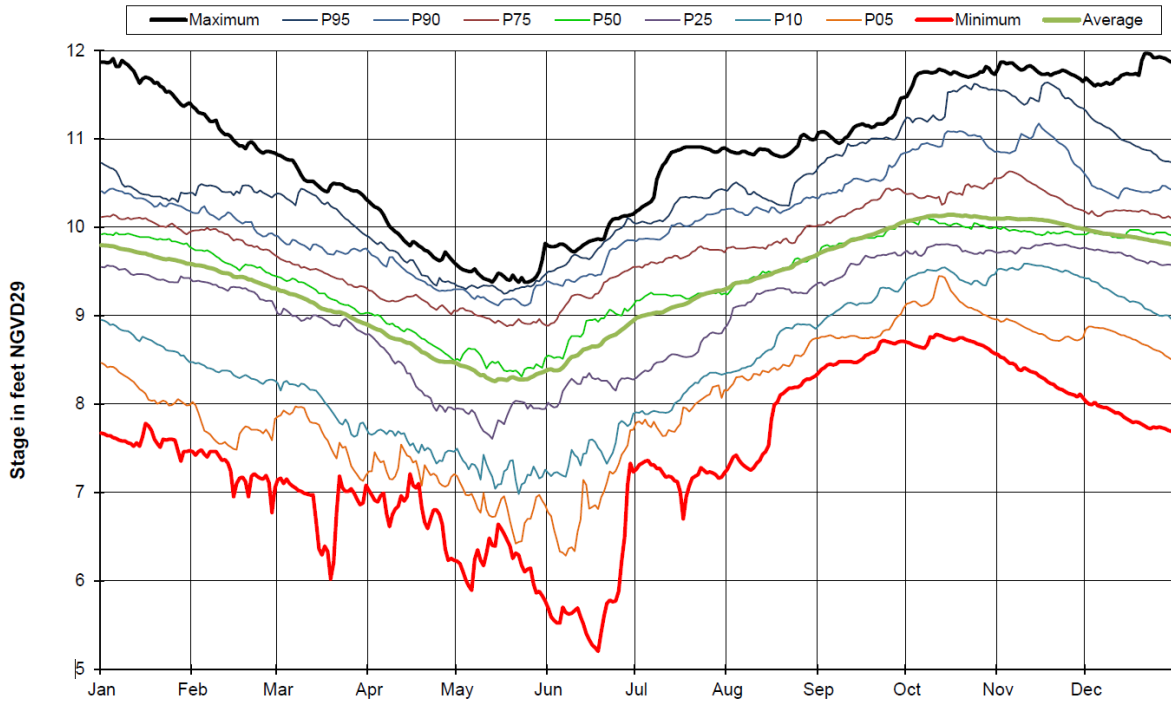
Figure A-1. Cyclic analysis of daily mean headwater stage (1978–2021) at S-333.
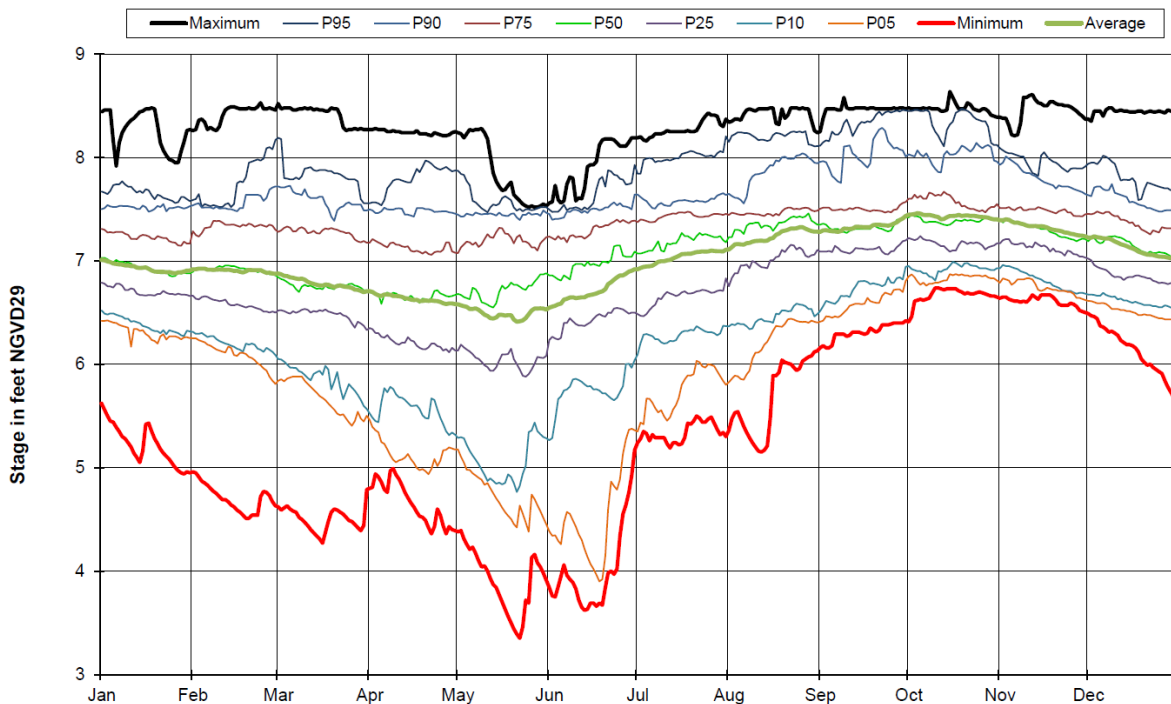
Figure A-2. Cyclic analysis of daily mean tailwater stage (1978–2021) at S-333.
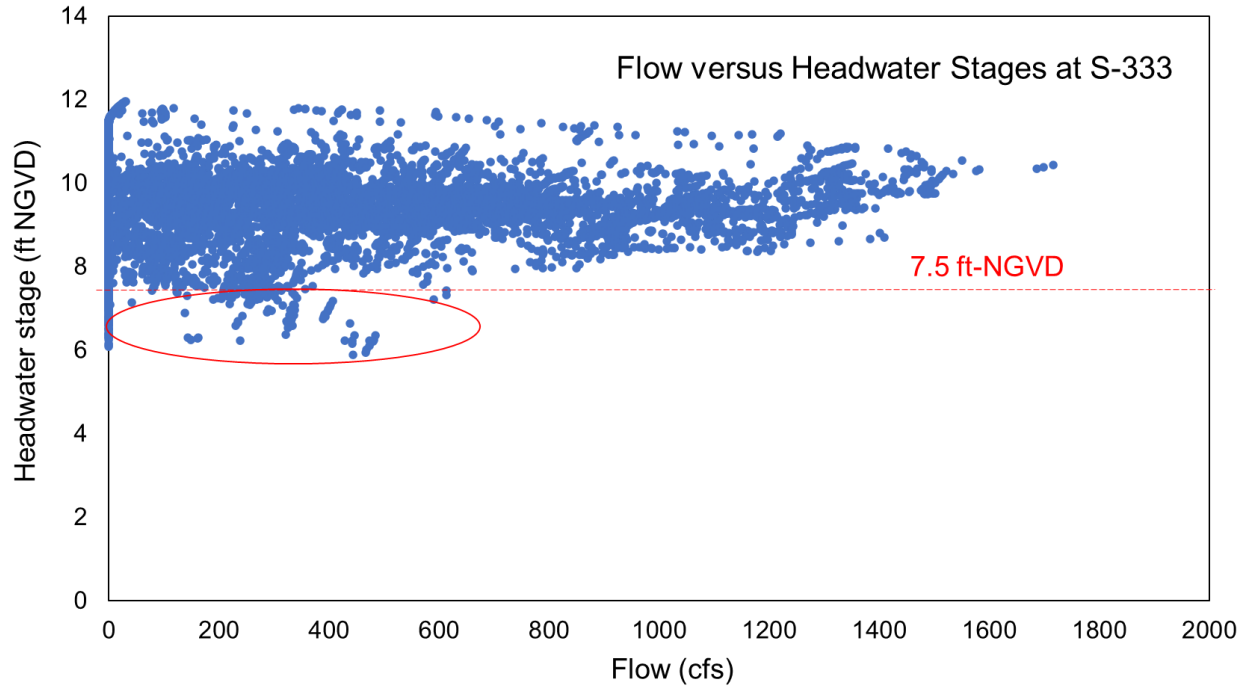
Figure A-3. Historic daily mean headwater stage versus flow at S-333.

APPENDIX B: VELOCITY VERSUS PARTICAL DIAGRAMS

SIZE OF RIPRAP TO BE USED DOWNSTREAM FROM STILLING BASINS
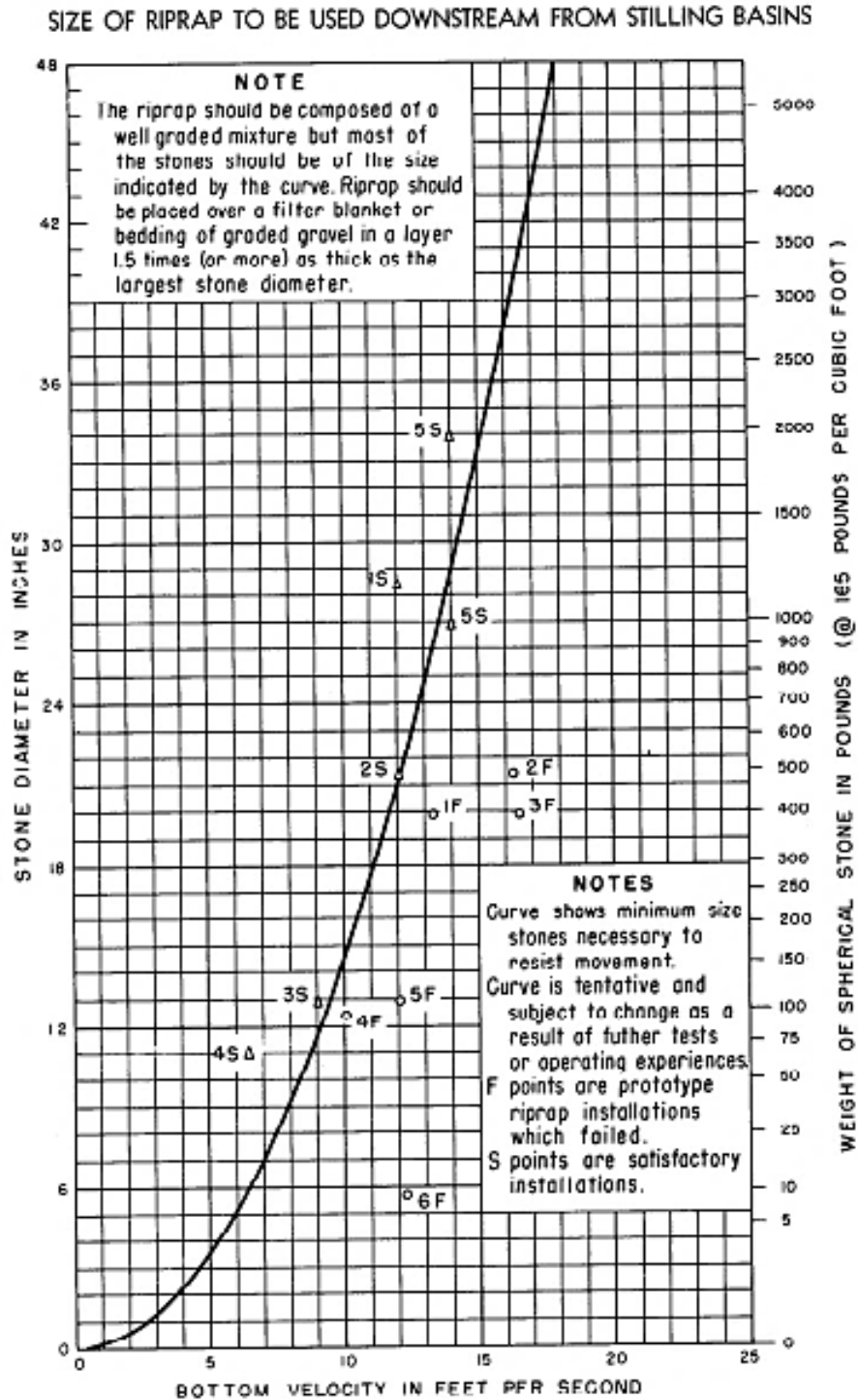
Figure B-1. Velocity versus particle diameter diagram
from the United States Bureau of Reclamation (USBR 1974).
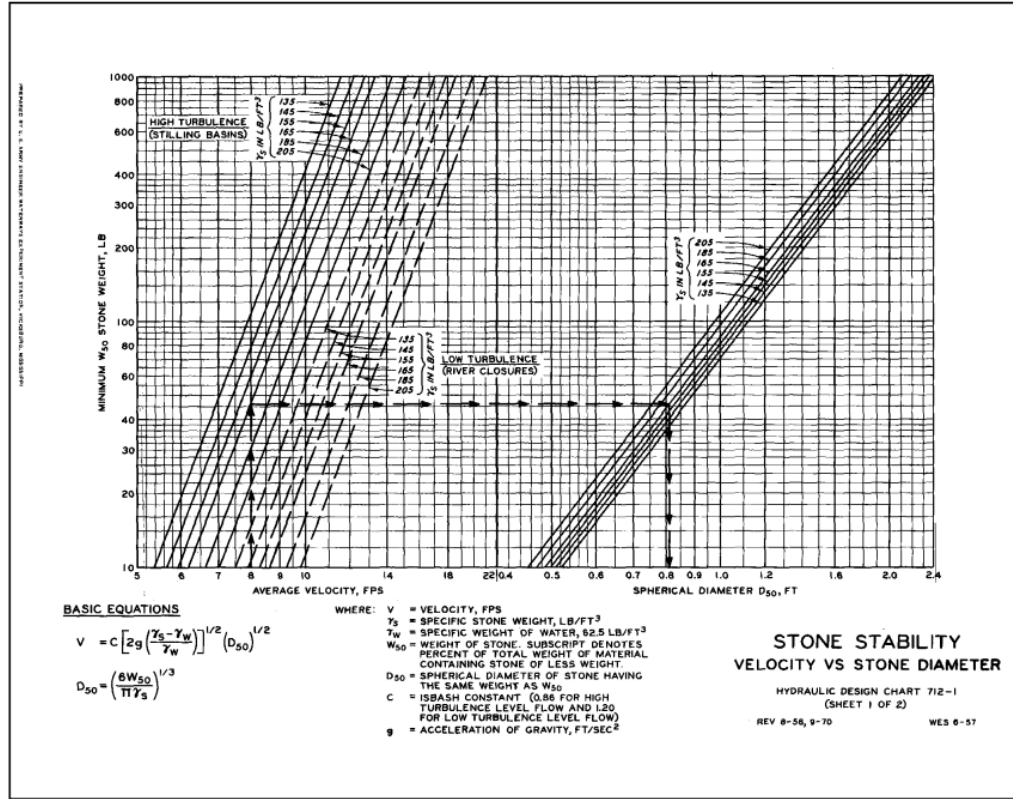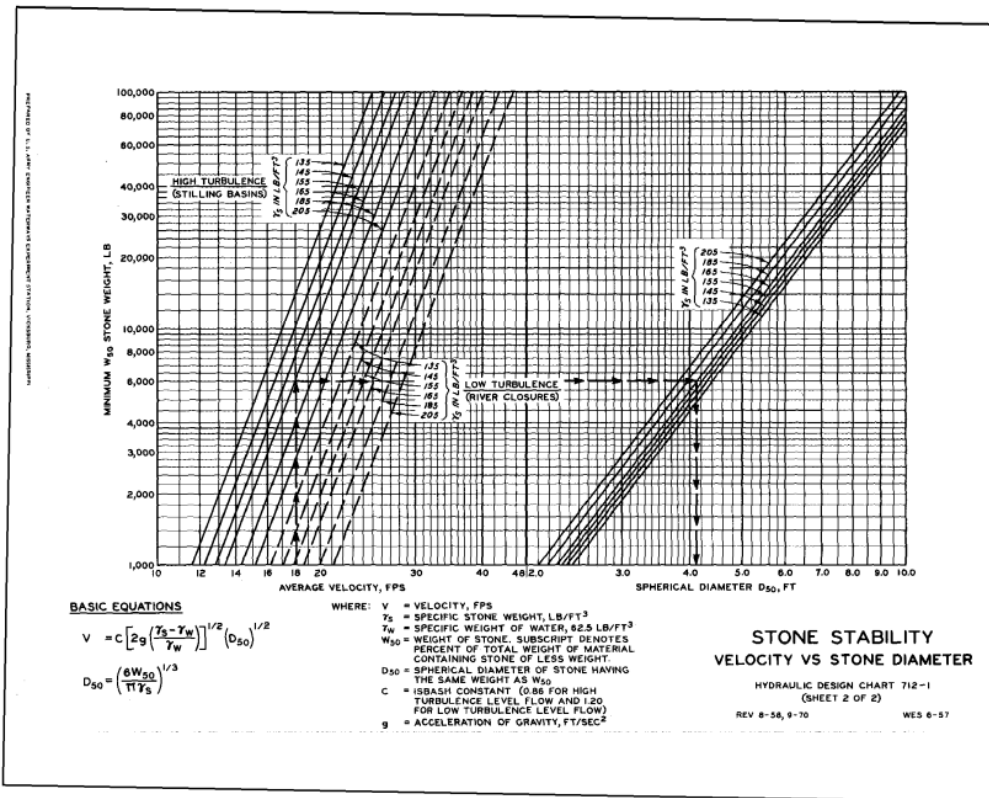
Figure B-2. Velocity versus particle diameter diagram from the United States Army Corps of Engineers (USACE 1991).

SECTION 2: CONSOLIDATED COMMENTS AND RESPONSES

Commenter Name	Agency	Page Number	Comment/Question	Response from SFWMD	Commenter Response
Chelsea Qiu	SFWMD	general	The 3-D CFD analysis examined the local velocity fields under low and high stages in the S-333 complex and within immediate proximity of the canals and marsh areas around the structures. Engineering measures for reducing sediment and TP transport, such as sediment trap or low-sill weir, and marsh vegetation buffer were also evaluated. However, the evaluation for sediment transport is based on sediment composed of primarily mineral particles. The Everglades is a system dominated by organic soils and floc materials with very low particle density. Transport of these materials would be much easier than conventional sediment. Critical velocity for entrainment of these materials would be lower and should be considered in Phase 2 study.	Average D_{50} was used in our analysis. More characteristics info such as sediment density, weight is needed for organic soil, that could be extended in phase 2. In the domain area for phase 1, soil material is mostly sandy. So, we picked the lowest conservative literature suggested critical near bed velocity as for sandy soil.	
Jose Guardiario	SFWMD	Page 6, 1st paragraph	On the statement, "At onset of the wet season, when flows are increased, the elevated energy in water column brings the phosphorus loaded sediments in suspension which contribute to increased TP peaks that gets flushed downstream." This statement is contrary to the decades of water quality samples that show TP spikes during low flows.	At onset of wet season, the flows are initially low, and it gradually increases based on the operations. It is the first flush low flows when high TP occurs. It is suspected that TP accumulates during the period of low or no flow. The statement has been reworded to clear the confusion.	
Jose Guardiario	SFWMD	Page 6, 2nd paragraph	On the staement, "(2) sediment core samples taken near the S-333 and S-333N complex in the L-67A and L-29 canals were very sandy, while fine and organic-rich material was found at a site west of S-12D in the L-29 Canal." With fows throughout the year, there is not enough time for the floc to settle. Unlike the S-12D, particulalry the other structures to the west, there are are long hiatus of no flow which allows deposition of organic rich material.	The sediment trap is aimed to promote reduction of flow velocity so that it allows settlement of sediment flocs. If it is not settled, the sediment in the trap would move as bedload, which would be removed routinely for maintenance. Low sill weir combined with sediment trap will promote trapping of floating flocs.	
Jose Guardiario	SFWMD	Page 6, 2nd paragraph	On the staement, "(4) fractionating the TP species found in canal floc and sediments suggest that TP spikes originate from bottom sediments, floc and possibly from peat soils in the marshes" This statement needs to be proven by hydrodynamic model during low flows with TP spikes. Samples are taken 1.5 feet below the canal water surface and the canal bed is approximately 17.0 feet below.	This is beyond the scope of the hydrodynamic study. This could perhaps be addressed from the sediment characterization study.	
Jose Guardiario	SFWMD	Page 6, 3rd paragraph	On the statement, "These studies will assess the mechanisms responsible for the transport of sediment particulates and TP within the portion of the water column that is highly influenced by near-bed velocity, water depth and other hydrodynamic features. Relate this to water quality sampling depth. Once again, this needs to be proven by hydrodynamic model during low flows with TP spikes.	It may be added based on schedule constraints	

Commenter Name	Agency	Page Number	Comment/Question	Response from SFWMD	Commenter Response
Jose Guardiario	SFWMD	Page 14, 1st paragraph	On the statement, "This set of model simulations considered flow in upstream canals when water levels are below the marsh ground elevation (approximately 7.5 ft NGVD) ..... When water stages were lower than the marsh ground elevation, the CFD simulations considered in-canal flows only." How could this be when water is present on the marsh and the ground surface elevation is +6.1 ft NGVD29 based on the USACE as-built plans? There will be contributions from the marsh as overland flow.	The marsh ground elevation from recent survey is about 7~7.5 ft-NGVD. At about 7.5 ft-NGVD, the canal flow starts to separate from the marsh flow. It is also a significant cut off number in the regulation schedule of WCA3A. Water supply to South Dade Conveyance System at S333/S333N for stages at 7.5 ft NGVD or lower must be made up by equivalent amount from upstream water bodies (LOK). Hence, to simplify the model simulations, when water stages were lower than the marsh ground elevation, the CFD model setup considered in-canal flows only.	
Jose Guardiario	SFWMD	Page 16	On Figure 3. Assumed Sediment Trap and Low-sill Weir Upstream of S-333 and S-333N Complex. Based on the statement, "sediment core samples taken near the S-333 and S-333N complex in the L-67A and L-29 canals were very sandy, while fine and organic-rich material was found at a site west of S-12D in the L-29 Canal", how will a sediment trap be able to be successful when there are always high flows that does not allow deposition of organic rich material. The L-67A as-built survey indicates a -15 ft. NGVD29 invert at the S-333 location.	Same response as comment #4.	
Jose Guardiario	SFWMD	Page 17, 2nd paragraph	on the statement, "Near the water surface level, velocities were about 0.35 ft/s and 0.25 ft/s in L-67A and L-29, respectively." At a low stage scenario where the TP spikes the velocities are high near the surface. There is no settlement at this velocities, hence the solution should be geared towards addressing the suspended high TP particulates.		
Jose Guardiario	SFWMD	Page 42, 1st paragraph	On the statement, "...the low sill weirs can trap the resuspended sediments preventing it from being flushed to the downstream and thereby reducing the probability of high TP occurrences." How high does these resuspended sediments go up in the water columns? Does it move or being salted from elevation -10.0ft NGVD29 to +6.0 ft. NGVD 29 where the high TPs are measured?	This may not be answered from the current hydrodynamic study. Beyond its scope. Sediment samples can provide more insight.	
Colin Saunders	SFWMD	pages 31, 33, 35	The figures with cross sections of velocity in the L29 canals show "East" and "West" above the figures - but since this canal runs east-west, the figures should instead show North and South above the graphics, correct?	East and west is the convention used to define bank sides, looking downstream (independent of universal north). Will be clarified in text.	Addressed.
Colin Saunders	SFWMD	page 35	The columns of figures on the left (I presume) should say L-67A cross section velocity, not L-29.	Yes, it has been corrected.	Addressed.
Colin Saunders	SFWMD	Page 9, paragraph 2, bullet point #4	addition of vegetation buffers along marsh-canal edge as a solution for reducing velocities and creating sediment traps should consider the long-term, biogeochemical effects of high sediment (and P) accumulation in these areas. Should these buffers become sites of cattail invasion, then there is the potential for positive feedbacks that generate P-enriched sediments (promoting more cattail) which eventually enter the canal and get transported downstream through S-333.	Recommendation added in the report	Addressed.

Commenter Name	Agency	Page Number	Comment/Question	Response from SFWMD	Commenter Response
	FDEP	14	Scenario 1(Low Water Existing Condition) is described as a scenario where water levels are below marsh ground elevations (below 7.5 feet NGVD) and considers 3 conditions for low flow at 750cfs, normal of 1,500 cfs, and high flows of 2,500 cfs. Please consider redefining the low, normal and high flow conditions to be representative of actual field conditions and current operational scenarios. The current operations are determined by the Tamiami Trail flow formula which typically has much reduced flows during dry conditions and flows of 2,500 cfs or even 1,500 cfs would not be delivered through the S-333 structure during these dry conditions. The maximum flows should be capped at the design discharge for S-333 which is 1350 cfs as there never are flows during low stage conditions that exceed this threshold (the only scenario that the S-333 would deliver up to 1350 cfs is if the structure is used in combination with opening S-334 for water supply as was done pre-COP). For the normal and low flow conditions real data from COP operations should be used to set the flow scenarios. Normal flows are at or typically less than 750 cfs, and low flows would be in the order of 300-400 cfs during low stage conditions when we have the higher TP concentrations.	The most common operations occur at headwater stages between 7.5 ft-NGVD and 9.5 ft-NGVD. The current operations determined by the Tamiami Trail flow formula typically has much reduced flows during dry conditions and flows of 2,500 cfs or even 1,500 cfs would likely not be delivered through the S-333 structure during the dry conditions (low stages). Since operations of the S-333 complex is currently limited to 1,500 cfs (per FDEP permit and COP operations manual), flows up to 1,500 cfs can be described as the current condition scenarios, while flows up to 2,500 cfs was considered under potential future condition where operations may be changed under future operation plans to a maximum flow of 2,500 cfs once rest of the CEPP South system comes online (such as, with increased capacity at S-356E).	
	FDEP	14-15	Scenario 2 (High Water Existing Condition) is described as a scenario where the up-steam water levels are higher than 9.5-10.5 feet NGVD and high flows of 2,500 cfs are delivered through the S-333 gates. Since the Operations of the S-333 complex is currently limited to 1,500 cfs (per FDEP permit and COP operations manual) we recommend describing the current condition scenario as flows up to 1,500 cfs and only considering the potential future 2,500 cfs conditions under a potential future condition where operations may be changed under future operation plans to a maximum flow of 2,500 cfs once the rest of the CEPP south system is online (with S-356E increased capacity etc).	Discharge close to the design flow of S-333 (1,350 cfs) was considered as normal flow, while about half of it was taken as low flow. The 750 cfs scenario was considered low in this study. Flow lower than this is not expected to be a discharge of much sediment transport to the structures. S-333N design flow (1,150 cfs) combined with that of S-333 flow was assumed as high flow condition. The low, normal, and high flows cover the existing and anticipated flow conditions, including operation of S-333N Spillway.	
	FDEP	16	Table 2 includes three different scenarios. Please recognize in your discussions that more common operation scenarios will occur at stages between 1 and 2 (between 7.5 ft and 9.5 ft). Only recent years have shown flows under 7.5 ft.	See response to previous two comments	
	FDEP	23	Table 3. Please recognize that flows of 2,500 cfs at low stage won't occur. Adding a low flow run of 400 cfs (currently we typically see these types of flows during low stages) will better represent operations. Future phases should investigate high stage condition using a 1,500 cfs run for both the 8.5 feet stage and the 9.0 feet stage (representing current conditions where the max allowable discharge is 1500 cfs). In this report, please consider adding an asterisk to the 2,000 cfs low stage and the 2,500 cfs high stage runs indicating that these are future conditions.	Thank you for the suggestions. This could be considered in phase 2	

Commenter Name	Agency	Page Number	Comment/Question	Response from SFWMD	Commenter Response
	FDEP	57	The Department agrees that the study shows that low sill weirs in canals coupled with vegetation buffer around marsh can be more effective in reducing both marsh and canal velocities during high stage high flow scenarios as shown in Figure 24 of the report. However, we do not necessarily agree that this may be helpful in terms of reducing TP transport from the marsh into the canal and would recommend rewording the first conclusion to state that a vegetation buffer along west bank of L-67A and north bank of L-29 significantly reduce velocities in the marsh during high stages, but will not limit the surface water exchange during low stage conditions. Inflows from the marsh during high stage conditions tend to improve water quality being delivered down the Miami Canal and the L-67A canal (water quality improves moving from the north end of the system southward), and that restricting inflows during these conditions may worsen the water quality being delivered at the S-333 structure (even if the sediment transport during these high stages and flows would be higher).	The recommendation on vegetation buffer has been revised in the report. The near bed velocities in the marsh for high stage scenarios are already below the critical incipient velocity in marsh. While the vegetation buffer is effective, it can be costly. The current condition w/o the buffer is sufficient to minimize sediment transport from the marsh.	
	FDEP	57	The Department recommends including in the Concluding Remarks Section the reasons why the backfilling of the S12E spur canal was not simulated. This could reference page 12/64 which stated: "A CFD model scenario involving backfill of the S-12E intake basin on the tailwater side of S-333 for the purpose of demonstrating whether it may enhance the flow and sediment transport characteristics downstream of S-333 (per recommendation from the S-333 Working Group Evaluation Matrix) was also considered. However, past CFD runs (Zeng et al. 2018) of the S-333/S-333N complex indicated a dead hydrodynamic zone in this area. Consequently, it is not expected to have any significant impact on the flow field."	It has been added in the concluding remarks	
	FDEP	15	The scenario matrix for the CFD simulations assumed flow direction of the L29 from west to east. Please distinguish in this report between L29 (east of S333) and L29 west.	It has been clarified in report	
	FDEP	7	Last paragraph mentions informing engineering measures. Should this also include maintenance and operational solutions?	Operational solutions have been suggested in the results discussion section	
	FDEP	36-37	reference Figures 5.3, 5.4, 5.6 and more but the figures in this section starts at Figure 17. The previous section had Figures labeled 4.1, 4.2 etc. Please check the Figure numbering throughout the report and fix the references as necessary.	The error has been fixed.	
Cristina Gauthier	NPS	10	"In addition, impacts from rainfall **WERE** not considered." There are other past/present, plural/singular discrepancies throughout the document. Additionally, table and figure numbers need to be revised as they do not match in text/captions/Table of Contents.	The document has undergone a technical editing. Any discrepancy has been resolved. Table numbers were fixed.	Thank you for addressing. No further comment.
Cristina Gauthier	NPS	17	Model Results - Canal bottom elevations are confusing for L-29 canal and L-29. Throughout the document, L-29 canal is referred to as L-29. In this paragraph, it seems as if there are two different depths for the same canal (L-29). Is L-29 meant to be L-29 East? If so, please clarify in the sentence.	L-29 east and L-29 (west of S-333) has been clarified in the text	Thank you for addressing. No further comment.
Cristina Gauthier	NPS	27	Unclear why the assumption of 0.23 ft/s is made throughout the whole system and a value range is not used.	The value was recommended conservatively based on the lowest literature suggested values; 0.25 ft/s for canals and 0.34 ft/s for marsh. Needed to pick a specific critical velocity for assessing the sediment trap.	Thank you for addressing. No further comment.

Commenter Name	Agency	Page Number	Comment/Question	Response from SFWMD	Commenter Response
Cristina Gauthier	NPS	35	L-29 Cross Section Velocity (Fig. 4.3) - Do the curved/W-shaped velocities indicate disturbance in the middle of the channel?	The W-shaped velocities in the middle of L-29 is due to a bump in the canal bottom that caused local disturbance. Indicated in figure caption.	Thank you for addressing. No further comment.
Cristina Gauthier	NPS	41	Confused by Fig 5.6 and 5.7. How does vegetation increase flows in the canals?	The vegetation buffer increased the velocity in the canals as the marsh becomes disconnected from canals due to the vegetation buffer and flows defined in the model boundary setup primarily moves through the canals.	Thank you for addressing. No further comment.
Cristina Gauthier	NPS	43	Would cutting into the sides of the canals (sediment trap option 2) cause a long term effect that woud affect erosion?	The concern is the impact to either the marsh or levee. This analysis is beyond the scope of the current SOW.	Thank you for addressing. No further comment.
Rajendra Paudel	NPS	36 - 56	Section 5 and 6 Figures - Consider providing the direction of velocity fields in HEC-RAS and CFD output maps. Unclear from the maps how different conditions and engineering measures affect the distribution of water within the marsh.	Velocity field directions have been added.	Addressed.
Rajendra Paudel	NPS	37	Figure 19 - From the Manning's Coefficients map, it can be observed that open water channels are not represented realistically in the model (see Reference Figure below). Connected open water channels would distribute water very differently than the emergent marsh as assumed in this study. Reference Figure 	The phase I flow domain is the first 1800 ft on each side of the canal. The open water in this region was minimal and was not considered. Also, the open water channels mentioned in the comment are outside of the phase 1 model domain, hence no impact to the model results.	From satellite imagery, there is significant presence of open water chanels (not minimal). These channels create short-circuiting flows and transport nutrient preferentially. This will have impacts on the accuracy of flow distribution. Given the nature of the problem, it is critical to simulate the effects of these features in the model.
Rajendra Paudel	NPS	37	How were Manning's Coefficients obtained? - Were they calibrated, obtained from empirical modeling, obtained from the literature? - It is surprising that the "wet prairie" has 2.4 times higher resistance coefficient than the "emergent marsh". Is that reasonable? Please provide a clear explanation. Manning's n is a key parameter of flow dynamics in the modelling performed.	The manning's coefficients were defined based on the vegetation distribution in the model domain by adding spatially varying land use classification versus Manning's n value layer in RAS-Mapper. Canal and marsh flow resistance values were based on the vegetation resistance coefficients referred from literature and the Blue Shanty Flow Way Project, in which the Environmental Fluid Dynamics Code (EFDC) model has been calibrated. The questionable manning's n for the 'wet prairie' is outside the phase I model domain, hence no impact to results. However, this will be scrutinized further in Phase II.	Please elaborate on the second question. If it was derived from the literature, please provide references that show "wet prairie" has 2.4 times higher resistance coefficient than the "emergent marsh" in conditions similar to this study.
Rajendra Paudel	NPS	HEC-RAS Model General Question	From Google Maps, it can be seen that there exist higher elevation lands or thick vegetation along the edge of the marsh (banks of L-67 and L-29 canals). - How were these features represented in the model? - How were the interactions of flow between canals and marsh captured in the model? Please provide explanation.	They are treated as wall boundary in the model, the hydraulics between marsh and canal were driven by the flow physics of the CFD model, water follows the path of least resistance. Having said that, the regions considered in Phase I did not have sediment mound except on the north side of the L-29 canal.	What type of wall boundary? Interaction of flows depend on the natural of wall such as impermeable, porous, semi-porous etc. If the wall is not corretcly represented in the model, the flow physics of CFD model won't produce accurate results.

Commenter Name	Agency	Page Number	Comment/Question	Response from SFWMD	Commenter Response
Rajendra Paudel	NPS	HEC-RAS Model General Question	Was the canal simulated with the same model mesh of the marsh but with a difference in flow resistance and topography? If so, are those assumptions valid and reasonable? Please explain, a discussion would clarify concerns. Was coupling a 3-D canal model with a 2-D marsh model considered as a potential approach?	Canal and marsh had different resistance n-values. Mesh details have been added. No coupling of 2D and 3D, 2D hec-ras was an independent study for conceptual testing only	
Rajendra Paudel	NPS	HEC-RAS Model General Question	Please clarify how stage boundary conditions at the marsh were derived and set in the model for different HEC-RAS simulation runs (high stage/low stage, high/low discharge, and management/engineering measures). These different simulation scenarios would have different hydrologic conditions (i.e., stages) at the marsh boundary.	The upstream and downstream boundaries for each scenario were defined by the agreed upon stages identified in the report. Flows through S-333 and S-333N were set by flow hydrographs. A table in the report summarizes these scenarios.	My question was whether boundary conditions were iteratively identified for differnet management measures and stages that would produce different hydrologic conditions in the boundary OR was it treated as a sensitivity run by using management measures or stages and keeping everything same. I wanted to interpret results based on boundary conditions. Please specify the table you make reference to.
Rajendra Paudel	NPS	Throughout Document	Figure numbers do not match text (e.g. Figs. 5.5, 5.6, 5.7 are captioned as Fig. 21, 22, 23)	This has been fixed.	Addressed.
Rajendra Paudel	NPS	39	Before applying the model for evaluating management/engineering measures, it is essential to validate the model against observational data and ensure the robustness of the model. Provide more explanation regarding this important step. Current statement ("2D HEC-RAS model results compared well with the CFD results") is insufficient.	Calibration and validation of the CFD model is beyond the scope of this report. Having said that the CFD RANS model used was calibrated in numerous previous SFWMD studies (G420 pump station field measurements, peer-reviewed articles where this model was compared with laboratories measurements at gated structures and through bends). In Phase I, limited validation of 3D CFD was done using field measurements at S-333N. HEC-RAS results are depth averaged and is intended for proof of concept only. Mean velocity from CFD were compared to 2D depth averaged velocity in hec-ras to evaluate general agreement between two models.	It is essential that the model needs to be calibrated and/or validated before applications. If reasonable model parameter values are available from the literature, then validation may be adequate. Calibrated parameters may produce inaccurate results if applied to a field condion than is sufficiently different from the condition used in calibration because model parameters depend on local conditions. It is difficult to ascertain the applicability of this model without proper validation using field observations. I know CFD parameters have been calibrated in numerous studies. If they are valid in this study, please demonstrate how parameters obtained from laboratories or derived from other studies are reasonable by comparing their conditions. Please clarify what is meant by "limited validation".
Rajendra Paudel	NPS	39	What are the Manning's resistance coefficients used for for Vegetation 1 (low density) and Vegetation 2 (high density) buffers along the edge of the marsh?	Two vegetation densities defined by artificial manning's roughness region were simulated for the vegetation buffer, indicated as vegetation 1 (low density, manning's n=0.6) and vegetation 2 (high density, n=1.2). Deliberately high n-values were used to block marsh flow into the canals as a test of concept.	Partially addressed. Please provide this information in the report. Deliberately assigning high resistance value to block the flow makes sense but how do you know n=1.2 is reasobale? Why not 1.5 or 0.8? It begs clear justification because small changes in this parameter can have big impacts on flow volumes and distribution.
Rajendra Paudel	NPS	40	It can be seen that vegetation buffers reduce flow velocities in the marsh. - What would be the significance of reduction in marsh velocity? - Would there be increased flow velocity in both L-29 and L-67 canals? - What does it mean for TP concentrations upstream of S333 and what are the implications?	1. Yes, reduction in marsh velocity indicate less potential for sediment transport from marsh, i.e., lower likelihood of sediment entrainment in the marsh; 2. It increased the velocity in the canals as the marsh becomes disconnected from canals due to the vegetation buffer and flows defined in the model boundary setup primarily moves through the canals; less sediment transport indicate lower TP peaks; 3. potentially lower TP due to overall lower sediment entrainment rate.	Addressed.
Rajendra Paudel	NPS	42	HEC-RAS is a 2D model. How were "low sill weirs" represented in the model? - What are the assumptions behind simulating "low sill weirs"? - Was the ground surface elevation of the canal simply raised at the sill location? Please clarify.	To represent the low sill weirs in HEC-RAS, canal bed elevation was raised at the sill location. They were placed across the canal (about 90 ft wide, thickness 6 ft, slope: 1:2.5, top elevation -7.5 ft-NAVD) at 500 ft upstream from the structures	Addressed.
Rajendra Paudel	NPS	42	What is "meaningful improvement"? How is it being defined?	Reworded	Addressed.

Commenter Name	Agency	Page Number	Comment/Question	Response from SFWMD	Commenter Response
Rajendra Paudel	NPS	43	It is interesting to see the flow velocity reductions due to sediment traps. - Were sediment traps represented with different flow resistance values? - What would be the mechanism behind reducing the flow velocity?	No. resistance in channel and in the sediment trap were the same. Velocities reduced due to larger cross-sectional area of the flow at the sediment trap.	Addressed.
Rajendra Paudel	NPS	CFD Model General Question	It is not clear how stage boundary conditions at the marsh were derived and set for different CFD simulation runs (high stage/low stage, high/low discharge, and management/engineering measures)?	The headwater and tailwater elevations, treated as pressure inlet and outlet, were used for upstream and downstream boundary conditions. Desired flow through each structure was attained by controlling the gate opening estimated using site-specific rating equations. Agreed upon stage boundary for different scenarios were used as upstream boundary conditions. A table in the report summarizes these scenarios.	My question is misinterpreted (perhaps not clear). I wanted to know whether you adjusted stage boundary conditions in upstream of L-67A and L-29 when you simulated high and low stages at S-333? When there were high stages at S-333, you would also have high stages at upstream of these canals. My question was - did you adjust L-67A and L-29 canal unstream boundary conditions in response to changes in stages in S-333 and other management actions. Or, how did you capture such effects in the model scenario simulations?
Donatto Surratt	NPS	6	Third sentence "Frequent occurrences" consider referring to it as "Cyclic ocurrences"	Reworded	Accepted
Donatto Surratt	NPS	6	"the stage-TP inverse relationship is region-wide and applicable to canals that are not directly connected to Lake Okeechobee or the EAA". Where was this investigated. Please provide a reference.	All references were cited on page 6	It would have been preferred to have the citations go with each concept so that it becomes simpler to link each citation to its respective concept.
Donatto Surratt	NPS	9	Objective Section Question 1 - What are the future and anticipated stage and flow conditions based on?	CEPP South flow conditions	CEPP is not mentioned in this report. Discussion of this point should be provided so it is not left to the imagination of the reader.
Donatto Surratt	NPS	9	The marsh near the canal edge is already densely vegetated. Is this proposing a different vegetation than the existing one? (i.e. remove existing dense vegetation and replace with another type?	Deliberately high n-values were used to disconnect the marsh from canal and block marsh flow into the canals as a test of concept. We are not proposing a particular veg. type.	An explanation of present density, and if that is actually already serving this purpose, is missing.
Donatto Surratt	NPS	11	If there is is local and recent topography for the marsh, sharing the data would be helpful. Including a figure would also be helpful.	The topo is from the DTM that was provided by Miami Dade and USACE, and was put together by sfwmd geospatial staff.	A figure helping the reader understand the topography was not included. The explanation provided was also not included in the final report provided. This will continue to leave the reader assuming the district has data that is not available to the reader. The response provided does not match the report text, the district states they did the survey.
Donatto Surratt	NPS	11	The term DTM for surface elevations needs to be defined. Is this similar to Digital Elevation Model?	Reworded. digital elevation model (DEM)	Based on the final report we received, it is not reworded to DEM, instead a glossary is provide for DTM.
Donatto Surratt	NPS	13	CFD Model Applications - Model was used to simulate the improved flow field. What determines an improved flow field?	Reworded in the updated report. Lower velocities, ideally lower than incipient velocities = improved flow field.	Accepted
Donatto Surratt	NPS	14	Scenario 1 - How is 7.5 ft NGVD determined? Considering that the marsh itself is not flat, what assumptions are embedded in the "below marsh ground elevation" statement?	From terrain data, used average marsh elevation of 7.5 ft-ngvd. 7.5 ft NGVD is the stage at which the marsh starts to meaningfully separate from the canal. It is also a significant cut off number in the regulation schedule of WCA3A. Water supply to South Dade Conveyance System at S333/S333N for stages at 7.5 ft NGVD or lower must be made by equivalent amount from upstream water bodies (LOK).	Appreciate this response. This really needs to be field tested.
Donatto Surratt	NPS	14	Scenario 1 - Why is 750 cfs described as low? During the NPS study, flows were half this value.	Discharge close to the design flow of S-333 (1,350 cfs) was considered as normal flow, while about half of it was taken as low flow. S-333N design flow (1,150 cfs) combined with that of S-333 flow was assumed as high flow condition. These are conservative selections to obtain more critical velocity fields.	Appreciate the response. This would be bettered determined from observed flow to get us close to reality as possible.

Commenter Name	Agency	Page Number	Comment/Question	Response from SFWMD	Commenter Response
Donatto Surratt	NPS	14	Scenario 1 - Please describe how "normal flow" was determined. Define what is normal and if the flows selected were based on empirical data.	Discharge close to the design flow of S-333 (1,350 cfs) was considered as normal flow, while about half of it was taken as low flow. S-333N design flow (1,150 cfs) combined with that of S-333 flow was assumed as high flow condition. These are conservative selections to obtain more critical velocity fields.	Appreciate the response. This would be bettered determined from observed flow to get us close to reality as possible.
Donatto Surratt	NPS	14	Scenario 1 - When water stages were lower than the marsh, CFD simulations considered in-canal flows only. Doesn't this kind of gradient promote flow from marsh to canal? In the Refuge, when this condition occurs, particularly at the airboat cuts, we see waterfalls coming off the marsh.	At about 7.5 ft-NGVD, the canal flow starts to separate from the marsh flow. When headwater stages are lower than the marsh ground elevation, the predominant flow is the canal flow only. We expect possibly some limited flow from the marsh into the canal (mostly as groundwater contribution), but it is expected to be insignificant as far as sediment transport.	Appreciate this response. This really needs to be field tested.
Donatto Surratt	NPS	14	Scenario 2 - Simulations consider higher upstream water levels and overflow. - Is there anyway to include marsh runoff for Scenario 1 given you considered the marsh for Scenario 2? - At these higher stages (9.5, 10.5ft NGVD), concentrations at S333 tend to be low. Please explain how this scenario contributes to our understanding of the dynamics described in the objectives?	In scenario 1, there is no runoff from marsh to the canal. CEPP South operations need to be considered for future flows. At higher stages, discharges also tend to be higher. We needed to make sure these higher discharges do not translate into higher near bed velocities (erosive).	Response is acknowledged
Donatto Surratt	NPS	14	This exercise was focused on determining whether high TP is due to near or far field issues, or both. However, we generally do not have high TP under this higher stage water configuration.	Discussions were added in this regard	Response is acknowledged
Donatto Surratt	NPS	14	It is assumed L-67A flows north to south and L-29 flows west to east. Was empirical data used to guide this desicion? There seems to be an inherent bias that impacts the potential insights these model scenarios could provide if they were calibrated to empirical data.	No empirical data were used. This phase of the study focused on assessing velocities that induce sediment transport into S333/S333N in the vicinity of these structures. As such flow towards these structures in both L29 and L67A canals were considered. For scenario runs, an assumption needed to be made based on the objectives. There can be different flow direction split in field. L-29 can flow east to west, while L-67A north to south. Such cases were covered under NPS scenarios.	Response is acknowledged
Donatto Surratt	NPS	16	Table 2 - NPS provided an analysis of empirical data as a guideline to be used in these scenarios. We have suggested that empirically based assumptions be used but that suggestion does not appear to be incorporated.	Table 2 summarize the conditions agreed upon when we scoped Phase I of this study. The suggested additional scenarios from DOI (your field experiments) were subsequently simulated and are presented in Table 4.	In this response, it is not clear who agreed to these conditions. We objected and provided rationale for our objection. The table was modified some, but the scenarios continued to support evaluating high stage and high flow conditions.
Donatto Surratt	NPS	17	Model Results - The average ground elevation is stated as 7 ft-NGVD in the marsh on page 17, but 7.5 ft on page 14. How do the canal and marsh separate at 7.5 ft if the marsh is 0.5 ft lower? Is this suggesting that the disconnect ocurrs when there is less than 0.5 ft of water on the marsh surface?	At about 7.5 ft-NGVD, the canal flow starts to separate from the marsh flow. Hence, to simplify the model simulations, when water stages were lower than the marsh ground elevation, the CFD model setup considered in-canal flows only.	Response is acknowledged
Donatto Surratt	NPS	17	Low Stage Scenario - This section states that simulations considered in-canal flows only, as water stage was lower than the marsh ground elevation. An earlier statement in the report mentions the marsh floor is 7 ft, yet canal levels are being modeled at 7.5 ft. It would seem canal levels are higher than the marsh floor in this scenario. Please clarify.	At about 7.5 ft-NGVD, the canal flow starts to separate from the marsh flow. Hence, to simplify the model simulations, when water stages were lower than the marsh ground elevation, the CFD model setup considered in-canal flows only. Texts have been corrected. Also, see responses above regarding the 7.5 ft NGVD cutoff.	Response is acknowledged
Donatto Surratt	NPS	17	Low Stage Scenario - Near bed velocities in L-67A and L-29 decreased just upstream of the structures. Are the gates not able to move all the flows, resulting in some reverse turbulence at the gate and slowing of the velocities?	The decrease in near bed velocity near S-333 is due to deeper canal bed upstream of structures.	Response is acknowledged
Donatto Surratt	NPS	18	Low Stage Scenario - What does mean velocity represent? Does it include the entire vertical canal profile or is this talking about surface flow?	Mean velocity indicates the cross-sections averaged velocity, V=Q/A. clarified in text.	Response is acknowledged

Commenter Name	Agency	Page Number	Comment/Question	Response from SFWMD	Commenter Response
Donatto Surratt	NPS	18	Low Stage Scenario - It is stated that the approaching flow at the spillways was uniformly distributed without any strong potential of eddy formations. Based on visual observations during NPS study sampling events in 2022, eddies were apparent even at the low flows with one gate open. Please clarify what the 'no-eddy-formation assumption' is based on. Can a reference to past surveys supporting this assumption be provided?	What is meant here is there are no large recirculating eddies. There are some flow nonuniformity across the channel as expected. The report was clarified.	Response is acknowledged
Donatto Surratt	NPS	19	Please define and describe Froude number's importance. Seems to be related to wave making resistance or the Eddie statement below, but no thresholds of importance are provided to help the reader support statements about no Eddies, minimal Eddies, etc.	Froude number is a key nondimensional parameter in open channel flow. It is the ratio of initial forces to gravitational forces. It encompasses the effect of both depth and flow velocity. It is used to characterize flow in canals: Fr<1 subcritical flow, Fr= critical flow and Fr>1 supercritical flow. Since it strongly characterizes the flow physics (in gravity driven open channel flow) it is also useful to relate it to other parameters of interest.	We meant that it should be added to the report when having the identified discussion.
Donatto Surratt	NPS	20	Figure 3.7 shows the model results for headwater and tailwater at 2,500 cfs discharge, representative of high (design) flow condition. Previously in the text, 2000 cfs was defined as high flow for these same stage configuration. Unclear as to what is being defined as high. Please clarify.	high flows covers the 2000~2500 cfs range, clarified in text	Response is acknowledged
Donatto Surratt	NPS	20	Are we to assume Froude numbers in L67 and L29 are high and Eddies are formed?	No, Fr is relatively small as the flow is very subcritical	Response is acknowledged
Donatto Surratt	NPS	21	Simulations considered overflow within the marsh area. Please define "overflow". - Is this defined as flow over the brim? If so, what is it flowing over and to where?	Meant flow from the marsh into the canal. These simulations considered marsh-canal interaction.	Response is acknowledged
Donatto Surratt	NPS	23	Table 3 - Can marsh velocities be summarized here side-by-side?	There are only two cases (high stage scenarios) where marsh velocity is reported, mentioned in text.	Response is acknowledged
Donatto Surratt	NPS	27	Sediment size in the marsh was 0.45mm, translating to an incipient velocity of 0.34 ft/s. Is that velocity the threshold necessary to move 0.45 mm sized particles? How is this being decided? The nomograph appears to provide a range of velocities at each particle size. How is this being decided?	See the Mavis and Laushey (1948) equation, that is based on bottom velocity. This threshold velocity is based on Mavis and Laushey (1948) relation presented in the report. Yes, the other nomogram (Hjulstrom) provides a range. However, for practical purposes Mavis and Laushey is used in this statement.	Response is acknowledged
Donatto Surratt	NPS	27	The near bed velocities should be limited to 0.25 ft/s to avoid sediment transport at S-333/S-333N. What does this all mean in terms of real world operations? - Does this mean decrease flow rates? - Does it mean flows observed during low stage and empirical low flow conditions are not entraining sediments?	1. It means current real-world operations at times are conducive to sediment transport. 2. No decrease in flow rates, but create conditions where flow is unaffected, but velocities are reduced to acceptable levels (by widening or deepening of the canal, or both). The engineering solutions were geared towards reducing flow velocities in marsh and canals, not the discharge itself, the sediment trap or low sill weir is not expected to impact flows to the ENP. 3. No, low flow conditions are still entraining sediments, that is why remedial measures are developed.	Accepted
Donatto Surratt	NPS	28	"S-333 DBHYDRO flows, gate openings, and head and tailwater stages given in the table show average for the duration of the ADCP measurement taken in front of S-333." Please review this statement. The table shows the values for the sample event dates. Using the term "average" may mislead the reader to believe all measurements shown on the table are averages.	Edited in table	Accepted
Donatto Surratt	NPS	30	Figure 14 - Can the colors be described relative to entrainment thresholds? Red would be considerable entrainment, yellow would be moderate, etc.	This can be misleading; color scheme depends on range of velocities and number of color selected in the figure.	Response is acknowledged

Commenter Name	Agency	Page Number	Comment/Question	Response from SFWMD	Commenter Response
Donatto Surratt	NPS	36 - 37	Figures 17 through 19 - Please make sure legends are legible	Figures have been improved	Accepted
Donatto Surratt	NPS	37	Figure 19 - Why does Wet Prairie have a higher roughness coefficient than Emergent Marsh or Mixed Marsh? What assumptions were made? Is it based on empirical data? Please consider adding a reference.	Agreed - this is due to the oversimplification of HEC-RAS in this region. The 'wet prairie' is outside the selected near field model domain in this phase, hence no impact to the results. Again as stated above HEC-RAS was not rigorously developed for design purposes. Future phases of the project (HEC-RAS 2D for large area of WCA3A) will rigorously treat open prairies differently than was done in this study.	Response is acknowledged
Donatto Surratt	NPS	38	Upstream and downstream boundary conditions were defined by stages, using uniform time series. What stage measurements were used (on either canal) at 2000 ft upstream of S333? Do they have gages? Is this empirically verified?	The HW/TW stages indicated in table 2 are the stages assigned in model. No measurements are needed for this purpose	Response is acknowledged.
Donatto Surratt	NPS	38	The same scenarios identified for Phase I (Table 3.2) were simulated using HEC-RAS. If this statement is referring to Table 2, that table has assumptions and cannot be defined as Existing Conditions. Perhaps this statement is referring to Table 4, which depicts real world conditions. Please clarify.	reworded	Response is acknowledged
Donatto Surratt	NPS	38	Figure 20 - What is the information in the legend (unitless)? How is the extreme contrast between red and blue in the marsh explained? Does the blue in the marsh have anything to do with the legends?	Edited in fig. caption. Blue in the marsh are velocities less than 0.8 ft/s. The red colors in the marsh are topo and beyond the flow domain.	Response is acknowledged
Donatto Surratt	NPS	39	"Based on preliminary discussions with the Working Group, some engineering measures were identified" Please re-write the sentence as the engineering solutions identified to be modeled were selected by SFWMD staff. NPS staff raised concerns about the use of a vegetation buffer to managing marsh pulls to the canal.	reworded. Unless I misunderstood this, my recollection is that NPS strong objections were about the use of berms to separate the marsh from the canal. Vegetation buffer were the compromise. Are you saying NPS is not comfortable with the use of vegetation buffer either?	We did not support marsh or marsh vegetation modifications.
Donatto Surratt	NPS	39	Vacuum dredging is another potential engineering solution now discussed for several years - not being considered here. It needs to be considered as an engineering solution to remove loose sediments in the canal bed.	We don't have enough info to say we are or not opposed to this. We just need to discuss further to clarify what is meant by vacuum dredging, its potential benefits, Impact on flow field, its constructability and any potential permitting challenges.	This response is appreciated and interpreted to mean that dredging could be modeled.
Donatto Surratt	NPS	39	Can vegetation densities (Vegetation 1, Vegetation 2) be stated in terms of the roughness coefficients? The highest coefficient was defined for wet prairie, so is Vegetation 2 denser than wet prairie? Please note, in the real world, vegetation along the marsh-canal interface is exceptionally dense. It is dense to the point that NPS could not access the marsh through these boundaries to collect samples. We had to enter through L29 along the forced airboat trails.	Two vegetation densities defined by artificial manning's roughness region were simulated for the vegetation buffer, indicated as vegetation 1 (low density, manning's n=0.6) and vegetation 2 (high density, n=1.2). Deliberately high n-values were used to block marsh flow into the canals as a test of concept. See comments above on wet prairies.	Response is acknowledged
Donatto Surratt	NPS	39	Results show that the vegetation buffer can reduce flow velocities significantly in the marsh. Is this relative to existing conditions? How can one make the marsh boundary more dense than it already is?	They are relative to baseline scenarios. Vegetation buffer scenario is for conceptual testing only. Use wider vegetation strip along the banks if it cannot be made denser than it is now.	Response is acknowledged
Donatto Surratt	NPS	39	There are some sediments mounds along the north bank of L-29 Canal and west bank of L67A that can locally affect flow from the marsh into the canals. These mounds are loaded with shrubby vegetation denser than wet prairie and emergent vegetation. How is that accounted for?	Mounds along the north bank of L29 are in the model as seen from the topo data. They are treated as wall boundary in the model, and the hydraulics between marsh and canal were driven by the flow physics in CFD model, water follows the path of least resistance.	This response is appreciated. Hopefully the text was adjusted to clarify.

Commenter Name	Agency	Page Number	Comment/Question	Response from SFWMD	Commenter Response
Donatto Surratt	NPS	39	Sediment mounds on the west bank of L-67A canal were outside the modeling domain for Phase I. Smaller built up vegetation mounds (shrubby, trees, etc.) appear to be within the model domain based on Google Earth. Are these not considered?	All features captured in the DTM terrain data were considered in the model.	Response is acknowledged
Donatto Surratt	NPS	40	Figure 22 - It would be excellent if this was empirically evaluated as there seems to be some disconnect between model assumptions and real world dynamics.	Again see comments on HEC-RAS 2D. Was used it as a mean to test a concept and do reality check on the subsequent CFD and to provide relative impact of proposed features. It was not rigorously developed for design purposes.	Response is acknowledged
Donatto Surratt	NPS	42	The low sill weirs were found to reduce the canal velocities slightly (Figure 5.8). Does this account for potential stratification of the canal velocities? Can this be used to assert that near canal bed velocities are more reduced?	Low sill weir is not modeled yet in CFD	Response is acknowledged
Donatto Surratt	NPS	42	Figure 24 - HW 9.5 ft-NGVD, TW 9.0 ft-NGVD, Q total 2500 cfs. These configurations seem exactly the same as for the two plots above. How did the W/O low sill weir maps come out with different results?	Corrected	Accepted
Donatto Surratt	NPS	43	Figure 25 - HW 9.5 ft-NGVD, TW 9.0 ft-NGVD, Q total 2500 cfs. Is 0.18 ft/s already below the entrainment threshold according to the nomograph? This report referenced 0.34 ft s-1.	Yes, that's the right interpretation	Response is acknowledged
Donatto Surratt	NPS	44	Low sill weirs upstream of the spillways could prevent bedload movement from flushing to the downstream. Given the modeled reductions in flow rates, how does this impact flow to the park, particularly during the dry season?	The flow rates did not decrease, flow velocity did. Engineering solutions were geared towards reducing flow velocities in marsh and canals, not the discharge itself, the sediment trap or low sill weir is not expected to impact flows to the ENP.	Response is acknowledged
Donatto Surratt	NPS	47	With higher discharges, the decrease in near bed velocities is not as large due to the sudden drop in canal bed at the sediment trap. Not as large as what?	Clarified	Response is acknowledged
Donatto Surratt	NPS	57	"THE" objective of this project…	Corrected	Response is acknowledged
Dilip Shinde	NPS	6	Outcome # 2 of previous investigations makes reference to fine and organic-rich materials at a site west of S-12D in the L-29 Canal. We do not recall a sample west of S12D. We did take samples in L29 west, but they were away near S12C and S12B.	It is out of phase 1 CFD model domain	Not addressed. Please cite reference.
Dilip Shinde	NPS	9	Phase I Objective 4 - What is exactly meant by horizontal velocity distribution and does it consider variation in only X & Y directions? Is Z direction considered to have no variation? At least in the canal, this is not true (based on ADCP data).	near bed velocity	Addressed.
Dilip Shinde	NPS	11	The text notes that the CFD model domain was extended to about 1,500 ft of the inflow canals, however, further down it says that the upstream boundary was situated about 1800 ft upstream. Please correct this inconsistency.	Corrected	Addressed.
Dilip Shinde	NPS	13	Table 1 - What does AARE stands for? Please show the equation.	Equation was added, AARE abbreviation has been added	Addressed.
Dilip Shinde	NPS	14	Cyclic analysis of stages at S-333 - The duration presented is 1978-2021. However, this duration should have been limited to ERTP+COP period to represent current and recent past conditions, which probably should have been more appropriate.	It will be added based on schedule constraints	

Commenter Name	Agency	Page Number	Comment/Question	Response from SFWMD	Commenter Response
Dilip Shinde	NPS	15	High Stage Scenario - Evaluating this scenario is fine based on gates total discharge capacity. However, the frequency of this scenario occurring should be discussed. In addition, when does the probability of this scenario occur (month) and does it coincide with TP peaks?	The current operations determined by the Tamiami Trail flow formula typically has much reduced flows during dry conditions and flows of 2,500 cfs or even 1,500 cfs would likely not be delivered through the S-333 structure during the dry conditions (low stages). Since operations of the S-333 complex is currently limited to 1,500 cfs (per FDEP permit and COP operations manual), flows up to 1,500 cfs can be described as the current condition scenarios, while flows up to 2,500 cfs was considered under potential future condition where operations may be changed under future operation plans to a maximum flow of 2,500 cfs once rest of the CEPP South system comes online (such as, with increased capacity at S-356E).	Not addressed. Response is not related to comment on frequency of scenario occurrence in the past and projected future, and the probability of the scenario occurrence during TP peak period.
Dilip Shinde	NPS	15	Figure 3 needs improvement. These are very important measures of sediment transport control and they are decribed ambiguosly. "Probable sediment trap locations" can be misleading. Please state what was actually simulated. Is the red line running around the canals a sediment trap or is the sediment trap located somewhere within that area? Also, the low sill weir is barely noticeable in the figure. Two different enlarged section maps clearly showing the details of the sediment trap and low sill weir, with their dimensions and orientations, are needed. A supplementary table (or Table 2) should include key data such as dimensions, which are missing in the methods section.	Discussion has been added, figure caption was updated	Addressed.
Dilip Shinde	NPS	15	Figure 3 - Why does this figure show 1000 ft in both sections when the simulation domain was 1850 and 2000 ft in L67A and L29 canals, respectively.	Corrected	Addressed.
Dilip Shinde	NPS	15	The statement that flows from L29 are from west to east is unrealistic. Our field measurements for two years (2021-2022) show flows also happen from east to west in high volumes. These field measurements have been shared multiple times. In addition, Table 2 must show how much flows are coming from L29 and L67A.	This phase of the study focused on assessing velocities that induce sediment transport into S333/S333N and in the vicinity of these structures. As such flow towards these structures in both L29 and L67A were considered. Hence, for the CFD scenario modeling, it is assumed that the flow direction in L-67A is from north to south, while in L-29 is from west to east. There can be real-time occurrences when flow in L-29 moves from east to west. Modeling results of such field conditions are presented in Section 4.0.	For engineering solutions purpose if flows in L29 are considered to occur towards S333, one would then consider building sediment trap and weirs in L29 to stop sediment transport towards S333, which would be unrealistic.
Dilip Shinde	NPS	16	Table 2 - Add inflows from L29 and L67A	They are computed in model based on hydraulics.	Computed flows from model based on hydraulics can be shown in Table or in text.
Dilip Shinde	NPS	17-21	Near bed velocities at the Low Stage Scenario - For all simulations in this scenario, please specify at what distance from gate the velocity decreased. This decrease can be misleading because cross-sectional area reduces as water moves through the gate. If possible, please report what were the values at 10, 30, and 50 ft in front of the gates.	It will be added based on schedule constraints	
Dilip Shinde	NPS	17-21	For all simulations in this scenario, please specify at what height from the canal bed are these reported "near bed velocities" measured (i.e. 5 cm, 10 cm)?	Added in the report	Addressed.
Dilip Shinde	NPS	18 - 21	Figures 5, 6, 7 - Needs to show 1) inflows (cfs) at L67A and L29 inlets, 2) outflows (cfs) going out of S333 gates, 3) gate openings and stages. This would provide a complete and easy to follow picture of the simulation.	It will be added based on schedule constraints	

Commenter Name	Agency	Page Number	Comment/Question	Response from SFWMD	Commenter Response
Dilip Shinde	NPS	18 - 21	Figures 5, 6, 7 - The bottom graph does not convey much if the intent is to show cross-sectional flows. One recommendation is to include a couple of cross-sectional graphs (i.e. one closer to the gate, one in middle and another closer to the inlets) to improve upon this figure.	It will be added based on schedule constraints	
Dilip Shinde	NPS	21	High Stage Scenario - The statement "These simulations considered overflow within the marsh area" is a bit ambiguous. Is this meant to say overflow from marsh to canal or from canal to marsh?	Reworded in the updated report, meant exchange between canal and marsh	Addressed.
Dilip Shinde	NPS	22	Figures 9 & 10 - From these velocity contour plots, it appears water is flowing from canal to marsh. Can we see flow vectors also in the plots, mainly in marsh area to get a clear sense of direction of flows. What was the marsh stage set to? Please clarify. Also please show inlet flows from L29 and L67A.	It will be added based on schedule constraints	
Dilip Shinde	NPS	23	Table 3 - Please show the near bed velocities at 10, 30, and 50 ft in front of the gates.	It will be added based on schedule constraints	
Dilip Shinde	NPS	27	It is stated that flow conditions between 1500-2000cfs are less likely to occur based on the typical operation of the S-333 and S-333N. It is worth noting that high flow conditions only occur later during the season at high stage, when TP peaks have already receded. Results from high flows scenarios, though useful, should not be related to TP peaks period, early wet season.	Please see previous responses. Related discussion were added in report	
Dilip Shinde	NPS	27	The statement "there is less potential of sediment transport from the marsh into the canals" is not evident from Figures 9 & 10. In the figures, it is not clear which direction is the flow. It appears from velocity contours that it is from canal to marsh. In that condition, if transport occurs, it will be sediment to the marsh. Please show flow vectors on Figures 9 & 10.	Flow directions were added on all figures	This comment relates to flow direction in marsh portion not in canal.
Dilip Shinde	NPS	27	For the statement "the near bed velocities should be limited to about 0.25 ft/s to avoid the adverse sediment transport concerns at S-333/S-333N." Was this conclusion reached based on some analysis or is it referring to published literature. Please provide a reference.	The critical velocity value was recommended conservatively based on the lowest literature suggested values; 0.25 ft/s for canals and 0.34 ft/s for marsh. See Mavis and Laushey (1948).	Addressed.
Dilip Shinde	NPS	28	Note: The NPS team collected sediment AND WATER samples in the study area during April-June 2022. The objective was to characterize the sediments in the marsh, canal , AND IN WATER.	Added in the report	Addressed.
Dilip Shinde	NPS	31	Figure 4.1, 4.2, 4.3 - L29 should be marked North and South. In addition, it would be of value to examine how the cross-sectional velocities look like near the S333 gate due to its lift gate configuration. Is it possible to add cross-sectional graphs at 30, 50, and 75 ft from the gate? This would allow for some comparison to ADCP data.	East and west is the convention used to define bank sides, looking downstream (independent of universal north). It has been clarified in text. The rest of the comment will be added based on schedule constraints.	Addressed.
Dilip Shinde	NPS	36	Shouldn't the manning's coefficients be defined based on vegetation distribution in the model domain? Why is it the other way round?	corrected	Addressed.
Dilip Shinde	NPS	36	Figure 17 - Please enlarge text and color ramp. Consider adding colors to the table in Figure 19.	Figures have been improved	Addressed.

Commenter Name	Agency	Page Number	Comment/Question	Response from SFWMD	Commenter Response
Dilip Shinde	NPS	36	Model Development - Application of HEC-RAS limits the results from simulations, particularly in canal sections. Being a 2D model, the 'z' dimension is considered uniform velocity. This appears to be a questionable assumption, specifically in the canal section. We already saw the variation in CFD simulations in the canal cross-sections vertical profile (near bed vs surface velocity). Figure 9 & 10 show the CFD model has covered the same model domain as the HEC-RAS and it does not have this assumption and limitation. It is not clear what extra information HEC-RAS brings to the table by relaxing the crucial "z" dimension velocity distribution, specially in the canal. Can HEC-RAS be restricted to marsh region only up to canal edges and use the results to set boundary conditions for CFD model in L29 and L67A along the marsh edges? Using HEC-RAS to describe what is happening in canal at close vicinity to S333 gate can be misleading as it does not decsribe the velocity variation in vertical profile ("z" dimension).	HEC-RAS was done as a reality check on the CFD and were quick simulations intended only for primary proof of concepts before establishing additional CFD models. HEC-RAS was not rigorously developed for design purposes. All recommendations were made based on CFD results.	Recommendation on the effectiveness of weir is based on HEC-RAS. It is suggested that weirs are not much effective based on HEC-RAS simulation. The provided response that all recommendations were made based on CFD results is not correct.
Dilip Shinde	NPS	37	Figure 19 - Please enlarge the text. ID Marker should be marked on the map to orient the reader. It is not clear what color is which ID. As an observation, the NE corner of WCA3A has dense vegetation near the edge of the canal. Manning's N should be high there.	Figures have been improved	Addressed.
Dilip Shinde	NPS	39	More details should be provided to support the statement "2D HEC-RAS model results compared well with the CFD results." What was actually compared and at what locations? How were differences in compared parameters evaluated? Futher, please provide details on the run times cited.	2D HEC-RAS model results (depth averaged velocity) compared well with the CFD results (mean velocity). Overall, similar flow field patterns were observed in both models.	No response on details of run times for CFD model. Run times are implied as limitation for CFD model application and reason for using HEC-RAS for low sill weir evaluation.
Dilip Shinde	NPS	39	Vegetation Densities - Please provide more details on the dimensions of vegetation buffers used and roughness coefficients assigned to bufferred and non-buffered areas.	Discussion has been added. Also see previous responses	Addressed.
Dilip Shinde	NPS	42	Low sill weirs - Please provide detales on weir sizes. In Figure 3, the weir location shown is in front of S333. What distance was it located from S333 and how high was the weir sill from the canal bed?	To represent the low sill weirs in HEC-RAS, canal bed elevation was raised at the sill location. They were placed across the canal (about 90 ft wide, thickness 6 ft, slope: 1:2.5, top elevation -7.5 ft-NAVD) at 500 ft upstream from the structures.	Addressed.
Dilip Shinde	NPS	42	Figure 24 - Do the mean velocities in these figures refer to: The whole flow system? Paticular canal sytem? Marsh sytem?	Mean velocity over the model domain indicates the whole flow system including canals and marsh. It was omitted in the final report to avoid any confusion.	Addressed.
Dilip Shinde	NPS	47	CFD Modelling - Why was low sill weir not evaluated using CFD? HEC-RAS is 2-D only, whereas CFD evaluates the verticle flow profile which is important in the canal section, especially close to the gate. Without thoroughly investigating influence of weir on verticle profile using CFD, which is more appropriate tool, weir can not be discounted as not a useful measure in reducing sediment transport. We can not rely on 2-D model results for discounting low-sill weir's efficiency.	Low sill weir is yet to be modeled in CFD.	Comment #114 states that "All recommendations were made based on CFD results". However, this response contradicts the earlier one.
Dilip Shinde	NPS	47	For the statement "sediment trap decreased near bed velocities from 0.76 ft/s to 0.58 ft/s" please clarify if this is the average drop value, the drop at a particular location, or the drop within the trap.	Clarified in text	Addressed.

Commenter Name	Agency	Page Number	Comment/Question	Response from SFWMD	Commenter Response
Dilip Shinde	NPS	47	For the statement "Comparing the velocity magnitudes with Hjulstrom's curves", Hjulstrom's curves are mentioned to be appropriate for flow depth of 1 m. How appropriate is to derive conclusions for flows several meters higher?	Hjulstrom's curves were used for comparison. The nomogram (Hjulstrom) provides a range. However, for practical purposes, the suggested critical velocity criteria based on Mavis and Laushey (1948) were lower than what Hjulstrom's curves suggests.	Addressed.
Dilip Shinde	NPS	57	Concluding Remark #3 - Low sill weir was not appropriately evaluated using CFD? HEC-RAS is 2-D only, whereas CFD evaluates the vertical flow profile which is important in the canal section, especially close to the gate and also where the weir is located. Without thoroughly investigating the influence of low sill weir on verticle profile using CFD, the conclusion is not appropriate. We can not rely on 2-D model results for discounting low-sill weir's efficiency. We recommend CFD to evaluate low sill weir before removing it from consideration as not being effective. Additionally, near bed velocities mentioned here can not be evaluated from HEC-RAS 2-D model.	Low sill weir is yet to be modeled in CFD.	Comment #114 states that "All recommendations were made based on CFD results". However, this response contradicts the earlier one.
Lori Miller	USFWS	Overview	When the studies were in development, the intent, as I remember, was to find the source of high TP being "released" from the S-333 complex during primarily low water stages and to evaluate the hydro-dynamics involved. Where is the higher TP coming from to begin with? The surrounding marsh of WCA-3 generally speaking has lower TP so that leads us to canal source or some other localized sources directly around the pump station and spillways. Is it a "localized driver" directly located at the S-333 complex? Or is it ultimately a "regional driver" with upstream sources moving into and through the L-67 canal, for example? If the source is regional then we have to include the assumption that high TP could be entering the L-67 near the S-9 or even higher upstream. Lake O and the EAA waters are not out of the question due to the connecting canals from the L-37 all the way through the EAA and up to Lake O or the Miami Canal. So, I don't think we can discount this connection YET. I am not attempting to make the connection to Lake O and the EAA. I just don't think we are ready to discount some influence from these areas just yet.	Identifying regional sources of TP was not a component of the Phase I hydrodynamic study. Having said that, Phase I hydrodynamic findings do show erosive velocities in L67A and L29 when stages are low and discharge are 750 cfs and 1500 cfs. This, at a minimum, suggests a potential localized source of TP (from entrained near bed sediment) under certain flow conditions. That, of course, does not discount additional potential regional sources of TP (Yet To be determined from subsequent phases of this joint hydrodynamic/sediment study).	
Lori Miller	USFWS	4.0 Field Conditions	An interesting find within the study was the fact that the S-333 complex can and does flow westward during higher discharges. This could explain some of the higher TP also found at times at the S-12D and perhaps even S-12C.	Just to be clear, S333 complex does not flow westward (i.e., no reverse flow at S333 complex). Rather the flow in L67A under certain conditions such as those encountered during NPS sampling can split between what S333 complex takes and what loops around the junction of L67A and L29 and head west towards S12D. That is by design; in order words, Tamiami Flow Formula (on which releases from WCA3A are based on) intent at times is to split flow between S333 and S12D.	
Lori Miller	USFWS	6.0 Engineering Measures	I'm trying to remember which WG meeting it was decided to further evaluate sediment traps upstream as stated in the study?	Sediment traps is number 1 of the initial 11 engineering, maintenance, and operational solutions to be evaluated in either phase I or phase II. Sediments traps was included in the phase I SOW to be evaluated.	

Commenter Name	Agency	Page Number	Comment/Question	Response from SFWMD	Commenter Response
Lori Miller	USFWS	7.0 Conclusions	Modeling conclusions are beginning to show some promise for sediment maintenance strategies for the incitement of higher TP during low flow and low stage conditions at the S-333 complex. Some maintenance strategies are mentioned in the study's conclusion including vegetation buffers and sediment traps. I'm still hoping that all current and future studies will lead to corrective strategies if sources of the higher TP are found in a regional connection. This should be our next step.	Noted. Thank you.	

ATTACHMENT 3: ALTERNATIVE RECOMMENDATIONS FOR ENGINEERING AND MAINTENANCE SOLUTIONS

Alternative implementation options of the recommended engineering and maintenance solutions are described below. **Figures 1** through **7** depict the alternative options. **Table 1** provides a breakdown of the alternative options, including cost estimates and an implementation schedule. The implementation schedule is based on standard industry durations for design, permitting, and construction.

CANAL MAINTENANCE DREDGING

Four distinct segment canal maintenance dredging options upstream of the S-333 structures are presented below.

- Option 1 includes maintenance dredging 750 feet directly upstream of the S-333 structures in both the L-67A and L-29 canals (**Figure 1**).

- Option 2 includes maintenance dredging 1,500 feet directly upstream of the S-333 structures in both the L-67A and L-29 canals (**Figure 2**).

- Option 3 includes canal maintenance dredging 750 feet upstream of the S-333 structures in the L-67A canal or L-29 canal (**Figures 3** and **4**).

- Option 4 includes canal maintenance dredging 1,500 feet upstream of the S-333 structures in the L-67A canal or L-29 canal (**Figures 5** and **6**).

CANAL MAINTENANCE DREDGING ACTIVITIES AND DURATIONS

The identified durations below for design, permitting, and construction are standard industry durations and could be reduced and fast tracked by establishing priorities and additional resources.

- Pre-Maintenance Dredging Survey (Option 1, Option 2, Option 3, or Option 4) – 45 days

- Pre-Maintenance Geotechnical Testing (Option 1, Option 2, Option 3, or Option 4) – 45 days

- Project Plans and Specifications (Option 1, Option 2, Option 3, or Option 4) – 60 days

- Florida Department of Environmental Protection (FDEP) State 404 General Permit for Maintenance per 62-331.210, Florida Administrative Code – 60 days

- FDEP exemption per 403.813(1)f, Florida Statutes – 30 days (to be completed in parallel with the FDEP State 404 General Permit)

- United States Army Corps of Engineers (USACE) Section 408 not required for maintenance dredging; however, this determination will be made following development of the detailed scope of work – 30 days (to be completed in parallel with the FDEP State 404 General Permit)

- Dredging Contract Solicitation/Construction (Option 1, Option 2, Option 3, or Option 4) – 60 days

- Maintenance Dredging:
  - Option 1 – 180 days
  - Option 2 – 240 days
  - Option 3 – 90 days
  - Option 4 – 120 days

- Post-Maintenance Dredging Survey (Option 1, Option 2, Option 3, or Option 4) – 45 days

Total Project Duration:

- Option 1 – 495 days
- Option 2 - 555 days
- Option 3 - 405 days
- Option 4 - 435 days

CANAL MAINTENANCE DREDGING COST ESTIMATES

- Option 1: Maintenance Dredging Cost Estimate 750 feet upstream of the S-333/333N complex in both the L-67A and L-29 canals – $1,651,573.38.

- Option 2: Maintenance Dredging Cost Estimate 1,500 feet upstream of the S-333/333N complex in both the L-67A and L-29 canals – $2,313,574.01

- Option 3: Maintenance Dredging Cost Estimate 750 feet upstream of the S-333/333N complex in the L-67A canal or L-29 canal – L-67A canal only: $1,063,167; L-29 canal only: $1,241,229.

- Option 4: Maintenance Dredging Cost Estimate 1,500 feet upstream of the S-333/333N complex in the L-67A canal or L-29 canal – L-67A canal only: $1,273,821; L-29 canal only: $1,752,734.

LOW-SILL WEIR PILOT TEST

Three distinct low-sill weir placement options are presented below. All weir configurations can be optimized to synchronize with any selected dredging option identified above. The placement of the low-sill weirs (GeoTubes) as identified in the following options with figures are approximate, subject to minor field adjustments and range from 4 to 7.5 feet high. Exact locations and height will be determined during the design and permitting phase for the low-sill weirs (GeoTubes).

- Option 1 includes the installation of GeoTubes (short height) along the canal bottom in both the L-67A and L-29 canals at the upstream terminus of the maintenance dredging upon dredging completion (**Figure 7**). This option includes GeoTubes placed in two locations.

- Option 2 (includes Option 1 above) includes the installation of GeoTubes (short height) across the canal bottom in both the L-67A and L-29 canal at the upstream terminus of the maintenance dredging upon dredging completion, and another set of GeoTubes (tall height) across the canal bottom in both the L-67A and L-29 Canals 300 feet upstream of the S-333/S-333N complex (**Figure 7**). This option includes GeoTubes placed in four locations.

- Option 3 (includes Option 1 and Option 2 above) includes the installation of GeoTubes (short height) along the canal bottom in both the L-67A and L-29 canals at the upstream terminus of the maintenance dredging upon dredging completion, another set of GeoTubes (intermediate height) in both the L-67A and L-29 canals 900 feet upstream of the S-333/S-333N complex, and another set of GeoTubes (tall height) along the canal bottom in both the L-67A and L-29 canals 300 feet upstream of the S-333/S-333N complex (**Figure 7**). This option includes GeoTubes placed in six locations.

LOW-SILL WEIR ACTIVITIES AND DURATIONS

The identified durations below for design, permitting and construction are standard industry durations and could be reduced and fast tracked by establishing priorities and additional resources.

- Project Plans and Specifications - Option 1, Option 2 or Option 3 – 60 Days
- Permitting - Option 1, Option 2 or Option 3 - 270 Days
  - FDEP State 404 – 120 Days
  - FDEP - General Permit - 30 Days (To be completed in parallel with the FDEP State 404)
  - USACE - Section 408 -90 - 270 days
- Low-Sill Weir Contract Solicitation/Construction - Option 1, Option 2 or Option 3 - 60 Days
- Low-Sill Weir Installation:
  - Option 1 - 60 Days
  - Option 2 - 90 Days
  - Option 3 - 120 Days

Total Project Duration:

- Option 1 – 450 days
- Option 2 – 480 days
- Option 3 – 510 days

LOW-SILL WEIR COST ESTIMATES

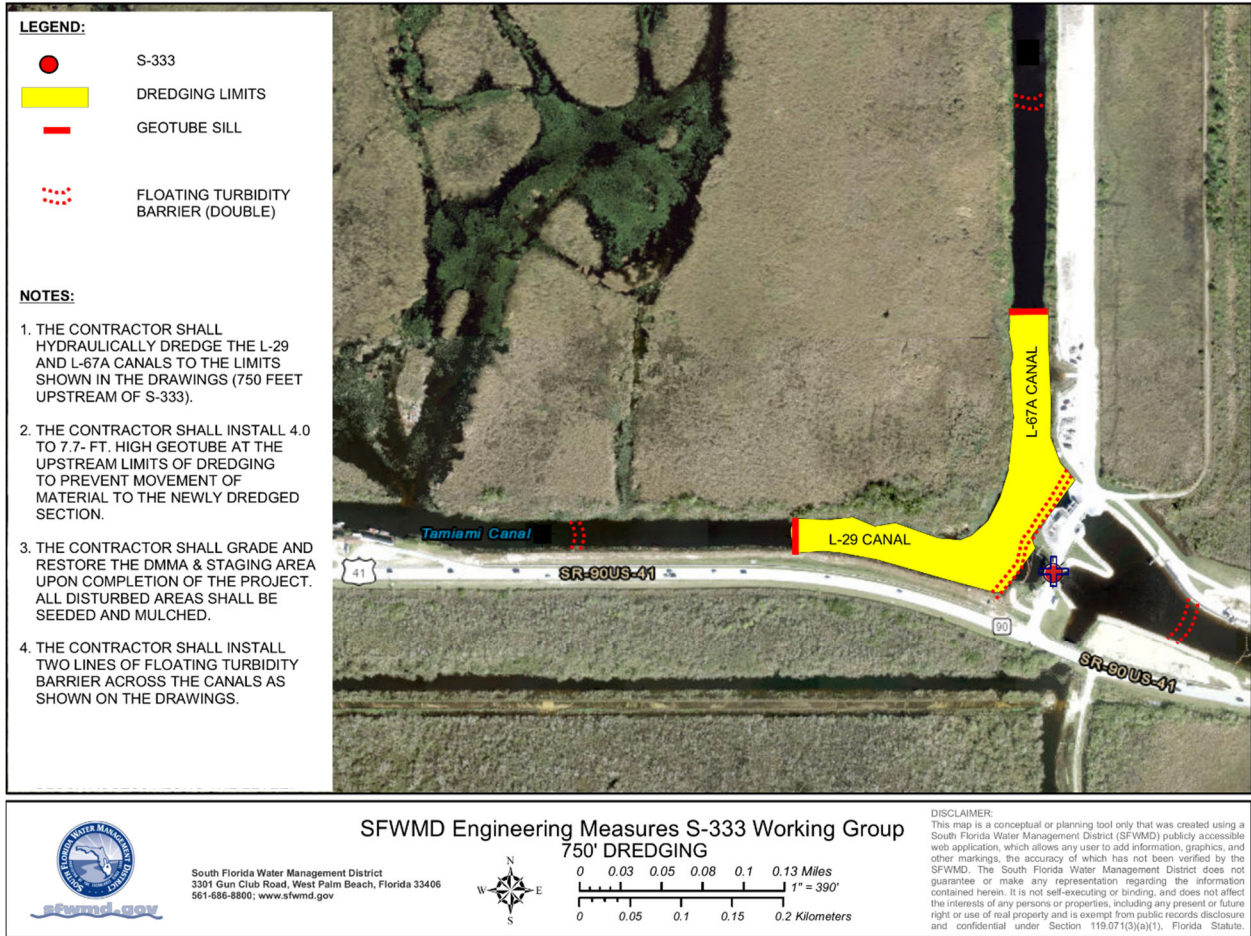Option 1 – $137,964.34
Option 2 – $259,000.00
Option 3 – $479,629.63

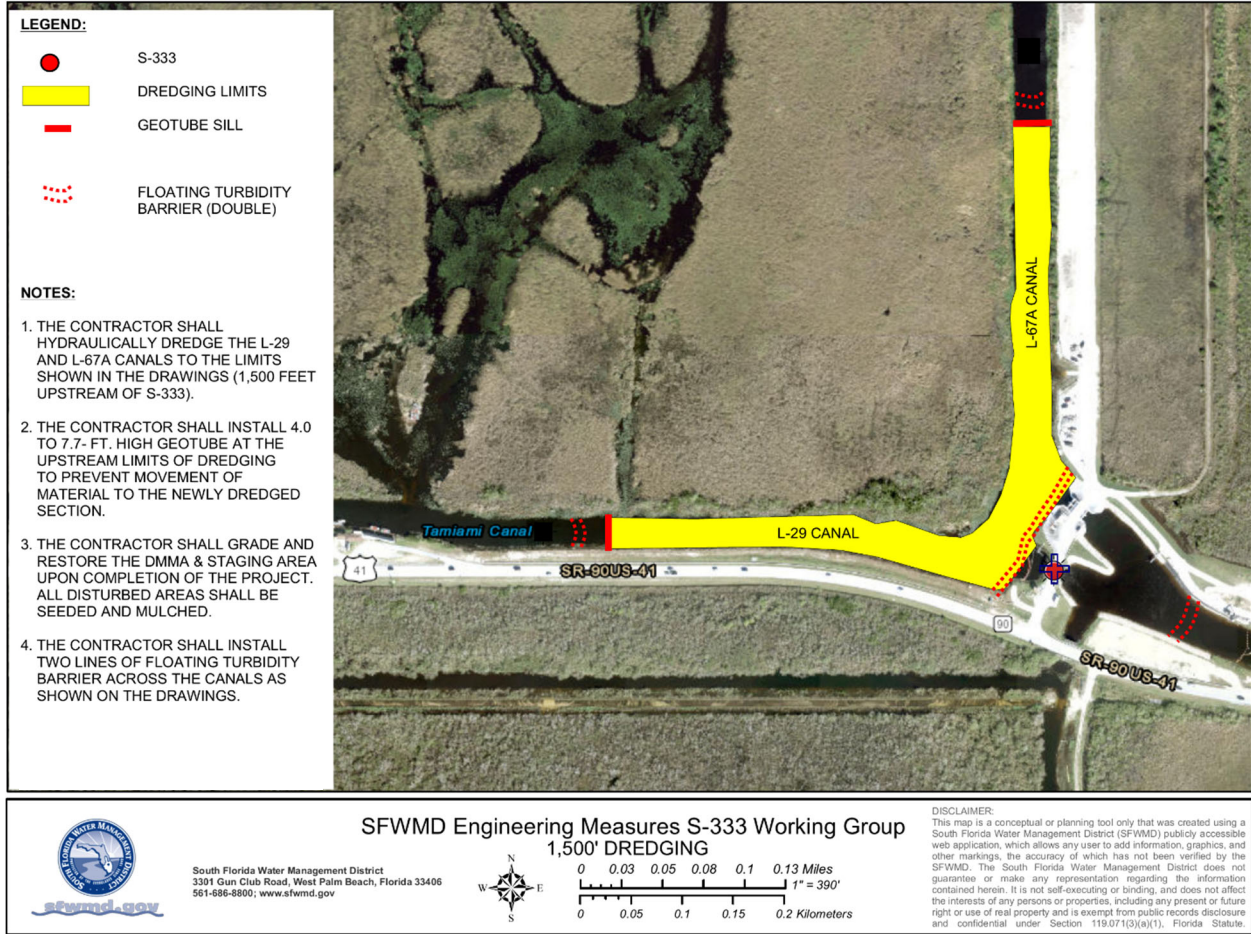**Figure 1.** Dredging of L-29 and L-67A canals 750 linear feet upstream of S-333.

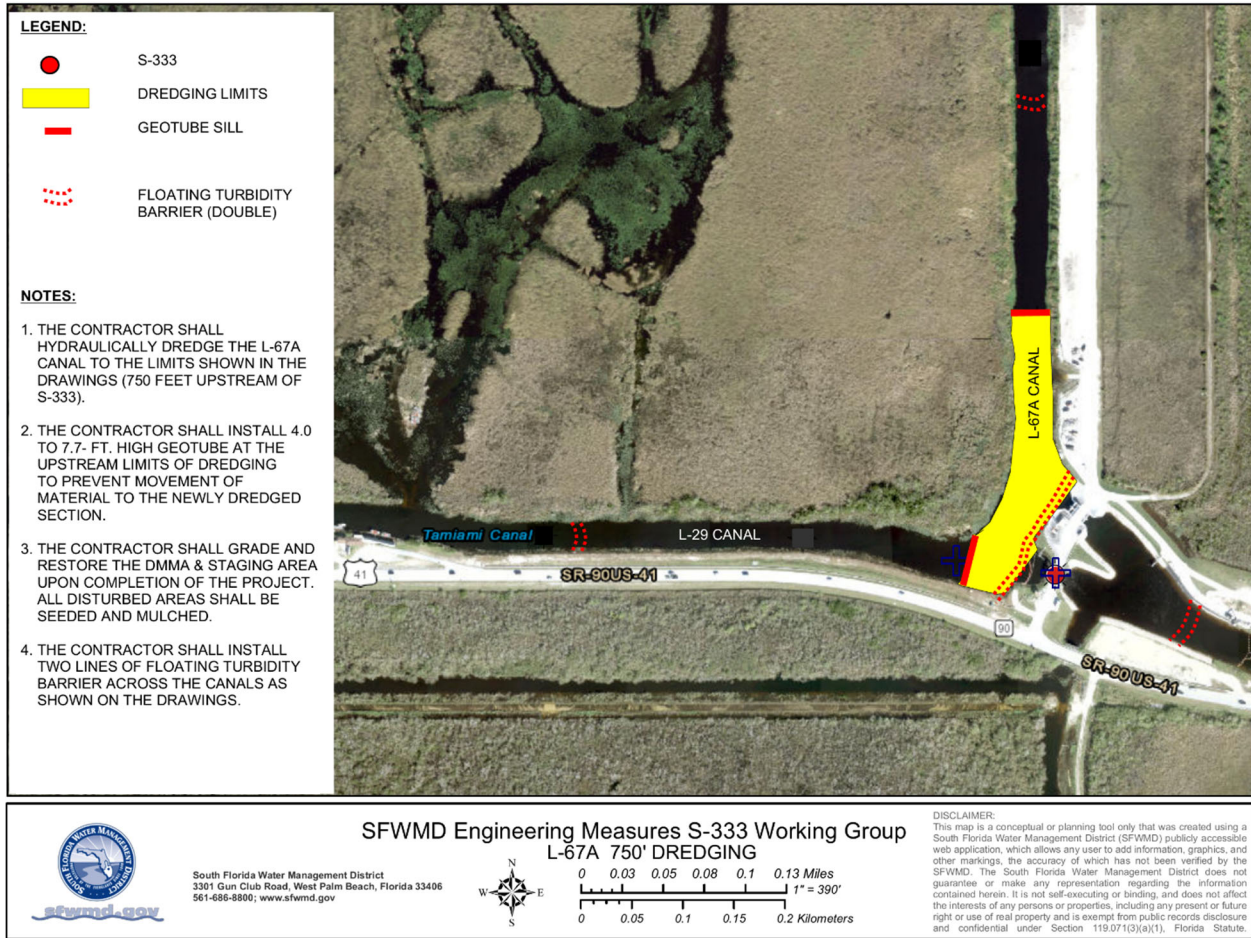**Figure 2.** Dredging of L-29 and L-67A canals 1,500 linear feet upstream of S-333.

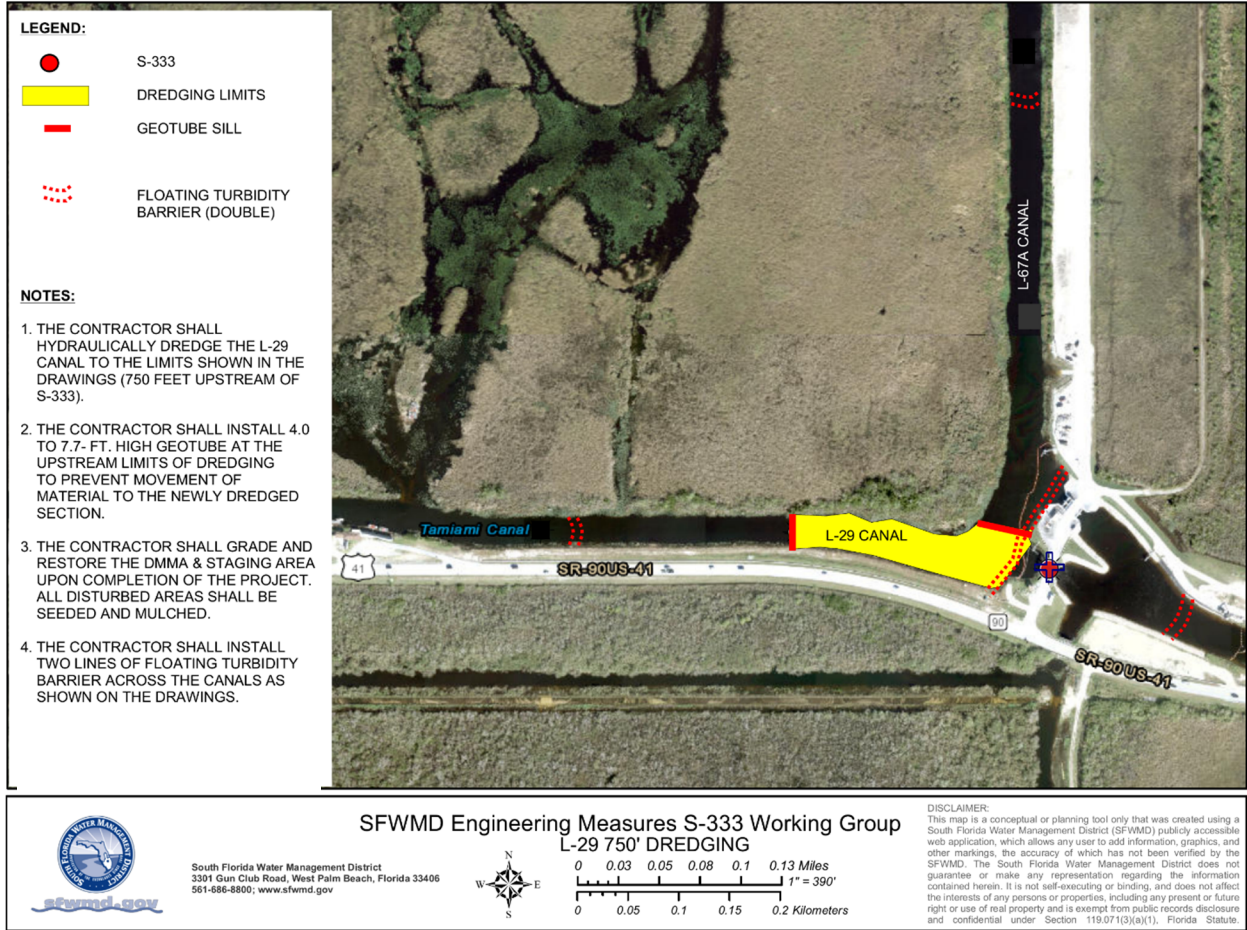**Figure 3.** Dredging of L-67A canal only 750 linear feet upstream of S-333.

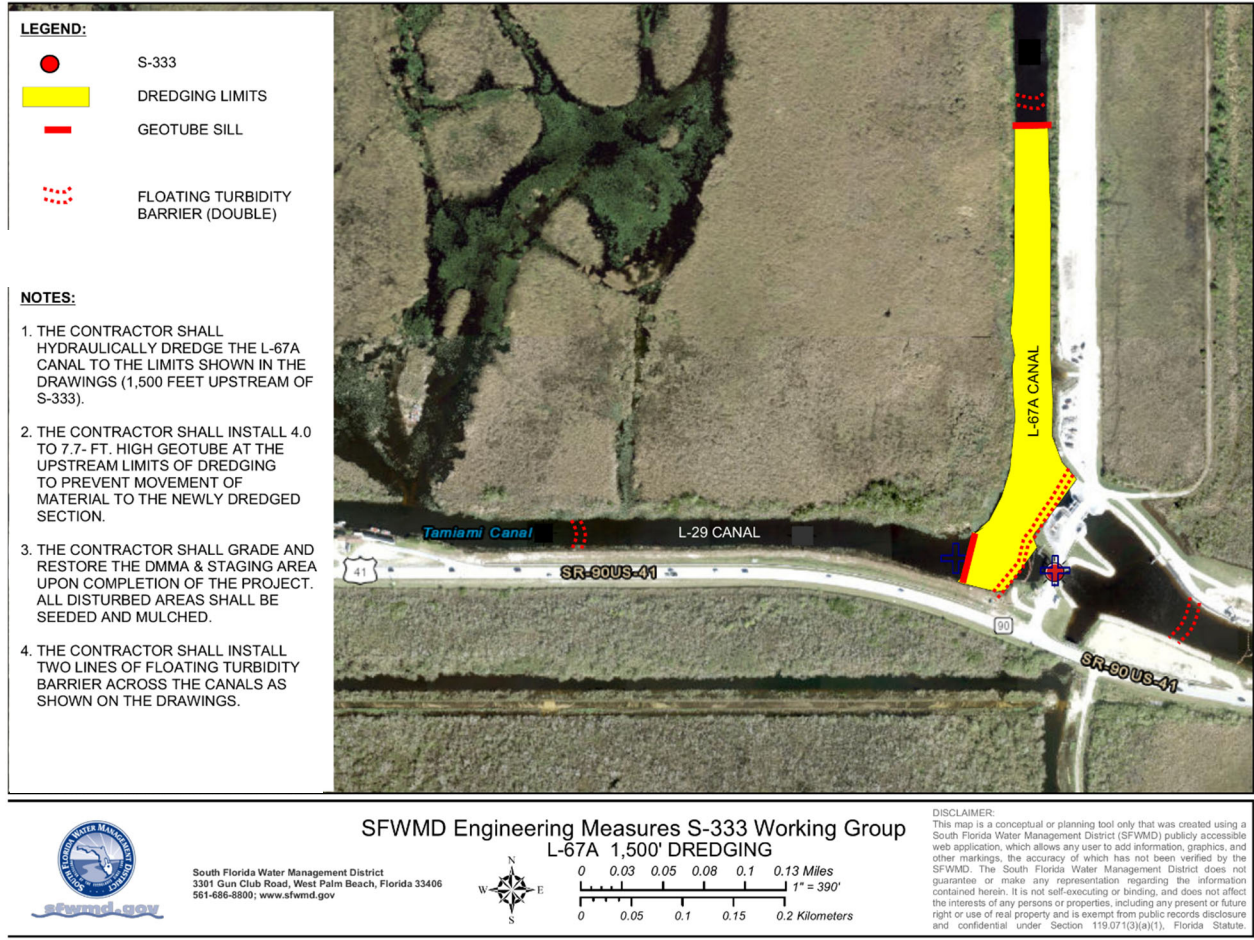**Figure 4.** Dredging of L-29 canal only 750 linear feet upstream of S-333.

Figure 5. Dredging of L-67A canal only 1,500 linear feet upstream of S-333.
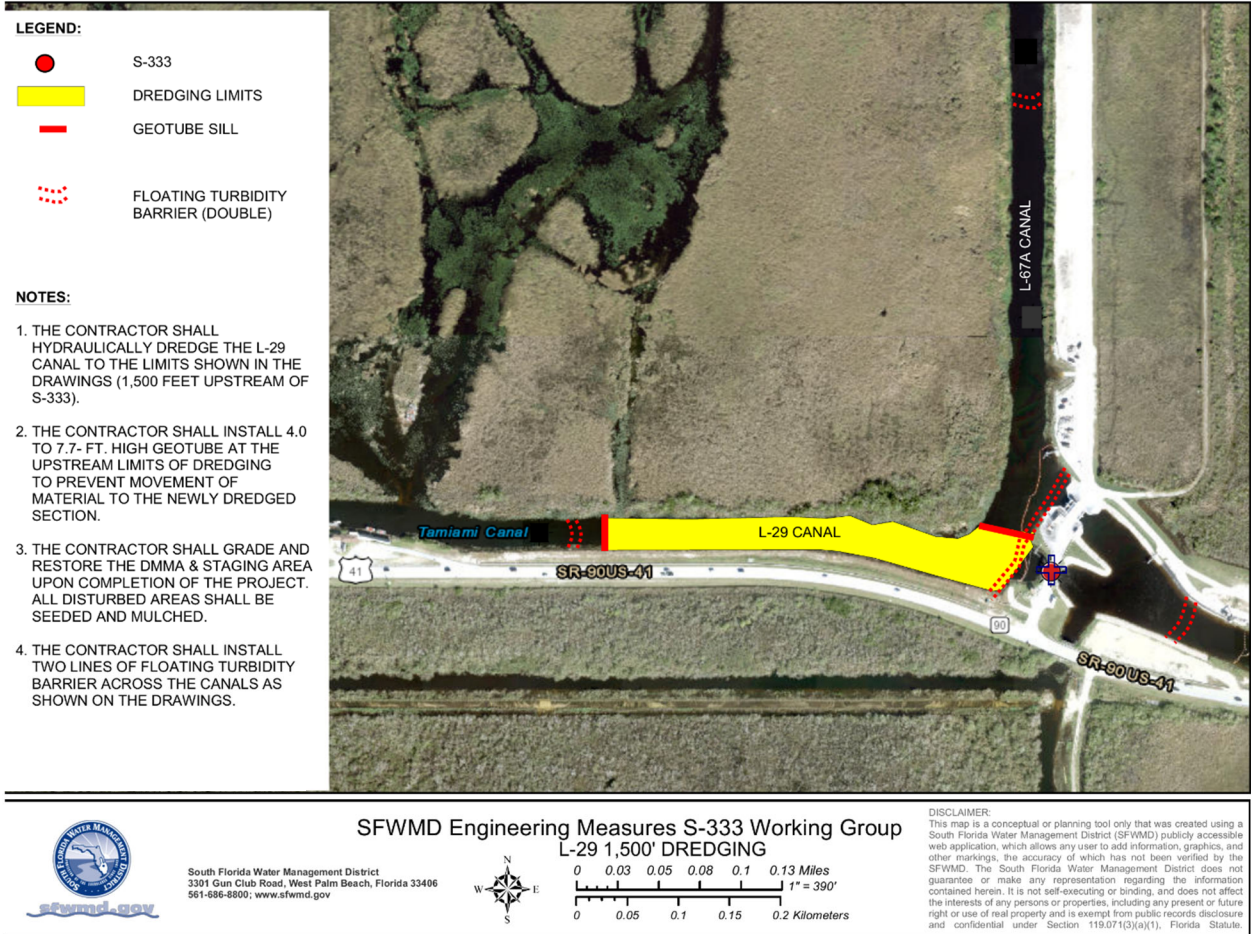
Figure 6. Dredging of L-29 canal only 1,500 linear feet upstream of S-333.
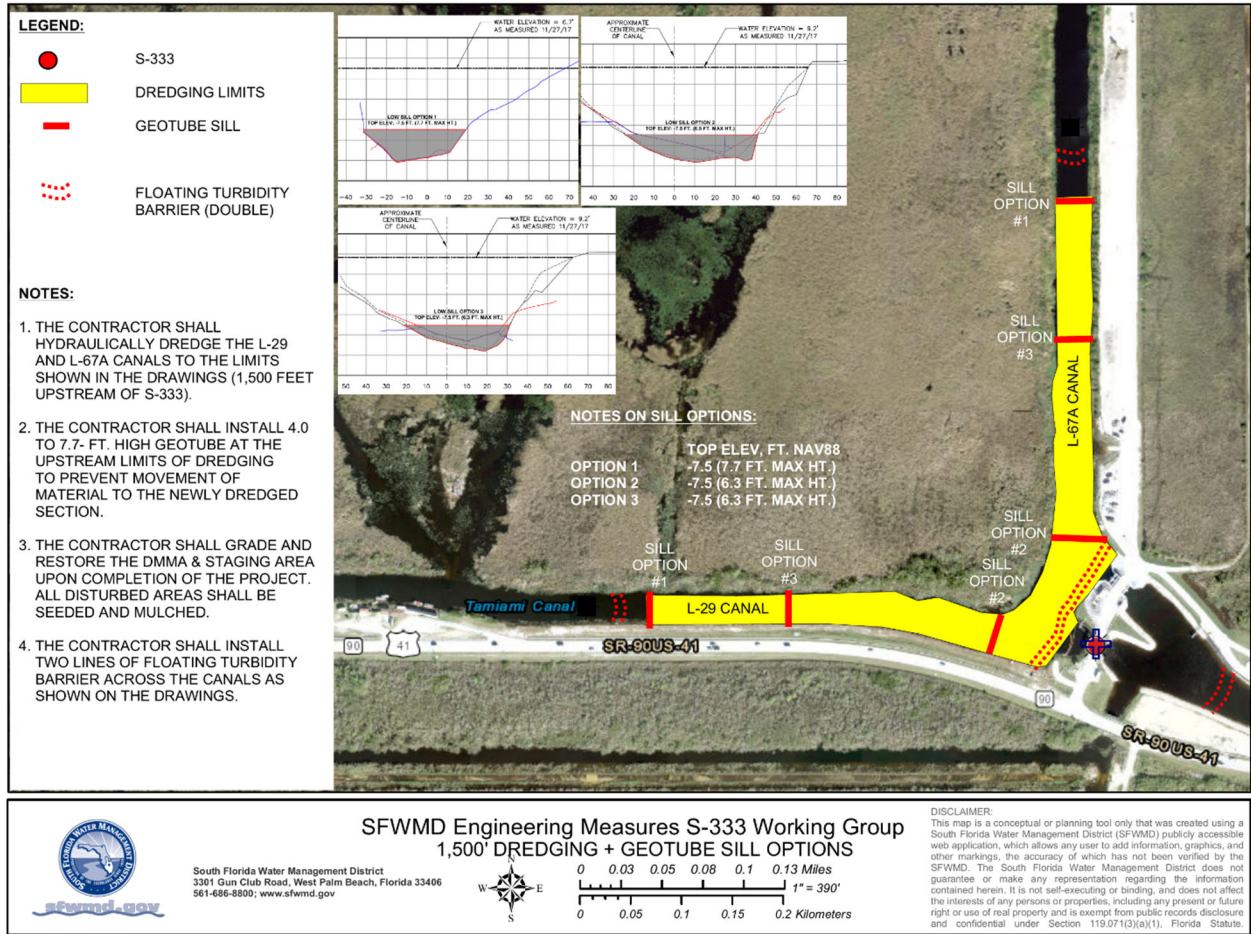
Figure 7. Low-sill weir options along the canal bottom in both
the L-67A and L-29 canals upstream of the S-333/S-333N complex.

Table 1. Cost estimate and implementation timeline.

	2023			2024												2025					Costs[2,3]
	Oct	Nov	Dec	Jan	Feb	Mar	Apr	May	Jun	Jul	Aug	Sep	Oct	Nov	Dec	Jan	Feb	Mar	Apr	May	
Canal Maintenance Dredging																					
Option 1 - dredging 750' upstream of the S-333 structures in both the L-67A and L-29 Canals[1]																					$1,651,573
Option 2 - dredging 1,500' upstream of the S-333 structures in both the L-67A and L-29 Canals[1]																					$2,313,574
Option 3 - dredging 750' upstream of the S-333 structures in the L-67A Canal or L-29 Canal[1]																					$1,063,167[3a] or $1,241,229[3b]
Option 4 - dredging 1,500' upstream of the S-333 structures in the L-67A Canal or L-29 Canal[1]																					$1,273,821[3a] or $1,752,734[3b]
Low-Sill Weir Pilot Test																					
Option 1 - Two placement locations[1]																					$137,964
Option 2 - Four placement locations[1]																					$259,000
Option 3 - Six placement locations[1]																					$479,629

Notes:
1. Includes design, permitting and construction durations that are standard industry durations.
2. The cost estimate provided includes planning, permitting, design, and construction.
3. Two cost estimates are provided for canal maintenance dredging options 3 and 4 since the Phase I studies concluded a greater sediment volume in the L-29 Canal vs. the L-67A canal. (a)Cost for L-67A Canal, (b)Cost for L-29 Canal.